RĪGAS TEHNISKĀ UNIVERSITĀTE

Ralfs Pomilovskis

MAIKLA KOMPONENTU SINTĒZE NO TALEĻĻAS TAUKSKĀBĒM UN TO IZMANTOŠANA POLIMĒRMATERIĀLU IEGUVEI

Promocijas darbs

SYNTHESIS OF THE MICHAEL COMPONENTS FROM TALL OIL FATTY ACIDS AND THEIR VALORISATION FOR POLYMER MATERIALS DEVELOPMENT

Doctoral Thesis

RTU Izdevniecība
RTU Press
Rīga 2024

RĪGAS TEHNISKĀ UNIVERSITĀTE

Dabaszinātņu un tehnoloģiju fakultāte

Ķīmijas un ķīmijas tehnoloģijas institūts

RIGA TECHNICAL UNIVERSITY

Faculty of Natural Sciences and Technology

Institute of Chemistry and Chemical Technology

Ralfs Pomilovskis

Doktora studiju programmas "Ķīmija, materiālzinātne un tehnoloģijas" doktorants

Doctoral Student of the Study Programme "Chemistry, Materials Science and Engineering"

MAIKLA KOMPONENTU SINTĒZE NO TALEĻĻAS TAUKSKĀBĒM UN TO IZMANTOŠANA POLIMĒRMATERIĀLU IEGUVEI

Promocijas darbs

SYNTHESIS OF THE MICHAEL COMPONENTS FROM TALL OIL FATTY ACIDS AND THEIR VALORISATION FOR POLYMER MATERIALS DEVELOPMENT

The Doctoral Thesis

Zinātniskie vadītāji / Scientific supervisors

Ph. D. Miķelis Kirpļuks

Dr. chem. Inese Mieriņa

Rīga / Riga 2024

Pomilovskis, R. Maikla komponentu sintēze no taleļļas taukskābēm un to izmantošana polimērmateriālu ieguvei. Promocijas darbs. Rīga: RTU Izdevniecība, 2024. 202 lpp.

Publicēts saskaņā ar RTU promocijas padomes "P-01" 2024. gada 8. aprīļa lēmumu, protokols Nr. 04030-9.1/61.

Promocijas darbs izstrādāts Latvijas Valsts koksnes ķīmijas institūtā un Rīgas Tehniskajā universitātē.

LATVIJAS VALSTS KOKSNES ĶĪMIJAS INSTITŪTS

1862 RTU DABASZINĀTŅU UN TEHNOLOĢIJU FAKULTĀTE

Promocijas darbs izstrādāts FLPP "Augsta atjaunojamo vielu satura termoreaktīvo polimēru izstrāde no augu izcelsmes eļļām (*Bio-Mer*)" ietvarā.

FLPP FUNDAMENTĀLO UN LIETIŠĶO PĒTĪJUMU PROJEKTI

Promocijas izstrādāts ar Eiropas Sociālā fonda atbalstu darbības programmas "Izaugsme un nodarbinātība" 8.2.2. specifiskā atbalsta mērķa "Stiprināt augstākās izglītības institūciju akadēmisko personālu stratēģiskās specializācijas jomās" projektā Nr. 8.2.2.0/20/I/008 "Rīgas Tehniskās universitātes un Banku augstskolas doktorantu un akadēmiskā personāla stiprināšana stratēģiskās specializācijas jomās" un ar Rīgas Tehniskās universitātes Doktorantūras grantu programmas atbalstu.

NACIONĀLAIS ATTĪSTĪBAS PLĀNS 2020

EIROPAS SAVIENĪBA
Eiropas Sociālais fonds

IEGULDĪJUMS TAVĀ NĀKOTNĒ

PROMOCIJAS DARBS IZVIRZĪTS ZINĀTNES DOKTORA GRĀDA IEGŪŠANAI RĪGAS TEHNISKAJĀ UNIVERSITĀTĒ

Promocijas darbs zinātnes doktora (*Ph. D.*) grāda iegūšanai tiek publiski aizstāvēts 2024. gada 13. jūnijā plkst. 16.30 Rīgas Tehniskās universitātes Dabaszinātņu un tehnoloģiju fakultāte fakultātē, Paula Valdena ielā 3/7, 272. auditorijā. Atklātajā sēdē būs iespējams piedalīties arī tiešsaistē *Zoom* platformā (https://rtucloud1.zoom.us/j/9352086644).

OFICIĀLIE RECENZENTI

Tenūrprofesors *Dr. sc. ing.* Sergejs Gaidukovs,
Rīgas Tehniskās universitāte

Asistentprofesors *Ph. D. Ondřej Sedláček*,
Kārļa Universitāte, Čehija

Profesore *Dr. Arantxa Eceiza*,
Basku Zemes universitāte, Spānija

APSTIPRINĀJUMS

Apstiprinu, ka esmu izstrādājis šo promocijas darbu, kas iesniegts izskatīšanai Rīgas Tehniskajā universitātē zinātnes doktora (*Ph. D.*) grāda iegūšanai. Promocijas darbs zinātniskā grāda iegūšanai nav iesniegts nevienā citā universitātē.

Ralfs Pomilovskis ……...
(paraksts)

Datums: ……

Promocijas darbs sagatavots kā tematiski vienotu zinātnisko publikāciju kopa ar kopsavilkumu latviešu un angļu valodā. Tajā ietverti septiņi zinātniskie oriģinālraksti angļu valodā. Promocijas darba kopējais apjoms, ieskaitot septiņus pielikumus, ir 202 lpp.

SAĪSINĀJUMI

AA	acetoacetāts
BD	1,4-butāndiols
BPAEDA	bisfenola A etoksilātdiakrilāts
cvKMR	cietvielu kodolu magnētiskā rezonanse
DMA	dinamiski mehāniskā analīze
DSC	diferenciālā skenējošā kalorimetrija
$E_{(\text{spiede})}$	spiedes modulis noteikts no spiedes testiem
$E_{(\text{uzkrājuma})}$	uzkrājuma modulis, kas noteikts ar dinamiski mehāniskās analīzes palīdzību
$E_{(\text{stiepe})}$	stiepes modulis, kas noteikts ar stiepes testu palīdzību
$E^{IR}TOFA$	epoksidētas taleļļas taukskābes
ESOA	epoksidētas sojas eļļas akrilāts
f	funkcionalitāte
FTIR	Furjē transformācijas infrasarkanās spektroskopija
GPC	gēla caurlaidības hromatogrāfija
KMR	kodolu magnētiskā rezonanse
MALDI-TOF MS	matricas saistītā lāzera desorbcijas/jonizācijas lidojuma laika masspektrometrija
M_c	molekulmasa starp šķērssaitēm
NIPU	bez izocianāta poliuretāns
PETA	pentaeritritoltetraakrilāts
T_g	stiklošanās temperatūra
TGA	termogravimetriskā analīze
TMP	trimetilolpropāns
TMPTA	trimetilolpropāntriakrilāts
ε	stiepes pagarinājums
λ	siltumvadītspējas koeficients
ν_e	šķērssaistīšanās blīvums
ρ	blīvums
σ	stiepes stiprība

SATURS

PROMOCIJAS DARBA VISPĀRĒJS RAKSTUROJUMS

Ievads

Pēdējos gados arvien lielāka zinātniskā interese tiek izrādīta par inovatīvu putu polimērmateriālu izstrādi. Šo pieaugošo interesi veicina putu materiālu plašais lietojums daudzās nozarēs. Mūsdienās šie materiāli ir kļuvuši neaizstājami tādās nozarēs kā būvniecībā (nodrošina izolāciju) [1], iepakojuma ražošanā (piedāvājot vieglus aizsargmateriālus) [2], autobūvē (samazinot masu un paaugstinot drošību) [3–5], un, īpaši šobrīd, aktualizējas putu polimērmateriālu izmantošanas iespējas militārajā aizsardzības nozarē [6]. Plašo putu polimērmateriālu lietojumu nodrošina to unikālās īpašības, kas ietver zemu blīvumu, labu stiprības un masas attiecību, kā arī izcilu siltumizolāciju [7–10]. Tomēr pašreizējie globālie izaicinājumi, kas galvenokārt saistīti ar fosilo resursu izsīkšanu, vides piesārņojumu un klimata pārmaiņām, rada nepieciešamību steidzīgi rast ilgtspējīgus no atjaunojamiem resursiem iegūtus alternatīvus materiālus [11–17].

Tradicionālie putu polimērmateriāli, tostarp visplašāk lietotie poliuretāna materiāli, sen ir kļuvuši par neaizstājamu materiālu daudzās nozarēs [5, 18]. Tomēr šo tradicionālo poliuretāna materiālu plašā izmantošana ir viens no iepriekš minēto globālo problēmu izraisītājiem un neatbilst mūsdienu ilgtspējības prasībām [19–23]. Poliuretāna putu polimērmateriālu ražošanai izmanto toksiskos izocianātus, ko galvenokārt iegūst no fosilajiem resursiem [24, 25], un patlaban nav ekonomiski pamatotu no atjaunojamiem resursiem iegūstamu alternatīvu [26]. Maikla reakcijas izmantošana putu polimērmateriālu ieguvei varētu būt inovatīvs risinājums problēmām, kas saistītas ar tradicionālo putu polimērmateriālu izmantošanu, jo paver iespēju polimērmateriālu ieguvei no bioresursiem [27].

Maikla reakcija ir zināma ķīmiskā reakcija, ko plaši izmanto dažādās ķīmijas nozarēs. Taču polimēru ķīmijā tā ir jauna pieeja materiālu sintēzei [27–30]. Viens no pazīstamākajiem Maikla reakciju veidiem ietver reakciju starp acetoacetātu kā Maikla donoru un akrilātu kā Maikla akceptoru [31–34]. Acetoacetātam ir aktīva metilēngrupa, kas kalpo kā nukleofīlais centrs un katalizatora klātbūtnē viegli reaģē ar elektroniem "nabadzīgo" akrilāta grupu dubultsaiti, veidojot oglekļa-oglekļa (C-C) saiti [31, 35]. Maikla reakcija sniedz iespēju sintezēt polimērmateriālus ar pielāgotām īpašībām, kas to padara par perspektīvu pieeju inovatīvu putu polimērmateriālu izveidē.

Taleļļas izmantošana ir daudzsološs ceļš polimēru ķīmijas nozares attīstībā. Tā ir vērtīga otrās paaudzes izejviela, ko iegūst kā blakusproduktu koksnes pārstrādes, celulozes ražošanas procesā [36, 37]. Destilēta taleļļa galvenokārt sastāv no oleīnskābes un linolskābes ar nelielu daudzumu citu taukskābju, sveķskābju un sterolu piemaisījumu. Epoksidētas taleļļas taukskābju polioli ir veiksmīgi izmantoti poliuretānu materiālu ieguvē daļēji no atjaunojamajiem resursiem [38]. No epoksidētas taleļļas iegūtos poliolus var izmantot kā prekursorus tādu komponentu sintēzei, kas piemēroti polimērmateriālu ieguvē, izmantojot Maikla reakciju (1. att.).

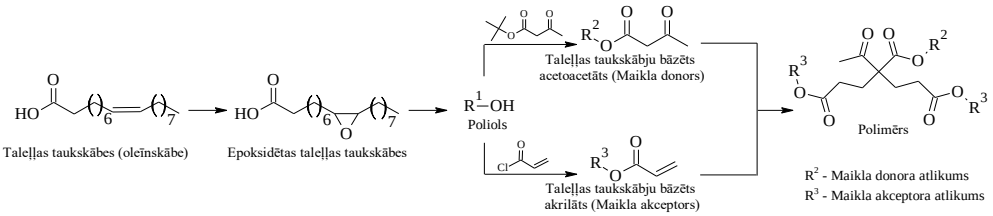

1. att. Piedāvātais dizains polimērmateriālu ieguvei no taleļļas taukskābēm, izmantojot Maikla reakciju.

Pētījuma mērķis un uzdevumi

Promocijas darba mērķis bija izstrādāt jaunu konceptu Maikla komponentu (acetoacetātu un akrilātu) sintēzei no atjaunojamajiem resursiem, kā arī iegūt polimērmateriālus (t. sk. putu polimērmateriālus), izmantojot Maikla reakciju. Galvenais uzdevums bija izstrādāt mūsdienu ilgtspējības kritērijiem atbilstošus putu polimērmateriālus, kā izejvielu izmantojot otrās paaudzes izejvielu – taleļļu, kas ir celulozes ražošanas blakusprodukts. Pētījums ietvēra taleļļas acetoacetātu (Maikla donora) un atšķirīgas izcelsmes akrilātu (Maikla akceptoru) izmantošanu gan elastīgu, gan cietu putu polimērmateriālu ieguvei ar plašu lietojumu, jo īpaši siltumizolācijai.

Darba mērķa īstenošanai definēti vairāki uzdevumi.

1. Sintezēt Maikla komponentus (Maikla donoru un Maikla akceptoru) no taleļļas, vispirms iegūstot prekursorus (poliolus), veicot taleļļas taukskābju dubultsaišu epoksidēšanu un sekojošu oksirāna gredzenu šķelšanu un karboksilgrupu esterificēšanu ar spirtu. Pēc tam no poliola iegūt Maikla donoru, veicot pāresterificēšanu ar *terc*-butilacetoacetātu, un Maikla akceptoru, akrilējot ar akriloilhlorīdu.
2. Iegūt polimērmateriālus, izmantojot sintezētos taleļļas Maikla donorus un komerciāli pieejamos Maikla akceptorus, lai pārbaudītu sintezētā donora piemērotību polimerizācijas reakcijai un izpētītu iegūto polimērmateriālu termiskās un mehāniskās īpašības.
3. Iegūt polimērmateriālus, izmantojot sintezētos taleļļas Maikla donorus un taleļļas Maikla akceptorus, un izpētīt iegūto polimērmateriālu termiskās un mehāniskās īpašības.
4. Iegūt putu polimērmateriālus, izmantojot sintezētos taleļļas Maikla donorus un taleļļas Maikla akceptorus, un izpētīt iegūto putu polimērmateriālu mehāniskās un termiskās īpašības.

Aizstāvamās tēzes

1. Maikla donorus un Maikla akceptorus var sintezēt no taleļļas, veicot taleļļas taukskābju epoksidēšanu, pēc tam – oksirāna gredzenu šķelšanu un karboksilgrupu esterificēšanu ar spirtiem, kam seko acetoacetilēšana, lai iegūtu Maikla donorus (acetoacetātus), vai akrilēšana, lai iegūtu Maikla akceptorus (akrilātus).

2. Taleļļas Maikla donori ir piemēroti polimēru iegūšanai reakcijā ar dažādiem komerciāli pieejamiem akrilātiem, turklāt termiskās un mehāniskās īpašības var pielāgot, mainot izmantoto komponentu funkcionalitāti, tādējādi iegūstot tādus polimērus, kas spēj konkurēt ar patlaban plaši lietotiem polimēriem.
3. Polimērus var iegūt no taleļļas acetoacetātiem un akrilātiem, turklāt termiskās un mehāniskās īpašības var pielāgot, mainot izmantoto komponentu funkcionalitāti, tādējādi iegūstot tādus polimērus, kas spēj konkurēt ar patlaban plaši lietotiem polimēriem.
4. Putu polimērmateriālus var iegūt, izmantojot taleļļas acetoacetātu un dažādas izcelsmes akrilātus, turklāt termiskās un mehāniskās īpašības var pielāgot, mainot izmantoto komponentu funkcionalitāti, tādējādi iegūstot putu polimērmateriālu dažādiem lietojumiem, īpaši – kā siltumizolācijas materiāliem.

Zinātniskā novitāte

Veikto pētījumu rezultātā izstrādāta jauna stratēģija vērtīgu ķīmisku vielu un inovatīvu polimērmateriālu ieguvei no taleļļas, sniedzot nozīmīgu pienesumu mežsaimniecībā balstītas ekonomikas attīstībā un zināšanas mūsdienu ilgtspējības prasībām atbilstošu polimērmateriālu, t. sk. putu polimērmateriālu, izstrādē.

Pētījums ir viens no pirmajiem nozarē, kurā iegūti Maikla komponenti no taleļļas brīvajām taukskābēm, tādējādi dažādojot Maikla komponentu iegūšanas iespējas līdztekus tradicionāli izmantotajiem triglicerīdiem. Pirmo reizi Maikla komponenti sintezēti no taleļļas polioliem ar atšķirīgu funkcionālo grupu skaitu. Maikla donori (acetoacetāti) tika sintezēti, poliolos esošās hidroksilgrupas pārvēršot acetoacetāta esteros. Polioli sintezēti no taleļļas, epoksidējot dubultsaites, kā katalizatoru izmantojot jonapmaiņas sveķus, pēc tam šķeļot oksirāna gredzenu un esterificējot skābes grupas ar daudzfunkcionāliem spirtiem. Sintezēto taleļļas poliolu priekšrocība ir to plašās funkcionalizēšanas iespējas, tai skaitā tie paši polioli var kalpot arī kā prekursori daudzfunkcionālu akrilātu sintezēšanai. Veiksmīgi tika iegūti arī Maikla akceptori (akrilāti) no taleļļas taukskābēm. Šī pētījuma novitāte bija abu Maikla komponentu (Maikla donora un Maikla akceptora) sintēze no vienas un tās pašas atjaunojamās izejvielas – taleļļas taukskābēm. Sintezētie Maikla komponenti veiksmīgi izmantoti polimēru ieguvei, izmantojot Maikla reakciju. Turklāt no taleļļas taukskābēm sintezētie akrilāti varētu būt potenciāli izmantojami citu veidu polimēru ražošanā, piemēram, UV ierosinātajā brīvo radikāļu polimerizācijā pārklājumu ražošanā.

Darbā izpētīts sintezēto taleļļas acetoacetātu potenciāls putu polimērmateriālu izstrādē reakcijā ar taleļļas akrilātu. Putu polimērmateriālu ieguvē tika izmantoti arī tādi komerciāli pieejami akrilāti kā bisfenola A etoksilātdiakrilāts, trimetilolpropāntriakrilāts, pentaeritritoltetraakrilāts un epoksidētas sojas eļļas akrilāts. Tika salīdzinātas šo inovatīvo materiālu mehāniskās, termomehāniskās un termiskās īpašības.

Promocijas darbs sniedz pirmās nozīmīgās atziņas par polimēru sveķu formulāciju izstrādi un putu polimērmateriālu ieguvi, izmantojot Maikla reakciju, no komponentiem, kas sintezēti no taleļļas taukskābēm. Putu polimērmateriāli, kas iegūti no taleļļas acetoacetāta un taleļļas akrilāta, varētu būt daudzsološa alternatīva pašreiz plaši lietotiem poliuretāna putu polimērmateriāliem, iezīmējot īstenojamu ceļu, lai samazinātu atkarību no fosilajiem resursiem un polimēru ražošanas industrijas ietekmi uz vidi.

Promocijas darba struktūra un apjoms

Promocijas darbs sagatavots kā tematiski vienota zinātnisko publikāciju kopa, kas veltīta polimērmateriālu izstrādei no taleļļas taukskābēm, izmantojot Maikla reakciju. Promocijas darbs apkopo septiņas oriģinālpublikācijas *Scopus* indeksētos žurnālos.

Promocijas darba aprobācija un publikācijas

Zinātniskās publikācijas

1. **R. Pomilovskis**, E. Kaulina, A. Abolins, I. Mierina, I. Heinmaa, V. Rjabovs, A. Fridrihsone, M. Kirpluks, Fast-curing bio-based thermoset foams produced *via* the Michael 1,4-addition using fatty acid-based acetoacetate and acrylate, Eur. Polym. J. 210 (2024) 112968. 10.1016/j.eurpolymj.2024.112968. (*IF* 6,0, *CiteScore* 9,6).

2. **R. Pomilovskis**, E. Kaulina, I. Mierina, A. Abolins, O. Kockova, A. Fridrihsone, M. Kirpluks, Wood pulp industry by-product valorization for acrylate synthesis and bio-based polymer development *via* Michael addition reaction, J. Bioresour. Bioprod. 8 (2023) 265–279. 10.1016/j.jobab.2023.06.001. (*CiteScore* 30,6).

3. **R. Pomilovskis**, I. Mierina, A. Fridrihsone, M. Kirpluks, Bio-based polymer developments from tall oil fatty acids by exploiting Michael addition, Polymers (Basel). 14 (2022) 4068. 10.3390/polym14194068. (*IF* 5,0, *CiteScore* 6,6).

4. **R. Pomilovskis**, I. Mierina, H. Beneš, O. Trhlíková, A. Abolins, A. Fridrihsone, M. Kirpluks, The synthesis of bio-based Michael donors from tall oil fatty acids for polymer development, Polymers (Basel). 14 (2022). 10.3390/polym14194107. (*IF* 5,0, *CiteScore* 6,6).

5. A. Abolins, D. Eihe, **R. Pomilovskis**, A. Fridrihsone, M. Kirpluks, Rapeseed oil as feedstock for the polymeric materials *via* Michael addition reaction, Ind. Crops Prod. 204 (2023) 117367. 10.1016/j.indcrop.2023.117367. (*IF* 5,9, *CiteScore* 9,7).

6. M. Kirpluks, **R. Pomilovskis**, E. Vanags, A. Abolins, I. Mierina, A. Fridrihsone, Influence of different synthesis conditions on the chemo-enzymatic epoxidation of tall oil fatty acids, Process Biochem. 122 (2022) 38–49. 10.1016/j.procbio.2022.08.024. (*IF* 4,4, *CiteScore* 7,9).

7. K. Polaczek, E. Kaulina, **R. Pomilovskis**, A. Fridrihsone, M. Kirpluks, Epoxidation of tall oil fatty acids and tall oil fatty acids methyl esters using the Spinchem® rotating bed reactor, J. Polym. Environ. (2022). 10.1007/s10924-022-02556-5. (*IF* 5,3, *CiteScore* 8,0).

Starptautiskais patenta pieteikums

Latvijas Valsts koksnes ķīmijas institūts. Miķelis Kirpļuks, **Ralfs Pomilovskis**, Arnis Āboliņš, Anda Fridrihsone. Plant oil-based polymer foam and method of manufacture thereof. Pieteikuma datums: 22.03.2023. Pieteikuma numurs: PCT/IB2022/052590. Publikācijas numurs: WO 2023/180786 A1.

Konferences, kurās prezentēti pētījumu rezultāti

1. **R. Pomilovskis**, E. Kaulina, I. Mierina, A. Abolins, O. Kockova, A. Fridrihsone, M. Kirpluks "Tall oil fatty acids valorization for acrylate synthesis and bio-based polymer development *via* Michael addition reaction", 2nd Conference on Green Chemistry and Sustainable Coatings. June 28–30, 2023, Pisa, Italy.

2. **R. Pomilovskis**, I. Mierina, E. Kaulina, A. Fridrihsone, M. Kirpluks, "By-product of the wood pulp industry – tall oil – utilisation for acrylate synthesis", International Conference on Renewable Resources & Biorefineries 2023 (RRB2023). May 31–June 2, 2023, Riga, Latvia.

3. **R. Pomilovskis**, I. Mierina, M. Kirpluks, "Polymer Developments from Tall Oil Fatty Acids using Michael Addition". Materials Science and Applied Chemistry. October 21, 2022, Riga, Latvia.

4. **R. Pomilovskis**, A. Fridrihsone, M. Kirpluks, "Tall oil fatty acids-based Michael donor monomer synthesis for thermoset polymers". EPF European Polymer Congress. June 26–July 1, 2022, Prague, Czech Republic.

5. **R. Pomilovskis**, I. Mierina, E. Kaulina, A. Fridrihsone, M. Kirpluks, "Bio-based polymer development from tall oil fatty acids by exploiting Michael reaction. Polymer development and characterization". International Conference on Renewable Resources & Biorefineries 2022 (RRB2022). June 1–3, 2022, Bruges, Belgium.

6. **R. Pomilovskis**, A. Fridrihsone, M. Kirpluks, "Bio-Based Polymer Development from tall oil fatty acids by exploiting Michael addition". International Conference for Young Scientists on Biorefinery Technologies and Products 2022 (BTechPro 2022!). April 27–29, 2022, Riga, Latvia.

7. **R. Pomilovskis**, A. Fridrihsone, A. Abolins, M. Kirpluks, "Michael donor monomer synthesis from tall oil fatty acids". International Conference on Renewable Resources & Biorefineries 2021 (RRB2021). September 6–8, 2021, Aveiro, Portugal.

8. A. Fridrihsone, A. Abolins, **R. Pomilovskis**, M. Kirpluks, "Bio-based Michael monomers from tall oil: life cycle assessment". The 11th International Conference on Life Cycle Management. September 6–8, 2023, Lille, France.

9. M. Kirpluks, **R. Pomilovskis**, A. Fridrihsone, "Tall oil fatty acids based thermoset foams obtained using Michael addition reaction". EPF European Polymer Congress. June 26–July 1, 2022, Prague, Czech Republic.

10. M. Kirpluks, **R. Pomilovskis**, "Bio-Based Thermoset Polymer as Viable Alternative for Rigid Polyurethane Foams". Polymers 2022: Turina New Trends in Polymer Science Health of the Planet, Health of the People. May 25–27, 2022, Turin, Italy.

PROMOCIJAS DARBA GALVENIE REZULTĀTI

Promocijas darba galvenie rezultāti apkopoti četrās daļās.

- Darba pirmajā daļā galvenā uzmanība pievērsta Maikla komponentu sintēzei no taleļļas taukskābēm, aprakstot sintēzes procesus, raksturojot iegūtos produktus un uzsverot atjaunojamo resursu izmantošanas nozīmību polimēru ķīmijā.
- Darba otrajā daļā aprakstīta polimērmateriālu ieguve no taleļļas Maikla donora un komerciāli pieejamajiem Maikla akceptoriem. Raksturoti iegūtie polimērmateriāli, uzsverot polimerizācijā izmantoto komponentu dažādās funkcionalitātes ietekmi uz materiāla īpašībām.
- Darba trešajā daļā pētīti polimērmateriāli ar dažādu šķērssaistīšanās blīvumu, kas sintezēti no taleļļas Maikla donora un akceptora, izceļot to augsto termisko stabilitāti un mehāniskās īpašības, pozicionējot tos kā potenciālu alternatīvu plaši lietotajiem termoreaktīvajiem sveķiem.
- Darba pēdējā daļā izzināta putu polimērmateriālu izstrāde no Maikla donoriem un akceptoriem, kas iegūti no atjaunojamajām izejvielām, analizējot šo materiālu daudzpusību un piemērotību dažādiem lietojumiem, īpaši – siltumizolācijā.

Promocijas darbā izstrādāto metožu mērķis bija izstrādāt jaunu pieeju Maikla komponentu (acetoacetātu un akrilātu) sintezēšanai no taleļļas brīvajām taukskābēm un izveidot polimēru matricu, kas piemērota dažādu materiālu ieguvei, īpaši uzsverot to potenciālās izmantošanas iespējas siltumizolējoša putu polimērmateriālu ražošanā.

1. Maikla komponentu sintēze no taleļļas taukskābēm

Galvenā Maikla reakcijas izmantošanas priekšrocība polimēru ķīmijā ir iespēja izmantot Maikla donoru un Maikla akceptoru, kas sintezēti no tādiem atjaunojamiem resursiem kā taukskābēm, piemēram, taleļļas taukskābēm. Taleļļas taukskābju izmantošanai ir vairāki pozitīvi vērtējami ieguvumi, piemēram, atkarības samazināšana no fosilajiem resursiem, turklāt taleļļas ieguve nekonkurē ar pārtikas un dzīvnieku barības ražošanu [37].

Taleļļa sastāv no nepiesātinātajām taukskābēm, kas satur dubultsaites, kas dod iespēju ķīmisko modifikāciju ceļā iegūt acetoacetātus. Process ir vairākpakāpju sintēze, kas ietver dubultsaites epoksidēšanu un pēcāk oksirāna gredzenu atvēršanu ar daudzfunkcionālu spirtu [39]. Pēc tam hidroksilgrupu acetoacetilēšanu īsteno, veicot transesterifikācijas ar tādiem savienojumiem kā *terc*-butilacetoacetāts un etilacetoacetāts [40–42]. Izvēloties atbilstošu spirtu, daudzpusīgā pieeja nodrošina iespēju iegūt vielas ar tādām pielāgotām īpašībām kā funkcionalitāte, molekulmasa, molekulas sazarotības pakāpe un ķīmiskais sastāvs. Šie pielāgojamie parametri sniedz iespēju ražot polimērmateriālus ar atšķirīgām īpašībām, padarot tos piemērotus daudziem dažādiem lietojumiem.

Taleļļas polioli var būt arī prekursori daudzfunkcionālu akrilātu sintēzei. Šajā procesā poliola hidroksilgrupas var akrilēt ar akriloilhlorīdu [43–45]. Iegūtos daudzfunkcionālos akrilātu tālāk var izmantot kā Maikla akceptorus. Ņemot vērā iepriekš minēto, abu Maikla komponentu sintēzei ir iespējams izmantot vienu un to pašu otrās paaudzes atjaunojamo izejvielu.

1.1. Maikla donoru sintēze no taleļļas taukskābēm

Taukskābju un to poliolu acetoacetilēšana vēl nav plaši pētīta. Ir publicēti tikai daži pētījumi par bioloģiskas izcelsmes poliolu acetoacetilēšanu. Zinātniskajā literatūrā atrodama informācija par veiksmīgu sojas pupiņu eļļas poliolu [46], rīcineļļas un rīcineļļas poliolu [41, 47–51] acetoacetilēšanu. Taukskābju poliolu hidroksilgrupas ir salīdzinoši viegli acetoacetilējamas transesterifikācijas reakcijā ar *terc*-butilacetoacetātu, iegūstot *β*-ketoesterus. Reakcija galvenokārt tiek īstenota 110–130 °C temperatūrā [46–49, 52, 53].

Patlaban tiek uzskatīts, ka *terc*-butilacetoacetāts ir vispiemērotākais reaģents acetoacetilēšanas reakcijai, jo tas ir efektīvs salīdzinoši maigos apstākļos, salīdzinot ar citiem analogiem, piemēram, metilacetoacetātu, etilacetoacetātu vai izopropilacetoacetātu. Turklāt *terc*-butilacetoacetāta izmantošanai ir vairākas priekšrocības, piemēram, stabilitāte uzglabāšanā, salīdzinoši zemas izmaksas un plaša komerciālā pieejamība, kas padara to par pievilcīgu izejvielu rūpnieciskajā ražošanā [53].

Pirmo reizi no taleļļas taukskābēm iegūtie polioli izmantoti, lai sintezētu Maikla donorus, pārvēršot poliolos esošās hidroksilgrupas acetoacetāta esteros. Idealizēta sintēzes shēma redzama 1.1. attēlā. Polioli sintezēti no taleļļas taukskābēm, izmantojot jonapmaiņas sveķu katalizētu epoksidēšanu un pēc tam sekojošu oksirāna gredzenu šķelšanu un skābes grupu esterificēšanu ar daudzfunkcionālu spirtu. Šajā darbā acetoacetāti tika sintezēti no diviem taleļļas polioliem un diviem komerciāli pieejamiem polioliem – *Lupranol 3300* (*L3300*), kas ir oksipropilēts glicerīns, un *Neopolyol 380* (*NEO380*), kas iegūts no rūpnieciskiem PET atkritumiem.

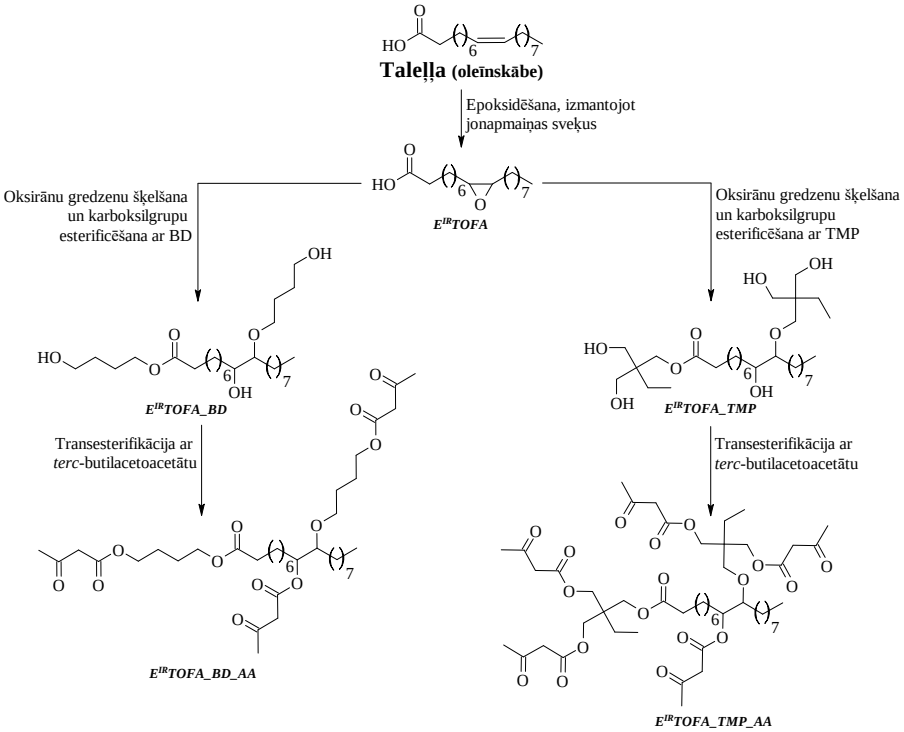

1.1. att. Idealizēta Maikla donora sintēzes shēma no taleļļas taukskābēm (oleīnskābes).

Sintezētie acetoacetāti, kā arī visi iegūtie starpprodukti raksturoti, izmantojot dažādas titrimetrijas metodes, lai noteiktu skābes, hidroksilgrupu, epoksīda un joda vērtības. Ķīmiskā struktūra tika analizēta, izmantojot *GPC* hromatogrammas, *FTIR,* KMR un *MALDI-TOF MS* spektrus. Iegūtajām vielām noteikta arī viskozitāte un tās atkarība no lietotās bīdes ātruma. 1.1. tabulā apkopots pārskats par raksturlielumiem, kas noteikti ar titrimetriskajām metodēm.

1.1. tabula

Sintezēto un komerciāli pieejamo poliolu un atbilstošā acetoacetāta raksturojums

	Viela	Skābes skaitlis, mg KOH/g	Hidroksil-skaitlis, Mg KOH/g	Joda skaitlis, g I_2/100 g	Mitrums, %	AA grupas, mol/100 g	Hidroksilgrupu konversija, mol%
Taleļļas atvasinājumi	*TOFA*	195	–	157	0,50	–	–
	E^{IR}TOFA	159	–	52,4	0,32	–	–
	E^{IR}TOFA_BD	5,8	258	–	0,20	–	–
	E^{IR}TOFA_BD_AA	< 5	36,2	–	0,025	0,3307	80,5
	E^{IR}TOFA_TMP	6,9	415	–	0,049	–	–
	E^{IR}TOFA_TMP_AA	< 5	41,6	–	0,037	0,4562	83,7
Komerciāli pieejamo poliolu	*NEO380*	<5	371	–	0,068	–	–
	NEO380_AA	< 5	40,7	–	0,048	0,4242	82,9
	L3300	< 5	400	–	0,060	–	–
	L3300_AA	< 5	26,2	–	0,021	0,4456	89,5

Oksirāna gredzenu šķelšanai izmantoto dažādo spirtu dēļ, iegūto *E^{IR}TOFA* poliolu hidroksilgrupu daudzums atšķīrās gandrīz divas reizes. Augstākais hidroksilgrupu saturs bija poliolam, kas iegūts, oksirāna gredzenus šķeļot un karboksilgrupas esterificējot ar TMP (f = 3). Oksirāna gredzenu šķelšanai un karboksilgrupu esterificēšanai izmanotjot BD (f = 2), tika iegūts poliols ar mazāku hidroksilgrupu saturu.

Lai iegūtu poliolu ar vēl augstāku hidroksilgrupu saturu, taleļļas taukskābes pirms epoksidēšanas var metilēt. Epoksidējot taleļļas taukskābju metilesterus, var novērst nevēlamas blakusreakcijas (oksirāna gredzenu šķelšanos ar taukskābju karboksilgrupām), un tas ļauj iegūt produktu ar augstāku epoksīda vērtību. Vēl viena pārbaudīta metode, lai iegūtu poliolu ar lielāku hidroksilgrupu saturu, ir epoksidēšanai kā katalizatorus izmantot enzīmus. Arī tas ievērojami palielina oksirāna iznākumu. Abām metodēm ir savi trūkumi – metilesteru izmantošana epoksidēšanai prasa papildu sintēzes posmu, savukārt enzīmi ir dārgi un būtiski palielina produkta pašizmaksu.

Pēc acetoacetilēšanas hidroksilgrupu saturs ievērojami samazinājās, jo *E^{IR}TOFA* poliolu hidroksilgrupas tika aizstātas ar acetoacetāta grupām. Tāda pati sakarība tika novērota arī komerciālo poliolu acetoacetilēšanas procesā. Komerciālie polioli izvēlēti, lai varētu salīdzināt sintēzes procesu norisi, produktu īpašības un piemērotību polimērmateriālu ieguvē ar sintezētajiem taleļļas polioliem. Acetoacetāta grupu saturs tika aprēķināts, ņemot vērā izmantoto acetoacetāta daudzumu un iegūtā produkta iznākumu.

Noteikts, ka komponentu viskozitāte nebija atkarīga no lietotā bīdes ātruma, kas liecina, ka iegūtās vielas bija Ņūtona šķidrumi (1.2. att.). Sintezētajiem Maikla donoriem piemītošās Ņūtona šķidruma īpašības ievērojami atvieglo šo acetoacetātu izmantošanu rūpniecībā, jo nav jāņem vērā lietotās bīdes ātruma ietekme uz vielu viskozitāti.

Polioliem, kas sintezēti no atjaunojamajām izejvielām, ir salīdzinoši augsta viskozitāte [54]. Vislielākā viskozitāte bija *E^{IR}TOFA_TMP* poliolam, kas sintezēts, atverot oksirāna gredzenus

un esterificējot ar TMP. *E*^{IR}*TOFA_TMP* viskozitāte bija lielāka par 118 000 mPa·s, kas ir salīdzinoši augsta viskozitāte un var apgrūtināt produkta izmantošanu rūpniecībā. *E*^{IR}*TOFA_TMP* poliola augstā viskozitāte galvenokārt skaidrojama ar lielo starpmolekulāro ūdeņraža saišu daudzumu. Tomēr pēc *E*^{IR}*TOFA_TMP* poliola acetoacetilēšanas viskozitāte būtiski samazinājās, un *E*^{IR}*TOFA_TMP_AA* viskozitāte bija 5500 mPa·s. Līdz ar to *E*^{IR}*TOFA_TMP_AA* lietošana rūpniecībā varētu būt vienkāršāka.

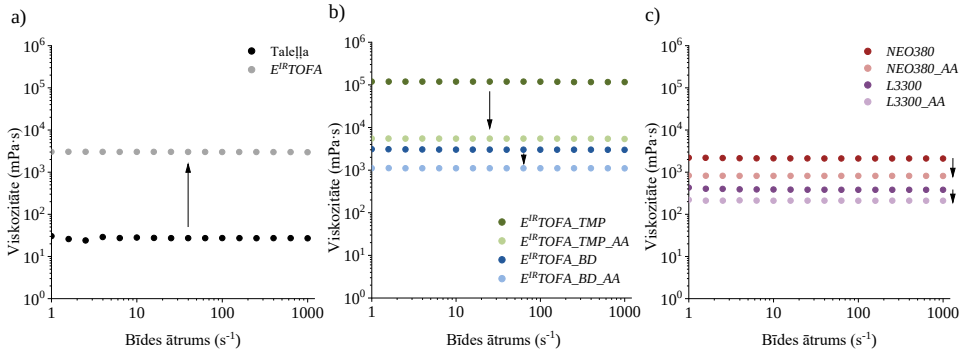

1.2. att. Reoloģiskie mērījumi (konusa-plātne sistēma, attālums 48 μm, 25 °C): a) taleļļa un *E*^{IR}*TOFA*; b) *E*^{IR}*TOFA* polioli un to acetoacetāti; c) komerciālie polioli un to acetoacetāti.

Kopumā acetoactetātiem, salīdzinot ar komerciālajiem un taleļļas polioliem, bija ievērojami mazāka viskozitāte. Viskozitātes pazemināšanos pēc acetoacetilēšanas varētu skaidrot ar hidroksilgrupu daudzuma samazināšanos un līdz ar to starpmolekulāro ūdeņraža saišu izzušanu [46, 47, 51, 55, 56]. Tas ievērojami uzlabo no atjaunojamiem resursiem iegūtu acetoacetātu potenciālo izmantošanu rūpniecībā. Zemāka viskozitāte ļauj vieglāk pielāgot jau esošās iekārtas un sūkņu jaudas. Acetoacetātus varētu transportēt pa cauruļvadiem, patērējot mazāk enerģijas transportēšanai nekā polioliem, kam ir sliktāka plūstamība.

Sintēzes gaita un ar molekulu funkcionālajām grupām saistītās izmaiņas noteiktas, izmantojot *FTIR* spektroskopiju (1.3. att.). Pēc taleļļas taukskābju epoksidēšanas *FTIR* spektrā parādījās jauns absorbcijas joslas maksimums pie 831 cm^{-1}, kas raksturīgs oksirāna gredzenu absorbcijas joslai (1.3. a att.). Tas norādīja, ka epoksidēšana, izmantojot jonapmaiņas sveķu *Amberlite IR-120 H* kā katalizatoru, bija veiksmīga. Par dubultsaišu izzušanu norādīja izmaiņas spektrā pie ~ 1654 cm^{-1} un ~ 3009 cm^{-1}, kas atbilst attiecīgi C=C valentajām svārstībām un =CH valentajām svārstībām. Šo absorbcijas joslu intensitāte *E*^{IR}*TOFA* spektrā bija ievērojami mazāka. *E*^{IR}*TOFA* spektrā jauna, salīdzinoši vāja, bet pamanāma absorbcijas josla tika novērota intervālā no 3600 cm^{-1} līdz 3150 cm^{-1}, kas parasti raksturo hidroksilgrupu svārstības.

Šis novērojums liecināja, ka epoksidēšanas laikā notikušas nevēlamas blakusreakcijas, kas galvenokārt saistītas ar oksirāna gredzenu šķelšanos. Kā redzams spektrā, karboksilgrupu absorbcijas joslas intensitāte pie ~ 1705 cm^{-1} samazinājās galvenokārt esteru veidošanās dēļ, kas apliecina nevēlamu blakusreakciju norisi. Hidroksilgrupas un esteri veidojās oksirāna gredzenu šķelšanās reakcijā ar taleļļas taukskābju vai etiķskābes karboksilgrupām.

Hidroksilgrupu absorbcijas joslas intensitāte ievērojami palielinājās sintezētajiem polioliem. Turklāt šī josla bija intensīvāka poliolam, kas iegūts *E*^{IR}*TOFA* reakcijā ar TMP spirtu, jo TMP satur vairāk hidroksilgrupu (f = 3) nekā BD (f = 2). Poliola spektros netika novērotas oksirāna gredzeniem raksturīgās absorbcijas joslas pie 831 cm^{-1}. Šajos spektros mazāka intensitāte novērota karboksilgrupām raksturīgajai absorbcijas joslai, bet lielāka

intensitāte konstatēta esteru saitēm raksturīgajām absorbcijas joslām pie ~ 1738 cm^{-1}, kas norādīja, ka taleļļas taukskābju skābes grupas esterifikācijas reakcija veiksmīgi realizējusies.

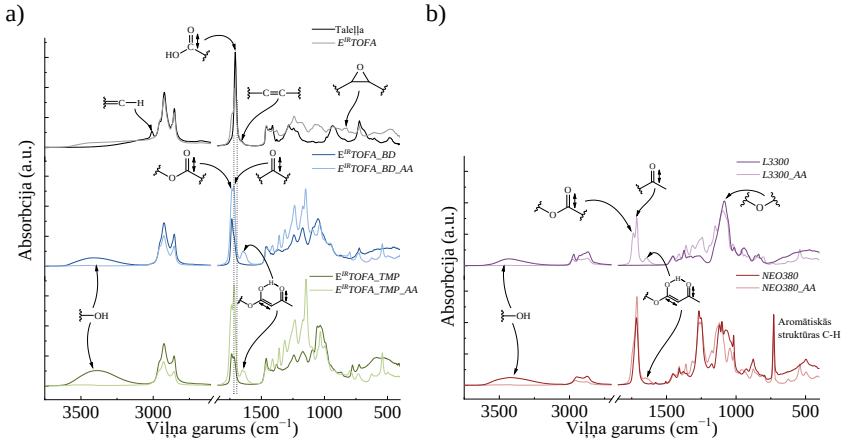

1.3. att. *FTIR* spektri (ATR režīms, 32 skenējumi, izšķirtspēja 4 cm^{-1}): a) taleļļai, $E^{IR}TOFA$, sintezētājiem polioliem un attiecīgajiem acetoacetātiem; b) komerciālajiem polioliem un attiecīgajiem acetoacetātiem.

FTIR spektros hidroksilgrupu valentajām svārstībām raksturīgajai absorbcijas joslai intensitāte bija ievērojami mazāka acetoacetilētiem polioliem. Joslas intensitāte bija gandrīz nenosakāma. Šis novērojums ir viens no galvenajiem veiksmīgas acetoacetilēšnas reakcijas radītājiem. Acetoacetilētu poliolu *FTIR* spektros novērota vēl lielāka esteru grupām raksturīgās absorbcijas joslas intesnitāte pie ~ 1738 cm^{-1} un ketona grupām raksturīgās absorbcijas joslas intensitāte pie ~ 1715 cm^{-1}. Tika novērota salīdzinoši spēcīgas, jaunas absorbcijas joslas parādīšanās spektrā intervālā no 1670 cm^{-1} līdz 1580 cm^{-1}. Acetoacetātiem raksturīga keto-enola tautomērija, kas rada karbonilgrupām raksturīgās absorbcijas joslas parādīšanos zemākā frekvencē iekšmolekulārās ūdeņraža saites enola formā dēļ. Tādas pašas izmaiņas *FTIR* spektros tika novērotas arī acetoacetilētajiem komerciālajiem polioliem (1.3. b att.).

^{1}H KMR spektri skaidri parādīja (1.4. att.) oksirāna gredzenu veidošanos (signāli pie 2,8−3,2 ppm), kā arī atklāja, ka daļa oksirāna gredzenu sašķēlās sintēzes procesā (signāli pie 3,4−4,1 ppm). Šis novērojums ir saskaņā ar iepriekš apskatītajiem rezultātiem (1.3. att.), kuros arī tika novērota nevēlama oksirāna šķelšanās un esterifikācijas reakciju norise. KMR spektri pierādīja poliolu veiksmīgu sintēzi oksirāna gredzenu šķelšanās un karboksilgrupu esterifikācijas reakcijā ar BD un TMP, par ko liecināja oksirāna grupām raksturīgo signālu izzušana (3,14−2,84 ppm). Jauni signāli KMR spektrā konstatēti pie 4,0−4,5 ppm, kas raksturīgi -O-CH_2- grupām. Esteru saišu veidošanos ar BD un TMP apstiprināja arī ^{13}C spektri; karbonilgrupu signāls nobīdījās no 180 ppm (karbonskābei) uz 174 ppm, kas raksturīgs esterim.

Acetoacetilēta $E^{IR}TOFA\_TMP$ poliola spektrā mazos daudzumos novērots arī aizvietots TMP. Par to liecināja vairāki signāli, piemēram, signāls pie 65,5−63,5 ppm, kas raksturīgs TMP molekulas -CH_2- grupām, kā arī signāls pie 43−42 ppm, kas raksturīgs ceturtējam ogleklim TMP molekulā. Vairākas izmaiņas ^{13}C KMR spektros apstiprināja arī taleļļas poliolu un komerciālo poliolu *NEO380* un *L3300* veiksmīgu acetoacetilēšanu. Acetoacetilgrupu CH_2 grupām raksturīgais signāls novērots pie 3,4 ppm.

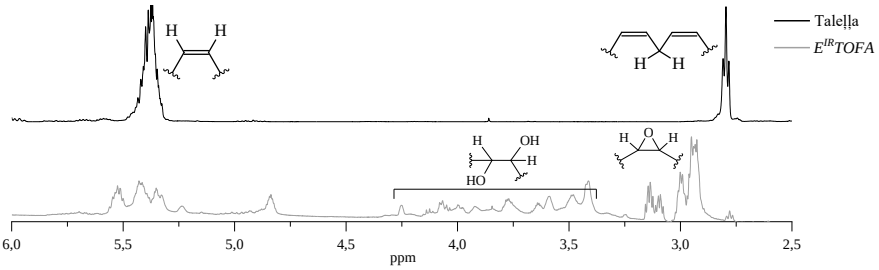

1.4. att. Taleļļas un $E^{IR}TOFA$ ^{1}H-NMR spektri (500 MHz, $CDCl_3$).

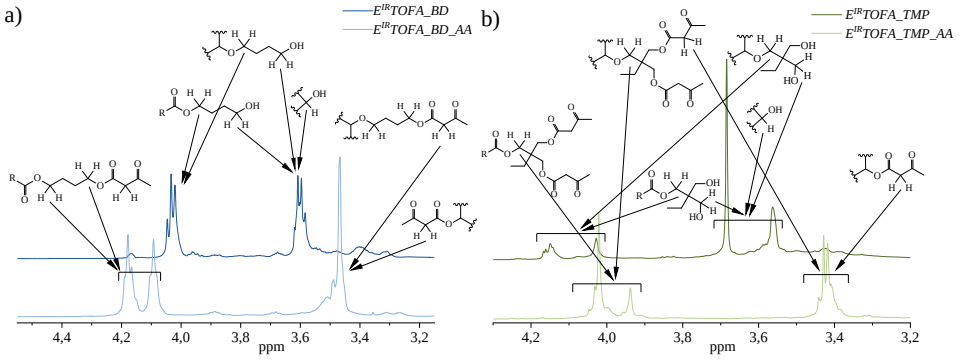

1.5. att. ^{1}H-NMR spektri (500 MHz, $CDCl_3$): a) $E^{IR}TOFA\_BD$ un $E^{IR}TOFA\_BD\_AA$; b) $E^{IR}TOFA\_TMP$ un $E^{IR}TOFA\_TMP\_AA$.

Saskaņā ar *GPC* rezultātiem (1.6. att.), taleļļas taukskābju epoksidēšanas procesā, kā katalizatoru izmantojot joapmaiņas sveķus, veidojās ļoti liels daudzums dažādu nevēlamu blakusproduktu. Hromatogrammā redzamas joslas, kas varētu atbilst dimēriem, trimēriem un citiem oligomēriem, kas veidojušies kā oksirāna gredzenu šķelšanās produkti. Āboliņš ar līdzautoriem arī identificēja līdzīgu blakusproduktu veidošanos taleļļas taukskābju epoksidācijā [38]. Oksirāna gredzenu šķelšanās produktu ar mazmolekulārām vielām aiztures laiks bija ~ 23,5 min., savukārt dimēri un trimēri tika identificēti ar aiztures laiku ~ 22,6 min. un ~ 22,0 min. Poliolu hromatogramma parādīja, ka joslu aiztures laiks samazinājās, salīdzinot ar *ETOFA*. Tas liecināja par molekulmasas palielināšanos.

$E^{IR}TOFA\_BD$ poliola spektrā novērojama jauna josla ar aiztures laiku ~ 25,4 min., kas liecināja par neizreaģējušu BD. *$E^{IR}TOFA\_TMP$* poliola gadījumā neizreaģējušā TMP joslas maksimums bija pie aiztures laika ~ 23 min. Pēc acetoacetilēšanas molekulmasa palielinājās, tādējādi samazinot molekulu aiztures laiku. Tas bija arī skaidri redzams *GPC* hromatogrammā un apstiprināja veiksmīgu acetoacetilēšanas norisi.

Komerciāli pieejamais poliols *NEO380* ir vairāku komponentu maisījums. Pēc acetoacetilēšanas visas *NEO380* joslas *GPC* hromatogrammā nobīdījās uz mazāku aiztures laiku (1.6. b att.), kas liecināja, ka lielākā daļa savienojumu šajā maisījumā pēc acetoacetilēšanas saturēja acetoacetāta grupas. *L3300* poliola spektrā ir tikai viena josla ar izteiktu maksimumu (1.6. b att.). Tāpat kā visos iepriekšējos gadījumos, arī acetoacetilēta *L3300 GPC* hromatogrammā josla parādījās pie mazāka aiztures laika, kas liecināja par molekulmasas palielināšanos un veiksmīgu acetoacetilēšanu.

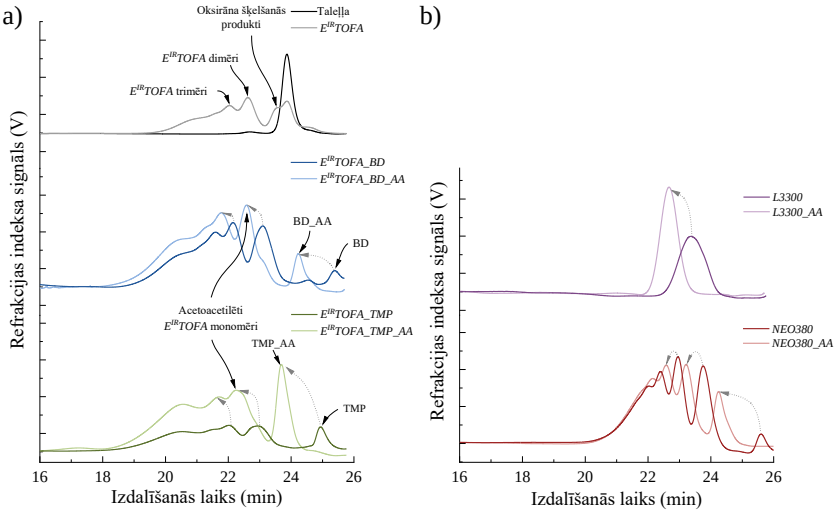

1.6. att. Sintezēto vielu *GPC* hromatogrammas (trīs PLgel kolonnas, daļiņu izmērs 10 µm, poru izmēri 104 Å, 103 Å un 50 Å, 300 mm × 7,5 mm, THF, 25 °C): a) no taleļļas; b) no komerciāli pieejamajiem polioliem.

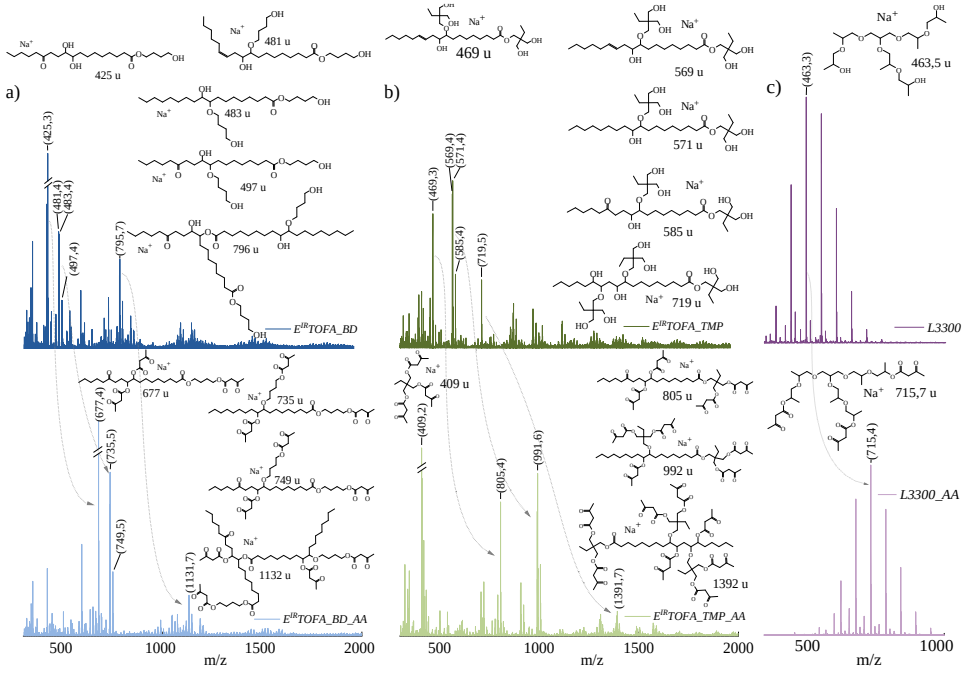

1.7. att. *MALDI-TOF MS* spektri (2000 Hz, 355 nm, jonizējošais aģents: CF_3COONa): a) *E^IRTOFA_BD* un *E^IRTOFA_BD_AA*; b) *E^IRTOFA_TMP* un *E^IRTOFA_TMP_AA*; c) *L3300* un *L3300_AA*.

Spektri parādīja, ka epoksidēšanas procesā, poliolu sintēzē un to acetoacetilēšanā veidojās dažādu savienojumu maisījums (1.7. att.). Spektrs tika uzņemts arī *E^IRTOFA*, taču to bija grūti interpretēt, jo epoksidētas oleīnskābes un linolskābes joniem atbilstošās joslas pārklājās ar

matricas joslām. Spektros joslas visbiežāk bija pa pāriem ar starpību 2 u. Tas atbilst oleīnskābes un linolskābes molekulmasas atšķirībai. *MALDI-TOF MS* spektros skaidri redzamas dominējošo sintezēto poliolu monomēru un to acetoacetātu jonu atbilstošās joslas. E^{IR}*TOFA_BD MALDI-TOF MS* spektrā identificētas joslas, kas atbilst poliolu dimēru, kā arī tiem atbilstošo acetoacetātu jona molekulmasām.

MALDI-TOF MS spektri norādīja arī uz poliolu veiksmīgu acetoacetilēšanas norisi. Pēc acetoacetilēšanas visintensīvākās joslas nobīdījās par tik m/z vienībām, kas atbilst masas pieaugumam, ja visas molekulā esošās hidroksilgrupas aizstātu ar acetoacetāta grupu. Piemēram, epoksidētas oleīnskābes TMP poliolam raksturīgā jona atbilstošās joslas maksimums bija pie 571 m/z $[C_{30}H_{60}O_8+Na]^+$. Pēc acetoacetilēšanas šī poliola acetoacetātam atbilstošā jona joslas maksimums bija pie 991 m/z. Atšķirība bija 420 m/z, kas precīzi atbilst piecu acetoacetāta grupu masai un pilnībā atbilst attiecīgā sintezētā poliola hidroksilgrupu skaitam (funkcionalitātei). Tas nozīmē, ka šis savienojums satur piecas funkcionālās grupas (E^{IR}*TOFA_TMP_AA f* = ~ 5). Pilnībā acetoacetilēti savienojumi, kas satur trīs funkcionālās grupas, tika atrasti arī acetoacetilētas epoksidētas oleīnskābes BD poliola spektros (E^{IR}*TOFA_BD_AA f* = ~ 3)

Pēc acetoacetilēšanas arī dimēru trimēru un citu blakusproduktu jonu atbilstošo joslu parādīšanās pie lielākām vērtībām norādīja, ka acetoacetilēšanas process noritējis veiksmīgi un molekulas satur acetoacetāta grupas. No tā var secināt, ka šie blakusprodukti arī pilnībā piemēroti polimērmateriālu ieguvei, izmantojot Maikla reakciju. Būtiski, ka šos dimēru, trimēru un citu blakusproduktu lielās un sazarotās struktūras dēļ var tikt paaugstināta acetoacetāta viskozitāte, kas var apgrūtināt tā izmantošanas iespējas.

Maz joslas novērotas *L3300* poliola un tā acetoacetāta *MALDI-TOF MS* spektrā, salīdzinot ar taleļļas acetoacetātu spektriem. *L3300* ir trifunkcionāls poliētera poliols, kura pamatā ir glicerīns. Rūpnieciski tas iegūts, glicerīna molekulai pievienojot 2-hidroksipropoksigrupas oksipropilēšanas reakcijā. *L3300* ir salīdzinoši tīra viela, kas atvieglo spektra interpretāciju. Intervāls starp intensīvāko joslu maksimumiem bija 58 m/z, kas atbilst 2-hidroksipropoksigrupas masai. *L3300* poliola spektrs atspoguļoja, cik vienmērīgi ir notikusi oksipropilēšana. Pēc acetoacetilēšanas visi atbilstošo joslu maksimumi nobīdījās precīzi par 252 m/z, kas atbilst trīs acetoacetāta grupu molmasai un liecināja par gandrīz pilnīgu *L3300* hidroksilgrupu aizvietošanu.

1.2. Maikla akceptora sintēze no taleļļas taukskābēm

Salīdzinoši plaši izmantoti ir tikai daži sintēzes ceļi, lai iegūtu akrilātus no atjaunojamajām izejvielām. Viens no visvairāk pētītiem un izmantotajiem sintēzes ceļiem ir dubultsaišu epoksidēšana un sekojoša oksirāna gredzenu šķelšana ar akrilskābi [57–62]. Vēl viena iespēja iegūt akrilātu ir vienas stadijas reakcija starp eļļu, kas satur dubultsaites, un akrilskābi bora trifluorīda dietileterāta šķīduma klātbūtnē [63–65]. Ja eļļas molekula dabiski jau satur hidroksilgrupas (piemēram, rīcineļļa), ir iespējama hidroksilgrupu akrilēšana ar akriloilhlorīdu [44, 62, 66].

Šīs metodes ir piemērotas izejvielām, kas satur vismaz divas dubultsaites katrā molekulā, jo veiksmīgai polimerizācijas reakcijai ir nepieciešams, lai katra molekula saturētu vismaz divas funkcionālās grupas. Diglicerīdi un triglicerīdi satur vairākas dubultsaites, kas padara šīs vielas piemērotas polimēru izejvielu sintēzei. Publicētie pētījumi liecina, ka triglicerīdus saturošas eļļas ir visplašāk izmantotās eļļas akrilātu sintēzei.

Dažas brīvās taukskābes, piemēram, linolskābe, satur divas dubultsaites, bet pēc epoksidēšanas katra molekula parasti satur tikai vienu oksirāna grupu blakusreakciju ar etiķskābi vai nepilnīgas epoksidācijas dēļ. Tāpēc epoksidēšana un oksirāna gredzenu atvēršana ar akrilskābi vai tieša dubultsaites akrilēšana ir neefektīva brīvās taukskābes saturošām eļļām, piemēram, taleļļai. Eļļām, kas satur brīvās taukskābes, ir jāizmanto cita pieeja.

Šajā darbā izstrādāta daudzsološa metode akrilātu sintēzei no taleļļas, izmantojot dubultaistes epoksidēšanu, kam seko oksirāna gredzenu atvēršana ar daudzfunkcionālu spirtu un pēc tam hidroksilgrupu akrilēšana ar akriloilhlorīdu (1.8. att.).

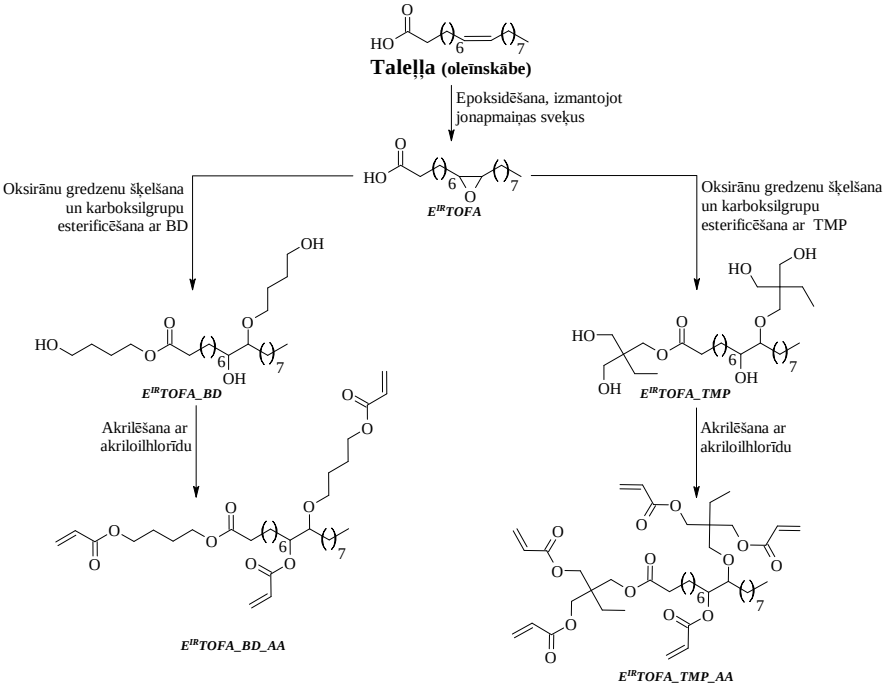

1.8. att. Idealizēta Maikla akceptora sintēzes shēma no taleļļas taukskābēm (oleīnskābes).

Pēc poliola akrilēšanas novēroja būtisku hidroksilgrupu vērtības samazināšanos, kas bija pirmais rādītājs, ka akrilāta sintēze bijusi veiksmīga (1.2. tabula). Lai gan titrimetrijas dati uzrādīja nelielu hidroksilgrupu klātbūtni, akrilātos hidroksilgrupu saturs bija tik mazs, salīdzinot ar poliolu, ka tas būtiski neietekmēja turpmāko polimērmateriālu iegūšanu.

1.2. tabula

Sintezēto taleļļas akrilātu raksturojums

Sintezētais akrilāts	Skābes skaitlis, mg KOH/g	Hidroksilskaitlis, mg KOH/g	Mitrums, %	Akrilgrupu saturs,* mmol/g
E^IRTOFA_BD_Acryl	< 5	28,8	0,022	3,9
E^IRTOFA_TMP_Acryl	< 5	46,2	0,027	3,5

*kvantitatīvais KMR (500 MHz, $CDCl_3$) izmantojot 1,2,3-trimetoksibenzolu kā iekšējo standartu.

Reoloģiskie mērījumi (1.9. att.) uzrādīja ievērojami mazāku viskozitāti akrilātiem nekā polioliem, no kuriem šie akrilāti sintezēti. Pēc *E^IRTOFA_TMP* poliola akrilēšanas viskozitāte samazinājās vairāk nekā 25 reizes līdz 4560 mPa·s. Tāda pati tendence bija novērojama

E^{IR}*TOFA_BD* akrilēšanas gadījumā. *E*^{IR}*TOFA_BD_Acryl* viskozitāte bija 315 mPa·s. Viskozitātes samazināšanās galvenokārt saistīta ar ūdeņraža saišu izzušanu starp molekulām hidroksilgrupu esterificēšanas dēļ. Viskozitāte nebija atkarīga no lietotā bīdes ātruma, tāpēc sintezētās vielas varēja klasificēt kā Ņūtona šķidrumus.

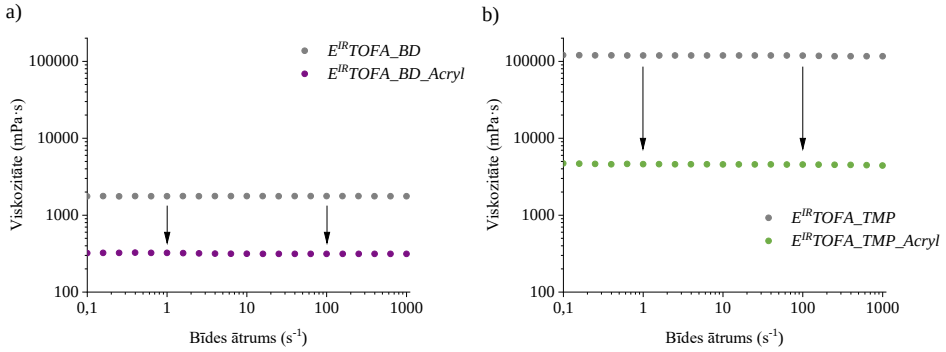

1.9. att. Reoloģiskie mērījumi (konusa-plātne sistēma, attālums 48 μm, 25 °C): a) *E*^{IR}*TOFA_BD* un *E*^{IR}*TOFA_BD_Acryl*; b) *E*^{IR}*TOFA_TMP* un *E*^{IR}*TOFA_TMP_Acryl*.

Salīdzinot poliola *E*^{IR}*TOFA_BD FTIR* spektru ar akrilāta *E*^{IR}*TOFA_BD_Acryl* spektru, skaidri redzama joslas pie 3600−3150 cm^{-1}, kas atbilst hidroksilgrupām raksturīgajām deformācijas svārstībām, izzušana (1.10. att.). Savukārt jaunas joslas novērotas pie 1640−1620 cm^{-1}, 1407 cm^{-1} un 810 cm^{-1}, kas atbilst attiecīgi akrilgrupām raksturīgajām deformācijas svārstībām un liecināja par veiksmīgu akrilēšanas norisi. Tādu pašu tendenci varēja novērot, salīdzinot poliola *E*^{IR}*TOFA_TMP* un akrilāta *E*^{IR}*TOFA_TMP_Acryl* spektrus.

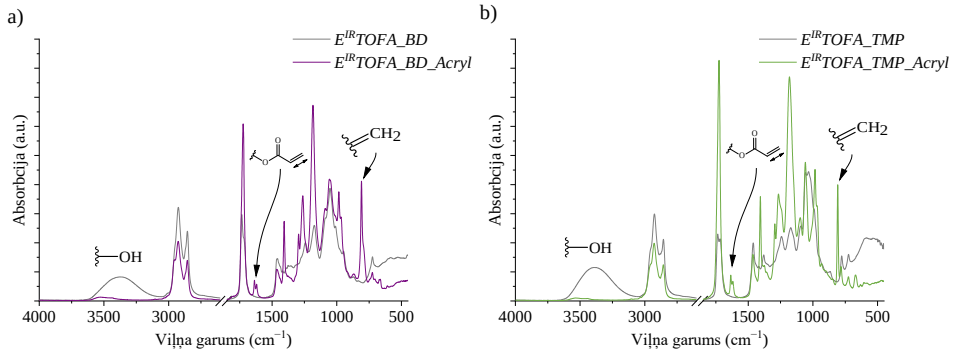

1.10. att. *FTIR* spektri (ATR režīms, 32 skenējumi, izšķirtspēja 4 cm^{-1}): a) *E*^{IR}*TOFA_BD* un *E*^{IR}*TOFA_BD_Acryl*; b) *E*^{IR}*TOFA_TMP* un *E*^{IR}*TOFA_TMP_Acryl*.

FTIR spektrus, kas apstiprināja ķīmiskās struktūras maiņu sintēzes procesā, pilnībā apstiprināja un papildināja KMR spektri (1.11. att.). Akrilētā taleļļas poliola ^{1}H KMR spektros bija redzami vinilgrupām tipiski signāli (6,4 ppm, 6,1 ppm un 5,8 ppm). Esteru veidošanās tika pierādīta ar signāliem pie 4,22−4,13 ppm, kas raksturoja –CH$_2$OCOR daļu (kur R ir vinilgrupa). Savukārt signāla, kas raksturīga HOCH$_2$– grupām pie 3,7−3,6 ppm, intensitāte bija būtiski mazāka, tādējādi liecinot par brīvo hidroksilgrupu esterificēšanu. Turklāt jauni signāli, kas raksturīgi akrilāta karbonilgrupām pie 166 ppm ^{13}C KMR spektrā, pierādīja veiksmīgu akrilātu veidošanos.

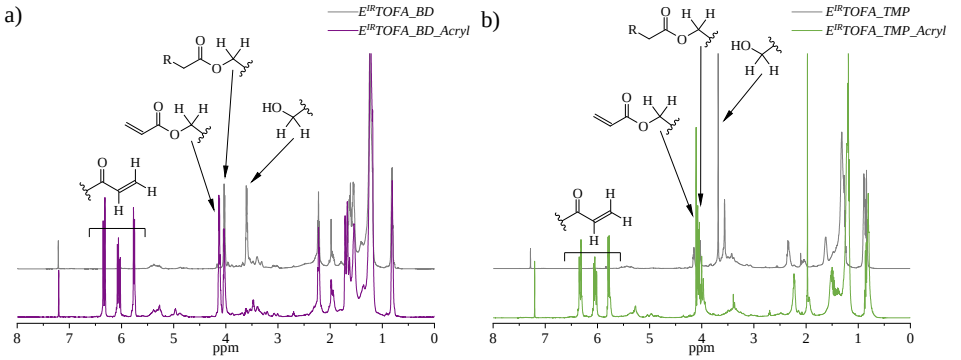

1.11. att. ^{1}H KMR spektri (500 MHz, $CDCl_3$) a) *E*^{IR}*TOFA_BD* un *E*^{IR}*TOFA_BD_Acryl*; b) *E*^{IR}*TOFA_TMP* un *E*^{IR}*TOFA_TMP_Acryl*.

GPC rezultāti (1.12. att.) apstiprināja, ka taleļļas taukskābju polioli sastāv no monomēru, dimēru, trimēru un oligomēru maisījuma [38]. Salīdzinot akrilētu taleļļas poliolu un taleļļas poliolu *GPC* hromatogrammas, joslu maksimumi bija pie nedaudz īsāka aiztures laika, kas liecināja par molekulmasas palielināšanos. Molekulmasas palielināšanās saistīta ar hidroksilgrupu aizstāšanu ar akrilgrupām, kas liecināja par veiksmīgu akrilēšanas reakcijas norisi.

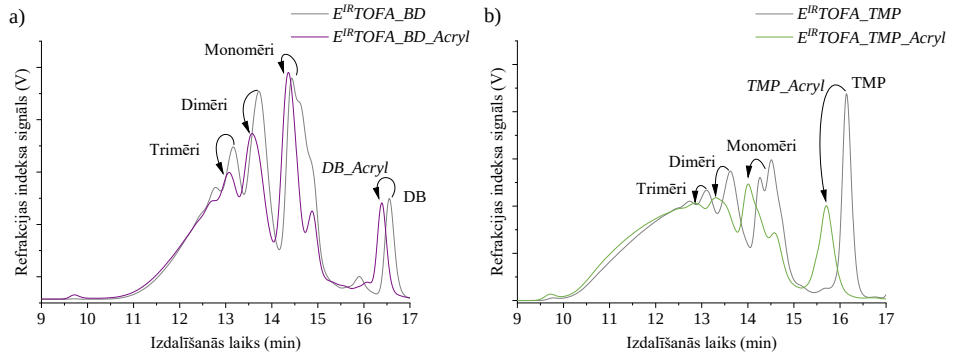

1.12. att. Sintezēto vielu *GPC* hromatogrammas (divas *PLgel Mixed-E* kolonnas, daļiņu izmērs 3 μm, 300 mm × 7,5 mm, THF, 35 °C): a) *E*^{IR}*TOFA_BD* and *E*^{IR}*TOFA_BD_Acryl*; b) *E*^{IR}*TOFA_TMP* and *E*^{IR}*TOFA_TMP_Acryl*.

Līdztekus *GPC* analīzei izmaiņas vielu ķīmiskajā struktūrā noteiktas arī ar *MALDI-TOF MS* spektrometrijas palīdzību (1.13. un 1.14. att.). *MALDI-TOF MS* dati apstiprināja *GPC* novēroto, ka taleļļas polioli sastāv no sarežģīta maisījuma, kas spektrā redzams kā liels daudzums zemas intensitātes joslas.

Galvenais izaicinājums *MALDI-TOF MS* spektru analīzē bija noteikt akrilētu taleļļas taukskābju poliolu joniem atbilstošās joslas. *MALDI-TOF MS* spektros visintensīvākās joslas akrilātiem novērotas pie lielākām m/z vērtībām nekā to attiecīgajiem polioliem. Salīdzinot poliola un atbilstošā akrilāta *MALDI-TOF MS* spektrus, tika identificētas vairākas joslas ar starpību, kas dalās ar 54. Šis vienību skaits (54 m/z) atspoguļo masas pieaugumu par vienu akrilgrupu. Lielākā daļa joslu pēc akrilēšanas spektrā nobīdījās par 108 m/z, 162 m/z, 216 m/z,

270 m/z un 324 m/z vienībām, kas liecināja, ka katra molekula satur attiecīgi vismaz divas, trīs, četras un piecas akrilgrupas. Spektrā tika identificētas joslas, kas atbilst pilnībā akrilētu *E*^{IR}*TOFA_BD* un *E*^{IR}*TOFA_TMP* poliolu jonu masām.

Pilnībā akrilēts *E*^{IR}*TOFA_BD* poliols satur trīs akrilgrupas katrā molekulā. Spektrā varēja novērot relatīvi intensīvus atbilstošās joslas maksimumus pie 643,4 m/z un 645,4 m/z, kas atbilst pilnībā akrilētam *E*^{IR}*TOFA_BD*, kas satur trīs akrilgrupas (*E*^{IR}*TOFA_BD_Acryl* f = ~ 3). *E*^{IR}*TOFA_BD_Acryl* gadījumā dimēru akrilēšanās rezultātā izveidojās savienojumi arī ar četrām akrilgrupām molekulā, par ko liecināja atbilstošās jona joslas pie 1009,7 m/z un 1011,7 m/z. Šo joslu intensitāte gan bija salīdzinoši neliela. Turklāt no iegūtajiem spektriem tika secināts, ka maisījums satur arī daļēji akrilētus savienojumus.

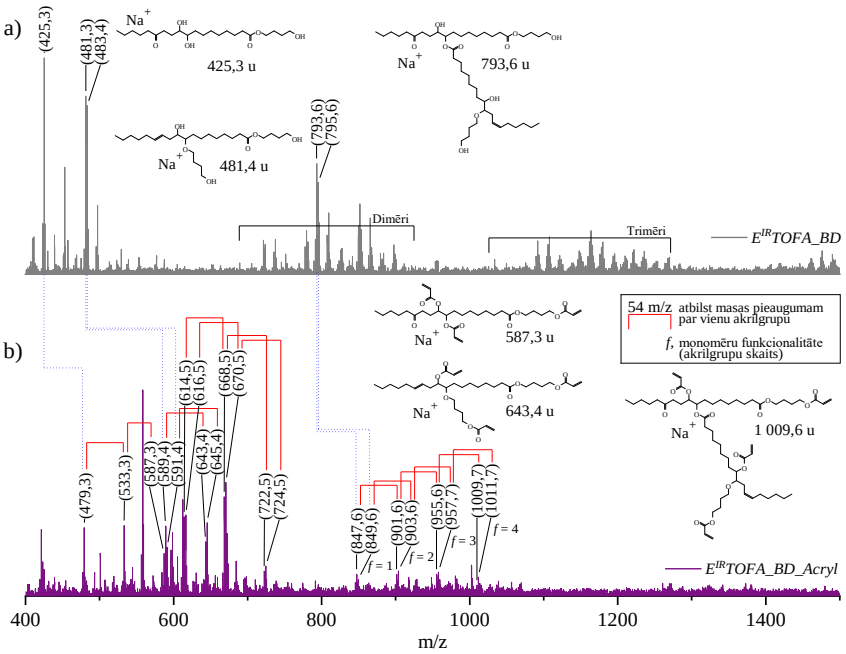

1.13. att. *MALDI-TOF MS* spektri (2000 Hz, 355 nm, jonizējošais aģents: CF_3COONa): a) *E*^{IR}*TOFA_BD*; b) *E*^{IR}*TOFA_BD_Acryl*.

E^{IR}*TOFA_TMP_Acryl* akrilāta spektrā intensīvas joslas bija pie 839,5 m/z un 841,5 m/z, kas atbilst savienojumiem, kas satur piecas akrilgrupas vienā molekulā (*E*^{IR}*TOFA_TMP_Acryl* f = ~ 5) (1.14. att.). Tāpat kā *E*^{IR}*TOFA_BD_Acryl* gadījumā, daļēji akrilētie savienojumi tika novēroti arī *E*^{IR}*TOFA_TMP_Acryl* spektrā. Joslu intensitāte palielinājās līdz ar akrilgrupu skaita pieaugumu molekulā, un visintensīvākās joslas atbilda pilnībā akrilētam poliolam. Pateicoties augstajai funkcionalitātei, sintezētos taleļļas Maikla donorus var izmantot, lai iegūtu ļoti šķērssaistītu polimēru matricu, kas var palielināt polimēra matricas mehāniskās īpašības. Sintezētie akrilāti no taleļļas taukskābju polioliem satur vairākas akrilgrupas molekulā, kas ir galvenais priekšnoteikums, lai tos izmantotu polimerizācijas reakcijā.

Ņemot vērā reoloģijas mērījumus, *FTIR*, KMR, *GPC* un *MALDI-TOF MS* datus, iegūtie taleļļas poliola akrilāti ir piemēroti polimēru sintēzei ar Maikla reakciju. Turklāt sintezētie taleļļas poliola akrilāti varētu būt potenciāli piemēroti citu polimēru ražošanā, piemēram, UV ierosinātajā brīvo radikāļu polimerizācijā pārklājumu ražošanā.

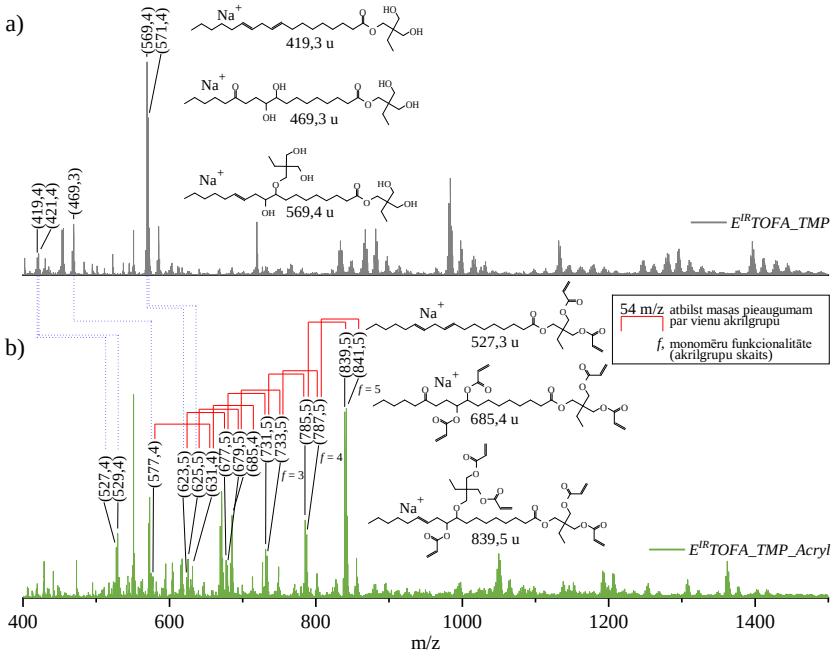

1.14. att. *MALDI-TOF MS* spektri (2000 Hz, 355 nm, jonizējošais aģents: CF_3COONa): a) *E*^{IR}*TOFA_TMP*; b) *E*^{IR}*TOFA_TMP_Acryl*.

2. Polimēru sveķi no taleļļas Maikla donoriem un petroķīmiskiem Maikla akceptoriem

Maikla reakcijas mehānisms ir daudz pētīts un zināms. Vispirms bāzisks katalizators deprotonē acetoacetātu, kā rezultātā veidojas enolāta anjons. Pēc tam enolāta anjons reaģē ar akrilātu 1,4-pievienošanās reakcijā. Pirmās Maikla reakcijas produkts satur vēl vienu aktīvo protonu acetoacetāta metilēngrupā, ko var pievienot citam akrilātam [23, 31], kas nozīmē, ka Maikla donors divreiz reaģē ar diviem Maikla akceptoriem [67], protams, ja reaģentu molārā attiecība to atļauj. Polimērs var veidoties tikai tad, ja Maikla akceptora katra molekula satur vismaz divas funkcionālās grupas.

Reakcija starp akrilātiem un aktīvo acetoacetātu metilēngrupu ir ātra, un sistēma pēc samaisīšanas ar katalizatoru sacietē istabas temperatūrā. Šī reakcija ir bāzes katalizēta pievienošanās [31, 35, 68]. Maikla reakcijai vispiemērotākie ir amīnu, amidīna un guanidīna bāzes katalizatori [31, 35, 46, 49, 68–72].

Iepriekš sintezētie divi taleļļas un divi komerciālo poliolu acetoacetāti tika izmantoti, lai iegūtu polimērus Maikla reakcijā (2.1. tab.), izmantojot 1,1,3,3-tetrametilguanidīnu (TMG) kā katalizatoru. Iepriekš sintezētājiem acetoacetātiem bija atšķirīga ķīmiskā struktūra un funkcionalitāte, kas polimerizācijas reakcijās dažādiem akrilātiem ļāva izstrādāt polimērus ar atšķirīgu šķērssaistīšanās blīvumu. Tika izmantoti trīs komerciāli pieejami akrilāti ar dažādu akrilgrupu skaitu molekulā jeb funkcionalitāti – *BPAEDA* (*f* = 2), *TMPTA* (*f* = 3) un *PETA* (*f* = 4).

2.1. tabula

Iegūtie polimēri

	Maikla donori			
	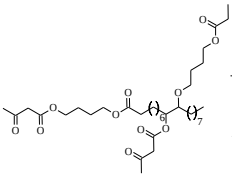	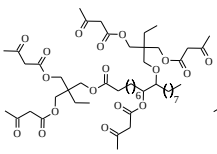	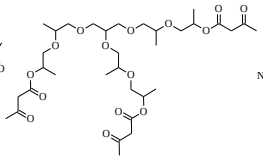	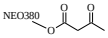
Maikla akceptori	***E^{IR}TOFA_BD_AA* (*f* = ~ 3)**	***E^{IR}TOFA_TMP_AA* (*f* = ~ 5)**	***L3300_AA* (*f* = 3)**	***NEO380_AA***
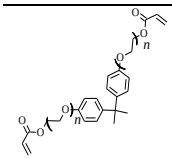 ***BPAEDA* (*f* = 2)**	*E^{IR}TOFA_BD_AA_BPAEDA*	*E^{IR}TOFA_TMP_AA_BPAEDA*	*L3300_AA_BPAEDA*	*NEO380_AA_BPAEDA*
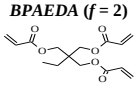 ***TMPTA* (*f* = 3)**	*E^{IR}TOFA_BD_AA_TMPTA*	*E^{IR}TOFA_TMP_AA_TMPTA*	*L3300_AA_TMPTA*	*NEO380_AA_TMPTA*
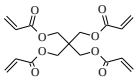 ***PETA* (*f* = 4)**	*E^{IR}TOFA_BD_AA_PETA*	*E^{IR}TOFA_TMP_AA_PETA*	*L3300_AA_PETA*	*NEO380_AA_PETA*

Iegūtajiem polimēriem tika veikta TGA (2.1. att.). No taleļļas poliolu acetoacetātiem iegūtajiem polimēriem būtisks masas zudums netika novērots līdz pat 300 °C temperatūrai; tie bija termiski stabili. Tā ir priekšrocība, jo, piemēram, plaši lietotie poliuretāna materiāli bez pievienotiem termostabilizatoriem sadalās temperatūras diapazonā no 200 °C līdz 300 °C [73, 74]. Turklāt arī organiskā stikla polimetilmetakrilāta sadalīšanās sākas temperatūrā zem 300 °C [75, 76].

Salīdzinot Maikla donora ietekmi, polimēriem, kas iegūti no TMP polioliem, bija augstāka termiskā stabilitāte. Savukārt, salīdzinot Maikla akceptoru ietekmi, termiski stabilākie polimēri tika iegūti no bisfenola A atvasinājuma *BPAEDA* akrilāta. To var izskaidrot ar bisfenola A aromātisko struktūru. Polimēriem, kas iegūti, kā akrilātu izmantojot *BPAEDA*, tika novēroti divi masas zuduma ātruma maksimumi. Pārējiem polimēriem atvasinājuma līkņu profilu līdzību noteica izmantotais poliols un mazāk – akrilāts.

Polimēriem no komerciāli pieejamo poliolu acetoacetātiem bija līdzīgi TGA masas zuduma līkņu un to atvasinājumu līkņu profili. Polimēriem, kas iegūti no taleļļas poliolu acetoacetātiem ar *BPAEDA* akrilātu, bija augstāka termiskā stabilitāte (salīdzinot temperatūru, kur masas zudums sasniedza 5 %) nekā polimēriem no komerciāli pieejamo poliolu acetoacetātiem ar tādu pašu akrilātu. 5 % masas zuduma temperatūru lielā mērā noteica izmantotais akrilāts, taču šī ietekme mazāk izteikta bija augstākā temperatūrā.

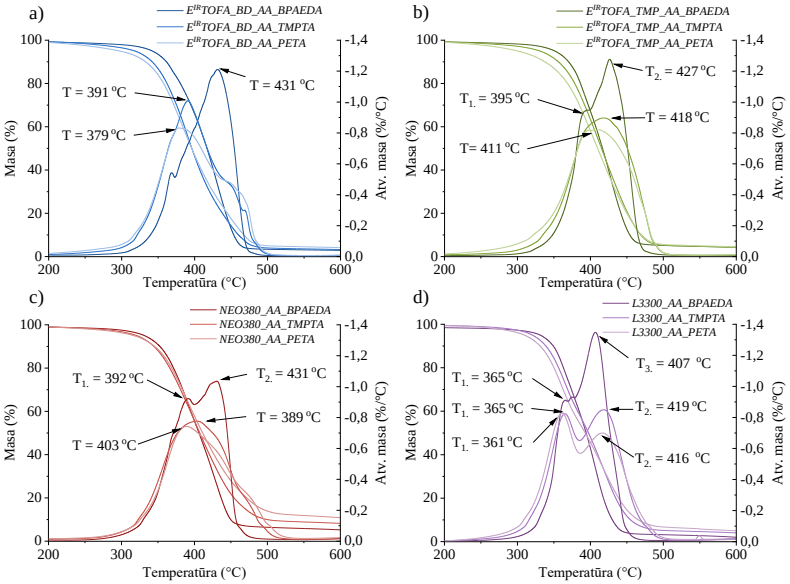

2.1. att. TGA (10 °C·min^{-1}) masas zuduma līknes un TGA līkņu atvasinājums polimēriem no sintezētiem acetoacetātiem un *BPAEDA*, *TMPTA*, *PETA* akrilātiem: a) *E^{IR}TOFA_BD_AA* polimēri; b) *E^{IR}TOFA_TMP_AA* polimēri; c) *NEO380_AA* polimēri; d) *L3300_AA* polimēri.

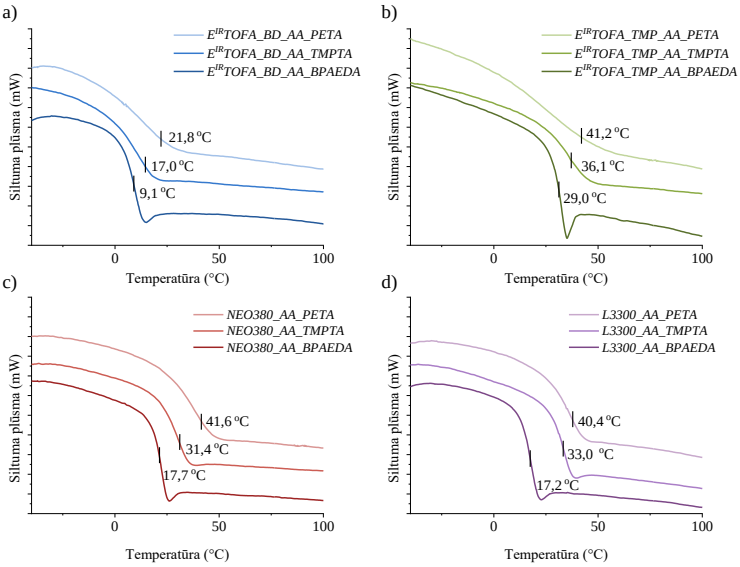

2.2. att. *DSC* (10 °C·min^{-1}) līknes polimēriem no sintezētiem acetoacetātiem un *BPAEDA*, *TMPTA*, *PETA* akrilātiem: a) *E^{IR}TOFA_BD_AA* polimēri; b) *E^{IR}TOFA_TMP_AA* polimēri; c) *NEO380_AA* polimēri; d) *L3300_AA* polimēri.

Iegūtajiem polimēriem tika veikta *DSC* analīze, lai noteiktu stiklošanās temperatūru (T_g) (2.2. att.). $T_{g(DSC)}$ tika noteikta kā viduspunkts starp stiklošanās procesa sākuma temperatūru un stiklošanās procesa beigu temperatūru.

Polimēriem, kas iegūti no komerciāli pieejamo poliolu acetoacetātiem (*L3300_AA* un *NEO380_AA*), $T_{g(DSC)}$ galvenokārt ietekmēja izmantotais akrilāts. Salīdzinot no tiem pašiem akrilātiem iegūtos polimērus, $T_{g(DSC)}$ atšķīrās par mazāk nekā 2 °C (2.1. c, d att.). Izmantotie komerciāli pieejamie poliolu acetoacetāti būtiski neietekmēja polimēra $T_{g(DSC)}$. Atkarībā no izmantotā akrilāta $T_{g(DSC)}$ palielinājās šādā secībā: *BPAEDA* < *TMPTA* < *PETA*. Secināts, ka izmantotā akrilāta funkcionalitāte ietekmēja $T_{g(DSC)}$. Jo lielāka funkcionalitāte izmantotajam akrilātam, jo augstāka bija polimēra $T_{g(DSC)}$. Tas skaidrojams ar lielāku šķērssaistīšanās blīvumu [77]. Tāda pati tendence tika novērota arī polimēriem, kas iegūti no sintezētajiem taleļļas poliolu acetoacetātiem (2.1. a, b att.), bet šiem polimēriem redzama arī būtiska taleļļas poliola acetoacetāta ietekme uz polimēra $T_{g(DSC)}$.

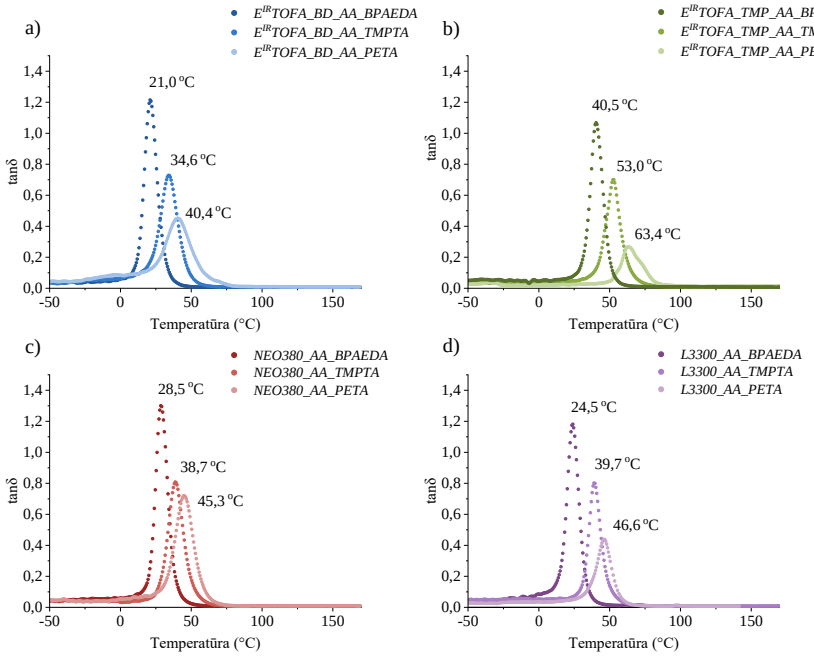

2.3. att. DMA (3 °C·min^{-1}, 1 Hz, 5 N) tanδ līknes polimēriem no sintezētiem acetoacetātiem un *BPAEDA*, *TMPTA*, *PETA* akrilātiem: a) *E^{IR}TOFA_BD_AA* polimēri; b) *E^{IR}TOFA_TMP_AA* polimēri; c) *NEO380_AA_TMPTA* polimēri; d) *L3300_AA* polimēri.

Lai noteiktu polimēru dinamiski mehāniskās īpašības, tika veikta DMA. Visu iegūto polimēru tanδ (2.3. att.) līknēs bija novērojams tikai viens skaidri izteikts maksimums, turklāt simetriskais līkņu profils (joslas profils) attiecībā pret to maksimumu liecināja par polimēru viendabīgo struktūru. Šī sakarība starp joslas platumu, simetriju un polimēra struktūru viendabīgumu ir aprakstīta arī vairākos citos publicētajos pētījumos [68, 78–80].

Lai gan attiecīgajiem polimēriem $T_{g(DMA)}$ atšķīrās no $T_{g(DSC)}$, tendences tika novērotas tādas pašas. $T_{g(DMA)}$ bija augstāka par $T_{g(DSC)}$. Tas skaidrojams ar to, ka DMA gadījumā tiek lietots spēks un mērīta parauga pretošanās spēja piemērotajam spēkam, savukārt *DSC* metode pamatojas uz siltumietilpības izmaiņām paraugā [81, 82]. DMA metode ir daudz piemērotāka T_g noteikšanai polimēriem ar grūti nosakāmu T_g un ļoti šķērssaistītiem polimēriem [83]. Polimēriem ar lielāku šķērssaistīšanās blīvumu bija augstāka stiklošanās temperatūra (2.2. tab.).

Par šo sakarību starp lielāku šķērssaistīšanās blīvumu un augstāku polimēra $T_{g(DSC)}$ ir ziņojusi arī Vanga zinātniskā grupa *(Wang et al.)* [51].

2.2. tabula

No taleļļas poliolu vai komerciāli pieejamo poliolu acetoacetātiem un *BPAEDA*, *TMPTA*, *PETA* akrilātiem iegūto polimēru raksturojums

	Paraugs	Max. tanδ	$T_{g(DMA)}$, °C	$E_{(uzkrājuma)}$ ($T_{g(DMA)}$ + 50), MPa	ν_e, moles·cm^{-3}	ρ, g·cm^{-3}	M_c, g·mol^{-1}
No taleļļas acetoacetātiem	*E^{IR}TOFA_BD_AA_BPAEDA*	1,21	21,0	5,1	$0{,}59\cdot10^{-3}$	1,167	1695
	E^{IR}TOFA_BD_AA_TMPTA	0,73	34,6	17,7	$1{,}98\cdot10^{-3}$	1,211	505
	E^{IR}TOFA_BD_AA_PETA	0,45	40,4	24,2	$2{,}67\cdot10^{-3}$	1,219	375
	E^{IR}TOFA_TMP_AA_BPAEDA	1,07	40,5	17,1	$1{,}89\cdot10^{-3}$	1,116	529
	E^{IR}TOFA_TMP_AA_TMPTA	0,70	53,0	19,1	$2{,}04\cdot10^{-3}$	1,177	490
	E^{IR}TOFA_TMP_AA_PETA	0,27	63,4	30,6	$3{,}17\cdot10^{-3}$	1,235	315
No komerciāli pieejamo poiolu acetoacetātiem	*NEO380_AA_BPAEDA*	1,30	28,5	8,2	$0{,}93\cdot10^{-3}$	1,257	1075
	NEO380_AA_TMPTA	0,81	38,7	18,4	$2{,}04\cdot10^{-3}$	1,328	490
	NEO380_AA_PETA	0,72	45,3	23,4	$2{,}55\cdot10^{-3}$	1,330	392
	L3300_AA_BPAEDA	1,18	24,5	9,8	$1{,}13\cdot10^{-3}$	1,171	885
	L3300_AA_TMPTA	0,80	39,7	19,9	$2{,}20\cdot10^{-3}$	1,202	455
	L3300_AA_PETA	0,44	46,6	24,9	$2{,}70\cdot10^{-3}$	1,247	369

No DMA datiem tika noteikta $T_{g(DMA)}$ un uzkrājuma modulis elastīgajā diapazonā ($E_{(uzkrājuma)}$ temperatūrā $T_{g(DMA)}$ + 50). Šie dati izmantoti, lai aprēķinātu šķērssaistīšanās blīvumu un molekulmasu starp šķērssaitēm (2.2. tab.). Aprēķinātie rezultāti liecināja, ka šķēssaišu blīvums un molekulmasa starp šķērssaitēm bija ļoti atkarīga no izmantotā akrilāta un acetoacetāta funkcionalitātes. Izmantojot komponentus ar lielāku funkcionalitāti, tika iegūti polimēri ar lielāku šķēssaistīšanās blīvumu, kā arī ar mazāku molekulmasu starp šķēssaitēm, kas būtiski ietekmē polimēra mehāniskās īpašības. Tas atbilst Raula *(Rahul)* un Kitija *(Kitey)* zinātniskās grupas novērojumiem, ka polimēra šķērssaistīšanās blīvums ietekmē $T_{g(DMA)}$ [84]. Arī stiepes testi apstiprināja mehānisko īpašību atkarību no šķērssaistīšanās blīvuma.

Lielākais škērssaistīšanās blīvums ($3{,}17\cdot10^{-3}$ mol·cm^{-3}) un mazākā molekulmasa starp šķērssaitēm (315 g·mol^{-1}) bija polimēram, kas iegūts no *E^{IR}TOFA_TMP_AA* un *PETA*. Tas skaidrojams ar abu – Maikla donora un Maikla akceptora – lielāko funkcionalitāti. Vismazākais škērssaistīšanās blīvums un lielākā molekulmasa starp šķērssaitēm bija polimēriem, kas iegūti no mazākas funkcionalitātes acetoacetāta un difunkcionālā akrilāta – *BPAEDA*.

Polimēru paraugi, kas iegūti no poliolu acetoacetātiem un *PETA* ($f = 4$), uzrādīja visaugstākās stiepes moduļa un stiepes stiprības vērtības (2.4. att.). To var izskaidrot ar izmantotā akrilāta lielo funkcionalitāti, kā rezultātā tiek iegūts polimērs ar lielāku šķērssaistīšanās blīvumu (2.2. tab.), kā arī šiem polimēriem bija visaugstākā stiepes moduļa vērtība. Tika novērota sakarība starp izmantotā akrilāta funkcionalitāti un iegūstamā polimēra stiepes moduļa vērtībām – izmantojot lielākas funkcionalitātes komponentus, varēja iegūt polimērus ar lielākām stiepes moduļa un stiepes stiprības vērtībām.

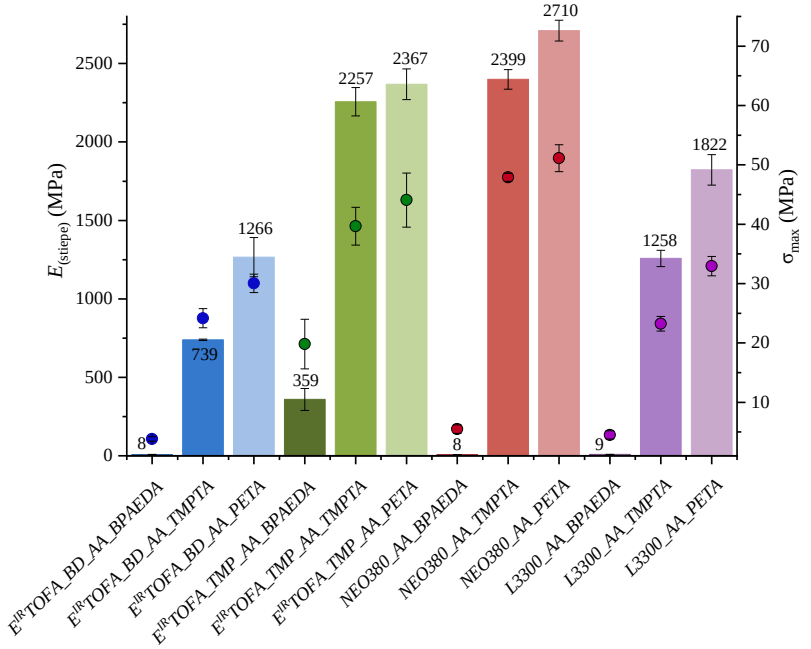

2.4. att. $E_{(stiepe)}$ un σ_{max} (2 mm·min^{-1}, 22 °C) polimēriem no taleļļas poliolu vai komerciālo poliolu acetoacetātiem un *BPAEDA*, *TMPTA* vai *PETA* akrilātiem.

NEO380_AA_PETA polimēra stiepes stiprība bija 51 MPa, stiepes moduļa vērtība sasniedza 2710 MPa, kas bija vislielākā starp visiem paraugiem. Salīdzinoši augstas moduļa un stiepes stiprības vērtības bija arī taleļļas polimēriem *E^{IR}TOFA_TMP_AA_TMPTA* ($E_{(stiepe)}$ = 2250 MPa, σ_{max} = 40 MPa) un *E^{IR}TOFA_TMP_AA_PETA* ($E_{(stiepe)}$ = 2370 MPa, σ_{max} = 44 MPa). Iegūto polimērmateriālu mehāniskās īpašības var tikt salīdzinātas ar citiem inovatīviem materiāliem, piemēram, Fleišera zinātniskās grupas *(Fleischer et al.)* izstrādātajiem bezizocianāta poliuretāna materiāliem (*NIPU*) no heksametilēndiamīna, glicerīna cikliskajiem karbonātiem un TMP. Šo *NIPU* stiepes stiprība bija 68 MPa, un stiepes moduļa vērtība sasniedza 2100 MPa [85]. Iegūto polimēru mehāniskās īpašības bija līdzīgas poliuretānu materiālu [86, 87] un polimetilmetakrilāta materiālu īpašībām. Šiem materiāliem stiepes stiprība ir aptuveni 55 MPa, stiepes moduļa vērtība – aptuveni 2700 MPa [88, 89]. Tas apliecina, ka polimēri, kas iegūti Maikla reakcijā, izmatojot no taleļļas iegūtus komponentus, var būt daudzsološa un konkurētspējīga alternatīva jau zināmajiem polimērmateriāliem.

Stiepes testos tika noteikta arī polimēru paraugu pagarinājums līdz pārplīšanai, un secināts, ka tas korelē ar konkrēto paraugu stiepes moduļa un stiepes stiprības vērtībām Jo augstākas moduļa un stiepes izturības vērtības, jo mazāks bija pagarinājums. Vismazākie pagarinājumi novērti *E^{IR}TOFA_TMP_AA_PETA* (ε = 1,9 %), *NEO380_AA_PETA* (ε = 2,7 %) un *L3300_AA_PETA* (ε = 2,9 %) polimēriem, savukārt vislielākās pagarinājuma vērtības bija *E^{IR}TOFA_BD_AA_BPAEDA* (ε = 55 %), *NEO380_AA_BPAEDA* (ε = 53 %) un *L3300_AA_BPAEDA* (ε = 47 %) polimēriem.

Tika novērota tā pati sakarība starp mehāniskajām īpašībām un molekulmasu starp šķērssaistēm un šķēssaistīšanās blīvumu. Jo lielāks ir šķērssaistīšanās blīvums (2.2. tab.), jo attiecīgi lielāks stiepes modulis un stiepes stiprība.

Rezultāti apliecināja, ka, izmantojot akrilātus ar atšķirīgām funkcionalitātēm, ir iespējams iegūt ļoti dažādus polimērus. Izmantojot zemākas funkcionalitātes komponentus, varēja iegūt polimērus, kas pēc īpašībām bija līdzīgi gumijām. Bija iespējams iegūt arī tādus polimērus, kas pēc īpašībām līdzīgi organiskajam stiklam [88–90]. Apkopojot literatūru par līdzīgiem materiāliem un to īpašībām, var apgalvot, ka šajā pētījumā iegūtie polimēri ir konkurētspējīgi ar vairākiem citiem alternatīviem materiāliem. Polimēru ražošana no brīvajām taukskābēm, izmantojot Maikla reakciju, bija vienkārša un tika veikta daudz maigākos apstākļos, salīdzinot ar citām inovatīvu polimēru iegūšanas metodēm, piemēram, *NIPU* sintēzi.

Maikla 1,4-pievienošanās polimerizāciju var īstenot īsā laika periodā istabas temperatūrā un atmosfēras spiedienā. Izejvielas, ko izmanto polimēru sintezēšanai, izmantojot Maikla reakciju, ir mazāk toksiskas nekā izocianāti, kas ir viena no galvenajām izejvielām poliuretāna ražošanā. Maikla reakcijā sintezēto polimēru mehāniskās un termiskās īpašības bija līdzvērtīgas vai pat labākas, salīdzinot ar citiem literatūrā aprakstītiem inovatīviem materiāliem. Turklāt polimēru īpašības var pielāgot, mainot polimerizācijai izmantotos komponentus.

3. Polimēru sveķi no taleļļas Maikla donora un Maikla akceptora

Literatūrā ir atrodamas tikai dažas publikācijas, kurās pētīta acetoacetātu sintēze no atjaunojamajām izejvielām un to izmantošana dažādu polimērmateriālu ieguvei. Sjuja zinātniskā grupa (*Xu et al.*) izstrādāja pārklājuma plēves no acetoacetilētas rīcineļļas un aldehīdgrupu un akrilgrupu saturošām vielām polimerizācijā pēc Maikla reakcijas mehānisma [49]. Vana zinātniskā grupa *(Wang et al.)* izveidoja sacietējošus pārklājumus no acetoacetilētas rīcineļļas un daudzfunkcionāliem akrilātiem (heksametilēndiakrilāts, *TMPTA, PETA*), izmantojot Maikla rekciju [51]. Noordovera zinātniskā grupa *(Noordover et al.)* izstrādāja malonāta grupas saturošus poliestera pārklājumus no atjaunojamajiem resursiem, iegūtiem Maikla donoriem reakcijā ar ditrimetilolpropāntetraakrilātu [91]. Nagas zinātniskā grupa *(Naga et al.)* pētīja reakciju starp daudzfunkcionāliem acetoacetātiem (*mezo*-eritritoltetraacetoacetāta, trimetilolpropāntriacetoacetāta) un diakrilātiem (1,4-butāndioldiakrilātu, 1,6-heksāndioldiakrilātu, 1,9-nonāndioldiakrilātu), iegūstot gelus [92]. Nedaudz vēlāk Nagas zinātniskā grupa izstrādāja porainus polimērmateriālus no *mezo*-eritritoltetraacetoacetāta vai D-sorbītheksaacetoacetāta reakcijā ar polietilēnglikoldiakrilātu šķīdinātāju vidē [93]. Visos šajos pētījumos ir izmantots no atjaunojamajiem resursiem iegūts Maikla donors un petroķīmisks Maikla akceptors.

Šajā darbā iepriekš sintezētie taleļļas akrilāti un acetoacetāti tika izmantoti, lai iegūtu šķērssaistītu polimēru (3.1. att.). Iegūtajiem polimēriem bija augsta termiskā stabilitāte un labas mehāniskās īpašības, lai tos varētu izmantot kā alternatīvu plaši lietotajiem termoreaktīvajiem sveķiem, piemēram, epoksīda, poliesteru vai vinilesteru sveķiem.

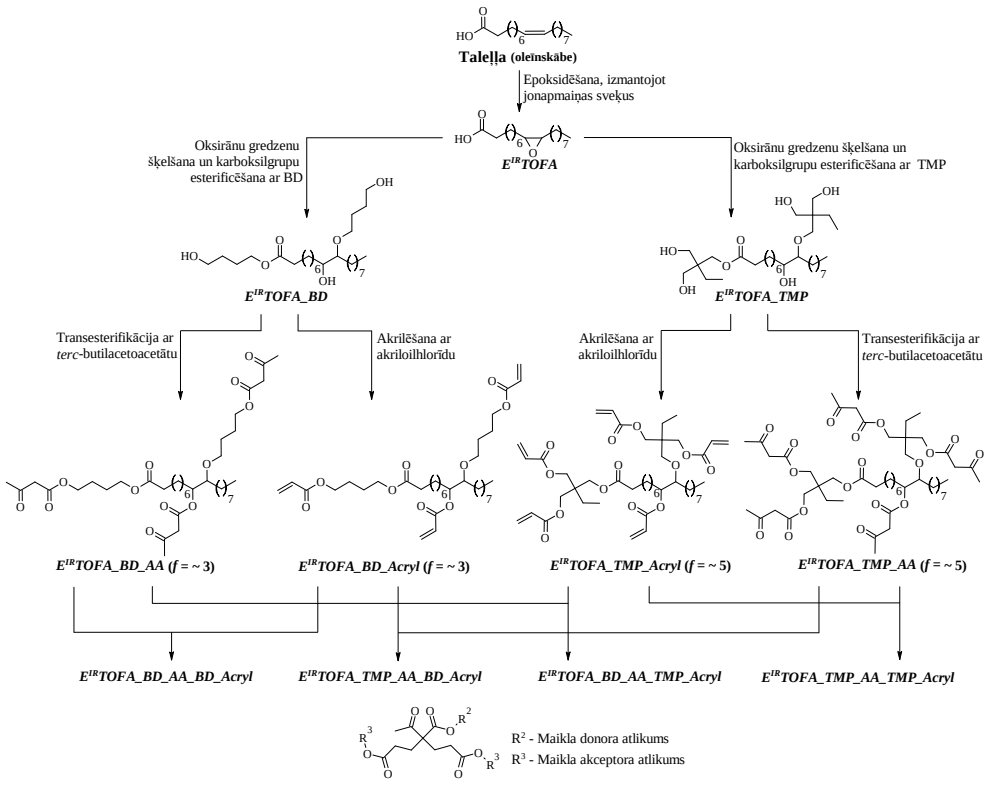

3.1. att. Konceptuāla shēma polimēru ieguvei no taleļļas taukskābju Maikla donora un Maikla akceptora.

No *E^IRTOFA_BD_Acryl* iegūtie polimēri bija elastīgi, līdzīgi gumijai. Polimēri, kas iegūti no *E^IRTOFA_TMP_Acryl*, bija cieti, līdzīgi organiskajam stiklam. Visi sintezētie polimēri bija caurspīdīgi un dzidri ar brūnganīgu vai dzeltenīgu nokrāsu.

Izstrādāto polimēru ķīmiskā struktūra tika analizēta, izmantojot *FTIR* spektroskopiju (3.2. a att.). Akrilātam raksturīgās absorbcijas joslas pie 1640–1620 cm^{-1} un 1407 cm^{-1} nevarēja izmantot interpretācijai, jo tās pārklājas ar donora funkcionālajām grupām raksturīgajām absorbcijas joslām. Akrilgrupām $=CH_2$ raksturīga vēl viena absorbcijas josla *FTIR* spektrā pie 810 cm^{-1}.

Polimēriem, kas iegūti no *E^IRTOFA_BD_Acryl* akrilāta, *FTIR* spektrā absorbcijas joslas pie 810 cm^{-1} netika novērotas. Tas liecināja par augstu konversijas pakāpi un pilnīgu reakcijas norisi. Bet šī absorbcijas josla bija novērojamas abiem polimēriem, kas iegūti no *E^IRTOFA_TMP_Acryl* akrilāta. Salīdzinot *E^IRTOFA_BD_AA_TMP_Acryl* un *E^IRTOFA_TMP_AA_TMP_Acryl* polimēru *FTIR* spektrus, akrilgrupu absorbcijas josla pie 810 cm^{-1} bija intensīvāka *E^IRTOFA_TMP_AA_TMP_Acryl* polimēra spektrā. Tas varētu nozīmēt nepilnīgu konversiju augstās viskozitātes, augstas funkcionalitātes un molekulas sazarotības, kā arī stērisku efektu dēļ.

Polimēru paraugu ķīmiskā struktūra tika analizēta, izmantojot arī cvKMR ^{13}C spektroskopiju (3.2. b att.). Spektros bija redzams gaidītās ^{13}C ķīmiskās nobīdes. Visiem iegūtajiem polimēriem bija redzamas >CH-O- grupām raksturīgi signāli diapazonā no 63,0 ppm līdz 83,5 ppm. >CH-O- grupas radās, oksirāna gredzeniem šķeļoties ar spirtiem. Arī ^{13}C spektrā

atbilstošo ceturtējo oglekļu raksturīgais signāls bija tajā pašā diapazonā no 63,0 ppm līdz 83,5 ppm, kas apliecināja, ka ir notikusi divu akrilgrupu reakcija ar acetoacetāta metilēngrupu pēc Maikla reakcijas mehānisma.

Var novērot arī vairāku signālu pārklāšanos 26,5−42,9 ppm diapazonā. Šajā diapazonā spektrā varēja identificēt ^{13}C signālu, kas raksturīgs trešējiem oglekļiem. Arī trešējo oglekļu esamība bija būtisks rādītājs polimerizācijas konstatēšanai, jo tas parādīja to, ka viena acetoacetāta grupa ir reaģējusi tikai ar vienu akrilgrupu. Maikla donora acetoacetāta daļas –C(=O)–CH_3 grupām raksturīgais ^{13}C signāls bija tajā pašā diapazonā no 24,0 ppm līdz 24,4 ppm.

Akrilgrupām raksturīgo signālu esamība dažu paraugu cvKMR spektros pie 130,2−131,2 ppm norādīja uz nepilnīgu reakcijas norisi. Līdzīgi kā *FTIR* spektros, arī cvKMR spektros akrilgrupu signāla intensitāte polimēros, kas iegūti no *E^{IR}TOFA_BD_Acryl*, bija zema. Toties tā bija salīdzinoši intensīva polimēru spektros, kas iegūti no *E^{IR}TOFA_TMP_Acryl*. Daudz sazarotāka struktūra un lielāks akrilgrupu skaits molekulā samazināja *E^{IR}TOFA_TMP_Acryl* un *E^{IR}TOFA_TMP_AA* reaģētspēju stērisko efektu dēļ. Polimēru sintēzē izmantotais akceptors un donors ir iegūti no taukskābēm, tāpēc tie saturēja dubultsaites nepilnīgas epoksidācijas reakcijas dēļ. Divkāršās saites signāls pārklājas ar signālu, kas raksturīgs akrilāta grupām. Tas jāņem vērā, interpretējot iegūtos spektrus. cvKMR un *FTIR* spektri apstiprināja, ka polimēri no taleļļas donoriem un akceptoriem ir iegūti Maikla reakcijā.

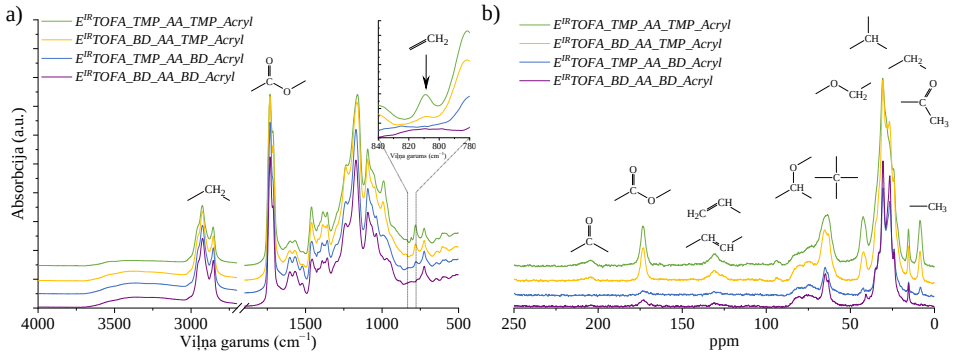

3.2. att. Struktūras analīze polimēriem no taleļļas Maikla donora un akceptora: a) *FTIR* spektri; b) cvKMR ^{13}C spektri.

Iegūto polimēru termiskā stabilitāte analizēta ar TGA (3.3. att.). Sākotnējais nelielais masas zudums temperatūrā līdz 300 °C saistīts ar katalizatora un citu iespējamu mazmolekulāru vielu izdalīšanos. Temperatūrā virs 300 °C iegūtajiem polimēriem sadalīšanās gaita noritēja atšķirīgi, ko labi varēja novērot masas zuduma atvasinājumu līknēs. *E^{IR}TOFA_BD_AA_BD_Acryl* polimēram TGA masas zuduma atvasinājuma līkne bija simetriska ar tikai vienu skaidru maksimumu pie 389,3 °C.

E^{IR}TOFA_TMP_AA_BD_Acryl masas zuduma atvasinājuma līkne nebija simetriska, maksimumam bija "plecs" pie aptuveni 450 °C. Otrais sadalīšanās maksimums kļuva izteiktāks, ja polimērs saturēja vairāk TMP saturošus komponentus. *E^{IR}TOFA_TMP_AA_TMP_Acryl* polimēram masas zuduma atvasinājuma līknē bija divi izteikti maksimumi (400 °C un 445 °C temperatūrā) ar gandrīz vienādu svara zuduma ātrumu. Pirmo atvasinājuma līknes maksimumu varēja saistīt ar esteru un ēteru saišu šķelšanos, veidojoties CO_2 un citiem zemas molekulmasas

savienojumiem [47, 51]. Otro atvasinājuma maksimumu varēja attiecināt uz polimēra ķīmiskās struktūras TMP daļas sadalīšanos [94].

Rezultāti apliecināja, ka izstrādātie termoreaktīvie polimēri no taleļļas bija termiski stabili. Visiem paraugiem bija ļoti līdzīgas svara zuduma līknes sākuma temperatūrā līdz 300 °C. Paraugi uzrādīja svara zudumu mazāk nekā 10 % līdz 300 °C. Visstraujākā polimēru termiskā sadalīšanās noritēja temperatūras intervālā no 300 °C līdz 475 °C. Polimēra paraugs *E*^{IR}*TOFA_TMP_AA_TMP_Acryl* uzrādīja nedaudz labāku termisko stabilitāti nekā citi paraugi.

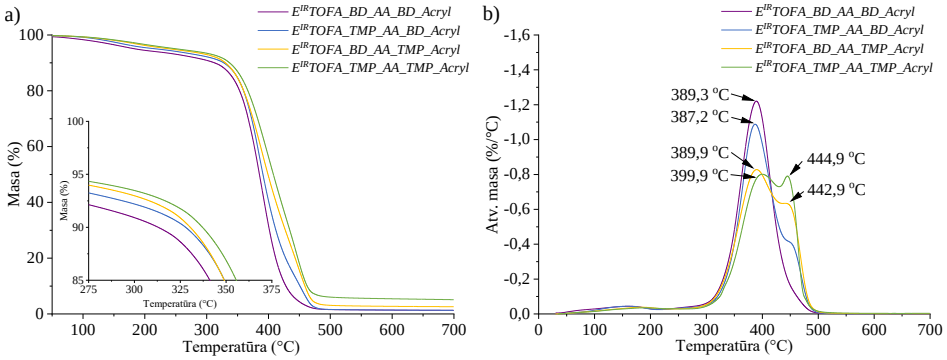

3.3. att. TGA (10 °C·min^{-1}) polimēriem no taleļļas Maikla donora un akceptora: a) TGA līknes; b) TGA atvasinājuma līknes.

Lielāks šķērssaistīšanās blīvums veicināja karbonizāciju, kā rezultātā radās lielāks cieto atlikumu daudzums [63, 95]. No visiem iegūtajiem termoreaktīvo polimēru paraugiem vislielākais cietā atlikuma iznākums bija *E*^{IR}*TOFA_TMP_AA_TMP_Acryl* polimēram – 5,10 % 675 °C temperatūrā.

Iegūto polimēru termiskās īpašības tika pētītas arī, izmantojot *DSC* (3.4. a att.). $T_{g(DSC)}$ tika noteikta visiem polimēriem. Novērots, ka $T_{g(DSC)}$ palielinājās, palielinoties TMP saturošu komponentu saturam polimēra sastāvā. Tas, visticamāk, bija saistīts ar šo polimēru lielāku šķērssaistīšanās blīvumu.

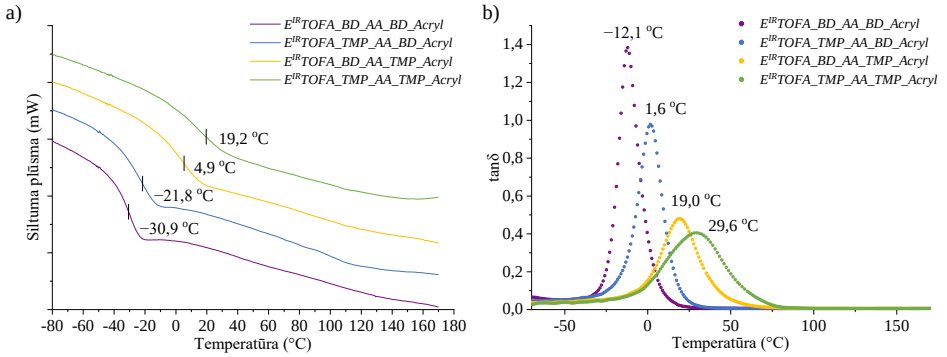

3.4. att. *DSC* un DMA līknes iegūtajiem polimēriem no taleļļas Maikla donora un akceptora: a) *DSC* līknes; b) DMA tanδ līknes.

DSC un DMA rezultāti polimēriem no taleļļas Maikla komponentiem

Sample	T_g, °C		ρ, g·cm^{-3}	$E_{(uzkrājuma)}$ ($T_{g(DMA)}$ + 50), MPa	ν_e, mol·cm^{-3}	M_c, g·mol^{-1}
	$T_{g(DSC)}$	$T_{g(DMA)}$				
E^{IR}TOFA_BD_AA_BD_Acryl	−30,9	−12,1	1,071	5,3	0,69·10^{-3}	1562
E^{IR}TOFA_TMP_AA_BD_Acryl	−21,8	1,6	1,085	5,8	0,71·10^{-3}	1518
E^{IR}TOFA_BD_AA_TMP_Acryl	4,9	19,0	1,104	11,4	1,33·10^{-3}	829
E^{IR}TOFA_TMP_AA_TMP_Acryl	19,2	29,6	1,125	13,7	1,55·10^{-3}	724

Iegūto polimēru tanδ līknes redzamas 3.4. b attēlā, nozīmīgākie dati apkopoti 3.1. tabulā. 3.4. b attēlā redzams, ka *BD_Acryl* saturošu polimēru tanδ joslas bija šaurākas un tanδ vērtības bija lielākas nekā *TMP_Acryl* saturošiem polimēriem. Sakarība starp $T_{g(DMA)}$ un $T_{g(DSC)}$ saglabājās tāda pati kā polimēriem no petroķīmiskiem komerciāli pieejamajiem akrilātiem (3.1. tab.). Zemākā stiklošanās temperatūra tika noteikta *E^{IR}TOFA_BD_AA_BD_Acryl* polimēram, kas bija −12,1 °C. Savukārt augstākā stiklošanās temperatūra – 29,6 °C – tika noteikta *E^{IR}TOFA_TMP_AA_TMP_Acryl* paraugam.

Sprieguma-deformācijas līknes un pagarinājums līdz pārrāvumam (3.5. att.) raksturo iegūto polimēru stiepes moduli un stiepes stiprību. Polimēriem, kas iegūti no *E^{IR}TOFA_BD_Acryl*, līknes bija līdzīgas viskoelastīgu materiālu raksturīgām līknēm. Savukārt polimēra *E^{IR}TOFA_TMP_AA_TMP_Acryl* sprieguma-deformācijas līkne līdz aptuveni 5 % deformācijai līdzinājās līknēm, kas raksturīgas cietai, stiklveidam polimērmateriālam.

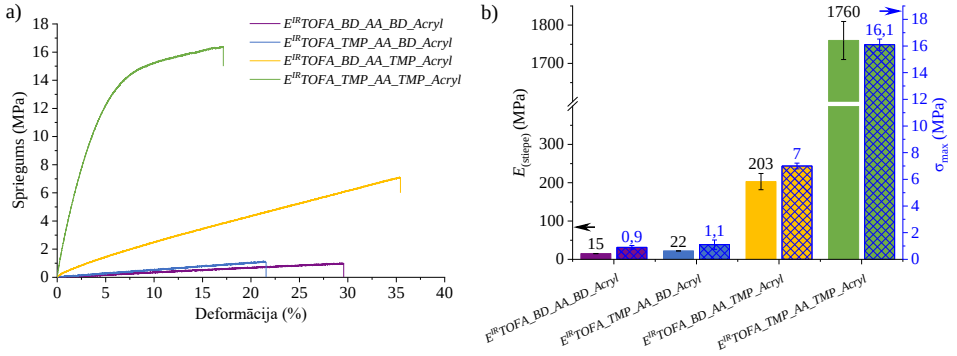

3.5. att. Stiepes testi (2 mm·min^{-1}, 18 °C) iegūtajiem polimēriem no taleļļas Maikla donora un akceptora: a) sprieguma-deformācijas līknes; b) $E_{(stiepe)}$ and σ_{max}.

No iegūtajiem datiem (3.1. tab. un 3.5. a att.) varēja secināt, ka polimēriem no *E^{IR}TOFA_TMP_Acryl* bija lielāks stiepes modulis, kas skaidrojams ar lielāku šķērssaistīšanās blīvumu. *E^{IR}TOFA_TMP_AA_TMP_Acryl* polimēram bija visaugstākā stiepes moduļa vērtība (1760 MPa) un stiepes stiprība (16,1 MPa), kā arī mazākais pagarinājums līdz pārrāvumam (17 %). *E^{IR}TOFA_TMP_AA_TMP_Acryl* polimērs bija ļoti līdzīgas polimēram, kas iegūts no *L3300_AA* un *PETA* ($E_{(stiepe)}$ = 1822 MPa; σ_{max} = 30 MPa). Mehāniskie testi apstiprināja, ka izstrādātie polimēri bija konkurētspējīgi ar polimēriem, kas iegūti no petroķīmiskiem komerciāli pieejamajiem akrilātiem. Starp polimēru paraugiem *E^{IR}TOFA_BD_AA_BD_Acryl* bija viszemākās stiepes moduļa (15 MPa) un stiepes stiprības (0,9 MPa) vērtības, kā arī vislielākais stiepes pagarinājmus (27 %); polimēram bija gumijai līdzīgas īpašības.

4. Putu polimērmateriāli no taleļļas Maikla donora un Maikla akceptora

Ir publicēti vairāki pētījumi, kuros izmantoti dažādi Maikla reakcijas veidi putu polimērmateriālu izstrādei. Kostes zinātniskā grupa *(Koste et al.)* ieguva mīkstās putas *aza*-Maikla reakcijā no akrilētas sojas pupiņu eļļas un no atjaunojamām izejvielām sintezētiem amīniem [27]. Savukārt Lī zinātniskā grupa *(Li et al.)* pētīja viena soļa tiolīna "klikšķa" ķīmiju (angļu val. – *click chemistry*) un Maikla reakciju, lai izveidotu cietu superhidrofobu/superoleofīlu melamīna putu polimērmateriālu [96]. Dažās publikācijās ir aprakstīta putu polimērmateriālu izstrāde, izmantojot oglekļa-oglekļa Maikla reakciju. Zonnenšeina zinātniskā grupa (*Sonnenschein et al.)* iedziļinājās Maikla ķīmijas izmantošanā dažādu putu polimērmateriālu, tai skaitā cieto un viskoelastīgo, kā arī elastomēru ražošanā. Viņa pētījumos kā izejviela izmantots acetoacetilēts glicerīns un petroķīmiski akrilāti [68]. Nagas darba grupa *(Naga et al.)* izstrādāja porainus polimērmateriālus, izmantojot Maikla reakciju starp daudzfunkcionālu acetoacetātu un polietilēnglikoldiakrilātu [93]. Reakciju rezultātā iegūti poraini polimērmateriāli ar savienotām sfērām, un pētījums izceļ iespēju pielāgot šo polimērmateriālu morfoloģiju un īpašības, mainot polimerizācijas apstākļus. Tomēr arī polietilēnglikoladiakrilāta, petroķīmiska atvasinājuma, lietošana rada bažas par ilgtspējību, ņemot vērā polimēru nozares mērķi pāriet uz atjaunojamo izejvielu plašāku izmantošanu. Par putu polimērmateriālu izstrādi, izmantojot Maikla reakciju, ir atrodami daži patenti [97] un patentu pieteikumi [98, 99]. Katrs piedāvā dažādas pieejas putu polimērmateriāla ražošanai gan no petroķimikālijām, gan pirmās paaudzes atjaunojamajām izejvielām. To kopējais trūkums ir otrās paaudzes atjaunojamo izejvielu, īpaši otrās paaudzes brīvo taukskābju, neizmantošana. Šie patenti kopumā liecina par nozares tendenci meklēt ilgtspējīgākus materiālus, bet arī izceļ otrās paaudzes atjaunojamu izejvielu neizmantošanu, piemēram, izejvielas, kas atvasinātas no brīvajām taukskābēm.

Šajā promocijas darba daļā tika izpētīts taleļļas acetoacetāta potenciāls putu polimērmateriālu izstrādē, kombinējot to ar taleļļas akrilātu. Papildus tika izmantoti tādi komerciāli pieejami akrilāti no petroķimikālijām kā *BPAEDA, TMPTA, PETA* un no sojas pupiņu eļļas kā *ESOA*. 1,1,3,3-tetrametilguanidīns tika izmantots kā katalizators. Lai izveidotu putu materiālam nepieciešamo poru struktūru, bija nepieciešams pievienot tādas piedevas kā virsmaktīvo vielu (silikona virsmaktīvā viela *Niax Silicone L-6915*) un uzputošanās aģentu (*Opteon™ 1100*, kura pamatsastāvā ir hidrofluorolefīni ar zemu globālās sasilšanas potenciālu).

Pirms putu polimērmateriālu izstrādes tika noteiktas dielektriskās polarizācijas izmaiņas cietēšanas laikā izvēlētajām formulācijām bez virsmaktīvās vielas un uzputošanās aģenta. Polimēri uzrādīja dažādas dielektriskās polarizācijas pakāpes, un cietēšanas procesā tie sasniedza atšķirīgas maksimālās temperatūras (4.1. att.). Analizējot cietēšanas parametrus polimēriem, kas iegūti no E^{IR}*TOFA_TMP_AA* reakcijā ar dažādiem akrilātiem, noteikta saistība starp akrilāta funkcionalitāti un cietēšanas parametriem. Pieaugot akrilāta funkcionalitātei, cietēšana noritēja ātrāk un tika sasniegta augstāka maksimālā temperatūra. Piemēram, polimērs no četrvērtīgā *PETA* sacietēja visātrāk (70 s) un sasniedza augstāko temperatūru (133 °C). Polimēram no trīsvērtīgā *TMPTA* bija nedaudz ilgāks cietēšanas laiks (116 s) un zemāka maksimālā temperatūra (122 °C). Vērts atzīmēt, ka komerciāli pieejamajiem petroķīmiskiem akrilātiem ir tendence sacietēt ātrāk un augstākās temperatūrās nekā akrilātiem no

atjaunojamām izejvielām. Konkrētāk, sojas pupiņu eļļas *ESOA* un taleļļas *E^{IR}TOFA_BD_Acryl* polimēri cietēja ilgāk un sasniedza zemāku maksimālo temperatūru. Tas uzsver gan akrilāta izcelsmes, gan funkcionalitātes ietekmi uz šo polimēru sacietēšanas parametriem.

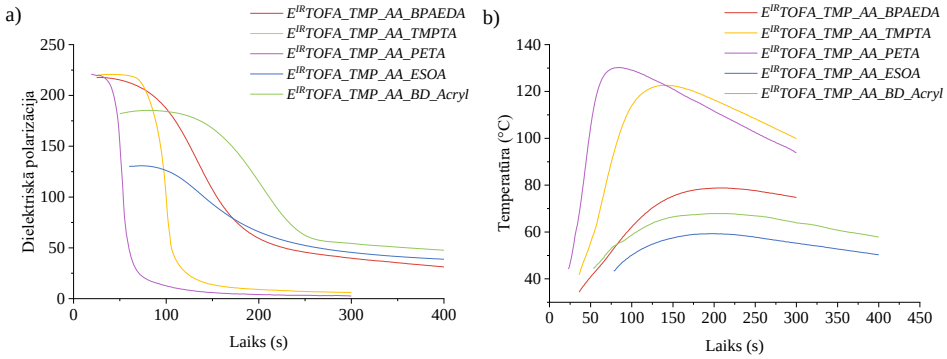

4.1. att. Iegūto polimēru cietēšanas parametri: a) dielektriskās polarizācijas līknes; b) polimēra temperatūras līknes.

Petroķīmisku akrilātu saturošu polimēru cietēšanas parametrus ietekmēja to molekulārā struktūra. Petroķīmisko akrilātu molekulas parasti ir mazākas, līdz ar to akrilgrupu koncentrācija ir lielāka. Lielāka pieejamo akrilgrupu koncentrācija paātrināja reakciju, veicinot cietēšanas procesu. Turpretim akrilātiem no atjaunojamām izejvielām, taleļļas un sojas pupiņu eļļas molekulārā struktūra ir sazarotāka un sarežģītāka.

Novērtējot putu polimērmateriālu uzputošanās līknes un raksturlielumus (4.2. att. un 4.1. tab.), bija redzams, ka putu polimērmateriāli, kas tika iegūti, kombinējot donoru no atjaunojamām izejvielām ar petroķīmisku akceptoru, uzputošanās sākuma un beigu laiki bija īsāki. No tiem *E^{IR}TOFA_TMP_AA_PETA* putu polimērmateriālam bija visātrākie uzputošanās sākuma un beigu laiki, kas liecina par ātrāku putu polimērmateriāla uzputošanās procesu. Putu polimērmateriāli no taleļļas donora un no atjaunojamām izejvielām iegūta akceptora (*ESOA* un *E^{IR}TOFA_BD_Acryl*) uzrādīja lielākus uzputošanās sākuma un beigu laikus, liecinot par lēnāku putu polimērmateriāla izplešanos. No visiem paraugiem vislielāko uzputošanās sākuma un beigu laiku uzrādīja *E^{IR}TOFA_TMP_AA_BD_Acryl* putu polimērmateriāls, kas iegūts, izmantojot taleļļas akrilātu un acetoacetātu. Novērota būtiska izmantotā komponenta izcelsmes ietekme uz izstrādāto putu polimērmateriālu uzputošanās parametriem.

Lēnāku augšanas ātrumu var skaidrot ar garāku alkilķēžu klātbūtni abos akceptoros no atjaunojamām izejvielām. Šī strukturālā īpašība ietekmē cietēšanas procesu, radot lēnāku putu polimērmateriāla uzputošanos. Turklāt struktūras sarežģītība rada stēriskus efektus, kas varēja traucēt reakcijas procesu. Šo molekulu sazarotais raksturs padara akrilgrupas grūtāk pieejamas, palēninot uzputošanos un cietēšanu.

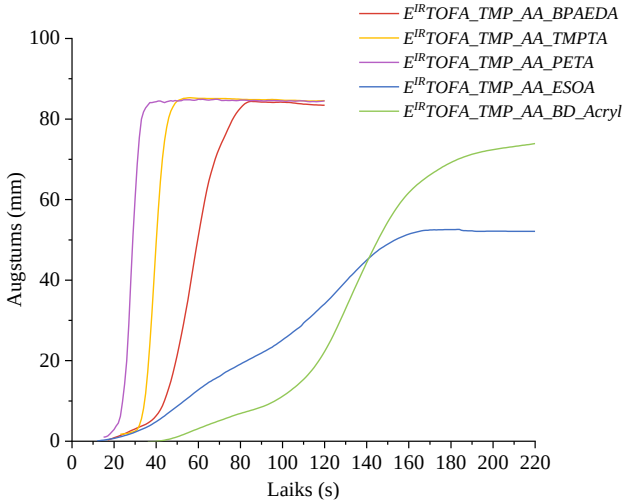

4.2. att. Izstrādāto putu polimērmateriālu paraugu uzputošanās līkne.

4.1. tabula

Iegūto putu polimērmateriālu uzputošanās parametri

Putu polimērmateriāla paraugs		**Uzputošanās sākuma laiks, s**	**Uzputošanās beigu laiks, s**
Taleļļas donors un petroķīmisku akceptors	*E^{IR}TOFA_TMP_AA_BPAEDA*	42,9	79,5
	E^{IR}TOFA_TMP_AA_TMPTA	34,2	56,6
	E^{IR}TOFA_TMP_AA_PETA	20,5	34,8
Taleļļas donors un atjaunojamo resursu akrilāts	*E^{IR}TOFA_TMP_AA_ESOA*	57,9	163,7
	E^{IR}TOFA_TMP_AA_BD_Acryl	87,6	187,8

Kā redzams no *DSC* rezultātiem (4.3. a att.), putu polimērmateriāliem, kas iegūti no atjaunojamo izejvielu donoriem un petroķīmiskiem akceptoriem, $T_{g(DSC)}$ vērtības svārstījās no 16,8 °C *E^{IR}TOFA_TMP_AA_BPAEDA* paraugam līdz pat 85,5 °C *E^{IR}TOFA_TMP_AA_PETA* paraugam. *E^{IR}TOFA_TMP_AA_PETA* putu polimērmateriālam, kas iegūts no četrvērtīga akrilāta, bija vislielākā $T_{g(DSC)}$, jo tā struktūra bija šķērssaistītāka. Turpretim putu polimērmateriāliem, kas iegūti no atjaunojamo resursu donoriem un akceptoriem, bija zemākas $T_{g(DSC)}$ vērtības, sasniedzot pat negatīvas temperatūras *E^{IR}TOFA_TMP_AA_ESOA* un *E^{IR}TOFA_TMP_AA_BD_Acryl* putu polimērmateriāliem, attiecīgi –1,9 °C un –9,7 °C. Šīs atšķirības izceļ izejvielu izcelsmes (atjaunojamas vai naftas ķīmijas) un ķīmisko struktūru (funkcionalitāte, sazarotības, molekulmasa) ietekmi uz iegūto putu polimērmateriālu īpašībām. Tāda pati tendence tika novērota DMA rezultātos, nosakot $T_{g(\mathrm{DMA})}$ no tanδ līknēm (4.3. b att.).

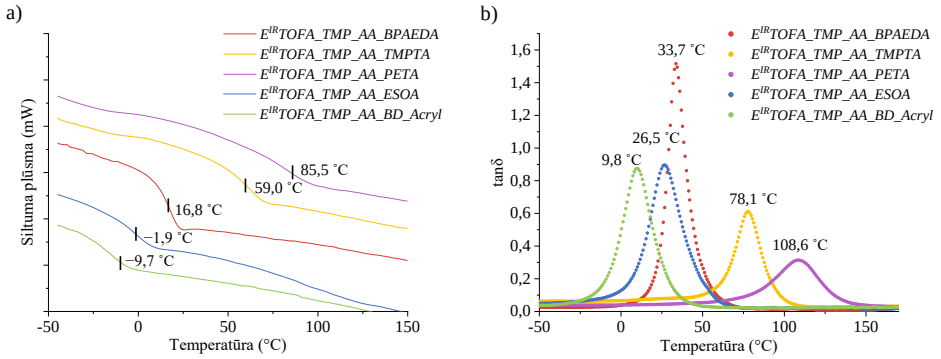

4.3. att. Iegūto putu polimērmateriālu *DSC* (10 °C·min^{-1}) un DMA (3 °C·min^{-1}, 1 Hz, 5 N) līknes: a) *DSC* līknes; b) DMA tanδ.

Polimēru termisko sadalīšanās procesu norisi analizēja ar TGA (4.4. att.). Putu polimērmateriāliem, kas iegūti no atjaunojamu izejvielu donoriem un petroķīmiskiem akceptoriem, sadalīšanās sākuma temperatūru galvenokārt ietekmēja akrilāta funkcionalitāte. Lai gan temperatūras bija diezgan līdzīgas, *E^{IR}TOFA_TMP_AA_PETA* putu polimērmateriālam, kas iegūts no četrvērtīga akrilāta, bija visaugstākā sadalīšanās sākuma temperatūra (374,6 °C), tam sekoja *E^{IR}TOFA_TMP_AA_TMPTA* putu polimērmateriāls, kas iegūts no trīsvērtīgā akrilāta, un *E^{IR}TOFA_TMP_AA_BPAEDA*, kas iegūts no divvērtīgā akrilāta. Akrilāta funkcionalitātes un šķērssaistīšanās blīvuma palielināšanās uzlabo termisko stabilitāti [100].

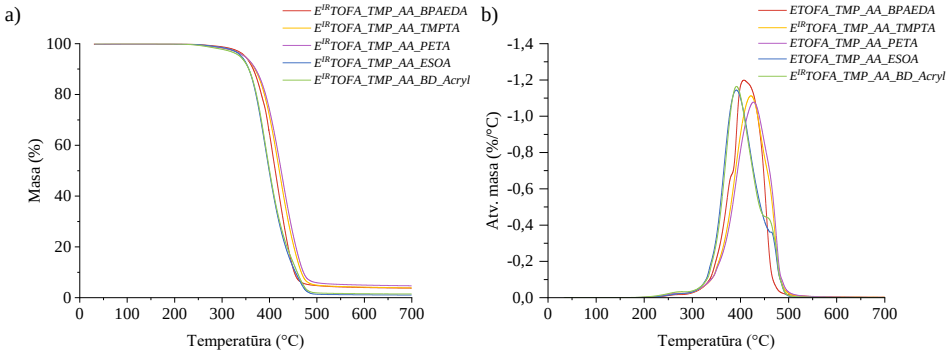

4.4. att. Iegūto putu polimērmateriālu TGA (10 °C·min^{-1}): a) TGA līknes; b) TGA atvasinājuma līknes.

E^{IR}TOFA_TMP_AA_ESOA un *E^{IR}TOFA_TMP_AA_BD_Acryl* degradēšanās sākuma temperatūras bija attiecīgi 354,8 °C un 359,6 °C. Tās ir zemākas nekā putu polimērmateriāliem, kas iegūti daļēji no petroķīmiskām izejvielām. Tas liecina par nedaudz samazinātu termisko stabilitāti putu polimērmateriāliem no atjaunojamām izejvielām.

Putu polimērmateriāliem, kam Maikla donors un Maikla akceptors bija iegūts no atjaunojamajiem resursiem, bija ievērojami mazāks cietais atlikums 675 °C temperatūrā. Putu polimērmateriālam *E^{IR}TOFA_TMP_AA_ESOA* un *E^{IR}TOFA_TMP_AA_BD_Acryl* cietais atlikums bija attiecīgi 1,02 % un 1,50 %. Putu polimērmateriāliem no petroķīmiskiem komerciāli pieejamajiem akrilātiem cietā atlikuma iznākums bija ievērojami lielāks. Vislielākais tas bija *E^{IR}TOFA_TMP_AA_PETA* (4,65 %), tam sekoja

E^{IR}*TOFA_TMP_AA_TMPTA* un *E*^{IR}*TOFA_TMP_AA_BPAEDA*. Tas liecināja, ka putu polimērmateriāliem, kas iegūti no lielākas funkcionalitātes akrilātiem, termiskās degradācijas laikā ir tendence veidot stabilāku ogles struktūru.

Putu polimērmateriālu siltumvadītspējas koeficients (λ) bija atkarīgs no izmantotajiem komponentiem (4.2. tab.). Proti, putu polimērmateriāliem no petroķīmiskiem akrilātiem bija zemākas λ vērtības, kas liecināja par labākām siltumizolācijas spējām. Viens no iespējamiem skaidrojumiem varētu būt lielāks slēgto poru saturs (*E*^{IR}*TOFA_TMP_AA_TMPTA*, *E*^{IR}*TOFA_TMP_AA_PETA*). Piemēram, *E*^{IR}*TOFA_TMP_AA_PETA* ar λ 30,7 mW·(m·K)$^{-1}$ apliecināja, ka petroķīmisko izejvielu izmantošana būtiski uzlabo materiāla siltumizolācijas īpašības. Turpretī putu polimērmateriāliem, kas iegūti no atjaunojamo resursu Maikla komponentiem, bija lielākas λ vērtības (46,7 mW·(m·K)$^{-1}$ un 44,5 mW·(m·K)$^{-1}$). No otras puses, izstrādāto putu polimērmateriālu siltumizolācijas īpašības ir vērtējamas kā labas, salīdzinot ar citiem inovatīviem izolācijas materiāliem, kas ražoti no bioloģiskām un/vai otrreizēji pārstrādātām izejvielām. Liao zinātniskā grupa *(Liao et al.)* izstrādāja daudzfunkcionālus putu polimērmateriālus no celulozes ar λ 48,2 mW·(m·K)$^{-1}$, uzsverot labās siltumizolācijas īpašības [101]. Pala zinātniskā grupa *(Pal et al.)* ziņoja par citiem siltumizolācijas materiāliem ar zemu siltumvadītspēju, izceļot korķa materiālu (40 mW·(m·K)$^{-1}$), pārstrādātu stikla materiālu (44 mW·(m·K)$^{-1}$), pārstrādātu kokvilnu (42 mW·(m·K)$^{-1}$) un stikla vati (40 mW·(m·K)$^{-1}$) kā efektīvus alternatīvus materiālus, kas izmantojami būvniecībā [102].

Kā redzams 4.2. tabulā, λ ir atkarīgs gan no blīvuma, gan no slēgto poru satura. Putu polimērmateriāliem ar lielāku slēgto poru saturu parasti bija labākas siltumizolācijas īpašības. Putu polimērmateriāliem, kas iegūti no petroķīmiska akrilāta (*TMPTA* un *PETA*), bija augstāks slēgto poru saturs, piemēram, *E*^{IR}*TOFA_TMP_AA_PETA* slēgto poru saturs bija 72,4 %. Tas liek domāt, ka, iekļaujot petroķīmiskos komponentus, var iegūt putu polimērmateriālu ar slēgtāku poru struktūru. Lielāks šķietamais blīvums novērots putu polimērmateriāliem, kas iegūti tikai no atjaunojamo resursu Maikla komponentiem, salīdzinot ar putu polimērmateriāliem, kas iegūti no taleļļas Maikla donora un petroķīmiska akceptora. Šo šķietamā blīvuma atšķirību varētu skaidrot ar bioloģiskas izcelsmes izejvielu dabu, kas rezultējas kompaktākā struktūrā, kas savukārt pasliktina siltumizolācijas īpašības.

4.2. tabula

Izstrādāto putu polimērmateriālu siltumvadītspēja, šķietamais blīvums un slēgto poru saturs

Iegūtie putu polimērmateriāli		**λ, mW·(m·K)$^{-1}$**	**Šķietamais ρ, kg·m^{-3}**	***V*$_{closed}$, %**
Taleļļas donors un petroķīmisks akceptors	*E*^{IR}*TOFA_TMP_AA_BPAEDA*	38,8	110,1	7,7
	E^{IR}*TOFA_TMP_AA_TMPTA*	32,3	111,1	68,7
	E^{IR}*TOFA_TMP_AA_PETA*	30,7	108,1	72,4
Taleļļas donors un atjaunojamo resursu akrilāts	*E*^{IR}*TOFA_TMP_AA_ESOA*	46,7	173,8	32,7
	E^{IR}*TOFA_TMP_AA_BD_Acryl*	44,5	143,9	45,3

Lai uzlabotu putu polimērmateriālu, kas iegūts tikai no atjaunojamo resursu Maikla komponentiem, siltumizolāciju, būtu nepieciešams atrast piemērotākas piedevas. Citu uzputošanās aģentu un virsmaktīvo vielu izpētei varētu būt izšķiroša nozīme, lai izveidotu putu polimērmateriālu, kas būtu vēl piemērotāks izolācijas nolūkiem. Šis pētījums sniedz tikai ieskatu putu polimērmateriālu ieguvē no atjaunojamajiem resursiem, izmantojot Maikla

reakciju un izmantojot piedevas, kas piemērotas populārākajiem slēgto poru putu materiāliem – cietajām poliuretānu putu polimērmateriāliem [103].

SEM attēli (4.3. tab.) parāda iegūto termoreaktīvo putu polimērmateriālu morfoloģiju. SEM attēlos redzams, ka poru forma un to izvietojums ir vienmērīgs, kas ir būtiski, apsverot putu polimērmateriāla potenciālos lietojumus.

4.3. tabula

Putu polimērmateriāla SEM attēli, kas uzņemti paralēli un perpendikulāri putu polimērmateriāla augšanas virzienam

Putu polimērmateriāla paraugs	X griezums perpendikulāri augšanas virzienam	Z griezums paralēli augšanas virzienam
E^{IR}TOFA_TMP_AA_BPAEDA	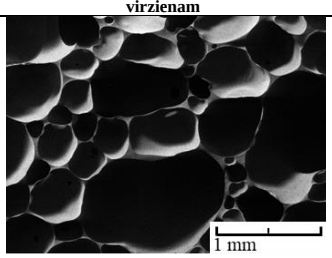	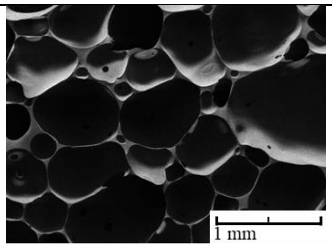
E^{IR}TOFA_TMP_AA_TMPTA	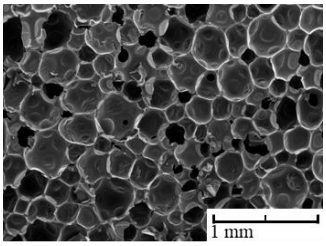	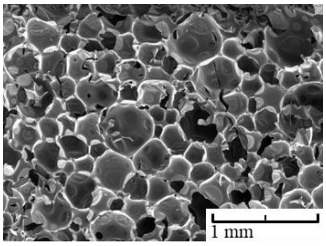
E^{IR}TOFA_TMP_AA_PETA	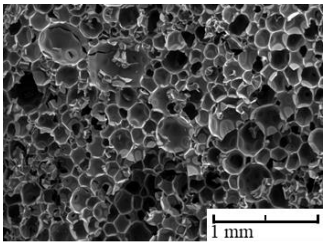	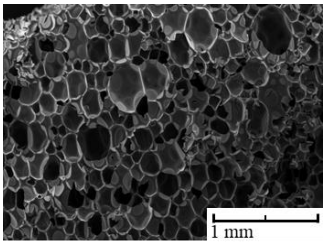
E^{IR}TOFA_TMP_AA_ESOA	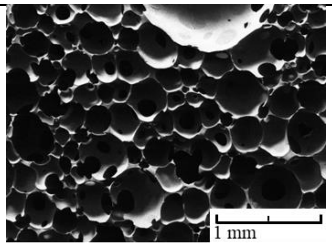	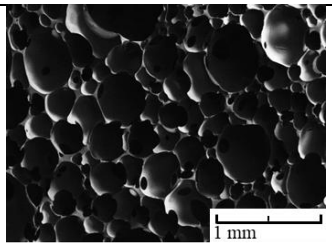
E^{IR}TOFA_TMP_AA_BD_Acryl	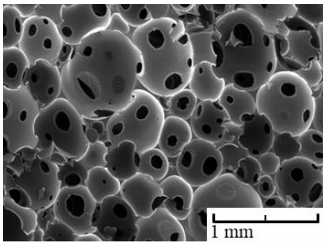	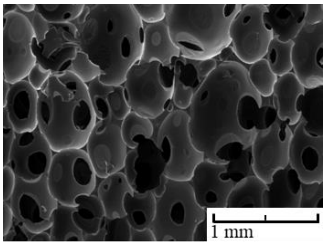

E^{IR}TOFA_TMP_AA_BPAEDA putu polimērmateriālam bija izteikti lielas poras (~ 410 µm). *E^{IR}TOFA_TMP_AA_TMPTA* putu polimērmateriālam bija blīvāka, vienmērīgāka poru struktūra ar redzami mazākām porām (~ 260 µm) nekā *E^{IR}TOFA_TMP_AA_BPAEDA* putu polimērmateriālam.

Bija skaidri redzams, ka izmantotā monomēra funkcionalitāte būtiski ietekmēja putu polimērmateriāla poru izmēru. Izmantojot monomērus ar augstāku funkcionalitāti, piemēram, *PETA* (*f* = 4), varēja iegūt ļoti blīvi saistītu struktūru, kas rezultējās mazāka izmēra porās (~ 150 µm). Turpretim, izmantojot monomērus ar zemāku funkcionalitāti, piemēram, *BPAEDA* (*f* = 2), bija iespējams iegūt putu polimērmateriālu ar lielāka izmēra porām, jo ir mazāk šķērssaistīšanās punktu, kas atļāva ievērojami vairāk izplesties un iegūt mīkstu putu polimērmateriālu. Savukārt, izmantojot *TMPTA* ar vidēju funkcionalitāti (*f* = 3), varēja iegūt putu polimērmateriālu ar vidēju poru izmēru.

Iegūtajiem putu polimērmateriāliem, īpaši *E^{IR}TOFA_TMP_AA_BPAEDA* un putu polimērmateriāliem no abiem atjaunojamajiem Maikla komponentiem, bija atvērta poru struktūra. Putu polimērmateriāli ar lielu poru izmēru izkliedi un savstarpēji saistītam porām var būt īpaši efektīvi skaņas absorbcijai. Poru izmēru nevienmērīgums un savstarpēji savienotās poras var uzlabot skaņas viļņu uztveršanu un izkliedēt skaņas viļņus dažādās frekvencēs, padarot putu polimērmateriālu par skaņas izolācijai potenciāli izmantojamu materiālu [104]. Šo materiālu potenciālais lietojums varētu būt arī kā polsterējuma materiāls vai izolācija, kur ir vēlama gaisa cirkulācija, jo atvērtās poras var sniegt gaisa caurlaidību, kas var nodrošināt termisko komfortu [105].

Analizējot iegūto putu polimērmateriālu morfoloģiju, atšķirība starp griezumiem paralēli un perpendikulāri putu polimērmateriāla augšanas virzienam bija nenozīmīga. Poru struktūra, izmērs un sadalījums bija līdzīgs abās orientācijās, kas liecina par samērā izotropiskām putu polimērmateriāla īpašībām. Tikai *E^{IR}TOFA_TMP_AA_BD_Acryl* putu polimērmateriāla paraugs norādīja uz iespējamu poru izmēra anizotropiju griezumam, kas paralēls putu polimērmateriāla augšanas virzienam. *E^{IR}TOFA_TMP_AA_BD_Akrila* putu polimērmateriālam vidējais poru izmērs perpendikulāri putošanas virzienam bija 360 µm, paralēli putošanas virzienam vidējais platums bija 360 µm, savukārt vidējais garums bija 560 µm.

Spiedes stiprība un spiedes modulis tika noteikts gan paralēli (Z), gan perpendikulāri (X) putu polimērmateriālu augšanas virzienam (4.5. att. un 4.4. tab.). *E^{IR}TOFA_TMP_AA_BPAEDA, E^{IR}TOFA_TMP_AA_TMPTA* un *E^{IR}TOFA_TMP_AA_PETA* putu polimērmateriāliem bija dažādas spiedes stiprības. *E^{IR}TOFA_TMP_AA_BPAEDA* putu polimērmateriālam spiedes stiprība bija 0,0073 MPa X virzienā un 0,0092 MPa Z virzienā, kas liecināja par mazāku stiprību, tās bija mīkstākas ar mīkstajiem materiāliem potenciālu lietojumu. Turpretim *E^{IR}TOFA_TMP_AA_TMPTA* un *E^{IR}TOFA_TMP_AA_PETA* putu polimērmateriāliem bija daudz lielāka spiedes stiprība (attiecīgi ~ 0,27 MPa un ~ 0,40 MPa), kas liecināja par stingrāku struktūru. Šāda stiprība ir piemērota, lai iegūto putu polimērmateriālu izmantotu kā siltumizolācijas materiālu vai citur būvniecībā. Šī stiprība padara šos materiālus piemērotus lietošanai tur, kur būtiska ir lielāka mehāniskā izturība un slodzes nestspēja.

Nelielās spiedes stiprības atšķirības starp X un Z virzieniem, galvenokārt *E^{IR}TOFA_TMP_AA_BD_Acryl* putu polimērmateriāliem, liecināja par šo materiālu nelielo anizotropisko raksturu. Tas atbilda arī SEM attēlos novērotajam, un to var skaidrot ar poru izmēra (garums un platums) atšķirībām augšanas virzienā. Šo anizotropiju ir svarīgi apzināties materiāla lietojumos, kur pieliktā spēka virziens ir atšķirīgs. Pretēji tam, *E^{IR}TOFA_TMP_AA_TMPTA, E^{IR}TOFA_TMP_AA_PETA* un *E^{IR}TOFA_TMP_AA_ESOA* putu polimērmateriāliem atšķirības starp virzieniem un pielikto spēku netika konstatētas.

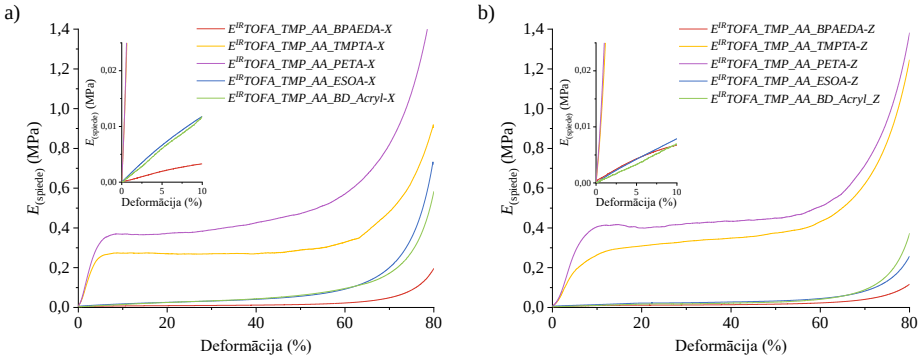

4.5. att. Spiedes testu (priekšslodze 2 N, 2 %·min^{-1}) līknes iegūtajiem putu polimērmateriāliem: a) perpendikulari (X) augšanas virzienam; b) paralēli (Z) augšanas virzienam.

Āboliņa zinātniskā grupa izstrādāja cietos putupoliuretāna materiālus, kas iegūti no dažādiem taleļļas polioliem ar λ aptuveni 22 mW·(m·K)$^{-1}$ un spiedes stiprību aptuveni 0,2 MPa, kas ir tipiska vērtība materiāliem, ko izmanto inženierbūvēs [38]. Lai gan cietajiem putupoliuretānaiem ir nedaudz labākas siltumizolācijas īpašības un mazāks šķietamais blīvums, ir pamats uzskatīt, ka šajā darbā iegūtie putu polimērmateriāli var konkurēt ar daļēji no atjaunojamajiem resursiem iegūtajiem poliuretāna putu polimērmateriāliem. Iegūtajiem putu polimērmateriāliem bija ievērojami labāka spiedes stiprība, sasniedzot pat 0,4 MPa. Savukārt blīvumu varētu samazināt, optimizējot putošanas procesu, piemeklējot atbilstošākus katalizatorus un uzputošanās aģentus.

4.4. tabula

Izstrādāto putu polimērmateriālu mehāniskās īpašības gan perpendikulāri (X), gan paralēli (Z) putu polimērmateriāla augšanas virzienam

Putu polimērmateriāla paraugi		**X**		**Z**	
		$E_{(spiede)}$, MPa	**$\sigma_{10\%}$, MPa**	**$E_{(spiede)}$, MPa**	**$\sigma_{10\%}$, MPa**
Taleļļas donors un petroķīmisks akceptors	*E^{IR}TOFA_TMP_AA_BPAEDA*	0,041	0,0073	0,079	0,0092
	E^{IR}TOFA_TMP_AA_TMPTA	7,6	0,274	5,1	0,263
	E^{IR}TOFA_TMP_AA_PETA	9,7	0,39	7,6	0,400
Taleļļas donors un atjaunojamo resursu akrilāts	*E^{IR}TOFA_TMP_AA_ESOA*	0,10	0,0158	0,12	0,0147
	E^{IR}TOFA_TMP_AA_BD_Acryl	0,12	0,0111	0,09	0,0074

SECINĀJUMI

1. Maikla komponentu prekursorus (poliolu) var sintezēt no taleļļas taukskābēm, veicot taukskābju dubultsaišu epoksidāciju un sekojošu oksirāna gredzenu šķelšanu un karboksilgrupu esterificēšanu ar spirtiem. Tālāk no prekursoriem var sintezēt:
    - Maikla donorus (acetoacetātus), veicot poliolu hidroksilgrupu acetoacetilēšanu transesterifikācijas reakcijā ar *terc*-butilacetoacetātu;
    - Maikla akceptorus (akrilātus), veicot poliolu hidroksilgrupu akrilēšanu ar akriloilhlorīdu.

2. Iegūti polimēri no taleļļas Maikla donoriem un petroķīmiskiem Maikla akceptoriem (bisfenola A etoksilātdiakrilāta, trimetilolpropāntriakrilāta, pentaeritritoltetraakrilāta). Izmantojot komponentus ar zemāku funkcionalitāti, var sintezēt mīkstus polimērmateriālus ar gumijai līdzīgām īpašībām (*E*^{IR}*TOFA_BD_AA_BPAEDA*: $E_{(stiepe)}$ = 8 MPa, σ_{max} = 4 MPa, ε = 55 %), savukārt augstākas funkcionalitātes komponentu izmantošana ļauj iegūt stingrus, cietus, organiskajam stiklam līdzīgus polimērmateriālus (*E*^{IR}*TOFA_TMP_AA_PETA*: $E_{(stiepe)}$ = 2370 MPa, σ_{max} = 44 MPa, ε = 1,9 %).

3. Iegūti polimērmateriāli no taleļļas Maikla komponentiem. Polimēri, kas iegūti no *E*^{IR}*TOFA_BD_Acryl*, bija mīksti (*E*^{IR}*TOFA_BD_AA_BD_Acryl*: $E_{(stiepe)}$ = 15 MPa, σ_{max} = 0,9 MPa, ε = 27 %), savukārt *E*^{IR}*TOFA_TMP_Acryl* polimēri bija cieti, organiskajam stiklam līdzīgi (*E*^{IR}*TOFA_TMP_AA_TMP_Acryl*: $E_{(stiepe)}$ = 1760 MPa, σ_{max} = 16,1 MPa, ε = 17 %).

4. Iegūti putu polimērmateriāli no taleļļas Maikla donoriem un dažādas izcelsmes Maikla akceptoriem (petroķīmiskām vielām – bisfenola A etoksilātdiakrilāta, trimetilolpropāntriakrilāta, pentaeritritoltetraakrilāta – un bioloģiskas izcelsmes – epoksidētas sojas eļļas akrilāta, sintezētā taleļļas akrilāta), izmantojot Maikla reakciju. Putu polimērmateriāliem, kas iegūti no taleļļas Maikla donoriem un petroķīmiskiem Maikla akceptoriem, bija augsta stiklošanās temperatūra ($T_{g(DSC)}$ līdz 85,5 °C, $T_{g(DMA)}$ līdz 108,6 °C), laba siltumizolācija (līdz 30,7 mW/(m·K)), liela mehāniskā izturība (~ 0,40 MPa). Putu polimērmateriāli no abiem biobāzētiem komponentiem bija mīksti. Visiem iegūtajiem putu polimērmateriāliem bija augsta termiskā stabilitāte – līdz 350 °C.

LITERATŪRAS SARAKSTS

[1] D. Feldman, Polymeric foam materials for insulation in buildings, Mater. Energy Effic. Therm. Comf. Build. (2010) 257–273. https://doi.org/10.1533/9781845699277.2.257.

[2] M. Niaounakis, Foaming and Foamed Products, in: Biopolym. Process. Prod., Elsevier Science, 2015: pp. 327–359. https://doi.org/10.1016/B978-0-323-26698-7.00009-X.

[3] A. Baroutaji, A. Arjunan, A. Niknejad, T. Tran, A.-G. Olabi, Application of Cellular Material in Crashworthiness Applications: An Overview, Elsevier Ltd., 2019. https://doi.org/10.1016/b978-0-12-803581-8.09268-7.

[4] M. Y. Lyu, T. G. Choi, Research trends in polymer materials for use in lightweight vehicles, Int. J. Precis. Eng. Manuf. 16 (2015) 213–220. https://doi.org/10.1007/s12541-015-0029-x.

[5] F. M. De Souza, Y. Desai, R. K. Gupta, Introduction to Polymeric Foams, ACS Symp. Ser. 1439 (2023) 1–23. https://doi.org/10.1021/bk-2023-1439.ch001.

[6] S. Siengchin, A review on lightweight materials for defence applications: Present and future developments, Def. Technol. 24 (2023) 1–17. https://doi.org/10.1016/j.dt.2023.02.025.

[7] F. L. Jin, M. Zhao, M. Park, S. J. Park, Recent trends of foaming in polymer processing: A review, Polymers (Basel). 11 (2019). https://doi.org/10.3390/polym11060953.

[8] G. Wu, P. Xie, H. Yang, K. Dang, Y. Xu, M. Sain, L. S. Turng, W. Yang, A review of thermoplastic polymer foams for functional applications, J. Mater. Sci. 56 (2021) 11579–11604. https://doi.org/10.1007/s10853-021-06034-6.

[9] L. Li, D. Xu, S. Bai, N. Chen, Q. Wang, Progress in preparation of high-performance and multi-functional polymer foams, J. Polym. Sci. (2023) 1–15. https://doi.org/10.1002/pol.20230490.

[10] Z. Wang, C. Wang, Y. Gao, Z. Li, Y. Shang, H. Li, Porous Thermal Insulation Polyurethane Foam Materials, Polymers (Basel). 15 (2023) 3818. https://doi.org/10.3390/polym15183818.

[11] S. B. Murmu, Alternatives derived from renewable natural fibre to replace conventional polyurethane rigid foam insulation, Clean. Eng. Technol. 8 (2022) 100513. https://doi.org/10.1016/j.clet.2022.100513.

[12] A. Agrawal, R. Kaur, R. S. Walia, PU foam derived from renewable sources: Perspective on properties enhancement: An overview, Eur. Polym. J. 95 (2017) 255–274. https://doi.org/10.1016/j.eurpolymj.2017.08.022.

[13] N. Singh, O. A. Ogunseitan, M. H. Wong, Y. Tang, Sustainable materials alternative to petrochemical plastics pollution: A review analysis, Sustain. Horizons. 2 (2022). https://doi.org/10.1016/j.horiz.2022.100016.

[14] J. G. Rosenboom, R. Langer, G. Traverso, Bioplastics for a circular economy, Nat. Rev. Mater. 7 (2022) 117–137. https://doi.org/10.1038/s41578-021-00407-8.

[15] European Commission, The European Green Deal, Eur. Comm. 53 (2019) 24. https://doi.org/10.1017/CBO9781107415324.004.

[16] A. Di Bartolo, G. Infurna, N. T. Dintcheva, A Review of Bioplastics and Their Adoption in the Circular Economy, Polymers (Basel). 13 (2021) 1229. https://doi.org/10.3390/polym13081229.

[17] M. Kircher, Bioeconomy: Markets, Implications and Investment Opportunities, 2019.

[18] S. A. Madbouly, Novel recycling processes for thermoset polyurethane foams, Curr. Opin. Green Sustain. Chem. 42 (2023) 100835. https://doi.org/10.1016/j.cogsc.2023.100835.

[19] S. E. Dechent, A. W. Kleij, G. A. Luinstra, Fully bio-derived CO2 polymers for non-isocyanate based polyurethane synthesis, Green Chem. 22 (2020) 969–978. https://doi.org/10.1039/c9gc03488a.

[20] J. Sternberg, S. Pilla, Materials for the biorefinery: High bio-content, shape memory Kraft lignin-derived non-isocyanate polyurethane foams using a non-toxic protocol,

Green Chem. 22 (2020) 6922–6935. https://doi.org/10.1039/d0gc01659d.
[21] C. D. Lindsay, C. M. Timperley, TRPA1 and issues relating to animal model selection for extrapolating toxicity data to humans, Hum. Exp. Toxicol. 39 (2020) 14–36. https://doi.org/10.1177/0960327119877460.
[22] M. Kathalewar, A. Sabnis, D. D'Mello, Isocyanate free polyurethanes from new CNSL based bis-cyclic carbonate and its application in coatings, Eur. Polym. J. 57 (2014) 99–108. https://doi.org/10.1016/j.eurpolymj.2014.05.008.
[23] M. S. Kathalewar, P. B. Joshi, A. S. Sabnis, V. C. Malshe, Non-isocyanate polyurethanes: From chemistry to applications, RSC Adv. 3 (2013) 4110–4129. https://doi.org/10.1039/c2ra21938g.
[24] S. Sambhudevan, H. S, A. Reghunadhan, Polyurethane from Sustainable Routes, in: Polyurethane Chem. Renew. Polyols Isocyanates, American Chemical Society, 2021: pp. 75–106. https://doi.org/10.1021/bk-2021-1380.ch004.
[25] M. Włoch, K. Błażek, Isocyanate-Free Polyurethanes, in: 2021: pp. 107–166. https://doi.org/10.1021/bk-2021-1380.ch005.
[26] J. Niesiobędzka, J. Datta, Challenges and recent advances in bio-based isocyanate production, Green Chem. 25 (2023) 2482–2504. https://doi.org/10.1039/d2gc04644j.
[27] G. Coste, C. Negrell, L. Averous, S. Caillol, Green Synthesis of Biobased Soft Foams by the Aza-Michael Reaction, ACS Sustain. Chem. Eng. 10 (2022) 8549–8558. https://doi.org/10.1021/acssuschemeng.2c01885.
[28] A. O. Konuray, F. Liendo, X. Fernández-Francos, À. Serra, M. Sangermano, X. Ramis, Sequential curing of thiol-acetoacetate-acrylate thermosets by latent Michael addition reactions, Polymer (Guildf). 113 (2017) 193–199. https://doi.org/10.1016/j.polymer.2017.02.072.
[29] Q. Jiang, Y. L. Zhang, Y. Du, M. Tang, L. Jiang, W. Huang, H. Yang, X. Xue, B. Jiang, Preparation of hyperbranched polymers by oxa-Michael addition polymerization, Polym. Chem. 11 (2020) 1298–1306. https://doi.org/10.1039/c9py01686d.
[30] Z. Ma, Y. Zeng, X. He, S. Pan, Y. Wei, B. Wang, L. Tao, Introducing the aza-Michael addition reaction between acrylate and dihydropyrimidin-2(1H)-thione into polymer chemistry, Polym. Chem. 13 (2022) 6322–6327. https://doi.org/10.1039/D2PY01130A.
[31] S. R. Williams, K. M. Miller, T. E. Long, Michael addition reaction kinetics of acetoacetates and acrylates for the formation of polymeric networks, Prog. React. Kinet. Mech. 32 (2007) 165–194. https://doi.org/10.3184/146867807X247730.
[32] M. Iwamura, Y. Gotoh, T. Hashimoto, R. Sakurai, Michael addition reactions of acetoacetates and malonates with acrylates in water under strongly alkaline conditions, Tetrahedron Lett. 46 (2005) 6275–6277. https://doi.org/10.1016/j.tetlet.2005.07.045.
[33] A. O. Konuray, A. Ruiz, J. M. Morancho, J. M. Salla, X. Fernández-Francos, À. Serra, X. Ramis, Sequential dual curing by selective Michael addition and free radical polymerization of acetoacetate-acrylate-methacrylate mixtures, Eur. Polym. J. 98 (2018) 39–46. https://doi.org/10.1016/j.eurpolymj.2017.11.003.
[34] M. Gould, T. Hammond, S. Narayan-Sarathy, Radiation Curable Michael Addition Resins Having Built-In Photoinitiators, US20050261388A1, 2005.
[35] B. D. Mather, K. Viswanathan, K. M. Miller, T. E. Long, Michael addition reactions in macromolecular design for emerging technologies, Prog. Polym. Sci. 31 (2006) 487–531. https://doi.org/10.1016/j.progpolymsci.2006.03.001.
[36] V. Aryan, A. Kraft, The crude tall oil value chain: Global availability and the influence of regional energy policies, J. Clean. Prod. 280 (2021) 124616. https://doi.org/10.1016/j.jclepro.2020.124616.
[37] L. Vevere, A. Fridrihsone, M. Kirpluks, U. Cabulis, A review of wood biomass-based fatty acids and rosin acids use in polymeric materials, Polymers (Basel). 12 (2020) 1–17. https://doi.org/10.3390/polym12112706.
[38] A. Abolins, R. Pomilovskis, E. Vanags, I. Mierina, S. Michalowski, A. Fridrihsone, M. Kirpluks, Impact of different epoxidation approaches of tall oil fatty acids on rigid polyurethane foam thermal insulation, Materials (Basel). 14 (2021) 1–17.

https://doi.org/10.3390/ma14040894.
[39] A. Saputra, P. Satwikanitya, F. Puspita, M. W. Sya'bani, M. F. Agustian, W. Pambudi, Synthesis of epoxy oil from Waste Cooking Oil (WCO) using acetic acid and amberlite resin IR-120 as catalyst, Eng. Appl. Sci. Res. 50 (2023) 335–342. https://doi.org/10.14456/easr.2023.36.
[40] M. C. Hennessy, T. P. O'Sullivan, Recent advances in the transesterification of β-keto esters, RSC Adv. 11 (2021) 22859–22920. https://doi.org/10.1039/d1ra03513d.
[41] H. Zuo, Z. Cao, J. Shu, D. Xu, J. Zhong, J. Zhao, T. Wang, Y. Chen, F. Gao, L. Shen, Effect of structure on the properties of ambient-cured coating films prepared via a Michael addition reaction based on an acetoacetate-modified castor oil prepared by thiol-ene coupling, Prog. Org. Coatings. 135 (2019) 27–33. https://doi.org/10.1016/j.porgcoat.2019.05.032.
[42] R. K. Pandey, P. Kumar, A facile procedure for transesterification of β-keto esters promoted by ceria-yttria based Lewis acid catalyst, Catal. Commun. 8 (2007) 1122–1125. https://doi.org/10.1016/j.catcom.2006.10.031.
[43] R. A. Omer, A. Hughes, J. R. Hama, W. Wang, H. Tai, Hydrogels from dextran and soybean oil by UV photo-polymerization, J. Appl. Polym. Sci. 132 (2015) 1–10. https://doi.org/10.1002/app.41446.
[44] A. Luo, X. Jiang, H. Lin, J. Yin, "Thiol-ene" photo-cured hybrid materials based on POSS and renewable vegetable oil, J. Mater. Chem. 21 (2011) 12753–12760. https://doi.org/10.1039/c1jm11425e.
[45] D. Kim, S. Kim, S. Jeong, M. Kim, W. K. Hong, H. B. Jeon, H. Y. Cho, S. M. Noh, H. jong Paik, Thermally latent vinyl crosslinking of polymers via sulfoxide chemistry, Eur. Polym. J. 179 (2022) 111520. https://doi.org/10.1016/j.eurpolymj.2022.111520.
[46] Z. Cao, F. Gao, J. Zhao, X. Wei, Q. Cheng, J. Zhong, C. Lin, J. Shu, C. Fu, L. Shen, Bio-based coating materials derived from acetoacetylated soybean oil and aromatic dicarboxaldehydes, Polymers (Basel). 11 (2019). https://doi.org/10.3390/polym11111809.
[47] X. He, J. Zhong, Z. Cao, J. Wang, F. Gao, D. Xu, L. Shen, An exploration of the Knoevenagel condensation to create ambient curable coating materials based on acetoacetylated castor oil, Prog. Org. Coatings. 129 (2019) 21–25. https://doi.org/10.1016/j.porgcoat.2018.12.015.
[48] A. S. Trevino, D. L. Trumbo, Acetoacetylated castor oil in coatings applications, Prog. Org. Coatings. 44 (2002) 49–54. https://doi.org/10.1016/S0300-9440(01)00223-5.
[49] D. Xu, Z. Cao, T. Wang, J. Zhong, J. Zhao, F. Gao, X. Luo, Z. Fang, J. Cao, S. Xu, L. Shen, An ambient-cured coating film obtained via a Knoevenagel and Michael addition reactions based on modified acetoacetylated castor oil prepared by a thiol-ene coupling reaction, Prog. Org. Coatings. 135 (2019) 510–516. https://doi.org/10.1016/j.porgcoat.2019.06.026.
[50] Y. Zhu, F. Gao, J. Zhong, L. Shen, Y. Lin, Renewable castor oil and DL-limonene derived fully bio-based vinylogous urethane vitrimers, Eur. Polym. J. 135 (2020) 109865. https://doi.org/10.1016/j.eurpolymj.2020.109865.
[51] T. Wang, J. Wang, X. He, Z. Cao, D. Xu, F. Gao, J. Zhong, L. Shen, An Ambient Curable Coating Material Based on the Michael Addition Reaction of Acetoacetylated Castor Oil and Multifunctional Acrylate, Coatings. 9 (2019) 37. https://doi.org/10.3390/coatings9010037.
[52] E. M. Krall, E. M. Serum, M. P. Sibi, D. C. Webster, Catalyst-free ligin valorization by acetoacetylation. Structural elucidation by comparison with model compounds, Green Chem. 20 (2018) 2959–2966. https://doi.org/10.1039/c8gc01071d.
[53] J. S. Witzeman, W. D. Nottingham, Transacetoacetylation with tert-Butyl Acetoacetate: Synthetic Applications, J. Org. Chem. 56 (1991) 1713–1718. https://doi.org/10.1021/jo00005a013.
[54] M. Kirpluks, E. Vanags, A. Abolins, S. Michalowski, A. Fridrihsone, U. Cabulis, High functionality bio-polyols from tall oil and rigid polyurethane foams formulated solely

using bio-polyols, Materials (Basel). 13 (2020) 38–53. https://doi.org/10.3390/MA13081985.
[55] R. de V. V. Lopes, J. R. Zamian, I. S. Resck, M. J. A. Sales, M. L. Dos Santos, F. R. Da Cunha, Physicochemical and rheological properties of passion fruit oil and its polyol, Eur. J. Lipid Sci. Technol. 112 (2010) 1253–1262. https://doi.org/10.1002/ejlt.201000098.
[56] W. T. Petroskey, L. Gott, T. E. Carter, Acetoacetylation: a Process for Polyol Viscosity Reduction, J. Cell. Plast. 29 (1993) 458–459. https://doi.org/10.1177/0021955X9302900565.
[57] J. Sung, X. S. Sun, Cardanol modified fatty acids from camelina oils for flexible bio-based acrylates coatings, Prog. Org. Coatings. 123 (2018) 242–253. https://doi.org/10.1016/j.porgcoat.2018.02.008.
[58] J. La Scala, R. P. Wool, The effect of fatty acid composition on the acrylation kinetics of epoxidized triacylglycerols, J. Am. Oil Chem. Soc. 79 (2002) 59–63. https://doi.org/10.1007/s11746-002-0435-4.
[59] A. M. Salih, M. Bin Ahmad, N. A. Ibrahim, K. Z. HjMohd Dahlan, R. Tajau, M. H. Mahmood, W. M. Z. W. Yunus, Synthesis of radiation curable palm oil-based epoxy acrylate: NMR and FTIR spectroscopic investigations, Molecules. 20 (2015) 14191–14211. https://doi.org/10.3390/molecules200814191.
[60] G. Wuzella, A. R. Mahendran, U. Müller, A. Kandelbauer, A. Teischinger, Photocrosslinking of an Acrylated Epoxidized Linseed Oil: Kinetics and its Application for Optimized Wood Coatings, J. Polym. Environ. 20 (2012) 1063–1074. https://doi.org/10.1007/s10924-012-0511-9.
[61] Y. Xia, R. C. Larock, Vegetable oil-based polymeric materials: Synthesis, properties, and applications, Green Chem. 12 (2010) 1893–1909. https://doi.org/10.1039/c0gc00264j.
[62] Y. Gan, X. Jiang, Photo-cured materials from vegetable oils, RSC Green Chem. 2015-Janua (2015) 1–27. https://doi.org/10.1039/9781782621850-00001.
[63] Y. Su, H. Lin, S. Zhang, Z. Yang, T. Yuan, One-Step synthesis of novel renewable vegetable oil-based acrylate prepolymers and their application in UV-curable coatings, Polymers (Basel). 12 (2020) 1–13. https://doi.org/10.3390/POLYM12051165.
[64] P. Zhang, J. Xin, J. Zhang, Effects of catalyst type and reaction parameters on one-step acrylation of soybean oil, ACS Sustain. Chem. Eng. 2 (2014) 181–187. https://doi.org/10.1021/sc400206t.
[65] P. Zhang, J. Zhang, One-step acrylation of soybean oil (SO) for the preparation of SO-based macromonomers, Green Chem. 15 (2013) 641–645. https://doi.org/10.1039/c3gc36961g.
[66] R. Müller, G. Wilke, Synthesis and radiation curing of acrylated castor oil glycerides, J. Coatings Technol. Res. 11 (2014) 873–882. https://doi.org/10.1007/s11998-014-9596-5.
[67] N. Liu, New polymers synthesis by organocatalyzed step-growth polymerization of aldehydic monomers : polyaldols, linear polybenzoin and hyperbranched polyacetals, (2014). https://tel.archives-ouvertes.fr/tel-01081197.
[68] M. F. Sonnenschein, J. B. Werness, K. A. Patankar, X. Jin, M. Z. Larive, From rigid and flexible foams to elastomers via Michael addition chemistry, Polymer (Guildf). 106 (2016) 128–139. https://doi.org/10.1016/j.polymer.2016.10.054.
[69] G. Ozturk, T. E. Long, Michael addition for crosslinking of poly(caprolactone)s, J. Polym. Sci. Part A Polym. Chem. 47 (2009) 5437–5447. https://doi.org/10.1002/pola.23593.
[70] T. Balotupi, T. Lanta, D. A. N. P. K. Rzwpk, WO 2013/101682 Al, 2016.
[71] M. Y. Zhaoo, C.-P. Hsu, S. L. Voeks, R. Landtiser, WO 2013/132077 Al, 2013.
[72] I. Bureau, FUNCTIONALIZED OLIGOMERS, WO/2014/052081, 2014.
[73] J. C. Q. Amado, Thermal Resistance Properties of Polyurethanes and its Composites: A Short Review, J. Res. Updat. Polym. Sci. (2019) 66–84. https://doi.org/10.6000/1929-

5995.2019.08.10.
[74] L. Shufen, J. Zhi, Y. Kaijun, Y. Shuqin, W. K. Chow, Studies on the thermal behavior of polyurethanes, Polym. – Plast. Technol. Eng. 45 (2006) 95–108. https://doi.org/10.1080/03602550500373634.
[75] F. A. Zhang, D. K. Lee, T. J. Pinnavaia, PMMA-mesocellular foam silica nanocomposites prepared through batch emulsion polymerization and compression molding, Polymer (Guildf). 50 (2009) 4768–4774. https://doi.org/10.1016/j.polymer.2009.08.007.
[76] T. Rajkumar, N. Muthupandiyan, C. T. Vijayakumar, Synthesis and investigation of thermal properties of PMMA-maleimide-functionalized reduced graphene oxide nanocomposites, J. Thermoplast. Compos. Mater. 33 (2020) 85–96. https://doi.org/10.1177/0892705718804595.
[77] J. S. Bermejo, C. M. Ugarte, Influence of cross-linking density on the glass transition and structure of chemically cross-linked PVA: A molecular dynamics study, Macromol. Theory Simulations. 18 (2009) 317–327. https://doi.org/10.1002/mats.200900032.
[78] M. K. Hassan, S. J. Tucker, A. Abukmail, J. S. Wiggins, K. A. Mauritz, Polymer chain dynamics in epoxy based composites as investigated by broadband dielectric spectroscopy, Arab. J. Chem. 9 (2016) 305–315. https://doi.org/10.1016/j.arabjc.2015.07.016.
[79] V. J. Dave, H. S. Patel, Synthesis and characterization of interpenetrating polymer networks from transesterified castor oil based polyurethane and polystyrene, J. Saudi Chem. Soc. 21 (2017) 18–24. https://doi.org/10.1016/j.jscs.2013.08.001.
[80] S. Chen, Q. Wang, X. Pei, T. Wang, Dynamic mechanical properties of castor oil-based polyurethane/epoxy graft interpenetrating polymer network composites, J. Appl. Polym. Sci. 116 (2010) n/a-n/a. https://doi.org/10.1002/app.32518.
[81] P. K. Menard, Dynamic analysis a practical introduction, CRC Press, New York, 1999.
[82] R. Hagen, L. Salmén, H. Lavebratt, B. Stenberg, Comparison of dynamic mechanical measurements and Tg determinations with two different instruments, Polym. Test. 13 (1994) 113–128. https://doi.org/10.1016/0142-9418(94)90020-5.
[83] C. A. Gracia-Fernández, S. Gómez-Barreiro, J. López-Beceiro, J. Tarrío Saavedra, S. Naya, R. Artiaga, Comparative study of the dynamic glass transition temperature by DMA and TMDSC, Polym. Test. 29 (2010) 1002–1006. https://doi.org/10.1016/j.polymertesting.2010.09.005.
[84] R. Rahul, R. Kitey, Effect of cross-linking on dynamic mechanical and fracture behavior of epoxy variants, Compos. Part B Eng. 85 (2016) 336–342. https://doi.org/10.1016/j.compositesb.2015.09.017.
[85] M. Fleischer, H. Blattmann, R. Mülhaupt, Glycerol-, pentaerythritol- and trimethylolpropane-based polyurethanes and their cellulose carbonate composites prepared via the non-isocyanate route with catalytic carbon dioxide fixation, Green Chem. 15 (2013) 934–942. https://doi.org/10.1039/c3gc00078h.
[86] A. Abolins, V. Yakushin, D. Vilsone, Properties of polyurethane coatings based on linseed oil phosphate ester polyol, J. Renew. Mater. 6 (2018) 737–745. https://doi.org/10.32604/JRM.2018.00119.
[87] V. Yakushin, A. Abolins, D. Vilsone, I. Sevastyanova, Polyurethane coatings based on linseed oil phosphate ester polyols with intumescent flame retardants, Fire Mater. 43 (2019) 92–100. https://doi.org/10.1002/fam.2672.
[88] W. Xie, S. Guo, Y. Liu, R. Chen, Q. Wang, Organic-inorganic hybrid strategy based on ternary copolymerization to prepare flame retardant poly(methyl methacrylate) with high performance, Compos. Part B Eng. 203 (2020) 108437. https://doi.org/10.1016/j.compositesb.2020.108437.
[89] U. Ali, K. J. B. A. Karim, N. A. Buang, A Review of the Properties and Applications of Poly (Methyl Methacrylate) (PMMA), Polym. Rev. 55 (2015) 678–705. https://doi.org/10.1080/15583724.2015.1031377.
[90] A. Ishigami, K. Watanabe, T. Kurose, H. Ito, Physical and morphological properties of

tough and transparent PMMA-based blends modified with polyrotaxane, Polymers (Basel). 12 (2020). https://doi.org/10.3390/polym12081790.
[91] B. Noordover, W. Liu, E. McCracken, B. DeGooyer, R. Brinkhuis, F. Lunzer, Michael addition curable coatings from renewable resources with enhanced adhesion performance, J. Coatings Technol. Res. 17 (2020) 1123–1130. https://doi.org/10.1007/s11998-020-00351-2.
[92] N. Naga, M. Satoh, T. Magara, K. Ahmed, T. Nakano, Synthesis of gels by means of Michael addition reaction of multi-functional acetoacetate and diacrylate compounds and their application to ionic conductive gels, J. Polym. Sci. 59 (2021) 2129–2139. https://doi.org/10.1002/pol.20210388.
[93] N. Naga, M. Satoh, T. Magara, K. Ahmed, T. Nakano, Synthesis of porous polymers by means of Michael addition reaction of multifunctional acetoacetate and poly(ethylene glycol) diacrylate, Eur. Polym. J. 162 (2022) 110901. https://doi.org/10.1016/j.eurpolymj.2021.110901.
[94] M. Y. Cheong, Z. A. A. Hasan, Z. Idris, Characterisation of epoxidised trimethylolpropane trioleate:NMR and thermogravimetric analysis, J. Oil Palm Res. 31 (2019) 146–158. https://doi.org/10.21894/jopr.2018.0066.
[95] B. Liang, S. Kuang, J. Huang, L. Man, Z. Yang, T. Yuan, Synthesis and characterization of novel renewable tung oil-based UV-curable active monomers and bio-based copolymers, Prog. Org. Coatings. 129 (2019) 116–124. https://doi.org/10.1016/j.porgcoat.2019.01.007.
[96] M. Li, Y. Fang, C. Liu, M. Zhou, X. Miao, Y. Pei, Y. Yan, W. Xiao, H. Qiu, L. Wu, Facile generation of highly durable thiol-functionalized polyhedral oligomeric silsesquioxane based superhydrophobic melamine foam, Front. Chem. Sci. Eng. 16 (2022) 1247–1258. https://doi.org/10.1007/s11705-021-2124-0.
[97] D. Trumbo, N. Krogman, D. Nelson, A Method for Applying a Foam Composition Using Spray Foam Equipment, EP3783048A1, 2021.
[98] J. O. L. Robert, L.K.-E. Michelle, O.F. Nassreen, One-Part Non-Toxic Spray Foam, US2008281006A1, 2008.
[99] T. F. Kauffman, D. W. Whitman, M. J. Zajaczkowski, V. David Elmer, Biomass Based Michael Addition Compositions, US 2006/0069234 A1, 2006.
[100] G. F. Levchik, K. Si, S. V. Levchik, G. Camino, C. A. Wilkie, Correlation between cross-linking and thermal stability: Cross-linked polystyrenes and polymethacrylates, Polym. Degrad. Stab. 65 (1999) 395–403. https://doi.org/10.1016/S0141-3910(99)00028-2.
[101] J. Liao, Y. Hou, J. Li, M. Zhang, Y. Dong, X. Chen, Lightweight and recyclable hybrid multifunctional foam based cellulose fibers with excellent flame retardant, thermal, and acoustic insulation property, Compos. Sci. Technol. 244 (2023) 110315. https://doi.org/10.1016/j.compscitech.2023.110315.
[102] R. K. Pal, P. Goyal, S. Sehgal, Effect of cellulose fibre based insulation on thermal performance of buildings, Mater. Today Proc. 45 (2021) 5778–5781. https://doi.org/10.1016/j.matpr.2021.02.749.
[103] J. Andersons, R. Grūbe, L. Vēvere, P. Cābulis, M. Kirpluks, Anisotropic thermal expansion of bio-based rigid low-density closed-cell polyurethane foams, J. Mater. Res. Technol. 16 (2022) 1517–1525. https://doi.org/10.1016/j.jmrt.2021.12.094.
[104] A. Abbad, K. Jaboviste, M. Ouisse, N. Dauchez, Acoustic performances of silicone foams for sound absorption, J. Cell. Plast. 54 (2018) 651–670. https://doi.org/10.1177/0021955X17732305.
[105] B. E. Obi, Overview of Applications of Polymeric Foams, Polym. Foam. Struct. (2018) 3–14. https://doi.org/10.1016/b978-1-4557-7755-6.00001-x.

Pomilovskis, R. Synthesis of the Michael Components from Tall Oil Fatty Acids and Their Valorisation for Polymer Materials Development. The Doctoral Thesis. Riga: RTU Press, 2024. 202 p.

Published in accordance with the decision of the RTU Promotion Council "P-01" of 8 April 2024, Minutes No. 04030-9.1/61.

The Doctoral Thesis was developed at the Latvian State Institute of Wood Chemistry and Riga Technical University.

LATVIAN STATE INSTITUTE OF WOOD CHEMISTRY

1862 RTU FACULTY OF NATURAL SCIENCES AND TECHNOLOGY

The Doctoral Thesis was supported by the FLPP project "High bio-based content thermoset polymer foam development from plant origin oils (Bio-Mer)".

FLPP FUNDAMENTAL AND APPLIED RESEARCH PROJECTS

The Doctoral Thesis was supported by European Social Fund within Project "Strengthening of PhD students and academic personnel of Riga Technical University and BA School of Business and Finance in the strategic fields of specialization" (No. 8.2.2.0/20/I/008) of the Specific Objective 8.2.2, "To Strengthen Academic Staff of Higher Education Institutions in Strategic Specialization Areas" of the Operational Programme "Growth and Employment" and Riga Technical University's Doctoral Grant programme.

NATIONAL DEVELOPMENT PLAN 2020

EUROPEAN UNION European Social Fund

INVESTING IN YOUR FUTURE

DOCTORAL THESIS PROPOSED TO RIGA TECHNICAL UNIVERSITY FOR PROMOTION TO THE SCIENTIFIC DEGREE OF DOCTOR OF SCIENCE

To be granted the scientific degree of Doctor of Science (Ph. D.), the present Doctoral Thesis has been submitted for defence at the open meeting of RTU Promotion Council on 13 June 2024 16.30 at the Faculty of Natural Sciences and Technology of Riga Technical University, 3/7 Paula Valdena Street, Room 272. It will be possible to participate in the open meeting online on the Zoom platform (https://rtucloud1.zoom.us/j/9352086644).

OFFICIAL REVIEWERS

Tenured Professor Dr. sc. ing. Sergejs Gaidukovs
Riga Technical University

Assistant Professor Ph. D. Ondřej Sedláček
Charles University, Czech Republic

Professor Dr. Arantxa Eceiza
University of the Basque Country, Spain

DECLARATION OF ACADEMIC INTEGRITY

I hereby declare that the Doctoral Thesis submitted for review to Riga Technical University for promotion to the scientific degree of Doctor of Science (Ph. D.) is my own. I confirm that this Doctoral Thesis has not been submitted to any other university for promotion to a scientific degree.

Ralfs Pomilovskis ……...
(signature)

Date: ……

The Doctoral Thesis has been prepared as a collection of thematically related scientific publications complemented by summaries in Latvian and English. The Doctoral Thesis unites seven scientific publications written in English. The total volume of the Doctoral Thesis is 202 pages, including seven appendices.

ABBREVIATIONS

AA	acetoacetate
BD	1,4-butanediol
BPAEDA	bisphenol A ethoxylate diacrylate
DMA	dynamic mechanical analysis
DSC	differential scanning calorimetry
$E_{(comp.)}$	compression modulus from compression tests
$E_{(storage)}$	storage modulus from dynamic mechanical analysis
$E_{(tensile)}$	tensile modulus from tensile tests
E^{IR}TOFA	epoxidized tall oil fatty acids
ESOA	epoxidized soybean oil acrylate
f	component functionality
FTIR	Fourier-transform infrared spectroscopy
GPC	gel permeation chromatography
MALDI-TOF MS	matrix-assisted laser desorption/ionization-time-of-flight mass spectrometry
M_c	molecular weight between cross-links
NIPU	non-isocyanate polyurethanes
NMR	nuclear magnetic resonance spectroscopy
PETA	pentaerythritol tetraacrylate
ssNMR	solid-state nuclear magnetic resonance spectroscopy
T_g	glass transition temperature
TGA	thermogravimetric analysis
TMP	trimethylolpropane
TMPTA	trimethylolpropane triacrylate
ε	elongation at break
λ	thermal conductivity coefficient
ν_e	cross-link density
ρ	density
σ	tensile stress

CONTENTS

GENERAL OVERVIEW OF THE THESIS

Introduction

In recent years, the pursuit of innovative polymer foam materials has garnered significant attention and research interest, driven by a growing recognition of their multifaceted applications across industries. Today, these materials have become indispensable in sectors such as construction (providing insulation) [1], packaging (offering lightweight and protective materials) [2], automotive (contributing to weight reduction and enhanced safety) [3]–[5], and increasingly relevant for defence applications [6]. Polymer foams, with their remarkable properties, including low density, exceptional strength-to-weight ratios, and outstanding insulation capabilities, enable these diverse applications [7]–[10]. However, the current global context underscores the urgency to explore sustainable alternatives, firmly rooted in bio-based materials, to address pressing challenges such as the depletion of fossil resources, environmental degradation, and climate change [11]–[17].

Conventional polymer foams, including the most widely used materials like polyurethane foams, have long been integral to various industries [5], [18]. However, conventional polyurethane's extensive use has brought global challenges to the forefront and does not meet modern sustainability requirements [19]–[23]. Notably, the production of polyurethane foams requires hazardous isocyanates, primarily derived from fossil resources [24], [25], with no commercially viable renewable alternatives currently [26]. The Michael reaction is an innovative approach that leverages bio-based resources to address the sustainability issues associated with traditional polymer foams [27].

The Michael reaction is a known chemical reaction utilised in various fields. However, in polymer chemistry, it is emerging as a novel approach [27]–[30]. One notable variant of the Michael reaction involves the reaction between acetoacetates as the Michael donor and acrylates as the Michael acceptor [31]–[34]. Acetoacetates possess active methylene groups that serve as nucleophilic centres, readily engaging with the electron-poor double bond of acrylates in the presence of a catalyst. This reaction leads to forming a carbon-carbon (C-C) bond [31], [35]. The versatility of the Michael reaction lies in its ability to facilitate the controlled synthesis of polymers with tailored properties, making it a promising strategy for the development of innovative polymer foam materials.

The utilisation of tall oil represents a promising avenue for advancing polymer chemistry. Tall oil is a valuable second-generation by-product of the wood biomass pulping process [36], [37]. Distilled tall oil consists mainly of oleic and linoleic acids with small amounts of other fatty acids, resin acids, and unsaponifiable sterols. It has been demonstrated that tall oil polyols can be successfully used to develop bio-based polyurethanes [38]. Polyols obtained from tall oil can be used as a precursor for the synthesis of components suitable in use form polymerisation *via* the Michael reaction (Fig. 1).

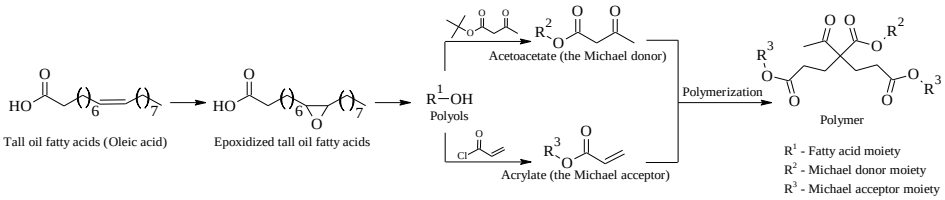

Fig. 1. Proposed design of polymer development from tall oil *via* the Michael reaction.

Aims and tasks

The aim of the Thesis was to develop a novel strategy for the synthesis of the bio-based Michael components (acetoacetates and acrylates) and to obtain polymers (polymer foams) exploiting the Michael reaction. This approach focused on using a second-generation bio-based feedstock – tall oil, a by-product of wood pulping, to develop polymer foams meeting modern sustainability requirements. The study explored combining tall oil-based acetoacetates (Michael donor) with various origin acrylates (Michael acceptor) to create flexible and rigid foams with a range of properties suitable for different applications, particularly as thermal insulation materials.

The following tasks were defined.

1. To synthesise the Michael components (Michael donors and Michael acceptors) from tall oil by, first, synthesising precursors from tall oil unsaturated fatty acids by double bonds epoxidation and subsequent oxirane rings cleavage and esterification of carboxyl groups with alcohol. The second step involved transforming the obtained polyols into the Michael donors through transesterification with *tert*-butyl acetoacetate, and into the Michael acceptors through acrylation with acryloyl chloride.
2. To develop polymers using tall oil-based Michael donors and commercially available Michael acceptors, test the synthesised donor's suitability for polymerization reaction, and investigate the thermal and mechanical properties of the created polymers.
3. To develop polymers from tall oil-based both Michael components and investigate the chemical composition, thermal and mechanical properties of the obtained polymers.
4. To obtain polymer foams using a tall oil-based Michael donor and various origin Michael acceptors and to investigate the mechanical and thermal properties of the developed foams.

Thesis statements to be defended

1. Michael donors and Michael acceptors can be synthesised from tall oil through tall oil fatty acids epoxidation, then oxirane ring cleavage, and carboxyl groups esterification with alcohol, followed by acetoacetylation to obtain Michael donors (acetoacetates) or acrylation to produce Michael acceptors (acrylates).
2. Tall oil-based Michael donors are suitable for obtaining polymers with various commercially available acrylates with adjustable thermal and mechanical properties by changing the functionality of the used components, thereby obtaining polymers competitive with conventional polymers.

3. Polymers can be obtained from tall oil-based acetoacetates and acrylates with adjustable thermal and mechanical properties by changing the functionality of the used components, thereby obtaining polymers competitive with conventional polymers.
4. Polymer foams can be obtained using tall oil-based acetoacetates and various origins acrylates, with adjustable thermal and mechanical properties by changing the functionality of the used components, thereby obtaining polymer foams for different applications, particularly as thermal insulation materials.

Scientific novelty

As a result of this Doctoral Thesis, a novel strategy has been developed for valuable chemicals and innovative polymer material production from tall oil in an entirely new way, making a significant contribution to the development of a forest-based bioeconomy and providing knowledge of polymer foam development that meets today's sustainability requirements.

This research pioneers the derivation of Michael components from the unsaturated free fatty acids present in tall oil, diverging from the traditional reliance on triglycerides. For the first time, different tall oil-based polyols were used to synthesise the Michael components. The Michael donors (acetoacetates) were synthesised by converting the hydroxyl groups present in polyols into acetoacetate esters. Polyols were synthesised from tall oil by catalytical epoxidation using ion exchange resin and subsequent cleavage of the oxirane rings and esterification of the acid groups with polyfunctional alcohol. Synthesised tall oil-based polyols offered remarkable versatility – the same polyols can also serve as a precursor for synthesising polyfunctional acrylates. Tall oil-based multifunctional Michael acceptors (acrylates) were developed. The novelty of the proposed approach was that the same renewable raw material, tall oil-based polyols, was used for the synthesis of both Michael components (Michael donor and Michael acceptor). Polymers have been successfully obtained from synthesised components using the Michael reaction. Furthermore, synthesised tall oil polyol-based acrylates could be promising in producing other polymers, for example, in UV-initiated free radical polymerization in the production of coatings.

The potential of tall oil-based acetoacetates as key components in polymer foam development, combining them with a tall oil-based acrylate, was explored. Additionally, commercially available acrylates such as bisphenol A ethoxylate diacrylate, trimethylolpropane triacrylate, pentaerythritol tetraacrylate, and epoxidized soybean oil acrylate were used. The Thesis delved into comparing these innovative materials' mechanical, thermos-mechanical, and thermal properties.

The Thesis provides the first insights into the development of bio-based polymer and polymer foams from tall oil-based components using the Michael reaction. Foam was formulated from tall oil-based acetoacetate and tall oil-based acrylate, offering a promising pathway towards reducing reliance on non-renewable resources and mitigating environmental impact in the polymer industry.

Structure and volume of the Thesis

This Doctoral Thesis was prepared as a collection of thematically related scientific publications by the author dedicated to the development of polymer materials from tall oil *via* the Michael reaction. The Thesis unites 7 original publications in Scopus-indexed journals.

Publications and approbation of the Thesis

Scientific publications

1. **R. Pomilovskis**, E. Kaulina, A. Abolins, I. Mierina, I. Heinmaa, V. Rjabovs, A. Fridrihsone, M. Kirpluks, Fast-curing bio-based thermoset foams produced *via* the Michael 1,4-addition using fatty acid-based acetoacetate and acrylate, Eur. Polym. J. 210 (2024) 112968. 10.1016/j.eurpolymj.2024.112968. (IF 6.0, CiteScore 9.6).

2. **R. Pomilovskis**, E. Kaulina, I. Mierina, A. Abolins, O. Kockova, A. Fridrihsone, M. Kirpluks, Wood pulp industry by-product valorization for acrylate synthesis and bio-based polymer development *via* Michael addition reaction, J. Bioresour. Bioprod. 8 (2023) 265–279. 10.1016/j.jobab.2023.06.001. (CiteScore 30.6).

3. **R. Pomilovskis**, I. Mierina, A. Fridrihsone, M. Kirpluks, Bio-based polymer developments from tall oil fatty acids by exploiting Michael addition, Polymers (Basel). 14 (2022) 4068. 10.3390/polym14194068. (IF 5.0, CiteScore 6.6).

4. **R. Pomilovskis**, I. Mierina, H. Beneš, O. Trhlíková, A. Abolins, A. Fridrihsone, M. Kirpluks, The synthesis of bio-based Michael donors from tall oil fatty acids for polymer development, Polymers (Basel). 14 (2022). 10.3390/polym14194107. (IF 5.0, CiteScore 6.6).

5. A. Abolins, D. Eihe, **R. Pomilovskis**, A. Fridrihsone, M. Kirpluks, Rapeseed oil as feedstock for the polymeric materials *via* Michael addition reaction, Ind. Crops Prod. 204 (2023) 117367. 10.1016/j.indcrop.2023.117367. (IF 5.9, CiteScore 9.7).

6. M. Kirpluks, **R. Pomilovskis**, E. Vanags, A. Abolins, I. Mierina, A. Fridrihsone, Influence of different synthesis conditions on the chemo-enzymatic epoxidation of tall oil fatty acids, Process Biochem. 122 (2022) 38–49. 10.1016/j.procbio.2022.08.024. (IF 4.4, CiteScore 7.9).

7. K. Polaczek, E. Kaulina, **R. Pomilovskis**, A. Fridrihsone, M. Kirpluks, Epoxidation of tall oil fatty acids and tall oil fatty acids methyl esters using the Spinchem® rotating bed reactor, J. Polym. Environ. (2022). 10.1007/s10924-022-02556-5. (IF 5.3, CiteScore 8.0).

International patent application

Latvijas Valsts koksnes ķīmijas institūts. Miķelis Kirpļuks, **Ralfs Pomilovskis**, Arnis Āboliņš, Anda Fridrihsone. Plant oil-based polymer foam and method of manufacture thereof. Application date: 22.03.2023. Application number: PCT/IB2022/052590. International publication number: WO 2023/180786 A1.

Conferences where research results are presented

1. **R. Pomilovskis**, E. Kaulina, I. Mierina, A. Abolins, O. Kockova, A. Fridrihsone, M. Kirpluks "Tall oil fatty acids valorization for acrylate synthesis and bio-based polymer development *via* Michael addition reaction", 2nd Conference on Green Chemistry and Sustainable Coatings. June 28–30, 2023, Pisa, Italy.

2. **R. Pomilovskis**, I. Mierina, E. Kaulina, A. Fridrihsone, M. Kirpluks, "By-product of the wood pulp industry – tall oil – utilisation for acrylate synthesis", International Conference on Renewable Resources & Biorefineries 2023 (RRB2023). May 31–June 2, 2023, Riga, Latvia.

3. **R. Pomilovskis**, I. Mierina, M. Kirpluks, "Polymer Developments from Tall Oil Fatty Acids using Michael Addition". Materials Science and Applied Chemistry. October 21, 2022, Riga, Latvia.

4. **R. Pomilovskis**, A. Fridrihsone, M. Kirpluks, "Tall oil fatty acids-based Michael donor monomer synthesis for thermoset polymers". EPF European Polymer Congress. June 26–July 1, 2022, Prague, Czech Republic.

5. **R. Pomilovskis**, I. Mierina, E. Kaulina, A. Fridrihsone, M. Kirpluks, "Bio-based polymer development from tall oil fatty acids by exploiting Michael reaction. Polymer development and characterization". International Conference on Renewable Resources & Biorefineries 2022 (RRB2022). June 1–3, 2022, Bruges, Belgium.

6. **R. Pomilovskis**, A. Fridrihsone, M. Kirpluks, "Bio-Based Polymer Development from tall oil fatty acids by exploiting Michael addition". International Conference for Young Scientists on Biorefinery Technologies and Products 2022 (BTechPro 2022!). April 27–29, 2022, Riga, Latvia.

7. **R. Pomilovskis**, A. Fridrihsone, A. Abolins, M. Kirpluks, "Michael donor monomer synthesis from tall oil fatty acids". International Conference on Renewable Resources & Biorefineries 2021 (RRB2021). September 6–8, 2021, Aveiro, Portugal.

8. A. Fridrihsone, A. Abolins, **R. Pomilovskis**, M. Kirpluks, "Bio-based Michael monomers from tall oil: life cycle assessment". The 11th International Conference on Life Cycle Management. September 6–8, 2023, Lille, France.

9. M. Kirpluks, **R. Pomilovskis**, A. Fridrihsone, "Tall oil fatty acids based thermoset foams obtained using Michael addition reaction". EPF European Polymer Congress. June 26–July 1, 2022, Prague, Czech Republic.

10. M. Kirpluks, **R. Pomilovskis**, "Bio-Based Thermoset Polymer as Viable Alternative for Rigid Polyurethane Foams". Polymers 2022: Turina New Trends in Polymer Science Health of the Planet, Health of the People. May 25–27, 2022, Turin, Italy.

MAIN RESULTS OF THE THESIS

The summary of the main results of the Doctoral Thesis is presented in four main chapters.

- Chapter 1 focuses on the synthesis of the Michael components from tall oil fatty acids, characterizing the synthesised products, detailing the process and importance of using renewable raw materials in polymer chemistry.
- Chapter 2 describes the development of polymers combining tall oil-based Michael donors with petrochemical Michael acceptors, polymer characterization emphasizing the influence of components' varied functionality used for polymerization.
- Chapter 3 explores polymers with varied cross-link densities synthesised from both tall oil-based Michael components, highlighting their high thermal stability and mechanical properties, positioning them as alternatives to traditional thermoset resins.
- Chapter 4 discusses the development of polymer foams from bio-based Michael donors and acceptors, illustrating the versatility and sustainability of these materials for various applications, particularly in thermal insulation.

The synthetic methods investigated during the Doctoral Thesis aimed to develop a novel strategy for synthesising bio-based Michael components (acetoacetates and acrylates) from tall oil-free fatty acids and to create a polymer suitable for various applications through the Michael reaction, with a special focus on polymer foams, particularly for thermal insulation applications.

1. Synthesis of the Michael components from tall oil fatty acids

A key advantage of utilising the Michael reaction in polymer chemistry is its ability to incorporate the Michael donor and the Michael acceptor from tall oil fatty acids. The use of tall oil offers several advantages, such as reducing dependence on fossil resources. Also, tall oil fatty acids do not compete with food and feed production [37].

Acetoacetates can be synthesised from tall oil due to its rich content of unsaturated fatty acids. The process involves several chemical steps, including epoxidation of double bonds and subsequent oxirane ring opening reaction with polyfunctional alcohols [39]. Hydroxyl group's acetoacetylation is then achieved through transesterification with compounds like *tert*-butyl acetoacetate and ethyl acetoacetate [40]–[42]. This versatile approach of selecting different alcohols provides the means to customize various characteristics, such as functionality, branching, molecular weight, and chemical composition. These adaptable properties enable the production of materials with a wide range of properties, making them suitable for diverse applications in polymer development.

The same tall oil-based polyols can also be as a precursor for synthesising polyfunctional acrylates. In this transformation, the hydroxyl groups react with acryloyl chloride [43]–[45]. This process leads to the formation of polyfunctional acrylates that can be used as a Michael acceptor. Considering the above, it is possible to utilise the same second-generation bio-based raw material for synthesising both Michael components.

1.1. Synthesis of the Michael donor from tall oil

The acetoacetylation of natural fatty acids and their polyols has not been broadly studied yet. A limited number of studies on acetoacetylation of bio-based polyols have been published. Acetoacetylation has been successfully demonstrated in the synthesis of soybean oil-based polyols [46], castor oil and castor oil-based polyols [41], [47]–[51]. Hydroxyl groups of fatty acids polyols are relatively easy to acetoacetylate with *tert*-butyl acetoacetate by a transesterification reaction, thereby obtaining β-ketoesters. The reaction is mostly carried out at a temperature of 110–130 °C [46]–[49], [52], [53].

It is currently believed that *tert*-butyl acetoacetate is the most suitable reagent for the acetoacetylation reaction due to its effectiveness under relatively mild conditions, in contrast to other analogues such as methyl acetoacetate, ethyl acetoacetate or isopropyl acetoacetate. Additionally, *tert*-butyl acetoacetate has several advantages, such as stability in storage, a relatively low cost and wide commercial availability, making it attractive from an industrial viewpoint [53].

For the first time, different tall oil-based polyols were used to synthesise the Michael donors by converting the hydroxyl groups present in polyols into acetoacetate esters. Idealized scheme of synthesis is shown in Fig. 1.1. Polyols were synthesised from tall oil by catalytical epoxidation using ion exchange resin and subsequent cleavage of the oxirane rings and esterification of the acid groups with polyfunctional alcohol. Acetoacetates were synthesised from two tall oil polyols and two commercially available polyols – Lupranol 3300 (L3300), which is oxyporpylated glycerine, and Neopolyol 380 (NEO380) based on pure industrial PET waste.

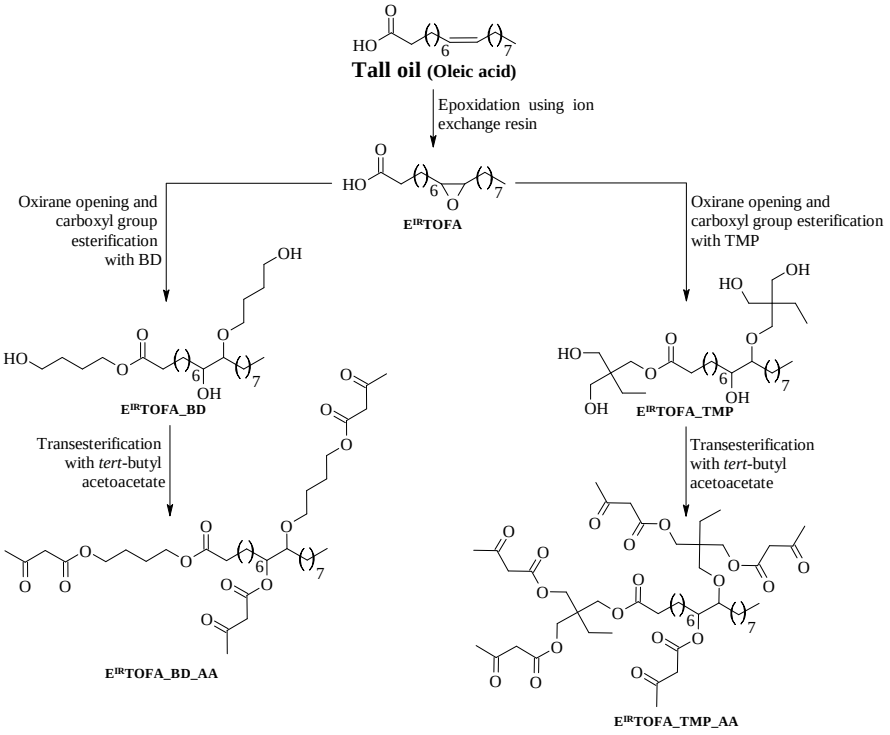

Fig. 1.1. Idealized scheme of tall oil (oleic acid) based Michael donor development.

Synthesised acetoacetates and intermediates were characterized using different titration methods to determine acid, hydroxyl, epoxy, and iodine values. The chemical structure was analysed using GPC chromatograms, FTIR, NMR and MALDI-TOF MS spectra. The viscosity and its dependence on the applied shear rate were also determined. Table 1.1 lists an overview of the characteristics determined using titrimetric methods and can be used to describe the synthesis process.

Table 1.1

Characteristics of the Synthesised and Commercially Available Polyols and Corresponding Acetoacetates

	Components	Acid value, mg KOH·g^{-1}	Hydroxyl value, mg KOH·g^{-1}	Iodine value, g I_2·100 g^{-1}	Moisture, %	AA groups, mol·100 g^{-1}	Conversion of hydroxyl, mol%
Tall oil-based	TOFA	195	-	157	0.50	-	-
	E^{IR}TOFA	159	-	52.4	0.32	-	-
	E^{IR}TOFA_BD	5.8	258	-	0.20	-	-
	E^{IR}TOFA_BD_AA	< 5	36.2	-	0.025	0.3307	80.5
	E^{IR}TOFA_TMP	6.9	415	-	0.049	-	-
	E^{IR}TOFA_TMP_AA	< 5	41.6	-	0.037	0.4562	83.7
Commercial polyols-based	NEO380	< 5	371	-	0.068	-	-
	NEO380_AA	< 5	40.7	-	0.048	0.4242	82.9
	L3300	< 5	400	-	0.060	-	-
	L3300_AA	< 5	26.2	-	0.021	0.4456	89.5

Due to different oxirane ring's opening reagents, the hydroxyl value of the obtained E^{IR}TOFA polyols differed almost twice. The polyol obtained with a TMP (f = 3) oxirane ring's opening reagent had the highest hydroxyl value. The use of BD (f = 2) as an oxirane ring's opening and acid groups esterification reagent yielded a smaller hydroxyl value. To obtain a polyol with higher functionality, tall oil fatty acids can be methylated before epoxidation. Epoxidation of tall oil fatty acids methyl ester helps to reduce the occurrence of undesirable side reactions (cleavage of the oxirane rings by the carboxyl groups of fatty acids) and allows obtaining a product with a higher epoxy value. Another proven possibility to increase the functionality of polyols is to use enzyme catalysts for epoxidation. Using enzymes as catalysts also significantly increases the yield of oxirane. Both methods have their disadvantages: using methyl esters for epoxidation requires an additional synthesis step, while enzymes are expensive and significantly increase the cost of the product.

After acetoacetylation, the hydroxyl number decreased significantly as the hydroxyl groups were replaced with the β-ketoester groups for tall oil polyols. The same relationship was observed for commercial polyols, which were selected to compare the synthesis process, the properties of the products and the suitability for the further development of polymeric materials. The content of acetoacetate groups was determined by calculations from the amounts of used acetoacetate and the yield of the product.

The viscosity of components did not depend on the applied shear rate, indicating that the obtained substances were Newtonian fluids (Fig. 1.2). The Newtonian behaviour of the developed Michael donors greatly facilitates the use of these acetoacetates in the industry, as the effect of the applied shear rate on the viscosity properties does not have to be taken into account.

Fatty acid-based polyols, including tall oil-based polyols, are known for their relatively high viscosities [54]. The most significant increase in viscosity was observed for the E^{IR}TOFA_TMP polyol that was synthesised by opening the oxirane rings and by the esterification of E^{IR}TOFA with TMP. The viscosity of E^{IR}TOFA_TMP was higher than 118 000 mPa·s, which is a relatively high viscosity and makes it difficult to use the product in the industry. E^{IR}TOFA_TMP polyol exhibits such a high viscosity mainly due to increased intermolecular hydrogen bonding. However, after E^{IR}TOFA_TMP polyol was acetoacetylated, the viscosity significantly decreased to 5500 mPa·s. Therefore, the E^{IR}TOFA_TMP_AA is more suitable for industrial use.

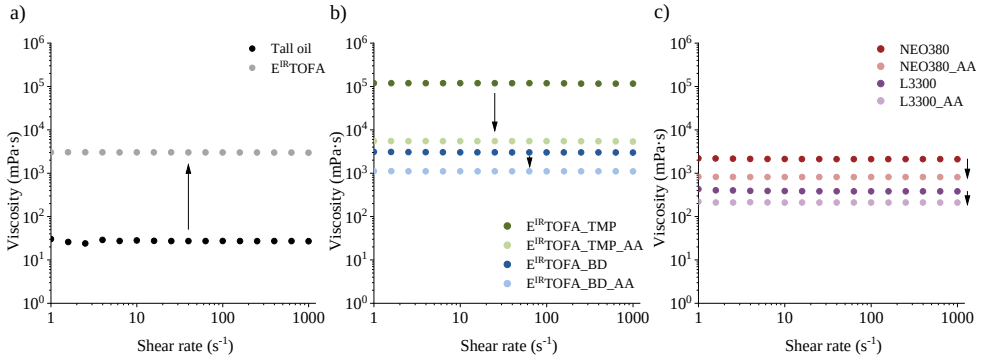

Fig. 1.2. Rheological measurements (cone-plate system, gap of 48 μm, 25 °C) of a) tall oil and E^{IR}TOFA; b) tall oil polyols and their acetoacetates; c) commercial polyols and their acetoacetates.

Compared to commercial or bio-based polyols, acetoacetates showed a significant decrease in viscosity due to the decrease in hydroxyl groups and, hence, the disappearance of intermolecular hydrogen bonds [46], [47], [51], [55], [56]. This significantly improves the potential use of bio-polyol acetoacetates in the industry. In the adjustment of existing equipment, in pump capacity alteration and in easier transportation through pipelines, they exhibit better flowability compared to neat polyols using less energy for transfer.

The course of synthesis and the changes associated with the functional groups of the molecules were determined using FTIR spectroscopy (Fig. 1.3). A new peak appeared at 831 cm^{-1} in the FTIR spectrum after the epoxidation of tall oil fatty acids, which corresponded to the vibrations of the oxirane rings (Fig. 1.3 a). This indicated that the epoxidation in the presence of ion exchange resin Amberlite IR-120 H was successful. Transformations of double bonds were also indicated by the peaks at ~ 1654 cm^{-1} and ~ 3009 cm^{-1}, corresponding to C=C stretching vibrations and =C-H stretching vibrations, respectively. The intensities of these peaks for E^{IR}TOFA decreased. The spectrum of E^{IR}TOFA also showed the appearance of a new, relatively weak but noticeable absorbance band between 3600 cm^{-1} and 3150 cm^{-1}, which typically characterizes vibrations of the hydroxyl groups. This indicated that the opening of the oxirane rings occurred as an undesirable side reaction during the epoxidation process. As seen in the spectrum, the intensity of the absorption band of the carbonyl groups of the acid moiety at ~ 1705 cm^{-1} decreased mainly due to ester formation, resulting in undesired by-products. Hydroxyl groups and esters were formed from the cleavage of the oxirane rings in the reaction with the carboxyl groups of tall oil or acetic acid.

The absorption of the hydroxyl group bands significantly increased for synthesised polyols. Moreover, this band was more intense for the polyols obtained by the E^{IR}TOFA reaction with TMP alcohol because the TMP polyol contained more hydroxyl functional groups (f = 3) than BD (f = 3). The spectrum also reflected the disappearance of the oxirane ring absorbance band at ~ 831 cm^{-1}. A decrease in the intensity of the peaks of the acid groups stretching vibration and an increase in the ester carbonyl groups at ~ 1738 cm^{-1} indicated that the esterification reaction was successful.

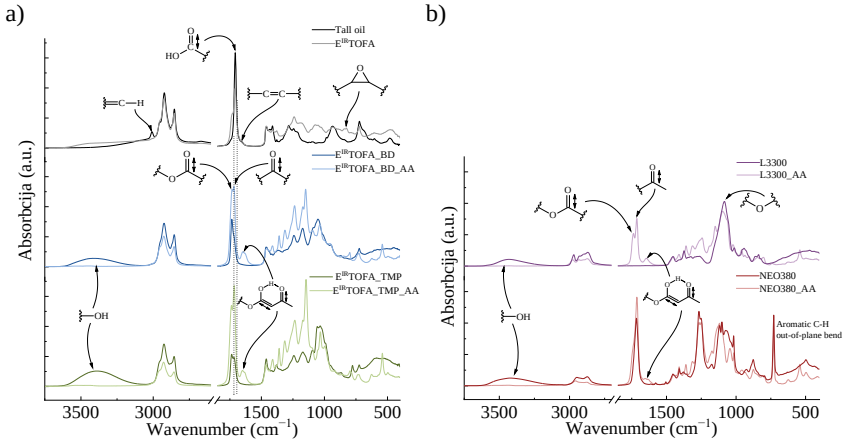

Fig. 1.3. FTIR spectra (ATR mode, 32 scans, resolution of 4 cm^{-1}) of: a) tall oil, E^{IR}TOFA, synthesised polyols and corresponding acetoacetates; b) commercial polyols and corresponding acetoacetates.

In the FTIR spectra, the intensity of the hydroxyl group's stretching vibration absorbance band decreased significantly for acetoacetylated polyols. They were nearly imperceptible. This is a very important indicator of a successful acetoacetylation reaction. The spectrum of acetoacetylated polyols showed an increase in the intensity of the carbonyl stretching vibration peak of ester at ~ 1738 cm^{-1} and ketone at ~ 1715 cm^{-1}. The appearance of a relatively strong, new absorption band between 1670 cm^{-1} and 1580 cm^{-1} was observed. Acetoacetates exhibited keto-enol tautomerism, and the carbonyl groups appeared at a lower frequency due to intramolecular hydrogen bonding in the enol form. The same changes in the FTIR spectra were also observed for the acetoacetylated commercial polyols (Fig. 1.3 b).

^{1}H NMR spectra clearly demonstrated (see Fig. 1.4) the formation of the epoxide moiety (signals at 2.8–3.2 ppm), although partial cleavage of the oxirane moiety occurred (signals at 3.4–4.1 ppm). The above-mentioned results (see Fig. 1.3) of the simultaneous cleavage of the oxirane rings and esterification were smoothly accompanied by NMR spectra, as well. As a result of the oxirane ring's cleavage, the signals (^{1}H-NMR: 3.14–2.84 ppm) raised from epoxide both disappeared when the BD and TMP were used for cleavage. New signals, characteristic of the -O-CH$_2$- groups at 4.0–4.5 ppm, were found. The formation of the ester bonds with BD and TMP was confirmed by ^{13}C spectra, as well; the signal of the carbonyl groups shifted from 180 ppm (for the carboxylic acid) to 174 ppm (for the ester).

The polysubstituted derivatives of TMP in small quantities were also observed in the spectrum of E^{IR}TOFA_TMP. The last one was deducted in the ^{13}C spectrum from several small signals at 65.5−3.5 ppm (-CH$_2$- from TMP moiety) and 43–42 ppm (quaternary carbon from TMP moiety). Several changes in the NMR spectra confirmed the successful acetoacetylation

and commercial polyols NEO380 and L3300. The signal characteristic of the methylene moiety of the acetoacetyl groups appeared at 3.4 ppm.

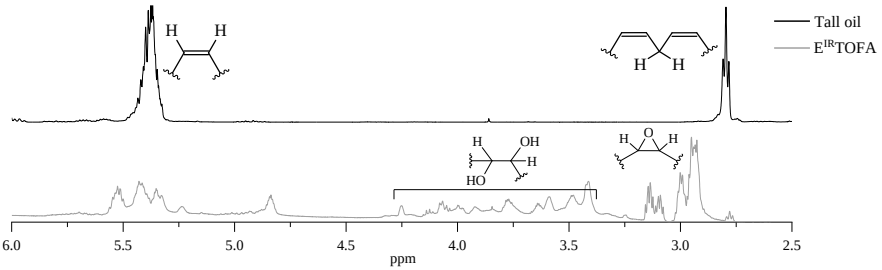

Fig. 1.4. ^{1}H-NMR spectra (500 MHz, $CDCl_3$) of tall oil and E^{IR}TOFA.

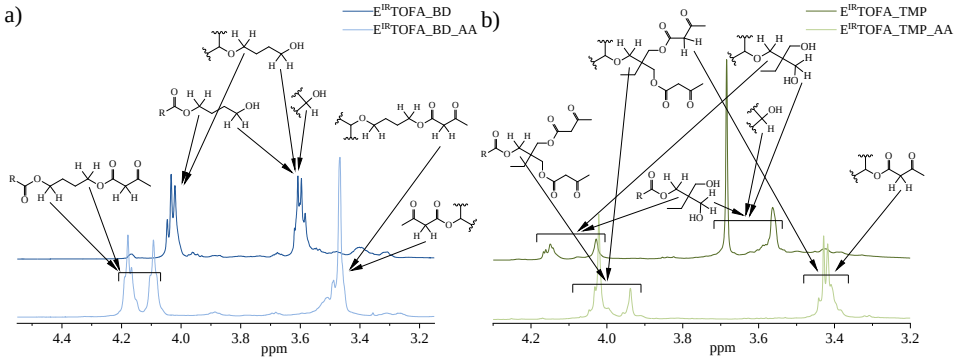

Fig. 1.5. ^{1}H-NMR spectra (500 MHz, $CDCl_3$) of a) E^{IR}TOFA_BD and E^{IR}TOFA_BD_AA; b) E^{IR}TOFA_TMP and E^{IR}TOFA_TMP_AA.

According to the chromatogram (Fig. 1.6), the ion exchange resin-catalysed epoxidation process of tall oil fatty acids produced a significant number of by-products. The formation of dimers, trimers and other oligomers and oxirane cleavage products were clearly visible in the spectrum. Abolins et al. also identified similar by-product formation in the epoxidation of tall oil fatty acids [38]. The retention time for the oxirane cleavage products was ~ 23.5 min, but dimers and trimers were identified at retention times of ~ 22.6 min and ~ 22.0 min. The chromatogram of polyols showed that the peaks shifted, and their retention times decreased. This indicated an increase in molecular weight.

In the spectrum of E^{IR}TOFA_BD polyol, a new peak appeared at a retention time of ~ 25.4 min, which characterized the free unreacted BD. In the case of E^{IR}TOFA_TMP polyol, the free TMP peak appeared at the retention time of ~ 23 min. After acetoacetylation, the molecular weight increased, thus reducing the retention times. It was distinctly visible in the chromatogram.

The commercial polyol NEO380 consisted of a mixture of several components. All peaks of NEO380 shifted after acetoacetylation, and the retention time decreased (Fig. 1.6 b), indicating that most of the compounds in this mixture contained acetoacetate groups after acetoacetylation. There was only one pronounced peak in the L3300 polyol spectrum (Fig. 1.6 b). There was a clearly identifiable shift in the spectrum of products, indicating an increase in molecular weight after acetoacetylation.

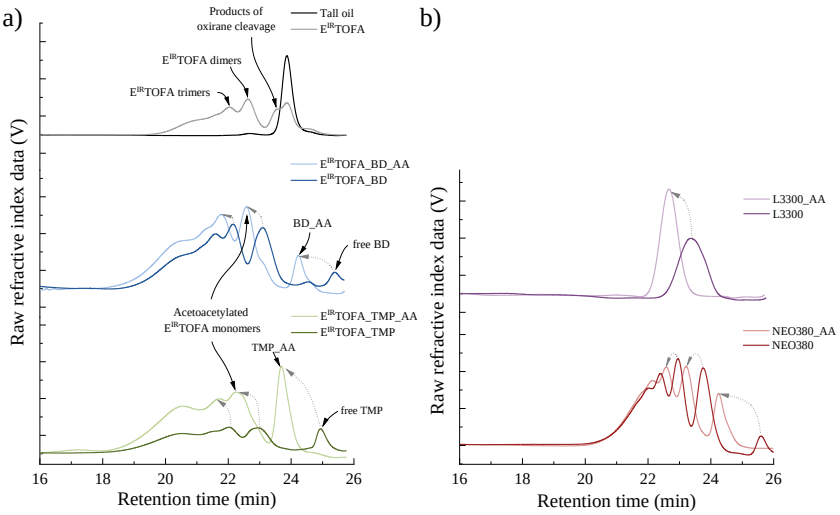

Fig. 1.6. GPC chromatograms (three PLgel columns, particle size – 10 μm, pore sizes – 104 Å, 103 Å and 50 Å, 300 mm × 7.5 mm, THF, 25 °C) of synthesised components a) based on tall oils; b) based on commercial polyols.

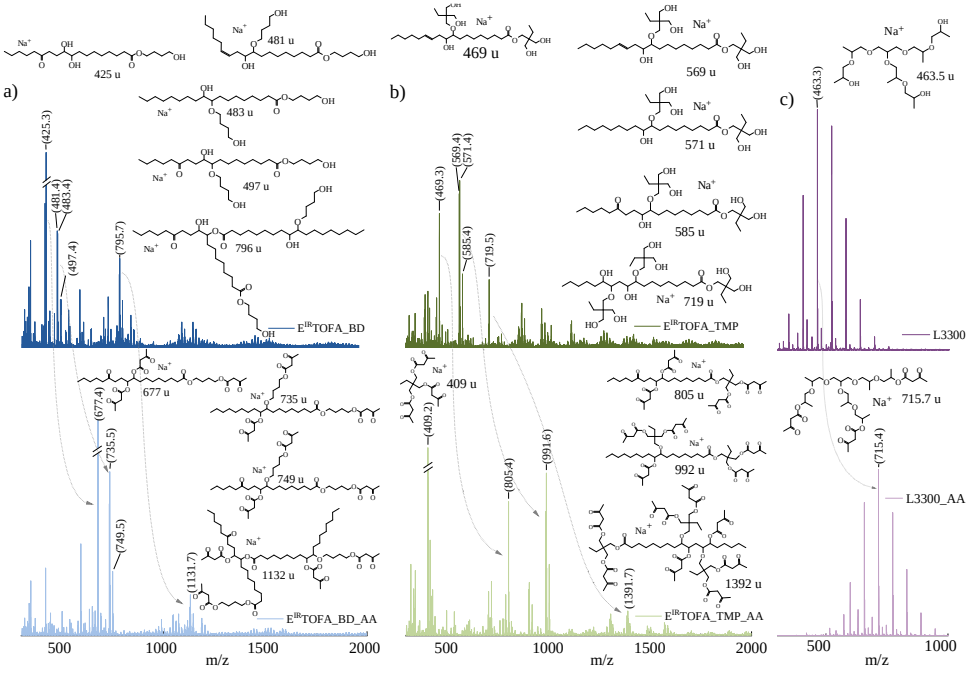

Fig. 1.7. MALDI-TOF MS spectra (2000 Hz, 355 nm, ionizing agent: CF_3COONa) of a) E^{IR}TOFA_BD and E^{IR}TOFA_BD_AA; b) E^{IR}TOFA_TMP and E^{IR}TOFA_TMP_AA; c) L3300 and L3300_AA.

The MALDI-TOF MS spectra showed that a mixture consisting of various compounds was formed in the epoxidation process and in the polyol synthesis and their subsequent acetoacetylation (Fig. 1.7). The spectrum was also registered for E^{IR}TOFA, but it was difficult

to interpret because the peak corresponding to epoxidized oleic and linoleic acids overlaps with the peaks of the matrix. In the spectra, typically, the peaks were in pairs with a difference of 2 m/z. This corresponds to the difference in the weight of oleic acid and linoleic acid. The dominant monomers of synthesised polyols and their acetoacetates are clearly visible in the spectrum. Dimers in the case of E^{IR}TOFA_BD polyol and its corresponding acetoacetate were identified in the MALDI-TOF MS spectrum.

The MALDI-TOF MS spectra show that the acetoacetylation process was successful. After acetoacetylation, the most intense polyol peaks shifted by such units of m/z that correspond to the increase in mass, which corresponds to the replacement of all hydroxyl groups of the molecule with the acetoacetate groups. For example, the characteristic peak of epoxidized oleic acid TMP polyol appeared at 571 m/z $[C_{30}H_{60}O_8+Na]^+$. After acetoacetylation, the peak of this polyol acetoacetate shifted to 991 m/z. The difference of 420 m/z corresponds exactly to the molar mass of the five acetoacetate groups and fully correlates with synthesised polyol functionality. This compound contains five functional groups (E^{IR}TOFA_TMP_AA f = ~ 5). Fully acetoacetylated compounds containing three functional groups were also found in the spectra of epoxidized oleic acid BD polyol (E^{IR}TOFA__AA f = ~ 3)

As the peaks of dimers, trimers and the other by-products were shifted after acetoacetylation, acetoacetate groups were successfully introduced into the molecules. It can be concluded that these by-products were also fully suitable for producing polymer materials by the Michael reaction. Increased viscosity could adversely affect these dimers, trimers and by-products due to the large and branched structure.

Relatively few peaks appeared in the MALDI-TOF MS spectrum of L3300 polyol and its acetoacetate, compared to bio-polyol acetoacetate. L3300 is a trifunctional polyether polyol based on glycerine, and 2-hydroxypropoxy groups are added to the glycerol molecule by oxypropylation in industrial synthesis. The L3300 is a relatively pure substance, making the spectrum easier to interpret. The most intensive characteristic peaks of the compounds were with an interval of 58 m/z, which corresponds to the molar mass of the 2-hydroxypropoxy group. This spectrum distinctly shows how evenly the oxypropylation had taken place. After acetoacetylation, all peaks shifted by 252 m/z, corresponding to the molar mass of the three acetoacetate groups.

1.2. Synthesis of the Michael acceptor from tall oil

There are a few main synthetic routes to obtain bio-based acrylates. One of the most studied reactions is the epoxidation of the double bonds and subsequent opening of the oxirane rings with acrylic acid [57]–[62]. Another possibility is the one-step reaction between unsaturated oil and acrylic acid in the presence of boron trifluoride diethyl etherate solution [63]–[65]. If the molecule of oil contains naturally occurring hydroxyl groups (e.g., castor oil), acrylation of the hydroxyl groups with acrylic chloride is possible [44], [62], [66].

These methods are appropriate for feedstocks with two or more double bonds, as polymerization necessitates at least two functional groups per molecule. Multiple double bonds are present in diglycerides and triglycerides. The literature review suggests that triglyceride-containing oils are the most widely used raw materials for acrylate synthesis.

Some free fatty acids, like linoleic acid, have two double bonds, but due to side reactions with acetic acid or incomplete epoxidation, each molecule is typically left with only one oxirane group. Therefore, epoxidation and oxirane ring's opening with acrylic acid or direct double

bond acrylation are ineffective for free fatty acids containing oils such as tall oil. For oils containing free fatty acids, a different strategy must be adopted.

A promising method for synthesising acrylates from tall oil fatty acids *via* epoxidation followed by oxirane rings opening with a polyfunctional polyol and subsequent acrylation of the hydroxyl groups with acryloyl chloride was developed (see Fig. 1.8).

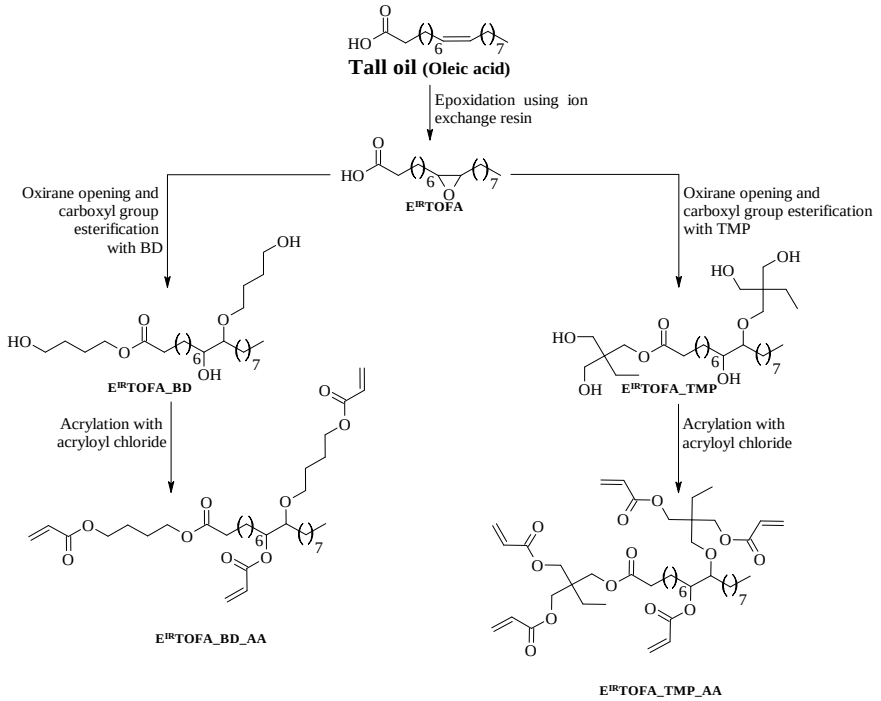

Fig. 1.8. Idealized scheme of tall oil (oleic acid) based Michael acceptor development.

After polyol acrylation, a significant decrease in the hydroxyl value was observed, which was the first indicator that the acrylate synthesis was successful (Table 1.2). Results showed that the samples still contained relatively small amounts of hydroxyl groups after the acrylation. The hydroxyl values of the acrylates were small compared to the hydroxyl values of the polyol and did not substantially impact further polymer production.

Table 1.2

Characteristics of the Synthesised Acrylates

Sample	Acid value, mg KOH·g^{-1}	Hydroxyl value, mg KOH·g^{-1}	Moisture, %	Acryl groups*, mmol·g^{-1}
E^{IR}TOFA_BD_Acryl	< 5	28.8	0.022	3.9
E^{IR}TOFA_TMP_Acryl	< 5	46.2	0.027	3.5

*qNMR (500 MHz, $CDCl_3$) using 1,2,3-trimethoxybenzene as an internal standard.

Rheological measurements (Fig. 1.9) showed a viscosity decreased after introducing acrylate groups into polyols. After the polyol was acrylated, the viscosity decreased more than 25 times to 4560 mPa·s. The same trend can be observed in the case of E^{IR}TOFA_BD acrylation. The viscosity of E^{IR}TOFA_BD_Acryl was 315 mPa·s. The decrease in viscosity was due to a decrease in hydrogen bonding between chains caused by the substitution of the

hydroxyl groups. Since the viscosity was independent of the shear rate applied, the synthesised substances can be categorized as Newtonian fluids.

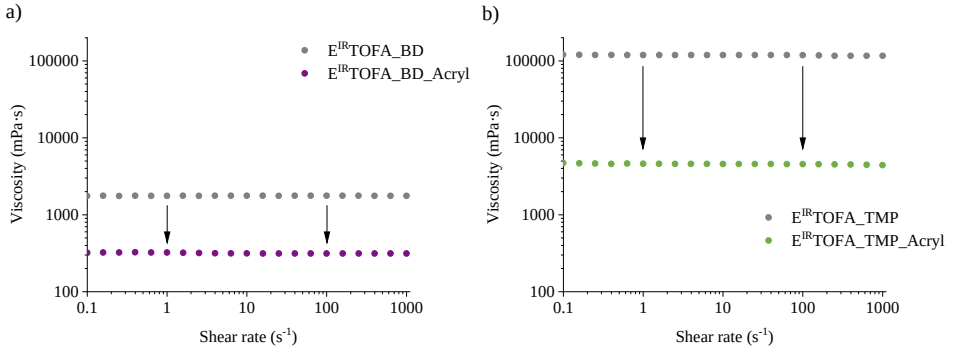

Fig. 1.9. Rheological measurements (cone-plate system, gap of 48 μm, 25 °C) of a) E^{IR}TOFA_BD and E^{IR}TOFA_BD_Acryl; b) E^{IR}TOFA_TMP and E^{IR}TOFA_TMP_Acryl.

Comparing the FTIR spectrum of polyol E^{IR}TOFA_BD to the spectrum of acrylate E^{IR}TOFA_BD_Acryl, results showed that the peak at 3600–3150 cm^{-1} corresponding to the hydroxyl groups disappeared (Fig. 1.10). New peaks appeared at 1640–1620 cm^{-1}, 1407 cm^{-1}, and 810 cm^{-1} were corresponding to the acrylate C=C vibration, scissoring vibration for HC=CH$_2$, and =CH$_2$ twisting vibration of acrylic groups, respectively, which indicated successful acylation reaction. The same trend could be observed when the spectra of polyol E^{IR}TOFA_TMP and acrylate E^{IR}TOFA_TMP_Acryl were compared.

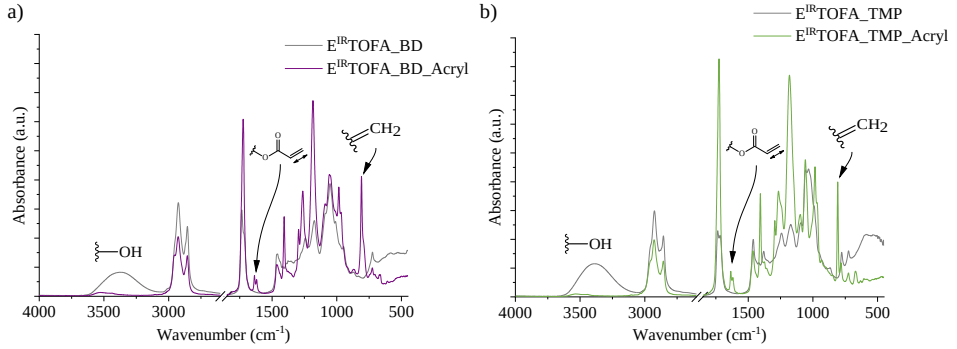

Fig. 1.10. FTIR spectra (ATR mode, 32 scans, resolution of 4 cm^{-1}) of a) E^{IR}TOFA_BD and E^{IR}TOFA_BD_Acryl; b) E^{IR}TOFA_TMP and E^{IR}TOFA_TMP_Acryl.

The FTIR spectra, which confirmed the chemical structures, have an exceptional correlation with NMR spectra (Fig. 1.11). In the ^{1}H NMR spectrum for the acrylated tall oil polyols, typical signals for vinyl moiety (6.4 ppm, 6.1 ppm and 5.8 ppm) were visible. The formation of ester bound was proved by new signals at 4.22−4.13 ppm characterizing –CH$_2$OCOR moiety (where R is vinyl groups). Meanwhile, the intensity of the signal arising from HOCH$_2$– at 3.7−3.6 ppm was reduced, thus indicating the esterification of free hydroxyl groups. Additionally, new signals characterizing the carbonyl groups of acrylate at 166 ppm in the ^{13}C NMR spectrum proved the formation of acrylates.

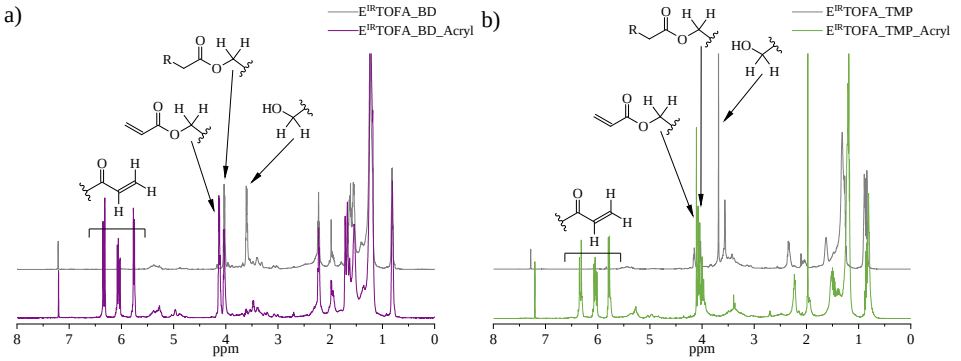

Fig. 1.11. ^{1}H NMR spectra (500 MHz, $CDCl_3$) for a) E^{IR}TOFA_BD and E^{IR}TOFA_BD_Acryl; b) E^{IR}TOFA_TMP and E^{IR}TOFA_TMP_Acryl.

The GPC results (Fig. 1.12) confirmed that tall oil polyols consist of a composition of monomers, dimers, trimers, and oligomers [38]. Comparing the GPC curves of acrylated tall oil polyols and tall oil polyols, the main peaks have slightly shifted to a shorter retention time indicating an increase in molecular weight. An increase in molecular weight was due to the replacement of hydroxyl groups with acrylic groups in the structure. The increase in molecular weight confirmed the successful acrylation.

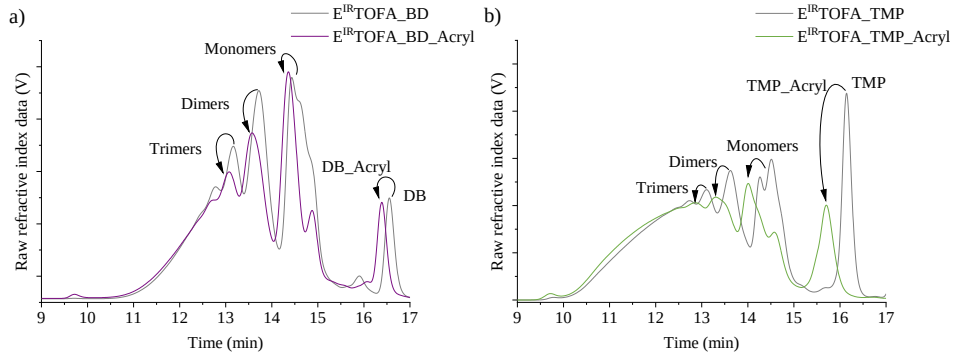

Fig. 1.12. GPC chromatogram (two PLgel Mixed-E columns, particle size of 3 µL, 300 mm × 7.5 mm, THF, 35 °C) of a) E^{IR}TOFA_BD and E^{IR}TOFA_BD_Acryl; b) E^{IR}TOFA_TMP and E^{IR}TOFA_TMP_Acryl.

Along with GPC measurements, synthesised substances were further analysed using MALDI-TOF MS spectrometry to identify changes in the chemical structure of the components (Figs. 1.13 and 1.14). The MALDI-TOF MS data also confirmed that synthesised tall oil polyols consist of a complex mixture, that appeared as an extensive amount of minor intensity mass peaks in the spectra.

The main challenge in analysing MALDI-TOF MS spectra was identifying peaks for acrylated tall oil polyols. In MALDI-TOF MS spectra, the most intense peaks for acrylates were at higher m/z values than for polyols. When comparing the MALDI-TOF MS spectra of polyol and the corresponding acrylate, several peaks were identified with the difference divisible by 54. This number of units (54 m/z) represented an increase in mass from one acrylic group. Since most peaks were shifted by 108 m/z, 162 m/z, 216 m/z, 270 m/z, and 324 m/z units, there were

at least two, three, four, and five acrylic groups per molecule after acrylation. Ion masses corresponding to fully acrylated polyols, E^{IR}TOFA_BD and E^{IR}TOFA_TMP, were found in the spectrum.

Fully functionalized E^{IR}TOFA_BD polyol contains three functional groups per molecule. Relatively intense corresponding peaks at 643.4 m/z and 645.4 m/z for three functional acrylates could be seen in the spectrum (E^{IR}TOFA_BD_Acryl f = ~ 3). In the case of E^{IR}TOFA_BD_Acryl, acrylation of dimers resulted in the formation of compounds with four functional groups at 1009.7 m/z and 1011.7 m/z. The intensity of the corresponding peaks was relatively small. Also, it could be concluded that the mixture also contained partially acrylated compounds.

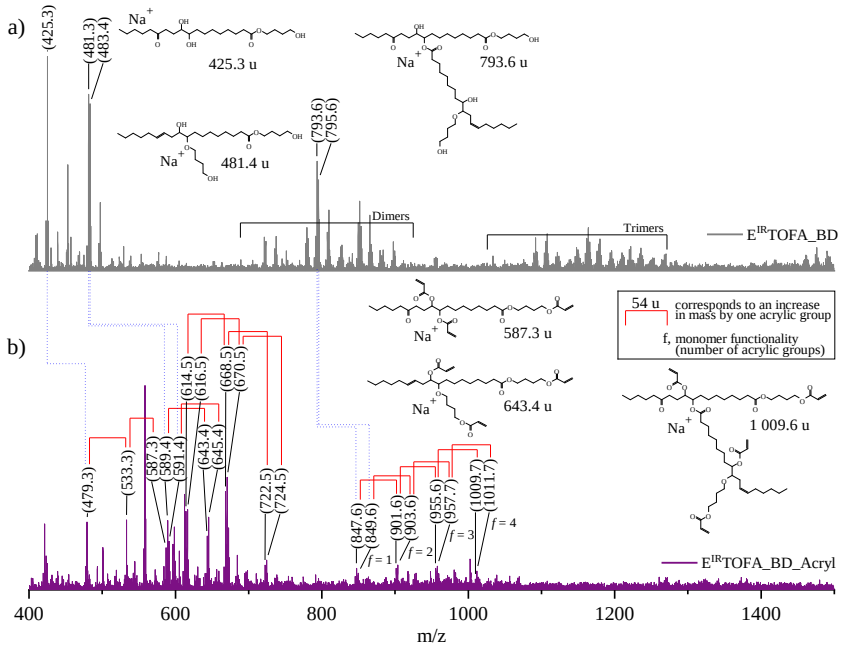

Fig. 1.13. MALDI-TOF MS spectra (2000 Hz, 355 nm, ionizing agent: CF_3COONa) of a) E^{IR}TOFA_BD; b) E^{IR}TOFA_BD_Acryl.

In the case of acrylate E^{IR}TOFA_TMP_Acryl, the intense bands at 839.5 m/z and 841.5 m/z correspond to compounds containing five functional groups per molecule (E^{IR}TOFA_TMP_Acryl f = ~ 5) (Fig. 1.14). As in the case of E^{IR}TOFA_BD_Acryl, the partially acrylated compounds were also observed for E^{IR}TOFA_TMP_Acryl. The peak intensity increased with the number of acrylic groups introduced per molecule, and the most intense bands corresponded to a fully acrylated polyol. Due to high functionality, the synthesised tall oil-based Michael donors can be used to obtain a highly cross-linked polymer, which may increase the polymer's mechanical properties. The synthesised acrylates from tall oil polyols contain several acrylic groups required for polymerization.

Considering the data of rheology, FTIR, NMR, GPC, and MALDI-TOF MS, the obtained tall oil-based acrylates are suitable for polymer synthesis by the Michael reaction. Moreover, the synthesised tall oil-based acrylates are promising in producing other polymers, for example, in UV-initiated free radical polymerization in the production of coatings.

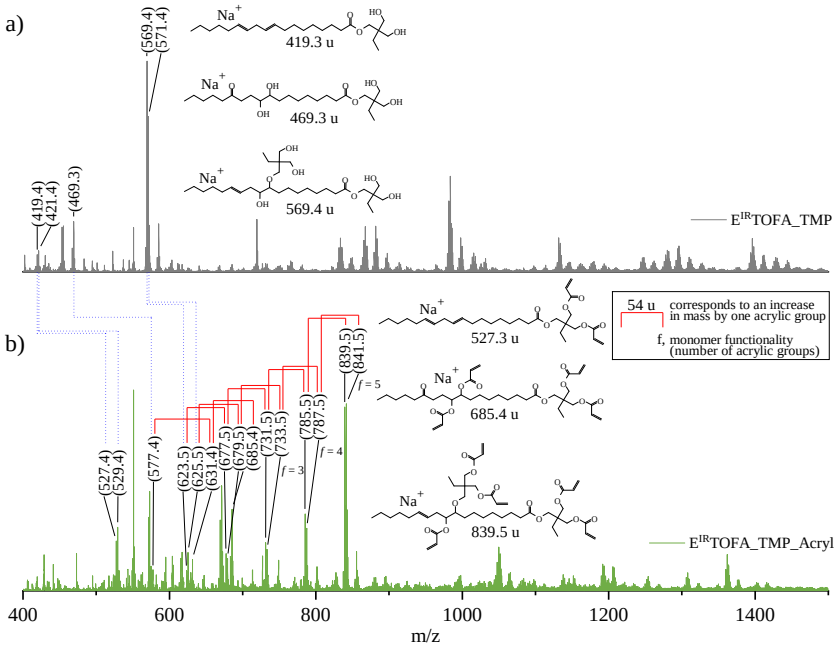

Fig. 1.14. MALDI-TOF MS spectra (2000 Hz, 355 nm, ionizing agent: CF_3COONa) of a) E^{IR}TOFA_TMP; b) E^{IR}TOFA_TMP_Acryl.

2. Polymer resins from tall oil-based Michael donor and petrochemical acceptor

The mechanism of the Michael reaction is well-studied. The base catalyst deprotonates the acetoacetate, resulting in an enolate anion. The enolate anion then reacts with the acrylate in a 1,4-conjugate addition. The product of the first Michael reaction contains active methylene hydrogen that can be added to another acrylate in a second step [23], [31], which means that the Michael donor reacts twice with two Michael acceptors [67], of course, if the ratio allows it. The polymeric material can only be formed if the molecule of the Michael acceptor component contains at least two functional groups.

The reaction between acrylates and the active methylene group of acetoacetates is quick, and the system cures at room temperature after mixing it in the presence of catalysts. This reaction is a base-catalysed addition [31], [35], [68]. For the Michael reaction amine, amidine- and guanidine-based catalysts may be the most suitable [31], [35] ,[46], [49], [68]–[72].

Previously developed acetoacetates of two tall oil-based and two commercial polyols were used to obtain polymers by the Michael reaction using 1,1,3,3-tetramethylguanidine as a catalyst. The previously developed acetoacetates had different chemical structures and functionalities. In conjunction with the use of various acrylates in polymerization reactions, it allowed the development of polymer formulations with varied cross-link densities. Three acrylates with different functionalities – BPAEDA (f = 2), TMPTA (f = 3) and PETA (f = 4) – were used (Table 2.1).

Table 2.1

Developed polymers

	Michael donor			
	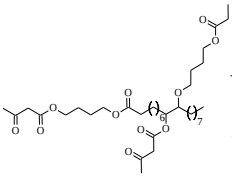	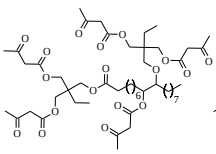	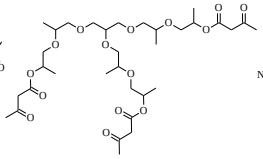	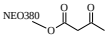
Michael acceptor	**E^{IR}TOFA_BD_AA (*f* = ~ 3)**	**E^{IR}TOFA_TMP_AA (*f* = ~ 5)**	**L3300_AA (*f* = 3)**	**NEO380_AA**
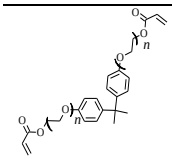 **BPAEDA (*f* = 2)**	E^{IR}TOFA_BD_AA_BPAEDA	E^{IR}TOFA_TMP_AA_BPAEDA	L3300_AA_BPAEDA	NEO380_AA_BPAEDA
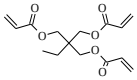 **TMPTA (*f* = 3)**	E^{IR}TOFA_BD_AA_TMPTA	E^{IR}TOFA_TMP_AA_TMPTA	L3300_AA_TMPTA	NEO380_AA_TMPTA
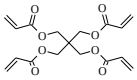 **PETA (*f* = 4)**	E^{IR}TOFA_BD_AA_PETA	E^{IR}TOFA_TMP_AA_PETA	L3300_AA_PETA	NEO380_AA_PETA

TGA analysis was performed for the obtained polymers (Fig. 2.1). No significant weight loss was observed up to almost 300 °C for polymers derived from tall oil polyols; they were thermally stable. This is an advantage because, e.g., classic polyurethane materials without special thermal stabilizer additives decompose in the temperature range from 200 °C to 300 °C [73], [74]. Moreover, organic glass poly(methyl methacrylate) onset decomposition temperatures are under 300 °C [75], [76].

Polymers derived from TMP polyols had higher thermal stability. The most thermally stable polymers were obtained from bisphenol A-derivative BPAEDA acrylate. This could be explained by the aromatic structure of bisphenol A. Two distinct peaks were observed for polymers obtained using BPAEDA as the acrylate. For other polymers, the similarity of the curves was determined by the used polyol and less by the acrylate.

Polymers from commercial polyol acetoacetates also showed similar characteristics in TGA mass triglyceride containing oils loss curves and their derivative curves. Polymeric materials derived from tall oil-based acetoacetates with BPAEDA acrylate had higher thermal stability (when comparing the temperature for weight loss of 5 %) than commercial polyols with the same acrylate. The temperature depended significantly on the used acrylate for a weight loss of 5 %, but this effect was less pronounced for weight losses at higher temperatures.

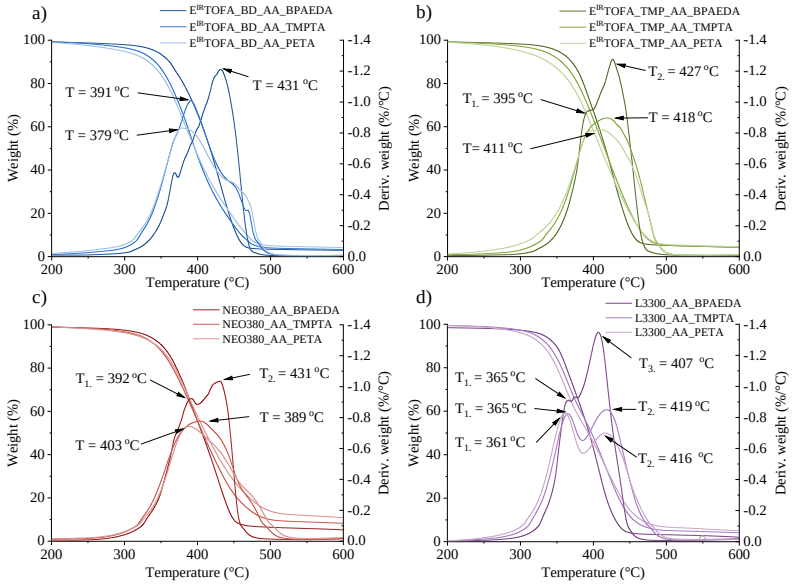

Fig. 2.1. TGA (10 °C·min^{-1}) mass loss curve and TGA derivative of polymers from synthesised acetoacetates and BPAEDA, TMPTA, PETA acrylates: a) E^{IR}TOFA_BD_AA polymers; b) E^{IR}TOFA_TMP_AA polymers; c) NEO380_AA polymers; d) L3300_AA polymers.

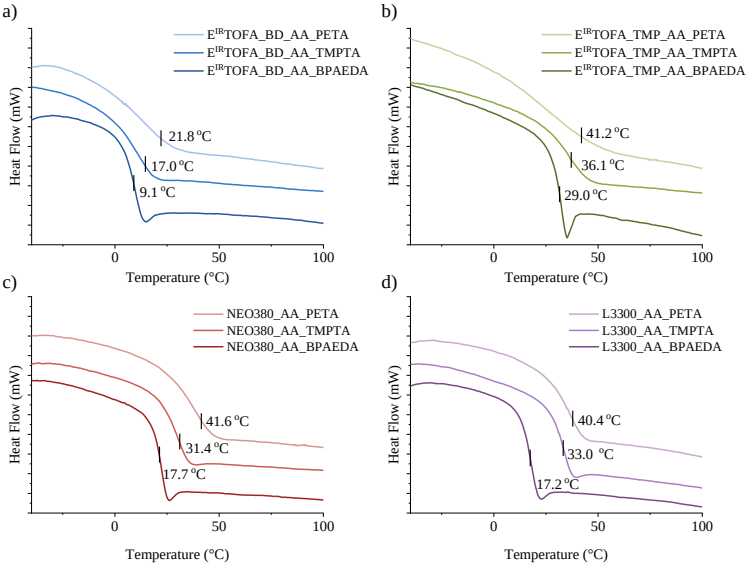

Fig. 2.2. DSC (10 °C·min^{-1}) curves of polymers from synthesised acetoacetates and BPAEDA, TMPTA, PETA acrylates: a) E^{IR}TOFA_BD_AA polymers; b) E^{IR}TOFA_TMP_AA polymers; c) NEO380_AA polymers; d) L3300_AA polymers.

The obtained polymers were subjected to DSC analysis to determine the glass transition temperature (T_g) (Fig. 2.2). $T_{g(DSC)}$ was determined as the midpoint between the onset temperature and endset temperature of the glass transition region.

For polymers obtained from commercial polyol acetoacetate (L3300_AA and NEO380_AA), $T_{g(DSC)}$ was mainly influenced by the used acrylate. $T_{g(DSC)}$ differed by less than 2 °C when polymers obtained with the same acrylates were compared (Fig. 2.2 c, d). The difference in T_g was relatively small when considering the effect of the commercial polyol acetoacetate used. Depending on the used acrylate, $T_{g(DSC)}$ increased as follows: BPAEDA < TMPTA < PETA. The functionality of the used acrylate impacted the glass transition temperature. When acrylate with higher functionality was used to obtain polymers, the polymer exhibited higher $T_{g(DSC)}$ due to a higher cross-link density in the polymer [77]. The same trend was observed for polymers obtained from acetoacetylated tall oil polyols (Fig. 2.2 a, b). The use of tall oil polyol acetoacetate had a significant effect on the $T_{g(DSC)}$ of the obtained polymer.

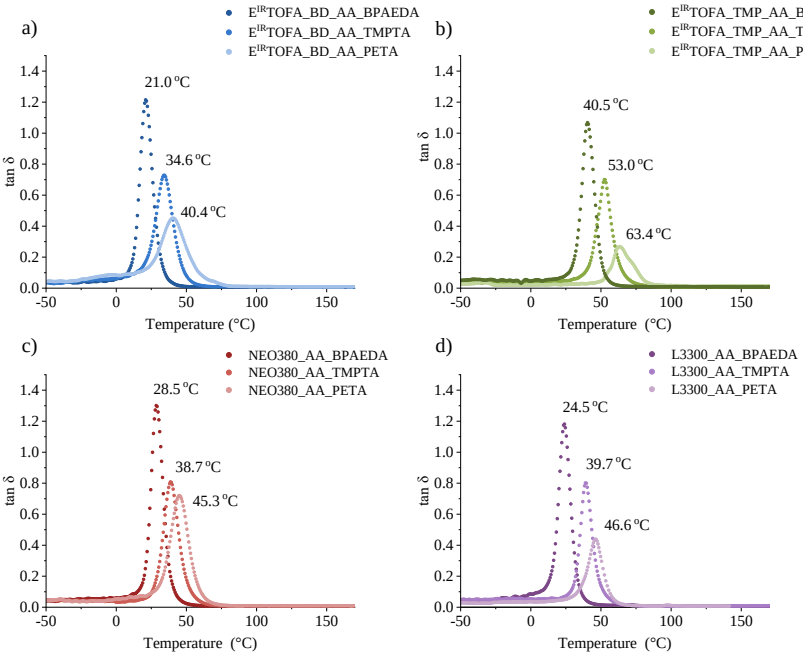

Fig. 2.3. DMA (3 °C·min^{-1}, 1 Hz, 5 N) tanδ curves of polymer from synthesised acetoacetates and BPAEDA, TMPTA, PETA acrylates: a) E^{IR}TOFA_BD_AA polymers; b) E^{IR}TOFA_TMP_AA polymers; c) NEO380_AA_TMPTA polymers; d) L3300_AA polymers.

DMA test was performed to determine the dynamic mechanical properties of polymer materials. Based on the tanδ data (Fig. 2.3), there was only one relatively narrow peak with a clear maximum, indicating that all samples had a quite homogeneous structure. These relationships between peak width, symmetry and structure, and the homogeneity of the structure have been described in several studies [68], [78]–[80].

Although $T_{g(DMA)}$ were different from DSC data, the same trends between them were observed. $T_{g(DMA)}$ was measured from the peak value of tanδ. T_g, determined using the DMA

method, were higher than those determined using the DSC analysis. Also, different effects were measured in the DSC and DMA methods. In the case of DMA, stress was applied and mechanical properties were measured, while DSC measures changed in heat capacity [81], [82]. DMA is beneficial for polymers with hard-to-find glass-transition temperatures and heavily cross-linked polymers [83]. Polymer samples with higher cross-link density exhibited higher T_g (Table 2.2). The correlation between increasing cross-link density and higher $T_{g(DSC)}$ of the polymer was also reported by Wang et al. [51], similarly as in the case of $T_{g(DMA)}$.

Table 2.2

Characteristics of Polymers from Tall Oil Polyol or Commercial Polyol-Based Acetoacetates and BPAEDA, TMPTA, and PETA Acrylate

	Sample	Max. tanδ	$T_{g(DMA)}$, °C	$E_{(storage)}$ ($T_{g(DMA)}$ + 50), MPa	ν_e, mol·cm^{-3}	ρ, g·cm^{-3}	M_c, g·mol^{-1}
Tall oil-based	E^{IR}TOFA_BD_AA_BPAEDA	1.21	21.0	5.1	$0.59\cdot10^{-3}$	1.167	1695
	E^{IR}TOFA_BD_AA_TMPTA	0.73	34.6	17.7	$1.98\cdot10^{-3}$	1.211	505
	E^{IR}TOFA_BD_AA_PETA	0.45	40.4	24.2	$2.67\cdot10^{-3}$	1.219	375
	E^{IR}TOFA_TMP_AA_BPAEDA	1.07	40.5	17.1	$1.89\cdot10^{-3}$	1.116	529
	E^{IR}TOFA_TMP_AA_TMPTA	0.70	53.0	19.1	$2.04\cdot10^{-3}$	1.177	490
	E^{IR}TOFA_TMP_AA_PETA	0.27	63.4	30.6	$3.17\cdot10^{-3}$	1.235	315
Commercial polyols-based	NEO380_AA_BPAEDA	1.30	28.5	8.2	$0.93\cdot10^{-3}$	1.257	1075
	NEO380_AA_TMPTA	0.81	38.7	18.4	$2.04\cdot10^{-3}$	1.328	490
	NEO380_AA_PETA	0.72	45.3	23.4	$2.55\cdot10^{-3}$	1.330	392
	L3300_AA_BPAEDA	1.18	24.5	9.8	$1.13\cdot10^{-3}$	1.171	885
	L3300_AA_TMPTA	0.80	39.7	19.9	$2.20\cdot10^{-3}$	1.202	455
	L3300_AA_PETA	0.44	46.6	24.9	$2.70\cdot10^{-3}$	1.247	369

The DMA tests were used to determine $T_{g(DMA)}$ and storage modulus in the rubbery plateau region ($E_{(storage)}$ at $T_{g(DMA)}$ + 50 temperature) for calculations of cross-link density and molecular weight between cross-links (Table 2.2). Results showed that cross-link density and molecular weight between cross-links of the polymers were highly dependent on the functionality of the used acrylate and acetoacetate. If higher functionalized monomers were used, the cross-link density of the obtained polymer was higher, and the molecular weight between cross-links was smaller, which significantly affects the polymer's mechanical properties. This is in line with Rahul and Kitey [84] observations that $T_{g(DMA)}$ was affected by the polymer cross-link density. Also, tensile tests confirmed the dependence of mechanical properties on the cross-link density.

The highest cross-link density ($3.17\cdot10^{-3}$ mol·cm^{-3}) and the lowest molecular weight between cross-links (315 g·mol^{-1}) were obtained from E^{IR}TOFA_TMP_AA and PETA. It can be explained by the higher functionality of both – the Michael donor and the Michael acceptor compound. The lowest cross-link density and biggest molecular weight between cross-links were for the polymers derived from the lower functionalized acetoacetate and difunctional acrylate – BPAEDA.

Polymer samples obtained by the reaction of polyol acetoacetates with PETA (f = 4) showed the highest tensile (Young's) modulus values (Fig. 2.4). The results of tensile strength showed the same trend. This could be explained by the higher functionality of the acrylate and, thus, the higher cross-link density (see Table 2.2), resulting in the highest tensile modulus value. A

correlation between the functionality of acrylate used in polymer formulations and the tensile modulus values was observed: the higher functionality of the used acrylate yielded polymers with higher tensile module values.

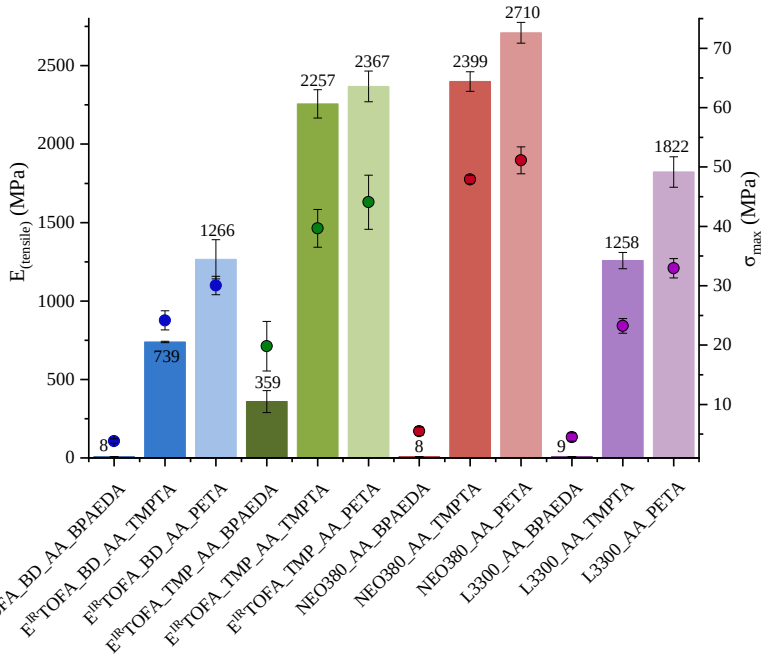

Fig. 2.4. $E_{(tensile)}$ and σ_{max} (2 mm·min^{-1}, 22 °C) for the polymers from tall oil polyol or commercial polyol-based acetoacetates and BPAEDA, TMPTA or PETA acrylates.

The highest tensile modulus and tensile strength were for NEO380_AA_PETA polymer, respectively, 51 MPa and 2710 MPa. Relatively high modulus values were also obtained for polymers from tall oil from E^{IR}TOFA_TMP_AA_TMPTA and E^{IR}TOFA_TMP_AA_PETA, respectively, 2250 MPa and 2370 MPa, and tensile strength was 40 MPa and 44 MPa. These materials can be compared to other innovative materials, e.g, Fleischer et al. prepared non-filled non-isocyanate polyurethanes (NIPU) from hexamethylene diamine, glycerol cyclic carbonates and TMP. This NIPU showed a tensile strength of 68 MPa and a tensile modulus of 2100 MPa [85]. The mechanical properties of obtained polymers are also comparable to polyurethane materials [86], [87], and poly(methyl methacrylate), which had a tensile strength value of at least 55 MPa and a tensile modulus of about 2700 MPa [88], [89]. This shows that tall oil-based polymer materials obtained by the Michael reaction are competitive and promising alternatives.

The elongation at break correlates with the modulus value and the tensile strength. The higher the modulus and tensile strength values, the smaller the elongation. The smallest elongations at breaks were 1.9 %, 2.7 %, and 2.9 % for polymers E^{IR}TOFA_TMP_AA_PETA, NEO380_AA_PETA, and L3300_AA_PETA, and the highest elongations at breaks were 55 %, 53 % and 47 % for polymers E^{IR}TOFA_BD_AA_BPAEDA, NEO380_AA_BPAEDA, and L3300_AA_BPAEDA, respectively.

The relationship between mechanical properties and the molecular weight between cross-links was observed. The lower the molecular weight between cross-links, the higher the

cross-link density (see Table 2.2) and the correspondingly higher tensile modulus and tensile strength.

Results indicated that it was possible to obtain vastly different polymeric materials by changing the chemical structure of the used acrylate. Polymeric materials that are similar in properties to rubbers can be obtained by using lower functionality monomers. It was also possible to obtain materials that were similar in their properties even to organic glass [88]–[90]. By compiling the literature on similar materials and their characteristics, the polymer materials obtained in this study are competitive with several other alternative materials. The production of polymers from free fatty acid-based monomers by the Michael reactions was simple and was carried out in milder conditions compared to other methods, such as NIPU synthesis.

The Michael 1,4-addition polymerizations can be realized in a short period of time, at room temperature, and at atmospheric pressure. The chemicals used to synthesise polymers *via* the Michael reaction are less toxic than isocyanates, which is one of the main raw materials for polyurethane production. The mechanical and thermal properties of synthesised polymers by the Michael reaction are equal to or even better than materials shown in the literature. Moreover, the properties of polymers can be tailored by varying the components used for polymerization.

3. resins from tall oil-based both Michael components

There are a few studies on synthesising and using bio-based acetoacetates for different polymer materials. Xu et al. developed a coating film by reacting acetoacetylated castor oil with a cross-linker that had both aldehyde and acrylate groups by the Michael reaction [49]. Wang et al. created curable coatings from acetoacetylated castor oil and a multifunctional acrylate using the Michael reaction (hexamethylene diacrylate, TMPTA, PETA) [51]. Noordover et al. proposed malonate-functional polyester coatings from synthesised bio-based Michael donors cured through the Michael reaction with di(trimethylolpropane) tetraacrylate [91]. Naga et al. demonstrated a reaction between multifunctional acetoacetates (*meso*-erythritol tetraacetoacetate, trimethylolpropane triacetoacetate) and diacrylate monomers (1,4-butanediol diacrylate, 1,6-hexanediol diacrylate, 1,9-nonanediol diacrylate), resulting in the formation of corresponding gels [92]. Later, Naga et al. investigated the Michael reaction between *meso*-erythritol tetra acetoacetate or D-sorbitol hexaacetoacetate and poly(ethylene glycol) diacrylate in solvents to create a porous polymer [93]. All previous studies share the use of a bio-based Michael donor and a petrochemical-based Michael acceptor.

In this work, previously synthesised tall oil-based acrylates and tall oil-based acetoacetates were successfully used to develop a highly cross-linked polymer (Fig. 3.1). The polymer material has high thermal stability and mechanical properties and may be used as an alternative to industrially used thermoset resins, such as epoxy, polyesters, and vinyl esters resins.

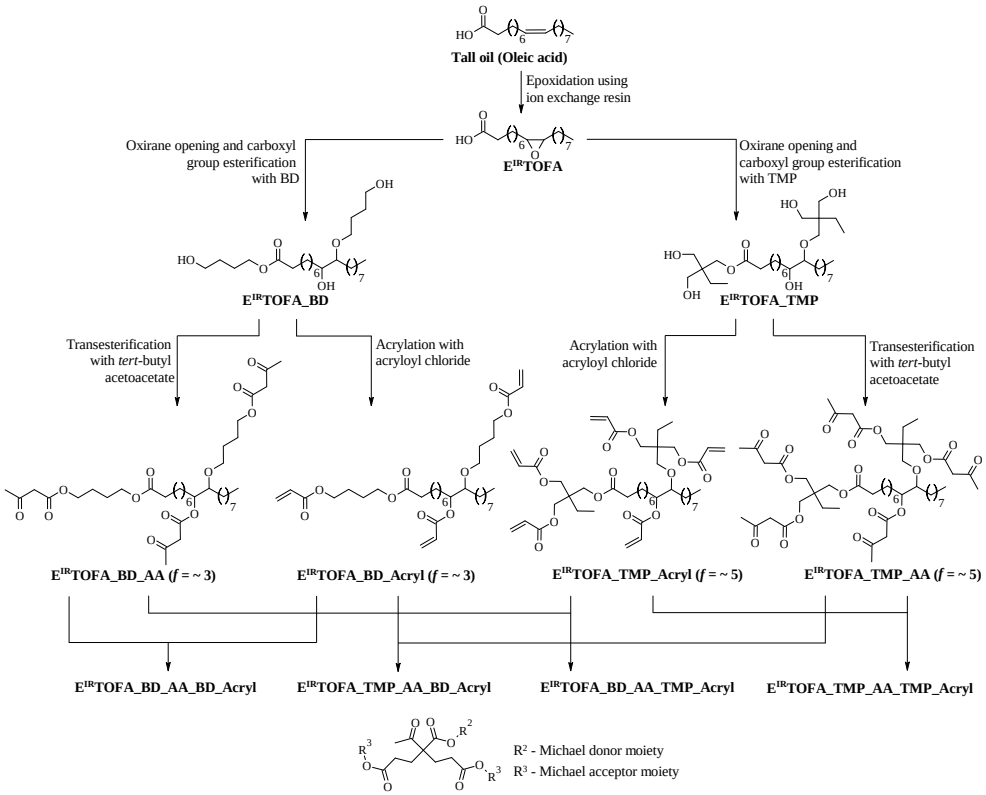

Fig. 3.1. Conceptual scheme of polymer development from synthesised Michael donor and Michael acceptor.

By tactile perception, the polymer materials obtained from E^{IR}TOFA_BD_Acryl were flexible, similar to hard rubber. The resulting polymer materials based on E^{IR}TOFA_TMP_Acryl were solid, with an organic glass-like feel to the hand. All synthesised polymers were transparent and clear with a slight brown or yellow tint.

The structure of the developed polymer materials was characterized by FTIR spectroscopy (Fig. 3.2 a). The characteristic absorption bands of acrylate at 1640−1620 cm^{-1} and 1407 cm^{-1} cannot be evaluated because of overlapping with the absorption bands typical of the functional groups of the donor. The FTIR spectrum well represented the content of acrylic groups by the characteristic absorption of =CH$_2$ twisting vibration bands at about 810 cm^{-1}.

Polymers obtained from acrylate E^{IR}TOFA_BD_Acryl had no absorption band at 810 cm^{-1}. This could indicate a good conversion and complete reaction of the acrylic groups. The absorption band was observable for both polymers synthesised from E^{IR}TOFA_TMP_Acryl. When comparing FTIR spectra of E^{IR}TOFA_BD_AA_TMP_Acryl and E^{IR}TOFA_TMP_AA_TMP_Acryl, the absorption band of the acrylic groups at 810 cm^{-1} was more intense for the last. This could mean an incomplete conversion because of high viscosity, high functionality, branched structure, as well as steric effects.

The polymer samples were also characterized using ssNMR ^{13}C spectroscopy (Fig. 3.2 b) The spectra exhibited anticipated ^{13}C chemical shifts. The analysis of the ssNMR spectrum showed signals corresponding to the >CH-O- groups in the range of 63.0−83.5 ppm for all the

developed polymers. The >CH-O- groups were a result of oxirane rings opening with alcohols. Also, the characteristic signal of ^{13}C corresponding quaternary carbon was in the same range of 63.0−83.5 ppm, indicating that the reaction of two acrylic groups with the methylene group of acetoacetate *via* the Michael reaction had occurred.

Overlapping of several signals can also be observed in the range of 26.5−42.9 ppm. The characteristic signal of ^{13}C corresponding tertiary carbon can be observed in this range. Also, tertiary carbon was essential for the detection of polymerization, representing a situation where one acetoacetate group has reacted with only one acrylic group. The characteristic signal of ^{13}C in the –C(=O)–CH_3 groups was in the same range of 24.0−24.4 ppm, which represented the acetoacetate groups in the Michael donor compound.

The signals of the acrylate groups at 130.2−131.2 ppm indicated an incomplete reaction. The ssNMR ^{13}C spectra were consistent with FTIR data. While the signal intensity of acrylic groups in polymers obtained from E^{IR}TOFA_BD_Acryl was low, it was relatively intense in spectra of polymers obtained from E^{IR}TOFA_TMP_Acryl. A much more branched structure and multiple acrylic groups per molecule decreased the reactivity of the E^{IR}TOFA_TMP_Acryl and E^{IR}TOFA_TMP_AA because of steric hindrance effects. Since the acceptor and donor used in polymer synthesis are derived from fatty acids, they contain double bonds because of an incomplete epoxidation reaction. The double bond signal overlaps with the signal characteristic of acrylate groups. This must be considered when evaluating the results. Hence, the ssNMR and FTIR results confirmed that polymers from tall oil-based donors and acceptors *via* the Michael reaction were successfully synthesised.

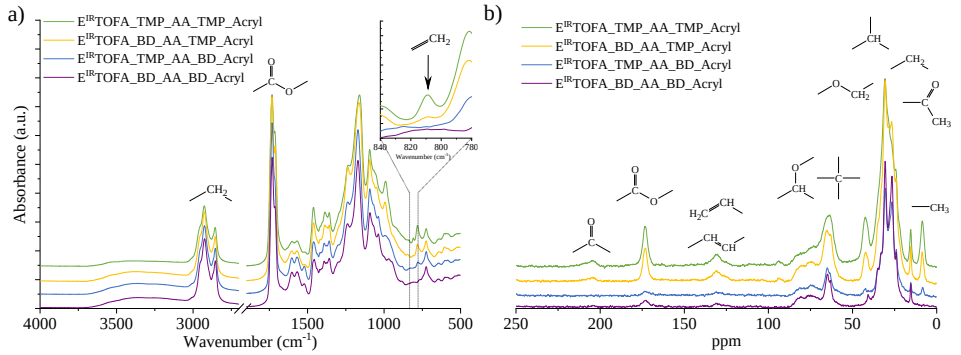

Fig. 3.2. Structure analysis of polymers from tall oil-based Michael donor and acceptor: a) FTIR spectra; b) ssNMR ^{13}C spectra.

The thermal stability of synthesised polymers was assessed by TGA (Fig. 3.3) The initial degradation stage occurred up to 300 °C because of the decomposition of the catalyst and some leftover raw materials. Polymer samples showed different degradation processes at temperatures above 300 °C, which could be very well seen in the mass loss derivative curves. The E^{IR}TOFA_BD_AA_BD_Acryl TGA mass loss derivative curve showed one symmetrical peak with only one clear maximum at 389.3 °C.

The peak of the E^{IR}TOFA_TMP_AA_BD_Acryl mass loss derivative curve has a shoulder at about 450 °C. The second degradation peak became more pronounced when the composition of the polymer contained more TMP derivatives. Both derivative peaks of the E^{IR}TOFA_TMP_AA_TMP_Acryl mass loss derivative curve at 400 °C and 445 °C had almost the same rate of change in weight loss. The first derivative peak can be linked to the ester and

ether bonds cleavage to form CO_2 and other low molecular weight compounds [47], [51]. The second derivative peak can be attributed to the degradation of the TMP of the polymer chemical structure [94].

The results showed that the developed bio-based thermoset polymer samples were thermally stable. All samples had very similar weight loss curves at the start up to 300 °C. The samples represented weight loss of less than 10 % up to 300 °C. The main degradation process of polymers occurred between 300 °C and 475 °C. Polymer sample E^{IR}TOFA_TMP_AA_TMP_Acryl exhibited slightly better thermal stability than other samples.

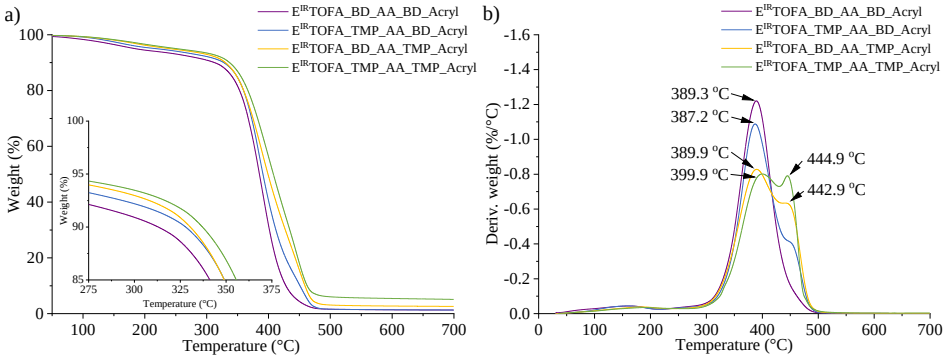

Fig. 3.3. TGA (10 °C·min^{-1}) of polymers from tall oil-based Michael donor and acceptor: a) TGA curves; b) TGA weight derivative curves.

Higher cross-link density favours the carbonation reaction, resulting in a greater amount of solid residue [63], [95]. From all the developed bio-based thermoset polymer samples, the solid residue yield was the highest for E^{IR}TOFA_TMP_AA_TMP_Acryl polymer. The solid residue yield was 5.10 % at 675 °C.

The thermal behaviours of the polymer samples were also studied using DSC (Fig. 3.4 a). $T_{g(DSC)}$ was identified for all obtained polymers. It was observed that $T_{g(DSC)}$ increased with the increased TMP-derivative content in the polymer composition. This was most likely due to a higher cross-link density of these polymers.

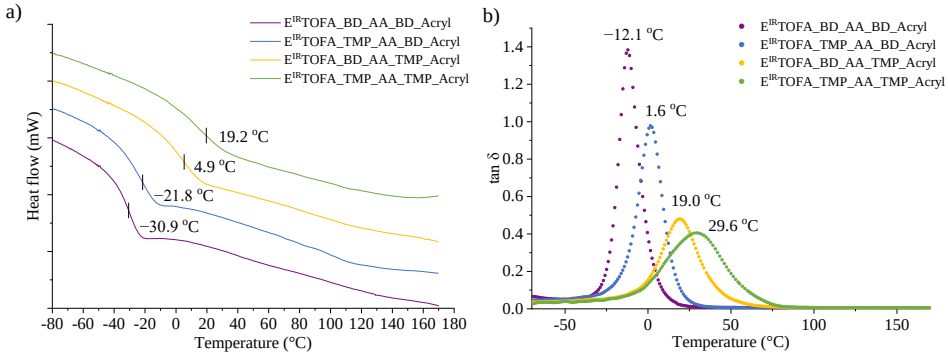

Fig. 3.4. DSC (10 °C·min^{-1}) and DMA (3 °C·min^{-1}, 1 Hz, 5 N) results of polymers from tall oil-based Michael donor and acceptor: a) DSC curves; b) DMA tanδ curves.

DSC and DMA Results of Polymers from Tall Oil-Based Michael Components

Sample	T_g, °C		ρ, g·cm^{-3}	$E_{(storage)}$ ($T_{g(DMA)}$ + 50), MPa	ν_e, mol·cm^{-3}	M_c, g·mol^{-1}
	$T_{g(DSC)}$	$T_{g(DMA)}$				
E^{IR}TOFA_BD_AA_BD_Acryl	−30.9	−12.1	1.071	5.3	0.69·10^{-3}	1562
E^{IR}TOFA_TMP_AA_BD_Acryl	−21.8	1.6	1.085	5.8	0.71·10^{-3}	1518
E^{IR}TOFA_BD_AA_TMP_Acryl	4.9	19.0	1.104	11.4	1.33·10^{-3}	829
E^{IR}TOFA_TMP_AA_TMP_Acryl	19.2	29.6	1.125	13.7	1.55·10^{-3}	724

The tanδ of the obtained samples is shown in Fig. 3.4 b, and the results are summarized in Table 3.1. In Fig. 3.4 b, the tanδ peaks of the BD_Acryl polymer systems were narrower, and the values of tanδ were higher than tanδ values of TMP_Acryl derived polymers.

The same trend was observed between $T_{g(DMA)}$ and $T_{g(DSC)}$, as in the case of polymers with petrochemical commercial acrylates (Table 3.1). The lowest and highest $T_{g(DMA)}$ values were determined to be −12.1 °C for polymer E^{IR}TOFA_BD_AA_BD_Acryl, and 29.6 °C for polymer sample E^{IR}TOFA_TMP_AA_TMP_Acryl.

The stress-strain curves and elongation at break, depicted in Fig. 3.5, showed the tensile modulus and tensile strength of the obtained thermoset polymers. The polymers derived from E^{IR}TOFA_BD_Acryl exhibited the elastic region. At the same time, polymer E^{IR}TOFA_TMP_AA_TMP_Acryl exhibited the stress-strain behaviour of more rigid polymer.

According to results in Table 3.1 and Fig. 3.5 a, the polymers obtained from E^{IR}TOFA_TMP_Acryl have higher tensile modulus because of higher cross-link density and lower molecular weight between cross-links. The highest tensile modulus, stress at break (σ_{max}), and the lowest elongation at break were 1760 MPa, 16.1 MPa, and 17 %, repectively, for the E^{IR}TOFA_TMP_AA_TMP_Acryl polymer. Properties of the E^{IR}TOFA_TMP_AA_TMP_Acryl polymer were very similar to the polymer obtained from L3300_AA and PETA ($E_{(tensile)}$ = 1822 MPa; σ_{max} = 30 MPa). Mechanical tests confirmed that developed polymer materials showed competitive properties to semi-petrochemical-based polymers. Among the polymer samples, E^{IR}TOFA_BD_AA_BD_Acryl had the lowest tensile properties. The tensile modulus, σ_{max}, and elongation for above-mentioned polymer were 15 MPa, 0.9 MPa, and 27 %, respectively which exhibited rubber-like properties.

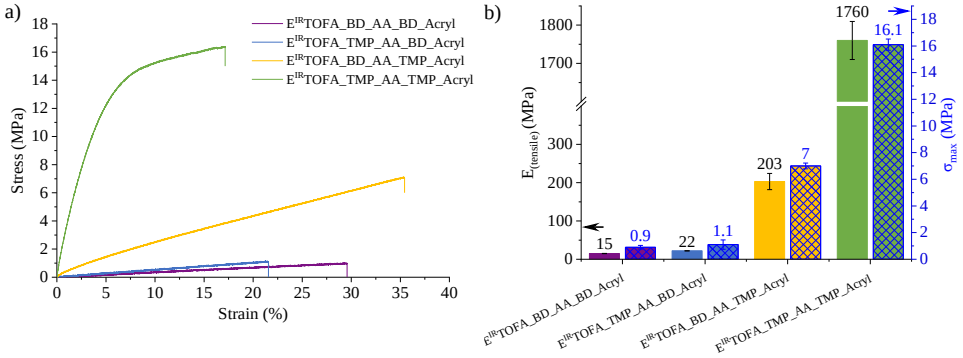

Fig. 3.5. Tensile properties (2 mm·min^{-1}, 18 °C) for polymers developed from tall oil-based Michael donor and acceptor: a) stress-strain curves; b) $E_{(tensile)}$ and σ_{max}.

4. Polymer foams from tall oil-based Michael donor and Michael acceptor

There are several publications that use different types of Michael reactions for the development of foam materials. Coste et al. investigated soft foams using acrylated soybean oils and biobased amines in the *aza*-Michael reactions [27]. Li et al. explored a one-step thiolene "click" chemistry and the Michael reaction to create a robust superhydrophobic/superoleophilic melamine foam [96]. Few publications describe the development of polymer foam materials using the carbon-carbon Michael reaction. Sonnenschein et al. delve into the utilisation of Michael chemistry for producing a range of foams, including rigid, viscoelastic, and flexible elastomers. Sonnenschein et al. investigation employs acetoacetylated glycerol and petrochemical acrylates as raw materials [68]. Despite the potential advantages of the Michael reaction approach, the choice of raw materials may not meet the contemporary requirements for a sustainable future. Naga et al. developed porous polymers through the Michael reactions between multifunctional acetoacetate and poly(ethylene glycol) diacrylate [93]. The resulting reactions lead to porous polymers with connected spheres, and the study highlights the ability to tailor the morphology and properties of these polymers by varying the polymerization conditions. However, the use of poly(ethylene glycol) diacrylate, a petrochemical derivative, also raises sustainability concerns as the polymer industry aims to shift towards more renewable raw materials.

There are few patents [97] and patent applications [98], [99] about the Michael foams. Each presents different approaches to foam production. A common drawback is the absence of second-generation raw materials in their formulations, specifically second-generation free fatty acids. These patents collectively point towards an industry trend of seeking more sustainable materials but also highlight a gap in the availability of fully renewable and bio-based feedstocks, such as those derived from free fatty acids.

In this chapter of the Thesis, the potential of tall oil-based acetoacetate as a key component in polymer foam development was explored, combining it with a synthesised tall oil-based acrylate. Additionally, commercially available acrylates such as BPAEDA, TMPTA, PETA, and ESOA were used. 1,1,3,3-tetramethylguanidine was used as a catalyst. The development of the foam required the addition of additives as a surfactant (silicone surfactant with the trade name Niax Silicone L-6915) and blowing agent (low global warming potential hydrofluoroolefin-based blowing agent with the trade name Opteon™ 1100) to form the cell structure.

Prior to foam development, dielectric polarization changes during curing were determined for selected foam formulations without surfactant and foaming agent. Different polymers exhibited varying degrees of dielectric polarization and reached different maximum temperatures during the curing process (Fig. 4.1). In analysing the curing parameters of polymer derived from tall oil trimethylolpropane acetoacetate combined with various acrylates, a clear relationship emerged between acrylate functionality and curing behaviour. Specifically, the curing process is expedited as acrylate functionality increases and a higher maximum temperature is achieved. For instance, the polymer formulated using the tetra-functional PETA polymer cured the fastest at 70 s and reached the highest temperature of 133 °C. The polymer formulated using the trifunctional TMPTA had a slightly prolonged curing time of 116 s and a temperature of 122 °C. Notably, when comparing commercially available petroleum-based

acrylates to bio-based ones, the former tend to cure more rapidly at elevated temperatures. Specifically, the soybean oil-based ESOA and tall oil-based E^{IR}TOFA_BD_Acryl polymers had longer curing durations and achieved lower maximum temperatures. This underscores the influence of both acrylate origin and functionality on the curing parameters of these polymers.

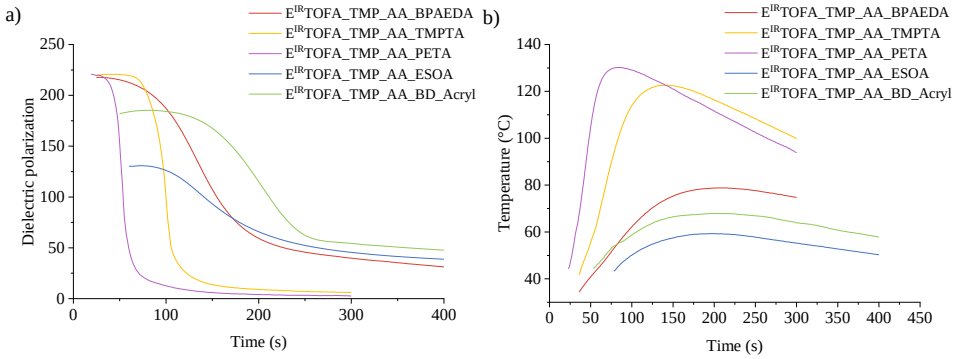

Fig. 4.1. Developed polymer curing parameters: a) dielectric polarization curves; b) temperature curves of the polymers.

The behaviour of petrochemical-based acrylates in the curing process can be attributed to their molecular structure. These acrylates are typically smaller molecules, meaning the acrylic group content is larger. The high concentration of accessible acrylic groups facilitates a more rapid reaction, enhancing the curing process. In contrast, the bio-based acrylates derived from tall and soybean oil have a more branched and complex molecular structure.

In evaluating the rise profiles (Fig. 4.2 and Table 4.1) of the developed polymer foams, those that combine a bio-based donor with a petrochemical-based acceptor typically initiated and completed their rise more rapidly. The E^{IR}TOFA_TMP_AA_PETA foam within this category exhibited the shortest start and rise times, indicative of a faster foam expansion process. Foams with tall oil-based donor and bio-based acceptor components displayed extended start and rise times, suggesting a slower foam expansion. Notably, the E^{IR}TOFA_TMP_AA_BD_Acryl foam formulated using tall oil-based acrylate and acetoacetate had the longest start and rise durations among all samples. The significant influence of monomer origin on the rising behaviour of the developed polymer foams was observed.

The slower rising profile can be attributed to the presence of longer alkyl chains in both bio-based acceptors. This structural characteristic influences the curing process, leading to a more gradual expansion of the foam. Also, this complexity introduces steric hindrance, which can interfere with the reaction process. The branched nature of these molecules makes the acrylic groups less accessible, slowing down the curing parameters.

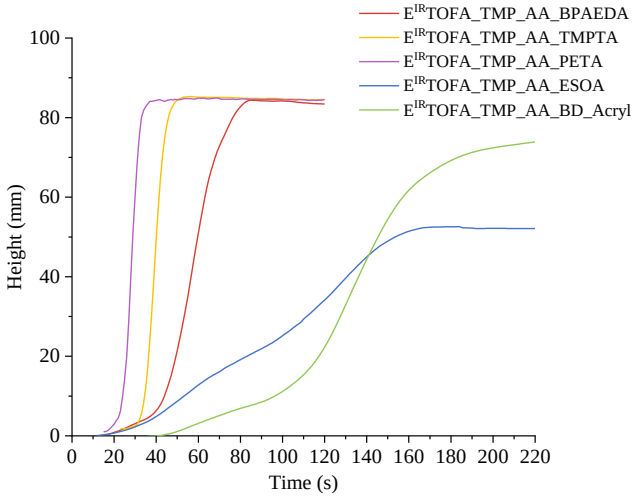

Fig. 4.2. The rise curve of the rise curve of developed polymer foam samples.

Table 4.1

Characteristic of Developed Foams Rising Profile

Polymer foam sample		Start time, s	Rise time, s
Bio-based donor and petrochemical-based acceptor	E^{IR}TOFA_TMP_AA_BPAEDA	42.9	79.5
	E^{IR}TOFA_TMP_AA_TMPTA	34.2	56.6
	E^{IR}TOFA_TMP_AA_PETA	20.5	34.8
Bio-based donor and bio-based acceptor	E^{IR}TOFA_TMP_AA_ESOA	57.9	163.7
	E^{IR}TOFA_TMP_AA_BD_Acryl	87.6	187.8

From DSC data (Fig. 4.3 a) for foams derived from a combination of bio-based donors and petrochemical-based acceptors, the $T_{g(DSC)}$ values ranged from 16.8 °C for E^{IR}TOFA_TMP_AA_BPAEDA to 85.5 °C for E^{IR}TOFA_TMP_AA_PETA. Notably, the E^{IR}TOFA_TMP_AA_PETA foam, which incorporated a tetra-functional acrylate, exhibited the highest $T_{g(DSC)}$ because of a more cross-linked and rigid structure. In contrast, foams with bio-based donor and bio-based acceptor components displayed lower $T_{g(DSC)}$ values, with E^{IR}TOFA_TMP_AA_ESOA and E^{IR}TOFA_TMP_AA_BD_Acryl registering negative $T_{g(DSC)}$ values of −1.9 °C and −9.7 °C, respectively. These differences highlight the influence of raw material sources (bio-based, petrochemical) and chemical structures (functionality, branching, molecular weight) on the properties of the resulting polymer foams. The same trend was observed in the case of DMA tests when determining $T_{g(DMA)}$ values from the tanδ curves (Fig. 4.3 b).

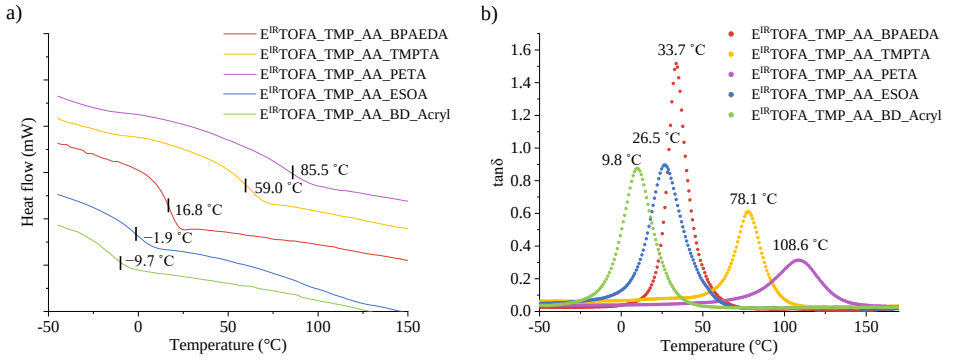

Fig. 4.3. DSC (10 °C·min^{-1}) and DMA (3 °C·min^{-1}, 1 Hz, 5 N) results of developed polymer foams: a) DSC curves; b) DMA tanδ.

The thermal degradation process of the developed polymer was determined by TGA (Fig. 4.4). For foams derived from bio-based donor and petrochemical-based acceptor, the functionality of the acrylate plays a pivotal role in determining the onset temperature. Although the temperatures were relatively similar, foam E^{IR}TOFA_TMP_AA_PETA formulated with a tetra-functional acrylate exhibited the highest onset temperature of 374.6 °C, followed by foam E^{IR}TOFA_TMP_AA_TMPTA formulated with the trifunctional acrylate, and E^{IR}TOFA_TMP_AA_BPAEDA with the difunctional acrylate. The increase in functionality of the acrylate and cross-link density of the polymer network results in enhanced thermal stability. This observation aligns with other studies found in the literature [100].

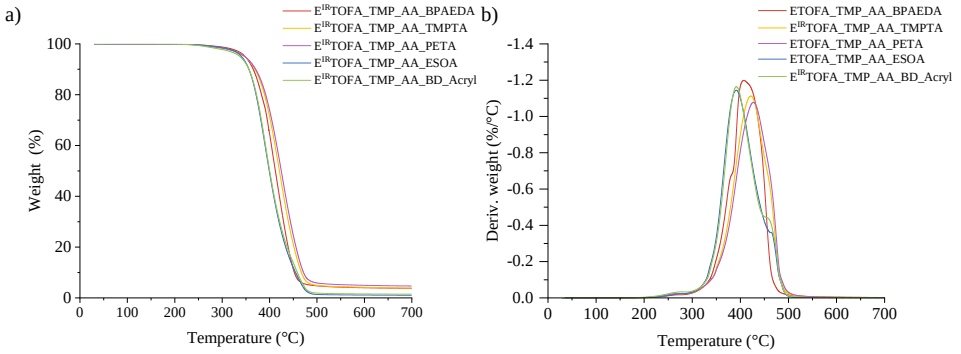

Fig. 4.4. TGA (10 °C·min^{-1}) weight loss and derivative curves of developed polymer foam samples.

E^{IR}TOFA_TMP_AA_ESOA and E^{IR}TOFA_TMP_AA_BD_Acryl exhibited onset temperatures of 354.8 °C and 359.6 °C, respectively. These values were slightly lower than those observed for partly petrochemical-based foams, suggesting a somewhat reduced thermal stability for the bio-based samples. This could be attributed to the inherent molecular structures of bio-based materials.

When considering the residue left at 675 °C, the bio-based foams leave significantly lower amounts, with E^{IR}TOFA_TMP_AA_ESOA and E^{IR}TOFA_TMP_AA_BD_Acryl registering residues of 1.02 % and 1.50 %, respectively. Among the partly petrochemical-based foams, E^{IR}TOFA_TMP_AA_PETA left the highest residue of 4.65 %, followed by E^{IR}TOFA_TMP_AA_TMPTA and E^{IR}TOFA_TMP_AA_BPAEDA. This indicates that

polymer foams obtained from higher functionality acrylates tend to form a more stable char structure during thermal degradation.

The thermal conductivity coefficient (λ) of the foams showed a clear correlation with their composition (Table 4.2). Notably, foams with petrochemical-based acceptors generally exhibited lower λ values, indicating better thermal insulation capabilities. One possible reason was the higher closed cell content (E^{IR}TOFA_TMP_AA_TMPTA, E^{IR}TOFA_TMP_AA_PETA). For instance, E^{IR}TOFA_TMP_AA_PETA, with a λ of 30.7 $mW\cdot(m\cdot K)^{-1}$, demonstrated the effectiveness of incorporating petrochemical components in enhancing thermal insulation. Conversely, foams from both bio-based Michael components exhibited higher λ values (46.7 $mW\cdot(m\cdot K)^{-1}$ and 44.5 $mW\cdot(m\cdot K)^{-1}$). On the other hand, the thermal insulation properties of the developed foams are good compared to other innovative insulation materials produced from bio-based and/or recycled feedstock. Liao et al. investigated cellulose-based multifunctional foam with a λ of 48.2 $mW\cdot(m\cdot K)^{-1}$, emphasizing good thermal insulation properties [101]. Pal et al. reported other insulation materials with good thermal conductivity, highlighting cork (40 $mW\cdot(m\cdot K)^{-1}$), recycled glass (44 $mW\cdot(m\cdot K)^{-1}$), recycled cotton (42 $mW\cdot(m\cdot K)^{-1}$), and glass wool (40 $mW\cdot(m\cdot K)^{-1}$) as effective alternatives making them suitable for various building applications [102].

As can be seen, λ depends on both the apparent density and the closed-cell content. Foams with higher closed-cell content typically demonstrate better thermal insulation properties. In this context, the partly petrochemical-based foams (from TMPTA and PETA) generally exhibited higher closed-cell contents, as seen in E^{IR}TOFA_TMP_AA_PETA with a V_{closed} of 72.4 %. This suggests that the incorporation of petrochemical components may contribute to a more closed-cell structure. Higher apparent density was observed in foams from both bio-based Michael components compared to foams from petrochemical Michael acceptor. This difference in apparent density can be attributed to the intrinsic material properties of both bio-based components, which might lead to a more compact structure, resulting in worse thermal insulation properties.

Table 4.2

The Thermal Cconductivity, Apparent Density, and Closed-Cell Content of Developed Foams

Polymer foam sample		**λ, $mW\cdot(m\cdot K)^{-1}$**	**Apparent ρ, $kg\cdot m^{-3}$**	**V_{closed}, %**
Bio-based donor and petrochemical-based acceptor	E^{IR}TOFA_TMP_AA_BPAEDA	38.8	110.1	7.7
	E^{IR}TOFA_TMP_AA_TMPTA	32.3	111.1	68.7
	E^{IR}TOFA_TMP_AA_PETA	30.7	108.1	72.4
Bio-based donor and bio-based acceptor	E^{IR}TOFA_TMP_AA_ESOA	46.7	173.8	32.7
	E^{IR}TOFA_TMP_AA_BD_Acryl	44.5	143.9	45.3

To enhance the thermal insulation of foams derived from both bio-based Michael components, exploring alternative, more suitable additives such as blowing agents and surfactants could be crucial in creating a foam structure more apt for insulation purposes. This research provides only an insight into the development of bio-based polymer foams using the Michael reaction as additives using chemicals suitable for the most popular closed-cell foam materials – rigid polyurethane foams [103].

The SEM images (Table 4.3) showed the morphology of the developed thermoset foams. Across the images, there was a noticeable consistency in cell shape and distribution, which is important for the foam's performance in its intended application.

E^{IR}TOFA_TMP_AA_BPAEDA foam was marked by its large pores (~ 410 µm). E^{IR}TOFA_TMP_AA_TMPTA foams present a tighter, more uniform pore structure with visibly smaller pores (~ 260 µm) than E^{IR}TOFA_TMP_AA_BPAEDA foam.

Table 4.3

SEM Images of the Foams, Taken Parallel and Perpendicular to the Direction of Foaming

Polymer foam sample	X perpendicular to the direction of foaming	Z parallel to the direction of foaming
E^{IR}TOFA_TMP_AA_BPAEDA	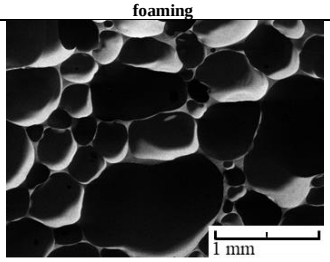	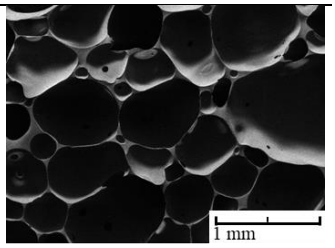
E^{IR}TOFA_TMP_AA_TMPTA	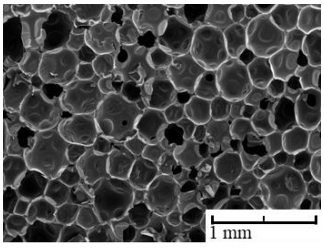	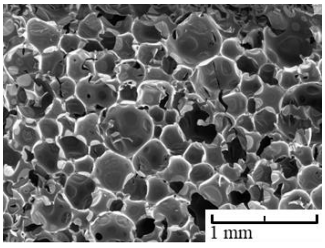
E^{IR}TOFA_TMP_AA_PETA	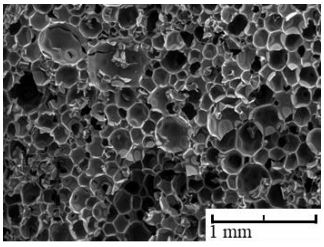	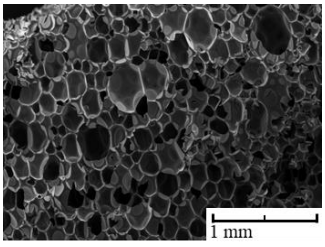
E^{IR}TOFA_TMP_AA_ESOA	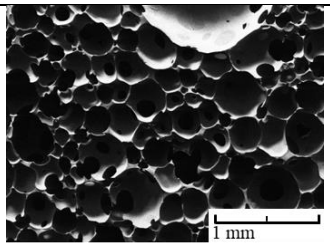	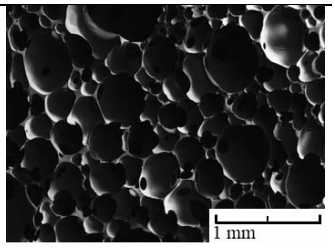
E^{IR}TOFA_TMP_AA_BD_Acryl	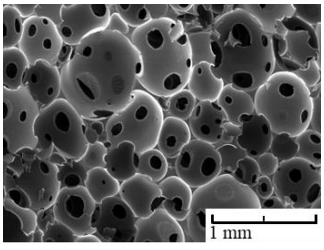	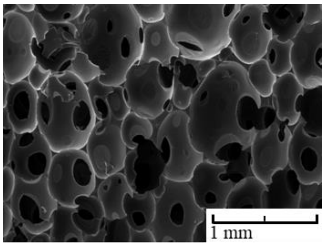

It was clearly visible that the functionality of the used monomer significantly influenced the cell size of polymer foams. Monomers with higher functionality, like PETA (f = 4), tended to form highly cross-linked networks, leading to smaller cells (~ 150 µm). In contrast, monomers with lower functionality, such as BPAEDA (f = 2), resulted in foam with larger cell sizes, as there were fewer cross-linking points, allowing more significant expansion and resulting in a softer foam. TMPTA with intermediate functionality (f = 3) produced a medium cell size.

The foams, especially E^{IR}TOFA_TMP_AA_BPAEDA and foams from bio-based donor and bio-based acceptor, had an open-cell structure. The varying sizes and interconnected nature of the cells can be particularly effective for sound absorption. The irregularities in cell size and inter-connected porosity can help trap and dissipate sound waves at different frequencies, making the foam a good candidate for acoustic insulation [104]. In applications like padding or insulation where air circulation is beneficial, the open cells provide breathability, which can contribute to thermal comfort [105].

There were no significant morphological differences between the cuts parallel and perpendicular to the direction of foam growth. The pore structure, size, and distribution appeared consistent across both orientations, suggesting quite isotropic foam characteristics. Only sample E^{IR}TOFA_TMP_AA_BD_Acryl indicated possible pore size anisotropy in parallel cut to the direction of foam growth. E^{IR}TOFA_TMP_AA_BD_Acryl foam had an average cell size of 360 µm in perpendicular to the direction of foaming, but in parallel to the direction of foaming the average width was 360 µm, but average length was 560 µm.

The compression strength and modulus were evaluated both parallel (Z) and perpendicular (X) to the direction of foam rise of developed polymer foams (Fig. 4.5 and Table 4.4). E^{IR}TOFA_TMP_AA_BPAEDA, E^{IR}TOFA_TMP_AA_TMPTA, and E^{IR}TOFA_TMP_AA_PETA foams demonstrated varying degrees of compression strength. E^{IR}TOFA_TMP_AA_BPAEDA foam, with compression strengths of 0.0073 MPa in the X direction and 0.0092 MPa in the Z direction, were less rigid and more flexible, potentially useful in applications where flexibility is a key requirement. In contrast, E^{IR}TOFA_TMP_AA_TMPTA and E^{IR}TOFA_TMP_AA_PETA foams exhibited much higher compression strengths (~ 0.27 MPa and ~ 0.40 MPa, respectively), indicating a more rigid structure. This allows for foams to be used as a thermal insulation material or other potential applications for civil engineering. This rigidity makes these materials suitable for applications where higher mechanical strength and load-bearing capability are essential.

Additionally, the variation in compression strength between the X and Z directions, especially for E^{IR}TOFA_TMP_AA_BD_Acryl foam, pointed to a slight anisotropic nature of these materials. The slight anisotropy of the materials can be explained by the differences in the cell morphology. This anisotropy is crucial in applications where the direction of stress application varies. Contrarily, E^{IR}TOFA_TMP_AA_TMPTA, E^{IR}TOFA_TMP_AA_PETA and E^{IR}TOFA_TMP_AA_ESOA foams showed isotropic compression strength properties.

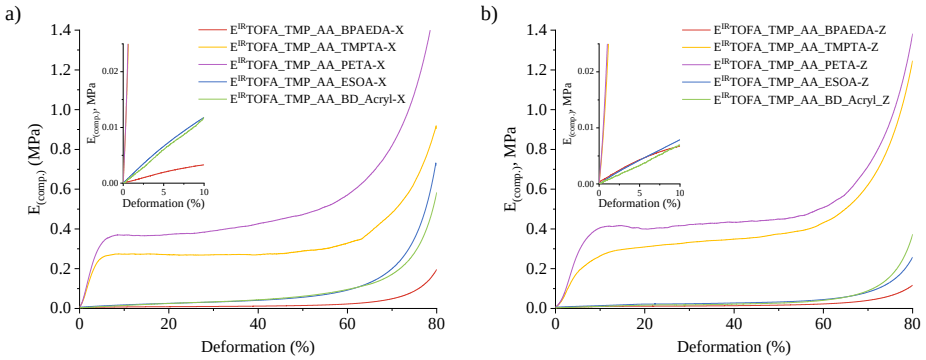

Fig. 4.5. Compression test (pre-load 2 N, 2 %·min^{-1}) curves of foam: a) perpendicular (X) to the direction of foam rise; b) parallel (Z) to the direction of foam.

Abolins et al. developed rigid polyurethane foams based on various formulations of tall oil polyols with a λ of around 22 mW·(m·K)$^{-1}$ and compression strength of around 0.2 MPa, a value typical for materials used in civil engineering applications [38]. Although rigid polyurethane foams have slightly better thermal insulation capabilities and lower apparent density, there is a reason to believe that in this work obtained materials can compete with partly bio-based polyurethane foam materials in this area because the foam materials obtained in this study have significantly better compressive strength in the case of foam, reaching up to 0.4 MPa. The decrease of the apparent density could be achieved by the optimization of the foaming process, catalyst package and blowing agent content.

Table 4.4

The Mechanical Properties of Developed Foams

Polymer foam sample		**X**		**Z**	
		***E*(comp.), MP**	**σ10%, MPa**	***E*(comp.), MPa**	**σ10%, MPa**
Bio-based donor and petrochemical-based acceptor	E^{IR}TOFA_TMP_AA_BPAEDA	0.041	0.0073	0.079	0.0092
	E^{IR}TOFA_TMP_AA_TMPTA	7.6	0.274	5.1	0.263
	E^{IR}TOFA_TMP_AA_PETA	9.7	0.39	7.6	0.400
Bio-based donor and bio-based acceptor	E^{IR}TOFA_TMP_AA_ESOA	0.10	0.0158	0.12	0.0147
	E^{IR}TOFA_TMP_AA_BD_Acryl	0.12	0.0111	0.09	0.0074

CONCLUSIONS

1. Precursors for the Michael components can be successfully synthesised from tall oil fatty acids through double bond epoxidation and subsequent cleavage of oxirane rings and esterification of carboxyl groups with alcohols. Further from precursors can be synthesised:
    - the Michael donors by a transesterification reaction of hydroxyl groups with *tert*-butyl acetoacetate;
    - the Michael acceptors by acylation reaction of hydroxyl groups with acryloyl chloride.

2. Polymers from tall oil-based Michael donors and petrochemical Michael acceptors (bisphenol A ethoxylate diacrylate, trimethylolpropane triacrylate, pentaerythritol tetraacrylate) were successfully developed. By using components with lower functionality, viscoelastic polymeric materials with rubber-like properties can be synthesised (E^{IR}TOFA_BD_AA_BPAEDA: $E_{(tensile)}$ = 8 MPa, σ_{max} = 4 MPa, ε = 55 %), while the use of higher functionality components allows to obtain rigid, glassy polymer materials (E^{IR}TOFA_TMP_AA_PETA: $E_{(tensile)}$ 2370 MPa, σ_{max} = 44 MPa, ε = 1.9 %).

3. Polymers from tall oil-based Michael donors and tall oil-based Michael acceptors were successfully developed. The polymers derived from E^{IR}TOFA_BD_Acryl exhibited the viscoelastic properties (E^{IR}TOFA_BD_AA_BD_Acryl: $E_{(tensile)}$ = 15 MPa, σ_{max} =0.9 MPa, ε = 27 %), while E^{IR}TOFA_TMP_Acryl exhibited properties more like rigid, glassy resins (E^{IR}TOFA_TMP_AA_TMP_Acryl: $E_{(tensile)}$ = 1760 MPa, σ_{max} = 16.1 MPa, ε = 17 %).

4. Polymer foams from tall oil-based Michael donor combined with various origins Michael acceptor (petrochemical-based – bisphenol A ethoxylate diacrylate, trimethylolpropane triacrylate, pentaerythritol tetraacrylate – and bio-based – epoxidized soybean oil acrylate, synthesised tall oil-based acrylate) were successfully developed *via* the Michael reaction. Bio-based donor and petrochemical-based acceptor foams demonstrated high glass transition temperatures (up to 85.5 °C by DSC, 108.6 °C by DMA), excellent thermal insulation (as low as 30.7 $mW \cdot (m \cdot K)^{-1}$), and great mechanical strength (around 0.40 MPa). Polymer foam from bio-based both Michael components was characterized by properties fitting for flexible foam applications. All foams exhibited high thermal stability up to 350 °C.

REFERENCES

[1] D. Feldman, Polymeric foam materials for insulation in buildings, Mater. Energy Effic. Therm. Comf. Build. (2010) 257–273. https://doi.org/10.1533/9781845699277.2.257.

[2] M. Niaounakis, Foaming and Foamed Products, in: Biopolym. Process. Prod., Elsevier Science, 2015: pp. 327–359. https://doi.org/10.1016/B978-0-323-26698-7.00009-X.

[3] A. Baroutaji, A. Arjunan, A. Niknejad, T. Tran, A.-G. Olabi, Application of Cellular Material in Crashworthiness Applications: An Overview, Elsevier Ltd., 2019. https://doi.org/10.1016/b978-0-12-803581-8.09268-7.

[4] M. Y. Lyu, T. G. Choi, Research trends in polymer materials for use in lightweight vehicles, Int. J. Precis. Eng. Manuf. 16 (2015) 213–220. https://doi.org/10.1007/s12541-015-0029-x.

[5] F. M. De Souza, Y. Desai, R. K. Gupta, Introduction to Polymeric Foams, ACS Symp. Ser. 1439 (2023) 1–23. https://doi.org/10.1021/bk-2023-1439.ch001.

[6] S. Siengchin, A review on lightweight materials for defence applications: Present and future developments, Def. Technol. 24 (2023) 1–17. https://doi.org/10.1016/j.dt.2023.02.025.

[7] F. L. Jin, M. Zhao, M. Park, S. J. Park, Recent trends of foaming in polymer processing: A review, Polymers (Basel). 11 (2019). https://doi.org/10.3390/polym11060953.

[8] G. Wu, P. Xie, H. Yang, K. Dang, Y. Xu, M. Sain, L. S. Turng, W. Yang, A review of thermoplastic polymer foams for functional applications, J. Mater. Sci. 56 (2021) 11579–11604. https://doi.org/10.1007/s10853-021-06034-6.

[9] L. Li, D. Xu, S. Bai, N. Chen, Q. Wang, Progress in preparation of high-performance and multi-functional polymer foams, J. Polym. Sci. (2023) 1–15. https://doi.org/10.1002/pol.20230490.

[10] Z. Wang, C. Wang, Y. Gao, Z. Li, Y. Shang, H. Li, Porous Thermal Insulation Polyurethane Foam Materials, Polymers (Basel). 15 (2023) 3818. https://doi.org/10.3390/polym15183818.

[11] S. B. Murmu, Alternatives derived from renewable natural fibre to replace conventional polyurethane rigid foam insulation, Clean. Eng. Technol. 8 (2022) 100513. https://doi.org/10.1016/j.clet.2022.100513.

[12] A. Agrawal, R. Kaur, R. S. Walia, PU foam derived from renewable sources: Perspective on properties enhancement: An overview, Eur. Polym. J. 95 (2017) 255–274. https://doi.org/10.1016/j.eurpolymj.2017.08.022.

[13] N. Singh, O. A. Ogunseitan, M. H. Wong, Y. Tang, Sustainable materials alternative to petrochemical plastics pollution: A review analysis, Sustain. Horizons. 2 (2022). https://doi.org/10.1016/j.horiz.2022.100016.

[14] J. G. Rosenboom, R. Langer, G. Traverso, Bioplastics for a circular economy, Nat. Rev. Mater. 7 (2022) 117–137. https://doi.org/10.1038/s41578-021-00407-8.

[15] European Commission, The European Green Deal, Eur. Comm. 53 (2019) 24. https://doi.org/10.1017/CBO9781107415324.004.

[16] A. Di Bartolo, G. Infurna, N. T. Dintcheva, A Review of Bioplastics and Their Adoption in the Circular Economy, Polymers (Basel). 13 (2021) 1229. https://doi.org/10.3390/polym13081229.

[17] M. Kircher, Bioeconomy: Markets, Implications and Investment Opportunities, 2019.

[18] S. A. Madbouly, Novel recycling processes for thermoset polyurethane foams, Curr. Opin. Green Sustain. Chem. 42 (2023) 100835. https://doi.org/10.1016/j.cogsc.2023.100835.

[19] S. E. Dechent, A. W. Kleij, G. A. Luinstra, Fully bio-derived CO2 polymers for non-isocyanate based polyurethane synthesis, Green Chem. 22 (2020) 969–978. https://doi.org/10.1039/c9gc03488a.

[20] J. Sternberg, S. Pilla, Materials for the biorefinery: High bio-content, shape memory Kraft lignin-derived non-isocyanate polyurethane foams using a non-toxic protocol,

Green Chem. 22 (2020) 6922–6935. https://doi.org/10.1039/d0gc01659d.
[21] C. D. Lindsay, C. M. Timperley, TRPA1 and issues relating to animal model selection for extrapolating toxicity data to humans, Hum. Exp. Toxicol. 39 (2020) 14–36. https://doi.org/10.1177/0960327119877460.
[22] M. Kathalewar, A. Sabnis, D. D'Mello, Isocyanate free polyurethanes from new CNSL based bis-cyclic carbonate and its application in coatings, Eur. Polym. J. 57 (2014) 99–108. https://doi.org/10.1016/j.eurpolymj.2014.05.008.
[23] M. S. Kathalewar, P. B. Joshi, A. S. Sabnis, V. C. Malshe, Non-isocyanate polyurethanes: From chemistry to applications, RSC Adv. 3 (2013) 4110–4129. https://doi.org/10.1039/c2ra21938g.
[24] S. Sambhudevan, H. S, A. Reghunadhan, Polyurethane from Sustainable Routes, in: Polyurethane Chem. Renew. Polyols Isocyanates, American Chemical Society, 2021: pp. 75–106. https://doi.org/10.1021/bk-2021-1380.ch004.
[25] M. Włoch, K. Błażek, Isocyanate-Free Polyurethanes, in: 2021: pp. 107–166. https://doi.org/10.1021/bk-2021-1380.ch005.
[26] J. Niesiobędzka, J. Datta, Challenges and recent advances in bio-based isocyanate production, Green Chem. 25 (2023) 2482–2504. https://doi.org/10.1039/d2gc04644j.
[27] G. Coste, C. Negrell, L. Averous, S. Caillol, Green Synthesis of Biobased Soft Foams by the Aza-Michael Reaction, ACS Sustain. Chem. Eng. 10 (2022) 8549–8558. https://doi.org/10.1021/acssuschemeng.2c01885.
[28] A. O. Konuray, F. Liendo, X. Fernández-Francos, À. Serra, M. Sangermano, X. Ramis, Sequential curing of thiol-acetoacetate-acrylate thermosets by latent Michael addition reactions, Polymer (Guildf). 113 (2017) 193–199. https://doi.org/10.1016/j.polymer.2017.02.072.
[29] Q. Jiang, Y. L. Zhang, Y. Du, M. Tang, L. Jiang, W. Huang, H. Yang, X. Xue, B. Jiang, Preparation of hyperbranched polymers by oxa-Michael addition polymerization, Polym. Chem. 11 (2020) 1298–1306. https://doi.org/10.1039/c9py01686d.
[30] Z. Ma, Y. Zeng, X. He, S. Pan, Y. Wei, B. Wang, L. Tao, Introducing the aza-Michael addition reaction between acrylate and dihydropyrimidin-2(1H)-thione into polymer chemistry, Polym. Chem. 13 (2022) 6322–6327. https://doi.org/10.1039/D2PY01130A.
[31] S. R. Williams, K. M. Miller, T. E. Long, Michael addition reaction kinetics of acetoacetates and acrylates for the formation of polymeric networks, Prog. React. Kinet. Mech. 32 (2007) 165–194. https://doi.org/10.3184/146867807X247730.
[32] M. Iwamura, Y. Gotoh, T. Hashimoto, R. Sakurai, Michael addition reactions of acetoacetates and malonates with acrylates in water under strongly alkaline conditions, Tetrahedron Lett. 46 (2005) 6275–6277. https://doi.org/10.1016/j.tetlet.2005.07.045.
[33] A. O. Konuray, A. Ruiz, J. M. Morancho, J. M. Salla, X. Fernández-Francos, À. Serra, X. Ramis, Sequential dual curing by selective Michael addition and free radical polymerization of acetoacetate-acrylate-methacrylate mixtures, Eur. Polym. J. 98 (2018) 39–46. https://doi.org/10.1016/j.eurpolymj.2017.11.003.
[34] M. Gould, T. Hammond, S. Narayan-Sarathy, Radiation Curable Michael Addition Resins Having Built-In Photoinitiators, US20050261388A1, 2005.
[35] B.D. Mather, K. Viswanathan, K.M. Miller, T.E. Long, Michael addition reactions in macromolecular design for emerging technologies, Prog. Polym. Sci. 31 (2006) 487–531. https://doi.org/10.1016/j.progpolymsci.2006.03.001.
[36] V. Aryan, A. Kraft, The crude tall oil value chain: Global availability and the influence of regional energy policies, J. Clean. Prod. 280 (2021) 124616. https://doi.org/10.1016/j.jclepro.2020.124616.
[37] L. Vevere, A. Fridrihsone, M. Kirpluks, U. Cabulis, A review of wood biomass-based fatty acids and rosin acids use in polymeric materials, Polymers (Basel). 12 (2020) 1–17. https://doi.org/10.3390/polym12112706.
[38] A. Abolins, R. Pomilovskis, E. Vanags, I. Mierina, S. Michalowski, A. Fridrihsone, M. Kirpluks, Impact of different epoxidation approaches of tall oil fatty acids on rigid polyurethane foam thermal insulation, Materials (Basel). 14 (2021) 1–17.

https://doi.org/10.3390/ma14040894.
[39] A. Saputra, P. Satwikanitya, F. Puspita, M. W. Sya'bani, M. F. Agustian, W. Pambudi, Synthesis of epoxy oil from Waste Cooking Oil (WCO) using acetic acid and amberlite resin IR-120 as catalyst, Eng. Appl. Sci. Res. 50 (2023) 335–342. https://doi.org/10.14456/easr.2023.36.
[40] M. C. Hennessy, T.P. O'Sullivan, Recent advances in the transesterification of β-keto esters, RSC Adv. 11 (2021) 22859–22920. https://doi.org/10.1039/d1ra03513d.
[41] H. Zuo, Z. Cao, J. Shu, D. Xu, J. Zhong, J. Zhao, T. Wang, Y. Chen, F. Gao, L. Shen, Effect of structure on the properties of ambient-cured coating films prepared via a Michael addition reaction based on an acetoacetate-modified castor oil prepared by thiol-ene coupling, Prog. Org. Coatings. 135 (2019) 27–33. https://doi.org/10.1016/j.porgcoat.2019.05.032.
[42] R. K. Pandey, P. Kumar, A facile procedure for transesterification of β-keto esters promoted by ceria-yttria based Lewis acid catalyst, Catal. Commun. 8 (2007) 1122–1125. https://doi.org/10.1016/j.catcom.2006.10.031.
[43] R. A. Omer, A. Hughes, J. R. Hama, W. Wang, H. Tai, Hydrogels from dextran and soybean oil by UV photo-polymerization, J. Appl. Polym. Sci. 132 (2015) 1–10. https://doi.org/10.1002/app.41446.
[44] A. Luo, X. Jiang, H. Lin, J. Yin, "Thiol-ene" photo-cured hybrid materials based on POSS and renewable vegetable oil, J. Mater. Chem. 21 (2011) 12753–12760. https://doi.org/10.1039/c1jm11425e.
[45] D. Kim, S. Kim, S. Jeong, M. Kim, W. K. Hong, H. B. Jeon, H. Y. Cho, S. M. Noh, H. jong Paik, Thermally latent vinyl crosslinking of polymers via sulfoxide chemistry, Eur. Polym. J. 179 (2022) 111520. https://doi.org/10.1016/j.eurpolymj.2022.111520.
[46] Z. Cao, F. Gao, J. Zhao, X. Wei, Q. Cheng, J. Zhong, C. Lin, J. Shu, C. Fu, L. Shen, Bio-based coating materials derived from acetoacetylated soybean oil and aromatic dicarboxaldehydes, Polymers (Basel). 11 (2019). https://doi.org/10.3390/polym11111809.
[47] X. He, J. Zhong, Z. Cao, J. Wang, F. Gao, D. Xu, L. Shen, An exploration of the Knoevenagel condensation to create ambient curable coating materials based on acetoacetylated castor oil, Prog. Org. Coatings. 129 (2019) 21–25. https://doi.org/10.1016/j.porgcoat.2018.12.015.
[48] A. S. Trevino, D.L. Trumbo, Acetoacetylated castor oil in coatings applications, Prog. Org. Coatings. 44 (2002) 49–54. https://doi.org/10.1016/S0300-9440(01)00223-5.
[49] D. Xu, Z. Cao, T. Wang, J. Zhong, J. Zhao, F. Gao, X. Luo, Z. Fang, J. Cao, S. Xu, L. Shen, An ambient-cured coating film obtained via a Knoevenagel and Michael addition reactions based on modified acetoacetylated castor oil prepared by a thiol-ene coupling reaction, Prog. Org. Coatings. 135 (2019) 510–516. https://doi.org/10.1016/j.porgcoat.2019.06.026.
[50] Y. Zhu, F. Gao, J. Zhong, L. Shen, Y. Lin, Renewable castor oil and DL-limonene derived fully bio-based vinylogous urethane vitrimers, Eur. Polym. J. 135 (2020) 109865. https://doi.org/10.1016/j.eurpolymj.2020.109865.
[51] T. Wang, J. Wang, X. He, Z. Cao, D. Xu, F. Gao, J. Zhong, L. Shen, An Ambient Curable Coating Material Based on the Michael Addition Reaction of Acetoacetylated Castor Oil and Multifunctional Acrylate, Coatings. 9 (2019) 37. https://doi.org/10.3390/coatings9010037.
[52] E. M. Krall, E. M. Serum, M. P. Sibi, D. C. Webster, Catalyst-free ligin valorization by acetoacetylation. Structural elucidation by comparison with model compounds, Green Chem. 20 (2018) 2959–2966. https://doi.org/10.1039/c8gc01071d.
[53] J. S. Witzeman, W. D. Nottingham, Transacetoacetylation with tert-Butyl Acetoacetate: Synthetic Applications, J. Org. Chem. 56 (1991) 1713–1718. https://doi.org/10.1021/jo00005a013.
[54] M. Kirpluks, E. Vanags, A. Abolins, S. Michalowski, A. Fridrihsone, U. Cabulis, High functionality bio-polyols from tall oil and rigid polyurethane foams formulated solely

using bio-polyols, Materials (Basel). 13 (2020) 38–53. https://doi.org/10.3390/MA13081985.
[55] R. de V. V. Lopes, J.R. Zamian, I. S. Resck, M. J .A. Sales, M. L. Dos Santos, F. R. Da Cunha, Physicochemical and rheological properties of passion fruit oil and its polyol, Eur. J. Lipid Sci. Technol. 112 (2010) 1253–1262. https://doi.org/10.1002/ejlt.201000098.
[56] W. T. Petroskey, L. Gott, T. E. Carter, Acetoacetylation: a Process for Polyol Viscosity Reduction, J. Cell. Plast. 29 (1993) 458–459. https://doi.org/10.1177/0021955X9302900565.
[57] J. Sung, X. S. Sun, Cardanol modified fatty acids from camelina oils for flexible bio-based acrylates coatings, Prog. Org. Coatings. 123 (2018) 242–253. https://doi.org/10.1016/j.porgcoat.2018.02.008.
[58] J. La Scala, R. P. Wool, The effect of fatty acid composition on the acrylation kinetics of epoxidized triacylglycerols, J. Am. Oil Chem. Soc. 79 (2002) 59–63. https://doi.org/10.1007/s11746-002-0435-4.
[59] A. M. Salih, M. Bin Ahmad, N. A. Ibrahim, K. Z. HjMohd Dahlan, R. Tajau, M. H. Mahmood, W. M. Z. W. Yunus, Synthesis of radiation curable palm oil-based epoxy acrylate: NMR and FTIR spectroscopic investigations, Molecules. 20 (2015) 14191–14211. https://doi.org/10.3390/molecules200814191.
[60] G. Wuzella, A. R. Mahendran, U. Müller, A. Kandelbauer, A. Teischinger, Photocrosslinking of an Acrylated Epoxidized Linseed Oil: Kinetics and its Application for Optimized Wood Coatings, J. Polym. Environ. 20 (2012) 1063–1074. https://doi.org/10.1007/s10924-012-0511-9.
[61] Y. Xia, R.C. Larock, Vegetable oil-based polymeric materials: Synthesis, properties, and applications, Green Chem. 12 (2010) 1893–1909. https://doi.org/10.1039/c0gc00264j.
[62] Y. Gan, X. Jiang, Photo-cured materials from vegetable oils, RSC Green Chem. 2015-Janua (2015) 1–27. https://doi.org/10.1039/9781782621850-00001.
[63] Y. Su, H. Lin, S. Zhang, Z. Yang, T. Yuan, One-Step synthesis of novel renewable vegetable oil-based acrylate prepolymers and their application in UV-curable coatings, Polymers (Basel). 12 (2020) 1–13. https://doi.org/10.3390/POLYM12051165.
[64] P. Zhang, J. Xin, J. Zhang, Effects of catalyst type and reaction parameters on one-step acrylation of soybean oil, ACS Sustain. Chem. Eng. 2 (2014) 181–187. https://doi.org/10.1021/sc400206t.
[65] P. Zhang, J. Zhang, One-step acrylation of soybean oil (SO) for the preparation of SO-based macromonomers, Green Chem. 15 (2013) 641–645. https://doi.org/10.1039/c3gc36961g.
[66] R. Müller, G. Wilke, Synthesis and radiation curing of acrylated castor oil glycerides, J. Coatings Technol. Res. 11 (2014) 873–882. https://doi.org/10.1007/s11998-014-9596-5.
[67] N. Liu, New polymers synthesis by organocatalyzed step-growth polymerization of aldehydic monomers : polyaldols, linear polybenzoin and hyperbranched polyacetals, (2014). https://tel.archives-ouvertes.fr/tel-01081197.
[68] M. F. Sonnenschein, J. B. Werness, K. A. Patankar, X. Jin, M. Z. Larive, From rigid and flexible foams to elastomers via Michael addition chemistry, Polymer (Guildf). 106 (2016) 128–139. https://doi.org/10.1016/j.polymer.2016.10.054.
[69] G. Ozturk, T. E. Long, Michael addition for crosslinking of poly(caprolactone)s, J. Polym. Sci. Part A Polym. Chem. 47 (2009) 5437–5447. https://doi.org/10.1002/pola.23593.
[70] T. Balotupi, T. Lanta, D.A.N.P.K. Rzwpk, WO 2013/101682 Al, 2016.
[71] M. Y. Zhaoo, C.-P. Hsu, S. L. Voeks, R. Landtiser, WO 2013/132077 Al, 2013.
[72] I. Bureau, FUNCTIONALIZED OLIGOMERS, WO/2014/052081, 2014.
[73] J. C. Q. Amado, Thermal Resistance Properties of Polyurethanes and its Composites: A Short Review, J. Res. Updat. Polym. Sci. (2019) 66–84. https://doi.org/10.6000/1929-5995.2019.08.10.
[74] L. Shufen, J. Zhi, Y. Kaijun, Y. Shuqin, W. K. Chow, Studies on the thermal behavior

of polyurethanes, Polym. – Plast. Technol. Eng. 45 (2006) 95–108. https://doi.org/10.1080/03602550500373634.
[75] F. A. Zhang, D. K. Lee, T .J. Pinnavaia, PMMA-mesocellular foam silica nanocomposites prepared through batch emulsion polymerization and compression molding, Polymer (Guildf). 50 (2009) 4768–4774. https://doi.org/10.1016/j.polymer.2009.08.007.
[76] T. Rajkumar, N. Muthupandiyan, C. T. Vijayakumar, Synthesis and investigation of thermal properties of PMMA-maleimide-functionalized reduced graphene oxide nanocomposites, J. Thermoplast. Compos. Mater. 33 (2020) 85–96. https://doi.org/10.1177/0892705718804595.
[77] J. S. Bermejo, C. M. Ugarte, Influence of cross-linking density on the glass transition and structure of chemically cross-linked PVA: A molecular dynamics study, Macromol. Theory Simulations. 18 (2009) 317–327. https://doi.org/10.1002/mats.200900032.
[78] M. K. Hassan, S. J. Tucker, A. Abukmail, J. S. Wiggins, K. A. Mauritz, Polymer chain dynamics in epoxy based composites as investigated by broadband dielectric spectroscopy, Arab. J. Chem. 9 (2016) 305–315. https://doi.org/10.1016/j.arabjc.2015.07.016.
[79] V. J. Dave, H. S. Patel, Synthesis and characterization of interpenetrating polymer networks from transesterified castor oil based polyurethane and polystyrene, J. Saudi Chem. Soc. 21 (2017) 18–24. https://doi.org/10.1016/j.jscs.2013.08.001.
[80] S. Chen, Q. Wang, X. Pei, T. Wang, Dynamic mechanical properties of castor oil-based polyurethane/epoxy graft interpenetrating polymer network composites, J. Appl. Polym. Sci. 116 (2010) n/a-n/a. https://doi.org/10.1002/app.32518.
[81] P. K. Menard, Dynamic analysis a practical introduction, CRC Press, New York, 1999.
[82] R. Hagen, L. Salmén, H. Lavebratt, B. Stenberg, Comparison of dynamic mechanical measurements and Tg determinations with two different instruments, Polym. Test. 13 (1994) 113–128. https://doi.org/10.1016/0142-9418(94)90020-5.
[83] C. A. Gracia-Fernández, S. Gómez-Barreiro, J. López-Beceiro, J. Tarrío Saavedra, S. Naya, R. Artiaga, Comparative study of the dynamic glass transition temperature by DMA and TMDSC, Polym. Test. 29 (2010) 1002–1006. https://doi.org/10.1016/j.polymertesting.2010.09.005.
[84] R. Rahul, R. Kitey, Effect of cross-linking on dynamic mechanical and fracture behavior of epoxy variants, Compos. Part B Eng. 85 (2016) 336–342. https://doi.org/10.1016/j.compositesb.2015.09.017.
[85] M. Fleischer, H. Blattmann, R. Mülhaupt, Glycerol-, pentaerythritol- and trimethylolpropane-based polyurethanes and their cellulose carbonate composites prepared via the non-isocyanate route with catalytic carbon dioxide fixation, Green Chem. 15 (2013) 934–942. https://doi.org/10.1039/c3gc00078h.
[86] A. Abolins, V. Yakushin, D. Vilsone, Properties of polyurethane coatings based on linseed oil phosphate ester polyol, J. Renew. Mater. 6 (2018) 737–745. https://doi.org/10.32604/JRM.2018.00119.
[87] V. Yakushin, A. Abolins, D. Vilsone, I. Sevastyanova, Polyurethane coatings based on linseed oil phosphate ester polyols with intumescent flame retardants, Fire Mater. 43 (2019) 92–100. https://doi.org/10.1002/fam.2672.
[88] W. Xie, S. Guo, Y. Liu, R. Chen, Q. Wang, Organic-inorganic hybrid strategy based on ternary copolymerization to prepare flame retardant poly(methyl methacrylate) with high performance, Compos. Part B Eng. 203 (2020) 108437. https://doi.org/10.1016/j.compositesb.2020.108437.
[89] U. Ali, K. J. B. A. Karim, N. A. Buang, A Review of the Properties and Applications of Poly (Methyl Methacrylate) (PMMA), Polym. Rev. 55 (2015) 678–705. https://doi.org/10.1080/15583724.2015.1031377.
[90] A. Ishigami, K. Watanabe, T. Kurose, H. Ito, Physical and morphological properties of tough and transparent PMMA-based blends modified with polyrotaxane, Polymers (Basel). 12 (2020). https://doi.org/10.3390/polym12081790.

[91] B. Noordover, W. Liu, E. McCracken, B. DeGooyer, R. Brinkhuis, F. Lunzer, Michael addition curable coatings from renewable resources with enhanced adhesion performance, J. Coatings Technol. Res. 17 (2020) 1123–1130. https://doi.org/10.1007/s11998-020-00351-2.
[92] N. Naga, M. Satoh, T. Magara, K. Ahmed, T. Nakano, Synthesis of gels by means of Michael addition reaction of multi-functional acetoacetate and diacrylate compounds and their application to ionic conductive gels, J. Polym. Sci. 59 (2021) 2129–2139. https://doi.org/10.1002/pol.20210388.
[93] N. Naga, M. Satoh, T. Magara, K. Ahmed, T. Nakano, Synthesis of porous polymers by means of Michael addition reaction of multifunctional acetoacetate and poly(ethylene glycol) diacrylate, Eur. Polym. J. 162 (2022) 110901. https://doi.org/10.1016/j.eurpolymj.2021.110901.
[94] M. Y. Cheong, Z. A. A. Hasan, Z. Idris, Characterisation of epoxidised trimethylolpropane trioleate:NMR and thermogravimetric analysis, J. Oil Palm Res. 31 (2019) 146–158. https://doi.org/10.21894/jopr.2018.0066.
[95] B. Liang, S. Kuang, J. Huang, L. Man, Z. Yang, T. Yuan, Synthesis and characterization of novel renewable tung oil-based UV-curable active monomers and bio-based copolymers, Prog. Org. Coatings. 129 (2019) 116–124. https://doi.org/10.1016/j.porgcoat.2019.01.007.
[96] M. Li, Y. Fang, C. Liu, M. Zhou, X. Miao, Y. Pei, Y. Yan, W. Xiao, H. Qiu, L. Wu, Facile generation of highly durable thiol-functionalized polyhedral oligomeric silsesquioxane based superhydrophobic melamine foam, Front. Chem. Sci. Eng. 16 (2022) 1247–1258. https://doi.org/10.1007/s11705-021-2124-0.
[97] D. Trumbo, N. Krogman, D. Nelson, A Method for Applying a Foam Composition Using Spray Foam Equipment, EP3783048A1, 2021.
[98] J. O. L. Robert, L. K.-E. Michelle, O.F. Nassreen, One-Part Non-Toxic Spray Foam, US2008281006A1, 2008.
[99] T. F. Kauffman, D. W. Whitman, M. J. Zajaczkowski, V. David Elmer, Biomass Based Michael Addition Compositions, US 2006/0069234 A1, 2006.
[100] G. F. Levchik, K. Si, S. V. Levchik, G. Camino, C. A. Wilkie, Correlation between cross-linking and thermal stability: Cross-linked polystyrenes and polymethacrylates, Polym. Degrad. Stab. 65 (1999) 395–403. https://doi.org/10.1016/S0141-3910(99)00028-2.
[101] J. Liao, Y. Hou, J. Li, M. Zhang, Y. Dong, X. Chen, Lightweight and recyclable hybrid multifunctional foam based cellulose fibers with excellent flame retardant, thermal, and acoustic insulation property, Compos. Sci. Technol. 244 (2023) 110315. https://doi.org/10.1016/j.compscitech.2023.110315.
[102] R. K. Pal, P. Goyal, S. Sehgal, Effect of cellulose fibre based insulation on thermal performance of buildings, Mater. Today Proc. 45 (2021) 5778–5781. https://doi.org/10.1016/j.matpr.2021.02.749.
[103] J. Andersons, R. Grūbe, L. Vēvere, P. Cābulis, M. Kirpluks, Anisotropic thermal expansion of bio-based rigid low-density closed-cell polyurethane foams, J. Mater. Res. Technol. 16 (2022) 1517–1525. https://doi.org/10.1016/j.jmrt.2021.12.094.
[104] A. Abbad, K. Jaboviste, M. Ouisse, N. Dauchez, Acoustic performances of silicone foams for sound absorption, J. Cell. Plast. 54 (2018) 651–670. https://doi.org/10.1177/0021955X17732305.
[105] B. E. Obi, Overview of Applications of Polymeric Foams, Polym. Foam. Struct. (2018) 3–14. https://doi.org/10.1016/b978-1-4557-7755-6.00001-x.

PIELIKUMI / APPENDICES

1. pielikums
Appendix 1

Fast-curing bio-based thermoset foams produced *via* the Michael 1,4-addition using fatty acid-based acetoacetate and acrylate

Ralfs Pomilovskis, Elīza Kauliņa, Arnis Āboliņš, Inese Mieriņa,
Anda Fridrihsone, Miķelis Kirpļuks

European Polymer Journal, 2024

European Polymer Journal 210 (2024) 112968

Contents lists available at ScienceDirect

European Polymer Journal

journal homepage: www.elsevier.com/locate/europolj

Fast-curing bio-based thermoset foams produced *via* the Michael 1,4-addition using fatty acid-based acetoacetate and acrylate

Ralfs Pomilovskis [a,b,*], Eliza Kaulina [a], Arnis Abolins [a], Inese Mierina [b], Ivo Heinmaa [c], Vitalijs Rjabovs [b], Anda Fridrihsone [a], Mikelis Kirpluks [a]

[a] Polymer Laboratory, Latvian State Institute of Wood Chemistry, Riga LV-1006, Latvia
[b] Institute of Chemistry and Chemical Technology, Faculty of Natural Sciences and Technology, Riga Technical University, Riga LV-1048, Latvia
[c] National Institute of Chemical Physics and Biophysics, Tallinn 12618, Estonia

ARTICLE INFO

Keywords:
Bio-based polymer foams
Free fatty acid-based polymer foams
The Michael 1,4-addition reaction
Michael monomers
Bio-based acetoacetates
Bio-based acrylates

ABSTRACT

This study introduces an approach for creating bio-based polymer foams exploiting the Michael reaction that could be utilized as thermal insulation. The thermoset foams were developed using a second-generation bio-based feedstock – tall oil. Tall oil is a by-product of wood pulping in paper manufacturing and mainly comprises unsaturated fatty acids like oleic and linoleic acid. The study explores the use of tall oil-based acetoacetates (Michael donor) combined with various acrylates (Michael acceptor), petrochemical-based (bisphenol-A ethoxylate diacrylate, trimethylolpropane triacrylate, pentaerythritol tetraacrylate), and bio-based (epoxidized soybean oil acrylate, epoxidized tall oil free fatty acids-based acrylate), to develop polymer foams that meet today's sustainability requirements. The developed polymer foams underwent extensive characterization. Matrix curing parameters were assessed by measuring changes in dielectric polarization during curing. Foaming parameters, including start and rise times, were precisely measured. The chemical composition of the foams was analysed using Fourier-transform infrared spectroscopy. Their thermal, thermo-mechanical, and mechanical properties were evaluated through thermal gravimetric analysis, differential scanning calorimetry (DSC), dynamic mechanical analysis (DMA), and compression tests. Additionally, the content of closed-cell and the coefficient of thermal conductivity were determined, further characterizing the foams as potential thermal insulation materials. Foams from bio-based donors with petrochemical-based acceptors exhibited a range of enhanced properties. They not only achieved high glass transition temperatures (up to 85 °C by DSC and up to 108 °C by DMA) but also displayed a spectrum of mechanical strengths (compression strength ranging from moderate to as high as ~ 0.40 MPa) and good thermal isolation properties (thermal conductivity coefficient ~ 31 mW/(m·K)). Bio-based foams, derived from renewable resources, were characterized by properties fitting for flexible foam applications, such as low glass transition temperatures (down to −9.7 °C by DSC and down to 9.8 °C by DMA), reduced compression strength (approximately 0.011 MPa), and increased thermal conductivity (up to 46.7 mW/(m·K)), indicating their potential utility in applications where flexibility is a key requirement.

Abbreviations for polymer foam samples	Full name
E^{IR}TOFA_TMP_AA_BPAEDA	Foam from epoxidized tall oil fatty acids trimethylolpropane polyol acetoacetate and bisphenol-A ethoxylate diacrylate
E^{IR}TOFA_TMP_AA_TMPTA	Foam from epoxidized tall oil fatty acids trimethylolpropane polyol acetoacetate and trimethylolpropane triacrylate
E^{IR}TOFA_TMP_AA_PETA	Foam from epoxidized tall oil fatty acids trimethylolpropane polyol acetoacetate and pentaerythritol tetraacrylate

(*continued on next column*)

(*continued*)

(*continued on next page*)

* Corresponding author at: Polymer Laboratory, Latvian State Institute of Wood Chemistry, Riga LV-1006, Latvia.
E-mail addresses: ralfs.pomilovskis@kki.lv (R. Pomilovskis), arnis.abolins@kki.lv (A. Abolins), inese.mierina@rtu.lv (I. Mierina), ivo.heinmaa@kbfi.ee (I. Heinmaa), vitalijs.rjabovs@rtu.lv (V. Rjabovs), anda.fridrihsone@kki.lv (A. Fridrihsone), mikelis.kirpluks@kki.lv (M. Kirpluks).

https://doi.org/10.1016/j.eurpolymj.2024.112968
Received 11 December 2023; Received in revised form 3 March 2024; Accepted 23 March 2024
Available online 25 March 2024
0014-3057/© 2024 The Authors. Published by Elsevier Ltd. This is an open access article under the CC BY license (http://creativecommons.org/licenses/by/4.0/).

(*continued*)

Abbreviations for polymer foam samples	Full name
E^{IR}TOFA_TMP_AA_ESOA	Foam from epoxidized tall oil fatty acids trimethylolpropane polyol acetoacetate and epoxidized soybean oil acrylate
E^{IR}TOFA_TMP_AA_BD_Acryl	Foam from epoxidized tall oil fatty acids trimethylolpropane polyol acetoacetate and epoxidized tall oil fatty acids 1,4-butanediol polyol acrylate

Note: Abbreviations are based on previous research to maintain a consistent style with previous publications. This publication is one of four consecutive publications developed within the project "High bio-based content thermoset polymer foam development from plant origin oils (Bio-Mer)" (No. lzp-2020/1-0385) and is part of a thematically united series of scientific publications.

1. Introduction

In recent years, the pursuit of innovative polymer foam materials has garnered significant attention and research interest, driven by a growing recognition of their multifaceted applications across industries. Today, these materials have become indispensable in sectors such as construction (providing insulation) [1], packaging (offering lightweight and protective materials) [2], automotive (contributing to weight reduction and enhanced safety) [3–5], and increasingly relevant for defence applications [6]. Polymer foams, with their remarkable properties, including low density, exceptional strength-to-weight ratios, and outstanding insulation capabilities, enable these diverse applications [7–10]. However, the current global context underscores the urgency to explore sustainable alternatives, firmly rooted in bio-based materials, to address pressing challenges such as the depletion of fossil resources, environmental degradation, and climate change [11–13].

Conventional polymer foams, including the most widely used materials like polyurethane foams, have long been integral to various industries [5,14]. However, their extensive use has brought environmental challenges to the forefront. Notably, the production of polyurethane foams relies heavily on isocyanates, primarily derived from fossil resources [15,16], with no commercially viable renewable alternatives currently [17]. Michael's reaction is an innovative approach that leverages bio-based resources to address the sustainability issues associated with traditional polymer foams [18].

The Michael 1,4-addition (also simply the Michael reaction) is a known chemical reaction utilized in various fields. However, in polymer chemistry, it is emerging as a novel approach [18–21]. One notable variant of Michael reaction involves the reaction between acetoacetates as the Michael donor and acrylates as the Michael acceptor [22–25]. Acetoacetates possess active methylene groups that serve as nucleophilic centres, readily engaging with the electron-poor double bond of acrylates in the presence of a catalyst. This reaction leads to forming a carbon–carbon (C-C) bond [22,26]. The versatility of the Michael reaction lies in its ability to facilitate the controlled synthesis of polymers with tailored properties, making it a promising strategy for the development of innovative polymer foam materials.

There are several publications that use different types of the Michael reactions for the development of foam materials. Coste et al. investigated soft foams using acrylated soybean oils and biobased amines in *aza*-Michael reactions [18]. Li et al. explored a one-step thiolene click chemistry and the Michael reaction to create a robust superhydrophobic/superoleophilic melamine foam [27]. Few publications describe the development of polymer foam materials using the carbon–carbon Michael reaction. Sonnenschein et al. delve into the utilization of Michael chemistry for producing a range of foams, including rigid, viscoelastic, and flexible elastomers [28]. The investigation employs acetoacetylated glycerol and petrochemical acrylates as raw materials. Despite the potential advantages of the Michael reaction approach, such as producing foams with properties like polyurethanes, the choice of raw materials may not meet the contemporary requirements for a sustainable future. Naga et al. developed porous polymers through the Michael reactions between multifunctional acetoacetate and poly(ethylene glycol) diacrylate [29]. The resulting reactions yield porous polymers with connected spheres, and the study highlights the ability to tailor the morphology and properties of these polymers by varying the polymerization conditions. However, the use of poly(ethylene glycol) diacrylate, a petrochemical derivative, also raises sustainability concerns as the polymer industry aims to shift towards more renewable raw materials.

There are a few patents (EP3783048A1 [30]) and patent applications (US20080281006A1 [31], US20060069234A1 [32]) about the Michael foams. Each present different approaches to foam production, with various degrees of biodegradability and chemical origin. A common drawback is the absence of second-generation raw materials in their formulations, specifically second-generation free fatty acids. These patents collectively point towards an industry trend of seeking more sustainable materials but also highlight a gap in the availability of fully renewable and bio-based feedstocks, such as those derived from free fatty acids.

A key advantage of utilizing the Michael reaction in polymer chemistry is its ability to incorporate the Michael donor and the Michael acceptor from renewable bio-resources, such as tall oil — a second-generation raw material derived from the pulp and paper industry [33]. The use of tall oil fatty acids offer several advantages, such as reducing dependence on fossil resources. Also, tall oil fatty acids are not competing with food and feed production [34].

Acetoacetates can be synthesized from tall oil due to its rich content of unsaturated fatty acids [35]. The process involves several chemical steps, including epoxidation of double bonds and subsequent oxirane ring opening reaction with polyfunctional alcohols [36,37]. Hydroxyl group acetoacetylation is then achieved through transesterification with compounds like *tert*-butyl acetoacetate [38–40]. This versatile approach of selecting different alcohols provides the means to customize various characteristics, such as functionality, branching, molecular weight, and chemical composition. These adaptable properties enable the production of materials with a wide range of properties, making them suitable for diverse applications in polymer foam development.

Polyols offer remarkable versatility — the same polyols can also serve as a precursor for synthesizing polyfunctional acrylates. Pomilovskis et al. demonstrated this characteristic with tall oil-based polyols [33]. In this transformation, the hydroxyl group within polyols acts as a nucleophile, reacting with acryloyl chloride [41–43]. This process leads to the formation of polyfunctional acrylates that can be used as a Michael acceptor. Considering the above, it is possible to utilize the same second-generation bio-based raw material for synthesizing both Michael components. The utilization of the Michael 1,4–addition polymerization in foam development from second-generation free fatty acids presents an innovative pathway for producing sustainable materials with versatile applications.

In this study, we explored the potential of tall oil-based acetoacetates as key components in polymer foam development, combining them with a tall oil-based acrylate synthesized in our previous research [33]. Additionally, commercially available acrylates such as bisphenol-A ethoxylate diacrylate (BPAEDA), trimethylolpropane triacrylate (TMPTA), pentaerythritol tetraacrylate (PETA), and epoxidized soybean oil acrylate (ESOA) were used. 1,1,3,3-tetramethylguanidine (TMG) was used as a catalyst. The development of the foam also required the addition of additives as a surfactant (silicone surfactant with the trade name Niax Silicone L-6915) and blowing agent (low global warming potential hydrofluoroolefin based blowing agent with the trade name Opteon™ 1100) to form the cell structure.

Fossil-based commercially available acrylates were used to benchmark our bio-based polymers against conventional materials. This approach not only tests the compatibility of bio-based and fossil-based materials in existing applications but also aids in the gradual shift

towards more sustainable alternatives, aligning with current industrial practices and advancing sustainable material development. Our research delved into comparing these innovative materials' mechanical, thermo-mechanical, and thermal properties. Thermo-mechanical properties were evaluated using dynamic mechanical analysis (DMA), and thermal properties were investigated using differential scanning calorimetry (DSC) and thermogravimetric analysis (TGA). The chemical composition of the foams was analysed using Fourier-transform infrared spectroscopy (FT–IR). Scanning electron microscopy (SEM) was employed to gather information about the foam structure, and the closed-cell content was determined to gauge foam porosity. This publication elucidates the potential of utilizing tall oil-based components in the development of polymer foams with a wide range of applications and tailored properties based on the used monomers. We provide only an insight into the development of bio-based polymer foams using the Michael reaction as additives using chemicals suitable for the most popular closed-cell foam materials – rigid polyurethane foams [44].

2. Materials and methods

2.1. Materials

For bio-based foam development, acetoacetate from epoxidized tall oil fatty acid tris(hydroxymethyl)propane polyol (E^{IR}TOFA_TMP_AA) was synthesized according to previous research by Pomilovskis et al. [35]. E^{IR}TOFA_TMP_AA had an acid value below 5 mg KOH/g, a hydroxyl value of 36 mg KOH/g, moisture content of 0.03 %, and acetoacetate groups of 0.00484 mol/g. Acrylate from epoxidized tall oil fatty acid 1,4-butanediol polyol (E^{IR}TOFA_BD_Acryl) was synthesized according to previous research by Pomilovskis et al. [33]. E^{IR}TOFA_BD_Acryl had an acid value below 5 mg KOH/g, a hydroxyl value of 29 mg KOH/g, moisture content of 0.02 %, and acryl groups of 0.0034 mol/g. BPAEDA, TMPTA, PETA, and ESOA, Catalyst 1,1,3,3-tetramethylguanigine (TMG) were ordered from Sigma-Aldrich (Steinheim, Germany). Silicone surfactant with the trade name Niax Silicone L-6915 (L-6915) was ordered from Momentive Performance Materials Inc. (Hamburg, Germany). Blowing agent 1,1,1,4,4,4-hexafluorobut-2-ene with the trade name Opteon™ 1100 was ordered from Chemours (Dordrecht, The Netherlands).

2.2. System formulations

E^{IR}TOFA_TMP_AA as the Michael donor and different Michael acceptors, such as BPAEDA, TMPTA, PETA, ESOA, and E^{IR}TOFA_TMP_Acryl, were used to obtain foams. The molar ratio of acetoacetate groups to acrylic groups was 1:2. In the foam system, TMG (5 wt% of acetoacetate and acrylate total mass) was used as catalyst, L-6915 (1 wt% of acetoacetate and acrylate total mass) was used as a surfactant for improved shear stability. Opteon™ 1100 (20 wt% of acetoacetate and acrylate total mass), which has low vapour thermal conductivity and permeation rate, was used as a physical blowing agent. The Hauschild SpeedMixer DAC 250 SP (Hauschild GmbH & Co. KG, Hamm, Germany) mixer was used to mix the components for around 10 s. The systems formulated are given in Table 1. Idealized structures of bio-based Michael components are shown in Fig. 1.

170 g of the total mass of acetoacetate and acrylate was used to make foam blocks to determine the coefficient of thermal conductivity and further test thermal, thermomechanical, and mechanical properties. The ratio between acetoacetate and acrylate groups was kept the same, i.e., 1:2, respectively. Also, catalyst, surfactant and blowing agent were kept at the same percentages of the total weight of acrylate and acetoacetate (TMG 5 wt%, L-6915 1 wt%, Opteon™ 1100 20 wt%).

The polymer matrix parameters were studied by the change of dielectric polarization. A total mass of 10 g of acetoacetate and acrylate without blowing agent and surfactant was used to cover the dielectric polarisation sensor.

2.3. Methods of analysis

The curing monitor device (CMD) (Messtechnik GmbH, Germany) sensor was used in the monitoring of materials' curing processes by detecting changes in dielectric polarization. CMD sensor is a component of the Foam Qualification System FOAMAT® 285 (Messtechnik GmbH, Germany), which is a device for measuring foam rising and curing.

The FOAMAT® 285, equipped with a sound centring blow tube (SCBT) (Messtechnik GmbH, Germany) specially designed for 60 ml cups, was also used to measure foaming parameters such as foaming start time, which is marked by the initiation of the expansion of the material due to the exothermic reaction between the components, rise time, which is the duration it takes for the foam to reach its maximum height, and foam rise height, which is the ultimate height the foam achieved at the end of its expansion. For all FOAMAT tests, the total mass of acrylate and acetoacetate was 10 g. Each measurement was repeated three times.

The Thermo Scientific Nicolet iS50 spectrometer (Thermo Fisher Scientific, USA) was used for FT-IR spectroscopy analysis to determine the functional groups in the sample. Spectral data within the 4000 cm^{-1} to 500 cm^{-1} range were acquired *via* attenuated total reflectance (ATR) mode using a diamond crystal. Each spectrum was the result of 32 accumulated scans at a spectral resolution of 4 cm^{-1}.

Bruker AVANCE-II spectrometer was used for ^{13}C CP MAS NMR spectra. Spectra were recorded at 14.1 T magnetic field using home built double resonance magic-angle-spinning probe for 4 x 25 mm Si3N4 rotors. The spinning speed of the sample was set to 12.5 kHz. The spectra were recorded with standard cross polarization (CP) pulse sequence, where the duration of ramped polarization transfer pulse was 2 ms, CP was followed by the acquisition in the presence of proton decoupling by a strong frequency modulated rf field in proton channel. The relaxation delay between the excitations was 5 s.

The Metler Toledo DSC 823e (Mettler Toledo, Switzerland) equipment was used for DSC to determine the glass transition temperatures ($T_{g(DSC)}$) of the polymer samples. The thermal procedure consisted of a controlled temperature program, where the samples were subjected to a heating sequence from –90 ℃ to 170 ℃ at a rate of 10 ℃ per minute.

Table 1
Systems for FOAMAT tests to characterise foam rise parameters.

Components	Foam system name E^{IR}TOFA_TMP_AA_BPAEDA	E^{IR}TOFA_TMP_AA_TMPTA	E^{IR}TOFA_TMP_AA_PETA	E^{IR}TOFA_TMP_AA_ESOA	E^{IR}TOFA_TMP_AA_BD_Acryl
BPAEDA, g	7.13	–	–	–	–
TMPTA, g	–	4.89	–	–	–
PETA, g	–	–	4.60	–	–
ESOA, g	–	–	–	7.46	–
E^{IR}TOFA_BD_Acryl, g	–	–	–	–	7.19
E^{IR}TOFA_TMP_AA, g	2.87	5.11	5.40	2.54	2.81
TMG, g	0.50	0.50	0.50	0.50	0.50
L-6915, g	0.10	0.10	0.10	0.10	0.10
Opteon™ 1100, g	2.00	2.00	2.00	2.00	2.00

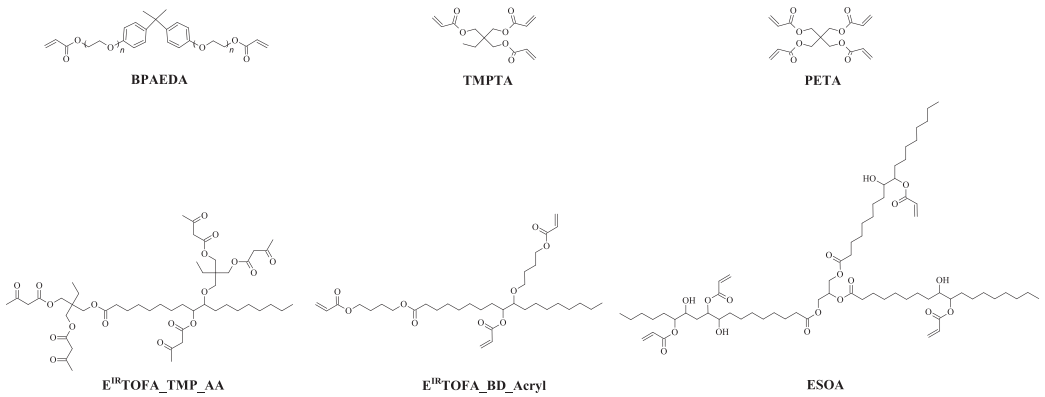

Fig. 1. Idealized structures of synthesised bio-based acetoacetate (E^{IR}TOFA_TMP_AA) and acrylate (E^{IR}TOFA_BD_Acryl), commercially available epoxidized soybean oil acrylate (ESOA) and commercially available petrochemical-based acrylates (BPAEDA, TMPTA, PETA).

This protocol was structured as a cyclic sequence of heating and cooling phases, and the $T_{g(DSC)}$ values were identified during the second heating cycle to prevent the effects of overlapping heat effects of curing chemical reactions [45].

The Mettler Toledo DMA/SDTA861e (Mettler Toledo, Switzerland) was used for the DMA to ascertain the glass transition temperatures ($T_{g\ (DMA)}$) of the materials. Samples, standardized to a diameter of 14.0 mm ± 0.5 mm and height of 7.5 mm ± 0.5 mm, underwent a thermal cycle comprising heating and cooling from –90 ℃ to 170 ℃. The temperature ramp of 3 ℃ per minute and an initial preload force applied at 5 N were used, all within the compression oscillation mode with an oscillation frequency set at 1 s^{-1}.

The Discovery TGA equipment (TA instruments, USA) was used for TGA to measure changes in the weight of a material as a function of temperature under a nitrogen atmosphere. Samples, with a mass of 10.0 mg ± 1.0 mg, were subjected to thermal scanning over a temperature spectrum of 30 ℃ to 700 ℃, employing a consistent heating rate of 10 ℃ per minute. For the analysis and interpretation of the collected data, TRIOS software version 5.0.0.44608 was utilized. Each measurement was performed twice.

The FOX 200 (TA instruments, USA) was used for the determination of the thermal conductivity coefficient (λ) adhered to the ISO 8301:1991 standard protocol [46]. Tests were executed with an average temperature differential set at 10 °C, which was achieved by maintaining the cold plate at 0 °C and the hot plate at + 20 °C. The samples tested had dimensions of 200 mm × 200 mm × 30 mm. Each measurement was performed twice.

The AccuPyc II 1340 pycnometer (Micromeritics Instrument Corporation, USA) was used for the determination of closed content. The content of closed cells within the specimens was quantified in compliance with ISO 4590:2016 [47], using samples measuring 30 mm × 30 mm × 55 mm. Each measurement was performed twice.

The TESCAN TS 5136 MM SEM (Tescan Orsay Holding, Czech Republic) was used for SEM to characterize foam morphology. Foam samples, with a form factor of 1 mm × 10 mm × 2 mm and oriented to align with the foam's rise and its transverse axes, were sectioned from larger foam blocks. The surfaces of these samples were coated with gold using an Emitech K550X (Emitech Ltd, UK) sputter coater to make them conducive to SEM imaging. Vega TC software was employed for image analysis. For the foam varieties under study, the dimensions of cell length and width in both the rise and transverse directions were measured across a dataset of over 100 cells. From these measurements, the ratios defining cell shape anisotropy, denoted as R, were derived based on the comparative lengths and widths of the cells (length/width).

The Zwick/Roell Z100 (ZwickRoell, Germany) was used for compression tests to determine compressive properties, including strength and modulus, in orientations both parallel and perpendicular to the direction of foam rise in accordance with ISO 844:2021 [48] standard protocol. Cylindrical test specimens, each approximately 20 mm in diameter and height, were prepared using a crown drill bit on a drill press. For each foam type, six such specimens underwent analysis.

3. Results and discussion

3.1. Curing parameters of matrix and the rise parameters of developed foam

From the data shown in Fig. 2, it can be inferred that different polymer matrices exhibited varying degrees of dielectric polarization and reached different maximum temperatures during the curing process. In analysing the curing parameters of polymer matrices derived from tall oil trimethylolpropane acetoacetate combined with various acrylates, a clear relationship emerged between acrylate functionality and curing behaviour. Specifically, the curing process is expedited as acrylate functionality increases and a higher maximum temperature is achieved. For instance, the foam matrix formulated using the tetra-functional PETA matrix cured the fastest at 70.3 s and reached the highest temperature of 132.6 °C. The foam matrix formulated using the trifunctional TMPTA had a slightly prolonged curing time of 116.1 s and a temperature of 122. °C, while the difunctional BPAEDA exhibited intermediate curing parameters. Notably, when comparing commercially available petroleum-based acrylates to bio-based ones, the former tend to cure more rapidly at elevated temperatures. Specifically, the soybean oil-based ESOA and tall oil-based E^{IR}TOFA_BD_Acryl matrices had longer curing durations and achieved lower maximum temperatures. This underscores the influence of both acrylate origin and functionality on the curing parameters of these polymer matrices.

The behaviour of petrochemical-based acrylates in the curing process can be attributed to their molecular structure. These acrylates are typically smaller molecules, meaning the acrylic group content is larger. The high concentration of accessible acrylic groups facilitates a more rapid reaction, enhancing the curing process. In contrast, the bio-based acrylates derived from tall and soybean oil have a more branched and complex molecular structure. The slower rising profile can be attributed to the presence of longer alkyl chains in both bio-based acceptors. This structural characteristic influences the curing process, leading to a more gradual expansion of the foam. Also, this complexity introduces steric hindrance, which can interfere with the reaction process. The branched

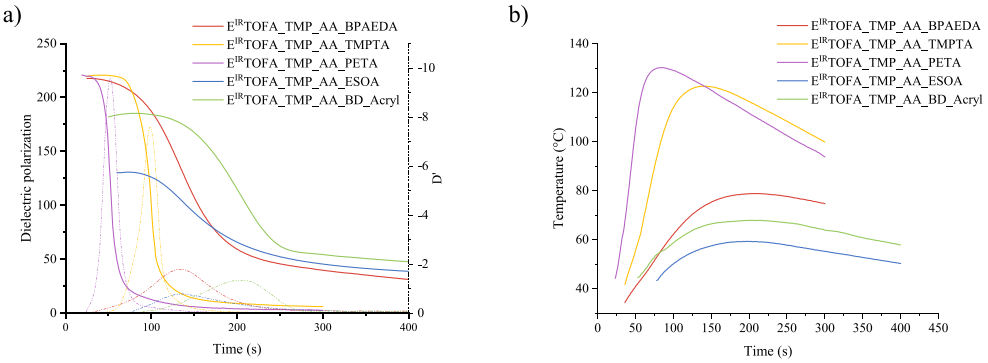

Fig. 2. Developed polymer curing parameters: a) dielectric polarization curves and derivatives of dielectric polarization curves; b) temperature curves of the polymer matrix.

nature of these molecules makes the acrylic groups less accessible, slowing down the curing parameters. The curing times of all matrices and the maximum temperatures reached during curing are shown in Table 2.

The rise profiles of polymer foams show that foams from tall oil–based donors and petrochemical acceptors expand faster than those from tall oil–based donors and acceptors. As in the dielectric polarization measurements, this indicates that the origin of the monomer significantly affects also foam rise profile. It is influenced by factors such as molecular size and functionality, functional group accessibility, structural complexity, and alkyl chain length, as depicted in Fig. 3 and Table 3.

3.2. Chemical characterization of developed bio-based polymer

FT-IR spectra of the obtained polymer foams are given in Fig. 4.b. The absorption bands at 810 cm^{-1}, characteristic of the $=CH_2$ twisting vibrations, measured the acrylic group's presence. The acrylate-specific absorption bands, which are also typically seen around 1630 cm^{-1} and 1410 cm^{-1}, are not analysable due to their overlap with the bands associated with the functional groups of the Michael donor. Observing a low intensity peak at 810 cm^{-1} within the spectra may indicate effective polymerization of the acrylic groups with acetoacetates, suggesting a high degree of conversion in the polymer formation process.

In solid state CP-MAS spectra (Fig. 4.a), signals of the characteristic groups can be observed. At 204 ppm, signals corresponding to a ketone present in the modified acetoacetate moiety is observed. It is present in all the analysed samples thus confirming successful addition reactions. Signal at ~ 173 ppm corresponds to carboxylic group within the ester

Table 2
Curing times and the maximum temperatures reached during the polymer matrix curing process.

Polymer foam sample		Curing time, s	Max. temperature, °C
Bio-based donor and petrochemical-based acceptor	E^IRTOFA_TMP_AA_BPAEDA	243.8 ± 5.8	78.0 ± 1.1
	E^IRTOFA_TMP_AA_TMPTA	116.1 ± 1.2	122.1 ± 0.8
	E^IRTOFA_TMP_AA_PETA	70.3 ± 2.7	132.6 ± 2.7
Bio-based donor and bio-based acceptor	E^IRTOFA_TMP_AA_ESOA	291.8 ± 29.4	57.3 ± 4.8
	E^IRTOFA_TMP_AA_BD_Acryl	275.75 ± 30.6	73.6 ± 8.0

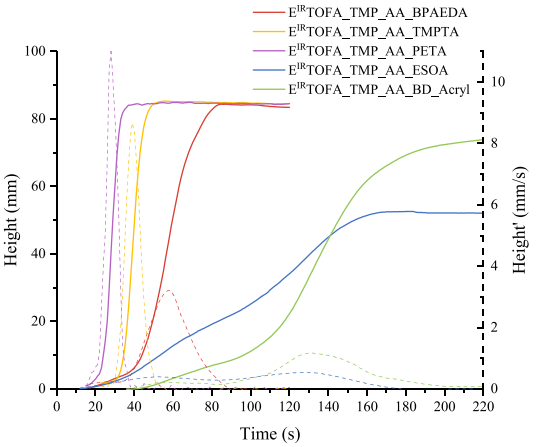

Fig. 3. The rise curve and derivative of the rise curve of developed polymer foam samples.

Table 3
Characteristic of developed foams rise profile.

Polymer foam sample		Start time, s	Rise time, s
Bio-based donor and petrochemical-based acceptor	E^IRTOFA_TMP_AA_BPAEDA	42.9 ± 3.5	79.5 ± 1.3
	E^IRTOFA_TMP_AA_TMPTA	34.2 ± 2.8	56.6 ± 5.6
	E^IRTOFA_TMP_AA_PETA	20.5 ± 1.3	34.8 ± 1.2
Bio-based donor and bio-based acceptor	E^IRTOFA_TMP_AA_ESOA	57.9 ± 4.5	163.7 ± 8.1
	E^IRTOFA_TMP_AA_BD_Acryl	87.6 ± 19.0	187.8 ± 4.9

moieties, while signals in the region from 160 to 110 ppm correspond to aromatic rings and double bonds. The signals of the latter are localized at ~ 130 ppm and are visible in the sample where PETA and TMPTA, and, to a much smaller degree, E^IRTOFA_BD_Acryl were used as Michael acceptors thus indicating incomplete reactions of the acrylate groups, most likely due to steric hindrance. In the spectral region from 80 to 60 ppm, signals of carbons of acylated or free alcohols and ethylene glycol

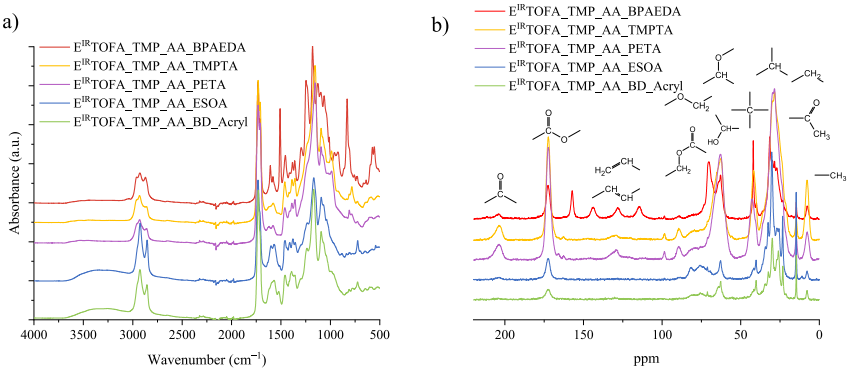

Fig. 4. Chemical structure analysis: a) Fourier-transform infrared spectroscopy spectra of obtained polymer foams; b) ^{13}C CP-MAS NMR spectra of studied samples. The asterisks denote spinning sidebands.

chains are observed. At ~ 43 ppm, quaternary carbons from both reagents manifest. Intensive signals in the region from 35 to 20 ppm are produced by –CH_2– groups of the aliphatic chains while signals at ~ 14 and ~ 7 ppm are characteristic of terminal –CH_3 groups in the acetoacetate moieties and TOFA chains.

3.3. Thermal and thermo-mechanical properties of polymer foam

Table 4 presents the glass transition temperatures (T_g) of developed polymer foam samples as determined by DSC and DMA and the cross-link density of a tall oil-based polymer matrix. DSC heating curves and DMA tanδ are shown in Fig. 5. From DSC data for foams derived from a combination of bio-based donors and petrochemical-based acceptors, the $T_{g(DSC)}$ values ranged from 16.8 °C for E^{IR}TOFA_TMP_AA_BPAEDA to 85.5 °C for E^{IR}TOFA_TMP_AA_PETA. Notably, the E^{IR}TOFA_TMP_AA_PETA foam, which incorporated a tetra-functional acrylate, exhibited the highest $T_{g(DSC)}$ because of a more cross-linked and rigid structure. In contrast, foams with bio-based donor and bio-based acceptor components displayed lower $T_{g(DSC)}$ values, with E^{IR}TOFA_TMP_AA_ESOA and E^{IR}TOFA_TMP_AA_BD_Acryl registering negative $T_{g(DSC)}$ values of −1.9 °C and −9.7 °C, respectively. These differences highlight the influence of raw material sources (bio-based, petrochemical) and chemical structures (functionality, molecular weight) on the properties of the resulting polymer foams.

When comparing the T_g of polymer foam samples as determined by DSC and DMA, distinct variations were evident. $T_{g(DMA)}$ values were consistently higher than those $T_{g(DSC)}$. For instance, the E^{IR}TOFA_TMP_AA_BPAEDA sample exhibited a T_g of 16.8 °C in DSC, while DMA reported a notably higher value of 33.7 °C. Similarly, the E^{IR}TOFA_TMP_AA_PETA foam formulated with the tetra-functional acrylate showed a T_g of 85.5 °C in DSC, but DMA detected a higher glass transition at 108.6 °C.

Table 5 provides insights into the thermal degradation behaviour of developed polymer foams determined by TGA. The TGA curves and derivatives are shown in Fig. 6. The parameters include the onset temperature of degradation, the temperature at which maximum degradation occurs, and the temperatures corresponding to 5 %, 10 %, and 50 % weight loss. Additionally, the residual content at 675 °C is provided. The onset temperature of degradation provides insights into the initial thermal stability of the polymer foams. For foams derived from a combination of bio-based donor and petrochemical-based acceptor, the functionality of the acrylate plays a pivotal role in determining the onset temperature. Although the temperatures were relatively similar, foam E^{IR}TOFA_TMP_AA_PETA formulated with a tetra-functional acrylate exhibited the highest onset temperature of 374.6 °C, followed by foam E^{IR}TOFA_TMP_AA_TMPTA formulated with the tri-functional acrylate, and E^{IR}TOFA_TMP_AA_BPAEDA with the difunctional acrylate. The increase in functionality of the acrylate and cross-link density of the polymer network results in enhanced thermal stability. This observation aligns with other studies found in the literature [50].

The residual content at 675 °C provided insight into the char-forming ability of the polymer foams. Among the partly petrochemical-based foams, E^{IR}TOFA_TMP_AA_PETA left the highest residue of 4.65 %, followed by E^{IR}TOFA_TMP_AA_TMPTA and E^{IR}TOFA_TMP_AA_BPAEDA. This indicates that polymers obtained from higher functionality acrylates tend to form a more stable char structure during thermal degradation. The increased cross-linking density, attributed to higher functionality, contributes to a larger amount of solid residue.

E^{IR}TOFA_TMP_AA_ESOA and E^{IR}TOFA_TMP_AA_BD_Acryl have little bit lower onset temperatures of thermal decomposition than partly petrochemical foams, indicating reduced thermal stability likely due to their complex molecular structures. These values are slightly subdued compared to the more uniform and high-purity petrochemical-based foams. Foams derived from tall oil-based donor and acceptor also leave

Table 4
Glass transition temperatures by differential scanning calorimetry (DSC), dynamic mechanical analysis (DMA) and cross-link density of tall oil-based polymer foams.

Polymer foam sample		$T_{g(DSC)}$, °C	$T_{g(DMA)}$, °C Loss modulus peak position	Tanδ max.	Matrix ν_e, mol/cm^3
Bio-based donor and petrochemical-based acceptor	E^{IR}TOFA_TMP_AA_BPAEDA	16.8	24.3	33.7	$1.89{\cdot}10^{-3}$ [49]
	E^{IR}TOFA_TMP_AA_TMPTA	59.0	68.1	78.1	$2.04{\cdot}10^{-3}$ [49]
	E^{IR}TOFA_TMP_AA_PETA	85.5	89.4	108.6	$3.17{\cdot}10^{-3}$ [49]
Bio-based donor and bio-based acceptor	E^{IR}TOFA_TMP_AA_ESOA	−1.9	9.3	26.5	$1{,}14{\cdot}10^{-3*}$
	E^{IR}TOFA_TMP_AA_BD_Acryl	−9.7	−6.3	9.8	$0.71{\cdot}10^{-3}$ [33]

Notes: ν_e – Cross-link density (mol·cm^{-3}) of the polymer matrix from previous research. ν_e is defined as the number of moles of elastically effective network chains per cubic centimetre of the sample (mol·cm^{-3}).
* The calculation is shown in the supplementary materials.

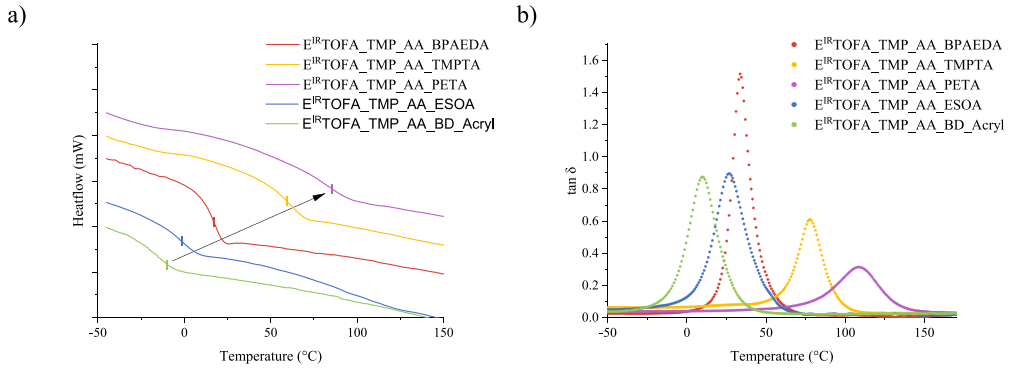

Fig. 5. Differential scanning calorimetry (DSC) and dynamic mechanical analysis (DMA) results: a) DSC analysis curves of developed polymer foam samples; b) DMA tanδ curves of developed polymer foam samples.

Table 5
Thermogravimetric analysis characteristics of developed polymer foams.

Polymer foam sample		Onset, ℃	Max, ℃	T 5 % weight loss, ℃	T 50 % weight loss, ℃	Residue at 675 °C, %
Bio-based donor and petrochemical-based acceptor	E^{IR}TOFA_TMP_AA_BPAEDA	358.8 ± 0.4	418.9 ± 3.0	349.2 ± 0.8	413.0 ± 1.1	3.81 ± 0.02
	E^{IR}TOFA_TMP_AA_TMPTA	368.0 ± 0.2	421.1 ± 0.8	347.9 ± 0.4	420.0 ± 1.0	4.02 ± 0.14
	E^{IR}TOFA_TMP_AA_PETA	374.6 ± 0.3	427.7 ± 0.4	348.2 ± 0.5	425.0 ± 0.4	4.65 ± 0.12
Bio-based donor and bio-based acceptor	E^{IR}TOFA_TMP_AA_ESOA	354.8 ± 0.7	391.8 ± 0.5	340.7 ± 0.1	399.9 ± 0.8	1.02 ± 0.05
	E^{IR}TOFA_TMP_AA_BD_Acryl	359.6 ± 0.3	392.0 ± 0.4	338.1 ± 0.2	400.4 ± 0.3	1.50 ± 0.07

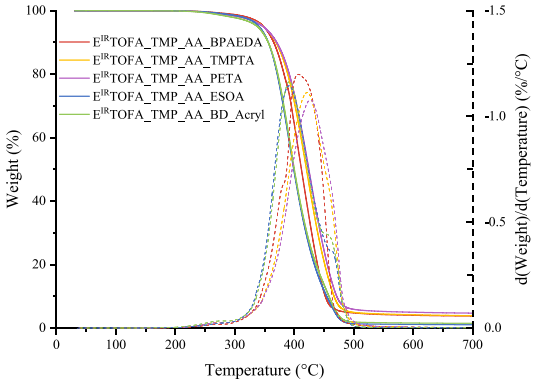

Fig. 6. Thermogravimetric analysis weight loss and derivative curves of developed polymer foam samples.

less residue at 675 °C, highlighting a lower char-forming ability compared to partly petrochemical-based foams, which may relate to differences in cross-linking density.

3.4. Thermal insulation properties

Table 6 provides a comparative parameter of the thermal conductivity, density, and closed-cell content of foams, distinguishing between foams formulated using a bio-based donor with petrochemical-based acceptors and foams formulated from a bio-based acceptor and bio-based donor. The thermal conductivity (λ) of the foams showed a clear correlation with their composition. Notably, foams with petrochemical-based acceptors generally exhibited lower λ values, indicating better thermal insulation capabilities. One possible reason is the higher closed cell content (E^{IR}TOFA_TMP_AA_TMPTA, E^{IR}TOFA_TMP_AA_PETA). For instance, E^{IR}TOFA_TMP_AA_PETA, with a λ of 30.7 mW/(m·K), demonstrated the effectiveness of incorporating petrochemical components in enhancing thermal insulation. Conversely, foams from both bio-based Michael components exhibited

Table 6
The thermal conductivity, apparent density, and closed-cell content of developed foams.

Polymer foam sample		λ, mW/(m·K)	ρ, kg/m^3	V_{closed}, %
Bio-based donor and petrochemical-based acceptor	E^{IR}TOFA_TMP_AA_BPAEDA	38.8 ± 0.3	110.1 ± 1.4	7.7 ± 0.4
	E^{IR}TOFA_TMP_AA_TMPTA	32.3 ± 0.2	111.1 ± 0.13	68.7 ± 2.1
	E^{IR}TOFA_TMP_AA_PETA	30.7 ± 0.5	108.1 ± 0.3	72.4 ± 1.4
Bio-based donor and bio-based acceptor	E^{IR}TOFA_TMP_AA_ESOA	46.7 ± 1.1	173.8 ± 1.6	32.7 ± 0.8
	E^{IR}TOFA_TMP_AA_BD_Acryl	44.5 ± 0.5	143.9 ± 10.2	45.3 ± 1.9

Notes: Rigid polyurethane foam: ρ = 37.4 kg/m^3, V_{closed} = 86 %, λ = 25.5 mW/(m·K). Data were taken from A. Septevani et al. (sample F_0) [53].
Expanded polystyrene: ρ = 28 kg/m^3; λ = 33 kg/m^3., Data were taken from K. T. Yucel et al. [54].

higher λ values (46.7 mW/(m·K)). On the other hand, the thermal insulation properties of the developed foams are well compared to other innovative insulation materials produced from bio-based and/or recycled feedstock. Liao et al. investigated cellulose-based multifunctional foam with a λ of 48.2 mW/(m·K), emphasizing good thermal insulation properties [51]. Pal et al. reported other insulation materials with good thermal conductivity, highlighting cork (40 mW/(m·K)), recycled glass (44 mW/(m·K)), recycled cotton (42 mW/(m·K)), and glass wool (40 mW/(m·K)) as effective alternativesmaking them suitable for various building applications [52].

As can be seen, λ depends on both the density and the closed-cell content. Foams with higher closed-cell content typically demonstrate better thermal insulation properties. In this context, the partly petrochemical-based foams generally exhibited higher closed-cell contents, as seen in E^{IR}TOFA_TMP_AA_PETA with a V_{closed} of 72.4 %. This suggests that the incorporation of petrochemical components may contribute to a more closed-cell structure. This effect is likely due to the smaller size and higher purity of petrochemical components, which promote uniform cell nucleation and stability, in contrast to bio-based components that, being mixtures of larger molecules, may lead to

Table 7
Scanning electron microscope images of the developed foams, taken both parallel and perpendicular to the direction of foaming.

Polymer foam sample	X perpendicular to the direction of foaming	Z parallel to the direction of foaming
E^{IR}TOFA_TMP_AA_BPAEDA	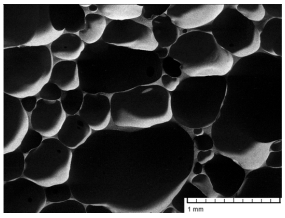	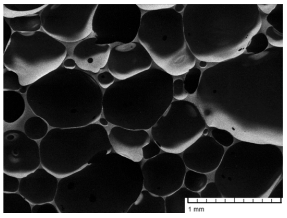
E^{IR}TOFA_TMP_AA_TMPTA	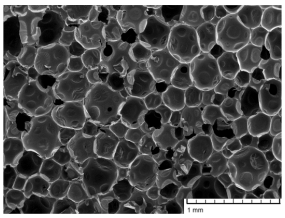	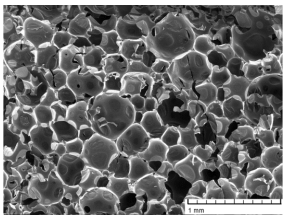
E^{IR}TOFA_TMP_AA_PETA	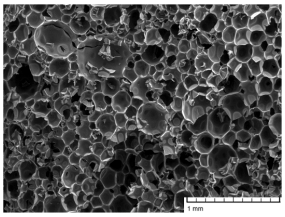	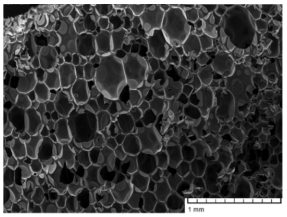
E^{IR}TOFA_TMP_AA_ESOA	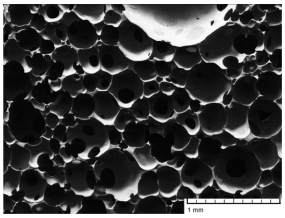	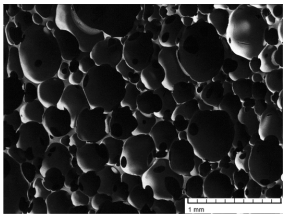
E^{IR}TOFA_TMP_AA_BD_Acryl	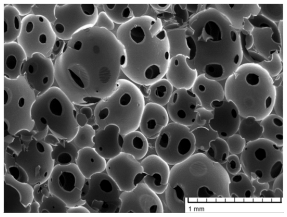	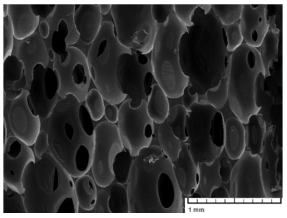

more varied cell sizes and open structures. Higher density was observed in foams from both bio-based Michael components compared to semi-bio-based polymer foams. This difference in density can be attributed to the intrinsic material properties of both bio-based components, which might lead to a more compact, resulting in worse thermal insulation properties.

The SEM images provided in Table 7 show the structural characteristics of the developed thermoset foams. Across the images, there is a noticeable consistency in cell shape and distribution, which is important for the foam's performance in its intended application.

E^{IR}TOFA_TMP_AA_BPAEDA foam is marked by its large pores (~410 μm) and high open-cell content. E^{IR}TOFA_TMP_AA_TMPTA foams presents a tighter, more uniform pore structure with visibly smaller pores (~260 μm) than E^{IR}TOFA_TMP_AA_BPAEDA foam. E^{IR}TOFA_TMP_AA_PETA foam shows the smallest pores with visible crack defects hinting at a brittle material. The high cross-link density of the E^{IR}TOFA_TMP_AA_PETA formulation delivers a cured polymer matrix while the foam is still expanding, which is the likely reason for the crack development during the foaming process. It is clearly visible that the functionality of the used monomer significantly influences the cell size of polymer foams. Monomers with higher functionality, like PETA (f = 4), tend to form highly cross-linked networks, leading to smaller cells (~150 μm). In contrast, monomers with lower functionality, such as BPAEDA (f = 2), resulted in foam with larger cell sizes (~410 μm), as there are fewer cross-linking points, allowing more significant expansion and resulting in a softer foam. TMPTA with intermediate functionality (f = 3) produced a medium cell size (~260 μm). Average cell size in foams directly influences their thermal conductivity. It was observed that larger cells lead to higher λ, while smaller cells enhance the foam heat insulation properties.

The foams, especially E^{IR}TOFA_TMP_AA_BPAEDA and foams from bio-based donor and bio-based acceptors, have an open-cell structure. The varying sizes and interconnected nature of the cells can be particularly effective for sound absorption. The irregularities in cell size and inter-connected porosity can help trap and dissipate sound waves at different frequencies, making the foam a good candidate for acoustic insulation [55]. In applications like padding or insulation where air circulation is beneficial, the open cells provide breathability, which can contribute to thermal comfort [56].

There were no significant morphological differences between the cuts parallel and perpendicular to the direction of foam growth. The pore structure, size, and distribution appeared consistent across both orientations, suggesting quite isotropic foam characteristics. Only sample E^{IR}TOFA_TMP_AA_BD_Acryl indicated possible pore size anisotropy (R = 1.6) in parallel cut to the direction of foam growth. The cell size anisotropy correlated with the compression strength of the developed foams, where it is similar regardless of the applied force axis in relation to the foaming direction. E^{IR}TOFA_TMP_AA_BD_Acryl foam had an average cell size of 360 μm in perpendicular to the direction of foaming, but in parallel to the direction of foaming the average width was 360 μm, but average length was 560 μm.

3.5. Mechanical properties of polymer foams

Table 8 presents the compression strength and modulus evaluated both parallel (Z) and perpendicular (X) to the direction of foam rise of developed polymer foams. The stress–strain curves of developed Michael polymer foams are given in Fig. 7. E^{IR}TOFA_TMP_AA_BPAEDA, E^{IR}TOFA_TMP_AA_TMPTA, and E^{IR}TOFA_TMP_AA_PETA foams demonstrated varying degrees of compression strength. E^{IR}TOFA_TMP_AA_BPAEDA foam, with compression strengths of 0.0073 MPa in the X direction and 0.0092 MPa in the Z direction, were less rigid and more flexible, potentially useful in applications where flexibility is a key requirement. In contrast, E^{IR}TOFA_TMP_AA_TMPTA and E^{IR}TOFA_TMP_AA_PETA foams exhibited much higher compression strengths (~0.27 MPa and ~ 0.40 MPa, respectively), indicating a more rigid structure. This allows for foams to be used as a thermal insulation material or other potential applications for civil engineering. This rigidity makes these materials suitable for applications where higher mechanical strength and load-bearing capability are essential.

Abolins et al. developed rigid polyurethane foams based on various formulations of epoxidized tall oil polyols with a λ of around 22 mW/(m·K) and compression strength of around 0.2 MPa, a value typical for materials used in civil engineering applications [57]. Although rigid polyurethane foams have slightly better thermal insulation capabilities and lower density, there is reason to believe that our obtained materials can compete with partly bio-based polyurethane foam materials in this area because the foam materials obtained in our study have significantly better compressive strength in the case of foam, reaching up to 0.4 MPa. The decrease of the apparent density could be achieved by the optimization of the foaming process, catalyst package and blowing agent content.

4. Conclusions

We believe this study provides the first valuable insights into the development of bio-based polymer foams using the Michael reaction. Foams were formulated from tall oil-based acrylate and tall oil-based acetoacetate, offering a promising pathway towards reducing reliance on non-renewable resources and mitigating environmental impact in the polymer industry.

Foams combining tall oil-based donors with petrochemical acceptors feature high glass transition temperatures, good thermal insulation, enhanced mechanical strength, and superior thermal stability up to 350 °C. E^{IR}TOFA_TMP_AA_PETA foams, exhibit the highest glass transition temperature and compression strength, along with the lowest thermal conductivity, making them good for high insulation and structural applications. Foams from tall oil-based both Michael components have lower glass transition temperatures, lower compression strength, and a little bit higher thermal conductivity compared to those incorporating a petrochemical-based acrylate. However, the thermal insulation properties of the developed foams are good compared to other innovative insulation materials produced from bio–based and/or recycled feedstock. Foams from tall oil-based both Michael components have a flexible nature, making them versatile for applications like packaging,

Table 8
The mechanical properties of developed foams.

	Polymer foam sample	X		Z	
		E, MPa	$\sigma_{10\%}$, MPa	E, MPa	$\sigma_{10\%}$, MPa
Bio-based donor and petrochemical-based acceptor	E^{IR}TOFA_TMP_AA_BPAEDA	0.041 ± 0.006	0.0073 ± 0.0003	0.079 ± 0.013	0.0092 ± 0.0007
	E^{IR}TOFA_TMP_AA_TMPTA	7.6 ± 0.3	0.274 ± 0.007	5.1 ± 0.5	0.263 ± 0.011
	E^{IR}TOFA_TMP_AA_PETA	9.7 ± 0.5	0.39 ± 0.02	7.6 ± 0.4	0.400 ± 0.010
Bio-based donor and bio-based acceptor	E^{IR}TOFA_TMP_AA_ESOA	0.10 ± 0.02	0.0158 ± 0.0017	0.12 ± 0.02	0.0147 ± 0.0004
	E^{IR}TOFA_TMP_AA_BD_Acryl	0.12 ± 0.02	0.0111 ± 0.0016	0.09 ± 0.02	0.0074 ± 0.0005

Notes: Rigid polyurethane foam: compression strength 0.21 MPa, compression modulus 5.1 MPa. Data were taken from A. Septevani et al. (sample F_0) [53].
Expanded polystyrene: compression strength 0.18–0.26 MPa, compression modulus 1.8–3.1 MPa. Data were taken from K. T. Yucel et al. [54].

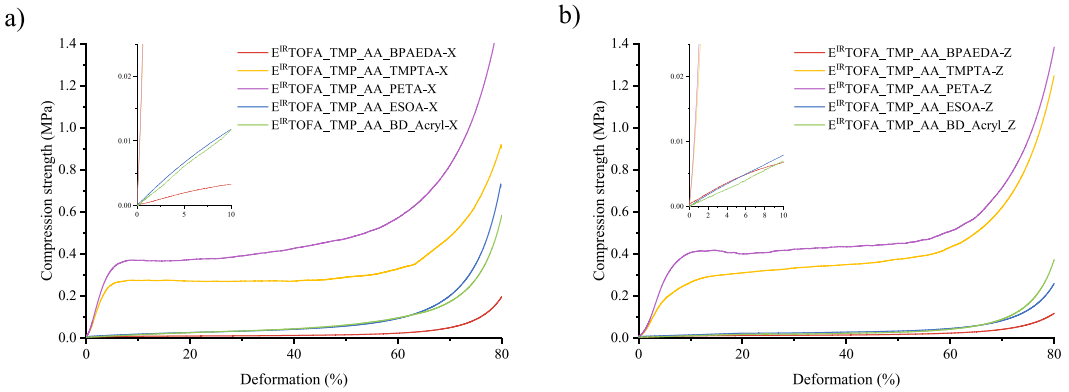

Fig. 7. Compression test curves of developed polymer foam: a) perpendicular (X) to the direction of foam rise of developed polymer foams; b) parallel (Z) to the direction of foam rise of developed polymer foams.

cushioning, automotive interiors, and certain construction uses where flexibility is beneficial.

The development of bio-based foams using the Michael components marks a significant step towards sustainable materials, thanks to their high renewable content. However, their higher thermal conductivity and density limit their use in lightweight, high-performance insulation applications. In contrast, partly petrochemical-based foams, offering superior insulation, fall short on environmental issues. This juxtaposition underscores the need for future research to enhance the properties of bio-based foams, exploring advanced blowing agents, surfactants, and tailored monomer functionality, which is crucial to achieving an optimal balance between today's sustainability and practical performance requirements.

Declaration of competing interest

No conflict of interest.

CRediT authorship contribution statement

Ralfs Pomilovskis: Writing – original draft, Visualization, Supervision, Software, Methodology, Investigation, Formal analysis, Data curation, Conceptualization. **Eliza Kaulina:** Writing – original draft, Formal analysis, Data curation. **Arnis Abolins:** Formal analysis, Data curation. **Inese Mierina:** Data curation. **Ivo Heinmaa:** Data curation, Formal analysis, Software, Visualization. **Vitalijs Rjabovs:** Data curation, Methodology, Software, Visualization. **Anda Fridrihsone:** Writing – review & editing, Project administration. **Mikelis Kirpluks:** Writing – review & editing, Supervision, Project administration, Investigation, Conceptualization.

Declaration of competing interest

The authors declare that they have no known competing financial interests or personal relationships that could have appeared to influence the work reported in this paper.

Data availability

Data will be made available on request.

Acknowledgements

This research was funded by the Latvian Council of Science, project "High bio-based content thermoset polymer foam development from plant origin oils (Bio-Mer)" (No. lzp-2020/1-0385). This research was supported by the Estonian Research Council grant No. PRG1702.

Appendix A. Supplementary data

Supplementary data to this article can be found online at https://doi.org/10.1016/j.eurpolymj.2024.112968.

References

[1] D. Feldman, Polymeric foam materials for insulation in buildings, Mater. Energy Effic. Therm. Comf. Build. (2010) 257–273, https://doi.org/10.1533/9781845699277.2.257.
[2] M. Niaounakis, Foaming and Foamed Products, in: Biopolym. Process. Prod., Elsevier Science, 2015: pp. 327–359. DOI: 10.1016/B978-0-323-26698-7.00009-X.
[3] A. Baroutaji, A. Arjunan, A. Niknejad, T. Tran, A.-G. Olabi, Application of Cellular material in crashworthiness applications: an overview, Elsevier Ltd. (2019), https://doi.org/10.1016/b978-0-12-803581-8.09268-7.
[4] M.Y. Lyu, T.G. Choi, Research trends in polymer materials for use in lightweight vehicles, Int. J. Precis. Eng. Manuf. 16 (2015) 213–220, https://doi.org/10.1007/s12541-015-0029-x.
[5] F.M. De Souza, Y. Desai, R.K. Gupta, Introduction to polymeric foams, ACS Symp. Ser. 1439 (2023) 1–23, https://doi.org/10.1021/bk-2023-1439.ch001.
[6] S. Siengchin, A review on lightweight materials for defence applications: present and future developments, Def. Technol. 24 (2023) 1–17, https://doi.org/10.1016/j.dt.2023.02.025.
[7] F.L. Jin, M. Zhao, M. Park, S.J. Park, Recent trends of foaming in polymer processing: a review, Polymers (Basel) 11 (2019), https://doi.org/10.3390/polym11060953.
[8] G. Wu, P. Xie, H. Yang, K. Dang, Y. Xu, M. Sain, L.S. Turng, W. Yang, A review of thermoplastic polymer foams for functional applications, J. Mater. Sci. 56 (2021) 11579–11604, https://doi.org/10.1007/s10853-021-06034-6.
[9] L. Li, D. Xu, S. Bai, N. Chen, Q. Wang, Progress in preparation of high-performance and multi-functional polymer foams, J. Polym. Sci. (2023) 1–15, https://doi.org/10.1002/pol.20230490.
[10] Z. Wang, C. Wang, Y. Gao, Z. Li, Y. Shang, H. Li, Porous thermal insulation polyurethane foam materials, Polymers (Basel) 15 (2023) 3818, https://doi.org/10.3390/polym15183818.
[11] S.B. Murmu, Alternatives derived from renewable natural fibre to replace conventional polyurethane rigid foam insulation, Clean. Eng. Technol. 8 (2022) 100513, https://doi.org/10.1016/j.clet.2022.100513.
[12] A. Agrawal, R. Kaur, R.S. Walia, PU foam derived from renewable sources: perspective on properties enhancement: an overview, Eur. Polym. J. 95 (2017) 255–274, https://doi.org/10.1016/j.eurpolymj.2017.08.022.
[13] N. Singh, O.A. Ogunseitan, M.H. Wong, Y. Tang, Sustainable materials alternative to petrochemical plastics pollution: a review analysis, Sustain. Horizons. 2 (2022), https://doi.org/10.1016/j.horiz.2022.100016.
[14] S.A. Madbouly, Novel recycling processes for thermoset polyurethane foams, Curr. Opin. Green Sustain. Chem. 42 (2023) 100835, https://doi.org/10.1016/j.cogsc.2023.100835.
[15] S. Sambhudevan, H. S, A. Reghunadhan, Polyurethane from Sustainable Routes, in: Polyurethane Chem. Renew. Polyols Isocyanates, Am. Chem. Soc., 2021: pp. 75–106. DOI: 10.1021/bk-2021-1380.ch004.
[16] M. Włoch, K. Błażek, Isocyanate-Free Polyurethanes, in: 2021: pp. 107–166. DOI: 10.1021/bk-2021-1380.ch005.

[17] J. Niesiobędzka, J. Datta, Challenges and recent advances in bio-based isocyanate production, Green Chem. 25 (2023) 2482–2504, https://doi.org/10.1039/d2gc04644j.
[18] G. Coste, C. Negrell, L. Averous, S. Caillol, Green synthesis of biobased soft foams by the Aza-Michael reaction, ACS Sustain. Chem. Eng. 10 (2022) 8549–8558, https://doi.org/10.1021/acssuschemeng.2c01885.
[19] A.O. Konuray, F. Liendo, X. Fernández-Francos, À. Serra, M. Sangermano, X. Ramis, Sequential curing of thiol-acetoacetate-acrylate thermosets by latent Michael addition reactions, Polymer (Guildf) 113 (2017) 193–199, https://doi.org/10.1016/j.polymer.2017.02.072.
[20] Q. Jiang, Y.L. Zhang, Y. Du, M. Tang, L. Jiang, W. Huang, H. Yang, X. Xue, B. Jiang, Preparation of hyperbranched polymers by oxa-Michael addition polymerization, Polym. Chem. 11 (2020) 1298–1306, https://doi.org/10.1039/c9py01686d.
[21] Z. Ma, Y. Zeng, X. He, S. Pan, Y. Wei, B. Wang, L. Tao, Introducing the aza-Michael addition reaction between acrylate and dihydropyrimidin-2(1H)-thione into polymer chemistry, Polym. Chem. 13 (2022) 6322–6327, https://doi.org/10.1039/D2PY01130A.
[22] S.R. Williams, K.M. Miller, T.E. Long, Michael addition reaction kinetics of acetoacetates and acrylates for the formation of polymeric networks, Prog. React. Kinet. Mech. 32 (2007) 165–194, https://doi.org/10.3184/146867807X247730.
[23] M. Iwamura, Y. Gotoh, T. Hashimoto, R. Sakurai, Michael addition reactions of acetoacetates and malonates with acrylates in water under strongly alkaline conditions, Tetrahedron Lett. 46 (2005) 6275–6277, https://doi.org/10.1016/j.tetlet.2005.07.045.
[24] A.O. Konuray, A. Ruiz, J.M. Morancho, J.M. Salla, X. Fernández-Francos, À. Serra, X. Ramis, Sequential dual curing by selective Michael addition and free radical polymerization of acetoacetate-acrylate-methacrylate mixtures, Eur. Polym. J. 98 (2018) 39–46, https://doi.org/10.1016/j.eurpolymj.2017.11.003.
[25] M. Gould, T. Hammond, S. Narayan-Sarathy, Radiation Curable Michael Addition Resins Having Built-In Photoinitiators, US20050261388A1, 2005.
[26] B.D. Mather, K. Viswanathan, K.M. Miller, T.E. Long, Michael addition reactions in macromolecular design for emerging technologies, Prog. Polym. Sci. 31 (2006) 487–531, https://doi.org/10.1016/j.progpolymsci.2006.03.001.
[27] M. Li, Y. Fang, C. Liu, M. Zhou, X. Miao, Y. Pei, Y. Yan, W. Xiao, H. Qiu, L. Wu, Facile generation of highly durable thiol-functionalized polyhedral oligomeric silsesquioxane based superhydrophobic melamine foam, Front. Chem. Sci. Eng. 16 (2022) 1247–1258, https://doi.org/10.1007/s11705-021-2124-0.
[28] M.F. Sonnenschein, J.B. Werness, K.A. Patankar, X. Jin, M.Z. Larive, From rigid and flexible foams to elastomers via Michael addition chemistry, Polymer (Guildf) 106 (2016) 128–139, https://doi.org/10.1016/j.polymer.2016.10.054.
[29] N. Naga, M. Satoh, T. Magara, K. Ahmed, T. Nakano, Synthesis of porous polymers by means of Michael addition reaction of multifunctional acetoacetate and poly (ethylene glycol) diacrylate, Eur. Polym. J. 162 (2022) 110901, https://doi.org/10.1016/j.eurpolymj.2021.110901.
[30] D. Trumbo, N. Krogman, D. Nelson, A Method for Applying a Foam Composition Using Spray Foam Equipment, EP3783048A1, 2021.
[31] J.O.L. Robert, L.K.-E. Michelle, O.F. Nassreen, One-Part Non-Toxic Spray Foam, US2008281006A1, 2008.
[32] T.F. Kauffman, D.W. Whitman, M.J. Zajaczkowski, V. David Elmer, Biomass Based Michael Addition Compositions, US 2006/0069234 A1, 2006.
[33] R. Pomilovskis, E. Kaulina, I. Mierina, A. Abolins, O. Kockova, A. Fridrihsone, M. Kirpluks, Wood pulp industry by-product valorization for acrylate synthesis and bio-based polymer development via Michael addition reaction, J. Bioresour. Bioprod. 8 (2023) 265–279, https://doi.org/10.1016/j.jobab.2023.06.001.
[34] L. Vevere, A. Fridrihsone, M. Kirpluks, U. Cabulis, A review of wood biomass-based fatty acids and rosin acids use in polymeric materials, Polymers (Basel) 12 (2020) 1–17, https://doi.org/10.3390/polym12112706.
[35] R. Pomilovskis, I. Mierina, H. Beneš, O. Trhlíková, A. Abolins, A. Fridrihsone, M. Kirpluks, The synthesis of bio-based Michael donors from tall oil fatty acids for polymer development, Polymers (Basel) 14 (2022), https://doi.org/10.3390/polym14194107.
[36] M. Kirpluks, R. Pomilovskis, E. Vanags, A. Abolins, I. Mierina, A. Fridrihsone, Influence of different synthesis conditions on the chemo-enzymatic epoxidation of tall oil fatty acids, Process Biochem. 122 (2022) 38–49, https://doi.org/10.1016/j.procbio.2022.08.024.
[37] A. Saputra, P. Satwikanitya, F. Puspita, M.W. Sya'bani, M.F. Agustian, W. Pambudi, Synthesis of epoxy oil from Waste Cooking Oil (WCO) using acetic acid and amberlite resin IR-120 as catalyst, Eng. Appl. Sci. Res. 50 (2023) 335–342. DOI: 10.14456/easr.2023.36.
[38] M.C. Hennessy, T.P. O'Sullivan, Recent advances in the transesterification of β-keto esters, RSC Adv. 11 (2021) 22859–22920, https://doi.org/10.1039/d1ra03513d.
[39] H. Zuo, Z. Cao, J. Shu, D. Xu, J. Zhong, J. Zhao, T. Wang, Y. Chen, F. Gao, L. Shen, Effect of structure on the properties of ambient-cured coating films prepared via a Michael addition reaction based on an acetoacetate-modified castor oil prepared by thiol-ene coupling, Prog. Org. Coatings. 135 (2019) 27–33, https://doi.org/10.1016/j.porgcoat.2019.05.032.
[40] R.K. Pandey, P. Kumar, A facile procedure for transesterification of β-keto esters promoted by ceria-yttria based Lewis acid catalyst, Catal. Commun. 8 (2007) 1122–1125, https://doi.org/10.1016/j.catcom.2006.10.031.
[41] R.A. Omer, A. Hughes, J.R. Hama, W. Wang, H. Tai, Hydrogels from dextran and soybean oil by UV photo-polymerization, J. Appl. Polym. Sci. 132 (2015) 1–10, https://doi.org/10.1002/app.41446.
[42] A. Luo, X. Jiang, H. Lin, J. Yin, "Thiol-ene" photo-cured hybrid materials based on POSS and renewable vegetable oil, J. Mater. Chem. 21 (2011) 12753–12760, https://doi.org/10.1039/c1jm11425e.
[43] D. Kim, S. Kim, S. Jeong, M. Kim, W.K. Hong, H.B. Jeon, H.Y. Cho, S.M. Noh, H. jong Paik, Thermally latent vinyl crosslinking of polymers via sulfoxide chemistry, Eur. Polym. J. 179 (2022) 111520. DOI: 10.1016/j.eurpolymj.2022.111520.
[44] J. Andersons, R. Grūbe, L. Vēvere, P. Cābulis, M. Kirpluks, Anisotropic thermal expansion of bio-based rigid low-density closed-cell polyurethane foams, J. Mater. Res. Technol. 16 (2022) 1517–1525, https://doi.org/10.1016/j.jmrt.2021.12.094.
[45] I. Bute, S. Tarasovs, S. Vidinejevs, L. Vevere, J. Sevcenko, A. Aniskevich, Thermal properties of 3D printed products from the most common polymers, Int. J. Adv. Manuf. Technol. 124 (2023) 2739–2753, https://doi.org/10.1007/s00170-022-10657-7.
[46] S. International Organization for Standardization, Geneva, ISO_8301_1991, Thermal insulation — Determination of steady-state thermal resistance and related properties Heat flow meter apparatus, (1991).
[47] S. International Organization for Standardization, Geneva, ISO 4590:2016, Rigid cellular plastics — Determination of the volume percentage of open cells and of closed cells, (2016).
[48] ISO 844:2021; Rigid cellular plastics — Determination of compression properties, International Organization for Standardization, Geneva, Switzerland, 2021.
[49] R. Pomilovskis, I. Mierina, A. Fridrihsone, M. Kirpluks, Bio-based polymer developments from tall oil fatty acids by exploiting Michael addition, Polymers (Basel) 14 (2022) 4068, https://doi.org/10.3390/polym14194068.
[50] G.F. Levchik, K. Si, S.V. Levchik, G. Camino, C.A. Wilkie, Correlation between cross-linking and thermal stability: cross-linked polystyrenes and polymethacrylates, Polym. Degrad. Stab. 65 (1999) 395–403, https://doi.org/10.1016/S0141-3910(99)00028-2.
[51] J. Liao, Y. Hou, J. Li, M. Zhang, Y. Dong, X. Chen, Lightweight and recyclable hybrid multifunctional foam based cellulose fibers with excellent flame retardant, thermal, and acoustic insulation property, Compos. Sci. Technol. 244 (2023) 110315, https://doi.org/10.1016/j.compscitech.2023.110315.
[52] R.K. Pal, P. Goyal, S. Sehgal, Effect of cellulose fibre based insulation on thermal performance of buildings, Mater. Today Proc. 45 (2021) 5778–5781, https://doi.org/10.1016/j.matpr.2021.02.749.
[53] A.A. Septevani, D.A.C. Evans, P.K. Annamalai, D.J. Martin, The use of cellulose nanocrystals to enhance the thermal insulation properties and sustainability of rigid polyurethane foam, Ind. Crops Prod. 107 (2017) 114–121, https://doi.org/10.1016/j.indcrop.2017.05.039.
[54] K.T. Yucel, C. Basyigit, C. Ozel, Thermal insulation properties of expanded polystyrene as construction and insulating materials, 15th symp Thermophys. Prop. (2003) 54–66.
[55] A. Abbad, K. Jaboviste, M. Ouisse, N. Dauchez, Acoustic performances of silicone foams for sound absorption, J. Cell. Plast. 54 (2018) 651–670, https://doi.org/10.1177/0021955X17732305.
[56] B.E. Obi, Overview of applications of polymeric foams, Polym. Foam. Struct. (2018) 3–14, https://doi.org/10.1016/b978-1-4557-7755-6.00001-x.
[57] A. Abolins, R. Pomilovskis, E. Vanags, I. Mierina, S. Michalowski, A. Fridrihsone, M. Kirpluks, Impact of different epoxidation approaches of tall oil fatty acids on rigid polyurethane foam thermal insulation, Materials (Basel) 14 (2021) 1–17, https://doi.org/10.3390/ma14040894.

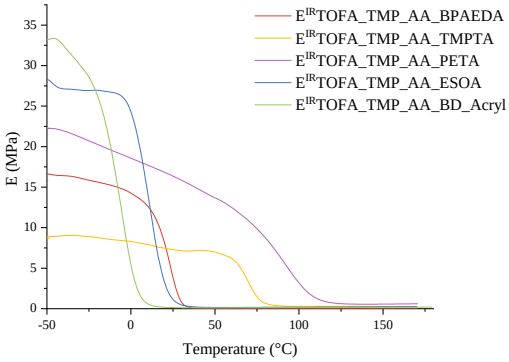

Fig. S1. DMA curves for storage modulus of developed polymer foam samples.

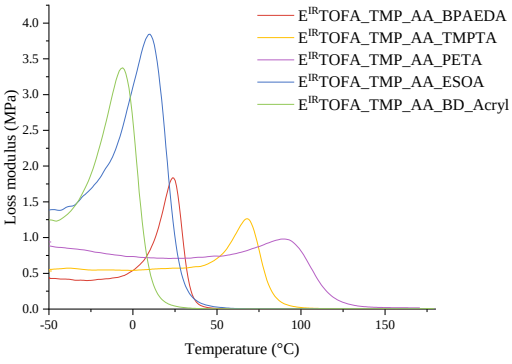

Fig. S2. DMA curves for loss modulus of developed polymer foam samples.

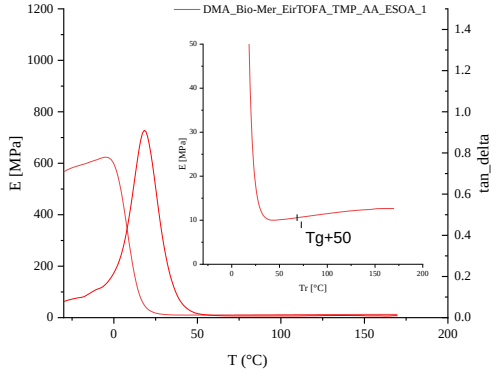

Fig. 3S. DMA curves for loss modulus and tanδ of for E^IRTOFA_TMP_AA_ESOA polymer sample.

Equation 1 was used to calculate the cross-link density using the results from the DMA test [1–4]:

$$\nu_e = \frac{E'_{rubbery}}{3RT} \quad (1)$$

where ν_e is the cross-link density (mol·cm^{-3}); $E'_{rubbery}$ is the storage modulus (MPa) at temperature $T_{g(DMA)}$+50 (K); R is the gas constant; T is the temperature that corresponds to the rubbery storage modulus (K).

According to Equation 2, the molecular weight between cross-links M_c (g·mol^{-1}) was found [5].

$$M_c = \frac{3RT\rho}{E'_{rubbery}} \quad (2)$$

References

[1] T.H. Kim, M. Kim, W. Lee, H.G. Kim, C.S. Lim, B. Seo, Synthesis and characterization of a polyurethane phase separated to nano size in an epoxy polymer, Coatings. 9 (2019). https://doi.org/10.3390/coatings9050319.

[2] K.K. Jena, K.V.S.N. Raju, Synthesis and characterization of hyperbranched polyurethane hybrids using tetraethoxysilane (TEOS) as cross-linker, Ind. Eng. Chem. Res. 47 (2008) 9214–9224. https://doi.org/10.1021/ie800884y.

[3] L.W. Hill, Calculation of crosslink density in short chain networks, Prog. Org. Coatings. 31 (1997) 235–243. https://doi.org/10.1016/S0300-9440(97)00081-7.

[4] C. Zhang, S.A. Madbouly, M.R. Kessler, Biobased polyurethanes prepared from different vegetable oils, ACS Appl. Mater. Interfaces. 7 (2015) 1226–1233. https://doi.org/10.1021/am5071333.

[5] I.M. Barszczewska-Rybarek, A. Korytkowska-Wałach, M. Kurcok, G. Chladek, J. Kasperski, DMA analysis of the structure of crosslinked poly(methyl methacrylate)s, Acta Bioeng. Biomech. 19 (2017) 47–53. https://doi.org/10.5277/ABB-00590-2016-01.

2. pielikums
Appendix 2

Wood pulp industry by-product valorization for acrylate synthesis and bio-based polymer development *via* Michael addition reaction

Ralfs Pomilovskis, Elīza Kauliņa, Inese Mieriņa, Arnis Āboliņš, Olga Kockova, Anda Fridrihsone, Miķelis Kirpļuks

Journal of Bioresources and Bioproducts, 2023

Journal of Bioresources and Bioproducts 8 (2023) 265–279

Contents lists available at ScienceDirect

Journal of Bioresources and Bioproducts

journal homepage: https://www.keaipublishing.com/en/journals/journal-of-bioresources-and-bioproducts/

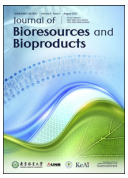

Research Article

Wood pulp industry by-product valorization for acrylate synthesis and bio-based polymer development via Michael addition reaction

Ralfs Pomilovskis[a,b,*], Eliza Kaulina[a,b], Inese Mierina[b], Arnis Abolins[a], Olga Kockova[c], Anda Fridrihsone[a], Mikelis Kirpluks[a]

[a] Polymer Laboratory, Latvian State Institute of Wood Chemistry, Riga LV-1006, Latvia
[b] Institute of Technology of Organic Chemistry, Faculty of Materials Science and Applied Chemistry, Riga Technical University, Riga LV-1048, Latvia
[c] Institute of Macromolecular Chemistry CAS, Prague 16200, Czech Republic

ARTICLE INFO

Keywords:
Tall oil fatty acid
Fatty acids-based michael acceptor
Bio-based acrylate
Michael addition
Bio-based polymer

ABSTRACT

It is crucial to adapt the processing of forest bio-resources into biochemicals and bio-based advanced materials in order to transform the current economic climate into a greener economy. Tall oil, as a by-product of the Kraft process of wood pulp manufacture, is a promising resource for the extraction of various value-added products. Tall oil fatty acids-based multifunctional Michael acceptor acrylates were developed. The suitability of developed acrylates for polymerization with tall oil fatty acids-based Michael donor acetoacetates to form a highly cross-linked polymer material via the Michael addition was investigated. With this novel strategy, valuable chemicals and innovative polymer materials can be produced from tall oil in an entirely new way, making a significant contribution to the development of a forest-based bioeconomy. Two different tall oil-based acrylates were successfully synthesized and characterized. Synthesized acrylates were successfully used in the synthesis of bio-based thermoset polymers. Obtained polymers had a wide variety of mechanical and thermal properties (glass transition temperature from –12.1 to 29.6 °C by dynamic mechanical analysis, Young's modulus from 15 to 1 760 MPa, and stress at break from 0.9 to 16.1 MPa). Gel permeation chromatography, Fourier-transform infrared (FT-IR) spectroscopy, matrix-assisted laser desorption/ionization-time of flight mass spectrometry, and nuclear magnetic resonance were used to analyse the chemical structure of synthesized acrylates. In addition, various titration methods and rheology tests were applied to characterize acrylates. The chemical composition and thermal and mechanical properties of the developed polymers were studied by using FT-IR, solid-state nuclear magnetic resonance, thermal gravimetric analysis, differential scanning calorimetry, dynamic mechanical analysis, and universal strength testing apparatus.

1. Introduction

The European Commission has initiated a new growth strategy the "European Green Deal" to transform the current economy of European Union countries into a circular bio-based economy, achieving climate neutrality and sustainable carbon cycles by 2050 (European Commission, 2019). Since polymer production occupies a large part of the global manufacturing sector and has a detrimental influence on the climate and environment, the development of bio-based polymers is crucial (Rosenboom et al., 2022). It is necessary to expand the synthesis of monomers from renewable bio-resources suitable for innovative and sustainable bio-based

* Corresponding author.
E-mail address: ralfs.pomilovskis@kki.lv (R. Pomilovskis).

https://doi.org/10.1016/j.jobab.2023.06.001
Received 4 March 2023; Received in revised form 16 April 2023; Accepted 22 April 2023
2369-9698/© 2023 The Authors. Publishing Services by Elsevier B.V. on behalf of KeAi Communications Co. Ltd. This is an open access article under the CC BY license (http://creativecommons.org/licenses/by/4.0/)

polymer production to establish that bio-based polymer manufacturing becomes a part of the bio-economy (Papageorgiou, 2018; Pellis et al., 2021).

Plant oil fatty acids are appealing for synthesizing versatile monomers due to their functional groups, i.e., double bonds, carboxyl groups, and, in some cases, hydroxyl groups. However, the growing demand for edible vegetable oils in food and feed production limits their use in chemical processing (Smeu et al., 2022; Claux et al., 2023). From the sustainability perspective, it would be preferable to use non-edible or used cooking oils as they do not compete with food and feed production for chemical processing (Perera et al., 2022).

One of the second-generation oils suitable for chemical conversions is tall oil (Vevere et al., 2020). Tall oil is a valuable by-product of the wood biomass pulping process (Aryan and Kraft, 2021). Distilled tall oil consists mainly of oleic and linoleic acids with small amounts of other fatty acids, resin acids, and unsaponifiable sterols. Tall oil is already used for the synthesis of high-value-added chemicals (Vevere et al., 2020). It has been demonstrated that epoxidized tall oil polyols can be successfully used to develop bio-based polyurethanes (Abolins et al., 2021; Kirpluks et al., 2022; Polaczek et al., 2022). However, because the production of polyurethanes requires hazardous isocyanates, conventional polyurethanes do not meet modern sustainability requirements (Kathalewar et al., 2013, 2014; Dechent et al., 2020; Lindsay and Timperley, 2020; Sternberg and Pilla, 2020). Pomilovskis et al. (2022a) reported that polyols obtained from epoxidized tall oil could be used as a precursor for the synthesis of monomers suitable for use in more advanced polymer production via the Michael addition reaction.

Hydroxyl groups of tall oil-based polyol can be converted into acetoacetate functional groups required by the Michael reaction in one-step synthesis. Hydroxyl groups can be acetoacetylated in a transesterification reaction with *tert*-butyl acetoacetate. Compounds containing acetoacetate groups are considered as Michael donors (Witzeman and Nottingham, 1991; Trevino and Trumbo, 2002; Krall et al., 2018; Cao et al., 2019; He et al., 2019; Xu et al., 2019). There are a few studies on synthesizing and using bio-based acetoacetates for different polymer materials. Xu et al. (2019) developed a coating film by reacting acetoacetylated castor oil with a cross-linker with both aldehyde and acrylate groups by the Michael addition. Wang et al. (2019) created curable coatings from acetoacetylated castor oil and a multifunctional acrylate using the Michael addition reaction (hexamethylene diacrylate, trimethylolpropane triacrylate, pentaerythritol tetraacrylate). Noordover et al. (2020) proposed malonate-functional polyester coatings from synthesized bio-based Michael donors cured through the Michael addition reaction with di(trimethylolpropane) tetraacrylate. Sonnenschein et al. (2016) provided procedures for foam production from multifunctional acetoacetates combined with the myriad of commercially available polyacrylates (di(trimethylolpropane) tetraacrylate, bisphenol A epoxy diacrylate, trimethylolpropane triacetoacetate). Naga et al. (2021) demonstrated a reaction between multifunctional acetoacetates (*meso*-erythritol tetraacetoacetate, trimethylolpropane triacetoacetate) and diacrylate monomers (1,4-butanediol diacrylate, 1,6-hexanediol diacrylate, 1,9-nonanediol diacrylate) resulting in the formation of corresponding gels. Later, Naga et al. (2022) investigated the Michael reaction between *meso*-erythritol tetraacetoacetate or *d*-sorbitol hexaacetoacetate and poly(ethylene glycol) diacrylate in solvents to create a porous polymer. All previous studies share the use of a bio-based Michael donor and a petrochemical-based Michael acceptor.

For nearly a century, acrylates, petroleum-based monomers, have been used for resins and coatings production (Hermens et al., 2020). Many different synthesis routes have been advanced, offering a large selection of suitable bio-based acrylates and methacrylates mostly for radical polymerization from saturated or unsaturated fatty acids (Lomège et al., 2019). Soybean oil-based acrylates (Xia and Larock, 2010; Rengasamy and Mannari, 2014; Zhang et al., 2014; Li and Sun, 2015; Ge et al., 2019; Hu et al., 2019; Liu et al., 2019; Tang et al., 2020; Baghban et al., 2022; Gapsari et al., 2022) and linseed oil-based acrylates (Wuzella et al., 2012; Boucher et al., 2021; Briede et al., 2022) have been studied most extensively. The acrylation of palm, olive, corn, peanut, canola, rapeseed, grapeseed, camelina, and tung oils has also been studied (Sung and Sun, 2018; Liang et al., 2019; Su et al., 2020). Although acrylates from the plant mentioned above oils have been used in UV-curable coatings, that does not limit their use as Michael acceptors.

There are a few main synthesis routes to obtain bio-based acrylates. One of the most studied reactions is the epoxidation of the double bonds and subsequent opening of the oxirane rings with acrylic acid (La Scala and Wool, 2002; Xia and Larock, 2010; Wuzella et al., 2012; Gan and Jiang, 2014; Salih et al., 2015; Sung and Sun, 2018). The one-step reaction between unsaturated oil and acrylic acid is in the presence of boron trifluoride diethyl etherate solution (Zhang and Zhang, 2013; Zhang et al., 2014; Su et al., 2020). If the molecule of oil contains naturally occurring hydroxyl groups (e.g., castor oil) acrylation of the hydroxyl groups with acrylic chloride is possible (Luo et al., 2011; Gan and Jiang, 2014; Müller and Wilke, 2014). These methods are appropriate for feedstocks with two or more double bonds, as polymerization necessitates at least two functional groups per molecule. Multiple double bonds are present in diglycerides and triglycerides. The literature review suggests that triglyceride-containing oils are the most widely used raw materials for acrylate synthesis. Some free fatty acids, like linoleic acid, have two double bonds, but due to side reactions with acetic acid or incomplete epoxidation, each molecule is typically left with only one oxirane group (Polaczek et al., 2022). Therefore, epoxidation and oxirane ring-opening with acrylic acid or direct double bond acrylation are ineffective for free fatty acids-containing oils such as tall oil. For oils containing free fatty acids, a different strategy must be adopted.

Tall oil fatty acids-based Michael donors were developed and characterized in our previous research (Pomilovskis et al., 2022a). This study investigated the synthesis of tall oil fatty acids-based acrylates. We presented a promising method for synthesizing acrylates from tall oil via epoxidation followed by oxirane ring-opening with a polyfunctional polyol and subsequent acrylation of the hydroxyl groups with acryloyl chloride. Further synthesized acrylates could be used to obtain a highly cross-linked polymer material from a two-component system based on fatty acids by using the Michael addition reaction. The novelty of the proposed approach is that the same renewable raw material, tall oil fatty acids-based polyols, is used for the synthesis of both Michael monomers. Gel permeation chromatography (GPC), Fourier-transform infrared (FT-IR) spectroscopy, matrix-assisted laser desorption/ionization-time of flight (MALDI-TOF) mass spectrometry (MS), and nuclear magnetic resonance (NMR) were used to analyse the chemical structure of synthesized acrylates. Michael addition was used to synthesize novel bio-based thermoset polymers from the developed tall oil

fatty acids-based acrylates and acetoacetates. The functional groups of obtained polymers were identified using FT-IR and solid-state nuclear magnetic resonance (ssNMR). Dynamic mechanical analysis (DMA), differential scanning calorimetry (DSC), thermal gravimetric analysis (TGA), and universal strength testing equipment were used to investigate the physical and thermal properties of developed bio-based thermoset polymers. The proposed polymer synthesis method may be used to prepare two-component systems suitable for resins, composite matrices, coatings, and polymer foams.

2. Materials and methods

2.1. Materials

2.1.1. Reagents for synthesis of monomers

Epoxidized tall oil fatty acids 1,4-butanediol polyol (E^{IR}TOFA_BD), acid value < 5 mg KOH per gram, –OH value of 258 mg KOH per gram, moisture of 0.199%; epoxidized tall oil fatty acids trimethylolpropane polyol (E^{IR}TOFA_TMP), acid value of 6.9 mg KOH per gram, –OH value of 415 mg KOH per gram, moisture of 0.049% were synthesized at Latvian State Institute of Wood Chemistry (LSIWC), Riga, Latvia. Superscript (^{IR}) means that an ion exchange resin was used to epoxidize tall oil fatty acids. Acryloyl chloride, ≥ 97%, contains ~400×10^{-6} phenothiazine as a stabilizer; triethylamine (TEA), puriss. pro analysis > 99.0%; ethyl acetate, American Chemical Society reagent, ≥ 99.5%, were purchased from Sigma-Aldrich, Schnelldorf, Germany.

2.1.2. Reagents for bio-based thermoset development

Acetoacetate of epoxidized tall oil fatty acids 1,4-butanediol polyol (E^{IR}TOFA_BD_AA), acid value < 5 mg KOH per gram, –OH value of 36 mg KOH per gram, moisture of 0.03%, acetoacetate groups of 0.331 mol per 100 g; acetoacetate of epoxidized tall oil fatty acids trimethylolpropane polyol (E^{IR}TOFA_TMP_AA), acid value < 5 mg KOH per gram,–OH value of 42 mg KOH per gram, moisture of 0.04%, acetoacetate groups of 0.456 mol per 100 g, were synthesized at LSIWC, Riga, Latvia. The N,N,N′,N′-tetramethylguanidine (TMG), 99%, was purchased from Sigma-Aldrich, Schnelldorf, Germany.

2.2. Synthesis of tall oil-based acetoacetates

The synthesis of tall oil-based polyols (E^{IR}TOFA_BD, E^{IR}TOFA_TMP) and acetoacetates (E^{IR}TOFA_BD_AA, E^{IR}TOFA_TMP_AA) was described and characterized in detail in our previous research by Pomilovskis et al. (2022a).

2.3. Synthesis of tall oil-based acrylate

Previously synthesized polyol, E^{IR}TOFA_BD or E^{IR}TOFA_TMP, and a corresponding amount of ethyl acetate and TEA were added to a round bottom flask with four necks equipped with a stirrer, thermocouple, and a reflux condenser. A dropping funnel was used for the slow, intermittent pouring of acryloyl chloride because of an exothermic reaction. The temperature was maintained –2 – 4 °C for 2 h and then acryloyl chloride was added in. Cooling was provided by a sodium chloride-containing ice bath. Synthesis was carried out under an internet atmosphere which was provided using nitrogen gas. Afterwards, the ice bath was removed, and synthesis was carried out for an additional 16 h at room temperature. The molar ratio of polyol hydroxyl groups to acryloyl chloride was 1:1.05. The molar ratio of TEA to acryloyl chloride was 1:1. The mass ratio of polyol to ethyl acetate was 1:5. After synthesis, the mixture was filtrated. The solution was washed with a 0.5% sodium hydroxide solution and warm distilled water (~35 °C) and dried for at least 12 h with anhydrous sodium sulfate. The solvent was removed using a rotary evaporator at low pressure. Depending on the used polyol, E^{IR}TOFA_BD or E^{IR}TOFA_TMP, the synthesized tall oil-based Micahel acceptors were named E^{IR}TOFA_BD_Acryl or E^{IR}TOFA_TMP_Acryl, respectively.

2.4. Solid polymer development

Polymer samples were obtained by mixing the tall oil-based acrylate, the catalyst (TMG), and acetoacetate. The molar ratio of acetoacetate groups to acrylic groups was 1:2. The mass of the catalyst was 1% of the total mass of the mixture. The Hauschild SpeedMixer DAC 250 SP (Hauschild GmbH & Co. KG, Hamm, Germany) mixer was used to mix the components for around 30 s. In one batch, 15 g of polymer mass was prepared. After mixing, the composition was filled into molds. For DMA tests, samples were prepared in plastic tubes with a diameter of 14 mm. Stainless steel molds were used for dog bone tensile test sample preparation. The sample gauge section size was 2.5 mm × 4 mm × 25 mm. Cured polymer samples were removed from the molds after 24 h. Polymer synthesis was repeated twice for each system.

2.5. Methods of analysis

The acid value and –OH value were analysed by volumetric titration according to ISO 2114:2000 and ISO 4629–2:2016. Karl Fischer titration was used to measure the moisture content using an automatic titrator Denver Instrument Model 275 KF (Denver Instrument, NY, USA).

The viscosity tests were performed on an Anton Paar Rheometer MCR 92 (Anton Paar, Graz, Austria). The experiments were carried out by using a cone-plate system with a gap of 48 μm. All tests were conducted at a constant temperature of 25 °C. The shear rate varied from 0.1 to 100 Hz.

The FT-IR spectra were recorded using a Thermo Scientific Nicolet iS50 spectrometer (Thermo Fisher Scientific, Waltham, MA, USA). The FT-IR spectra between 4 000 and 500 cm^{-1} were collected using a diamond crystal in attenuated total reflectance mode at a resolution of 4 cm^{-1} by 32 scans.

The proton nuclear magnetic resonance (^{1}H-NMR) and carbon-13 nuclear magnetic resonance (^{13}C-NMR) spectra were recorded with a Bruker spectrometer (Bruker BioSpin, Fällanden, Switzerland) at 500 and 126 MHz, respectively. Deuterated chloroform ($CDCl_3$) was used as the solvent. The ^{1}H-NMR spectra were used for the determination of acrylic group content using 1,2,3-trimethoxybenzene as an internal standard.

The MALDI-TOF MS measurements were carried out using the UltrafleXtreme TOF–TOF mass spectrometer (Bruker Daltonics, Bremen, Germany) with a 2 000 Hz smartbeam-II laser (355 nm) operating in positive ion mass reflectron mode. For molecular weight assignment, panoramic pulsed ion extraction and external calibration were used.

The GPC analysis was carried out using an Agilent Infinity 1260 HPLC system (Agilent Technologies, Inc., Santa Clara, CA, USA) with a refractive index detector and multi-angle static light scattering (miniDAWN) detector. Two GPC analytical columns PLgel Mixed-E (particle size: 3 μL, length 300 mm, diameter 7.5 mm) in series were used for the analysis. The refractive index detector was heated to 35 °C, and the flow rate was 1 mL/min. Tetrahydrofuran was used as a solvent. The GPC was only used to present the changes in the molecular weight. This method was not used to determine the exact molecular weight value.

The ssNMR ^{13}C spectra were acquired in an 18.8 T Bruker Avance III HD spectrometer at 16 kHz magic angle spinning using a 3.2 mm H/F X Bruker probe. Spectra were acquired with a relaxation delay of 3.5 s and 4 096 scans, leading to a total experimental time of 4 h. The spectra were analysed and plotted using the Topspin 3.6.5 program (Bruker Corporation, Billerica, MA, USA).

Thermogravimetric analysis (TGA) tests were performed using Discovery TGA equipment (TA instruments, New Castle, DE, USA). The sample weight was (10 ± 0.5) mg. The scanning temperature ranged from 30 to 700 °C under a nitrogen atmosphere at a heating rate of 10 °C·min^{-1}. Data processing was performed using TRIOS #5.0.0.44608 software. The measurements were carried out in duplicate.

Tensile (Young's) modulus and tensile strength were evaluated using a universal testing machine, an ElectroPuls E3000 from Instron (Norwood, Norfolk, MA, USA), and according to the ISO 14,125:1998 standard. The sample gauge section size was 2.5 mm × 4 mm × 25 mm. The deformation rate was 2 mm/min. The samples were tested at room temperature (18 °C). At least four parallel measurements were performed.

Glass transition temperatures ($T_{g(DSC)}$) were measured by DSC using Metler Toledo DSC 823e (Mettler Toledo, Greifensee, Switzerland) equipment. The samples were heated from –100 to 180 °C at a heating rate of 10 °C·min^{-1}. The tests were organized in a heating-cooling-heating-cooling regime. The $T_{g(DSC)}$ was detected in the second heating.

Mettler Toledo DMA/SDTA861e (Mettler Toledo, Greifensee, Switzerland) was used for the DMA. Glass transition temperatures ($T_{g(DMA)}$) were also measured using DMA. The samples were exposed to a heat-cool-heat cycle from –100 to 180 °C with 3 °C/min heating or cooling ramp at 1 Hz frequency and a preload force of 5 N. Tests were done in compression oscillation mode. Samples with a height of (7 ± 0.5) mm and a diameter of (14 ± 0.5) mm were used for tests. The measurements were carried out in duplicate.

The results of DSC and DMA were processed, including the determining glass transition temperature, using the program STARe Software ver. 9.00.

Eq. (1) was used to calculate the cross-link density using the results from the DMA test (Hill, 1997; Jena and Raju, 2008; Zhang et al., 2015; Kim et al., 2019):

$$\nu_e = \frac{E'_{rubbery}}{3RT} \quad (1)$$

where ν_e is the cross-link density (mol/cm^3); $E'_{rubbery}$ is the tensile storage modulus (MPa) at temperature $T_{g(DMA)} + 50$ K; R is the gas constant; T is the temperature that corresponds to the rubbery storage modulus (K).

According to Eq. (2), the molecular weight between cross-links M_c (g/mol) was calculated (Barszczewska-Rybarek et al., 2017).

$$M_c = \frac{3RT\rho}{E'_{rubbery}} \quad (2)$$

where the determination of the density ρ was based on the Archimedean principle using the Kern EMB-V balance with an integrated density determination function. Samples with a height of (7 ± 0.5) mm and a diameter of (14 ± 0.5) mm were used for tests. The measurement was carried out in triplicate.

All graphical figures representing the obtained data were composed using OriginPro 2021 9.8.0.200 program.

3. Results and discussion

The first stage of this study's framework was the synthesis of tall oil-based acrylates (Michael acceptors) from two tall oil-based polyols (E^{IR}TOFA_BD, E^{IR}TOFA_TMP). The second stage was obtaining polymers from tall oil fatty acids-based Michael donor (E^{IR}TOFA_BD_AA or E^{IR}TOFA_TMP_AA) and Michael acceptor (E^{IR}TOFA_BD_Acryl or E^{IR}TOFA_TMP_Acryl) by exploiting Michael addition. Fig. 1 shows the proposed concept of using free fatty acids to synthesize Michael monomers and obtain polymers through the Michael addition reaction. Synthesized materials are branched, close-meshed and highly cross-linked polymers. Polymer has an amorphous structure without ordered repeating units.

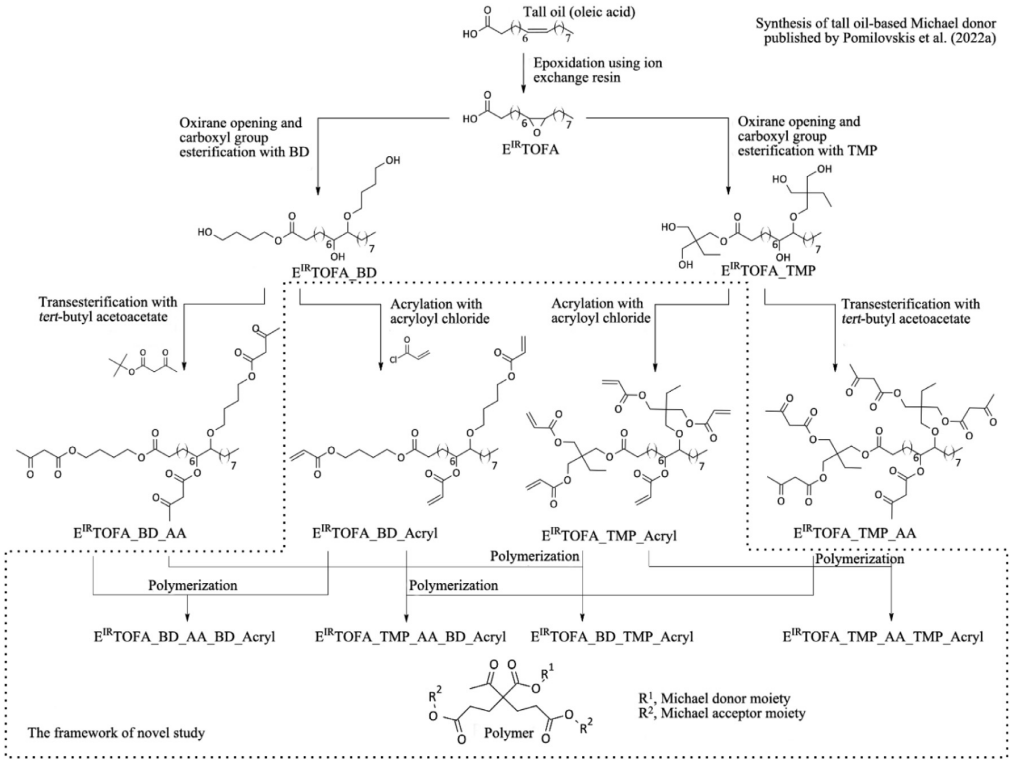

Fig. 1. Conceptual scheme of proposed design of polymer development from tall oil via the Michael reaction and the framework of this study. E^{IR}TOFA: epoxidized tall oil fatty acids; E^{IR}TOFA_BD: epoxidized tall oil fatty acids 1,4-butanediol polyol; E^{IR}TOFA_TMP: epoxidized tall oil fatty acids trimethylolpropane polyol; E^{IR}TOFA_BD_AA: epoxidized tall oil fatty acids 1,4-butanediol polyol acetoacetate; E^{IR}TOFA_TMP_AA: epoxidized tall oil fatty acids trimethylolpropane polyol acetoacetate; E^{IR}TOFA_BD_Acryl: epoxidized tall oil fatty acids 1,4-butanediol polyol acrylate; E^{IR}TOFA_TMP_Acryl: epoxidized tall oil fatty acids trimethylolpropane polyol acrylate; E^{IR}TOFA_BD_AA_BD_Acryl: polymer from epoxidized tall oil fatty acids 1,4-butanediol polyol acetoacetate and epoxidized tall oil fatty acids 1,4-butanediol polyol acrylate; E^{IR}TOFA_TMP_AA_BD_Acryl: polymer from epoxidized tall oil fatty acids trimethylolpropane polyol acetoacetate and epoxidized tall oil fatty acids 1,4-butanediol polyol acrylate; E^{IR}TOFA_BD_AA_TMP_Acryl: polymer from epoxidized tall oil fatty acids 1,4-butanediol polyol acetoacetate and epoxidized tall oil fatty acids trimethylolpropane polyol acrylate; E^{IR}TOFA_TMP_AA_TMP_Acryl: polymer from epoxidized tall oil fatty acids trimethylolpropane polyol acetoacetate and epoxidized tall oil fatty acids trimethylolpropane polyol acrylate.

Table 1
Acid and –OH values, moisture and content of acrylic group of tall oil-based acrylates.

Sample	Acid value (mg KOH per g)	–OH value (mg KOH per g)	Moisture (%)	Acryl groups (NMR, mol/g)
E^{IR}TOFA_BD	< 5	258 ± 5	0.20 ± 0.02	–
E^{IR}TOFA_TMP	6.9 ± 0.8	415 ± 4	0.049 ± 0.007	–
E^{IR}TOFA_BD_Acryl	< 5	28.8 ± 0.8	0.022 ± 0.004	0.003 9
E^{IR}TOFA_TMP_Acryl	< 5	46.2 ± 0.9	0.027 ± 0.003	0.003 5

Notes: E^{IR}TOFA_BD, epoxidized tall oil fatty acids 1,4-butanediol polyol; E^{IR}TOFA_TMP, epoxidized tall oil fatty acids trimethylolpropane polyol; E^{IR}TOFA_BD_Acryl, epoxidized tall oil fatty acids 1,4-butanediol polyol acrylate; E^{IR}TOFA_TMP_Acryl, epoxidized tall oil fatty acids trimethylolpropane polyol acrylate; NMR, nuclear magnetic resonance.

3.1. Characterization of michael acceptors

Different titration techniques were used to characterize the synthesized acrylates. Acid and –OH values and moisture were determined. The FT-IR, NMR, GPC, and MALDI-TOF were used to confirm the chemical structure. The content of acrylic groups was determined by NMR using 1,2,3-trimethoxybenzene as an internal standard. Additionally, the viscosity was determined.

Titration results and acrylic group content of the synthesized Michael acceptors were summarized in Table 1. After acrylation, a significant decrease in the –OH value was observed, which was the first indicator that the acrylate synthesis was successful. Results

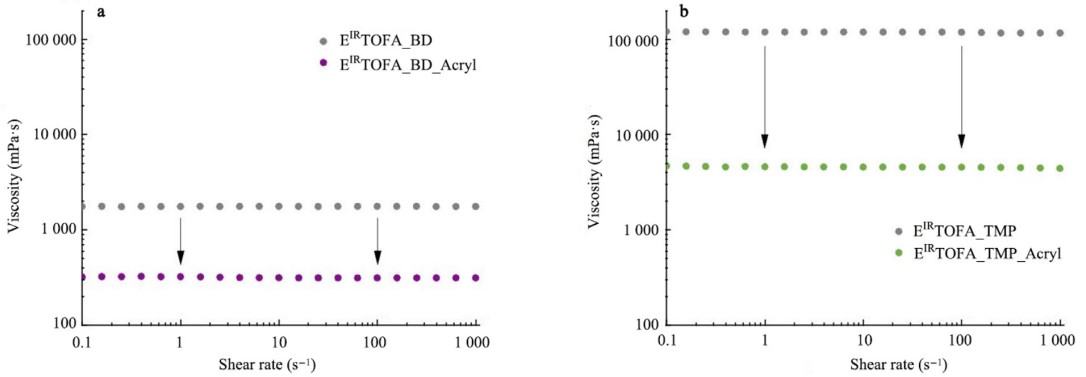

Fig. 2. Rheological measurements of tall oil-based polyols and tall oil-based acrylates: a) E^{IR}TOFA_BD and E^{IR}TOFA_BD_Acryl; b) E^{IR}TOFA_TMP and E^{IR}TOFA_TMP_Acryl.

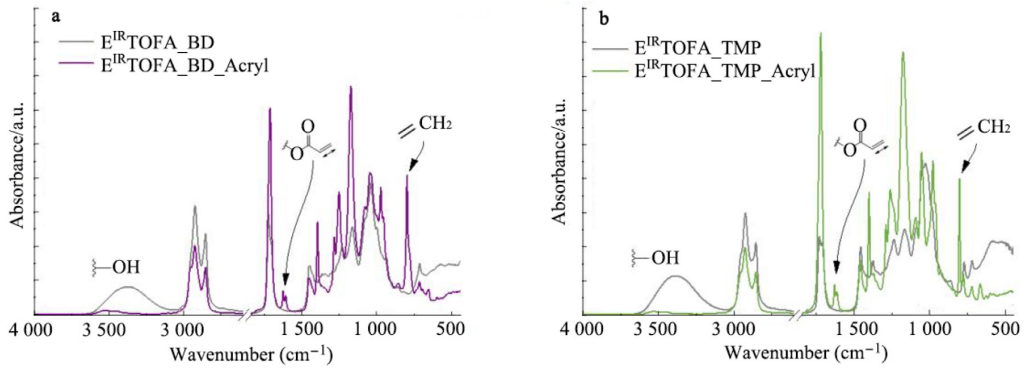

Fig. 3. Fourier-transform infrared (FT-IR) spectra of tall oil-based polyols and tall oil-based acrylates: a) spectra of E^{IR}TOFA_BD and E^{IR}TOFA_BD_Acryl; b) spectra of E^{IR}TOFA_TMP and E^{IR}TOFA_TMP_Acryl.

showed that the samples still contained relatively small amounts of hydroxyl groups after the acrylation. For E^{IR}TOFA_BD_Acryl, the –OH value dropped from (258 ± 5) to (28.8 ± 0.8) mg KOH per gram, while for E^{IR}TOFA_TMP_Acryl the value dropped from (415 ± 4) to (46.2 ± 0.9) mg KOH per gram. This indicated that the replacement of hydroxyl groups with acrylic groups had not been completed. However, the —OH values of the acrylates were small compared to the –OH values of the polyol and didn't substantially impact further polymer production.

The viscosities of polyols E^{IR}TOFA_BD and E^{IR}TOFA_TMP and their corresponding acrylates, E^{IR}TOFA_BD_Acryl and E^{IR}TOFA_TMP_Acryl, were presented in Fig. 2. Fatty acid-based polyols, including tall oil-based polyols, are known for their relatively high viscosities (Kirpluks et al., 2017). The viscosity of the E^{IR}TOFA_TMP polyol exceeded 118 000 mPa·s. Rheological measurements showed a viscosity decrease after introducing acrylate groups into polyols. After the polyol was acrylated, the viscosity decreased more than 25 times to 4 560 mPa·s. The same trend can be observed in the case of E^{IR}TOFA_BD acrylation. The viscosity of E^{IR}TOFA_BD_Acryl was 315 mPa·s. The decrease in viscosity is due to a decrease in hydrogen bonding between chains caused by the disappearance of the hydroxyl group.

Since the viscosity was independent of the shear rate applied, the synthesized substances can be categorized as Newtonian fluids. The Newtonian behaviour and lower viscosity of the acrylates make them more feasible for use in the industry. Lower viscosity and Newtonian behaviour would ensure smoother flow through pipelines and pumps, using less energy for transfer. It would be easier to mix synthesized acrylates with reagents and additives.

The FT-IR spectra of acrylates E^{IR}TOFA_BD_Acryl and E^{IR}TOFA_TMP_Acryl, along with polyols E^{IR}TOFA_BD and E^{IR}TOFA_TMP, were shown in Fig. 3. Comparing the spectrum of polyol E^{IR}TOFA_BD to the spectrum of acrylate E^{IR}TOFA_BD_Acryl, results showed that the peak at 3 600–3 150 cm^{-1} corresponding to the hydroxyl group disappeared. New peaks appeared at 1 640–1 620 cm^{-1}, 1 407 cm^{-1}, and 810 cm^{-1} were corresponding to the acrylate C = C vibration, scissoring vibration for HC=CH_2, and =CH_2 twisting vibration of acrylic group, respectively, which indicated successful acylation reaction (Paramarta and Webster, 2017). The same trend could be observed when the spectra of polyol E^{IR}TOFA_TMP and acrylate E^{IR}TOFA_TMP_Acryl were compared.

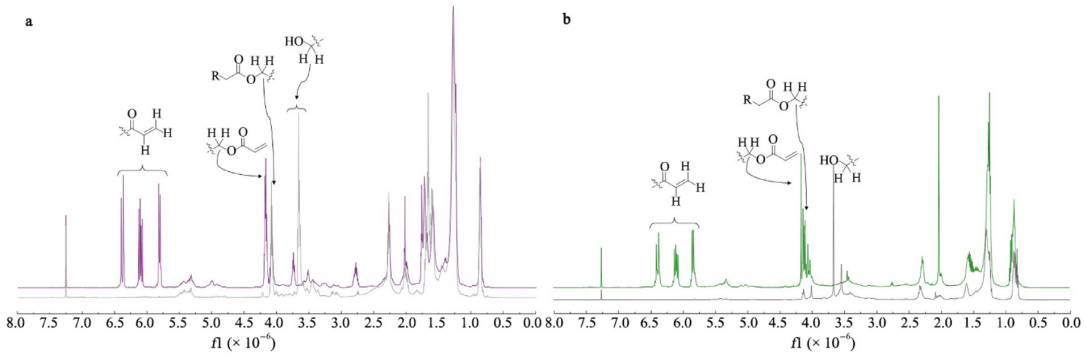

Fig. 4. Proton nuclear magnetic resonance (^{1}H NMR) spectra for a) E^{IR}TOFA_BD (in grey) and E^{IR}TOFA_BD_Acryl (in purple); b) E^{IR}TOFA_TMP (in grey) and E^{IR}TOFA_TMP_Acryl (in green). All spectra were recorded in $CDCl_3$ (500 MHz).

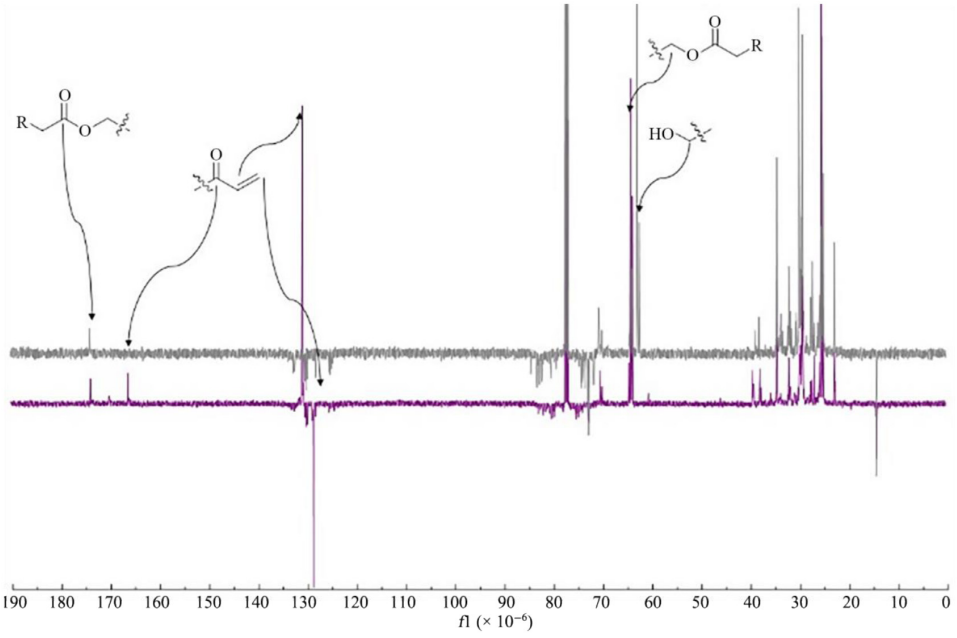

Fig. 5. The ^{13}C attached proton test NMR spectra for E^{IR}TOFA_BD (in grey) and E^{IR}TOFA_BD_Acryl (in purple). The spectra were recorded in $CDCl_3$ (125 MHz).

The FT-IR spectra, which confirmed the chemical structures, have an exceptional correlation with NMR spectra (Figs. 4 and 5). The monomers were also analysed by both ^{1}H and ^{13}C NMR spectra. The ^{13}C NMR spectra were registered in attached proton test regime. In the ^{1}H NMR spectrum for the acrylated E^{IR}TOFA-polyol, typical signals for vinyl moiety (6.4×10^{-6} (d, $J=17.0$ Hz), 6.1×10^{-6} (dd, $J=17.0$ Hz, $J=10.6$ Hz) and 5.8×10^{-6} (d, $J=10.6$ Hz) were visible. The corresponding signals of the vinyl moiety in ^{13}C spectra were at 1.28×10^{-4} (–CH=) and 1.30×10^{-4} (=CH_2). The formation of ester bound was proved by new signals at $4.22\times10^{-6}-4.13\times10^{-6}$ (^{1}H NMR spectrum) and 6.4×10^{-5} (^{13}C NMR spectrum), characterizing –CH_2COOR moiety (where R is vinyl group). Meanwhile, the intensity of signals arising from $HOCH_2$– at $3.7\times10^{-6}-3.6\times10^{-6}$ (^{1}H NMR spectrum) and $6.2\times10^{-5}-6.3\times10^{-5}$ (^{13}C NMR spectrum) were reduced, thus indicating the esterification of free hydroxyl groups. Additionally, new signals characterizing the carbonyl group of acrylate at 1.66×10^{-4} in ^{13}C NMR spectrum proved the formation of acrylates.

The GPC spectra of tall oil fatty acids-based acrylates, along with tall oil fatty acids-based polyols, are shown in Fig. 6. The GPC results confirmed the well known fact that tall oil fatty acid polyols consist of a composition of monomers, dimers, trimers, and oligomers (Abolins et al., 2021; Polaczek et al., 2022). Comparing the GPC curves of acrylated tall oil-based polyols and tall oil fatty

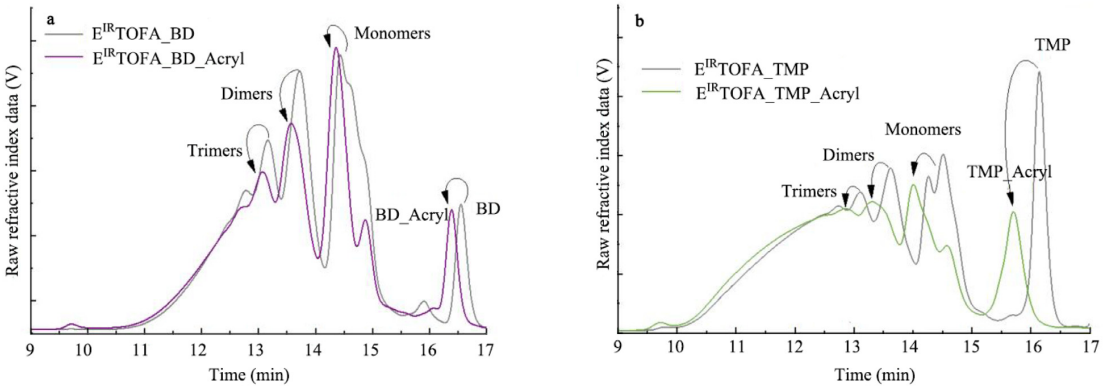

Fig. 6. Gel permeation chromatography (GPC) chromatogram of tall oil-based polyols and tall oil-based acrylates: a) E^IR TOFA_BD and E^IR TOFA_BD_Acryl; b) E^IR TOFA_TMP and E^IR TOFA_TMP_Acryl.

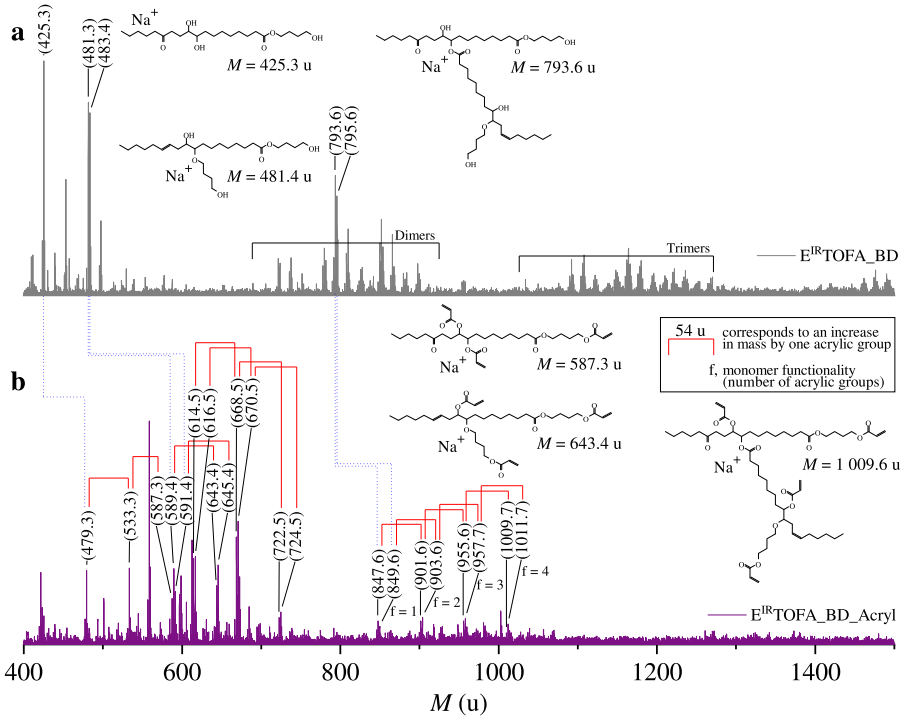

Fig. 7. Matrix-assisted laser desorption/ionization-time of flight (MALDI-TOF) spectra of tall oil-based polyol and tall oil-based acrylate: a) E^IR TOFA_BD; b) E^IR TOFA_BD_Acryl.

acid-based polyols, the main peaks have slightly shifted to a shorter retention time indicating an increase in molecular weight. An increase in molecular weight was due to the replacement of hydroxyl groups with acrylic groups in the structure. The increase in molecular weight confirmed the successful acrylation. The GPC results correlated well with the FT-IR (Fig. 3) and NMR (Figs. 4 and 5) data.

Along with GPC measurements, synthesized substances were further analysed using MALDI-TOF spectrometry to identify changes in the chemical structure of the components. MALDI-TOF spectra are shown in Figs. 7 and 8. The MALDI-TOF data also confirmed that tall oil fatty acid-based polyols consist of a complex mixture with an extensive amount of minor intensity mass peaks. Our previous study reported corresponding compounds for several major peaks in tall oil fatty acid polyols (Pomilovskis et al., 2022a).

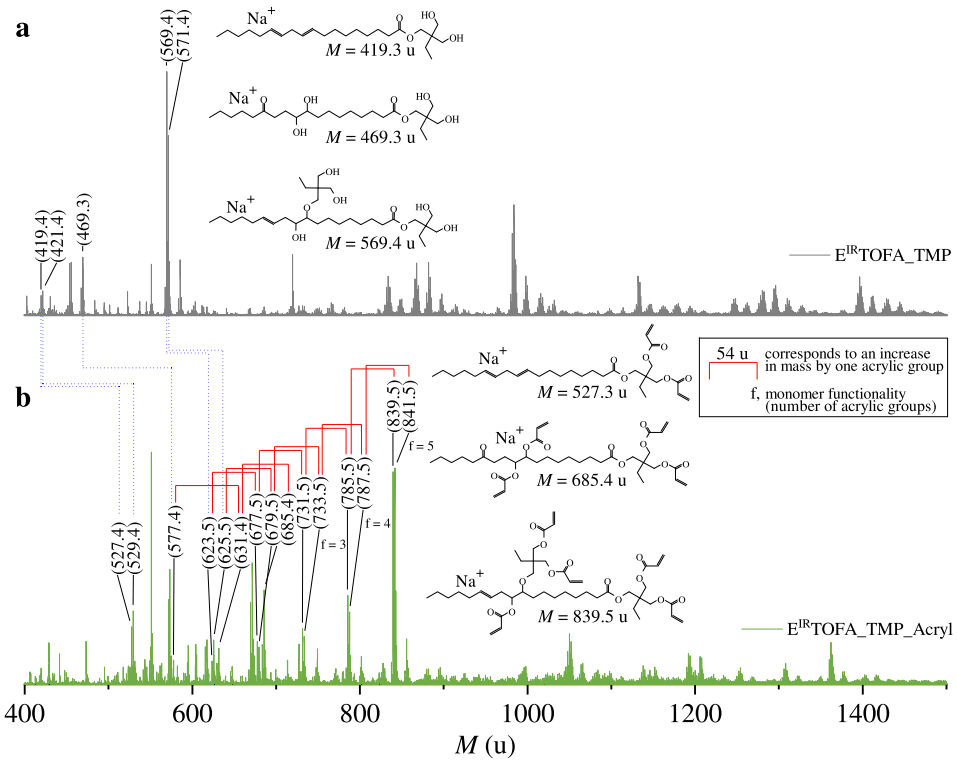

Fig. 8. The MALDI-TOF spectra of tall oil fatty acids-based polyol and tall oil fatty acids-based acrylate: a) E^{IR}TOFA_TMP; b) E^{IR}TOFA_TMP_Acryl.

The main challenge in analysing MALDI-TOF MS spectra was identifying peaks for acrylated tall oil fatty acid polyols. In the spectra, typically, the peaks are in pairs with a difference of 2 u. This corresponds to the difference in the molecular weight of linoleic acid and oleic acid. In the MALDI-TOF spectra (Figs. 7 and 8), the most intense peaks for acrylated polyols were at higher u values than for polyols. When comparing the MALDI-TOF spectra of polyol and the corresponding acrylate, several peaks were identified with the difference divisible by 54 in u unit. This number of units (54 u) represents an increase in mass from one acrylic group. Since most peaks are shifted by 108, 162, 216, 270, and 324 u units, there are at least two, three, four, and five acrylic groups per molecule after acrylation. Ion masses corresponding to fully acrylated polyols, E^{IR}TOFA_BD and E^{IR}TOFA_TMP, were found in the spectrum.

Fully functionalized E^{IR}TOFA_BD polyol contains three functional groups per molecule. Relatively intense corresponding peaks at 643.4 and 645.4 u for three functional acrylates could be seen in the spectrum (Fig. 7). In the case of E^{IR}TOFA_BD_Acryl, acrylation of dimers resulted in the formation of compounds with four functional groups at 1 009.7 and 1 011.7 u. The intensity of the corresponding peaks was relatively small. Also, it could be concluded that the mixture also contained partially acrylated compounds. Not all hydroxyl groups had been acrylated. This also correlated with the results of titration and FT-IR.

In the case of acrylate E^{IR}TOFA_TMP_Acryl, the intense bands at 839.5 and 841.5 u correspond to compounds containing five functional groups per molecule (Fig. 8). In the spectrum of E^{IR}TOFA_TMP_Acryl, an increase in the functionality of the molecules could be observed. As in the case of E^{IR}TOFA_BD_Acryl, the partially acrylated compounds were also observed for E^{IR}TOFA_TMP_Acryl. The peak intensity increased with the number of acrylic groups introduced per molecule, and the most intense bands corresponded to a fully acrylated polyol. Due to high functionality, the synthesized tall oil-based Michael donors can be used to obtain a highly cross-linked polymer matrix, which may increase the polymer matrix's mechanical properties. The synthesized acrylates from tall oil fatty acids-based polyols contain several acrylic groups required for polymerization according to the Michael reaction mechanism. Considering the data of rheology, FT-IR, NMR, GPC, and MALDI-TOF MS, the obtained tall oil polyol-based acrylates are suitable for polymer synthesis by the Michael reaction. Moreover, the synthesized tall oil polyol-based acrylates are promising in producing other polymers, for example, in UV-initiated free radical polymerization in the production of coatings.

3.2. Characterization of developed bio-based thermoset polymer

Two-component resins are widely applied in several industries, such as composite production and coatings, adhesive, and elastomer manufacturing. The present study proposed a new two-component bio-based polymer development method by exploiting the Michael

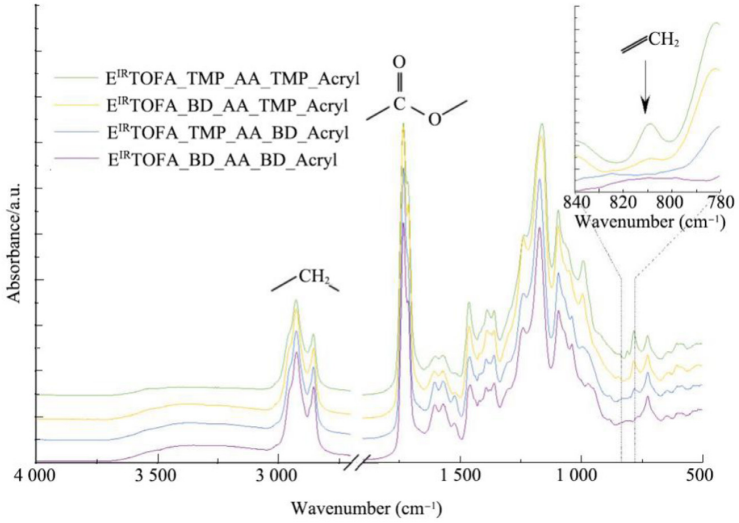

Fig. 9. The FT-IR spectra of polymers developed from tall oil-based Michael donor and acceptor.

addition. The synthesized tall oil-based acrylates and previously obtained tall oil-based acetoacetates have been successfully used to develop a highly cross-linked polymer matrix. The polymer material has high thermal stability and mechanical properties and may be used as an alternative to industrially used thermoset resins.

By tactile perception, the polymer materials obtained from 1,4-butanediol are flexible, similar to hard rubber. The resulting polymer materials based on trimethylolpropane are solid, with an organic glass-like feel to the hand. All synthesized polymers were transparent and clear with a slight brown or yellow tint.

3.2.1. Chemical structure characterization of synthesized thermoset polymers

The structure of the developed polymer materials was characterized by FT-IR spectroscopy. The spectra are shown in Fig. 9. The characteristic absorption bands of acrylate at 1 640–1 620 cm^{-1} and 1 407 cm^{-1} can not be evaluated because of overlapping with the absorption bands typical of the functional groups of the donor. The FT-IR spectrum well represented the content of acrylic groups by the characteristic absorption of $=CH_2$ twisting vibration bands at about 810 cm^{-1}.

Polymers obtained from acrylate E^{IR}TOFA_BD_Acryl had no absorption band at 810 cm^{-1}. This could indicate a good conversion and complete reaction of the acrylic groups. The absorption band was observable for both polymers synthesized from E^{IR}TOFA_TMP_Acryl. When comparing FT-IR spectra of E^{IR}TOFA_BD_AA_TMP_Acryl and E^{IR}TOFA_TMP_AA_TMP_Acryl, the absorption band of the acrylic group at 810 cm^{-1} was more intense for the last. This could mean an incomplete conversion because of high viscosity, high functionality, as well as steric effects.

The polymer samples were also characterized using ssNMR ^{13}C spectroscopy. The spectra are shown in Fig. 10. The spectra exhibited anticipated ^{13}C chemical shifts. The analysis of the ssNMR spectrum showed signals corresponding to the >CH–O– group in the range of $6.30\times10^{-5} - 8.35\times10^{-5}$ ^{13}C for all of the developed polymers. The >CH–O– group was a result of an oxirane ring opening with a polyol. Also, the characteristic signal of ^{13}C corresponding quaternary carbon was in the same range of $6.30\times10^{-5} - 8.35\times10^{-5}$ indicating that the reaction of two acrylic groups with the methylene group of acetoacetate via the Michael addition had occurred.

Overlapping of several signals can also be observed in the range of $2.65\times10^{-5} - 4.29\times10^{-5}$. The characteristic signal of ^{13}C corresponding tertiary carbon can be observed in this range. Also, tertiary carbon is essential for the detection of polymerization, representing a situation where one acetoacetate group has reacted with only one acrylic group. The characteristic signal of ^{13}C in the $–C(=O)–CH_3$ group was in the same range of $2.40\times10^{-5} - 2.44\times10^{-5}$, which represented the acetoacetate group in the Michael donor compound.

The signals of the acrylate groups at $1.302\times10^{-4} - 1.312\times10^{-4}$ indicated an incomplete reaction. The ssNMR ^{13}C spectra were consistent with FT-IR data. While the signal intensity of acrylic groups in polymers obtained from E^{IR}TOFA_BD_Acryl was low, it was relatively intense in spectra of polymers obtained from E^{IR}TOFA_TMP_Acryl. A much more branched structure and multiple acrylic groups per molecule decreased the reactivity of the E^{IR}TOFA_TMP_Acryl and E^{IR}TOFA_TMP_AA because of steric hindrance effects. Since the acceptor and donor used in polymer synthesis are derived from fatty acids, they contain double bonds because of an incomplete epoxidation reaction. The double bond signal overlaps with the signal characteristic of acrylate groups. This must be taken into account when evaluating the results. Hence, the NMR and FT-IR results confirmed that polymers from tall oil fatty acids-based donors and acceptors via the Michael addition were successfully synthesized.

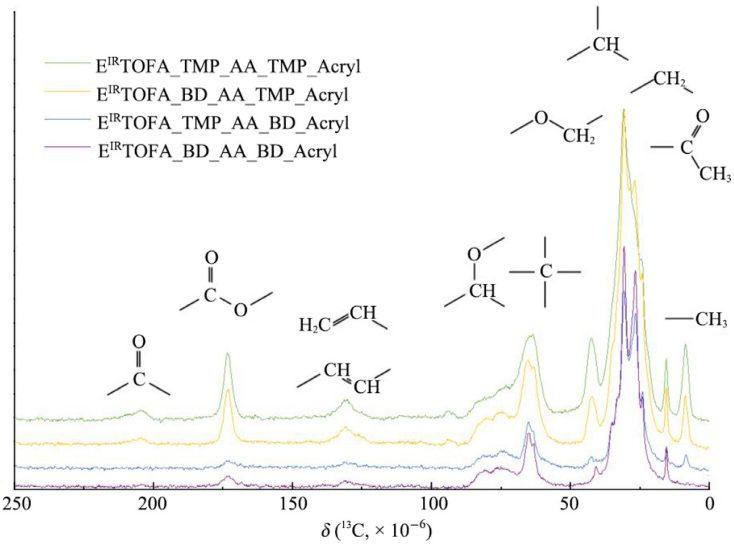

Fig. 10. Solid-state nuclear magnetic resonance (ssNMR) ^{13}C spectra of polymers developed from tall oil-based Michael donor and acceptor.

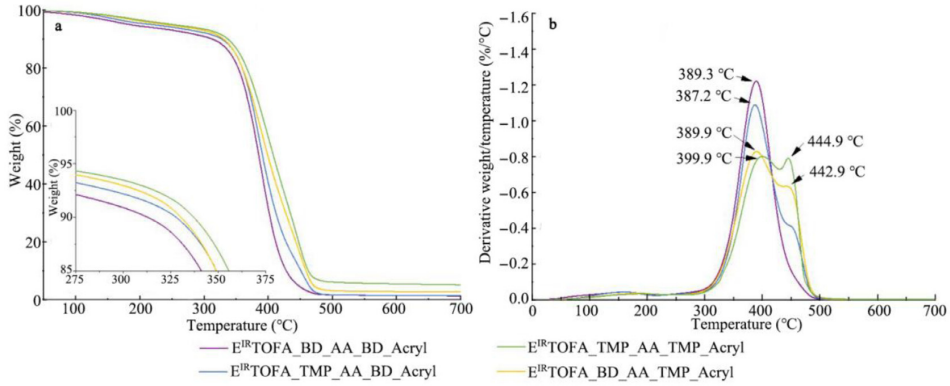

Fig. 11. Stability of thermosets from tall oil-based Michael donor and acceptor: a) thermal gravimetric analysis (TGA) thermograms; b) TGA weight derivative curves.

3.2.2. Thermal properties of synthesized bio-based thermoset polymers

The thermal stability of synthesized polymers was assessed by TGA. Thermograms and weight derivatives curves are shown in Fig. 11. The initial degradation stage occurred up to 300 °C because of the decomposition of the catalyst and some leftover raw materials. Polymer samples showed different degradation processes at temperatures above 300 °C, which could be very well seen in the mass loss derivative curves. The E^{IR}TOFA_BD_AA_BD_Acryl TGA mass loss derivative curve showed one symmetrical peak with only one clear maximum at 389.3 °C.

The peak of the E^{IR}TOFA_TMP_AA_BD_Acryl mass loss derivative curve has a shoulder at about 450 °C. The second degradation peak became more pronounced when the composition of the polymer contained more TMP derivatives. Both derivative peaks of the E^{IR}TOFA_TMP_AA_TMP_Acryl mass loss derivative curve at 399.9 °C and 444.9 °C had almost the same rate of change in weight loss. The first derivative peak can be linked to the ester and ether bonds dissociation to form CO_2 and other low molecular weight compounds (He et al., 2019; Wang et al., 2019). The second derivative peak can be attributed to the degradation of the TMP of the polymer chemical structure (Cheong et al., 2019).

The onset decomposition temperature (T_{onset}), the temperature at 10% weight loss ($T_{10\%}$), the temperature at 50% weight loss ($T_{50\%}$), and maxima of derivative peaks and residue are summarized in Table 2. The polymer's main degradation process occured between 300 and 475 °C. The T_{onset}, $T_{10\%}$, and $T_{50\%}$ were different between samples. The lowest T_{onset} was for the E^{IR}TOFA_BD_AA_BD_Acryl sample reaching 338.7 °C. The T_{onset} for samples E^{IR}TOFA_TMP_AA_BD_Acryl, E^{IR}TOFA_BD_AA_TMP_Acryl,

Table 2
Thermal gravimetric analysis and derivative thermogravimetry results of thermoset polymers from tall oil-based Michael monomers.

Sample	T_{onset} (°C)	$T_{10\%}$ (°C)	$T_{50\%}$ (°C)	T_{1max} (%/°C)	T_{2max} (%/°C)	Residue (%)
E^{IR}TOFA_BD_AA_BD_Acryl	338.7	312.9	385.3	389.3	–	1.28
E^{IR}TOFA_TMP_AA_BD_Acryl	341.0	327.9	391.0	387.2	–	1.30
E^{IR}TOFA_BD_AA_TMP_Acryl	348.2	330.5	399.2	389.9	442.9	2.59
E^{IR}TOFA_TMP_AA_TMP_Acryl	352.9	337.1	407.9	399.9	444.9	5.10

Notes: T_{onset}, $T_{10\%}$, $T_{50\%}$ refer to the onset decomposition temperature, the temperature at 10% weight loss, and the temperature at 50% weight loss, respectively; T_{1max} and T_{2max} refer to the maxima of derivative peaks.

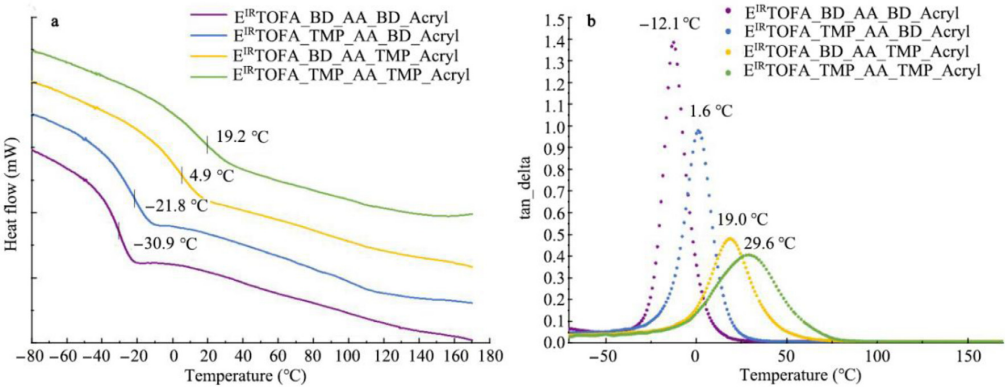

Fig. 12. Differential scanning calorimetry (DSC) and dynamic mechanical analysis (DMA) results of developed polymers from tall oil-based Michael donor and acceptor: a) DSC curves; b) DMA loss factor (tan δ) as a function of temperature curves.

and E^{IR}TOFA_TMP_AA_TMP_Acryl were 341.0, 348.2, and 352.9 °C, respectively. The same trend also persised for $T_{10\%}$ and $T_{50\%}$. Thermal stability was similar to polymers derived from bio-based acrylate and petrochemical acrylate (Pomilovskis et al., 2022b).

Polymer sample E^{IR}TOFA_TMP_AA_TMP_Acryl exhibited slightly better thermal stability than other samples. The relationship between higher cross-link density and high thermal stability is well known (Liang et al., 2019; Su et al., 2020). This relationship was also observed in our study. Thus, the higher thermal stability of the E^{IR}TOFA_TMP_AA_TMP_Acryl polymer sample compared to other polymers is explained by a higher cross-link density. Higher cross-linking density favours carbonation reaction resulting in a greater amount of solid residue (Su et al., 2020). Solid residue yield was measured at 675 °C. From all the developed bio-based thermoset polymer samples, the solid residue yield was the highest for E^{IR}TOFA_TMP_AA_TMP_Acryl polymer. The solid residue yield was 5.10%. The results showed that the developed bio-based thermoset polymer samples were thermally stable. All samples had very similar weight loss curves at the start up to 300 °C. The samples represented weight loss of less than 10% up to 300 °C.

The thermal behaviours of the polymer samples were also studied using DSC. The DSC thermograms of obtained bio-based thermoset polymers are shown in Fig. 12a. The $T_{g(DSC)}$ was identified for all obtained polymers. The $T_{g(DSC)}$ of polymer samples E^{IR}TOFA_BD_AA_BD_Acryl, E^{IR}TOFA_TMP_AA_BD_Acryl, E^{IR}TOFA_BD_AA_TMP_Acryl, and E^{IR}TOFA_TMP_AA_TMP_Acryl were found to be −30.9, −21.8, 4.9, and 19.2 °C, respectively. It was observed that $T_{g(DSC)}$ increased with the increased TMP-derivative content in the polymer composition. This was most likely due to a higher cross-link density of these polymers. The correlation between increasing cross-link density and higher $T_{g(DSC)}$ of the polymer was also reported by Wang et al. (2019), similarly as in the case of $T_{g(DMA)}$.

Different effects were measured in the DSC and DMA methods. In the case of DMA, stress was applied, and the strain in the constant, while DSC measures changed in heat capacity (Menard, 1999). The DMA tests were used to determine the $T_{g(DMA)}$ and storage modulus in the rubbery plateau region for calculations of cross-link density. The tan δ of the obtained samples is shown in Fig. 12b, and the results were summarized in Table 3. From Fig. 12b, the tan δ peaks of the BD_Acryl polymer systems were narrower, and the values of tan δ were higher than tan δ values of TMP_Acryl derived polymers, showing a network that was more homogeneously cross-linked.

The same trend was observed between $T_{g(DMA)}$ and $T_{g(DSC)}$ (Table 3), but the $T_{g(DMA)}$ values were higher than $T_{g(DSC)}$ values. The lowest and highest $T_{g(DMA)}$ values were determined to be −12.1 °C for polymer E^{IR}TOFA_BD_AA_BD_Acryl, and 29.6 °C for polymer sample E^{IR}TOFA_TMP_AA_TMP_Acryl. It was observed that polymer samples with higher cross-link density exhibited higher glass transition temperatures (Table 3). Rahul and Kitey (2016) also reported that $T_{g(DMA)}$ was effected by the polymer's cross-link density.

Table 3
Differential scanning calorimetry (DSC) and dynamic mechanical analysis (DMA) results of polymers from tall oil-based Michael monomers.

Sample	Glass transition temperature (°C)		ρ (g/cm^3)	E' (MPa)	ν_e (mol/cm^3)	M_c (g/mol)
	$T_{g(DSC)}$	$T_{g(DMA)}$				
E^{IR}TOFA_BD_AA_BD_Acryl	−30.9 ± 0.4	−12.1 ± 0.3	1.071 ± 0.002	5.3 ± 0.4	6.9×10^{-4}	1 562
E^{IR}TOFA_TMP_AA_BD_Acryl	−21.8 ± 0.7	1.6 ± 0.2	1.085 ± 0.002	5.8 ± 0.2	7.1×10^{-4}	1 518
E^{IR}TOFA_BD_AA_TMP_Acryl	4.9 ± 0.2	19.0 ± 0.2	1.104 ± 0.001	11.4 ± 0.8	1.33×10^{-3}	829
E^{IR}TOFA_TMP_AA_TMP_Acryl	19.2 ± 0.4	29.6 ± 0.2	1.125 ± 0.003	13.7 ± 0.3	1.55×10^{-3}	724

Notes: $T_{g(DSC)}$ and $T_{g(DMA)}$ refer to the glass transition temperatures of DSC and DMA, respectively; ρ refers to the density; ν_e refers to the cross-link density; E' refers to the storage modulus at $T_{g(DMA)}$+50 K; M_c refers to the molecular weight between cross-links.

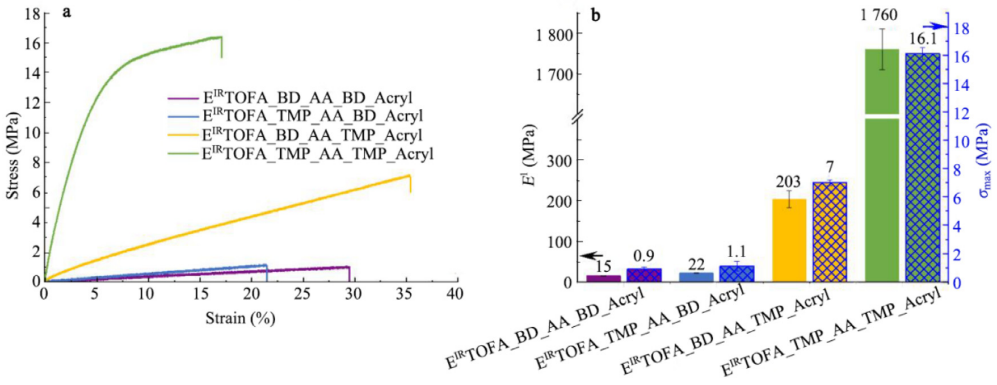

Fig. 13. Tensile properties for polymers developed from tall oil fatty acids-based Michael donor and acceptor: a) stress-strain curves; b) tensile (Young's) modulus (E^1) and stress at break (σ_{max}).

3.2.3. Mechanical properties of synthesized bio-based thermoset polymers

The stress-strain curves and elongation at break are depicted in Fig. 13a, and Fig. 13b showed the Young's modulus and tensile strength of the obtained thermoset polymers. Tensile tests confirmed the dependence of mechanical properties on the cross-link density. The polymers derived from E^{IR}TOFA_BD_Acryl exhibited the elastic region. At the same time, polymer E^{IR}TOFA_TMP_AA_TMP_Acryl exhibited the stress-strain behaviour of hard plastics, followed by strain softening before breaking.

According to results in Table 3 and Fig. 13a, the polymers obtained from E^{IR}TOFA_TMP_Acryl with higher tensile modulus because of higher cross-link density and lower molecular weight between cross-links. The highest Young's modulus (E^1), stress at break (σ_{max}), and the lowest elongation at break were 1 760 MPa, 16.1 MPa, and 17%, repectively, for the E^{IR}TOFA_TMP_AA_TMP_Acryl polymer. Properties of the E^{IR}TOFA_TMP_AA_TMP_Acryl polymer were very similar to the polymer obtained from Lupranol 3300 (trifunctional polyether polyol based on glycerine) acetoacetate and pentaeritol tetraacrylate (E^1 = 1 822 MPa; σ_{max} = 30 MPa) (Pomilovskis et al., 2022b). Mechanical tests confirmed the possibility of acquiring thermoset polymer materials by using Michael donors and acceptors that both are based on fatty acids. The developed polymer materials showed competitive properties to semi-petrochemical-based polymers. Amongst the polymer samples, E^{IR}TOFA_BD_AA_BD_Acryl had the lowest tensile properties. The E^1, σ_{max}, and elongation for above mentioned polymer were 15 MPa, 0.9 MPa, and 27%, respectively which exhibited rubber-like properties.

4. Conclusions

Two novel tall oil fatty acids-based Michael acceptor acrylates, E^{IR}TOFA_BD_Acryl and E^{IR}TOFA_TMP_Acryl, were prepared and characterized. These Michael acceptors were synthesized from two tall oil-based polyols (E^{IR}TOFA_BD and E^{IR}TOFA_TMP) by acrylation with acryloyl chloride. Several methods confirmed the successful synthesis of the Michael acceptor: titration, FT-IR, NMR, GPC, and MALDI-TOF MS. The characteristic of developed acrylates was fully suited for the synthesis of polymers via the Michael addition polymerization. Furthermore, synthesized acrylates were successfully used to develop polymers with tall oil fatty acids-based Michael donor acetoacetates (E^{IR}TOFA_BD_AA, E^{IR}TOFA_TMP_AA). The chemical composition and thermal and mechanical properties were determined for novel polymers. The functionality of the utilized monomers had a significant impact on the polymer's characteristics. Thermal stability of the developed polymers reached 300 °C. The glass transition temperatures varied from −30.9 °C for E^{IR}TOFA_BD_AA_BD_Acryl to 19.2 °C for E^{IR}TOFA_TMP_AA_TMP_Acryl obtained by DSC and from −12.1 °C for E^{IR}TOFA_BD_AA_BD_Acryl to 29.6 °C for E^{IR}TOFA_TMP_AA_TMP_Acryl obtained by DMA. Polymers with higher cross-link density had

higher glass transition temperatures. The tensile properties of polymers were also different because of different cross-linking densities. It was demonstrated that the mechanical properties of polymers can be customized when different functionalities of tall oil-based Michael monomers are used for polymer synthesis. It is possible to obtain rubber-like polymers from 1,4-butanediol-based components, while hard polymers can be obtained from trimethylolpropane-based components. The higher the amount of TMP-containing components in the composition, the harder the resulting polymer material is. The two-component polymer systems developed in this study can be used as resins, composite matrices, coatings, and polymer foams. It is also possible to use mixtures of several acrylates or acetoacetates to adjust desired properties of the polymers. This research has successfully provided completely new insight into the possibilities of a by-product valorization of the forestry and wood processing industry: tall oil. We believe the synthesis of advanced polymers from tall oil via the Michael reaction could make a significant contribution to the production of bio-based polymer materials.

Declaration of Competing Interest

No conflict of interest.

Acknowledgements

This research was funded by the Latvian Council of Science, project “High bio-based content thermoset polymer foam development from plant origin oils (Bio-Mer) ” (No. lzp-2020/1–0385). This publication was supported by LZA (Latvia) and CAS (Czech Republic) mobility project “Innovative bio-based polyols and advanced methods of their characterization, project no. LZA-22-02″. This work has been supported by ESF within Project “Strengthening of PhD students and academic personnel of Riga Technical University and BA School of Business and Finance in the strategic fields of specialization" (No 8.2.2.0/20/I/008) of the Specific Objective 8.2.2 “To Strengthen Academic Staff of Higher Education Institutions in Strategic Specialization Areas" of the Operational Programme “Growth and Employment”. This publication was supported by Riga Technical University’s Doctoral Grant programme.

References

Abolins, A., Pomilovskis, R., Vanags, E., Mierina, I., Michalowski, S., Fridrihsone, A., Kirpluks, M., 2021. Impact of different epoxidation approaches of tall oil fatty acids on rigid polyurethane foam thermal insulation. Materials. (Basel) 14, 894.
Aryan, V., Kraft, A., 2021. The crude tall oil value chain: global availability and the influence of regional energy policies. J. Clean. Prod. 280, 124616.
Baghban, S.A., Ebrahimi, M., Khorasani, M., 2022. A facile method to synthesis of a highly acrylated epoxidized soybean oil with low viscosity: combined experimental and computational approach. Polym. Test. 115, 107727.
Barszczewska-Rybarek, I.M., Korytkowska-Wałach, A., Kurcok, M., Chladek, G., Kasperski, J., 2017. DMA analysis of the structure of crosslinked poly(methyl methacrylate)s. Acta. Bioeng. Biomech. 19, 47–53.
Boucher, D., Ladmiral, V., Negrell, C., Caussé, N., Pébère, N., 2021. Partially acrylated linseed oil UV-cured coating containing a dihemiacetal ester for the corrosion protection of an aluminium alloy. Prog. Org. Coat. 158, 106344.
Briede, S., Jurinovs, M., Nechausov, S., Platnieks, O., Gaidukovs, S., 2022. State-of-the-art UV-assisted 3D printing via a rapid syringe-extrusion approach for photoactive vegetable oil acrylates produced in one-step synthesis. Mol. Syst. Des. Eng. 7, 1434–1448.
Cao, Z.Y., Gao, F., Zhao, J.Z., Wei, X., Cheng, Q., Zhong, J., Lin, C., Shu, J.B., Fu, C.Q., Shen, L., 2019. Bio-based coating materials derived from acetoacetylated soybean oil and aromatic dicarboxaldehydes. Polymers. (Basel) 11, 1809.
Cheong, M.Y., Hasan, Z.A.A., Idris, Z., 2019. Characterisation of epoxidised trimethylolpropane trioleate: NMR and thermogravimetric analysis. J. Oil. Palm. Res. 31, 146–158.
Claux, O., Rapinel, V., Abert-Vian, M., Chemat, F., 2023. Green Extraction of Vegetable Oils: From Tradition to Innovation. Reference Module in Food Science. Elsevier, Amsterdam.
Dechent, S.E., Kleij, A.W., Luinstra, G.A., 2020. Fully bio-derived CO_2 polymers for non-isocyanate based polyurethane synthesis. Green. Chem 22, 969–978.
European Commission, 2019. The European Green Deal. Available at: https://www.europarl.europa.eu/RegData/etudes/ATAG/2019/644205/EPRS_ATA(2019)644205_EN.pdf#:~:text=The%20European%20Green%20Deal%20is%20a%20programme%20outlined,an%20extraordinary%20plenary%20session%20on%2011%20December%202019.
Gan, Y.C., Jiang, X.S., 2014. Photo-cured materials from vegetable oils. In: Liu, Z.S., Kraus, G. (Eds.), Green Materials from Plant Oils. The Royal Society of Chemistry, London, pp. 1–27.
Gapsari, F., Djakfar, L., Handajani, R.P., Yusran, Y.A., Hidayatullah, S., Rangappa, S.M., Siengchin, S., 2022. The application of timoho fiber coating to improve the composite performance. Results. Eng 15, 100499.
Ge, X.Y., Yu, L., Liu, Z.S., Liu, H.S., Chen, Y., Chen, L., 2019. Developing acrylated epoxidized soybean oil coating for improving moisture sensitivity and permeability of starch-based film. Int. J. Biol. Macromol. 125, 370–375.
He, X.F., Zhong, J., Cao, Z.Y., Wang, J.L., Gao, F., Xu, D.D., Shen, L., 2019. An exploration of the Knoevenagel condensation to create ambient curable coating materials based on acetoacetylated castor oil. Prog. Org. Coat. 129, 21–25.
Hermens, J.G.H., Freese, T., van den Berg, K.J., van Gemert, R., Feringa, B.L., 2020. A coating from nature. Sci. Adv. 6, eabe0026.
Hill, L.W., 1997. Calculation of crosslink density in short chain networks. Prog. Org. Coat. 31, 235–243.
Hu, Y., Jia, P.Y., Shang, Q.Q., Zhang, M., Feng, G.D., Liu, C.G., Zhou, Y.H., 2019. Synthesis and application of UV-curable phosphorous-containing acrylated epoxidized soybean oil-based resins. J. Bioresour. Bioprod. 4, 183–191.
Jena, K.K., Raju, K.V.S.N., 2008. Synthesis and characterization of hyperbranched polyurethane hybrids using tetraethoxysilane (TEOS) as cross-linker. Ind. Eng. Chem. Res. 47, 9214–9224.
Kathalewar, M., Sabnis, A., D’Mello, D., 2014. Isocyanate free polyurethanes from new CNSL based bis-cyclic carbonate and its application in coatings. Eur. Polym. J. 57, 99–108.
Kathalewar, M.S., Joshi, P.B., Sabnis, A.S., Malshe, V.C., 2013. Non-isocyanate polyurethanes: from chemistry to applications. RSC. Adv 3, 4110–4129.
Kim, T.H., Kim, M., Lee, W., Kim, H.G., Lim, C.S., Seo, B., 2019. Synthesis and characterization of a polyurethane phase separated to nano size in an epoxy polymer. Coatings 9, 319.
Kirpluks, M., Kalnbunde, D., Walterova, Z., Cabulis, U., 2017. Rapeseed oil as feedstock for high functionality polyol synthesis. J. Renew. Mater. 5, 258–270.
Kirpluks, M., Pomilovskis, R., Vanags, E., Abolins, A., Mierina, I., Fridrihsone, A., 2022. Influence of different synthesis conditions on the chemo-enzymatic epoxidation of tall oil fatty acids. Process. Biochem. 122, 38–49.
Krall, E.M., Serum, E.M., Sibi, M.P., Webster, D.C., 2018. Catalyst-free lignin valorization by acetoacetylation. Structural elucidation by comparison with model compounds. Green. Chem 20, 2959–2966.
La Scala, J., Wool, R.P., 2002. The effect of fatty acid composition on the acrylation kinetics of epoxidized triacylglycerols. J. Am. Oil. Chem. Soc. 79, 59–63.

Li, Y.H., Sun, X.S., 2015. Synthesis and characterization of acrylic polyols and polymers from soybean oils for pressure-sensitive adhesives. RSC. Adv 5, 44009–44017.
Liang, B., Kuang, S.J., Huang, J.J., Man, L.M., Yang, Z.H., Yuan, T., 2019. Synthesis and characterization of novel renewable tung oil-based UV-curable active monomers and bio-based copolymers. Prog. Org. Coat. 129, 116–124.
Lindsay, C.D., Timperley, C.M., 2020. TRPA1 and issues relating to animal model selection for extrapolating toxicity data to humans. Hum. Exp. Toxicol. 39, 14–36.
Liu, P.F., Zhang, X.P., Liu, R., Liu, X.Y., Liu, J.C., 2019. Highly functional bio-based acrylates with a hard core and soft arms: from synthesis to enhancement of an acrylated epoxidized soybean oil-based UV-curable coating. Prog. Org. Coat. 134, 342–348.
Lomège, J., Lapinte, V., Negrell, C., Robin, J.J., Caillol, S., 2019. Fatty acid-based radically polymerizable monomers: from novel poly(meth)acrylates to cutting-edge properties. Biomacromolecules 20, 4–26.
Luo, A.F., Jiang, X.S., Lin, H., Yin, J., 2011. Thiol-ene" photo-cured hybrid materials based on POSS and renewable vegetable oil. J. Mater. Chem. 21, 12753–12760.
Menard, K.P., 1999. Dynamic Mechanical Analysis: A Practical Introduction. CRC Press, Boca Raton, Fla.
Müller, R., Wilke, G., 2014. Synthesis and radiation curing of acrylated castor oil glycerides. J. Coat. Technol. Res. 11, 873–882.
Naga, N., Satoh, M., Magara, T., Ahmed, K., Nakano, T., 2021. Synthesis of gels by means of Michael addition reaction of multi-functional acetoacetate and diacrylate compounds and their application to ionic conductive gels. J. Polym. Sci. 59, 2129–2139.
Naga, N., Satoh, M., Magara, T., Ahmed, K., Nakano, T., 2022. Synthesis of porous polymers by means of Michael addition reaction of multifunctional acetoacetate and poly(ethylene glycol) diacrylate. Eur. Polym. J. 162, 110901.
Noordover, B., Liu, W., McCracken, E., DeGooyer, B., Brinkhuis, R., Lunzer, F., 2020. Michael addition curable coatings from renewable resources with enhanced adhesion performance. J. Coat. Technol. Res. 17, 1123–1130.
Papageorgiou, G.Z., 2018. Thinking green: sustainable polymers from renewable resources. Polymers. (Basel) 10, 952.
Paramarta, A., Webster, D.C., 2017. The exploration of Michael-addition reaction chemistry to create high performance, ambient cure thermoset coatings based on soybean oil. Prog. Org. Coat. 108, 59–67.
Pellis, A., Malinconico, M., Guarneri, A., Gardossi, L., 2021. Renewable polymers and plastics: performance beyond the green. New. Biotechnol 60, 146–158.
Perera, M., Yan, J.Y., Xu, L., Yang, M., Yan, Y.J., 2022. Bioprocess development for biolubricant production using non-edible oils, agro-industrial byproducts and wastes. J. Clean. Prod. 357, 131956.
Polaczek, K., Kaulina, E., Pomilovskis, R., Fridrihsone, A., Kirpluks, M., 2022. Epoxidation of tall oil fatty acids and tall oil fatty acids methyl esters using the SpinChem® rotating bed reactor. J. Polym. Environ. 30, 4774–4786.
Pomilovskis, R., Mierina, I., Beneš, H., Trhlíková, O., Abolins, A., Fridrihsone, A., Kirpluks, M., 2022a. The synthesis of bio-based Michael donors from tall oil fatty acids for polymer development. Polymers. (Basel) 14, 4107.
Pomilovskis, R., Mierina, I., Fridrihsone, A., Kirpluks, M., 2022b. Bio-based polymer developments from tall oil fatty acids by exploiting Michael addition. Polymers. (Basel) 14, 4068.
Rahul, R., Kitey, R., 2016. Effect of cross-linking on dynamic mechanical and fracture behavior of epoxy variants. Compos. B. Eng. 85, 336–342.
Rengasamy, S., Mannari, V., 2014. UV-curable PUDs based on sustainable acrylated polyol: study of their hydrophobic and oleophobic properties. Prog. Org. Coat. 77, 557–567.
Rosenboom, J.G., Langer, R., Traverso, G., 2022. Bioplastics for a circular economy. Nat. Rev. Mater. 7, 117–137.
Salih, A.M., Ahmad, M.B., Ibrahim, N.A., Dahlan, K.Z.H.M., Tajau, R., Mahmood, M.H., Yunus, W.M.Z.W., 2015. Synthesis of radiation curable palm oil-based epoxy acrylate: NMR and FTIR spectroscopic investigations. Molecules 20, 14191–14211.
Smeu, I., Dobre, A.A., Cucu, E.M., Mustățea, G., Belc, N., Ungureanu, E.L., 2022. Byproducts from the vegetable oil industry: the challenges of safety and sustainability. Sustainability 14, 2039.
Sonnenschein, M.F., Werness, J.B., Patankar, K.A., Jin, X., Larive, M.Z., 2016. From rigid and flexible foams to elastomers via Michael addition chemistry. Polymer. (Guildf) 106, 128–139.
Sternberg, J., Pilla, S., 2020. Materials for the biorefinery: high bio-content, shape memory Kraft lignin-derived non-isocyanate polyurethane foams using a non-toxic protocol. Green. Chem 22, 6922–6935.
Su, Y.P., Lin, H., Zhang, S.T., Yang, Z.H., Yuan, T., 2020. One-step synthesis of novel renewable vegetable oil-based acrylate prepolymers and their application in UV-curable coatings. Polymers. (Basel) 12, 1165.
Sung, J., Sun, X.S., 2018. Cardanol modified fatty acids from camelina oils for flexible bio-based acrylates coatings. Prog. Org. Coat. 123, 242–253.
Tang, J.J., Zhang, J.S., Lu, J.Y., Huang, J., Zhang, F., Hu, Y., Liu, C.G., An, R.R., Miao, H.C., Chen, Y.Y., Huang, T., Zhou, Y.H., 2020. Preparation and properties of plant-oil-based epoxy acrylate-like resins for UV-curable coatings. Polymers. (Basel) 12, 2165.
Trevino, A.S., Trumbo, D.L., 2002. Acetoacetylated castor oil in coatings applications. Prog. Org. Coat. 44, 49–54.
Vevere, L., Fridrihsone, A., Kirpluks, M., Cabulis, U., 2020. A review of wood biomass-based fatty acids and rosin acids use in polymeric materials. Polymers. (Basel) 12, 2706.
Wang, T., Wang, J.L., He, X.F., Cao, Z.Y., Xu, D.D., Gao, F., Zhong, J., Shen, L., 2019. An ambient curable coating material based on the Michael addition reaction of acetoacetylated castor oil and multifunctional acrylate. Coatings 9, 37.
Witzeman, J.S., Nottingham, W.D., 1991. Transacetoacetylation with tert-butyl acetoacetate: synthetic applications. J. Org. Chem. 56, 1713–1718.
Wuzella, G., Mahendran, A.R., Müller, U., Kandelbauer, A., Teischinger, A., 2012. Photocrosslinking of an acrylated epoxidized linseed oil: kinetics and its application for optimized wood coatings. J. Polym. Environ 20, 1063–1074.
Xia, Y., Larock, R.C., 2010. Vegetable oil-based polymeric materials: synthesis, properties, and applications. Green. Chem 12, 1893–1909.
Xu, D.D., Cao, Z.Y., Wang, T., Zhong, J., Zhao, J.Z., Gao, F., Luo, X.Y., Fang, Z.L., Cao, J.S., Xu, S.Z., Shen, L., 2019. An ambient-cured coating film obtained via a Knoevenagel and Michael addition reactions based on modified acetoacetylated castor oil prepared by a thiol-ene coupling reaction. Prog. Org. Coat. 135, 510–516.
Zhang, C.Q., Madbouly, S.A., Kessler, M.R., 2015. Biobased polyurethanes prepared from different vegetable oils. ACS. Appl. Mater. Interfaces 7, 1226–1233.
Zhang, P., Xin, J.N., Zhang, J.W., 2014. Effects of catalyst type and reaction parameters on one-step acrylation of soybean oil. ACS. Sustainable. Chem. Eng. 2, 181–187.
Zhang, P., Zhang, J.W., 2013. One-step acrylation of soybean oil (SO) for the preparation of SO-based macromonomers. Green. Chem 15, 641–645.

3. pielikums
Appendix 3

Bio-based polymer developments from tall oil fatty acids by exploiting Michael addition

Ralfs Pomilovskis, Inese Mieriņa, Anda Fridrihsone, Miķelis Kirpļuks

Polymer, 2022

polymers

MDPI

Article

Bio-Based Polymer Developments from Tall Oil Fatty Acids by Exploiting Michael Addition

Ralfs Pomilovskis [1,2,*], Inese Mierina [2], Anda Fridrihsone [1] and Mikelis Kirpluks [1]

[1] Polymer Laboratory, Latvian State Institute of Wood Chemistry, Dzerbenes St. 27, LV-1006 Riga, Latvia
[2] Institute of Technology of Organic Chemistry, Faculty of Materials Science and Applied Chemistry, Riga Technical University, P. Valdena St. 3/7, LV-1048 Riga, Latvia
* Correspondence: ralfs.pomilovskis@kki.lv

Abstract: In this study, previously developed acetoacetates of two tall-oil-based and two commercial polyols were used to obtain polymers by the Michael reaction. The development of polymer formulations with varying cross-link density was enabled by different bio-based monomers in combination with different acrylates—bisphenol A ethoxylate diacrylate, trimethylolpropane triacrylate, and pentaerythritol tetraacrylate. New polymer materials are based on the same polyols that are suitable for polyurethanes. The new polymers have qualities comparable to polyurethanes and are obtained without the drawbacks that come with polyurethane extractions, such as the use of hazardous isocyanates or reactions under harsh conditions in the case of non-isocyanate polyurethanes. Dynamic mechanical analysis, differential scanning calorimetry, thermal gravimetric analysis, and universal strength testing equipment were used to investigate the physical and thermal characteristics of the created polymers. Polymers with a wide range of thermal and mechanical properties were obtained (glass transition temperature from 21 to 63 °C; tensile modulus (Young's) from 8 MPa to 2710 MPa and tensile strength from 4 to 52 MPa). The synthesized polymers are thermally stable up to 300 °C. The suggested method may be used to make two-component polymer foams, coatings, resins, and composite matrices.

Keywords: fatty acid-based Michael donor; Michael addition; bio-based polymer; tall oil

check for updates

Citation: Pomilovskis, R.; Mierina, I.; Fridrihsone, A.; Kirpluks, M. Bio-Based Polymer Developments from Tall Oil Fatty Acids by Exploiting Michael Addition. *Polymers* **2022**, *14*, 4068. https://doi.org/10.3390/polym14194068

Academic Editor: Nicolas Sbirrazzuoli

Received: 31 August 2022
Accepted: 24 September 2022
Published: 28 September 2022

Publisher's Note: MDPI stays neutral with regard to jurisdictional claims in published maps and institutional affiliations.

Copyright: © 2022 by the authors. Licensee MDPI, Basel, Switzerland. This article is an open access article distributed under the terms and conditions of the Creative Commons Attribution (CC BY) license (https://creativecommons.org/licenses/by/4.0/).

1. Introduction

The European Commission has set up a "European Green Deal" to tackle climate and environmental challenges. It is a new growth strategy that aims to transform the European Union into a prosperous society with a modern, resource-efficient, and competitive economy, achieving climate neutrality and a balance in carbon emissions and removals by 2050, which means reducing net greenhouse gas emissions to zero [1]. Improving the polymer industry by introducing innovative, sustainable, and knowledge-intensive technologies for producing materials from renewable bio-resources is also an essential field for achieving this goal [2].

In the polyurethane industry, sustainability has emerged as a major concern. Conventionally, polyurethanes are produced from two components—A (polyol) and B (isocyanate)—that are derived from petrochemicals. Particular attention is given towards the synthesis of polyols from biological fatty acids, diglycerides, and triglycerides [3–8]. Such bio-polyols are suitable for the production of polyurethanes as a method to make polyurethanes more sustainable [9]. However, the use of isocyanates still remains problematic as isocyanates are considered as toxic substances relative to the environment [10–14].

Recently, one of the extensive research topics is the development of non-isocyanate polyurethanes (NIPUs) materials as an alternative to polyurethanes. This technology has significant drawbacks, such as high pressure, high temperature, and long reaction times [15,16]. The polymer industry requires alternative methods for producing polymers

in relatively mild conditions with similar properties to polyurethanes. The Michael reaction can be used as a new synthesis pathway to yield bio-based polymers with a wide range of properties [2,17].

The Michael reaction is a versatile synthesis type for linking electron-poor olefins to a wide range of nucleophiles [18]. Enolates [19,20], nitrogen-containing [21–26] reagents, and thiols [26–32] are typical Michael donors, while alkyl acrylates are mainly used as Michael acceptors [33]. Adding an enolate anion to the α,β-unsaturated carbonyl compound to form a carbon–carbon bond is a Michael reaction [19,20,34]. A type of polymerization for the addition of hydroxyl monomers with electrophilic double or triple bonds is called the oxa-Michael reaction [35,36]. In the case of nitrogen and sulphur-containing donors, the reaction is called aza-Michael [21–26,37] and thio-Michael [26–32] addition reactions, respectively. In recent years, aza- and thio-Michael reactions have gained attention for polymerization [35,38]. However, carbon-Michael reactions have gained less attention.

The majority of the studies has been conducted on coating materials [39–43]. Recently, Naga et al. presented Michael-addition reactions of multi-functional acetoacetate and diacrylate monomers, yielding corresponding gels at room temperature in the presence of 1,8-diazabicyclo[5.5.0]undecane-7-ene as a catalyst [44]. Park reported how hydrophobic thin-film nanocomposite membranes could be successfully developed using only naturally occurring compounds by interfacial polymerization [45]. Sinha et al. has concluded that the nucleophilicity of the used enamines had a significant impact on the efficiency and total reaction yields. Moreover, photo-protecting amines with 2-(2-nitrophenyl)propyl chloroformate in the presence of a ketone create enamines in situ [46].

The Michael reaction can yield a variety of linear, graft, dendric, highly cross-linked, and hyperbranched polymer networks [18,33]. The mechanism of the reaction is relatively well-studied and straightforward. The thermodynamical mechanism depends on the base's relative strengths and the type of acetoacetate. The base deprotonates the acetoacetate, resulting in an enolate anion. The enolate anion then reacts with the acrylate in a 1,4-conjugate addition, and the carbonyl of the acrylate stabilizes, allowing the base to regenerate (see Figure 1). The enthalpic transition that occurs when a π-bond is replaced with a σ-bond is the overall driving force for conjugate addition. As a result, 1,4-addition is preferred over 1,2-addition. The product of the first Michael reaction contains active methylene hydrogen that can be added to another acrylate in a second step [14,34], which means that the Michael donor reacts twice with two Michael acceptors [33], of course, if the ratio allows it. The polymeric material can only be formed if the molecule of the Michael acceptor component contains at least two functional groups.

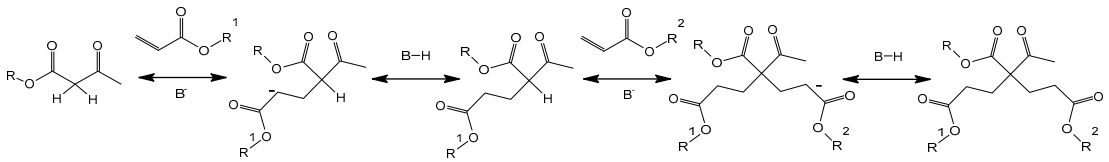

Figure 1. Mechanism of carbon–carbon Michael nucleophilic 1,4-addition reactions.

The reaction between acrylates and the active methylene group of β-ketoesters is quick, and the system cures at room temperature after mixing it in the presence of catalysts. This reaction is a strong base-catalyzed addition [18,20,34]. For the Michael reaction amine, amidine- and guanidine-based catalysts may be the most suitable [47,48] for example 1,1,3,3-tetramethylguanidine, triethylamine, 1,4-diazabicyclo[2.2.2]octane, (1,8-diazabicyclo[5.4.0]undec-7-ene), 4,4′-methylenebiscycloheexanamine, (1,5-diazabicyclo [4.3.0]non-5-ene), and 7-methyl-1,5,7-triazabicyclo[0,4,4]dec-5-ene [18,20,34,39,42,48–51].

In this study, we used previously developed acetoacetates of two tall-oil-based and two commercial polyols to obtain polymers by the Michael reaction. The previously developed acetoacetates had different chemical structures and functionalities. In conjunction with the

use of various acrylates in polymerization reactions, it allowed the development of polymer formulations with varied cross-link density. Three acrylates with different functionalities—bisphenol A ethoxylate diacrylate (BPAEDA), trimethylolpropane triacrylate (TMPTA), and pentaerythritol tetraacrylate (PETA)—were used. The physical and thermal properties of the developed polymers were studied using dynamic mechanical analysis (DMA), differential scanning calorimetry (DSC), thermal gravimetric analysis (TGA), and a universal strength testing machine. The chemical structure and functional groups present in the developed polymer were determined using Fourier-transform infrared spectroscopy (FTIR). The proposed technology has a potential in the production of two-component polymer foams, coatings, resins, and matrix for composites.

2. Materials and Methods

2.1. Materials

Epoxidized tall oil fatty acids 1,4-butanediol polyol acetoacetate (E^{IR}TOFA_DB_AA) were obtained from polyol that was synthesized from tall oil fatty acids via epoxidation using ion exchange resin (E^{IR}TOFA) followed by oxirane ring-opening and esterification with 1,4-butandiol and subsequent acetoacetylation with *tert*-butyl acetoacetate by a transesterification reaction, acid value < 5 mg KOH·g^{-1}, hydroxyl value 36.2 mg KOH·g^{-1}, moisture 0.025%, and acetoacetate groups 0.3307 mol·100 g^{-1}. Epoxidized tall oil fatty acids trimethylolpropane polyol acetoacetate (E^{IR}TOFA_TMP_AA) was obtained from E^{IR}TOFA by oxirane ring-opening and esterification with trimethylolpropane and subsequent acetoacetylation with *tert*-butyl acetoacetate by a transesterification reaction, acid value < 5 mg KOH·g^{-1}, hydroxyl value 41.6 mg KOH·g^{-1}, moisture 0.037%, and acetoacetate groups 0.4562 mol·100 g^{-1}. Acetoacetyled Neopolyol 380 (NEO380_AA) was synthesized from Neopolyol 380 (NEO380) by transesterification with *tert*-butyl acetoacetate from the NEO Group, acid value < 5 mg KOH·g^{-1}, hydroxyl value 40.7 mg KOH·g^{-1}, moisture 0.048%, and acetoacetate groups 0.4242 mol·100 g^{-1}. Acetoacetyled Lupranol 3300 (L3300_AA) was synthesized from Lupranol 3300 (L3300) by transesterification with *tert*-butyl acetoacetate, from BASF, acid value < 5 mg KOH·g^{-1}, hydroxyl value 26.2 mg KOH·g^{-1}, and moisture 0.021%, acetoacetate groups 0.4456 mol·100 g^{-1}. BPAEDA, average M_n~512, contains 1000 ppm monomethyl ether hydroquinone as an inhibitor from Sigma-Aldrich; TMPTA contains 600 ppm monomethyl ether hydroquinone as an inhibitor and is of technical grade from Sigma-Aldrich; PETA contains 350 ppm monomethyl ether hydroquinone as an inhibitor and is technical grade from Sigma-Aldrich (St. Louis, MO, USA). 1,1,3,3-tetramethylguanidine (TMG), assay 99%, was purchased from Sigma-Aldrich. Catalyst and acrylates were directly used as delivered without further purification.

2.2. Solid Polymer Development

The polymerization was carried out by mixing the acrylate with the catalyst (TMG), adding acetoacetate, and stirring the mixture rapidly until a homogeneous medium was obtained. Mixing was about 30 s. The ratio of acetoacetate to acrylic groups was 1:2 mol. The amount of TMG was 1% of the total mass of the mixture. After mixing, the mixture was quickly poured into a 15 mL centrifuge tube and centrifuged for 1 min to remove air bubbles and obtain a homogeneous polymer monolith. Samples were made with a weight of 14 g and solidified in a tube at room temperature and atmospheric pressure for 2 min to 3 min. Polymer syntheses were repeated twice. Samples were tested from both syntheses.

Tensile samples were prepared by immediately pouring the polymerization mixture into a mold after centrifugation. Samples were tested after 24 h curing at room temperature.

2.3. Characterization Methods

FTIR. Polymer chemical structure was analyzed using FTIR data, which was obtained with a Thermo Scientific Nicolet iS50 spectrometer (Thermo Fisher Scientific, Waltham, MA, USA) at a resolution of 4 cm^{-1} (32 scans). FTIR data were collected using the attenuated

total reflectance technique with diamond crystals. A sheet of the obtained polymer sample was pressed against the prism and analyzed.

DSC. Metler Toledo DSC 823^e (Mettler Toledo, Greifensee, Switzerland) was used to obtain DSC data. STAR^e Software ver. 9.00 (Mettler Toledo, Greifensee, Switzerland) and OriginPro 2021 9.8.0.200 programs (Northampton, MA, USA) were used for data processing. Specimens weighing approximately 0.2–2.0 mg were cut from the polymer sample. A total of 5 mg of samples were placed in an aluminium sample pan with an accuracy of ±0.5 mg. A Mettler Toledo sealing press for crucibles was used to crimp covers on DSC pans of aluminium. The test was organized in two cycles. The start temperature of the first cycle was 25 °C with heating up to 180 °C, followed by cooling to −50 °C. The second heating cycle was from −50 °C to 180 °C, and the temperature was reduced to 25 °C in the second cooling cycle. The heating rate used was 10 °C·min^{-1}. Two samples from each series were tested for DSC.

TGA. Thermogravimetric data were obtained using Discovery TGA equipment (TA instruments, New Castle, DE, USA). Data processing was performed using the OriginPro 2021 9.8.0.200 and TA Instruments TRIOS version #5.0.0.44608 software. A 10 mg sample consisting of similar size pieces (0.5–2.0 mg) was placed on a platinum scale sample pan with an accuracy of ±0.5 mg. Then, the sample on the sample pan was heated in a nitrogen atmosphere at 10 °C·min^{-1} in a temperature range between 30 °C and 700 °C. Two samples from each series were tested for TGA.

DMA. DMA was carried out with Mettler Toledo DMA/SDTA861^e (Mettler Toledo, Switzerland). The temperature range was from −100 °C to 180 °C, the ramp rate was 3 °C·min^{-1}, the frequency was 1 Hz, amplitude was 30 µm, and maximal force was 5 N. The compression oscillation mode was used. Polymer monolith samples with a diameter of 13 mm and a height of 7 mm, with an accuracy of ±0.2 mm, were used for DMA tests. Two samples from each series were tested for DMA.

The cross-link density was calculated from the data obtained in the DMA test according to Equation (1):

$$\nu_e = \frac{E'}{3RT} \quad (1)$$

where ν_e is the cross-link density (mol·cm^{-3}), E' is the tensile storage modulus (MPa), R is the gas constant (8.314 m^3·Pa·K^{-1}·mol^{-1}), and T is the temperature corresponding to the storage modulus value into the rubbery plateau (K) [52–55].

Knowing density ρ (g·cm^{-3}), the molecular weight between cross-links (M_c (g·mol^{-1})) was calculated according to Equation (2) [56].

$$M_c = \frac{3RT\rho}{E'_{rubbery}} \quad (2)$$

Tensile modulus (Young's) and compressive strength were determined from tests carried out at room temperature (22 °C) using a universal machine, an ElectroPuls E3000 from Instron (Norwood, Norfolk, MA, USA), following the ISO 14125:1998 standard. The sample size was 2.5 mm × 4 mm × 25 mm. The deformation rate for all samples was 2 mm·min^{-1}, and at least four samples from each series were tested.

3. Results and Discussion

A schematic overview of polymer syntheses performed, including information on the synthesis steps of the Michael donor monomers, is provided in Figure 2. Previously developed acetoacetates of two tall oil-based polyols (E^{IR}TOFA_DB_AA and E^{IR}TOFA_TMP_AA) and two commercial polyols (NEO380_AA and L3300_AA) were used to obtain polymers by the Michael reaction with three acrylates with different functionalities—BPAEDA, TMPTA, and PETA. Monomers of different degrees of functionalities were used to demonstrate that it was possible to obtain a polymeric material from tall oil polyol acetoacetates with various

acrylates. It also allowed the investigation of the effect of acrylate functionality on the properties of the obtained polymeric materials.

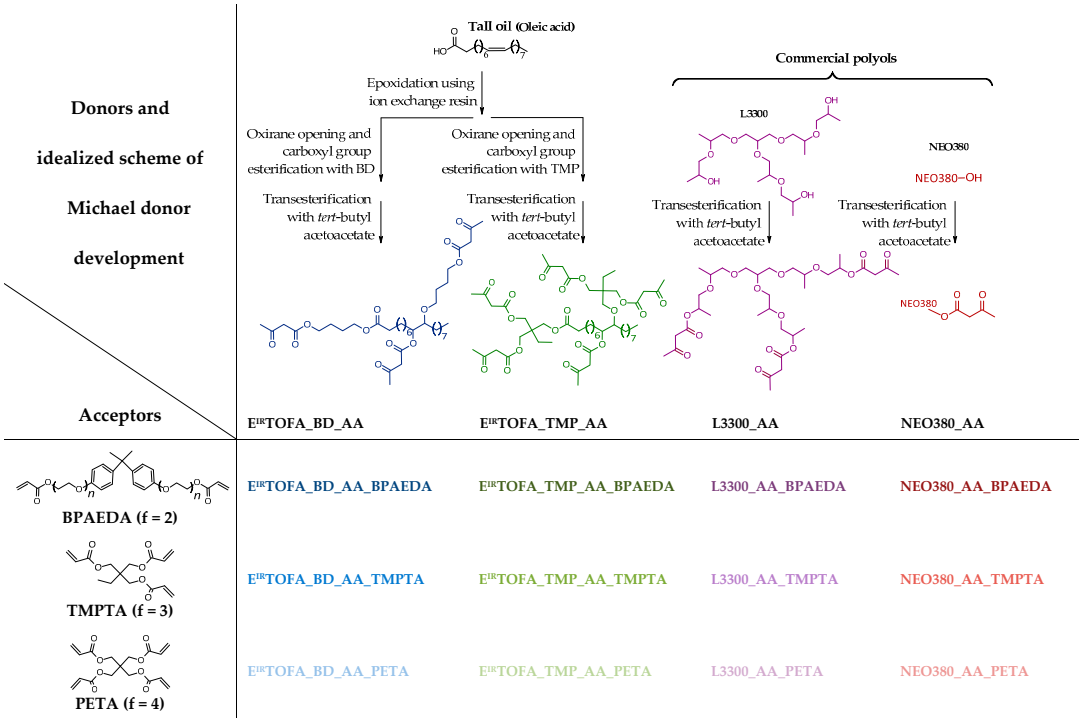

Figure 2. A schematic overview of polymer syntheses and synthesis of Michael donor monomers.

3.1. FTIR Analysis of Monoliths

The FTIR spectra of the film of obtained thin polymeric materials are shown in Figure 3. The FTIR spectra did not show very intensive peaks at ~1630 cm^{-1} and ~810 cm^{-1}, which are characteristic of the absorbance of acrylic group vibration. This indicated that the content of free acrylic groups in polymers was low [57]. Thus, a relatively high conversion occurred.

Polymers derived from BPAEDA have two intense peaks (at 830 cm^{-1} and 1510 cm^{-1}) corresponding to aromatic bonds characterizing bisphenol A in the FTIR spectrum. In the case of NEO380_AA-based polymers, an intense peak at 730 cm^{-1} was observed in the FTIR spectra, indicating the out-of-plane C-H bending of an aromatic ring (Figure 3c).

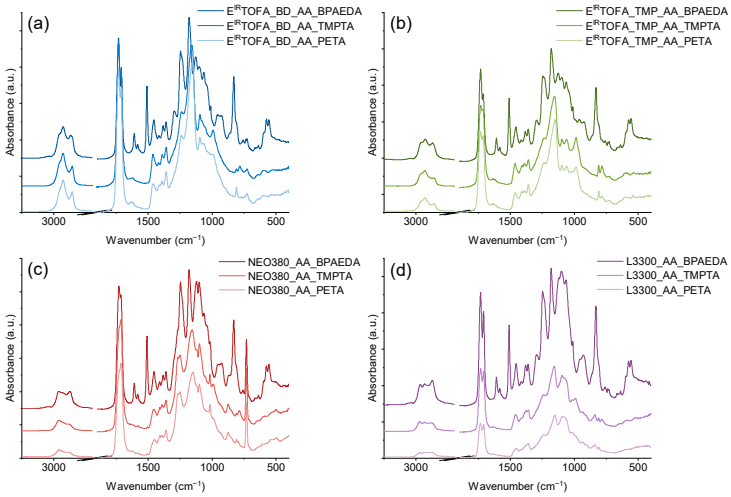

Figure 3. FTIR spectra of polymer monoliths from synthesized acetoacetates and BPAEDA, TMPTA, and PETA acrylates. (**a**) E^{IR}TOFA_BD_AA polymers; (**b**) E^{IR}TOFA_TMP_AA polymers; (**c**) NEO380_AA polymers; (**d**) L3300_AA polymers.

3.2. DSC Analysis of Monoliths

DSC heating curves are shown in Figure 4. The glass transition temperature can be very clearly identified in almost all DSC curves of the new polymeric materials. The exception was in the case of polymers from PETA acrylate. The glass transition temperature was less pronounced in the curves of these polymers by the used DSC analysis mode. For polymers synthesized using BPAEDA, the glass transition was clearly visible. The enthalpy relaxation peak also accompanied it.

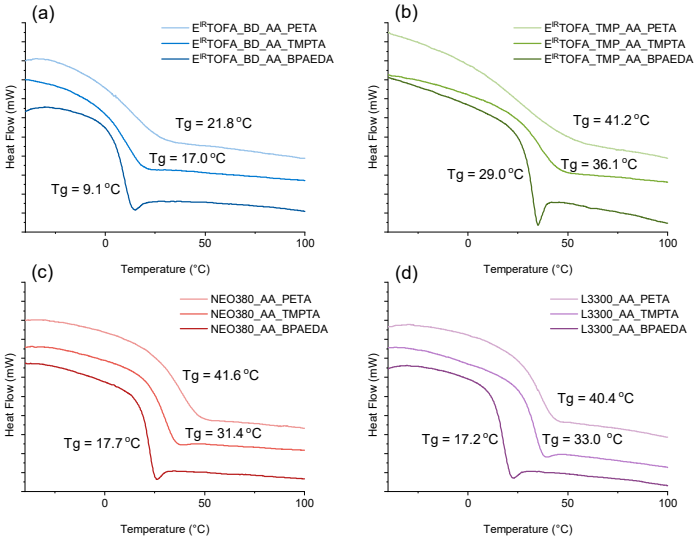

Figure 4. DSC curves of polymer monoliths from synthesized acetoacetates and BPAEDA, TMPTA, and PETA acrylates. (**a**) E^{IR}TOFA_BD_AA polymers; (**b**) E^{IR}TOFA_TMP_AA polymers; (**c**) NEO380_AA polymers; (**d**) L3300_AA polymers.

For polymers obtained from commercial polyol acetoacetate (L3300_AA and NEO380_AA), the glass transition temperature was mainly influenced by the used acrylate. The glass transition temperature differed by less than 2 °C when polymers obtained with the same acrylates were compared (Figure 4c,d). Depending on the used acrylate, the glass transition temperature increased as follows: BPAEDA < TMPTA < PETA. The functionality of the used acrylate impacted the glass's transition temperature. When acrylate with higher functionality was used to obtain polymers, the polymer exhibited higher glass transition temperature due to a higher cross-link density in the polymer matrix [58].

The same trend was observed for polymers obtained from acetoacetylated tall oil polyols (Figure 4a,b). The used tall oil polyol acetoacetate had a significant effect on the glass transition temperature of the obtained polymer. Higher glass transition temperature was observed for E^{IR}TOFA_TMP_AA, which was synthesized using a higher functionality polyol.

In the case of commercial polyol-based acetoacetate polymers, the difference in glass transition temperatures was relatively small when considering the effect of the polyol used. Of course, the previously established correlation between acrylate functionality and the glass transition temperature remained. A higher glass transition temperature was observed for polymers in which acrylate with higher functionalities was used (Figure 4c,d).

3.3. TGA Analysis of Monoliths

TGA curves and their derivatives of polymers obtained from tall oil-based and commercial polyol acetoacetates are shown in Figure 5. As shown in Figure 5a,b, no significant weight loss was observed up to almost 300 °C for polymers derived from tall oil polyols; they were thermally stable. This is an advantage because, for example, classic polyurethane materials without special thermal stabilizer additives decompose in the temperature range from 200 °C to 300 °C [59,60]. Moreover, organic glass poly(methyl methacrylate) (PMMA) onset decomposition temperatures are under 300 °C [61,62]. In Table 1, data of temperatures are summarized representing the temperatures at which the following mass losses were achieved: 5% ($T_{m5\%}$), 10% ($T_{m10\%}$), 25% ($T_{m25\%}$), and 50% ($T_{m50\%}$). If the influence of used polyol on thermal properties of polymer material was compared, then polymers derived from TMP polyols had higher thermal stability.

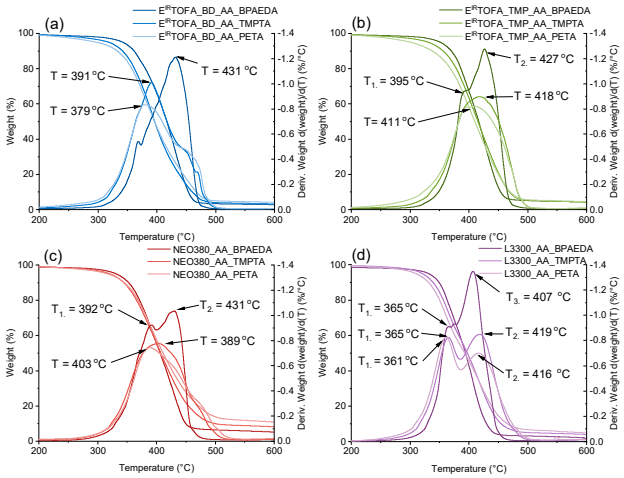

Figure 5. TGA mass loss curve of polymer monoliths from synthesized acetoacetates and BPAEDA, TMPTA, PETA acrylates, and derivative of the mass loss. (**a**) E^{IR}TOFA_BD_AA polymers; (**b**) E^{IR}TOFA_TMP_AA polymers; (**c**) NEO380_AA polymers; (**d**) L3300_AA polymers.

Table 1. Weight loss dependence on temperature of synthesized polymers from tall oil polyol or commercial polyol-based acetoacetates and BPAEDA, TMPTA, and PETA acrylates.

	Sample	First Onset, °C	$T_{m5\%}$, °C	$T_{m10\%}$, °C	$T_{m25\%}$, °C	$T_{m50\%}$, °C	Residue, %
Tall oil-based	E^{IR}TOFA_BD_AA_BPAEDA	349.0	342.0	361.5	388.1	417.0	2.0
	E^{IR}TOFA_BD_AA_TMPTA	342.2	318.3	341.8	369.0	396.2	1.8
	E^{IR}TOFA_BD_AA_PETA	340.2	297.2	332.9	365.2	396.1	2.6
	E^{IR}TOFA_TMP_AA_BPAEDA	360.9	351.2	370.2	391.8	416.7	3.0
	E^{IR}TOFA_TMP_AA_TMPTA	354.1	330.9	356.3	385.8	415.3	2.6
	E^{IR}TOFA_TMP_AA_PETA	344.7	300.3	337.7	377.7	410.0	2.8
Commercial polyols-based	L3300_AA_BPAEDA	342.5	331.3	349.2	368.5	394.2	0.1
	L3300_AA_TMPTA	418.8	320.8	339.0	362.8	397.4	2.1
	L3300_AA_PETA	332.3	309.7	331.2	356.6	393.0	2.7
	NEO380_AA_BPAEDA	347.1	331.6	352.7	378.1	406.3	2.1
	NEO380_AA_TMPTA	341.0	321.0	344.5	374.0	407.3	6.0
	NEO380_AA_PETA	347.5	317.0	345.4	376.5	411.3	8.2

On the other hand, if polymer materials were compared according to the used acrylate, then the most thermally stable polymers were obtained from BPAEDA acrylate. This could be explained by the aromatic structure of bisphenol A. It was observed that the temperature at which a 5% mass loss occurred was lower when acrylate with higher functionality was used.

The highest $T_{m5\%}$ was observed for polymers derived using difunctional BPAEDA, followed by trifunctional TMPTA. The lowest $T_{m5\%}$ was for polymers derived from tetrafunctional PETA. Thermal degradation continued up to almost 500 °C for all samples, after which no significant weight loss was observed.

The peaks indicate the point of the greatest rate of change on the weight loss curve (Figure 5). Two distinct peaks were observed for polymers obtained using BPAEDA as the acrylate. For other polymers, the similarity of the curves was determined by the used polyol and less by the acrylate.

Polymers from commercial polyols also showed similar characteristics in TGA mass-loss curves and their derivative curves (Figure 5c,d). Polymeric materials derived from tall oil polyols with BPAEDA acrylate had higher thermal stability (when comparing the temperature for weight loss of 5%) than commercial polyols with the same acrylate. The temperature depends significantly on the used acrylate for a weight loss of 5%, but this effect was less pronounced for weight losses at higher temperatures.

3.4. DMA Analysis of Monoliths

DMA test was performed to determine the dynamic mechanical properties of polymer materials. The obtained curves are shown in Figure 6. Based on the tanδ data, all samples had a quite homogeneous network structure because there was only one relatively narrow peak with a clear maximum, which appears in the graphs. These relationships between peak width, symmetry and structure, and the homogeneity of the structure have been described in several studies [20,63–65].

Wider peaks and with a lower maximum of tanδ value were observed in the case of the tall oil acetoacetate polymer with a tetrafunctional acrylate ester PETA (Figure 6a,b). This indicated a lower level of homogeneity in cross-link density. A symmetrical peak with the highest tanδ value was reached for all polymer samples obtained using the difunctional acrylate BPAEDA, indicating higher homogeneity of the cross-linked network.

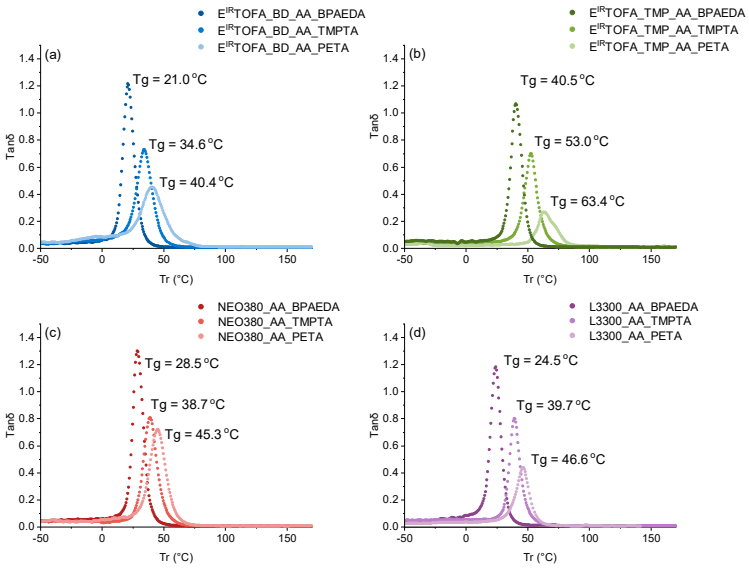

Figure 6. Tanδ curves of polymer monoliths from synthesized acetoacetates and BPAEDA, TMPTA, and PETA acrylates. (**a**) Polymers from E^{IR}TOFA_BD_AA; (**b**) polymers from E^{IR}TOFA_TMP_AA; (**c**) polymers from NEO380_AA_TMPTA; (**d**) polymers from L3300_AA.

The glass transition temperatures determined by the DMA method are summarized in Table 2. The glass transition temperatures obtained from DMA were compared with the glass transition temperatures of materials from DSC analysis. Although the glass transition temperatures were different, same trends between the glass transition temperatures were observed. The glass transition temperatures determined using the DMA method were higher than those determined using DSC analysis. DMA method has a higher sensitivity than DSC for detecting the glass transition temperature [66]. DMA is beneficial for polymers with hard-to-find glass-transition temperatures and heavily cross-linked polymers [67].

Table 2. Glass transition temperatures (T_g), cross-link density (ν_e) and molecular weight between cross-links (M_c) from DMA tests and density (ρ) of polymer monoliths from tall oil polyol or commercial polyol-based acetoacetates and BPAEDA, TMPTA, and PETA acrylate.

	Sample	Temperature Range, °C (Tanδ > 0.06 °C)	Max. Tanδ	T_g, °C	ν_e, moles·cm^{-3}	ρ, g·cm^{-3}	M_c, g·mol^{-1}
Tall oil-based	E^{IR}TOFA_BD_AA_BPAEDA	2.9–36.4	1.21	21.0	0.59×10^{-3}	1.167	1695
	E^{IR}TOFA_BD_AA_TMPTA	2.0–50.7	0.73	34.6	1.98×10^{-3}	1.211	505
	E^{IR}TOFA_BD_AA_PETA	−20.0–64.5	0.45	40.4	2.67×10^{-3}	1.219	375
	E^{IR}TOFA_TMP_AA_BPAEDA	21.9–54.5	1.07	40.5	1.89×10^{-3}	1.116	529
	E^{IR}TOFA_TMP_AA_TMPTA	32.6–68.9	0.70	53.0	2.04×10^{-3}	1.177	490
	E^{IR}TOFA_TMP_AA_PETA	52.2–80.2	0.27	63.4	3.17×10^{-3}	1.235	315
Commercial polyols-based	NEO380_AA_BPAEDA	9.9–43.9	1.30	28.5	0.93×10^{-3}	1.257	1075
	NEO380_AA_TMPTA	22.1–56.8	0.81	38.7	2.04×10^{-3}	1.328	490
	NEO380_AA_PETA	20.8–62.7	0.72	45.3	2.55×10^{-3}	1.330	392
	L3300_AA_BPAEDA	1.0–36.5	1.18	24.5	1.13×10^{-3}	1.171	885
	L3300_AA_TMPTA	22.5–55.1	0.80	39.7	2.20×10^{-3}	1.202	455
	L3300_AA_PETA	28.5–57.5	0.44	46.6	2.70×10^{-3}	1.247	369

Cross-link density and molecular weight between cross-links were calculated from the DMA data and are presented in Table 2. Results showed that cross-link density and molecular weight between cross-links of the polymers were highly dependent on the functionality of the used acrylate and acetoacetate. If higher functionalized monomers were used, the cross-link density of the obtained polymer was higher, and the molecular weight between cross-links was smaller, which significantly affects the polymer's mechanical properties.

The highest cross-link density (3.17×10^{-3} moles·cm^{-3}) and the lowest molecular weight between cross-links (315 g·mol^{-1}) were obtained from E^{IR}TOFA_TMP_AA and PETA (tetrafunctional acrylate). It can be explained by the higher functionality of both—the Michael donor and the Michael acceptor compound. The lowest cross-link density and molecular weight between cross-links were for the polymers derived from the lower functionalized acetoacetate and difunctional acrylate—BPAEDA.

3.5. Tensile Tests

Values of tensile modulus (Young's) and tensile strength for the samples are shown in Figure 7. Polymer monolith samples obtained by the reaction of polyol acetoacetates with tetraacrylate PETA showed the highest tensile modulus values. The results of tensile strength showed the same trend. This could be explained by the higher functionality of the acrylate and, thus, the higher cross-link density (see Table 2), resulting in the highest module value. A correlation between the functionality of acrylate used in polymer formulations and the tensile module values was observed: the higher functionality of the used acrylate yielded polymers with higher tensile module values.

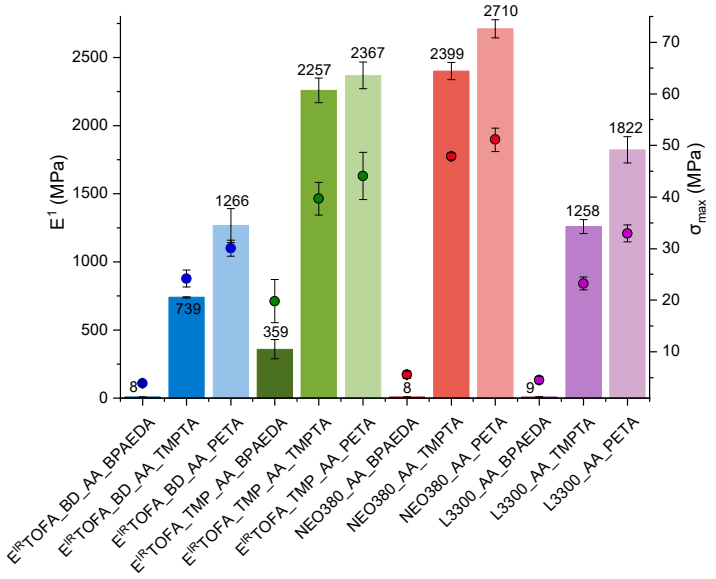

Figure 7. Tensile modulus (Young's) (E^1) and tensile strength (σ_{max}) for the polymers from tall oil polyol or commercial polyol-based acetoacetates and BPAEDA, TMPTA, and PETA acrylates.

The tensile strength for NEO380_AA_PETA polymer was 51 MPa. Relatively high modulus values were also obtained for polymers from tall oil from E^{IR}TOFA_TMP_AA_TMPTA and E^{IR}TOFA_TMP_AA_PETA, respectively, at 2250 MPa and 2370 MPa, and tensile strength was 40 MPa and 44 MPa. Slightly higher average tensile strength and modulus values were for the PETA acrylate, but they were lower for the TMPTA acrylate. These materials can be compared to PMMA, which had a tensile strength value of at least 55 MPa and a tensile modulus of about 2700 MPa [68,69]. Fleischer et al. prepared non-filled NIPU

from hexamethylene diamine and glycerol cyclic carbonates: trimethylolpropane. This NIPU showed a tensile strength of 68 MPa and Young's modulus of 2100 MPa [70]. The mechanical properties of obtained polymers are also comparable to polyurethane materials [71,72]. This shows that tall-oil-based polymer materials obtained by the Michael addition reaction are competitive and promising alternatives.

The highest tensile modulus values were for polymer materials obtained from triacrylate or tetraacrylate and NEO380_AA. A maximum average value of the modulus exceeds 2710 MPa for a NEO380_AA_PETA polymer. The polymers derived using BPAEDA had the lowest modulus value and tensile strength. These polymers (E^{IR}TOFA_BD_AA_BPAEDA, NEO380_AA_BPAEDA, and L3300_AA_BPAEDA) exhibited characteristics similar to rubber.

The elongation at break correlates with the modulus value and the tensile strength. The higher modulus and tensile strength values, the smaller the elongation. The smallest elongations at breaks were 1.9%, 2.7%, and 2.9% for polymers E^{IR}TOFA_TMP_AA_PETA, NEO380_AA_PETA, and L3300_AA_PETA, and the highest elongations at breaks were 55%, 53% and 47% for polymers E^{IR}TOFA_BD_AA_BPAEDA, NEO380_AA_BPAEDA, and L3300_AA_BPAEDA, respectively.

The relationship between mechanical properties and the molecular weight between cross-links was observed. The lower the molecular weight between cross-links, the higher the cross-link density (see Table 2) and the correspondingly higher tensile modulus (Young's) and tensile strength.

Results indicate that it is possible to obtain very different polymeric materials by changing the chemical structure of the used acrylate. Polymeric materials that are similar in properties to rubbers can be obtained by using lower functionality monomers. It is also possible to obtain materials that are similar in their properties even to organic glass [68,69,73]. By compiling the literature on similar materials and their characteristics, the polymer materials obtained in this study are competitive with several other alternative materials. The production of polymers from fatty-acid-based monomers by Michael reactions is relatively simple and is carried out in milder conditions compared to other methods, such as NIPU synthesis. Michael addition polymerizations can be realized in a short period of time, at room temperature, and at an atmospheric pressure. The chemicals used to synthesize polymers via Michael additions are less toxic than isocyanates, which is one of the main raw materials for polyurethane production. The mechanical and thermal properties of synthesized polymers by the Michael reaction are equal to or even better than materials shown in the literature. Moreover, the properties of polymers can be tailored by varying the monomers used for polymerization. For more information on other similar materials and their characteristics from the literature, see Supplementary Materials Table S1 "Characteristics (glass transition temperatures (T_g) by DMA, tensile (Young's) modulus (E^1), tensile strength and cross-link density (v_e)) of selected polymers for comparison".

4. Conclusions

Polymer materials were successfully obtained from the synthesized tall oil acetoacetates. The properties of synthesized bio-based polymer monoliths were comparable to polymeric materials obtained from commercially available acrylates. The modulus, tensile strength, and glass transition temperatures were determined for all obtained samples. The properties of the polymer were strongly dependent on the functionality of the monomers used. It was shown that a wide range of polymeric materials with different properties could be obtained by varying the functionality of the monomer. This study demonstrated that polymers can be synthesized with a wide range of mechanical properties, from rubber-like (E^1 = 8 MPa and σ_{max} = 4 MPa for E^{IR}TOFA_BD_AA_BPAEDA) to close to organic glass and NIPUs (E^1 = 2370 MPa and σ_{max} = 44 MPa for E^{IR}TOFA_TMP_AA_PETA). Glass transition temperatures varied from 21.0 °C for E^{IR}TOFA_BD_AA_BPAEDA to 63.4 °C for E^{IR}TOFA_TMP_AA_PETA obtained by DMA. The synthesized polymers were thermally stable up to 300 °C. Tall-oil-based polymers via the Michael nucleophilic 1,4-addition are an attractive alternative to poly(methyl methacrylate), conventional polyurethanes,

NIPUs, and other fossil-based polymer materials. The polymer formulations developed in this study may be suitable for two-component polymer foams, coatings, resins, and composite matrices.

Supplementary Materials: The following supporting information can be downloaded at: https://www.mdpi.com/article/10.3390/polym14194068/s1, Table S1: Characteristics (glass transition temperatures (T_g) by DMA, tensile (Young's) modulus (E^1), tensile strength, and cross-link density (v_e)) of the selected polymers for comparison. References [5,15,39,43,52,53,56,68,74,75] are cited in Supplementary Materials.

Author Contributions: Conceptualization, M.K.; data curation, R.P. and I.M.; formal analysis, R.P.; writing—original draft preparation, R.P. and I.M.; writing—review and editing, R.P., I.M., M.K. and A.F.; project administration, A.F.; software, R.P. and I.M.; supervision, M.K.; visualization R.P. and I.M. All authors have read and agreed to the published version of the manuscript.

Funding: This research was funded by the Latvian Council of Science, project "High bio-based content thermoset polymer foam development from plant origin oils (Bio-Mer)", project No. lzp-2020/1-0385. This publication was supported by Riga Technical University's Doctoral Grant programme (DOK.OĶTI/21).

Institutional Review Board Statement: Not applicable.

Informed Consent Statement: Not applicable.

Data Availability Statement: The raw data presented in this study are available on request from the corresponding author.

Conflicts of Interest: The authors declare no conflict of interest.

References

1. European Commission. *The European Green Deal*; Cambridge University Press: Cambridge, UK, 2019.
2. Rosenboom, J.G.; Langer, R.; Traverso, G. Bioplastics for a circular economy. *Nat. Rev. Mater.* **2022**, *7*, 117–137. [CrossRef] [PubMed]
3. Cifarelli, A.; Boggioni, L.; Vignali, A.; Tritto, I.; Bertini, F.; Losio, S. Flexible polyurethane foams from epoxidized vegetable oils and a bio-based diisocyanate. *Polymers* **2021**, *13*, 612. [CrossRef] [PubMed]
4. Sittinun, A.; Pisitsak, P.; Manuspiya, H.; Thiangtham, S.; Chang, Y.H.; Ummartyotin, S. Utilization of Palm Olein-Based Polyol for Polyurethane Foam Sponge Synthesis: Potential as a Sorbent Material. *J. Polym. Environ.* **2020**, *28*, 3181–3191. [CrossRef]
5. Chen, R.; Zhang, C.; Kessler, M.R. Polyols and polyurethanes prepared from epoxidized soybean oil ring-opened by polyhydroxy fatty acids with varying oh numbers. *J. Appl. Polym. Sci.* **2015**, *132*, 41213. [CrossRef]
6. Zhang, J.; Tang, J.J.; Zhang, J.X. Polyols prepared from ring-opening epoxidized soybean oil by a castor oil-based fatty diol. *Int. J. Polym. Sci.* **2015**, *2015*, 529235. [CrossRef]
7. Coman, A.E.; Peyrton, J.; Hubca, G.; Sarbu, A.; Gabor, A.R.; Nicolae, C.A.; Iordache, T.V.; Averous, L. Synthesis and characterization of renewable polyurethane foams using different biobased polyols from olive oil. *Eur. Polym. J.* **2021**, *149*, 110363. [CrossRef]
8. Liao, Y.-H.; Su, Y.-L.; Chen, Y.-C. The Influence of Neem Oil and Its Glyceride on the Structure and Characterization of Castor Oil-Based Polyurethane Foam. *Polymers* **2021**, *13*, 2020. [CrossRef] [PubMed]
9. Abolins, A.; Pomilovskis, R.; Vanags, E.; Mierina, I.; Michalowski, S.; Fridrihsone, A.; Kirpluks, M. Impact of different epoxidation approaches of tall oil fatty acids on rigid polyurethane foam thermal insulation. *Materials* **2021**, *14*, 894. [CrossRef] [PubMed]
10. Dechent, S.E.; Kleij, A.W.; Luinstra, G.A. Fully bio-derived CO_2 polymers for non-isocyanate based polyurethane synthesis. *Green Chem.* **2020**, *22*, 969–978. [CrossRef]
11. Sternberg, J.; Pilla, S. Materials for the biorefinery: High bio-content, shape memory Kraft lignin-derived non-isocyanate polyurethane foams using a non-toxic protocol. *Green Chem.* **2020**, *22*, 6922–6935. [CrossRef]
12. Lindsay, C.D.; Timperley, C.M. TRPA1 and issues relating to animal model selection for extrapolating toxicity data to humans. *Hum. Exp. Toxicol.* **2020**, *39*, 14–36. [CrossRef]
13. Kathalewar, M.; Sabnis, A.; D'Mello, D. Isocyanate free polyurethanes from new CNSL based bis-cyclic carbonate and its application in coatings. *Eur. Polym. J.* **2014**, *57*, 99–108. [CrossRef]
14. Kathalewar, M.S.; Joshi, P.B.; Sabnis, A.S.; Malshe, V.C. Non-isocyanate polyurethanes: From chemistry to applications. *RSC Adv.* **2013**, *3*, 4110–4129. [CrossRef]
15. Bähr, M.; Xie, W.; Łukaszewska, I.; Hebda, E.; Pielichowski, K. Recent advances in fabrication of non-isocyanate polyurethane-based composite materials. *Materials* **2021**, *14*, 3497. [CrossRef]

16. Gomez-Lopez, A.; Elizalde, F.; Sardon, H. Trends in non-isocyanate polyurethane (NIPU) development. *Chem. Commun.* **2021**, *57*, 12254–12265. [CrossRef]
17. Omer, R.A.; Hama, J.R.; Rashid, R.S.M. The Effect of Dextran Molecular Weight on the Biodegradable Hydrogel with Oil, Synthesized by the Michael Addition Reaction. *Adv. Polym. Technol.* **2015**, *36*, 120–127. [CrossRef]
18. Mather, B.D.; Viswanathan, K.; Miller, K.M.; Long, T.E. Michael addition reactions in macromolecular design for emerging technologies. *Prog. Polym. Sci.* **2006**, *31*, 487–531. [CrossRef]
19. Noordover, B.; Liu, W.; McCracken, E.; DeGooyer, B.; Brinkhuis, R.; Lunzer, F. Michael addition curable coatings from renewable resources with enhanced adhesion performance. *J. Coat. Technol. Res.* **2020**, *17*, 1123–1130. [CrossRef]
20. Sonnenschein, M.F.; Werness, J.B.; Patankar, K.A.; Jin, X.; Larive, M.Z. From rigid and flexible foams to elastomers via Michael addition chemistry. *Polymer* **2016**, *106*, 128–139. [CrossRef]
21. Yang, X.; Liu, H.; Qian, L.; Meng, Q.; Wu, H.; Li, Z.; Zhou, H. Surface functionalization of cellulose fibers via aza-Michael addition for CO_2-assisted water remediation. *Appl. Surf. Sci.* **2021**, *554*, 149593. [CrossRef]
22. Bhattacharjee, S.; Shaikh, A.A.; Ahn, W.S. Heterogeneous Aza-Michael Addition Reaction by the Copper-Based Metal–Organic Framework (CuBTC). *Catal. Lett.* **2021**, *151*, 2011–2018. [CrossRef]
23. Su, G.; Thomson, C.J.; Yamazaki, K.; Rozsar, D.; Christensen, K.E.; Hamlin, T.A.; Dixon, D.J. A bifunctional iminophosphorane squaramide catalyzed enantioselective synthesis of hydroquinazolines: Via intramolecular aza-Michael reaction to α,β-unsaturated esters. *Chem. Sci.* **2021**, *12*, 6064–6072. [CrossRef] [PubMed]
24. Mushtaque, M.; Avecilla, F.; Ahmad, I.; Alharbi, A.M.; Khan, P.; Ahamad, S.; Hassan, M.I. 5-Fluorouracil (5-FU)-based Aza-Michael addition product: A selective carbonic anhydrase IX inhibitor. *J. Mol. Struct.* **2021**, *1231*, 129977. [CrossRef]
25. Alaneed, R.; Golitsyn, Y.; Hauenschild, T.; Pietzsch, M.; Reichert, D.; Kressler, J. Network formation by aza-Michael addition of primary amines to vinyl end groups of enzymatically synthesized poly (glycerol adipate). *Polym. Int.* **2021**, *70*, 135–144. [CrossRef]
26. Gunay, U.S.; Cetin, M.; Daglar, O.; Hizal, G.; Tunca, U.; Durmaz, H. Ultrafast and efficient aza- and thiol-Michael reactions on a polyester scaffold with internal electron deficient triple bonds. *Polym. Chem.* **2018**, *9*, 3037–3054. [CrossRef]
27. Li, Q.F.; Chu, S.; Li, E.; Li, M.; Wang, J.T.; Wang, Z. Lanthanide-based hydrogels with adjustable luminescent properties synthesized by thiol-Michael addition. *Dye. Pigment.* **2020**, *174*, 108091. [CrossRef]
28. Chen, J.; Ma, X.; Edgar, K.J. A Versatile Method for Preparing Polysaccharide Conjugates via Thiol-Michael Addition. *Polymers* **2021**, *13*, 1905. [CrossRef]
29. Cespedes, S.; Hand, R.A.; Chmel, N.; Moad, G.; Keddie, D.J.; Schiller, T.L. Enhanced properties of well-defined polymer networks prepared by a sequential thiol-Michael-radical thiol-ene (STMRT) strategy. *Eur. Polym. J.* **2021**, *151*, 110440. [CrossRef]
30. Piñeiro-García, A.; Vega-Díaz, S.M.; Tristán, F.; Meneses-Rodríguez, D.; Labrada-Delgado, G.J.; Semetey, V. New insights in the chemical functionalization of graphene oxide by thiol-ene Michael addition reaction. *FlatChem* **2021**, *26*, 100230. [CrossRef]
31. Lenardão, E.J.; Trecha, D.O.; Ferreira, P.d.C.; Jacob, R.G.; Perin, G. Green Michael Addition of Thiols to Electron Deficient Alkenes using KF/Alumina and Recyclable Solvent or Solvent-free Conditions. *J. Braz. Chem. Soc.* **2009**, *20*, 93–99. [CrossRef]
32. Chatani, S.; Nair, D.P.; Bowman, C.N. Relative reactivity and selectivity of vinyl sulfones and acrylates towards the thiol-Michael addition reaction and polymerization. *Polym. Chem.* **2013**, *4*, 1048–1055. [CrossRef]
33. Liu, N. New Polymers Synthesis by Organocatalyzed Step-Growth Polymerization of Aldehydic Monomers: Polyaldols, Linear Polybenzoin and Hyperbranched Polyacetals. Ph.D. Thesis, Université Sciences et Technologies-Bordeaux I, Gradignan, France, 2014.
34. Williams, S.R.; Miller, K.M.; Long, T.E. Michael addition reaction kinetics of acetoacetates and acrylates for the formation of polymeric networks. *Prog. React. Kinet. Mech.* **2007**, *32*, 165–194. [CrossRef]
35. Jiang, Q.; Zhang, Y.L.; Du, Y.; Tang, M.; Jiang, L.; Huang, W.; Yang, H.; Xue, X.; Jiang, B. Preparation of hyperbranched polymers by oxa-Michael addition polymerization. *Polym. Chem.* **2020**, *11*, 1298–1306. [CrossRef]
36. Nising, C.F.; Bräse, S. The oxa-Michael reaction: From recent developments to applications in natural product synthesis. *Chem. Soc. Rev.* **2008**, *37*, 1218–1228. [CrossRef]
37. González, G.; Fernández-Francos, X.; Serra, À.; Sangermano, M.; Ramis, X. Environmentally-friendly processing of thermosets by two-stage sequential aza-Michael addition and free-radical polymerization of amine-acrylate mixtures. *Polym. Chem.* **2015**, *6*, 6987–6997. [CrossRef]
38. Farmer, T.J.; Comerford, J.W.; Pellis, A.; Robert, T. Post-polymerization modification of bio-based polymers: Maximizing the high functionality of polymers derived from biomass. *Polym. Int.* **2018**, *67*, 775–789. [CrossRef]
39. Cao, Z.; Gao, F.; Zhao, J.; Wei, X.; Cheng, Q.; Zhong, J.; Lin, C.; Shu, J.; Fu, C.; Shen, L. Bio-based coating materials derived from acetoacetylated soybean oil and aromatic dicarboxaldehydes. *Polymers* **2019**, *11*, 1809. [CrossRef]
40. He, X.; Zhong, J.; Cao, Z.; Wang, J.; Gao, F.; Xu, D.; Shen, L. An exploration of the Knoevenagel condensation to create ambient curable coating materials based on acetoacetylated castor oil. *Prog. Org. Coat.* **2019**, *129*, 21–25. [CrossRef]
41. Trevino, A.S.; Trumbo, D.L. Acetoacetylated castor oil in coatings applications. *Prog. Org. Coat.* **2002**, *44*, 49–54. [CrossRef]
42. Xu, D.; Cao, Z.; Wang, T.; Zhong, J.; Zhao, J.; Gao, F.; Luo, X.; Fang, Z.; Cao, J.; Xu, S.; et al. An ambient-cured coating film obtained via a Knoevenagel and Michael addition reactions based on modified acetoacetylated castor oil prepared by a thiol-ene coupling reaction. *Prog. Org. Coat.* **2019**, *135*, 510–516. [CrossRef]

43. Zuo, H.; Cao, Z.; Shu, J.; Xu, D.; Zhong, J.; Zhao, J.; Wang, T.; Chen, Y.; Gao, F.; Shen, L. Effect of structure on the properties of ambient-cured coating films prepared via a Michael addition reaction based on an acetoacetate-modified castor oil prepared by thiol-ene coupling. *Prog. Org. Coat.* **2019**, *135*, 27–33. [CrossRef]
44. Naga, N.; Satoh, M.; Magara, T.; Ahmed, K.; Nakano, T. Synthesis of gels by means of Michael addition reaction of multi-functional acetoacetate and diacrylate compounds and their application to ionic conductive gels. *J. Appl. Polym. Sci.* **2021**, *59*, 2129–2139. [CrossRef]
45. Park, S.-H.; Alammar, A.; Fulop, Z.; Pulido, B.A.; Nunes, S.P.; Szekely, G. Hydrophobic thin film composite nanofiltration membranes derived solely from sustainable sources. *Green Chem.* **2021**, *23*, 1175–1184. [CrossRef]
46. Sinha, J.; Soars, S.; Bowman, C.N. Enamine Organocatalysts for the Thiol-Michael Addition Reaction and Cross-Linking Polymerizations. *Macromolecules* **2021**, *54*, 1693–1701. [CrossRef]
47. Williams, S.R.; Mather, B.D.; Miller, K.M.; Long, T.E. Novel michael addition networks containing urethane hydrogen bonding. *J. Polym. Sci. Part A Polym. Chem.* **2007**, *45*, 4118–4128. [CrossRef]
48. Bureau, I. Functionalized Oligomers, WO 2014/052081 A2, 4 April 2014.
49. Ozturk, G.; Long, T.E. Michael addition for crosslinking of poly(caprolactone)s. *J. Polym. Sci. Part A Polym. Chem.* **2009**, *47*, 5437–5447. [CrossRef]
50. Balotupi, T.; Lanta, T.; Rzwpk, D.A.N.P.K. Non-Isocyanate Rigid Polymer Foams By Carbon-Michael Addition, and Foaming Process. WO 2013/101682 Al, 4 July 2013.
51. Zhaoo, M.Y.; Hsu, C.-P.; Voeks, S.L.; Landtiser, R. Acetoacetyl Thermosetting Resin for Zero Voc Gel Coat. WO 2013/132077, 12 September 2013.
52. Kim, T.H.; Kim, M.; Lee, W.; Kim, H.G.; Lim, C.S.; Seo, B. Synthesis and characterization of a polyurethane phase separated to nano size in an epoxy polymer. *Coatings* **2019**, *9*, 319. [CrossRef]
53. Jena, K.K.; Raju, K.V.S.N. Synthesis and characterization of hyperbranched polyurethane hybrids using tetraethoxysilane (TEOS) as cross-linker. *Ind. Eng. Chem. Res.* **2008**, *47*, 9214–9224. [CrossRef]
54. Hill, L.W. Calculation of crosslink density in short chain networks. *Prog. Org. Coat.* **1997**, *31*, 235–243. [CrossRef]
55. Zhang, C.; Madbouly, S.A.; Kessler, M.R. Biobased polyurethanes prepared from different vegetable oils. *ACS Appl. Mater. Interfaces* **2015**, *7*, 1226–1233. [CrossRef] [PubMed]
56. Barszczewska-Rybarek, I.M.; Korytkowska-Wałach, A.; Kurcok, M.; Chladek, G.; Kasperski, J. DMA analysis of the structure of crosslinked poly(methyl methacrylate)s. *Acta Bioeng. Biomech.* **2017**, *19*, 47–53. [CrossRef]
57. Omer, R.A.; Hughes, A.; Hama, J.R.; Wang, W.; Tai, H. Hydrogels from dextran and soybean oil by UV photo-polymerization. *J. Appl. Polym. Sci.* **2015**, *132*, 41446. [CrossRef]
58. Bermejo, J.S.; Ugarte, C.M. Influence of cross-linking density on the glass transition and structure of chemically cross-linked PVA: A molecular dynamics study. *Macromol. Theory Simul.* **2009**, *18*, 317–327. [CrossRef]
59. Amado, J.C.Q. Thermal Resistance Properties of Polyurethanes and its Composites: A Short Review. *J. Res. Updat. Polym. Sci.* **2019**, *8*, 66–84. [CrossRef]
60. Shufen, L.; Zhi, J.; Kaijun, Y.; Shuqin, Y.; Chow, W.K. Studies on the thermal behavior of polyurethanes. *Polym.-Plast. Technol. Eng.* **2006**, *45*, 95–108. [CrossRef]
61. Zhang, F.A.; Lee, D.K.; Pinnavaia, T.J. PMMA-mesocellular foam silica nanocomposites prepared through batch emulsion polymerization and compression molding. *Polymer* **2009**, *50*, 4768–4774. [CrossRef]
62. Rajkumar, T.; Muthupandiyan, N.; Vijayakumar, C.T. Synthesis and investigation of thermal properties of PMMA-maleimide-functionalized reduced graphene oxide nanocomposites. *J. Thermoplast. Compos. Mater.* **2020**, *33*, 85–96. [CrossRef]
63. Hassan, M.K.; Tucker, S.J.; Abukmail, A.; Wiggins, J.S.; Mauritz, K.A. Polymer chain dynamics in epoxy based composites as investigated by broadband dielectric spectroscopy. *Arab. J. Chem.* **2016**, *9*, 305–315. [CrossRef]
64. Dave, V.J.; Patel, H.S. Synthesis and characterization of interpenetrating polymer networks from transesterified castor oil based polyurethane and polystyrene. *J. Saudi Chem. Soc.* **2013**, *21*, 18–24. [CrossRef]
65. Chen, S.; Wang, Q.; Pei, X.; Wang, T. Dynamic mechanical properties of castor oil-based polyurethane/epoxy graft interpenetrating polymer network composites. *J. Appl. Polym. Sci.* **2010**, *116*, 1144–1151. [CrossRef]
66. Hagen, R.; Salmén, L.; Lavebratt, H.; Stenberg, B. Comparison of dynamic mechanical measurements and Tg determinations with two different instruments. *Polym. Test.* **1994**, *13*, 113–128. [CrossRef]
67. Gracia-Fernández, C.A.; Gómez-Barreiro, S.; López-Beceiro, J.; Tarrío Saavedra, J.; Naya, S.; Artiaga, R. Comparative study of the dynamic glass transition temperature by DMA and TMDSC. *Polym. Test.* **2010**, *29*, 1002–1006. [CrossRef]
68. Xie, W.; Guo, S.; Liu, Y.; Chen, R.; Wang, Q. Organic-inorganic hybrid strategy based on ternary copolymerization to prepare flame retardant poly (methyl methacrylate) with high performance. *Compos. Part B Eng.* **2020**, *203*, 108437. [CrossRef]
69. Ali, U.; Karim, K.J.B.A.; Buang, N.A. A Review of the Properties and Applications of Poly (Methyl Methacrylate) (PMMA). *Polym. Rev.* **2015**, *55*, 678–705. [CrossRef]
70. Fleischer, M.; Blattmann, H.; Mülhaupt, R. Glycerol-, pentaerythritol- and trimethylolpropane-based polyurethanes and their cellulose carbonate composites prepared via the non-isocyanate route with catalytic carbon dioxide fixation. *Green Chem.* **2013**, *15*, 934–942. [CrossRef]
71. Abolins, A.; Yakushin, V.; Vilsone, D. Properties of polyurethane coatings based on linseed oil phosphate ester polyol. *J. Renew. Mater.* **2018**, *6*, 737–745. [CrossRef]

72. Yakushin, V.; Abolins, A.; Vilsone, D.; Sevastyanova, I. Polyurethane coatings based on linseed oil phosphate ester polyols with intumescent flame retardants. *Fire Mater.* **2019**, *43*, 92–100. [CrossRef]
73. Ishigami, A.; Watanabe, K.; Kurose, T.; Ito, H. Physical and morphological properties of tough and transparent PMMA-based blends modified with polyrotaxane. *Polymers* **2020**, *12*, 1790. [CrossRef] [PubMed]
74. Zhu, Y.; Gao, F.; Zhong, J.; Shen, L.; Lin, Y. Renewable Castor Oil and DL-Limonene Derived Fully Bio-Based Vinylogous Urethane Vitrimers. *Eur. Polym. J.* **2020**, *135*, 109865. [CrossRef]
75. Bähr, M.; Mülhaupt, R. Linseed and Soybean Oil-Based Polyurethanes Prepared via the Non-Isocyanate Route and Catalytic Carbon Dioxide Conversion. *Green Chem.* **2012**, *14*, 483–489. [CrossRef]

Table S1. Characteristics (glass transition temperatures (T_g) by DMA, tensile (Young's) modulus (E^1), tensile strength and cross-link density (ν_e)) of selected polymers for comparison.

Materials(raw materials, short preparation method)	Samples	Characteristics				Ref.
		T_g (DMA), °C	E^1, (MPa)	Tensile strength, MPa	ν_e, mol·cm^{-3}	
On the basis of acetoacetylated soybean oil (AASBO), several bio-based coating materials were prepared using different aromatic dicarboxaldehydes (1,2-benzenedialdehyde (1,2-BDA), 1,3-benzenedialdehyde (1,3-BDA), 1,4-phthalaldehyde (1,4-BDA), 4,4′-biphenyldicarboxaldehyde (4,4′-BPDCA))	AASBO with 1,2-BDA	38	2.76	1.44	$1.4 \cdot 10^{-5}$	[39]
	AASBO with 1,3-BDA	39	6.27	3.54	$3.5 \cdot 10^{-5}$	
	AASBO with 1,4-BDA	42	15.07	3.85	$8.9 \cdot 10^{-5}$	
	AASBO with 4,4′-BPDCA	54	24.91	5.65	$9.0 \cdot 10^{-5}$	
Film materials prepared from acetoacetylated castor oil or modified castor oil (modified by different amount of 2-mercaptoethanol (Castrol oil:2-mercaptoethanol: 0.01:0.015 and 0.01:03)) and 4,4-diaminocyclohexylmethane (PACM) by Michael addition reaction	Film from acetoacetylated castor oil and PACM	2	0.028	0.68	$0.097 \cdot 10^{-3}$	[43]
	Film from modified castor oil (0.01:0.015) and PACM	27.6	0.041	1.06	$0.17 \cdot 10^{-3}$	
	Film from modified castor oil (0.01:0.015) and PACM	33.1	0.18	1.75	$0.27 \cdot 10^{-3}$	
Polyurethane (PU) films prepared from epoxidized soybean oil (ESBO) and epoxidized linseed oil (ELO) ring-opened by polyhydroxy fatty acids. Polyols were identified as SMS, SGS, LMS, and LGS, where the first letter "S" – ESBO, "L" – ELO; the second letter "M" – methanol , "G" – glycol; "S" refers to ESBO ring-opened by fatty acids.	SMS-PU	39.3	67.2	8.6	$0.0374 \cdot 10^{-3}$	[5]
	SGS-PU	49.9	123.4	11.5	$0.103 \cdot 10^{-3}$	
	LMS-PU	63.4	166.6	13.5	$0.31 \cdot 10^{-3}$	
	LGS-PU	80.5	315	17.2	$0.91 \cdot 10^{-3}$	
Bisphenol A epoxy resin was modified with a dimeric fatty acid and diglycidyl groups. The prepared polyol was mixed with polypropylene glycol and reacted with isophorone diisocyanate	PU	108	2035	~68	$1.03 \cdot 10^{-3}$	[52]
Hydroxyl-terminated fourth-generation hyperbranched polyester was synthesized from glycerol, 2,2-bis(Hydroxymethyl) propionic acid, 3-isocyanatopropyl triethoxysilane	PU	116.6	293		$2.97 \cdot 10^{-3}$	[53]
Vinylogous urethane vitrimer derived from renewable castor oil and DL-limonene	PU vitrimers	48	27.2	5.5	$0.99 \cdot 10^{-3}$	[74]

Materials(raw materials, short preparation method)	Samples	Characteristics				Ref.
		T_g (DMA), °C	E', (MPa)	Tensile strength, MPa	ν_e, mol·cm^{-3}	
Non-isocyanate polyurethane (NIPU) prepared from hexamethylene diamine and glycerol cyclic carbonates, trimethylolpropane	NIPU		2100	68		[15]
NIPU prepared by curing carbonated soybean (CSBO) and linseed (CLSO) oils with different diamines (1,2-ethane diamine (EDA), 1,4-butane diamine (BDA), isophorone diamine (IPDA))	NIPU (CSBO-EDA)	20	6	4		[75]
	NIPU (CSBO-BDA)	17	2	2		
	NIPU (CSBO-IPDA)	40	50	5		
	NIPU (CLSO-EDA)	55	180	18		
	NIPU (CLSO-BDA)	45	300	17		
	NIPU (CLSO-IPDA)	60	1460	10		
Methyl methacrylate (MMA)	Poly(methyl methacrylate) (PMMA)		2700	55		[68]
MMA	PMMA	126.5	1514		$0.081 \cdot 10^{-3}$	[56]

3

4. pielikums
Appendix 4

The synthesis of bio-based Michael donors from tall oil fatty acids for polymer development

Ralfs Pomilovskis, Inese Mieriņa, Hynek Beneš, Olga Trhlíková, Arnis Āboliņš, Anda Fridrihsone, Miķelis Kirpļuks

Polymers, 2023

polymers

MDPI

Article

The Synthesis of Bio-Based Michael Donors from Tall Oil Fatty Acids for Polymer Development

Ralfs Pomilovskis [1,2,*], Inese Mierina [2], Hynek Beneš [3], Olga Trhlíková [3], Arnis Abolins [1], Anda Fridrihsone [1] and Mikelis Kirpluks [1]

[1] Polymer Laboratory, Latvian State Institute of Wood Chemistry, Dzerbenes St. 27, LV-1006 Riga, Latvia
[2] Institute of Technology of Organic Chemistry, Faculty of Materials Science and Applied Chemistry, Riga Technical University, P. Valdena St. 3/7, LV-1048 Riga, Latvia
[3] Institute of Macromolecular Chemistry, CAS, Heyrovského nám. 2, 162 06 Prague 6, Czech Republic
* Correspondence: ralfs.pomilovskis@kki.lv

Abstract: In this study, the synthesis of a Michael donor compound from cellulose production by-products—tall oil fatty acids—was developed. The developed Michael donor compounds can be further used to obtain polymeric materials after nucleophilic polymerization through the Michael reaction. It can be a promising alternative method for conventional polyurethane materials, and the Michael addition polymerization reaction takes place under milder conditions than non-isocyanate polyurethane production technology, which requires high pressure, high temperature and a long reaction time. Different polyols, the precursors for Michael donor components, were synthesized from epoxidized tall oil fatty acids by an oxirane ring-opening and esterification reaction with different alcohols (trimethylolpropane and 1,4-butanediol). The addition of functional groups necessary for the Michael reaction was carried out by a transesterification reaction of polyol hydroxyl groups with *tert*-butyl acetoacetate ester. The following properties of the developed polyols and their acetoacetates were analyzed: hydroxyl value, acid value, moisture content and viscosity. The chemical structure was analyzed using Fourier transform infrared spectroscopy, gel permeation chromatography, size-exclusion chromatography and nuclear magnetic resonance. Matrix-assisted laser desorption/ionization analysis was used for structure identification for this type of acetoacetate for the first time.

Keywords: Michael addition components; Michael donor; tall oil fatty acids; bio-based acetoacetate

check for updates

Citation: Pomilovskis, R.; Mierina, I.; Beneš, H.; Trhlíková, O.; Abolins, A.; Fridrihsone, A.; Kirpluks, M. The Synthesis of Bio-Based Michael Donors from Tall Oil Fatty Acids for Polymer Development. *Polymers* **2022**, *14*, 4107. https://doi.org/10.3390/polym14194107

Academic Editor: Aleksander Hejna

Received: 31 August 2022
Accepted: 27 September 2022
Published: 30 September 2022

Publisher's Note: MDPI stays neutral with regard to jurisdictional claims in published maps and institutional affiliations.

Copyright: © 2022 by the authors. Licensee MDPI, Basel, Switzerland. This article is an open access article distributed under the terms and conditions of the Creative Commons Attribution (CC BY) license (https://creativecommons.org/licenses/by/4.0/).

1. Introduction

Bio-based polymer development is essential for the European Green Deal to transit into a circular bioeconomy as Europe strives to be climate neutral by 2050 [1]. It is quite clear that incentives will be given to the bio-based polymer industry to encourage it to expand, develop new technologies and materials and increase production quantities [2,3]. The bio-based polymer industry must overcome several challenges, such as changing the raw material base, implementing greener technology, modifying infrastructure and establishing new supply and value chains [4]. It is dire to find solutions to these challenges and to reorganize the carbon processing sector.

Tall oil is obtained as a side stream in pulp production. Tall oil is a second generation feedstock; thus, it does not compete with the food and feed supply chain. It is a complex mixture of tall oil fatty acids, mainly oleic and linoleic acid, rosin acids and unsaponifiables such as high-molecular alcohols, sterols and other alkyl hydrocarbon derivatives. Currently, its potential to produce high value-added bio-based substances and polymeric materials has been investigated relatively little [5]. Fatty acids of tall oil contain a double bond, making them attractive for introducing a reactive functional group and suitable for polymer production [6,7].

The modification of double bonds has been extensively studied. There are many publications on the double bond epoxidation of fatty acids by different methods for further synthesizing polyols by ring-opening reactions with alcohols [8–11]. In a couple of studies, these polyols are used as a part of component A to produce polyurethanes [3,7,12–15]. Isocyanates are used as component B in conventional polyurethane production. Isocyanates are considered to be highly toxic and environmentally hazardous substances [16–20]. Although non-isocyanate polyurethanes (NIPUs) are offered as an alternative to conventional polyurethanes and are considered a safe and sustainable way to extract polymers, the NIPU production technology also faces significant difficulties. For NIPUs, production occurs under harsh conditions—high pressure, high temperature and a long reaction time [21]. The industry needs to find more ways to obtain polymers under mild conditions. It is possible to obtain a two-component thermoset polymeric material with similar properties to polyurethane materials by exploiting the nucleophilic 1,4-addition reaction, which does not involve the application of isocyanates. Hydroxyl groups of polyols can be converted to β-ketoesters to obtain polymers with acrylates by the Michael reaction. Although the method is known, the research has mainly been conducted for coating materials [12,22–25].

Bio-based polymer development using β-ketoesters is an emerging field. Therefore, the acetoacetylation of natural fatty acids and their polyols is not broadly studied yet. A limited number of studies on acetoacetylation of bio-based polyols have been published. Acetoacetylation has been successfully demonstrated in the synthesis of soybean-oil-based polyols [12], castor oil and castor-oil-based polyols [22–27]. Hydroxyl groups of fatty acids polyols are relatively easy to acetoacetylate with *tert*-butyl acetoacetate by a transesterification reaction, thereby obtaining β-ketoesters. The reaction is mostly carried out at a temperature of 110–130 °C [12,22–24,28,29].

It is currently believed that *tert*-butyl acetoacetate is the most suitable reagent for the transacetoacetylation reaction due to its effectiveness under relatively mild conditions, in contrast to other analogs such as methyl acetoacetate, ethyl acetoacetate or isopropyl acetoacetate. Additionally, *tert*-butyl acetoacetate has several advantages, such as stability in storage, a relatively low cost and wide commercial availability, making it attractive from an industrial point of view [29].

In addition, the viscosity of polyol significantly decreases after acetoacetylation due to the disappearance of intermolecular hydrogen bonds. Thus, the obtained β-ketoesters are more easily handled in industrial products [12,22,27,30,31]. In the case of tall oil, lower viscosity is a particularly notable benefit for industrial use, as tall oil fatty acids polyols have a very high viscosity. It can be even above 100,000 mPa·s [7].

This study explores the suitability of cellulose production side stream—tall oils—to provide new insight into bioresource-based feedstocks for further bio-based polymer production. A Michael donor was synthesized, one of the components for a two-component system that cures at room temperature after mixing, forming a highly cross-linked and mechanically rigid polymer. It is a completely new way of valorizing a second generation feedstock—a tall oil.

For the first time, different tall-oil-based polyols were used to synthesize Michael donors by converting the hydroxyl groups present in polyols into acetoacetate esters. Polyols were synthesized from tall oil by catalytical epoxidation using ion exchange resin and subsequent cleavage of the oxirane ring and esterification of the acid group with polyfunctional alcohol. Acetoacetates were synthesized from two tall oil polyols and two commercially available polyols. The following properties of the developed polyols and their acetoacetates were analyzed: hydroxyl value, acid value, moisture content and viscosity. The chemical structure was determined using gel permeation chromatography and size-exclusion chromatography (GPC/SEC), Fourier-transform infrared spectroscopy (FTIR), matrix-assisted laser desorption/ionization (MALDI-TOF) spectra and nuclear magnetic resonance (NMR).

2. Materials and Methods

2.1. Materials and Reagents for Synthesis and Analysis

Reagents for synthesis: tall oil fatty acids (TOFA) (trade name "FOR2"), the content of TOFA: fatty acids > 96%, rosin acids 1.9% and unsaponifiables 1.8% from Forchem Oyj, Rauma, Finland; Amberlite IR-120 H, strongly acidic, hydrogen form from Fluka; glacial acetic acid, ACS reagent, ≥99.7%; hydrogen peroxide, purum p.a., ≥35%; *tert*-butyl acetoacetate, reagent grade, 98%; trimethylolpropane (TMP), reagent grade, 97%; and 1,4-butanediol (BD), reagent plus, ≥99% were purchased from Sigma-Aldrich, Schnelldorf, Germany; tetrafluoroboric acid solution, 48 wt.% in water, was purchased from Alfa Aesar, Kandel, Germany. Lupranol 3300 (L3300), hydroxyl value is 400 mg KOH/g, trifunctional, was purchased from BASF, Lemförde, Germany. Neopolyol 380 (NEO380), has a hydroxyl value of 370 mg KOH/g and a functionality of 3.3, purchased from NEO Group, Rimkai, Lithuania.

Reagents for analysis: 4-(dimethylamino)pyridine, reagent plus, ≥99%; acetic anhydride, puriss, ≥99%; anhydrous sodium sulfate, ACS reagent, granular, ≥99.0%; chloroform, puriss p.a., 99.0–99.4%; dichloromethane, puriss p.a., ACS reagent, ≥99.9%; methanol, puriss p.a., ACS reagent, ≥99.8%; N,N-dimethylformamide, ACS reagent, ≥99.8%, water content ≤150 ppm; perchloric acid, ACS reagent, 70%; potassium hydroxide, ACS reagent, pellets, ≥85%; potassium iodide, ACS reagent, ≥99%; tetraethylammonium bromide, reagent grade, 98%; 2,5-dihydroxybenzoic acid, ≥98%; sodium trifluoroacetate ≥99.5%; N,N-dimethylformamide, biotech. grade, ≥99.9%, purchased from Sigma Aldrich, Schnelldorf, Germany. Hanus solution, volumetric 0.1 M IBr, and sodium thiosulphate fixanals 0.1 M were purchased from Fluka, Seelze, Germany. Tetrahydrofuran, puriss p.a., 99.9%, was purchased from Lachner, Neratovice, Czech Republic.

2.2. Synthesis of Acetoacetylated Tall Oil Fatty Acid Polyols

2.2.1. Epoxidation of TOFA

The mixture of TOFA (700 g), acetic acid (126 g) and ion exchange resin (IR) Amberlite IR-120 H (20 wt.% of TOFA) was heated to 40 °C in a four-neck round flask, which was immersed in a thermostatic water bath. An inert environment was provided by argon gas. Then, slowly and evenly, the hydrogen peroxide (614 g) was added through the dropping funnel while watching the temperature; therefore, it did not exceed 60 °C. After adding hydrogen peroxide, the temperature was kept at 60 °C for 6 h, and the medium was stirred at 600 rpm. The obtained mixture was washed with ethyl acetate and warm distilled water (60 °C) and was dried using a rotatory vacuum evaporator to separate the epoxidized tall oil fatty acids (E^{IR}TOFA).

2.2.2. Synthesis of Polyols from E^{IR}TOFA

Polyols were obtained from the synthesized E^{IR}TOFA by opening the oxirane ring and subsequent esterification with alcohols. Two alcohols of different functionality were used for this step: BD and TMP.

E^{IR}TOFA (300 g) was added via a dropping funnel to a four-neck flask (1 L) already containing the mixture of the alcohol (amount of E^{IR}TOFA carboxyl and oxirane group to alcohol moles ratio of 1:1) and tetrafluoroboric acid solution (48 wt.% in H2O, 0.3 wt.% from E^{IR}TOFA) as a catalyst. The flask was immersed in a thermostatic oil bath. The temperature was maintained at 80 °C during the addition of the E^{IR}TOFA. In this step, the oxirane ring was opened. After all the epoxidized oil had been added, the temperature was raised to 180 °C. The stirring rate was 500 rpm. The water formed during the synthesis was removed with an inert carrier gas (nitrogen) and was condensed in a Liebig condenser. The duration of esterification was 6 h.

2.2.3. Acetoacetylation of Polyols

The polyol acetoacetylation was performed with *tert*-butyl acetoacetate by a transesterification reaction. Via dropping funnel, *tert*-butyl acetoacetate was added to E^{IR}TOFA

polyol (150 g) in a three-neck round bottom flask (500 mL). The amount of polyol hydroxyl groups to *tert*-butyl acetoacetate moles ratio was 1:1. The flask was immersed in a thermostatic oil bath, and the temperature was kept constant at about 120 °C throughout the synthesis. The *tert*-Butanol released during the reaction was condensed using a Liebig condenser. Water was used as a cooling agent in the Liebig condenser at a temperature of about 25–30 °C because the melting point of *tert*-butanol is 25 °C. If a lower temperature is used for cooling, there is a possibility that *tert*-butanol crystallizes in the cooler. The intense *tert*-butanol release ended after about 2 h. In total, the reaction was performed for 4 h to maximize conversions.

The amount of acetoacetate groups (*AA*) in the synthesized Michael donors was calculated according to Equation (1):

$$AA_{groups} = \frac{n_{tert-\text{butyl acetoacetate}}}{m_{yield}} \cdot 100 \quad (1)$$

where $n_{tert\text{-butyl acetoacetate}}$ is used for *tert*-butyl acetoacetate (mol), and m_{yield} is the product mass (g).

As a result of this step, the following Michael donors were obtained:

- epoxidized tall oil fatty acids 1,4-butanediol polyol acetoacetate (E^{IR}TOFA_BD_AA);
- epoxidized tall oil fatty acids trimethylolpropane polyol acetoacetate (E^{IR}TOFA_TMP_AA);
- Neopolyol 380 acetoacetate (NEO380_AA);
- Lupranol 3300 acetoacetate (L3300_AA).

2.3. Characterization of the Synthesized Michael Donor Components

All titration methods were used in accordance with the testing standards. The acid value and hydroxyl value were determined according to ISO 2114:2000 and ISO 4629-2:2016 standards, respectively. ISO 3961:2013 and ASTM D1652-04:2004 testing standards were used for epoxy and iodine value determination, respectively. The moisture content was measured using Karl Fischer titration using the Denver Instrument Model 275 KF automatic titrator (Denver Instrument, Bohemia, NY, USA).

The rheological measurements were made using the Anton Paar Modular Compact Rheometer MCR 92 (Anton Paar, Graz, Austria) with a cone-plate measuring system and a gap of 48 μm. Shear rate ramps were carried out from 1 to 1000 s^{-1}. The measurements were performed at a temperature of 25 °C, which was kept constant by the temperature hood.

The synthesized monomer structure was analyzed by FTIR. The spectra were registered with a Thermo Scientific Nicolet iS50 spectrometer (Thermo Fisher Scientific, Waltham, MA, USA) at a resolution of 4 cm^{-1} (32 scans). The FTIR data were collected using the attenuated total reflectance technique with diamond crystals. A drop of the synthesized components was dripped directly onto the prism and analyzed.

The NMR spectra for the samples were recorded on a Bruker spectrometer (Bruker BioSpin AG, Fällanden, Switzerland) at 500 MHz and 126 MHz for ^{1}H and ^{13}C spectra, respectively.

MALDI-TOF mass spectra were acquired with the UltrafleXtreme TOF–TOF mass spectrometer (Bruker Daltonics, Bremen, Germany) equipped with a 2000 Hz smartbeam-II laser (355 nm) using the positive ion reflectron mode. Panoramic pulsed ion extraction and external calibration were used for molecular weight assignment.

The dried droplet method was used, where the solutions of the sample (10 mg mL^{-1}), matrix 2,5-dihydroxybenzoic (20 mg mL^{-1}) and ionizing agent sodium trifluoroacetate (CF_3COONa; 10 mg mL^{-1}) in N,N-dimethylformamide were mixed in the volume ratio of 4:20:1. The mixture (1 mL) was deposited on the ground steel target.

SEC analyses were carried out in tetrahydrofuran at 25 °C and with a flow rate of 1 mL min^{-1} using a GPC system equipped with a refractive index detector (Shodex, Tokyo, Japan). A set of three PLgel columns with a particle size of 10 μm and pore sizes of 104, 103 and 50 Å, 300 × 7.5 mm (Polymer laboratories, Church Stretton, UK) were used. Polystyrene standards were used for calibration.

3. Results and Discussion

Ion exchange resin, an easily recyclable and reusable catalyst, was applied in the synthesis process as an alternative to commonly used inorganic acid catalysts [32]. Moreover, no solvent was used in the syntheses, nor were excess intermediates obtained, such as tall oil methyl esters. It made the synthesis process "greener" and more straightforward with fewer steps. A schematic overview for the synthesis of tall-oil-based Michael's donor components is shown in Figure 1.

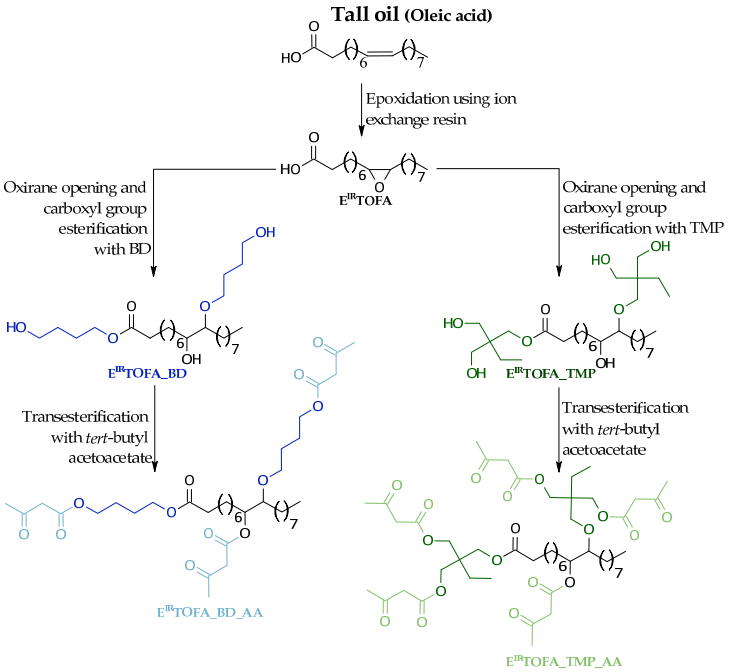

Figure 1. Idealized scheme of TOFA (oleic acid)-based Michael donor development.

3.1. Characteristics of Synthesized Michael Donor Components

Synthesized acetoacetates and intermediates were characterized using different titration methods to determine acid, hydroxyl, epoxy and iodine values. The chemical structure was analyzed using GPC/SEC, FTIR and MALDI-TOF spectra. The viscosity and its dependence on the applied shear rate were also determined. Table 1 lists an overview of the characteristics determined using titrimetric methods and can be used to describe the synthesis process.

For E^{IR}TOFA, the acid value decreased significantly compared to non-epoxidized tall oil. This was mainly because by-products were formed during the epoxidation process by oxirane ring opening with a carboxyl group of fatty acid to form dimers and even trimers. The GPC/SEC graphs and MALDI-TOF spectra confirmed the formation of by-products. The amount of double bonds significantly reduced during epoxidation, which indicated an effective conversion of double bonds into oxirane. The E^{IR}TOFA oxirane value was 2.142 mmol/g. The obtained polyols had a negligible acid value compared to epoxidized oil, which indicated a good yield of the esterification reaction.

Table 1. The acid, hydroxyl, epoxy and iodine values, as well as moisture and acetoacetate group content of: synthesized tall-oil-based polyols and their acetoacetates, and commercial polyols and their acetoacetates.

	Components	Acid Value, mg KOH/g	Hydroxyl Value, mg KOH/g	Iodine Value, g I_2/100 g	Moisture, %	AA Groups, mol/100 g	Conversion of Hydroxyl, mol%
Tall-oil-based	TOFA	195 ± 3	-	157 ± 7	0.50 ± 0.02	-	-
	E^{IR}TOFA	159 ± 2	-	52.4 ± 0.6	0.32 ± 0.01	-	-
	E^{IR}TOFA_BD	5.8 ± 0.2	258 ± 5	-	0.20 ± 0.02	-	-
	E^{IR}TOFA_BD_AA	<5	36.2 ± 0.8	-	0.025 ± 0.005	0.3307	80.5
	E^{IR}TOFA_TMP	6.9 ± 0.4	415 ± 4	-	0.049 ± 0.007	-	-
	E^{IR}TOFA_TMP_AA	<5	41.6 ± 0.3	-	0.037 ± 0.003	0.4562	83.7
Commercial polyols-based	NEO380	<5	371 ± 3	-	0.068 ± 0.002	-	-
	NEO380_AA	<5	40.7 ± 0.6	-	0.048 ± 0.002	0.4242	82.9
	L3300	<5	400 ± 5	-	0.060 ± 0.0012	-	-
	L3300_AA	<5	26.2 ± 0.4	-	0.021 ± 0.003	0.4456	89.5

Two different polyfunctional alcohols were used to introduce hydroxyl groups into the tall oil fatty acid structure and to design E^{IR}TOFA polyols with varied hydroxyl group functionality. Due to different oxirane-opening reagents, the hydroxyl value of the obtained E^{IR}TOFA polyols differed almost twice. The higher hydroxyl value was for a polyol obtained with a trifunctional TMP oxirane-opening reagent. The use of BD as an oxirane-opening reagent yielded a smaller hydroxyl value. Synthesized bio-polyols allow one to obtain bio-based polymers with varied physical properties further.

After acetoacetylation, the hydroxyl number decreased significantly as the hydroxyl groups were replaced with the β-ketoester groups for E^{IR}TOFA-based polyols. The same relationship was observed for commercial polyols, which were selected to compare the synthesis process, the properties of the products and the suitability for the further extraction of polymeric materials. The content of acetoacetate groups was determined by calculations from the amounts of used acetoacetate and polyol.

3.2. Viscosity Analysis of the Michael Donor Components

Viscosity was measured for TOFA, E^{IR}TOFA and E^{IR}TOFA-based polyols and subsequently synthesized acetoacetates and for commercial polyols and their acetoacetates. The results of the rheological measurements are presented in Figure 2.

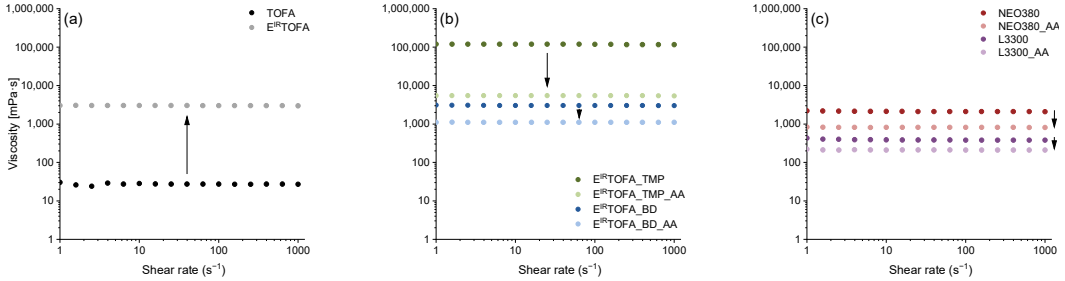

Figure 2. Rheological viscosity versus the shear rate at 25 °C for: (**a**) TOFA and E^{IR}TOFA; (**b**) E^{IR}TOFA-based polyols and their acetoacetates; (**c**) commercial polyols and their acetoacetates.

The viscosity did not depend on the applied shear rate, indicating that the obtained substances were Newtonian fluids. The Newtonian behavior of the developed Michael donors greatly facilitates the use of these acetoacetates in the industry, as the effect of the applied shear rate on the viscosity properties does not have to be taken into account.

The measured viscosities are summarized in Table 2. As can be seen, the viscosity of E^{IR}TOFA was significantly higher than that of TOFA. Firstly, the increased viscosity was caused by the formation of by-products (dimers and oligomers) with increased average molecular weight. Secondly, the opening of the oxirane ring resulted in the formation of hydroxyl groups that led to an intermolecular hydrogen bonding network.

Table 2. The rheological viscosity of synthesized components for tall-oil-based polyols and their acetoacetates, and for commercial polyols and their acetoacetates at a temperature of 25 °C.

Synthesized Components		Viscosity, mPa·s
Tall-oil-based	TOFA	27.0 ± 0.4
	E^{IR}TOFA	3012 ± 2
	E^{IR}TOFA_BD	3017 ± 5
	E^{IR}TOFA_BD_AA	1104 ± 3
	E^{IR}TOFA_TMP	118,400 ± 20
	E^{IR}TOFA_TMP_AA	5466 ± 12
Commercial polyols-based	L3300	382 ± 2
	L3300_AA	211.1 ± 0.8
	NEO380	2109 ± 8
	NEO380_AA	814 ± 3

The most significant increase in viscosity was observed for the E^{IR}TOFA_TMP polyol that was synthesized by opening the oxirane ring and by the esterification of E^{IR}TOFA with TMP. The viscosity of E^{IR}TOFA_TMP was higher than 118,000 mPa·s, which is considered to be relatively high viscosity and makes it difficult to use the product in the industry. E^{IR}TOFA_TMP polyol exhibits such a high viscosity mainly due to increased intermolecular hydrogen bonding. However, after E^{IR}TOFA_TMP polyol was acetoacetylated, the viscosity significantly decreased to 5500 mPa·s. Therefore, the E^{IR}TOFA_TMP_AA is more suitable for industrial use.

Compared to commercial or bio-based polyols, acetoacetates showed a significant decrease in viscosity due to the decrease in hydroxyl groups and hence the disappearance of intermolecular hydrogen bonds [12,22,27,30,31]. This significantly improves the potential use of bio-polyol acetoacetates in the industry. In the adjustment of existing equipment, in pump capacity alteration and in easier transportation through pipelines, they exhibit better flowability compared to neat polyols from the same raw material.

3.3. FTIR Analysis of the Michael Donor Components

FTIR spectra of TOFA, synthesized polyols, commercial polyols and acetoacetylated polyols are shown in Figure 3. The absorption bands of the FTIR spectrum characterize functional groups very well. The course of synthesis and the changes associated with the functional groups of the molecules can be determined.

A new peak appeared at 831 cm^{-1} in the FTIR spectrum after the epoxidation of TOFA, which corresponded to the vibrations of the oxirane ring (Figure 3a). This indicated that the epoxidation in the presence of ion exchange resin Amberlite IR-120 H was successful. Transformations of double bonds were also indicated by the peaks at ~1654 cm^{-1} and ~3009 cm^{-1}, corresponding to C=C stretching vibrations and =C-H stretching vibrations, respectively. The intensities of these peaks for E^{IR}TOFA decreased. The spectrum of E^{IR}TOFA also showed the appearance of a new, relatively weak but noticeable absorbance band between 3600 and 3150 cm^{-1}, which typically characterizes vibrations of the hydroxyl group. This indicated that the opening of the oxirane ring occurred as an undesirable side reaction during the epoxidation process. As seen in

the spectrum, the intensity of the absorption band of the carbonyl group of the acid moiety at ~1705 cm^{-1} decreased mainly due to ester formation, resulting in undesired by-products. Hydroxyl groups and esters were formed from the cleavage of the oxirane ring in the reaction with the carboxyl group of tall oil or acetic acid.

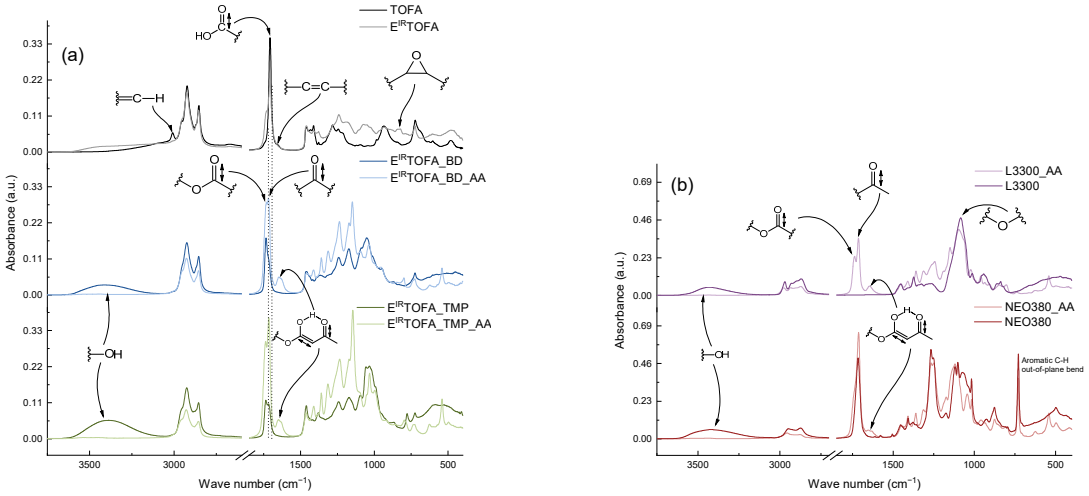

Figure 3. FTIR spectra of TOFA, E^{IR}TOFA, synthesized polyols, commercial polyols and acetoacetylated polyols: (**a**) based on tall oils; (**b**) based on commercial polyols.

The absorption of the hydroxyl group band significantly increased for synthesized polyols. Moreover, this band was more intense for the polyols obtained by the E^{IR}TOFA reaction with TMP alcohol because the TMP polyol contained more hydroxyl functional groups. The spectrum also reflected the disappearance of the oxirane ring absorbance band at ~831 cm^{-1}. A decrease in the intensity of the peaks of the acid group stretching vibration and an increase in the ester carbonyl group at ~1738 cm^{-1} indicated that the esterification reaction was successful.

In the FTIR spectra, the intensity of the hydroxyl group stretching vibration absorbance bands decreased significantly for acetoacetylated polyols. They were nearly imperceptible. This is a very important indicator of a successful acetoacetylation reaction. The spectrum of acetoacetylated polyols showed an increase in the intensity of the carbonyl stretching vibration peak of ester at ~1738 cm^{-1} and ketone at ~1715 cm^{-1}. The appearance of a relatively strong, new absorption band between 1670 and 1580 cm^{-1} was observed. Acetoacetates exhibited keto-enol tautomerism, and the carbonyl group appeared at a lower frequency due to intramolecular hydrogen bonding in the enol form. The same changes in the FTIR spectra were also observed for the acetoacetylated commercial polyols (Figure 3b).

3.4. MALDI-TOF Spectra of the Michael Donor Components

The MALDI-TOF spectra of synthesized polyols and their acetoacetates are shown in Figure 4. The spectra show that a mixture consisting of various compounds was formed in the epoxidation process and in the polyol synthesis and their subsequent acetoacetylation.

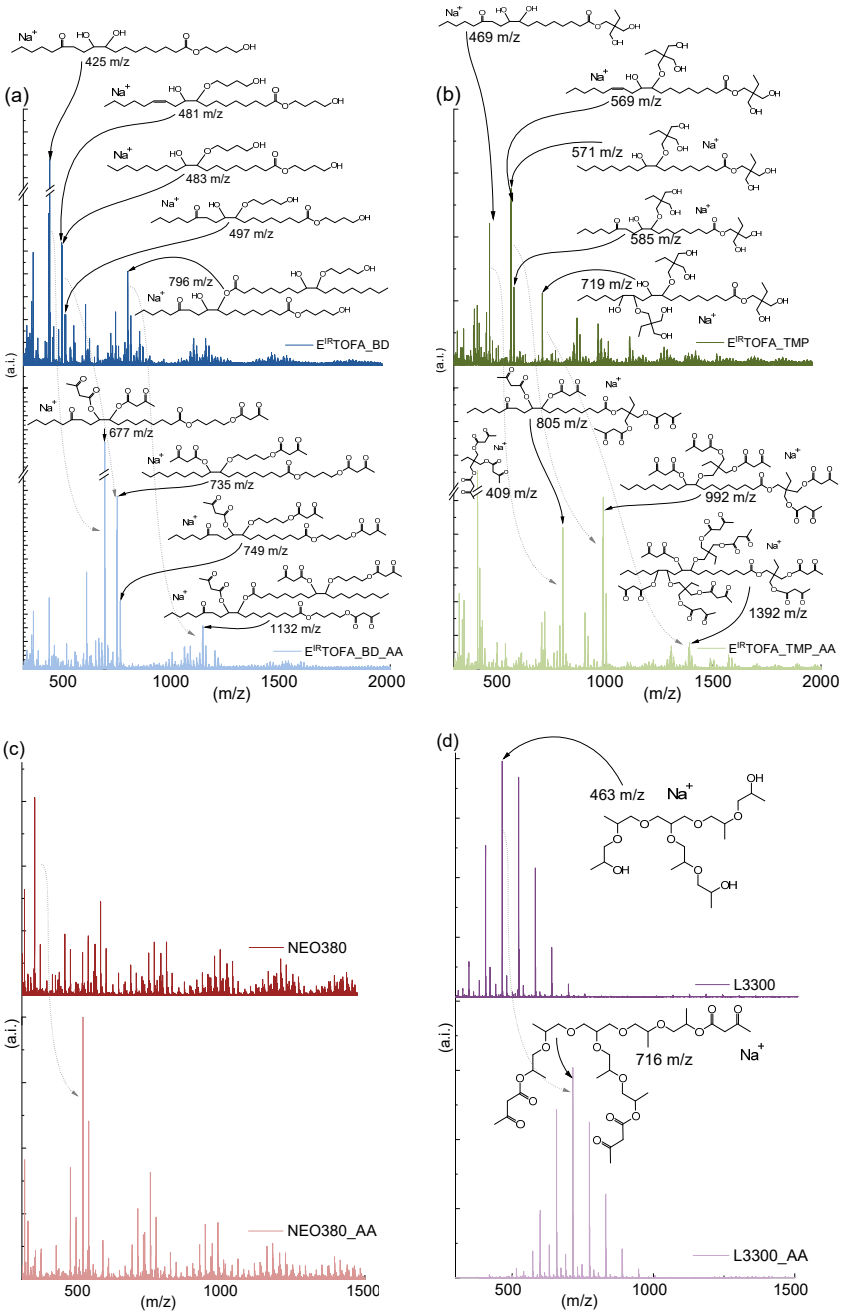

Figure 4. MALDI-TOF spectra of synthesized polyols and acetoacetylated polyols: (**a**) spectra of E^{IR}TOFA_BD and E^{IR}TOFA_BD_AA; (**b**) spectra of E^{IR}TOFA_TMP and E^{IR}TOFA_TMP_AA; (**c**) spectra of NEO380 and NEO380_AA; (**d**) spectra of L3300 and L3300_AA. For more information, see Supplementary Materials Table S1.

The spectrum was also taken for E^{IR}TOFA, but it was difficult to interpret because the peak corresponding to epoxidized oleic and linoleic acids overlaps with the peaks of the matrix. However, the spectrum of E^{IR}TOFA clearly shows that dimers and trimers were formed as by-products in the epoxidation process. The dominant monomers of synthesized polyols and their acetoacetates are clearly visible in the spectrum. Dimers in the case of E^{IR}TOFA_BD polyol and its corresponding acetoacetate were identified in the MALDI-TOF spectrum (see Figure 4a).

The MALDI-TOF spectra show that the acetoacetylation process was successful. After acetoacetylation, the most intense polyol peaks shifted by such units of m/z that correspond to the increase in mass, which corresponds to the replacement of all hydroxyl groups of the molecule with the acetoacetate group. For example, the characteristic peak of epoxidized oleic acid TMP polyol appeared at 571 m/z $[C_{30}H_{60}O_8{}^{+}Na]^{+}$. After acetoacetylation, the peak of this polyol acetoacetate shifted to 991 m/z (Figure 4b). The difference of 420 m/z corresponds exactly to the molar mass of the five acetoacetate groups and fully correlates with synthesized polyol functionality.

As the peaks of dimers, trimers and the other by-products were shifted after acetoacetylation, an acetoacetate group was successfully introduced into the molecules. It can be concluded that these by-products were also fully suitable for producing polymer materials by the Michael reaction. Increased viscosity could adversely affect these dimers, trimers and by-products due to the large and branched structure. For more information on the possible corresponding structures of the intense peaks in the MALDI-TOF spectra (Figure 4), see Supplementary Materials Table S1.

The MALDI-TOF spectra of NEO380 polyol (Figure 4c) show that the most intense peak appeared at 513 m/z after acetoacetylation. The difference (168 m/z) corresponds to two acetoacetate groups, which indicates that this compound was difunctional and contained two hydroxyl groups.

Relatively few peaks appeared in the MALDI-TOF spectrum of L3300 polyol (Figure 4d) and its acetoacetate, compared to bio-polyol acetoacetate and NEO380_AA spectra. L3300 is a trifunctional polyether polyol based on glycerine, and 2-hydroxypropoxy groups are added to the glycerol molecule by oxypropylation in industrial synthesis.

The L3300 is a relatively pure substance, making the spectrum easier to interpret. The most intensive characteristic peaks of the compounds were with an interval of 58 m/z, which corresponds to the molar mass of the 2-hydroxypropoxy group. This spectrum distinctly shows how evenly the oxypropylation had taken place. As shown in the spectrum in Figure 4d, after acetoacetylation, all peaks shifted by 252 m/z, corresponding to the molar mass of the three acetoacetate groups. This number is compatible with the free hydroxyl groups of the molecule.

3.5. GPC/SEC Analysis of the Michael Donor Components

The GPC/SEC chromatograms of the synthesized acetoacetates are shown in Figure 5. According to the chromatogram, the ion exchange resin catalyzed epoxidation process of TOFA produced a significant number of by-products (Figure 5a). The formation of dimers, trimers and other oligomers and oxirane cleavage products are clearly visible in the spectrum. Abolins et al. also identified similar by-product formation in the epoxidation of TOFA [7]. The retention time for the oxirane cleavage products was ~23.5 min, but dimers and trimers were identified at retention times of ~22.6 and ~22.0 min. The chromatogram of polyols showed that the peaks shifted, and their retention times decreased. This indicated an increase in molecular weight.

In the spectrum of E^{IR}TOFA_BD polyol, a new peak appeared at a retention time of ~25.4 min, which characterizes the free unreacted BD. In the case of E^{IR}TOFA_TMP polyol, the free TMP peak appeared at the retention time of ~23.7 min. After acetoacetylation, the molecular weight increased, thus reducing the retention times. It is distinctly visible in the chromatogram. The results of GPC/SEC correlate with the results of the MALDI-TOF analyses.

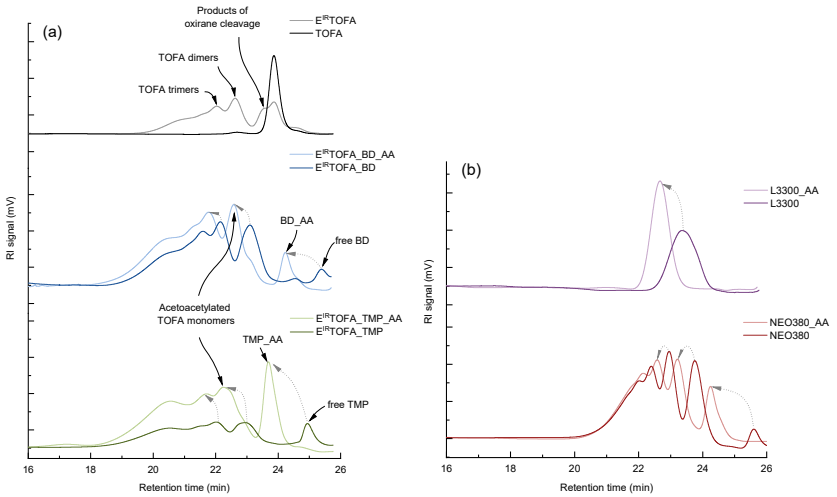

Figure 5. GPC/SEC chromatograms of TOFA, E^{IR}TOFA, synthesized polyols, commercial polyols and their corresponding acetoacetate: (**a**) based on tall oils; (**b**) based on commercial polyols.

Although synthesized E^{IR}TOFA-based polyols consist of a mixture of various derivatives, they contain free hydroxyl groups, which can be converted to β-ketoesters. The obtained substances with many acetoacetate groups are suitable for further use in polymer development.

A significant disadvantage of oligomerization by-products is that they are highly branched with a high molecular weight, resulting in a higher average molecular weight and viscosity. The TOFA epoxidation method can be improved to reduce the formation of oligomerization by-products. However, on the other hand, the obtained bio-based acetoacetates are fully suitable for the production of the polymer material by the Michael reaction. Polymers with higher cross-link densities can be obtained from dimers, trimers and oligomers, and it may be worth exploring their effect on cross-link density in detail.

The commercial polyol NEO380 also consists of a mixture of several components. All peaks of NEO380 shifted after acetoacetylation, and the retention time decreased (Figure 5b), indicating that most of the compounds in this mixture contained an acetoacetate group after acetoacetylation.

There is only one pronounced peak in the L3300 polyol spectrum (Figure 5b). There was a clearly identifiable shift in the spectrum of products, indicating an increase in molecular weight after acetoacetylation.

3.6. NMR Spectra of the Michael Donor Components

^{1}H NMR spectra clearly demonstrate (see Figure 6) the formation of the epoxide moiety (signals at 2.8–3.2 ppm), although partial cleavage of the oxirane moiety occurred (signals at 3.4–4.1 ppm). The above-mentioned results (see Figures 3–5) of the simultaneous cleavage of the oxirane ring and acid-catalyzed esterification were smoothly accompanied by NMR spectra, as well. As a result of the oxirane ring cleavage, the signals (^{1}H-NMR: 2.84–3.14 ppm) raised from epoxide both disappeared when the BD and TMP were used for cleavage. New signals, characteristic of the -O-CH_2- group at 4.0–4.5 ppm, were found (see Figure 7). The formation of the ester bonds with BD and TMP was confirmed by ^{13}C spectra, as well; the signal of the carbonyl group shifted from 180 ppm (for the carboxylic acid) to 174 ppm (for the ester). The polysubstituted derivatives of TMP in small quantities were also observed. The last one was deducted from several small signals at 65.5–63.5 ppm (-CH_2- from TMP moiety) and 43–42 ppm (quaternary carbon from TMP moiety) in the ^{13}C spectrum.

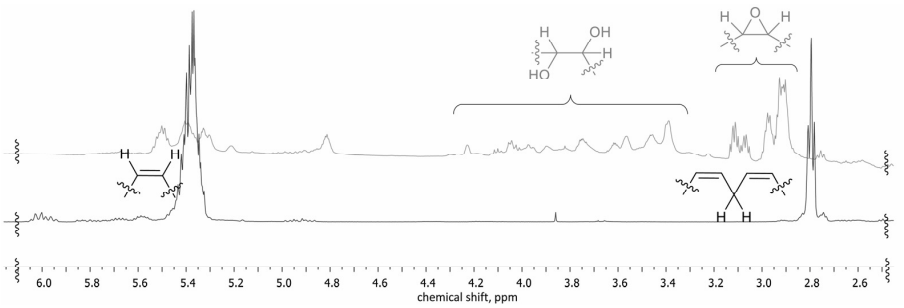

Figure 6. ^{1}H-NMR of TOFA and E^{IR}TOFA (500 MHz, $CDCl_3$).

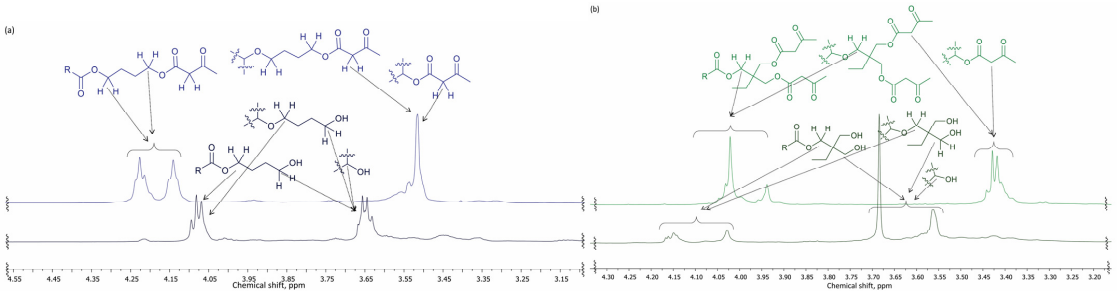

Figure 7. ^{1}H-NMR spectra of: (**a**) E^{IR}TOFA_BD and E^{IR}TOFA_BD_AA (500 MHz, $CDCl_3$); (**b**) E^{IR}TOFA_TMP and E^{IR}TOFA_TMP_AA (500 MHz, $CDCl_3$).

Several changes in the NMR spectra confirmed the successful acetoacetylation of the bio-based polyols and commercial polyols NEO380 and L3300 (see Figure 8). The signal characteristic of the methylene moiety of the acetoacetyl group appeared at 3.4 ppm. Clear signals assigning both the ketone (at 200 ppm) and the acetoacetic acid ester (at 167 ppm) moieties were detected in the ^{13}C spectra.

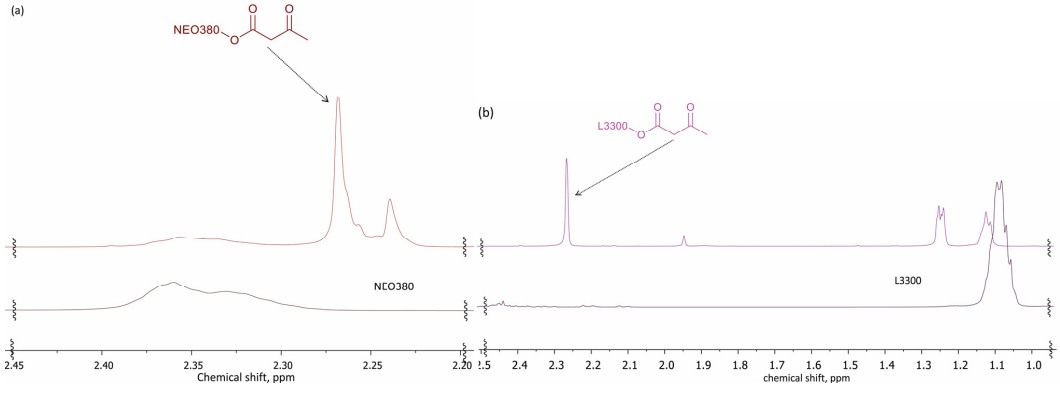

Figure 8. ^{1}H-NMR spectra of: (**a**) NEO380 polyol and NEO380_AA (500 MHz, $CDCl_3$); (**b**) L3300 polyol and L3300_AA (500 MHz, $CDCl_3$).

4. Conclusions

This paper reports the synthesis and characterization of different Michael donor components. For the first time, different tall-oil-based polyols were used to synthesize Michael donors. These donors were synthesized from bio-based polyols that were obtained from epoxidized tall oil fatty acids by oxirane ring-opening and esterification with alcohols and subsequent hydroxyl group acetoacetylation with *tert*-butyl acetoacetate by a transesterification reaction.

The successful synthesis of Michael donors from the cellulose production side stream—tall oil fatty acids—and commercial polyols was confirmed by FTIR, GPC/SEC, MALDI-TOF and NMR data. Moreover, after the polyols were acetoacetylated, the viscosity significantly decreased and made it more suitable for further use. Although synthesized substances are a mixture of various components—different monomers, dimers and other oligomers—they can be used as promising reagents for the synthesis of polymeric materials by the Michael reaction polymerization.

Different chemical structures and functionalities of the synthesized bio-based components can allow for the development of polymer formulations with varied cross-link density. In this study, the investigated tall oil and commercial polyol-based Michael donors can allow for the development of polymer formulations suitable for two-component polymer foams, coatings, resins and composite matrices. The obtained Michael donors were used by Pomilovskis et al. [33] for polymer synthesis.

Supplementary Materials: The following supporting information can be downloaded at: https://www.mdpi.com/article/10.3390/polym14194107/s1, Table S1. For possible structures that correspond to the peaks in the MALDI-TOF spectrum, see Figure 4.

Author Contributions: Conceptualization, M.K.; data curation, R.P., I.M., H.B., O.T. and A.A.; formal analysis, R.P. and A.A.; writing—original draft preparation, R.P. and I.M.; writing—review and editing, R.P., M.K. and A.F.; project administration, A.F.; software, R.P. and I.M.; supervision, M.K.; visualization, R.P. and I.M. All authors have read and agreed to the published version of the manuscript.

Funding: This research was funded by the Latvian Council of Science, project "High bio-based content thermoset polymer foam development from plant origin oils (Bio-Mer)", project No. lzp-2020/1-0385. This publication was supported by the Latvian Academy of Sciences and Czech Academy of Sciences mobility project "Innovative bio-based polyols and advanced methods of their characterization", project No. LZA-22-02. This publication was supported by Riga Technical University's Doctoral Grant program (DOK.OĶTI/21).

Institutional Review Board Statement: Not applicable.

Informed Consent Statement: Not applicable.

Data Availability Statement: The raw data presented in this study are available on request from the corresponding author.

Acknowledgments: A special thank you goes to Latvian State Institute of Wood Chemistry researcher *Mg. chem.* Laima Vevere for her contribution to the publication.

Conflicts of Interest: The authors declare no conflict of interest.

References

1. European Commission the European Green Deal. *Eur. Comm.* **2019**, *53*, 24. [CrossRef]
2. Di Bartolo, A.; Infurna, G.; Dintcheva, N.T. A Review of Bioplastics and Their Adoption in the Circular Economy. *Polymers* **2021**, *13*, 1229. [CrossRef] [PubMed]
3. Zhang, C.; Garrison, T.F.; Madbouly, S.A.; Kessler, M.R. Recent Advances in Vegetable Oil-Based Polymers and Their Composites. *Prog. Polym. Sci.* **2017**, *71*, 91–143. [CrossRef]
4. Kircher, M. Bioeconomy: Markets, Implications and Investment Opportunities. *Economies* **2019**, *7*, 73. [CrossRef]
5. Vevere, L.; Fridrihsone, A.; Kirpluks, M.; Cabulis, U. A Review of Wood Biomass-Based Fatty Acids and Rosin Acids Use in Polymeric Materials. *Polymers* **2020**, *12*, 2706. [CrossRef]
6. Lubguban, A.A.; Ruda, R.J.G.; Aquiatan, R.H.; Paclijan, S.; Magadan, K.O.; Balangao, J.K.B.; Escalera, S.T.; Bayron, R.R.; Debalucos, B.; Lubguban, A.A.; et al. Soy-Based Polyols and Polyurethanes. *Kimika* **2017**, *28*, 1–19. [CrossRef]

7. Abolins, A.; Pomilovskis, R.; Vanags, E.; Mierina, I.; Michalowski, S.; Fridrihsone, A.; Kirpluks, M. Impact of Different Epoxidation Approaches of Tall Oil Fatty Acids on Rigid Polyurethane Foam Thermal Insulation. *Materials* **2021**, *14*, 894. [CrossRef]
8. Zhang, J.; Tang, J.J.; Zhang, J.X. Polyols Prepared from Ring-Opening Epoxidized Soybean Oil by a Castor Oil-Based Fatty Diol. *Int. J. Polym. Sci.* **2015**, *2015*, 1–8. [CrossRef]
9. Kirpluks, M.; Kalnbunde, D.; Walterova, Z.; Cabulis, U. Rapeseed Oil as Feedstock for High Functionality Polyol Synthesis. *J. Renew. Mater.* **2017**, *5*, 258–270. [CrossRef]
10. Siti Munira, Y.; Ahmad Faiza, M.; Rahmah, M. Synthesis and Characterization of Palm Oil Based Polyol. *Adv. Mater. Res.* **2013**, *812*, 275–280. [CrossRef]
11. Furtwengler, P.; Avérous, L. Renewable Polyols for Advanced Polyurethane Foams from Diverse Biomass Resources. *Polym. Chem.* **2018**, *9*, 4258–4287. [CrossRef]
12. Cao, Z.; Gao, F.; Zhao, J.; Wei, X.; Cheng, Q.; Zhong, J.; Lin, C.; Shu, J.; Fu, C.; Shen, L. Bio-Based Coating Materials Derived from Acetoacetylated Soybean Oil and Aromatic Dicarboxaldehydes. *Polymers* **2019**, *11*, 1809. [CrossRef] [PubMed]
13. Kirpluks, M.; Vanags, E.; Abolins, A.; Michalowski, S.; Fridrihsone, A.; Cabulis, U. High Functionality Bio-Polyols from Tall Oil and Rigid Polyurethane Foams Formulated Solely Using Bio-Polyols. *Materials* **2020**, *13*, 1985. [CrossRef] [PubMed]
14. Sardari, A.; Sabbagh Alvani, A.A.; Ghaffarian, S.R. Castor Oil-Derived Water-Based Polyurethane Coatings: Structure Manipulation for Property Enhancement. *Prog. Org. Coatings* **2019**, *133*, 198–205. [CrossRef]
15. Zhang, C.; Madbouly, S.A.; Kessler, M.R. Biobased Polyurethanes Prepared from Different Vegetable Oils. *ACS Appl. Mater. Interfaces* **2015**, *7*, 1226–1233. [CrossRef]
16. Dechent, S.E.; Kleij, A.W.; Luinstra, G.A. Fully Bio-Derived CO2 Polymers for Non-Isocyanate Based Polyurethane Synthesis. *Green Chem.* **2020**, *22*, 969–978. [CrossRef]
17. Sternberg, J.; Pilla, S. Materials for the Biorefinery: High Bio-Content, Shape Memory Kraft Lignin-Derived Non-Isocyanate Polyurethane Foams Using a Non-Toxic Protocol. *Green Chem.* **2020**, *22*, 6922–6935. [CrossRef]
18. Lindsay, C.D.; Timperley, C.M. TRPA1 and Issues Relating to Animal Model Selection for Extrapolating Toxicity Data to Humans. *Hum. Exp. Toxicol.* **2020**, *39*, 14–36. [CrossRef]
19. Kathalewar, M.; Sabnis, A.; D'Mello, D. Isocyanate Free Polyurethanes from New CNSL Based Bis-Cyclic Carbonate and Its Application in Coatings. *Eur. Polym. J.* **2014**, *57*, 99–108. [CrossRef]
20. Kathalewar, M.S.; Joshi, P.B.; Sabnis, A.S.; Malshe, V.C. Non-Isocyanate Polyurethanes: From Chemistry to Applications. *RSC Adv.* **2013**, *3*, 4110–4129. [CrossRef]
21. Gomez-lopez, A.; Elizalde, F.; Sardon, H. Trends in Non-Isocyanate Polyurethane (NIPU) Development. *Chem. Commun.* **2021**, *57*, 12254–12265. [CrossRef]
22. He, X.; Zhong, J.; Cao, Z.; Wang, J.; Gao, F.; Xu, D.; Shen, L. An Exploration of the Knoevenagel Condensation to Create Ambient Curable Coating Materials Based on Acetoacetylated Castor Oil. *Prog. Org. Coatings* **2019**, *129*, 21–25. [CrossRef]
23. Trevino, A.S.; Trumbo, D.L. Acetoacetylated Castor Oil in Coatings Applications. *Prog. Org. Coatings* **2002**, *44*, 49–54. [CrossRef]
24. Xu, D.; Cao, Z.; Wang, T.; Zhong, J.; Zhao, J.; Gao, F.; Luo, X.; Fang, Z.; Cao, J.; Xu, S.; et al. An Ambient-Cured Coating Film Obtained via a Knoevenagel and Michael Addition Reactions Based on Modified Acetoacetylated Castor Oil Prepared by a Thiol-Ene Coupling Reaction. *Prog. Org. Coatings* **2019**, *135*, 510–516. [CrossRef]
25. Zuo, H.; Cao, Z.; Shu, J.; Xu, D.; Zhong, J.; Zhao, J.; Wang, T.; Chen, Y.; Gao, F.; Shen, L. Effect of Structure on the Properties of Ambient-Cured Coating Films Prepared via a Michael Addition Reaction Based on an Acetoacetate-Modified Castor Oil Prepared by Thiol-Ene Coupling. *Prog. Org. Coatings* **2019**, *135*, 27–33. [CrossRef]
26. Zhu, Y.; Gao, F.; Zhong, J.; Shen, L.; Lin, Y. Renewable Castor Oil and DL-Limonene Derived Fully Bio-Based Vinylogous Urethane Vitrimers. *Eur. Polym. J.* **2020**, *135*, 109865. [CrossRef]
27. Wang, T.; Wang, J.; He, X.; Cao, Z.; Xu, D.; Gao, F.; Zhong, J.; Shen, L. An Ambient Curable Coating Material Based on the Michael Addition Reaction of Acetoacetylated Castor Oil and Multifunctional Acrylate. *Coatings* **2019**, *9*, 37. [CrossRef]
28. Krall, E.M.; Serum, E.M.; Sibi, M.P.; Webster, D.C. Catalyst-Free Ligin Valorization by Acetoacetylation. Structural Elucidation by Comparison with Model Compounds. *Green Chem.* **2018**, *20*, 2959–2966. [CrossRef]
29. Witzeman, J.S.; Nottingham, W.D. Transacetoacetylation with Tert-Butyl Acetoacetate: Synthetic Applications. *J. Org. Chem.* **1991**, *56*, 1713–1718. [CrossRef]
30. Lopes, R.D.V.V.; Zamian, J.R.; Resck, I.S.; Sales, M.J.A.; Dos Santos, M.L.; Da Cunha, F.R. Physicochemical and Rheological Properties of Passion Fruit Oil and Its Polyol. *Eur. J. Lipid Sci. Technol.* **2010**, *112*, 1253–1262. [CrossRef]
31. Petroskey, W.T.; Gott, L.; Carter, T.E. Acetoacetylation: A Process for Polyol Viscosity Reduction. *J. Cell. Plast.* **1993**, *29*, 458–459. [CrossRef]
32. Milchert, E.; Malarczyk-Matusiak, K.; Musik, M. Technological Aspects of Vegetable Oils Epoxidation in the Presence of Ion Exchange Resins: A Review. *Polish J. Chem. Technol.* **2016**, *18*, 128–133. [CrossRef]
33. Pomilovskis, R.; Mierina, I.; Fridrihsone, A.; Kirpluks, M. Bio-Based Polymer Developments from Tall Oil Fatty Acids by Exploiting Michael Addition. *Polymers* **2022**, *14*, 4068. [CrossRef]

Table S1. Possible structures that could correspond to the peaks in the MALDI-TOF spectrum (see Figure 4.)

Synthesized component	Peaks, m/z	Theoretically probable structures	Molar mass (X+Na+), g/mol
E^{IR}TOFA_BD	425.33	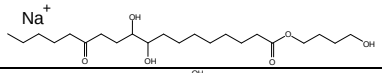	425.55
	481.31	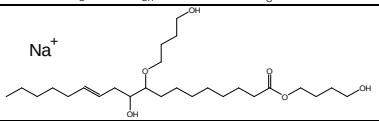	481.66
	483.41	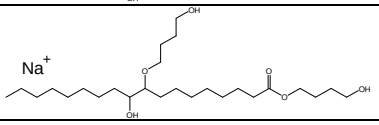	483.68
	497.39	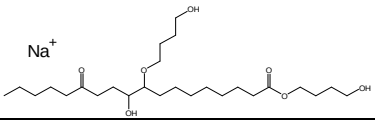	497.66
	795.65	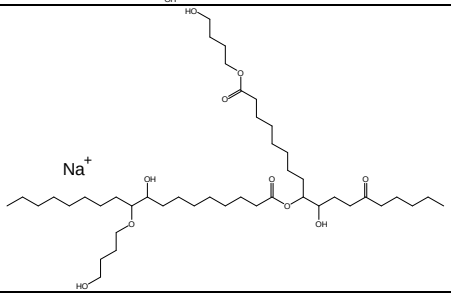	796.12
E^{IR}TOFA_BD_AA	677.39	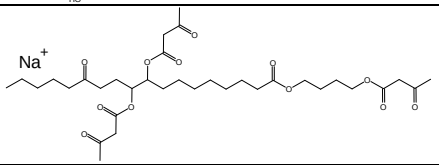	677.77
	733.45	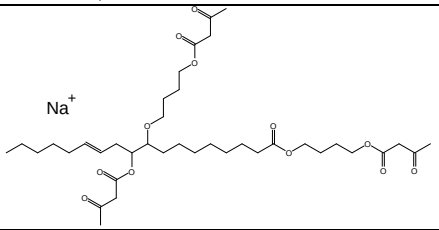	733.88

Synthesized component	Peaks, m/z	Theoretically probable structures	Molar mass (X+Na+), g/mol
	735.47	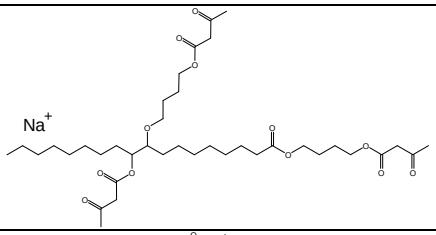	735.90
	749.45	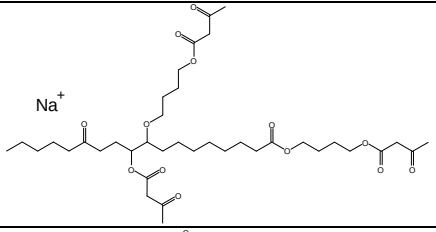	749.88
	1131.74	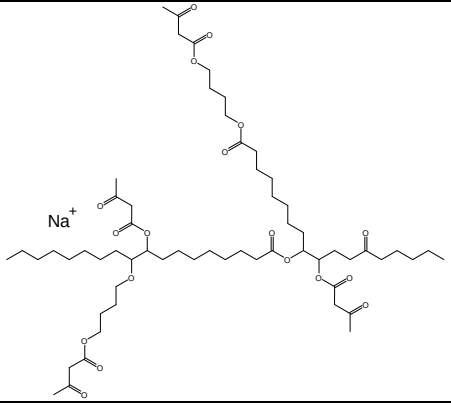	1132.41
E^{IR}TOFA_TMP	455.34	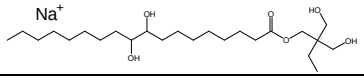	455.62
	469.33	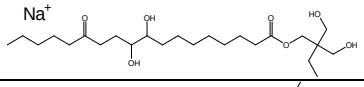	469.61
	569.42	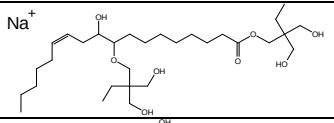	569.77
	571.43	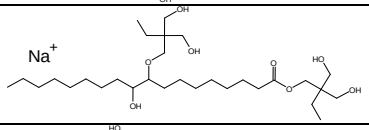	571.78
	585.41	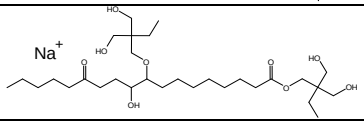	585.77

Synthesized component	Peaks, m/z	Theoretically probable structures	Molar mass (X+Na+), g/mol
	719.51	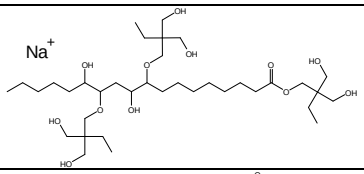	719.94
E^{IR}TOFA_TMP_AA	409.19	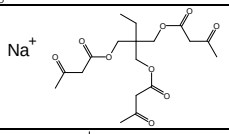	409.38
	804.44	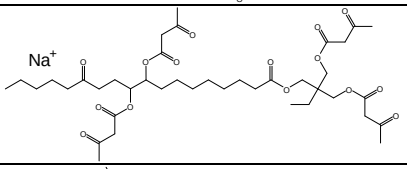	805.90
	989.56	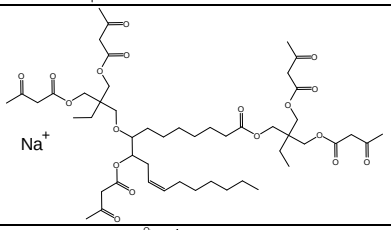	990.13
	991.57	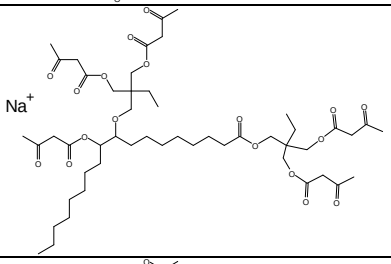	992.15
	1005.55	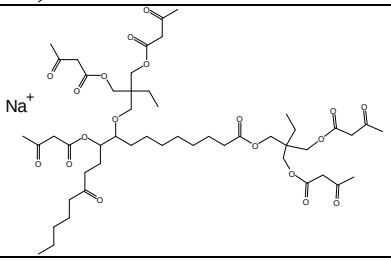	1006.13

Synthesized component	Peaks, m/z	Theoretically probable structures	Molar mass (X+Na+), g/mol
	1391.72	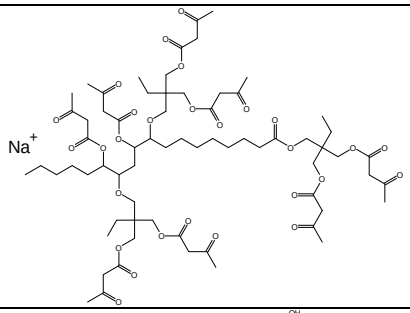	1392.53
L3300	463.31	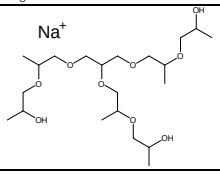	463.56
L3300_AA	715.40	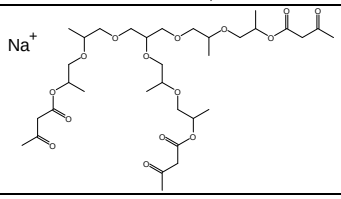	715.78

3

5. pielikums
Appendix 5

Rapeseed oil as feedstock for the polymeric materials *via* Michael addition reaction

Arnis Āboliņš, Dārta Eihe, Ralfs Pomilovskis, Anda Fridrihsone, Miķelis Kirpļuks

Industrial Crops and Products, 2023

Industrial Crops & Products 204 (2023) 117367

Contents lists available at ScienceDirect

Industrial Crops & Products

journal homepage: www.elsevier.com/locate/indcrop

Rapeseed oil as feedstock for the polymeric materials via Michael addition reaction

Arnis Abolins *, Darta Eihe, Ralfs Pomilovskis, Anda Fridrihsone, Mikelis Kirpluks

Polymer Laboratory, Latvian State Institute of Wood Chemistry, Dzerbenes str. 27, Riga, LV-1006, Latvia

ARTICLE INFO

Keywords:
Epoxidation
Rapeseed oil
Bio-polyols
Michael donor

ABSTRACT

Rapeseed oil was used to synthesize a Michael donor to obtain polymeric materials after nucleophilic polymerization via Michael reaction. Four different bio-polyols as precursors for the Michael donor monomer synthesis were synthesized from epoxidized rapeseed oil using an oxirane ring-opening reaction. Various alcohols such as methanol, butane-1,4-diol, 2,2′-oxydi(ethan-1-ol), and 2-ethyl-2-(hydroxymethyl)propane-1,3-diol were used to obtain bio-polyols with different OH group functionality. The transesterification reaction between the synthesised bio-polyol hydroxyl groups and *tert*-butyl acetoacetate ester introduced acetoacetate functional groups into their structure. The acid value, hydroxyl value, viscosity and moisture content of the synthesized polyols and corresponding acetoacetates were analyzed. Size-exclusion chromatography and Fourier transform infrared spectroscopy were used to study the chemical structure of polyols and acetoacetates. From developed acetoacetates and commercially available trimethylolpropane triacrylate, bio-based polymers were obtained via carbon-Michael reaction. The different chemical structures and functionalities of the synthesized bio-based monomers allowed for the development of polymer formulations with diverse cross-linking densities. The structural, physical and thermal properties of the developed polymers were analyzed using solid-state NMR, differential scanning calorimetry, dynamic mechanical analysis and thermal gravimetric analysis testing apparatus.

1. Introduction

A "European Green Deal" was established by the European Commission to address environmental and climate change issues, aiming to achieve climate neutrality which entails reducing net greenhouse gas emissions to zero until 2050. It is a new growth strategy that aims to create a flourishing society with a cutting-edge, resource-efficient, and prosperous economy in the European Union (European Commission, 2019). In the near future the bio-based polymer industry will be incentivized to grow, create new technologies and materials, and improve production levels (Di Bartolo et al., 2021; Zhang et al., 2017). Developing efficient, sustainable, and innovative technologies for creating materials from renewable bio-resources is also crucial for overcoming the polymer sector's challenges (Kircher, 2019).

Traditionally, polyurethanes are made of two components: component A, which consists of polyols, catalysts, surfactants and others, and component B, isocyanate. Fatty acids, diglycerides and triglycerides, which are found in plants, are one of the most suitable sources and have historically and currently been used as raw materials for the production of bio-based materials (Chen et al., 2015; Cifarelli et al., 2021; Liao et al., 2021; Sittinun et al., 2020; Biermann et al., 2011). Since almost all natural oils lack naturally occurring hydroxyl groups in their structure, they must first undergo chemical modification before they can be applied, for example, in manufacturing polyurethanes (Demirbas, 2011). Plant oils can be transformed into polyols through several processes, such as epoxidation and ring opening, transesterification, amidization, hydroformylation, ozonolysis, thiol-ene coupling, and others (Demirbas, 2011). All these modifications have been extensively studied. Polyols have been utilized in several studies as a part of component A to create polyurethanes (Abolins et al., 2021; Cao et al., 2019; Kirpluks et al., 2020; Sardari et al., 2019; Zhang et al., 2017, 2015). However, isocyanates are recognized to be environmentally hazardous and very toxic chemicals (Dechent et al., 2020; Kathalewar et al., 2014, 2013; Lindsay and Timperley, 2020; Sternberg and Pilla, 2020). The use of isocyanates is a significant drawback of polyurethane production and alternative methods of two-component polymer materials have to be investigated.

By utilizing the Michael addition process, which does not use

* Corresponding author.
E-mail address: arnis.abolins@kki.lv (A. Abolins).

https://doi.org/10.1016/j.indcrop.2023.117367
Received 17 March 2023; Received in revised form 17 August 2023; Accepted 20 August 2023
Available online 31 August 2023
0926-6690/© 2023 Elsevier B.V. All rights reserved.

isocyanates, it is possible to produce a polymeric material with properties comparable to polyurethane materials. By exploiting oxa-Michael (Jiang et al., 2020; Nising and Bräse, 2008), thio-Michael (Cespedes et al., 2021; Chatani et al., 2013; Chen et al., 2021; Gunay et al., 2018; Lenardão et al., 2009; Li et al., 2020; Piñeiro-García et al., 2021), aza-Michael (Alaneed et al., 2021; Bhattacharjee et al., 2021; González et al., 2015; Gunay et al., 2018; Mushtaque et al., 2021; Su et al., 2021; Yang et al., 2021) and carbon-Michael (Noordover et al., 2020; Pomilovskis et al., 2022a; Sonnenschein et al., 2016; Williams et al., 2007b) addition reactions a broad variety of polymers with a dendric, linear, graft, cross-linked and hyper branched network can be developed (Mather et al., 2006).

The two-component thermoset polymeric materials can be formed in a reaction between Michael donors (β-ketoesters) and Michael acceptors (mainly alkyl acrylates) in the presence of amine, amidine and guanidine-based catalysts (Cao et al., 2019; Mather et al., 2006; Ozturk and Long, 2009; Pomilovskis et al., 2022b; Sonnenschein et al., 2016; Williams et al., 2007a,b; Xu et al., 2019; Aripo, 2014; Zhaoo et al., 2013). More specifically, the hydroxyl groups of polyols can be converted to β-ketoesters via acetoacetylation to obtain a Michael donor. The field of bio-based polymer development using α,β-unsaturated carbonyl compound has not been broadly examined yet. However, several authors already report that successful acetoacetylation of castor oil and castor oil-based polyols (He et al., 2019; Trevino and Trumbo, 2002; Wang et al., 2019; Xu et al., 2019; Zhu et al., 2020; Zuo et al., 2019) and soybean oil-based polyols (Cao et al., 2019) can be achieved. Transacetoacetylation is most commonly done with *tert*-butyl acetoacetate as it allows the reaction to be carried out under relatively mild conditions of 110–130 °C. It is also attractive from an industrial standpoint due to its stability in storage, affordability, and widespread commercial availability (Cao et al., 2019; He et al., 2019; Krall et al., 2018; Trevino and Trumbo, 2002; Witzeman and Nottingham, 1991; Xu et al., 2019).

In this study, acetoacetates were synthesized from developed RO-based bio-polyols. Bio-polyols were synthesized from RO by catalytical epoxidation using ion exchange resin and subsequent cleavage of the oxirane ring with various functional alcohols. Then the RO-based bio-polyols were subsequently transacetoacetylated. As a result, Michael donors were obtained for further development of the polymer. Different chemical structures and functionalities of the developed bio-based Michael donors allowed the development of polymer with varied cross-linking densities. The following properties of the developed polyols and their acetoacetates were analyzed: acid value, hydroxyl value, viscosity and moisture content. The chemical structure was determined by size exclusion chromatography (SEC) and Fourier transform infrared spectroscopy (FTIR). The developed acetoacetates were used for polymerization reactions with commercially available trimethylolpropane triacrylate to obtain bio-based polymers. The chemical, physical and thermal properties of the developed polymers were studied using solid-state NMR (ssNMR), differential scanning calorimetry (DSC), dynamic mechanical analysis (DMA) and thermal gravimetric analysis (TGA).

2. Experimental

2.1. Materials

RO with an iodine value of 108 I_2 mg/100 g was ordered from Iecavnieks&Co (Iecava, Latvia). Hydrogen peroxide (H_2O_2), purum p.a., 35%; glacial acetic acid (AcOH), puriss, 99.8%; 4-(dimethylamino)pyridine (DMAP), reagent plus, 99%; acetanhydride, puriss, 99%; dichloromethane, puriss p.a., ACS reagent; N,N-dimethylformamide (DMF), ACS reagent, 99.8%, water content 150 ppm; potassium hydroxide, puriss, 85%; potassium iodide, ACS reagent, 99%; tetraethylammonium bromide, reagent grade, 98%; perchloric acid, ACS reagent, 70%; *tert*-butyl acetoacetate reagent grade, 98%; methanol (MeOH) puriss p.a., 99.0% (GC); 1,4-butanediol (BD), reagent plus, ≥ 99%; trimethylolpropane (TMP), reagent grade, 97%; diethylene glycol (DEG) puriss. p.a., 99.0% (GC); trimethylolpropane triacrylate (TMPTA), contains 600 ppm monomethyl ether hydroquinone as inhibitor, technical grade, *tert*-butyl acetoacetate, reagent grade, 98% and 1,1,3,3-tetramethylguanidine (TMG) ACS reagent, 99% were ordered from Sigma-Aldrich (Schnelldorf, Germany). Tetrafluoroboric acid solution, 48 wt % in water, from Alfa Aesar; Amberlite IR-120 H, strongly acidic, hydrogen form and sodium thiosulphate fixanals 0.1 M were ordered from Fluka (Bucharest, Romania).

2.2. RO epoxidation procedure

The mixture of RO (800 g), acetic acid (104 g) and ion exchange resin Amberlite IR-120 H (20 wt% of RO) was heated to 40 °C in a 2 L four-necked round flask which was immersed in a thermostatic water bath. Then 35% hydrogen peroxide (496 g) was added through a dropping funnel dropwise while not letting the temperature exceed 65 °C. After adding the hydrogen peroxide, the temperature was kept at 65 °C for 6 h, and the medium was stirred at 600 rpm. The obtained mixture was washed with warm distilled water (60 °C) and ethyl acetate and dried using a rotatory vacuum evaporator to separate epoxidized RO (ERO). The idealized epoxidation scheme of RO is depicted in (Fig. 1).

2.3. Synthesis of bio-polyols from ERO

Further bio-polyols, which are the precursors for Michael donor monomer synthesis, were synthesized from ERO by opening the oxirane ring with alcohols. For this step, four alcohols of different functionality were used: MeOH, BD, DEG, and TMP. The following acronyms were used for each synthesized bio-polyols: ERO_MeOH, ERO_BD, ERO_DEG, and ERO_TMP.

The synthesis was carried out in a 500 mL four-necked round bottom flask. The flask was immersed in a silicon oil bath and equipped with a mechanical stirrer, a reflux condenser, a thermocouple and a dropping funnel. The mixture of appropriate alcohol and tetrafluoroboric acid solution with a mass of 0.25% of ERO mass as a catalyst was added to epoxidized oil (100 g) via a dropping funnel. The amount of ERO oxirane group to alcohol molar ratio was 1:1. The synthesis temperature was maintained according to the alcohol used (Table 1). The reaction medium was stirred at 500 rpm. The reaction was carried out until the oxirane value dropped to 0 mmol/g. The idealized reaction of ERO-based bio-polyol synthesis is depicted in Fig. 2.

2.4. Acetoacetylation of bio-polyols

An acetoacetylation reaction was used to synthesize Michael donor monomers. Acetoacetylation was performed with *tert*-butyl acetoacetate by a transesterification reaction from the previously obtained bio-polyols ERO_MeOH, ERO_BD, ERO_DEG, and ERO_TMP. ERO bio-polyol (150 g) was charged to a four-neck round bottom flask (500 mL) equipped with a mechanical stirrer, a dropping funnel, a purge gas tube and a Liebig condenser. *Tert*-butyl acetoacetate was added to the flask via a dropping funnel. The amount of bio-polyol hydroxyl groups to *tert*-butyl acetoacetate moles ratio was 1:1. The flask was immersed in a thermostatic water bath, and the temperature was kept constant at about 130 °C throughout the synthesis. *Tert*-butanol released during the reaction was condensed using a Liebig condenser using water as a cooling agent at a temperature of about 25–30 °C since the melting point of *tert*-butanol is 25 °C. If a lower temperature is used for cooling, there is a possibility that *tert*-butanol will crystallize in the condenser. Intense *tert*-butanol release ended after about 2 h. In total, the reaction was performed for 4 h to maximize conversions. The idealized acetoacetylation reaction of ERO-based bio-polyols is depicted in Fig. 3. The following acronyms were used for each synthesized acetoacetate obtained from corresponding bio-polyol: ERO_MeOH_AA, ERO_BD_AA, ERO_DEG_AA, and ERO_TMP_AA.

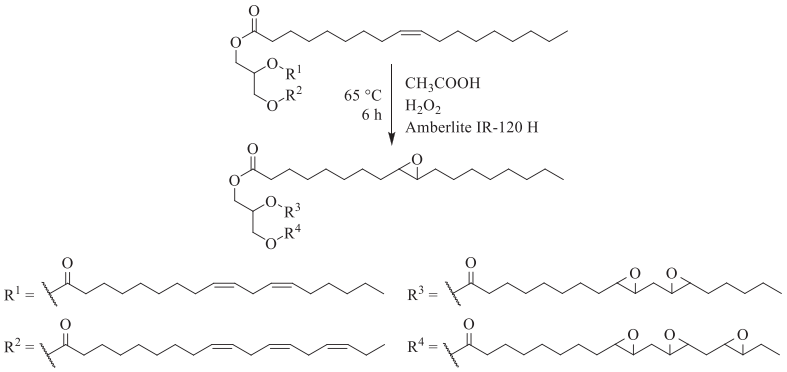

Fig. 1. Epoxidation of RO.

Table 1
The amount of polyfunctional alcohol used and temperature of synthesis.

Different functionality alcohols	Mass of different functionality alcohols for bio-polyol synthesis, g	Temperature, °C
MeOH	11.5	80 ± 5
BD	33.5	130 ± 5
DEG	40.1	180 ± 5
TMP	48.8	200 ± 5

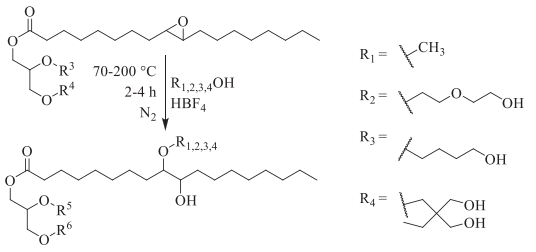

Fig. 2. Synthesis of the bio-polyols using ERO and different multifunctional alcohols.

2.5. Preparation of solid polymer material

Polymer samples were produced by combining the TMPTA, the catalyst TMG, and the synthesized ERO-based acetoacetate. Acetoacetate and acrylic groups had a molar ratio of 1:2. The mass of the catalyst was 1% of the total mass of the mixture. The components were mixed using the Hauschild SpeedMixer DAC 250 SP mixer (Hauschild GmbH & Co. KG, Hamm, Germany). In one batch, 15 g of polymer mass was prepared. The mixture was thoroughly mixed for 15 s before being poured into moulds. Samples were prepared in polypropylene tubes with a diameter of 14 mm. The following acronyms were used for each obtained polymeric material: P_MeOH_AA, P_BD_AA, P_DEG_AA, and P_TMP_AA.

2.6. Characterization methods of the synthesized bio-polyols and Michael donor monomers

The obtained bio-polyols were characterized based on the standards DIN EN ISO 4629–2:2016 (hydroxyl value) and DIN EN ISO 2114:2002–06 (acid value) using TitroLine® 7000 automatic titrator. ISO 3961:2013 and ASTM D1652–04:2004 testing standards were used for epoxy and iodine value determination. Using Karl Fisher titration, the moisture content was measured using the Denver Instrument Model 275KF automatic titrator (Denver Instrument, Bohemia, NY, USA).

FTIR measurements were taken using a Thermo Scientific Nicolet iS50 spectrometer (Thermo Fisher Scientific, Waltham, MA, USA) at a resolution of 4 cm^{-1} (32 scans) to analyze the synthesised monomer

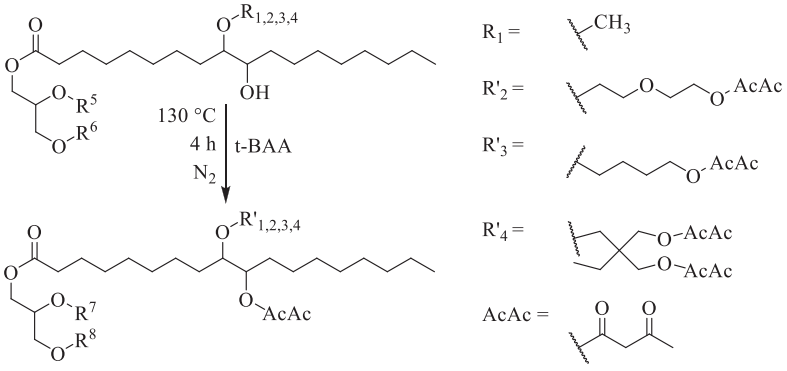

Fig. 3. Acetoacetylation of synthesized ERO_based multifunctional bio-polyols, where *t*-BAA – *tert*-butyl acetoacetate, AcAc – acetoacetate.

structure. The attenuated total reflectance technique with diamond crystals was used to gather the FTIR data.

The rheological tests were performed on an Anton Paar Rheometer MCR 92 (Anton Paar, Graz, Austria). The experiments were carried out by using a cone-plate system with a gap of 48 μm. Shear rate ramps ranging from 1 to 500 s^{-1} were performed. The measurements were carried out at a constant temperature of 25 °C, which was maintained by the temperature hood.

SEC analysis of the samples was conducted with Agilent Infinity 1260 HPLC system (Agilent Technologies, Inc., Santa Clara, CA, USA), equipped with degasser, autosampler, refractive index detector, and MALS (miniDAWN) detector. The refractive index detector was heated to 35 °C, and the flow rate was 1 mL/min. The mobile phase was tetrahydrofuran with a flow rate of 0.6 mL/min. Two analytical columns PLgel Mixed-E (3 uL, 300 7.5 mm) connected in series were used for the analysis.

2.7. Characterization methods of the developed bio-based polymers via Michael's addition

2.7.1. Solid state NMR

The ssNMR ^{1}H–^{13}C CP spectra were acquired in an 18.8 T Bruker Avance III HD spectrometer at 16 kHz MAS using a 3.2 mm H/F X Bruker probe. All spectra were acquired with a relaxation delay of 3.5 s and the number of scans of 4096, leading to a total experimental time of 4 h. The spectra were analyzed and plotted using Topspin 3.6.5 program.

2.7.2. DSC

The DSC data was acquired with the Metler Toledo DSC 823^{e} (Mettler Toledo, Switzerland) using STAR^{e} software ver. 9.00. The glass transition temperature T_g was determined by software as the midpoint temperature, corresponding to half of the heat flow difference between the extrapolated onset and the extrapolated end temperature (half-step method). Cuts from the polymer sample ranged in weight from 0.2 to 2.0 mg. With an accuracy of 0.15 mg, a total of 5 mg of the sample was put into an aluminium sample pan. Aluminum DSC pan coverings were crimped using a Mettler Toledo sealing press for crucibles. There were two cycles for the test. The first cycle began with a temperature of 25 °C, heated to 180 °C, and then cooled to − 50 °C. The temperature was raised to 180 °C in the second heating cycle and dropped to 25 °C in the second cooling cycle. A heating rate of 10 °C/min was used.

2.7.3. DMA

Mettler Toledo DMA/SDTA861^{e} was used for DMA (Mettler Toledo, Switzerland). The ramp rate was 3 °C/min, the amplitude 30 μm, the frequency 1 Hz, the maximum force 5 N, and the temperature range was − 100–180 °C. The oscillation compression mode was employed. For DMA experiments, 13 mm in diameter by 7 mm in height polymer monolith samples with an accuracy of 0.2 mm were tested.

Using the data from the DMA test and Eq. 1, the cross-linking density was determined:

$$\nu_e = \frac{E'_{rubbery}}{3RT} \quad (1)$$

where ν_e is the cross-linking density (mol/cm^3), T is the temperature corresponding to the storage modulus value into the rubbery plateau (K), R is the gas constant (8.314 m^3·Pa/(K·mol)), and $E'_{rubbery}$ is the compression storage modulus (MPa) at temperature $T_{g(DMA)}$ + 50 °C (Hill, 1997; Jena and Raju, 2008; Kim et al., 2019; Zhang et al., 2015).

The molecular weight between cross-links M_c (g/mol) was determined using Eq. 2 given the (Barszczewska-Rybarek et al., 2017):

$$M_c = \frac{3RT\rho}{E'_{rubbery}} \quad (2)$$

where ρ is the density of the polymer (g/cm^3).

2.7.4. TGA

The Discovery TGA device was used to perform thermogravimetric measurements (TA instruments, the USA). A 10 mg sample consisting of comparable-sized fragments was deposited into a platinum scale sample pan with a 0.5 mg precision. The sample was then heated between 30 °C and 700 °C at a rate of 10 °C/min in a nitrogen atmosphere.

3. Results and discussion

3.1. Characteristics of precursors and Michael donor monomers

After the epoxidation of RO, approximately 95% of the relative conversion from double bonds to oxirane was achieved. That gave 0.38 ± 0.01 mol/100 g of oxirane groups. In Table 2, an overview of synthesized RO-based bio-polyols and acetoacetates and their characteristics using different titration methods, such as the determination of acid and hydroxyl value as well as apparent viscosity at the shear rate 50 s^{-1} is presented. Because RO is a triglyceride with no free fatty acids, the acid value for all synthesized products was as expected - very low (below <5 mg KOH/g). Four different functional alcohols were chosen to introduce hydroxyl groups to the ERO structure and synthesize bio-polyols with various hydroxyl values. Due to different oxirane opening reagents, the hydroxyl value of the obtained ERO bio-polyols differed more than three times. The bio-polyol with the highest hydroxyl value (380 ± 10 mg KOH/g) was synthesized using a trifunctional TMP reagent, while the bio-polyol with the lowest hydroxyl value (120 ± 10 mg KOH/g) was obtained using MeOH as oxirane opening reagent.

After the acetoacetylation of ERO-based polyols, the synthesized acetoacetates will be used to obtain polymers and their physical and thermal characteristics were investigated.

3.2. Viscosity analysis of precursors and Michael monomer products

Viscosity was measured for ERO-based polyols and subsequently synthesized acetoacetates. The results of rheological measurements are presented in Fig. 4. The viscosity depended on the applied shear rate for all synthesized polyols and corresponding acetoacetates. All samples were non-Newtonian liquids and demonstrated pseudoplastic flow behaviour i.e. as the shear rate increased, the viscosity decreased. For ERO_DEG and ERO_TMP polyols and their corresponding acetoacetates, the viscosity greatly depended on the applied shear rate. However, polyols synthesized from MeOH and BD showed a more gradual decrease in viscosity as the shear rate increased. The viscosity decreased from 7500 to 7077 mPa·s for bio-polyol ERO_MeOH and from 7320 to 5900 mPa·s for acetoacetate ERO_MeOH_AA depending on the applied shear rate. As for bio-polyol ERO_BD, the viscosity decreased from 35500 to 31400 mPa·s and from 5300 to 4900 mPa·s for ERO_BD_AA. It was also observed that higher viscosity was for bio-polyols that also had higher hydroxyl values. This correlation could be explained due to the increased intermolecular hydrogen bonding (Cao et al., 2019). As can be

Table 2
Characteristics of obtained bio-polyols and corresponding acetoacetates.

Polyol and corresponding acetoacetate	Acid value, mg KOH/g	Hydroxyl value, mg KOH/g	Apparent viscosity, mPa·s (ẏ=50 s^{-1})
ERO_MeOH	< 5	120 ± 10	7425
ERO_MeOH_AA	< 5	25 ± 5	6300
ERO_BD	< 5	305 ± 5	34900
ERO_BD_AA	< 5	50 ± 5	5265
ERO_DEG	< 5	275 ± 5	22960
ERO_DEG_AA	< 5	50 ± 5	3780
ERO_TMP	< 5	380 ± 10	415000
ERO_TMP_AA	< 5	60 ± 5	25185

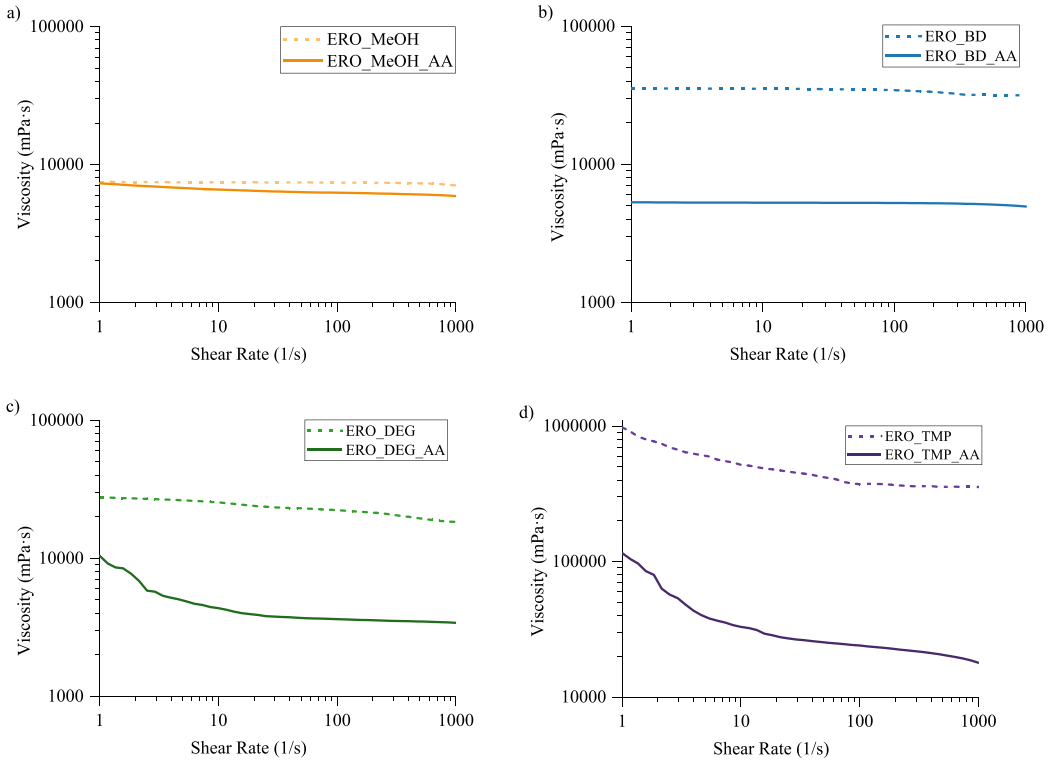

Fig. 4. Measured viscosities of synthesised bio-polyols using a) MeOH; b) BD; c) DEG and d) TMP as alcohols and their corresponding acetoacetates.

seen, after polyols were acetoacetylated, the viscosity showed a significant decrease. A number of authors have also observed that after acetoacetylation, viscosity decreased, which is due to the disappearance of hydroxyl groups that leads to an intermolecular hydrogen bond decrease (Cao et al., 2019; He et al., 2019; Lopes et al., 2010; Wang et al., 2019). The reduction of viscosity is relevant for further industrial applications of the developed material as it allows the use of simpler design pumps and higher efficiency of polymer component mixing.

3.3. FTIR analysis of precursors and Michael monomer products

Fig. 5 illustrates the FTIR spectra of ERO-based polyols and acetoacetylated polyols. Functional groups can be very well characterized by the FTIR spectra absorption bands. For all synthesized bio-polyols using ERO, typical symmetric and asymmetric stretching peaks of the $–CH_2–$ group were observed at ~2923 and 2853 cm^{-1}. Furthermore, all four bio-polyols demonstrated the carbonyl ester group C═O stretching vibration at ~1742 cm^{-1}. For all synthesized bio-polyols, a broad absorption peak was identified between 3600 and 3100 cm^{-1} as characteristic stretching vibrations of the -OH group. For synthesized bio-polyols, the -OH band absorption increased according to the different functionality of alcohols. The more functional alcohol was used, the more intense the hydroxyl group absorption peak was observed. Also, the intensity of peak between 3600 and 3100 cm^{-1} of synthesised bio-polyols correlated with the increase in hydroxyl value obtained from the titrimetric analysis of the polyols presented in Table 2.

For ERO-based polyol acetoacetates, the intensity of the hydroxyl group stretching vibration absorbance bands considerably decreased. As can be seen in FTIR spectra, they are almost undetectable. This is key evidence of a successful acetoacetylation process. The carbonyl stretching vibration peak of the ester at 1736 cm^{-1} and the ketone at 1715 cm^{-1} both showed an increase in intensity in the spectra of acetoacetylated polyols. Additionally, the decrease of the peak intensity of synthesized acetoacetylated bio-polyols in the range between 3600 and 3100 cm^{-1} correlated with the decrease in hydroxyl value detected by the titrimetric measurement of the polyols shown in Table 2. A significant absorption band for acetoacetates occurred from 1670 to 1580 cm^{-1}.

3.4. SEC analysis of precursors and Michael monomer products

The SEC chromatograms of the synthesized polyols and acetoacetates are shown in Fig. 6. It can be observed, that after oxirane group cleavage of ERO with different alcohols, the synthesized polyols formed monomers, dimers, trimers and oligomers and were visible in the spectrum. After the acetoacetylation reaction of polyols, the chromatograms showed that the peaks had shifted and retention times had decreased, thus indicating an increase in the molecular weight. From chromatograms in Fig. 6, the free unreacted alcohol peak was observed in the spectrum of polyols after ~16 min. After acetoacetylation, the corresponding product had reduced retention time, indicating that leftover alcohol has reacted with *tert*-butyl acetoacetate. Although the synthesized bio-polyols consist of a mixture of highly branched derivatives in the form of monomers, dimers, trimers and oligomers, they contain free hydroxyl groups, which can be converted to β-ketoesters. Furthermore, the products obtained after acetoacetylation have acetoacetate groups suitable for further use in polymeric material development.

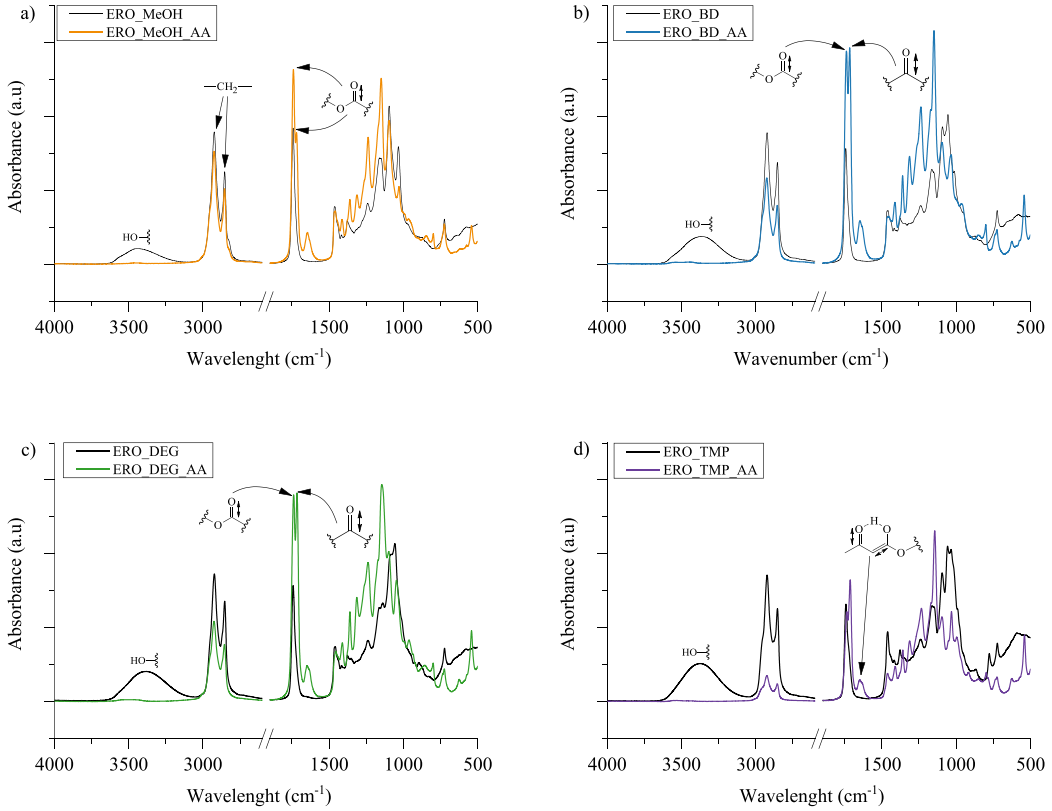

Fig. 5. FTIR spectra of synthesised bio-polyols and corresponding acetoacetates using a) MeOH; b) BD; c) DEG and d) TMP as alcohols.

Four different synthesized ERO-based acetoacetates and TMPTA acrylate were used to prepare thermoset polymer via Michael's addition reaction. The different functionality of the prepared ERO-based acetoacetates allows to tailor the crosslinking density and physical-mechanical properties of the developed polymer material. The reaction occurred at room temperature and was highly exothermic, which is convenient as it would allow for an easier upscale of the technology. The proposed polymer material synthesis technology could be an alternative to epoxy resin or polyurethane material production as these materials also are produced by mixing two components.

3.5. Solid-state NMR analysis of developed polymers

The ssNMR spectra of all significant ^{13}C chemical shifts of the developed polymer monoliths are depicted in Fig. 7. The chemical shift corresponding to methyl group ^{13}C of obtained polymer appeared at 8.4–8.9 and 15.3–15.6 ppm. The anticipated signal of ^{13}C corresponding to -C(=O)-CH_3 was present in the range of 24.1–24.3 ppm, which in this case can be associated with the Michael donor compound as a part of the acetoacetate group. It can be seen that there were several overlapping signals from 24.4 ppm to 42.7 ppm, which represent secondary and tertiary carbons of -CH_2-; >CH-; -O-CH_2- groups, respectively. Additionally, the >CH- group is crucial for the identification of polymerization, which occurs when one acetoacetate group and one acrylic group have reacted. Analysis of the ssNMR spectra for each of the obtained polymers revealed ^{13}C signals with a chemical shift from 51.1 to 84.4 ppm. This range corresponds to the distinctive signal of ^{13}C in the >CH-O- group, which is formed when the oxirane ring breaks down when synthesizing polyols. Additionally, the signal of the ^{13}C corresponding quaternary carbon (>C<) is in this same range, indicating the Michael addition reaction between the acrylic groups and the acetoacetate methylene group. The chemical shift corresponding to carbonyl ester group ^{13}C of obtained polymer appeared at 173.3–173.6 ppm. This ^{13}C signal intensified as the hydroxyl value rose because the acetoacetate groups reacted with hydroxyl group moieties. As a result, more carbonyl ester groups were acquired. Similarly, the chemical shift of ^{13}C at range 203.9–204.6 ppm can be described as carbonyl keto group carbon which increased with hydroxyl value as more acetoacetate groups were introduced into the molecule.

The more interesting ^{13}C signal was at 131.5 ppm and 130.5 ppm for developed polymers P_BD_AA and P_TMP_AA polymers, respectively. This ^{13}C chemical shift corresponds to double bonds in the material. As can be seen in P_MeOH_AA and P_DEG_AA polymer materials spectra, this signal is absent. However, the slight intensity of the double bond signal was noticeable for P_BD_AA and P_TMP_AA polymers. When evaluating ssNMR results, it must be taken into account that the chemical shift of ^{13}C double bonds from fatty acid chains and double bonds in acrylate can overlap. However, the conversion of double bonds to oxirane was almost 95% (Section 3.1) so we ruled out the probability that fatty acid chain double bonds give some visible signal in ssNMR spectra, and we presume that chemical shifts at 131.5 ppm and 130.5 ppm for P_BD_AA and P_TMP_AA polymers present only double bonds of unreacted TMP triacrylate. The idealized polymeric material structure after the reaction of Michael donor (ERO_MeOH_AA;

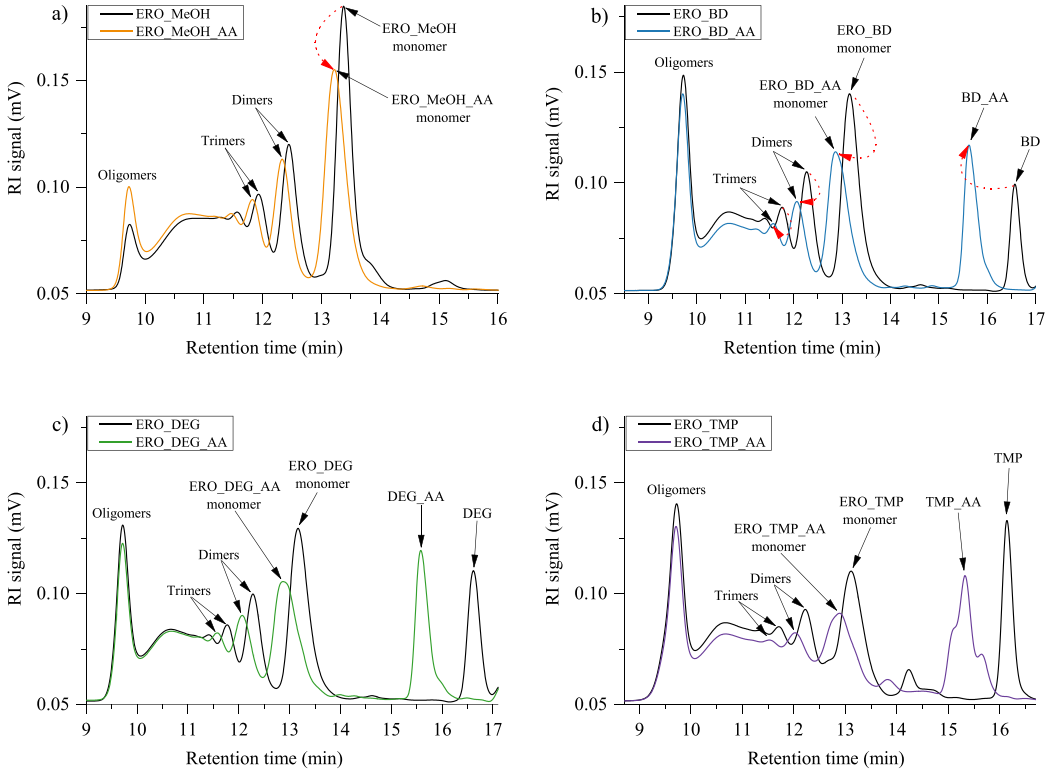

Fig. 6. SEC spectra of synthesised bio-polyols using a) MeOH; b) BD; c) DEG and d) TMP as alcohols and their corresponding acetoacetates.

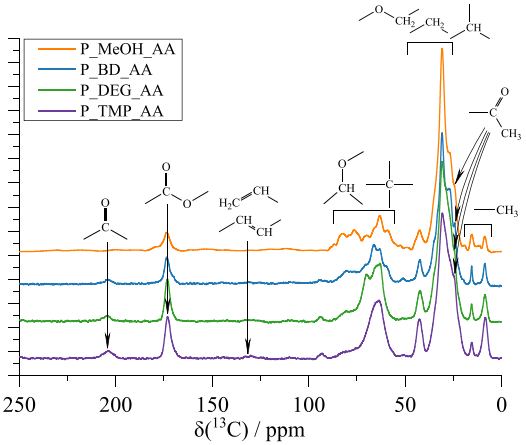

Fig. 7. ssNMR spectra of developed polymer monoliths synthesized from bio-polyol acetoacetates and TMPTA.

ERO_BD_AA; ERO_DEG_AA and ERO_TMP_AA) with Michael acceptor (TMPTA) is depicted in Fig. 8.

3.6. DSC analysis of developed polymers

DSC heating curves are displayed in Fig. 9. The DSC curves of new polymeric materials showed a stepwise change in heat capacity. The glass transition temperature T_g was determined as the midpoint temperature, corresponding to half of the heat flow difference between the extrapolated onset and the extrapolated end temperature. For polymeric materials, the glass transition temperature ranged from − 11.0–56.7 °C (Fig. 9). The glass transition temperature increased for the developed polymers as follows: P_MeOH_AA < P_BD_AA < P_DEG_AA with the highest for P_TMP_AA polymer. It was observed that the increase of alcohol functionality, thus obtaining different polyfunctional-based polyols used for polymer formulation, had a noticeable effect on the glass transition temperature. Higher crosslinking density of the polymer matrix (Table 4) was achieved when higher functionality alcohol was employed to create polymers, which correspondingly had higher glass transition temperatures. The presented results show that the developed polymer material can be tailored to suit the needs of the application. It is possible to obtain glassy polymer and polymer which is in a rubbery state at room temperature. Thus the proposed bio-based polymer can be applied as the resin for composite production where glassy polymers are required and also the bio-based feedstock can be used for elastomer development. Such flexibility of the material properties can be found in polyurethanes which have exceptionally broad applications.

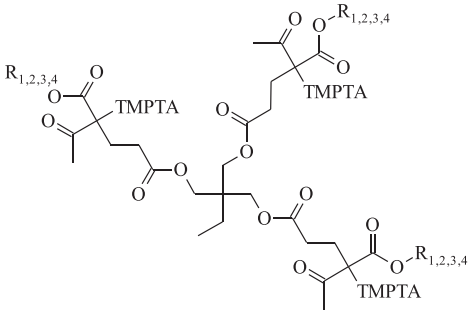

R_1 - ERO_MeOH_AA; R_2 - ERO_BD_AA; R_3 - ERO_DEG_AA and R_4 - ERO_TMP_AA moiety;
TMPTA - trimethylolpropane triacrylate

Fig. 8. The idealized polymeric material structure after the carbon-carbon Michael reaction.

Table 3
The ssNMR ^{13}C chemical shifts of developed polymer monoliths synthesized from bio-polyol acetoacetates.

Functional groups and moieties	Polymeric material			
	P_MeOH_AA	P_BD_AA	P_DEG_AA	P_TMP_AA
	^{13}C Chemical shifts/ppm			
$-CH_3$	8.9, 15.6	8.5, 15.5	8.6, 15.6	8.4, 15.3
$-C(=O)CH_3$	24.3	24.1	24.3	24.2
$-CH_2$-;>CH-;-O-CH_2-	26.4–42.4	26.5–42.2	24.4–42.3	25.9–42.7
>C< ; >CH-O-	58.8–84.4	51.2–80.5	51.1–80.6	56.5–83.0
CH_2 =CH-/-CH=CH-	-	131.5	-	130.5
-C(=O)-O-	173.6	173.6	173.3	173.3
>C=O	-	204.1	204.6	203.9

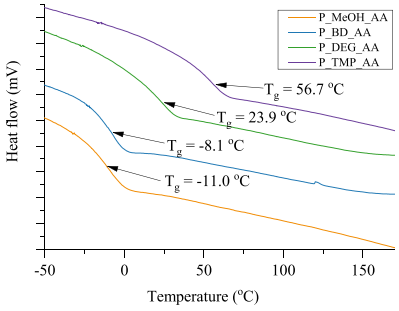

Fig. 9. DSC curves of developed polymer monoliths synthesized from bio-polyol acetoacetates and TMPTA.

3.7. DMA analysis of developed polymers

The dynamic mechanical characteristics of polymer materials were examined using the DMA (Fig. 10). Some researchers have discussed the connection between peak width, structure and symmetry, and uniformity of the structure (Chen et al., 2010; Dave and Patel, 2017; Hassan et al., 2016; Sonnenschein et al., 2016). As there was only one very narrow symmetrical peak with a distinct maximum, as shown in Fig. 10, the tan(δ) data indicated a good degree of homogeneity in the cross-linked network in all polymer samples.

Table 4 lists the glass transition temperatures as determined by the DMA technique. The materials glass transition temperatures determined by DSC analysis (Fig. 9) were compared to those obtained with DMA.

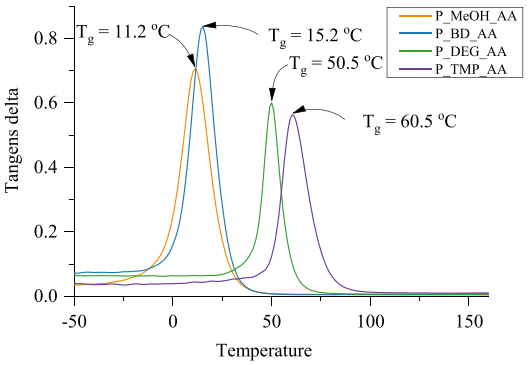

Fig. 10. DMA curves of developed polymer monoliths synthesized from bio-polyol acetoacetates and TMPTA.

Table 4
Glass transition temperatures (T_g), storage modulus value at T_g + 50 °C in rubbery plateau (E'rubbery), density (ρ), cross-link density (νe) and molecular weight between cross-links (Mc) from DMA tests of polymer monoliths from bio-polyol-based acetoacetates and TMPTA.

Sample	T_g, °C	Max. Tanδ	$E'_{rubbery}$, MPa	ρ, g/cm^3	ν_e, 10^{-3} moles/cm^3	M_c, g/mol
P_MeOH_AA	11.2	0.7035	8.98	1.0796	1.0768	1003
P_BD_AA	15.2	0.8374	9.95	1.1375	1.1790	965
P_DEG_AA	50.5	0.6009	22.7	1.1704	2.4357	481
P_TMP_AA	60.5	0.5636	26.7	1.1727	2.7902	420

Even though the glass transition temperatures varied, the same patterns between the temperatures gathered by DSC or DMA analysis were seen. DMA-derived glass transition temperatures were greater than those derived from DSC data because the two different techniques measure different effects, one is the change of the mechanical properties and the other is a thermal effect. It is known that the DMA approach can detect the glass transition temperature more accurately than the DSC method. DMA is advantageous for cross-linked and polymers with difficult-to-find glass transition temperatures (Gracia-Fernández et al., 2010; Hagen et al., 1994). For more information about DMA storage modulus and loss modulus see Supplementary Materials Fig. S1 and S2.

From the collected DMA data (Table 4), cross-link density and

molecular weight between cross-links were determined. The results demonstrated that the cross-link density and molecular weight between cross-links of the polymer matrix were significantly impacted by the functionality of the synthesized bio-polyols and, therefore, corresponding acetoacetate. When more highly functionalized Michael monomers were used, the crosslinking density of the resulting polymer was higher, and the molecular weight between cross-links was lower. This greatly affected the polymer's mechanical properties. Polymer from ERO_TMP_AA with TMPTA had the lowest molecular weight between cross-links (420 g/mol) and the maximum cross-link density ($2.7903 \cdot 10^{-3}$ moles/cm^3). Contrarily, the highest molecular weight between cross-links (1003 g/mol) and minimum cross-link density $1.0768 \cdot 10^{-3}$ moles/cm^3 was achieved using ERO_MeOH_AA as Michael donor.

3.8. TGA analysis of developed polymers

TGA curves for polymers prepared from different functionality bio-polyol acetoacetates and commercially available TMPTA are displayed in Fig. 11. All polymers made from ERO polyol acetoacetates except for P_BD_AA were thermally stable, and no noticeable weight loss was seen for up to about 300 °C. This can be beneficial because traditional polyurethane materials without particular thermal stabilizer additives degrade in the 200–300 °C range (Shufen et al., 2006), and organic–glass poly(methyl methacrylate) decomposition temperature is also lower than 300 °C (Rajkumar et al., 2020; Shufen et al., 2006; Zhang et al., 2009).

The temperature data for the following mass losses at which 5% ($T_{d5\%}$), 10% ($T_{d10\%}$), 25% ($T_{d25\%}$), and 50% ($T_{d50\%}$) were analysed are reported in Table 5. The first polymer material that lost 5% of the mass was developed using Michael donor ERO_BD_AA and TMPTA. The temperature at which 5% mass loss occurred was 275 °C. For all other polymers, the temperature at which 5% mass loss occurred was around 320 °C. It can be noticed that the polymer developed from ERO_BD_AA sooner reached temperatures corresponding to each decomposition weight loss, however, the main temperature range of the thermal degradation process of P_BD_AA was similar to other materials and exceeded 300 °C. Also, from TGA decomposition curves it can be seen that the degradation of polymers from Michael donors, ERO_DEG_AA and ERO_TMP_AA, are practically similar with only a few degree differences at $T_{d5\%}$ and $T_{d10\%}$. The highest char residue was left after decomposition from the ERO_DEG_AA polymer. Overall, the TGA decomposition curves are quite similar, as TMPTA was the only curing agent to obtain polymers. For future studies, the impact of different functionality acrylates on the TGA decomposition curves could be studied.

Table 5
Weight loss dependence on temperature of developed polymers from bio-polyol acetoacetates and commercial acrylate – TMPTA.

Sample	$T_{d5\%}$, °C	$T_{d10\%}$, °C	$T_{d25\%}$, °C	$T_{d50\%}$, °C	Residue, %
P_MeOH_AA	320.1	346.7	374.9	397.3	1.28
P_BD_AA	275.1	333.0	366.2	390.7	2.14
P_DEG_AA	319.7	348.8	377.7	402.4	4.08
P_TMP_AA	323.9	351.6	378.4	403.0	3.77

4. Conclusions

The synthesis and characterization of four Michael donor monomers developed from epoxidized rapeseed oils polyols were presented. The Michael donor monomers were synthesized with *tert*-butyl acetoacetate via a transesterification reaction of hydroxyl groups from previously obtained bio-based polyols from epoxidized rapeseed oil. Synthesized polyols were mixtures of various monomers, dimers, trimers, as well as a significant amount of oligomers which contributed to the increased viscosity. However, after the bio-polyols were acetoacetylated, the viscosity significantly decreased, making them more suitable for further material development. The use of different alcohols, hence various functionalities and chemical structures of the synthesized bio-based products, allowed the development of polymers with varied cross-linking densities.

Solid polymer monoliths were developed from Michael donor monomers, bio-polyol acetoacetates, and a commercially available acrylate. The structure and thermal properties of obtained bio-based polymer monoliths were determined. The glass transition temperatures of obtained polymers ranged from – 11.0–56.7 °C determined by DSC analysis and from 11.2° to 60.5°C when determined by DMA analysis. When a bio-based polyol with a higher OH group functionality was used as a precursor for Michael donor development, the storage modulus value of the resulting polymer monolith increased. The thermal stability of the developed polymers was up to 300 °C. When more highly functionalized monomers were utilized, the crosslinking density of the resulting polymer was higher, and the molecular weight between cross-link points was lower. The presented results show that it is possible to tailor the properties of the developed polymers by changing the cross-linking density of the polymer matrix. It was possible to obtain polymers that exhibit elastomer behaviour and that are rigid glassy materials. The varied physical-mechanical properties of the developed polymers open a broad range of their application.

CRediT authorship contribution statement

Arnis Abolins: Data curation, Formal analysis, Writing – original

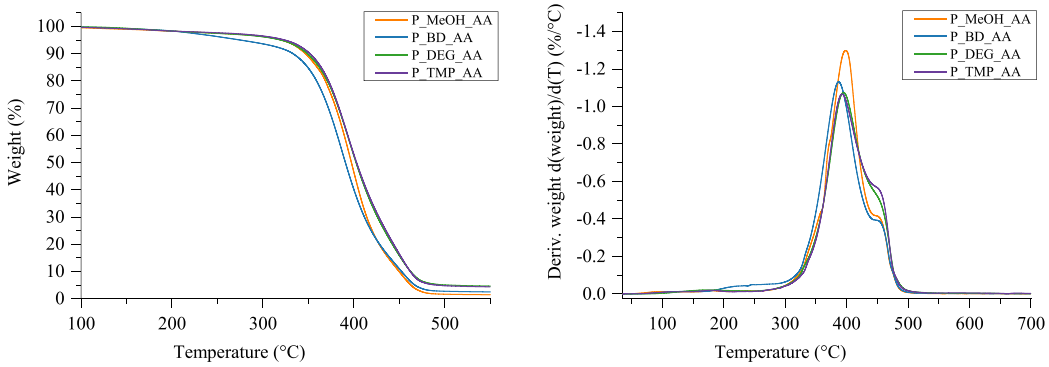

Fig. 11. TGA curves of developed polymer monoliths synthesized from bio-polyol acetoacetates and commercial acrylate – TMPTA.

draft, Writing – review & editing, Software, Visualization. **Darta Eihe**: Data curation, Formal analysis, Writing – review & editing, Visualization. **Ralfs Pomilovskis**: Data curation, Formal analysis, Writing – review & editing, Software. **Anda Fridrihsone**: Formal analysis, Writing – original draft, Writing – review & editing, Project administration. **Mikelis Kirpluks**: Conceptualization, Writing – original draft, Writing – review & editing, Software, Supervision.

Declaration of Competing Interest

The authors declare that they have no known competing financial interests or personal relationships that could have appeared to influence the work reported in this paper.

Data Availability

Data will be made available on request.

Acknowledgements

This research was funded by ERDF project No. 1.1.1.1/20/A/098 "100% Bio-based thermal insulation polymer development".

Appendix A. Supporting information

Supplementary data associated with this article can be found in the online version at doi:10.1016/j.indcrop.2023.117367.

References

Abolins, A., Pomilovskis, R., Vanags, E., Mierina, I., Michalowski, S., Fridrihsone, A., Kirpluks, M., 2021. Impact of different epoxidation approaches of tall oil fatty acids on rigid polyurethane foam thermal insulation. Materials 14, 1–17. https://doi.org/10.3390/ma14040894.

Alaneed, R., Golitsyn, Y., Hauenschild, T., Pietzsch, M., Reichert, D., Kressler, J., 2021. Network formation by aza-Michael addition of primary amines to vinyl end groups of enzymatically synthesized poly(glycerol adipate). Polym. Int. 70, 135–144. https://doi.org/10.1002/pi.6102.

Aripo (bw, Es Sd,;, St, S.L., Sz, T.Z., Euroasiática, Z.), Am, (, By, A.Z., Kg, K.Z., Tm), 2014. W P Ct.

Barszczewska-Rybarek, I.M., Korytkowska-Wałach, A., Kurcok, M., Chladek, G., Kasperski, J., 2017. DMA analysis of the structure of cross-linked poly(methyl methacrylate)s. Acta Bioeng. Biomech. 19, 47–53. https://doi.org/10.5277/ABB-00590-2016-01.

Bhattacharjee, S., Shaikh, A.A., Ahn, W.S., 2021. Heterogeneous Aza-Michael addition reaction by the copper-based metal–organic framework (CuBTC). Catal. Lett. 151, 2011–2018. https://doi.org/10.1007/s10562-020-03459-7.

Biermann, U., Bornscheuer, U., Meier, M.A.R., Metzger, J.O., Schäfer, H.J., 2011. Oils and fats as renewable raw materials in chemistry. Angew. Chem. - Int. Ed. 50, 3854–3871. https://doi.org/10.1002/anie.201002767.

Cao, Z., Gao, F., Zhao, J., Wei, X., Cheng, Q., Zhong, J., Lin, C., Shu, J., Fu, C., Shen, L., 2019. Bio-based coating materials derived from acetoacetylated soybean oil and aromatic dicarboxaldehydes. Polymers 11. https://doi.org/10.3390/polym11111809.

Cespedes, S., Hand, R.A., Chmel, N., Moad, G., Keddie, D.J., Schiller, T.L., 2021. Enhanced properties of well-defined polymer networks prepared by a sequential thiol-Michael - radical thiol-ene (STMRT) strategy. Eur. Polym. J. 151, 110440 https://doi.org/10.1016/j.eurpolymj.2021.110440.

Chatani, S., Nair, D.P., Bowman, C.N., 2013. Relative reactivity and selectivity of vinyl sulfones and acrylates towards the thiol-Michael addition reaction and polymerization. Polym. Chem. 4, 1048–1055. https://doi.org/10.1039/c2py20826a.

Chen, J., Ma, X., Edgar, K.J., 2021. A versatile method for preparing polysaccharide conjugates via thiol-michael addition. Polymers 13, 1–13. https://doi.org/10.3390/polym13121905.

Chen, R., Zhang, C., Kessler, M.R., 2015. Polyols and polyurethanes prepared from epoxidized soybean oil ring-opened by polyhydroxy fatty acids with varying oh numbers. J. Appl. Polym. Sci. 132, 1–10. https://doi.org/10.1002/app.41213.

Chen, S., Wang, Q., Pei, X., Wang, T., 2010. Dynamic mechanical properties of castor oil-based polyurethane/epoxy graft interpenetrating polymer network composites. J. Appl. Polym. Sci. 116, N./a-N./a. https://doi.org/10.1002/app.32518.

Cifarelli, A., Boggioni, L., Vignali, A., Tritto, I., Bertini, F., Losio, S., 2021. Flexible polyurethane foams from epoxidized vegetable oils and a bio-based diisocyanate. Polymers 13, 1–21. https://doi.org/10.3390/polym13040612.

Dave, V.J., Patel, H.S., 2017. Synthesis and characterization of interpenetrating polymer networks from transesterified castor oil based polyurethane and polystyrene. J. Saudi Chem. Soc. 21, 18–24. https://doi.org/10.1016/j.jscs.2013.08.001.

Dechent, S.E., Kleij, A.W., Luinstra, G.A., 2020. Fully bio-derived CO_2 polymers for non-isocyanate based polyurethane synthesis. Green. Chem. 22, 969–978. https://doi.org/10.1039/c9gc03488a.

Demirbas, A., 2011. Methylation of wood fatty and resin acids for production of biodiesel. Fuel 90, 2273–2279. https://doi.org/10.1016/j.fuel.2011.02.037.

Di Bartolo, A., Infurna, G., Dintcheva, N.T., 2021. A review of bioplastics and their adoption in the circular economy. Polymers 13. https://doi.org/10.3390/polym13081229.

European Commission, 2019. Eur. Green. Deal. Eur. Comm. 53, 24. https://doi.org/10.1017/CBO9781107415324.004.

González, G., Fernández-Francos, X., Serra, À., Sangermano, M., Ramis, X., 2015. Environmentally-friendly processing of thermosets by two-stage sequential aza-Michael addition and free-radical polymerization of amine-acrylate mixtures. Polym. Chem. 6, 6987–6997. https://doi.org/10.1039/c5py00906e.

Gracia-Fernández, C.A., Gómez-Barreiro, S., López-Beceiro, J., Tarrío Saavedra, J., Naya, S., Artiaga, R., 2010. Comparative study of the dynamic glass transition temperature by DMA and TMDSC. Polym. Test. 29, 1002–1006. https://doi.org/10.1016/j.polymertesting.2010.09.005.

Gunay, U.S., Cetin, M., Daglar, O., Hizal, G., Tunca, U., Durmaz, H., 2018. Ultrafast and efficient aza- and thiol-Michael reactions on a polyester scaffold with internal electron deficient triple bonds. Polym. Chem. 9, 3037–3054. https://doi.org/10.1039/c8py00485d.

Hagen, R., Salmén, L., Lavebratt, H., Stenberg, B., 1994. Comparison of dynamic mechanical measurements and Tg determinations with two different instruments. Polym. Test. 13, 113–128. https://doi.org/10.1016/0142-9418(94)90020-5.

Hassan, M.K., Tucker, S.J., Abukmail, A., Wiggins, J.S., Mauritz, K.A., 2016. Polymer chain dynamics in epoxy based composites as investigated by broadband dielectric spectroscopy. Arab. J. Chem. 9, 305–315. https://doi.org/10.1016/j.arabjc.2015.07.016.

He, X., Zhong, J., Cao, Z., Wang, J., Gao, F., Xu, D., Shen, L., 2019. An exploration of the Knoevenagel condensation to create ambient curable coating materials based on acetoacetylated castor oil. Prog. Org. Coat. 129, 21–25. https://doi.org/10.1016/j.porgcoat.2018.12.015.

Hill, L.W., 1997. Calculation of cross-link density in short chain networks. Prog. Org. Coat. 31, 235–243. https://doi.org/10.1016/S0300-9440(97)00081-7.

Jena, K.K., Raju, K.V.S.N., 2008. Synthesis and characterization of hyperbranched polyurethane hybrids using tetraethoxysilane (TEOS) as cross-linker. Ind. Eng. Chem. Res. 47, 9214–9224. https://doi.org/10.1021/ie800884y.

Jiang, Q., Zhang, Y.L., Du, Y., Tang, M., Jiang, L., Huang, W., Yang, H., Xue, X., Jiang, B., 2020. Preparation of hyperbranched polymers by oxa-Michael addition polymerization. Polym. Chem. 11, 1298–1306. https://doi.org/10.1039/c9py01686d.

Kathalewar, M., Sabnis, A., D'Mello, D., 2014. Isocyanate free polyurethanes from new CNSL based bis-cyclic carbonate and its application in coatings. Eur. Polym. J. 57, 99–108. https://doi.org/10.1016/j.eurpolymj.2014.05.008.

Kathalewar, M.S., Joshi, P.B., Sabnis, A.S., Malshe, V.C., 2013. Non-isocyanate polyurethanes: from chemistry to applications. RSC Adv. 3, 4110–4129. https://doi.org/10.1039/c2ra21938g.

Kim, T.H., Kim, M., Lee, W., Kim, H.G., Lim, C.S., Seo, B., 2019. Synthesis and characterization of a polyurethane phase separated to nano size in an epoxy polymer. Coatings 9. https://doi.org/10.3390/coatings9050319.

Kircher, M., 2019. Bioeconomy: markets, implications, and investment opportunities. Economies. https://doi.org/10.3390/economies7030073.

Kirpluks, M., Vanags, E., Abolins, A., Michalowski, S., Fridrihsone, A., Cabulis, U., 2020. High functionality bio-polyols from tall oil and rigid polyurethane foams formulated solely using bio-polyols. Materials 13, 38–53. https://doi.org/10.3390/MA13081985.

Krall, E.M., Serum, E.M., Sibi, M.P., Webster, D.C., 2018. Catalyst-free ligin valorization by acetoacetylation. Structural elucidation by comparison with model compounds. Green. Chem. 20, 2959–2966. https://doi.org/10.1039/c8gc01071d.

Lenardão, E.J., Trecha, D.O., Ferreira, P. da C., Jacob, R.G., Perin, G., 2009. Green Michael addition of thiols to electron deficient alkenes using KF/alumina and recyclable solvent or solvent-free conditions. J. Braz. Chem. Soc. 20, 93–99. https://doi.org/10.1590/S0103-50532009000100016.

Li, Q.F., Chu, S., Li, E., Li, M., Wang, J.T., Wang, Z., 2020. Lanthanide-based hydrogels with adjustable luminescent properties synthesized by thiol-Michael addition. Dye. Pigment. 174, 108091 https://doi.org/10.1016/j.dyepig.2019.108091.

Liao, Y.H., Su, Y.L., Chen, Y.C., 2021. The influence of neem oil and its glyceride on the structure and characterization of castor oil-based polyurethane foam. Polymers 13. https://doi.org/10.3390/polym13122020.

Lindsay, C.D., Timperley, C.M., 2020. TRPA1 and issues relating to animal model selection for extrapolating toxicity data to humans. Hum. Exp. Toxicol. 39, 14–36. https://doi.org/10.1177/0960327119877460.

Lopes, R., de, V.V., Zamian, J.R., Resck, I.S., Sales, M.J.A., Dos Santos, M.L., Da Cunha, F. R., 2010. Physicochemical and rheological properties of passion fruit oil and its polyol. Eur. J. Lipid Sci. Technol. 112, 1253–1262. https://doi.org/10.1002/ejlt.201000098.

Mather, B.D., Viswanathan, K., Miller, K.M., Long, T.E., 2006. Michael addition reactions in macromolecular design for emerging technologies. Prog. Polym. Sci. 31, 487–531. https://doi.org/10.1016/j.progpolymsci.2006.03.001.

Mushtaque, M., Avecilla, F., Ahmad, I., Alharbi, A.M., Khan, P., Ahamad, S., Hassan, M. I., 2021. 5-Fluorouracil (5-FU)-based Aza-Michael addition product: a selective carbonic anhydrase IX inhibitor. J. Mol. Struct. 1231, 129977 https://doi.org/10.1016/j.molstruc.2021.129977.

Nising, C.F., Bräse, S., 2008. The oxa-Michael reaction: from recent developments to applications in natural product synthesis. Chem. Soc. Rev. 37, 1218–1228. https://doi.org/10.1039/b718357g.
Noordover, B., Liu, W., McCracken, E., DeGooyer, B., Brinkhuis, R., Lunzer, F., 2020. Michael addition curable coatings from renewable resources with enhanced adhesion performance. J. Coat. Technol. Res. 17, 1123–1130. https://doi.org/10.1007/s11998-020-00351-2.
Ozturk, G., Long, T.E., 2009. Michael addition for cross-linking of poly(caprolactone)s. J. Polym. Sci. Part A Polym. Chem. 47, 5437–5447. https://doi.org/10.1002/pola.23593.
Piñeiro-García, A., Vega-Díaz, S.M., Tristán, F., Meneses-Rodríguez, D., Labrada-Delgado, G.J., Semetey, V., 2021. New insights in the chemical functionalization of graphene oxide by thiol-ene Michael addition reaction. FlatChem 26, 1–10. https://doi.org/10.1016/j.flatc.2021.100230.
Pomilovskis, R., Mierina, I., Beneš, H., Trhlíková, O., Abolins, A., Fridrihsone, A., Kirpluks, M., 2022a. The synthesis of bio-based michael donors from tall oil fatty acids for polymer development. Polymers 14. https://doi.org/10.3390/polym14194107.
Pomilovskis, R., Mierina, I., Fridrihsone, A., Kirpluks, M., 2022b. Bio-based polymer developments from tall oil fatty acids by exploiting Michael addition. Polymers 14, 1–15. https://doi.org/10.3390/polym14194068.
Rajkumar, T., Muthupandiyan, N., Vijayakumar, C.T., 2020. Synthesis and investigation of thermal properties of PMMA-maleimide-functionalized reduced graphene oxide nanocomposites. J. Thermoplast. Compos. Mater. 33, 85–96. https://doi.org/10.1177/0892705718804595.
Sardari, A., Sabbagh Alvani, A.A., Ghaffarian, S.R., 2019. Castor oil-derived water-based polyurethane coatings: structure manipulation for property enhancement. Prog. Org. Coat. 133, 198–205. https://doi.org/10.1016/j.porgcoat.2019.04.030.
Shufen, L., Zhi, J., Kaijun, Y., Shuqin, Y., Chow, W.K., 2006. Studies on the thermal behavior of polyurethanes. Polym. Plast. Technol. Eng. 45, 95–108. https://doi.org/10.1080/03602550500373634.
Sittinun, A., Pisitsak, P., Manuspiya, H., Thiangtham, S., Chang, Y.H., Ummartyotin, S., 2020. Utilization of palm olein-based polyol for polyurethane foam sponge synthesis: potential as a sorbent material. J. Polym. Environ. 28, 3181–3191. https://doi.org/10.1007/s10924-020-01834-4.
Sonnenschein, M.F., Werness, J.B., Patankar, K.A., Jin, X., Larive, M.Z., 2016. From rigid and flexible foams to elastomers via Michael addition chemistry. Polymers 106, 128–139. https://doi.org/10.1016/j.polymer.2016.10.054.
Sternberg, J., Pilla, S., 2020. Materials for the biorefinery: High bio-content, shape memory Kraft lignin-derived non-isocyanate polyurethane foams using a non-toxic protocol. Green. Chem. 22, 6922–6935. https://doi.org/10.1039/d0gc01659d.
Su, G., Thomson, C.J., Yamazaki, K., Rozsar, D., Christensen, K.E., Hamlin, T.A., Dixon, D.J., 2021. A bifunctional iminophosphorane squaramide catalyzed enantioselective synthesis of hydroquinazolines: Via intramolecular aza-Michael reaction to α,β-unsaturated esters. Chem. Sci. 12, 6064–6072. https://doi.org/10.1039/d1sc00856k.
Trevino, A.S., Trumbo, D.L., 2002. Acetoacetylated castor oil in coatings applications. Prog. Org. Coat. 44, 49–54. https://doi.org/10.1016/S0300-9440(01)00223-5.
Wang, T., Wang, J., He, X., Cao, Z., Xu, D., Gao, F., Zhong, J., Shen, L., 2019. An ambient curable coating material based on the michael addition reaction of acetoacetylated castor oil and multifunctional acrylate. Coatings 9. https://doi.org/10.3390/coatings9010037.
Williams, S.R., Miller, K.M., Long, T.E., 2007b. Michael addition reaction kinetics of acetoacetates and acrylates for the formation of polymeric networks. Prog. React. Kinet. Mech. 32, 165–194. https://doi.org/10.3184/146867807X247730.
Williams, S.R., Mather, B.D., Miller, K.M., Long, T.E., 2007a. Novel michael addition networks containing urethane hydrogen bonding. J. Polym. Sci. Part A Polym. Chem. 45, 4118–4128. https://doi.org/10.1002/pola.22236.
Witzeman, J.S., Nottingham, W.D., 1991. Transacetoacetylation with tert-Butyl acetoacetate: synthetic applications. J. Org. Chem. 56, 1713–1718. https://doi.org/10.1021/jo00005a013.
Xu, D., Cao, Z., Wang, T., Zhong, J., Zhao, J., Gao, F., Luo, X., Fang, Z., Cao, J., Xu, S., Shen, L., 2019. An ambient-cured coating film obtained via a Knoevenagel and Michael addition reactions based on modified acetoacetylated castor oil prepared by a thiol-ene coupling reaction. Prog. Org. Coat. 135, 510–516. https://doi.org/10.1016/j.porgcoat.2019.06.026.
Yang, X., Liu, H., Qian, L., Meng, Q., Wu, H., Li, Z., Zhou, H., 2021. Surface functionalization of cellulose fibers via aza-Michael addition for CO_2-assisted water remediation. Appl. Surf. Sci. 554, 149593 https://doi.org/10.1016/j.apsusc.2021.149593.
Zhang, C., Madbouly, S.A., Kessler, M.R., 2015. Biobased polyurethanes prepared from different vegetable oils. ACS Appl. Mater. Interfaces 7, 1226–1233. https://doi.org/10.1021/am5071333.
Zhang, C., Garrison, T.F., Madbouly, S.A., Kessler, M.R., 2017. Recent advances in vegetable oil-based polymers and their composites. Progress in Polymer Science. Elsevier B.V. https://doi.org/10.1016/j.progpolymsci.2016.12.009.
Zhang, F.A., Lee, D.K., Pinnavaia, T.J., 2009. PMMA-mesocellular foam silica nanocomposites prepared through batch emulsion polymerization and compression molding. Polymers 50, 4768–4774. https://doi.org/10.1016/j.polymer.2009.08.007.
Zhaoo, M.Y., Hsu, C.-P., Voeks, S.L., Landtiser, R., 2013. Acetoacetyl thermosetting resin for zero VOC gel coat.
Zhu, Y., Gao, F., Zhong, J., Shen, L., Lin, Y., 2020. Renewable castor oil and DL-limonene derived fully bio-based vinylogous urethane vitrimers. Eur. Polym. J. 135, 109865 https://doi.org/10.1016/j.eurpolymj.2020.109865.
Zuo, H., Cao, Z., Shu, J., Xu, D., Zhong, J., Zhao, J., Wang, T., Chen, Y., Gao, F., Shen, L., 2019. Effect of structure on the properties of ambient-cured coating films prepared via a Michael addition reaction based on an acetoacetate-modified castor oil prepared by thiol-ene coupling. Prog. Org. Coat. 135, 27–33. https://doi.org/10.1016/j.porgcoat.2019.05.032.

6. pielikums
Appendix 6

Influence of different synthesis conditions on the chemo-enzymatic epoxidation of tall oil fatty acids

Miķelis Kirpļuks, Ralfs Pomilovskis, Edgars Vanags, Arnis Āboliņš, Inese Mieriņa, Anda Fridrihsone,

Process Biochemistry, 2022

Process Biochemistry 122 (2022) 38–49

Contents lists available at ScienceDirect

Process Biochemistry

journal homepage: www.elsevier.com/locate/procbio

Influence of different synthesis conditions on the chemo-enzymatic epoxidation of tall oil fatty acids

Mikelis Kirpluks [a,*], Ralfs Pomilovskis [a,b], Edgars Vanags [a], Arnis Abolins [a], Inese Mierina [b], Anda Fridrihsone [a]

[a] Polymer Laboratory, Latvian State Institute of Wood Chemistry, str. Dzerbenes 27, Riga, LV-1006, Latvia
[b] Institute of Technology of Organic Chemistry, Faculty of Materials Science and Applied Chemistry, Riga Technical University, str. P. Valdena 3/7, Riga, LV-1048, Latvia

ARTICLE INFO

Keywords:
Tall oil
Epoxidation
Immobilised *Candida antarctica* lipase B

ABSTRACT

A side-stream of the cellulose pulping process – tall oil, was valorised for polyol precursor synthesis. The influence of various parameters on the tall oil self-epoxidation method was studied to increase the conversion towards oxirane rings while using a reduced amount of immobilised lipase catalyst – Novozym® 435 and hydrogen peroxide. The influence of synthesis time (0–7 h), process temperature (30–40 °C), hydrogen peroxide (20–50 wt. %) and Novozym® 435 catalyst concentration (1.5–4.5 wt. % of tall oil mass) on the tall oil fatty acid self-epoxidation process was studied and optimised using response surface method. The shift in relative conversion to oxirane and ethylenic unsaturation was used to track the epoxidation process. The chemical structure change of the epoxidised tall oil was investigated using FTIR, ^{1}H NMR and ^{13}C NMR spectroscopies. The maximum relative conversion to oxirane of 81 % was attained at a relatively high Novozym® 435 catalyst loading of 4.5 wt. %. In comparison, the optimised relative conversion to oxirane of 73 % was achieved at a more feasible catalyst content of 3.2 wt. % after 7 h of synthesis, at hydrogen peroxide and tall oil molar ratios of 2.0/1.0, hydrogen peroxide concentration of 28 wt. % and synthesis temperature of 44 °C.

1. Introduction

In academia and industry, creating new bio-based feedstock-based chemicals and materials is a constant focus. According to E. Jong et al., "a key factor in the deployment of a successful bio-based economy will be the development of biorefinery systems allowing highly efficient and cost-effective processing of biological feedstocks into a range of bio-based products and successful integration into existing infrastructure" [1]. The potential of the accessible renewable bioresources and their processing by-products in high value-added chemicals and materials needs to be maximised. The twelve principles of Green chemistry must also be followed more closely when introducing new approaches. Bio-based products and their production technologies need to be more atom efficient and achieve higher yields, along with focusing on waste minimisation and avoiding the use of hazardous chemicals and process conditions [2]. Valorisation of bio-residuals to minimise waste and knowledge-intensive production of chemicals, biofuels and polymers using highly efficient chemo- or biocatalysts are essential parts of the bio-economy [3,4].

Compared to other components in biomass, such as lignin, carbohydrate, and protein, fatty acids have several advantages. The most significant could be that fatty acids are relatively easy to adapt for use in existing hydrocarbon-based production infrastructure due to their usually liquid state and low oxygen content [1,5]. Currently, the work of many research groups is devoted to the epoxidation of the double-bonded fatty acids of plant oils. Epoxidised fatty acids are a thoroughly valuable intermediate with great potential for use in the production of alcohols, high-temperature environmentally friendly

Abbreviations: Novozym® 435, epoxidation catalyst based on immobilised lipase B of *Candida antarctica* enzyme; TOFA, tall oil fatty acids; ETOFA, epoxidised tall oil fatty acids; TMAH, tetramethylammonium hydroxide; H_2O_2, hydrogen peroxide; AcOH, acetic acid; FTIR, fourier transform infrared spectra; OO_{th}, theoretical maximum oxirane content in 100 g of oil; OO_{ex}, content of oxirane oxygen; RCO, relative conversion to oxirane; REU, relative ethylenic unsaturation; UBC, unsaturated bond conversion; EU_i, the initial degree of ethylenic unsaturation; EU_{ex}, remaining degree of ethylenic unsaturation during synthesis; S, synthesis selectivity; RSM, response surface modelling; ^{13}C NMR, ^{13}C nuclear magnetic resonance; $CDCl_3$, deuterated chloroform; ^{1}H NMR, ^{1}H nuclear magnetic resonance.

* Corresponding author.
E-mail addresses: mikelis.kirpluks@kki.lv (M. Kirpluks), ralfs.pomilovskis@kki.lv (R. Pomilovskis), edgarsvanags6@gmail.com (E. Vanags), arnis.abolins@kki.lv (A. Abolins), inese.mierina@rtu.lv (I. Mierina), anda.fridrihsone@kki.lv (A. Fridrihsone).

https://doi.org/10.1016/j.procbio.2022.08.024
Received 14 February 2022; Received in revised form 12 August 2022; Accepted 16 August 2022
Available online 18 August 2022
1359-5113/© 2022 Elsevier Ltd. All rights reserved.

bio-lubricants, plasticisers, polyols and polymers, e.g., polyurethanes and epoxy resins [6–12].

One of the most versatile and widely used polymeric compounds is polyurethane. Polyurethanes are synthesised by polycondensation reactions between isocyanates and polyols. In the polyurethane sector, the creation of bio-polyols from renewable resources is critical. Even though epoxidation of vegetable oil is a well-studied topic, research on epoxidation of different non-edible oils is very important to synthesise bio-polyols for different types of polyurethanes [13,14]. Prilezhaev epoxidation technique has been applied to various plant oils with the aim of obtaining plant-based polyols. Literature reports epoxidation of edible plant oils – palm [15], canola [16,17], castor [18], wild safflower [19], soybean [20–23], cottonseed [24,25], grape seed oil [26], sesame and non-edible oils – jatropha [27–29], tall oil [30], karanja oil [31,32], rice bran oil [33], moringa [34] and others.

According to Wai et al., the main epoxidation methods that are being studied are homogeneous catalysis by peroxy acids, heterogeneous catalysis using acidic ion exchange resin, epoxidation over phosphotungstate heteropolyacid catalysts and in the presence of phase-transfer catalysts, chemo-enzymatic epoxidation, metal-catalysed heterogeneous systems with H_2O_2, cumene, O_2, organic hydroperoxides as the oxidant and enzymatic catalysis [14]. The homogeneous chemical catalytic epoxidation process is the most extensively utilised method in the above-mentioned investigations, as well as for industrial production of epoxidised oil (the Prilezhaev epoxidation). There in-situ generated peroxy acids such as peroxyacetic acid, peroxyformic or perpropanoic acid have been used as the oxidising agent in the presence of a strong acidic catalyst. However, the undesirable acid-catalysed degradation of the oxirane ring occurs in this process, which results in a significant amount of unwanted by-products [14,35,36]. The inclusion of extra acid as an oxygen carrier also means that the acid must be removed from the reaction media following oil epoxidation. Acid removal is normally performed with hazardous chemicals, which is not ideal from a Green chemistry standpoint. Furthermore, oil epoxidation by homogeneous catalysis by peroxy acids poses a safety risk due to the reaction's potential for thermal runaway, which is highly undesired [21,23,37]. Several studies have been dedicated to finding optimal epoxidation conditions in terms of epoxide yield and reaction time while reducing the thermal risk in the semi-batch reactors [38–40].

As a more sustainable alternative to traditional chemical catalysis procedures, various chemo-enzymatic catalysis reactions have been investigated. Biocatalytic processes are extremely attractive for several reasons [41–46]. Biocatalysts such as enzymes are usually highly selective with an epoxidation conversion rate over 90 %, and epoxidation using biocatalysts can be routinely carried out at an ambient or relatively low temperature of 30–50 °C under atmospheric pressure. The above-mentioned factors could result in a smaller pollution level compared to chemical epoxidation [47–49].

At present, one of the hot research directions is enzymatic double-bond epoxidation using lipase as a catalyst for the peroxycarboxylic acid in-situ formation. Lipase has been shown to catalyze the synthesis of fatty acid peracids, such as perstearic acid [50,51] and peroleic [12,52], by several authors. This eliminates the need for formic and acetic acid during the epoxidation process. Lipase can be utilised to convert an unsaturated acid to an oxirane derivative through self-epoxidation [12]. Moreover, lipases are capable of recognizing many different substrates, and they can catalyze hydrolysis, acidolysis, esterification, transesterification and amination reactions [44,45,53–60].

Although the prospect of using lipase as a cleaner biocatalyst for epoxidation has long been known, there have been very few successful research in which oil was converted to polyols using a chemo-enzymatic epoxidation approach to be employed in polyurethane manufacture. The microbial oil was successfully converted to epoxidised oil with 85 % conversion, the epoxidation reaction was catalysed by lipase B of *Candida antarctica* immobilised on the acrylic resin (Novozym® 435), and the epoxidation was followed by a ring-opening reaction to produce polyols [61]. *Candida antarctica* lipase B is one of the most effective lipases for unsaturated bond epoxidation [12,62]. Kirpluks et al. used tall oil fatty acids (TOFA) as a bio-based feedstock for polyol precursor synthesis. TOFA are a by-product of wood biomass Kraft pulping processes. It is a second-generation bio-based feedstock. Distilled TOFA are a mixture of unsaturated free fatty acids that principally consist of oleic, linoleic, and linolenic acids [63]. TOFA were self-epoxidised in the presence of an immobilised lipase catalyst – Novozym® 435 and, as previously stated, valorised for polyol precursor synthesis [30].

The selectivity of chemo-enzymatic epoxidation of fatty acid derivatives, as well as oxirane oxygen production, is greatly influenced by the structure of the acyl donor. Longer linear alkyl chain carboxyl acids (C4-C18) are more suitable for epoxidation [64]. The medium in which the reaction takes place also has a significant effect on the desired product's yield. A promising method in the enzymatic epoxidation process of unsaturated fatty acid methyl esters is the use of ionic liquids, and employing this method Silva et al. reported a relative conversion to oxirane up to 89 % by employing ionic liquids [65]. The conversion up to 98 % was achieved when oleic acid was epoxidised in the presence of Novozym® 435 catalyst in acetonitrile [12]. However, the benefits of using organic solvents or other synthesis ingredients in the epoxidation process must be balanced against the cost of their creation, usage, and disposal. The ideally built approach must be as simple as possible, using as few raw resources as possible. Zhang et al. reported a relative conversion to oxirane up to 83 % in a solvent-free chemo-enzymatic epoxidation of *Sapindus mukurossi* fatty acids [66]. However, a higher relative conversion to oxirane of 95 % was achieved in the chemo-enzymatic epoxidation of 2-ethylhexyl oleic acid ester [11]. Thus, such a solvent-free approach ensures that no additional chemicals and materials are required. Moreover, Novozym® 435, as being an immobilised form of *Candida antarctica* B can be recovered and reused [12,67]. The reusability of Novozym® 435 was studied for the synthesis of epoxidised 2-ethylhexyl oleate from oleic acid and 2-ethyl hexanol, and no significant loss of activity was observed after 13 cycles in a solvent-free system [67]. Nevertheless, the use of Novozym® 435 in typical epoxidation where peroxy acid is generated in-situ from acid and hydroge peroxide may poses some problems on the process, as hydrogen peroxide is a enzyme inactivating agent. The use of organic hydroperoxide such as t-butyl hydroxyperoxide did yield in higher stability of Novozym® 435. However, no fatty acid epoxide formation was observed. A controlled addition of hydrogen peroxide is essential for the enzyme stability [68]. Lipase from Pseudomonas fluorescens immobilised on magnetic nanoparticles proved to be a robust biocatalyst and it was possible to reuse it up to five times [69]. The immobilization of the enzyme is essential for its economic use as it allows easy separation of catalyst from the reaction medium, reuse of the catalyst and improvement in the stability of the three-dimensional structure of the enzyme [70,71]. Moreover, the immobilization of an enzyme may increase its activity, increase the yields of the desired reaction and prevent the release of the catalyst into the product [72]. The key advantage of the immobilised enzyme bio-catalysts is their use in continuous operations, as well as their better stability across a wider range of pH and temperature. However, there are some drawbacks, including enzyme immobilization in an unfavourable shape formation, followed by a loss of activity, carrier costs, additional preparation materials and techniques, as well as time-consuming training tactics, mass transfer limitations, and difficult and time-consuming immobilization processes. Studies of enzyme immobilization, or the attachment of a biocatalyst to a material with desirable physical, chemical, electrical, or mechanical properties, have shown that immobilizing biocatalysts can increase their activity and stability over a wider range of operating parameters, with the increased functionality conferred being dependent on both the method of immobilization and the inherent features of the materials used in such immobilization [73].

In the previous research performed by the Polymer laboratory group at the Latvian State Institute of Wood Chemistry, one step solvent-free

chemo-enzymatic epoxidation of free TOFAs was developed [30]. The present paper aims to study synthesis temperature, hydrogen peroxide (H_2O_2) concentration, and molar ratios influence on the chemo-enzymatic epoxidation of free TOFAs. The aim is to reach as high as possible oxirane group yield using as low as possible amount of Novozym® 435 catalyst. Although Novozym® 435 catalyst is commercially produced, it is still the most expensive component in the TOFA epoxidation process and its minimal use is vital for commercially viable process development. Response surface methodology (RSM) was used to determine the different factor influence on the TOFA epoxidation process. The presented results describe optimal reaction conditions for epoxidised tall oil fatty acid (ETOFA) synthesis that can be further used for bio-polyol production.

2. Materials and methods

2.1. Materials

TOFA (trademark "FOR_2″ from Forchem Oyj (Finland)) composition: fatty acids ≥98 % (2.7 % linolenic acid, 50.4 % linoleic acid, 43.5 % oleic acid, 1.6 % stearic acid) and 1.8 % other fatty and rosin acids. The iodine value was 155 ± 2 g I_2/100 g. The acid value was 190 ± 3 mg KOH/g. The composition of fatty acids and resin acids in TOFA was calculated using capillary gas chromatography and ASTM D 5974–96 as a standard method. TOFA was derivatised with tetramethylamonium hydroxide (TMAH) [74].

Novozymes A/S (Denmark) generously provided immobilised lipase enzyme on acrylic resin for epoxidation with the trade name Novozym® 435. Novozym® 435 is a lipase enzyme immobilised on acrylic resin from *Candida antarctica* ≥5000 U/g, recombinant, expressed in *Aspergillus niger*. Acetic anhydride, assay ≥99 %, H_2O_2, assay ≥35 %, glacial acetic acid (AcOH), assay ≥99.8 %, dichloromethane, puriss.p.a., assay ≥99.9 %, chloroform, contains ethanol as a stabiliser, assay 99.0–99.4 %, potassium iodide, assay ≥99 %, tetraethylammonium bromide, assay 98 % and perchloric acid, assay 70 % were obtained from Sigma-Aldrich Chemie GmbH (Germany). Ampoules to make 1 L of 0.1 M sodium thiosulphate fixanals and 0.1 M Hanus solution, volumetric IBr were obtained from Honeywell Fluka (Germany). Deuterochloroform with 99.8 % content of D ($CDCl_3$) was ordered from Eurisotop (France). All the chemicals mentioned above were at least reagent grade and used untreated.

2.2. Tall oil fatty acid epoxidation procedure

The TOFA epoxidation was carried in the four-neck round bottom flask equipped with a dropping funnel, a thermocouple, a mechanical stirrer, and a reflux condenser and heated to a selected temperature using a thermostat with temperature control with a precision of ± 0.1 °C. A few dozen experiments were planned to determine the optimal conditions for TOFA epoxidation. The molar ratio of the unsaturated TOFA and hydrogen peroxide was selected to be 1.0/1.5, 1.0/2.0 and 1.0/2.5. In addition, the concentration of hydrogen peroxide used in synthesis was changed from 20 to 50 wt. %. Furthermore, the effect on the TOFA epoxidation process of the Novozym® 435 catalyst quantity was investigated at 1.5 wt. %, 3.0 wt. % and 4.5 wt. % catalyst load from TOFA mass. Lastly, the impact of temperature on the TOFA epoxidation reaction was studied at 30 °C, 40 °C and 50 °C. A more detailed plan of experiments is presented in paragraph 2.4. The masses of all reagents were calculated upon the mass of TOFA, which was 40 g.

The TOFA and Novozym® 435 were placed in the reactor, and the temperature was raised to the required level using a thermostat with a temperature controller. A certain amount of H_2O_2 water solution was applied to the reactants for 10 min period, maintaining the temperature with a precision ± 1 ºC. An anchor-style stirrer was used to stir the reaction mixture rapidly. The stirring speed was 450 rpm. After reagent addition, all parameters were kept constant until the end of the synthesis. The homogeneous reaction mixture was sampled every 60 min. The volume of the taken samples was 2 mL and poured into a separating funnel (100 mL). The samples were washed with warm demineralised water (20 mL) before being dried in a rotatory evaporator at 50 °C under a 3 mbar vacuum. The samples were placed in the freezer and stored at a temperature of −20 °C. Titration of oxirane rings and iodine value and Fourier transform infrared (FTIR) spectra were used to explore the process kinetics further.

2.3. Methods of compound characterization

The progress of TOFA epoxidation was monitored by the percentage of relative conversion to oxirane (RCO) and by the percentage of the relative level of ethylenic unsaturation (REU). The RCO and REU were calculated from epoxy group content (OO_{ex}) (the content of oxirane oxygen) and the samples' iodine value that was determined according to ISO 3961:2013 and ASTM D1652–11 standards, respectively. A detailed RCO and REU calculation, together with a calculation of the unsaturated bond conversion (UBC) and the TOFA epoxidation selectivity (S) is described in our previous study [30].

TOFA and ETOFA structures were analysed by FTIR spectrometry data obtained with Thermo Fisher Nicolet iS50 spectrometer at a resolution of 4 cm^{-1}, 32 scans. The FTIR data was collected using an attenuated total reflectance technique with a diamond crystal. ^1H NMR and $^{13}C\{^1H\}$ NMR spectra for the samples were recorded on a Bruker spectrometer at 500 and 126 MHz, respectively. The chemical shifts (δ) are reported in ppm. The residual chloroform peak was used as an internal reference (for ^1H NMR, 7.26 ppm, for ^{13}C NMR, 77.16 ppm).

2.4. Optimisation of tall oil fatty acid self-epoxidation with Novozym® 435

The previously studied TOFA epoxidation method by our group [30] was further optimised to increase the RCO and to achieve as high as possible yield of oxirane groups. The optimisation was performed using the response surface modelling (RSM) approach employing a modified Box-Behnken design. Design Expert V12.0.7.0 software was used. The influence of H_2O_2 and the TOFA double bond molar ratio, H_2O_2 concentration, Novozym® 435 content and the synthesis temperature on the TOFA epoxidation process was studied and optimised. The influence of different factors (H_2O_2 and the TOFA double bond molar ratio, H_2O_2 concentration, Novozym® 435 content and the synthesis temperature) on the TOFA epoxidation process was modelled at three coded levels, low (−1), high (+1) and mean (0), which resulted in 25 different experimental runs. Moreover, synthesis time as an additional factor influencing the TOFA epoxidation was investigated for each run. TOFA epoxidation kinetics were studied by measuring the double bond conversion and introduction of oxirane rings at the following intervals – 0, 0.5, 1, 2, 3, 4, 5, 6 and 7 h. The developed RSM design was further supplemented with additional data points by using the results of the previously obtained TOFA epoxidation kinetic curves [30]. An additional coded design level of −2 was ascribed to these data for the H_2O_2 and the TOFA double bond molar ratio of 1.0/1.1 and H_2O_2 concentration of 15 wt. %. The actual values of different coded Box-Behnken design levels (−2; −1; 0 and +1) and the optimised experimental factors are summarised in Table 1.

In total, 32 runs were carried out, 9 data points of TOFA epoxidation kinetic curves of RCO and REU were determined for each run. The summary of performed experiments is depicted in Table 2. The values of the different experimental levels – the molar ratio of H_2O_2 and TOFA double bonds, H_2O_2 concentration, Novozym® 435 content and the synthesis temperature – are shown. The data for runs 26–32 have been taken from our previous study [30].

Table 1
The levels of the optimised tall oil fatty acid epoxidation factors.

Factors	Units	Symbol	Actual and coded levels			
			-2	-1	0	+1
Time	h	A	n. a.	0.0	3.2	7.0
Molar ratio of H_2O_2/tall oil fatty acids		B	1.1	1.5	2.0	2.5
H_2O_2 concentration	wt. %	C	15	20	35	50
Novozym® 435 content	wt. %	D	n. a.	1.5	3.0	4.5
Temperature	°C	E	n. a.	30	40	50

3. Results and discussion

This paper is a continuation of previous work published by our group [30] and presents the optimisation of the TOFA epoxidation method. The chemo-enzymatic solvent-free TOFA self-epoxidation has several advantages from a sustainability perspective. It does not require solvents, additional chemicals for oxygen transfer and synthesis of intermediates, such as fatty acid methyl esters. However, the disclosed TOFA epoxidation process has drawbacks, the most significant of which is the loss of oxirane yield due to oxirane ring cleavage during synthesis. The change in TOFA structure during the epoxidation process is depicted in Fig. 1. FTIR spectroscopy confirmed that oxirane ring-opening side reactions occurred during the TOFA epoxidation. However, it was possible to find optimal TOFA epoxidation conditions with minimal occurrence of side reactions and relatively high RCO values.

Table 2
Different runs for determination of tall oil fatty acid epoxidation factors.

Run	H_2O_2/ Tall oil fatty acid molar ratio	Coded level	H_2O_2 conc., wt. %	Coded level	Novozym® 435 content, wt. %	Coded level	Temp., °C	Coded level
1	1.5	-1	35	0	4.5	+1	40	0
2	2.5	+1	35	0	3.0	0	50	+1
3	1.5	-1	50	+1	3.0	0	40	0
4	2.5	+1	35	0	3.0	0	30	-1
5	2.0	0	20	-1	4.5	+1	40	0
6	2.0	0	35	0	3.0	0	40	0
7	2.0	0	35	0	1.5	-1	50	+1
8	2.0	0	20	-1	3.0	0	50	+1
9	2.0	0	20	-1	1.5	-1	40	0
10	2.0	0	50	+1	1.5	-1	40	0
11	2.0	0	50	+1	3.0	0	30	-1
12	1.5	-1	35	0	3.0	0	30	-1
13	1.5	-1	20	-1	3.0	0	40	0
14	2.0	0	35	0	1.5	-1	30	-1
15	2.5	+1	35	0	1.5	-1	40	0
16	1.5	-1	35	0	3.0	0	50	+1
17	2.0	0	50	+1	4.5	+1	40	0
18	1.5	-1	35	0	1.5	-1	40	0
19	2.5	+1	50	+1	3.0	0	40	0
20	2.5	+1	20	-1	3.0	0	40	0
21	2.0	0	35	0	4.5	+1	50	+1
22	2.0	0	50	+1	3.0	0	50	+1
23	2.0	0	35	0	4.5	+1	30	-1
24	2.0	0	20	-1	3.0	0	30	-1
25	2.5	+1	35	0	4.5	+1	40	0
26*	1.1	-2	20	-1	1.5	-1	40	0
27	1.1	-2	20	-1	3.0	0	40	0
28	1.1	-2	20	-1	4.5	-1	40	0
29	1.1	-2	15	-2	3.0	0	40	0
30	1.1	-2	25	n.a.	3.0	0	40	0
31	1.1	-2	30	n.a.	3.0	0	40	0
32	1.1	-2	35	0	3.0	0	40	0

* The data for runs 26–32 have been taken from our previous study [30].

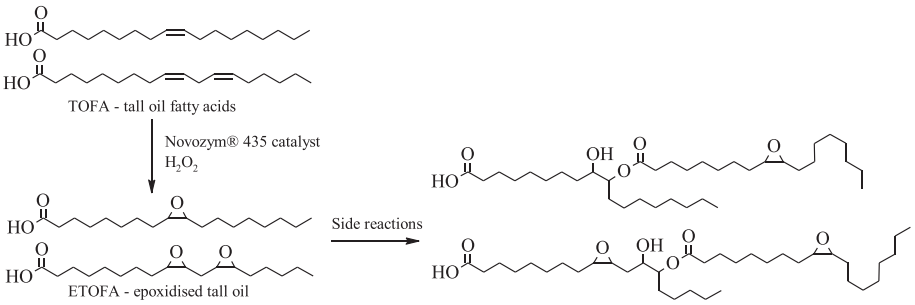

Fig. 1. Tall oil fatty acid epoxidation and the oxirane ring-opening side reactions.

3.1. Development of the RSM model for tall oil fatty acid epoxidation optimisation

The overall yield of oxirane groups during the epoxidation process depends on the synthesis time and the concentration of the used reagents. The applied Box-Behnken design allowed to determine the influence of different factors on the TOFA epoxidation process, which was approximated using the reduced second-order polynomial equation. The coefficients of the second-order polynomial equations in terms of the analysed factors for both RCO and REU responses are summarised in Table 3. The RCO and REU response surface model F-values of 164.8 and 203.4 imply that the developed models are significant. An F-value of this magnitude has a 0.01 % chance of occurring due to noise. The quadratic model of the RCO and REU responses was reduced to include only the significant factors with p-values less than 0.1. The adequate precision of the developed RCO and REU response surface models was much higher than 4 (52.4 and 57.3, respectively), which indicated adequate signals and that this model can be used to navigate the design space within the limits of set boundaries of optimised factors.

The developed model fitted the experimental data relatively well and allowed to navigate the five-dimensional space of TOFA epoxidation influencing factors to select the optimal process conditions. The predicted RCO and REU response surfaces are depicted in Figs. 2 and 3. Furthermore, the experimental outcomes are shown by red dots above the response surface and pink dots below it. The RCO values increased, and REU values decreased during the TOFA epoxidation process following a typical reaction's kinetic curves. A slight decrease of RCO after the peak value is reached. It is explained by the undesired oxirane ring-opening side reaction as depicted in Fig. 1. The developed polynomial model was validated by carrying out TOFA epoxidation experiments after the model was developed close to the optimized parameters. The validation experiment points are depicted as black points in Fig. 3.

3.2. The influence of different factors on the tall oil fatty acid epoxidation

The essential goal of the epoxidation process is to reach as high as possible yield of newly introduced oxirane groups into TOFA. It is represented as RCO values, and the higher the value, the better. The influence of H_2O_2 and TOFA double bond molar ratios on the RCO response surface is depicted in Fig. 4a. In the set constraints of the study of H_2O_2 and TOFA double bond molar ratios from 1.1 to 2.5 there was little influence on the RCO. Other experiment factors influenced RCO to a higher degree. The peak of the RCO surface appeared at H_2O_2/TOFA molar ratio of 2.0/1.0. The RCO increased with the increase of H_2O_2/TOFA molar ratios to the midpoint of the experiment design of the 2.0/1.0 of H_2O_2/TOFA. This could be explained by the ineffective formation of the TOFA-enzyme complex. During the reaction, TOFA bind to the enzyme catalyst active sites. At lower H_2O_2/TOFA molar ratios, there is a higher content of TOFA, which are binding to the enzyme active sites; however, the active sites are not vacant. The absence of the free catalyst sites will make the TOFA-enzyme complex ineffective, thus reducing the reactivity [75]. A further increase of H_2O_2/TOFA molar ratios beyond 2.0/1.0 resulted in a decrease in RCO. Inactivation of the enzyme catalyst occurred at higher quantities of H_2O_2. It has been reported that lipase enzyme catalysts are stable at moderate concentrations of H_2O_2 at relatively low temperatures. In contrast, lipase-based catalysts lose their activity at increased H_2O_2 concentrations due to the damaging effects of the H_2O_2 [68]. For the potential upscale of the TOFA epoxidation process to an industrial scale, the lowest possible usage of reagents is crucial; thus, only the necessary amount of H_2O_2 must be used.

The influence of H_2O_2 concentration on the RCO response surface is depicted in Fig. 4b. Similar conclusions can be made as for H_2O_2/TOFA molar ratios. Some minimal content of H_2O_2 is necessary for TOFA epoxidation, whereas epoxidation yield is decreased at higher H_2O_2 concentration due to the denaturation and inhibition of the enzyme catalyst. Meyer-Waßewitz et al. reported that the decrease of RCO was detected with the increased temperature at lower H_2O_2 concentrations due to more dominant catalyst deactivation [76]. The optimal value of H_2O_2 concentration is at ~28–36 wt. %, which is beneficial from an industrial perspective. A high concentration of H_2O_2 is hazardous and could introduce various risks during the industrial-scale epoxidation process, such as runaway of the reaction, explosion and risks associated with transportation and handling of hazardous chemicals [77].

The influence of Novozym® 435 catalyst content on the RCO response surface is depicted in Fig. 5a. The catalyst content had the most significant influence on the RCO yield, where the maximum RCO was reached at higher Novozym® 435 content at a shorter synthesis time. The catalyst content must be optimised as it is the most expensive component of the TOFA epoxidation process. Moreover, the repeated use of the catalyst is essential for a commercially feasible process. However, catalyst recycling was out of the scope of this article.

The influence of temperature on the TOFA epoxidation process and the RCO yield is depicted in Fig. 5b. Higher RCO values were reached with the increase in temperature from 30 °C to 40 °C at a shorter

Table 3
ANOVA and the equation in terms of actual factors for the relative conversion to oxirane (RCO) and percentage of the relative level of ethylenic unsaturation (REU) reduced quadratic response surface model and the R^2 values of the model.

Factors	Symbol	RCO equation	F-value	Sum of Squares	REU equation	F-value	Sum of Squares
Model			164.8	$1.47 \cdot 10^5$		203.4	$2.12 \cdot 10^5$
Intercept		-267.80			+290.39		
Time	A	+23.25	85520.7	1534.4	-24.56	128365.2	1605.0
H_2O_2/Tall oil fatty acid molar ratios	B	+46.63	471.97	8.5	-25.37	39.9	0.5
H_2O_2 concentration	C	+6.02	26.5	0.48	-6.28	32.8	0.4
Novozym® 435 content	D	+16.32	17053.2	306.0	-6.58	22760.7	284.6
Temperature	E	+4.52	760.9	13.7	-1.99	3262.6	40.8
Time H_2O_2 / Tall oil fatty acid molar ratios	A·B	+0.52	86.0	1.5	-0.53	87.6	1.1
Time H_2O_2 concentration	A·C	-0.11	1872.9	33.6	+0.08	1071.3	13.4
Time Novozym® 435 content	A·D	+0.98	1516.8	27.2	-0.75	875.3	10.9
Time Temperature	A·E	-0.09	583.7	10.5	+0.02	16.8	0.2
H_2O_2/ Tall oil fatty acid molar ratios·H_2O_2 concentration	B·C	-0.29	263.4	4.7	+0.87	3381.6	42.3
H_2O_2 concentration·Temperature	C·E	-0.04	1457.8	26.2	+0.04	1414.8	17.7
Time^2	A^2	-1.76	18334.5	329.0	+2.18	27910.8	349.0
H_2O_2/ Tall oil fatty acid molar ratios^2	B^2	-9.86	523.8	9.4			
H_2O_2 concentration^2	C^2	-0.05	6119.6	109.8	+0.04	5884.8	73.6
Novozym® 435 content^2	D^2	-1.98	880.3	15.8			
Temperature^2	E^2	-0.03	349.7	6.3			
R^2		0.909			0.910		
Adequate Precision		52.4			57.3		

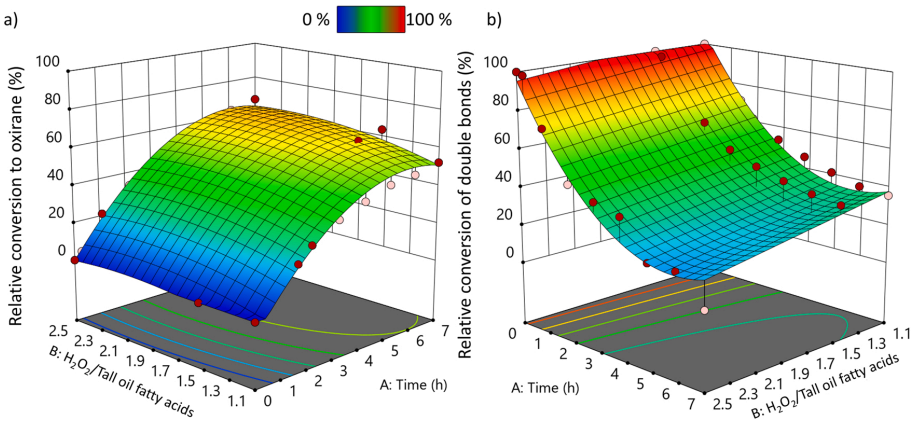

Fig. 2. a) Relative conversion to oxirane response surface b) Relative ethylenic unsaturation response surface at different H_2O_2 and tall oil fatty acid double bond molar ratios (T_{synth} = 40 °C; Novozym® 435 wt. % = 3.0 %; H_2O_2 wt. % = 20 %).

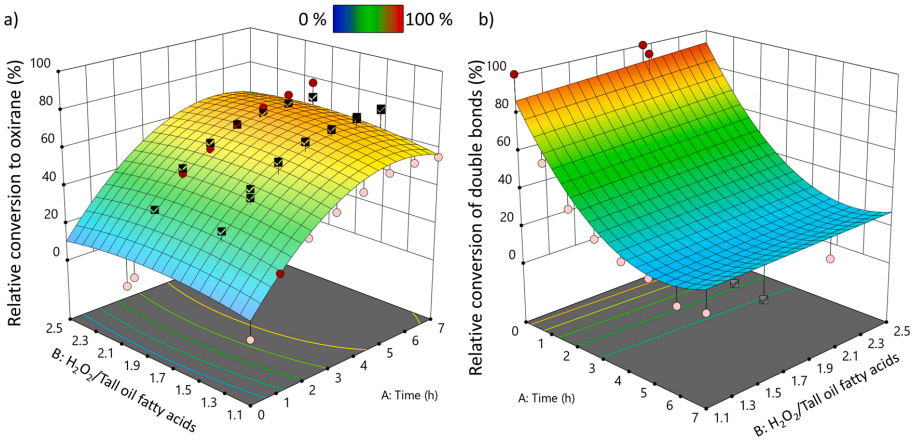

Fig. 3. a) Relative conversion to oxirane response surface b) Relative ethylenic unsaturation response surface at different H_2O_2 and tall oil fatty acid double bond molar ratios (T_{synth} = 40 °C; Novozym® 435 wt. % = 3.0 %; H_2O_2 wt. % = 35 %; black points are model validation experiments).

synthesis time, which is explained by the increase in the epoxidation rate due to the accelerated diffusion and the increase in the enzyme activity [51]. The RCO values slightly decreased with a further increase of the synthesis temperature to 50 °C due to the increase of the catalyst degradation and accelerated oxirane ring-opening side reactions. Overall the temperature had a minor effect on the increase of RCO in the selected constraints.

It is presumed, that the mass transfer limitations of the reagents during the TOFA epoxidation process are unessential and the system is ideally mixed. Nevertheless, the mixing speed influence on the TOFA epoxidation process was evaluated. by measuring the change of oxirane oxygen content and relative conversion to oxirane during the epoxidation process. The epoxidation of TOFA was carried out at the mixing speed of 200, 400, 600, 800 and 1000 revolutions per minute (rpm). The results of epoxidation at various mixing speeds are depicted in Fig. S1 or the Supplementary information. The epoxidation was done in the following conditions: H_2O_2/ Tall oil fatty acid molar ratio; concentration of H_2O_2 wt. % = 35 %; catalyst content Novozym® 435 wt. % = 3.0 %; T_{synth} = 40 °C. The mixing speed did not influence the reoxidation rate of the TOFA.

3.3. Finding optimal tall oil fatty acid epoxidation conditions

A mathematical approach to finding optimal TOFA epoxidation conditions is to calculate a desirability function *D(X)* which reflects the desirable range (d_i) for five different factors and obtained response. The desirable ranges from the least to most desirable are set from zero to one, respectively. Eq. 1 describes the simultaneous objective function, which is a geometric mean of all converted factors and responses, where n is the number of factors and responses. Moreover, a different value of importance was assigned for each factor or response to prioritise the more essential ones. The importance (ri) was scaled from 1 to 5, with 1 being the least significant and 5 being the most important. The overall function becomes 0 if the response or factors fall outside their desirability range [78]. The 3D surface plots of the desirability function can be used to explore the function in the factor space.

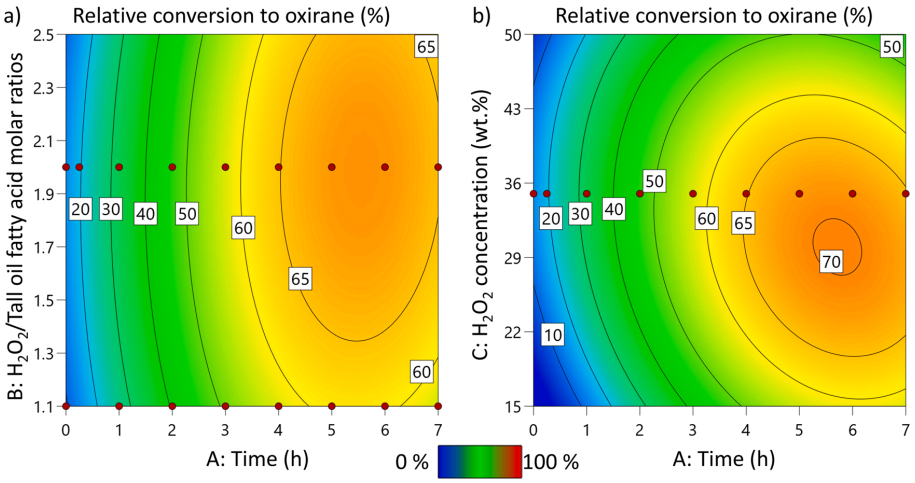

Fig. 4. Relative conversion to oxirane response surface at a) different H_2O_2 and tall oil fatty acid double bond molar ratios and b) different H_2O_2 concentrations at the midpoint of experimental levels •.

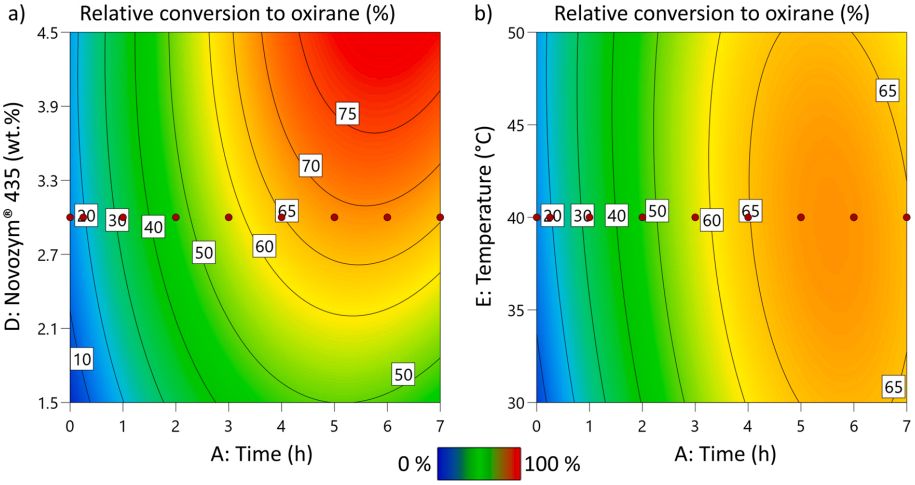

Fig. 5. Relative conversion to oxirane response surface at a) different Novozym® 435 catalyst content and b) synthesis temperatures at the midpoint of experimental levels.

$$D = (d_1{}^{r_1} \cdot d_2{}^{r_2} \cdot \ldots \cdot d_n{}^{r_n})^{\frac{1}{\sum r_i}} = \left(\prod_{i=1}^{n} d_i{}^{r_i}\right)^{\frac{1}{\sum r_i}} \quad (1)$$

The different factors influencing the TOFA epoxidation were optimised to reach as high as possible RCO values. The maximum importance factor of 5 was set for the RCO response. The limits of the RCO response were set from 67.4 % to 100 %, which is the maximum RCO value reached in the previous study [30] and the maximum theoretical RCO value, respectively. The TOFA epoxidation time was minimised with the importance factor of 1 to reach a shorter process time. The H_2O_2 and TOFA molar ratios and H_2O_2 concentration were also minimised with the importance factor of 1 to decrease the amount of reagents used in the synthesis process. Most importantly, the Novozym® 435 catalyst amount was minimised with an importance factor of 5 to be able to reduce the most expensive component of the TOFA epoxidation. The synthesis temperature was not optimised as it had little influence on the overall TOFA epoxidation process in the studied constraints. The REU was minimised with an importance factor of 1 to achieve as high as possible conversion degree of double bonds. Lastly, a maximum of the process selectivity was prioritised with an importance factor of 1. The obtained solution for the TOFA epoxidation influencing factor optimisation is summarised in Table 4.

In the present study, TOFA self-epoxidation in a solvent-free medium was developed, and a high RCO value of 80.6 % was achieved, which was significantly larger than the RCO of 67.4 % that was achieved in the previous study [30]. Achieving RCO values higher than 80.6 % was not feasible as the introduction of new epoxy groups is limited due to the lack of unreacted double bonds at the end of the epoxidation process. Furthermore, prolonging the epoxidation has an adverse effect on the RCO yield due to the undesired cleavage of oxirane moiety [79]. TOFA

Table 4
Constraints, importance levels and found solution for tall oil fatty acid epoxidation optimisation.

Factor/response	Goal	Lower limit	Upper limit	Importance	Solution
A: Time	Minimise	0	7	1	5.5 h
B: Molar ratios of H_2O_2/Tall oil fatty acids	Minimise	1.1	2.5	1	2.0
C: H_2O_2 concentration	Minimise	15	50	1	28 wt. %
D: Novozym® 435 content	Minimise	1.5	4.5	5	3.3 wt. %
E: Temperature	In range	30	50	1	44 °C
Relative conversion to oxirane	Maximise	67.4	100	5	73 %
Relative ethylenic unsaturation	Minimise	0	100	1	16 %
Selectivity	Maximise	0	100	1	91 %

epoxidation process factors have been optimised to reach as high as possible RCO value while keeping the Novozym® 435 content as low as possible. The optimised RCO yield was 73 % which was achieved after only 5.5 h of TOFA epoxidation. The RCO yield of 73 % corresponds to 6.6 % of the oxirane oxygen content in the compound, which is comparably high value. A comparable oxirane oxygen content of 6.4 % was achieved for epoxidation of Vietnam rubber seed oil, which has similar initial iodine value as TOFA of 147 g I_2/100 g [80]. The relatively high epoxy group yield allows using the developed ETOFA for bio-polyol synthesis, which will be explored in future studies.

3.4. Investigation of the tall oil fatty acid chemical changes during the epoxidation process

FTIR spectroscopy was used to investigate the chemical transformation of TOFA into ETOFA during the epoxidation process. Fig. 6a illustrates the overall FTIR spectra in the absorption spectrum for TOFA epoxidation using tailored synthesis parameters. The =C–H stretching peak of unsaturated TOFA at 3010 cm^{-1} dropped during the epoxidation process, while the C–O–C oxirane ring stretching vibration peak at 825 cm^{-1} increased. Absorption peaks characteristic for tall oil, $–CH_2–$ symmetric stretching at ~2936 cm^{-1} and asymmetric stretching at ~2865 cm^{-1}, were identified. Fig. 6b shows a close-up of the =C–H stretching peak at 3010 cm^{-1}, gradually decreasing during epoxidation. After 7 h of synthesis, the =C–H peak faded. This means that the double bonds were almost entirely converted. The measured unsaturated bond conversion of 84 % was calculated from the iodine value. By the 7th hour of synthesis, the iodine value of TOFA had fallen from 155 to 25 g I_2 per 100 g of oil. The progressive development of the C–O–C oxirane ring stretching vibration peak at 825 cm^{-1} indicated the introduction of the oxirane rings into the TOFA structure (Fig. 6c), which coincides with the data of RCO at the 7th synthesis hour of 78 % (OO_{ex} = 6.9 %; [OO_{ex}] = 4.32 mmol/g).

An undesired oxirane ring-opening side reactions with carboxylic groups of free TOFA occurred during the TOFA epoxidation. The distinctive change of the carboxyl group peak depicted in Fig. 6d confirms the dimerisation of the ETOFA. A single peak of the carboxyl group at 1707 cm^{-1} of neat TOFA developed a shoulder peak of the ester carboxyl group at 1737 cm^{-1} during the epoxidation process. The ETOFA dimerisation process is undesirable since it increases the end

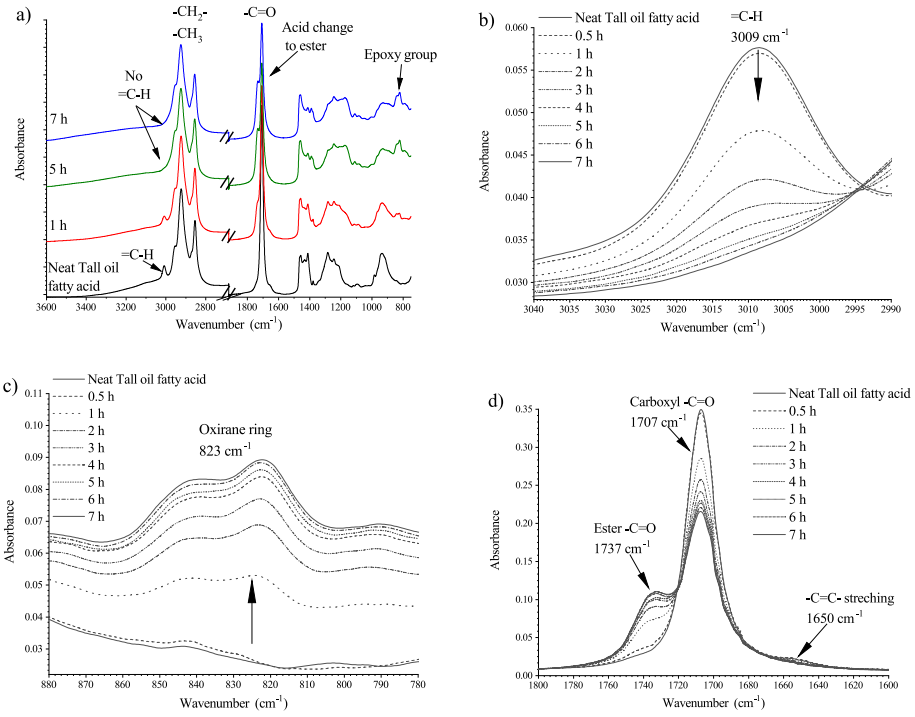

Fig. 6. FTIR spectra during tall oil fatty acid epoxidation for H_2O_2/C=C/ 2.0/1.1; H_2O_2 wt. % = 35 %; Novozym® 435 = 3.0 wt. %; temperature = 40 °C a) overall FTIR spectra b) change of =C–H at 3009 cm^{-1}, c) change of oxirane ring vibration, 823 cm^{-1}, d) change of –C=O stretching vibration absorption band, ~ 1707 cm^{-1}.

product's viscosity and reduces the yield of oxirane groups. The dimerisation of ETOFA could be circumvented by the initial derivatisation of TOFA to TOFA methyl esters. Nevertheless, the derivatisation of TOFA would be an additional synthesis step that is undesired from an economic nor sustainability perspective.

3.5. NMR analysis of synthesised epoxidised tall oil fatty acids

The change of TOFA during the epoxidation process was studied using ^{1}H and ^{13}C NMR spectra. The ^{1}H NMR spectra of TOFA and ETOFA in Fig. 7. shows the distinctive signal for linoleic acid, which is *bis*-allylic protons at 2.8 ppm. The signal intensity of allylic protons between 1.9 and 2.1 ppm was used to determine the amount of oleic acid. The ratio of fatty acids (oleic and linoleic) is 1:1, the oleic and linoleic acids form the majority of TOFA. The typical signal between 5.1 and 5.7 ppm was used to assess the presence of double bonds.

The ^{1}H NMR spectra of neat TOFA and two different ETOFA are compared in Fig. 7. ETOFA with the maximum RCO value of 80.9 % ($[OO_{ex}] = 4.48$ mmol/g) obtained in this study is compared with ETOFA with the RCO value of 41.5 % ($[OO_{ex}] = 2.31$ mmol/g), which was used for polyol synthesis with high OH group functionality [81]. Abbreviations of ETOFA_Novozym®_435 and ETOFA_Amberlite_IR-120_H are attributed to respective ETOFA. ETOFA_Amberlite_IR-120_H was synthesised using an ion exchange resin catalyst, which is far less effective than Novozym® 435.

The ^{1}H NMR spectra clearly demonstrated that the conversion of double bonds is complete when the epoxidation process was catalysed by Novozym® 435. The signals from epoxide moiety are located at 2.9–3.1 ppm. According to the ratio of integrals presenting oxirane moiety, around 80 % of double bonds are converted to epoxides, which agrees with the RCO value of 80.9 %. The absence of signals at 5.1–5.7 ppm establishes the complete conversion of double bonds. The rest of the double bonds have formed epoxides, but cleavage with *O*-nucleophile occurred, and various alcohols, esters or ethers were formed. The cleavage products are confirmed by small signals in the range of 3.3–4.5 ppm. According to ^{13}C NMR spectra (Fig. 8), up to 5 different oxirane moieties (9 different signals in the range 54–58 ppm) may form – monoepoxides with different stereocenters from oleic acid, diepoxides with different stereochemistry from linoleic, as well as monoepoxides from linoleic acid where one of the epoxide functions is cleaved.

When ion exchange resin was used as the catalyst, the yield of oxirane was significantly reduced (ETOFA_Amberlite_IR-120_H sample). Despite the formation of the oxirane moiety, a large amount of oxirane cleavage products were found. This was indicated by a signal between 3.3 and 4.5 ppm. The synthesised mixture contained less than 20 % epoxide moieties, as seen in the ^{1}H NMR spectra from the signal of double bonds. The double bond conversion was not complete. Not all double bonds were converted, as indicated by the signal between 5.1 and 5.7 ppm. The low amount of epoxide moieties could be explained by the old age of ETOFA_Amberlite_IR-120_H sample, as the NMR spectra were obtained after several months from the TOFA epoxidation with ion exchange resin.

4. Conclusions

A solvent-free chemo-enzymatic epoxidation of tall oil fatty acids was devised and optimised to reach as high as possible yield of oxirane groups while using as low as possible amount of *Candida antarctica* lipase B enzyme-based catalyst., It was possible to obtain a much higher conversion to oxirane (up to 80.9 %) using Novozym® 435 as an epoxidation catalyst than in the case of an ion exchange resin catalyst. Furthermore, the chemo-enzymatic epoxidation yielded a cleaner product with fewer undesired oxirane cleavage products. The optimal tall oil fatty acid epoxidation parameters were as follows: synthesis time of 5.5 h; TOFA/H_2O_2 molar ratios of 1.0/2.0; H_2O_2 concentration of 28

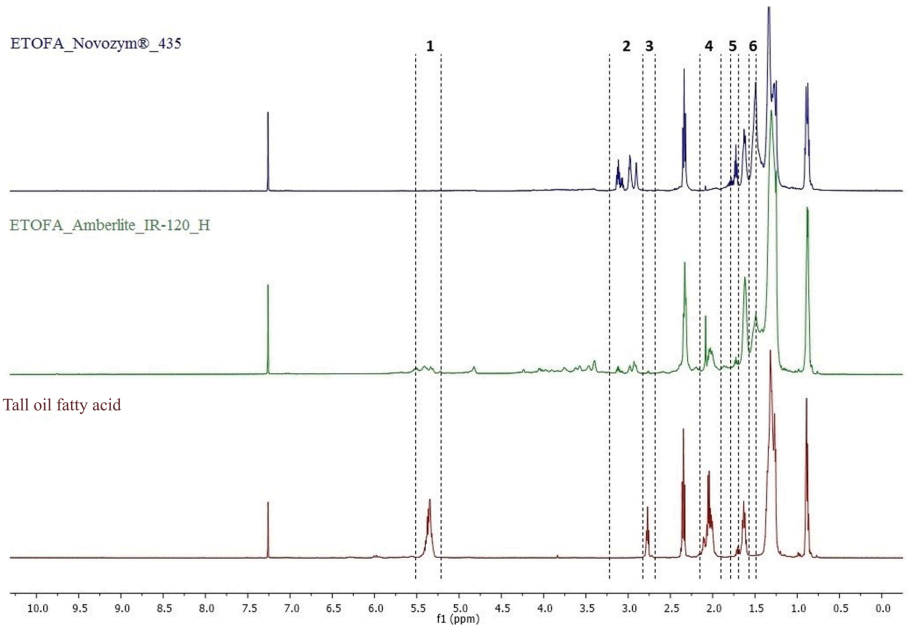

Fig. 7. ^{1}H NMR of tall oil fatty acid and epoxidised tall oil fatty acids (catalysed by ion-exchange resin (ETOFA_Amberlite_IR-120_H) and Lipase enzyme (ETOFA_Novozym®_435)) (500 MHz, $CDCl_3$). Abbreviations: 1 – protons of the double bond; 2 – protons at oxirane ring; 3 – protons of *bis*-allylic position; 4 – protons of allylic position; 5 – CH_2 protons of oxiran-2-yl moiety; 6 – CH_2 protons of *bis*-(oxiran-2-yl) moiety.

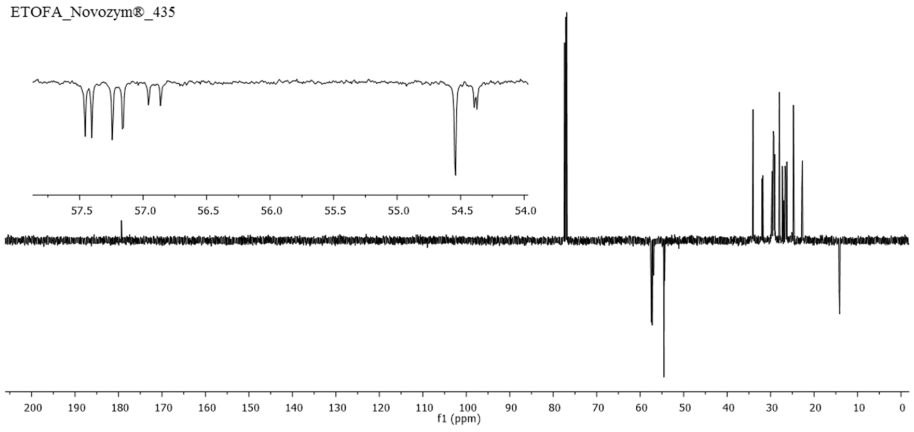

Fig. 8. ^{13}C NMR spectra of epoxidized tall oil fatty acid - ETOFA_Novozym®_435 (the signals of epoxide moiety are zoomed)) (126 MHz, $CDCl_3$).

%; Novozym® 435 content of 3.3 %, and synthesis temperature of 44 °C. Tall oil fatty acid epoxidation under such conditions yielded an RCO value of 73 % ($[OO_{ex}]$ = 4.06 mmol/g) which is high enough to be further used as a precursor for high functionality bio-polyol synthesis. Further development of TOFA epoxidation is necessary as the commercial viability of the proposed process is only possible if Novozym® 435 is recycled and reused for several batch syntheses.

CRediT authorship contribution statement

Conceptualisation, M.K.; formal analysis, M.K., E.V. and A.A.; investigation, A.A., E.V., R.P., I.M. and A.F.; writing—original draft preparation, M.K, R.P. and I.M.; writing—review and editing, A.F., I.M., and M.K.; visualisation, M.K.; supervision, M.K. All authors contributed to data analysis and manuscript writing.

Data availability

The authors declare that all data supporting the findings of this study are available within the article. Extra data are available from the corresponding author upon request.

Declaration of Competing Interest

The authors declare that they have no known competing financial interests or personal relationships that could have appeared to influence the work reported in this paper.

Data availability

No data was used for the research described in the article.

Acknowledgements

- This research is supported/funded by the Latvian Council of Science, project Forest industry by-product transformation into valuable biopolyols using advanced heterogeneous phase biocatalyst and characterization of the process kinetics (FORinPOL), grant No. lzp-2018/ 2-0020.
- Special acknowledgement to Novozymes A/S, Denmark who kindly supplied a sample of Novozym® 435 (on acrylic resin immobilised Lipase enzyme catalyst).

Appendix A. Supporting information

Supplementary data associated with this article can be found in the online version at doi:10.1016/j.procbio.2022.08.024.

References

[1] E. Jong, H. Stichnothe, G. Bell, H. Jørgensen, IEA Bioenergy Task 42 - Bio-Based Chemicals: a 2020 Update (2020).

[2] C. Zhang, T.F. Garrison, S.A. Madbouly, M.R. Kessler, Recent advances in vegetable oil-based polymers and their composites, Prog. Polym. Sci. 71 (2017) 91–143, https://doi.org/10.1016/j.progpolymsci.2016.12.009.

[3] J.S. Gregg, J. Jürgens, M.K. Happel, N. Strøm-Andersen, A.N. Tanner, S. Bolwig, A. Klitkou, Valorization of bio-residuals in the food and forestry sectors in support of a circular bioeconomy: a review, J. Clean. Prod. 267 (2020), 122093, https://doi.org/10.1016/j.jclepro.2020.122093.

[4] R.A. Sheldon, Green chemistry, catalysis and valorization of waste biomass, J. Mol. Catal. A Chem. 422 (2016) 3–12, https://doi.org/10.1016/j.molcata.2016.01.013.

[5] C. Caullet, J. Le Nôtre, Vegetable Oil Biorefineries, Elsevier B.V, 2015, https://doi.org/10.1016/B978-0-444-63453-5.00007-0.

[6] S.G. Tan, W.S. Chow, Biobased epoxidized vegetable oils and its greener epoxy blends: a review, Polym. - Plast. Technol. Eng. 49 (2010) 1581–1590, https://doi.org/10.1080/03602559.2010.512338.

[7] T. Saurabh, M. Patnaik, S.L. Bhagt, V.C. Renge, Epoxidation of vegetable oils: a review, Int. J. Adv. Eng. Technol. 2 (2011) 491–501.

[8] A. Campanella, E. Rustoy, A. Baldessari, M.A. Baltanás, Lubricants from chemically modified vegetable oils, Bioresour. Technol. 101 (2010) 245–254, https://doi.org/10.1016/j.biortech.2009.08.035.

[9] X. Wu, X. Zhang, S. Yang, H. Chen, D. Wang, Study of epoxidized rapeseed oil used as a potential biodegradable lubricant, J. Am. Oil Chem. Soc. 77 (2000) 561–563, https://doi.org/10.1007/s11746-000-0089-2.

[10] A.F. Aguilera, P. Tolvanen, J. Wärnå, S. Leveneur, T. Salmi, Kinetics and reactor modelling of fatty acid epoxidation in the presence of heterogeneous catalyst, Chem. Eng. J. 375 (2019), 121936, https://doi.org/10.1016/j.cej.2019.121936.

[11] W. Zhang, J. Wu, S. Yu, Y. Shen, Y. Wu, B. Chen, K. Nie, X. Zhang, Modification and synthesis of low pour point plant-based lubricants with ionic liquid catalysis, Renew. Energy 153 (2020) 1320–1329, https://doi.org/10.1016/j.renene.2020.02.067.

[12] E. Brenna, D. Colombo, G. Di Lecce, F.G. Gatti, M.C. Ghezzi, F. Tentori, D. Tessaro, M. Viola, Conversion of oleic acid into azelaic and pelargonic acid by a chemo-enzymatic route, Molecules 25 (2020) 1–11, https://doi.org/10.3390/molecules25081882.

[13] M.A. Sawpan, Polyurethanes from vegetable oils and applications: a review, J. Polym. Res. 25 (2018), https://doi.org/10.1007/s10965-018-1578-3.

[14] P.T. Wai, P. Jiang, Y. Shen, P. Zhang, Q. Gu, Y. Leng, Catalytic developments in the epoxidation of vegetable oils and the analysis methods of epoxidized products, RSC Adv. 9 (2019) 38119–38136, https://doi.org/10.1039/c9ra05943a.

[15] N.E. Marcovich, M. Kuranska, A. Prociak, E. Malewska, S. Bujok, The effect of different palm oil based bio-polyols on foaming process and selected properties of porous polyurethanes, Polym. Int. 66 (2017) 1522–1529, https://doi.org/DOI 10.1002/pi.5408.

[16] R. Mungroo, N.C. Pradhan, V.V. Goud, A.K. Dalai, Epoxidation of canola oil with hydrogen peroxide catalyzed by acidic ion exchange resin, J. Am. Oil Chem. Soc. 85 (2008) 887–896, https://doi.org/10.1007/s11746-008-1277-z.

[17] T.S. Omonov, E. Kharraz, J.M. Curtis, The epoxidation of canola oil and its derivatives, RSC Adv. 6 (2016) 92874–92886, https://doi.org/10.1039/c6ra17732h.
[18] S. Sinadinovic-Fiser, M. Jankovi, O. Borota, Epoxidation of castor oil with peracetic acid formed in situ in the presence of an ion exchange resin, Chem. Eng. Process. Process. Intensif. 62 (2012) 106–113, https://doi.org/10.1016/j.cep.2012.08.005.
[19] P.D. Meshram, R.G. Puri, H.V. Patil, Epoxidation of Wild Safflower (Carthamus oxyacantha) Oil with Peroxy acid in presence of strongly Acidic Cation Exchange Resin IR- 122 as Catalyst, Int. J. ChemTech Res 3 (2011) 1152–1163.
[20] E. Santacesaria, R. Tesser, M. Di Serio, R. Turco, V. Russo, D. Verde, A biphasic model describing soybean oil epoxidation with H2O2in a fed-batch reactor, Chem. Eng. J. 173 (2011) 198–209, https://doi.org/10.1016/j.cej.2011.05.018.
[21] V. Casson Moreno, V. Russo, R. Tesser, M. Di Serio, E. Salzano, Thermal risk in semi-batch reactors: the epoxidation of soybean oil, Process Saf. Environ. Prot. 109 (2017) 529–537, https://doi.org/10.1016/j.psep.2017.05.001.
[22] H. Lu, S. Sun, Y. Bi, G. Yang, R. Ma, H. Yang, Enzymatic epoxidation of soybean oil methyl esters in the presence of free fatty acids, Eur. J. Lipid Sci. Technol. 112 (2010) 1101–1105, https://doi.org/10.1002/ejlt.201000041.
[23] J.V. de Quadros, R. Giudici, Epoxidation of soybean oil at maximum heat removal and single addition of all reactants, Chem. Eng. Process. Process. Intensif. 100 (2016) 87–93, https://doi.org/10.1016/j.cep.2015.11.007.
[24] S. Dinda, A.V. Patwardhan, V.V. Goud, N.C. Pradhan, Epoxidation of cottonseed oil by aqueous hydrogen peroxide catalysed by liquid inorganic acids, Bioresour. Technol. 99 (2008) 3737–3744, https://doi.org/10.1016/j.biortech.2007.07.015.
[25] J.L. Zheng, J. Wärnå, T. Salmi, F. Burel, B. Taouk, S. Leveneur, Kinetic modeling strategy for an exothermic multiphase reactor system: Application to vegetable oils epoxidation using Prileschajew method, AIChE J. 62 (2016) 726–741, https://doi.org/10.1002/aic.15037.
[26] J.C. de Haro, I. Izarra, J.F. Rodríguez, Á. Pérez, M. Carmona, Modelling the epoxidation reaction of grape seed oil by peracetic acid, J. Clean. Prod. 138 (2016) 70–76, https://doi.org/10.1016/j.jclepro.2016.05.015.
[27] V.V. Goud, A.V. Patwardhan, S. Dinda, N.C. Pradhan, Kinetics of epoxidation of jatropha oil with peroxyacetic and peroxyformic acid catalysed by acidic ion exchange resin, Chem. Eng. Sci. 62 (2007) 4065–4076, https://doi.org/10.1016/j.ces.2007.04.038.
[28] A.S.A. Hazmi, M.M. Aung, L.C. Abdullah, M.Z. Salleh, M.H. Mahmood, Producing Jatropha oil-based polyol via epoxidation and ring opening, Ind. Crops Prod. 50 (2013) 563–567, https://doi.org/10.1016/j.indcrop.2013.08.003.
[29] B.W. Chieng, N.A. Ibrahim, Y.Y. Then, Y.Y. Loo, Epoxidized jatropha oil as a sustainable plasticizer to poly(lactic acid), Polymers (Basel) 9 (2017) 1–10, https://doi.org/10.3390/polym9060204.
[30] M. Kirpluks, E. Vanags, A. Abolins, A. Fridrihsone, U. Cabulis, Chemo-enzymatic oxidation of tall oil fatty acids as a precursor for further polyol production, J. Clean. Prod. 215 (2019) 390–398, https://doi.org/10.1016/j.jclepro.2018.12.323.
[31] A. Kadam, M. Pawar, O. Yemul, V. Thamke, K. Kodam, Biodegradable biobased epoxy resin from karanja oil, Polymer (Guildf.) 72 (2015) 82–92, https://doi.org/10.1016/j.polymer.2015.07.002.
[32] V.V. Goud, A.V. Patwardhan, S. Dinda, N.C. Pradhan, Epoxidation of karanja (Pongamia glabra) oil catalysed by acidic ion exchange resin, Eur. J. Lipid Sci. Technol. 109 (2007) 575–584, https://doi.org/10.1002/ejlt.200600298.
[33] P.G. Nihul, S.T. Mhaske, V.V. Shertukde, Epoxidized rice bran oil (ERBO) as a plasticizer for poly(vinyl chloride) (PVC), Iran. Polym. J. (Engl. Ed. 23 (2014) 599–608, https://doi.org/10.1007/s13726-014-0254-7.
[34] M.S. Silva, H. Arimatéia Júnior, G.F. Silva, A.A. Dantas Neto, T.N.Castro Dantas, New formulations for hydraulic biolubricants based on epoxidized vegetable oils: passion fruit (Passiflora edulis sims f. flavicarpa degener) and moringa (Moringa oleifera lamarck), Braz. J. Pet. Gas. 9 (2015) 27–36, https://doi.org/10.5419/bjpg2015-0004.
[35] A.E.V. Hagström, U. Törnvall, M. Nordblad, R. Hatti-Kaul, J.M. Woodley, Chemo-enzymatic epoxidation-process options for improving biocatalytic productivity, Biotechnol. Prog. 27 (2011) 67–76, https://doi.org/10.1002/btpr.504.
[36] X. Cai, J.L. Zheng, A.F. Aguilera, L. Vernières-Hassimi, P. Tolvanen, T. Salmi, S. Leveneur, Influence of ring-opening reactions on the kinetics of cottonseed oil epoxidation, Int. J. Chem. Kinet. 50 (2018) 726–741, https://doi.org/10.1002/kin.21208.
[37] H. Rakotondramaro, J. Wärnå, L. Estel, T. Salmi, S. Leveneur, Cooling and stirring failure for semi-batch reactor: application to exothermic reactions in multiphase reactor, J. Loss Prev. Process Ind. 43 (2016) 147–157, https://doi.org/10.1016/j.jlp.2016.05.011.
[38] S. Leveneur, Thermal safety assessment through the concept of structure-reactivity: application to vegetable oil valorization, Org. Process Res. Dev. 21 (2017) 543–550, https://doi.org/10.1021/acs.oprd.6b00405.
[39] S. Leveneur, M. Pinchard, A. Rimbault, M. Safdari Shadloo, T. Meyer, Parameters affecting thermal risk through a kinetic model under adiabatic condition: application to liquid-liquid reaction system, Thermochim. Acta 666 (2018) 10–17, https://doi.org/10.1016/j.tca.2018.05.024.
[40] N. Zora, T. Rigaux, J.-C. Buvat, D. Lefebvre, S. Leveneur, Influence assessment of inlet parameters on thermal risk and productivity: application to the epoxidation of vegetable oils, J. Loss Prev. Process Ind. 72 (2021), 104551, https://doi.org/10.1016/j.jlp.2021.104551.
[41] J.E. da, S. Souza, G.P. de Oliveira, J.Y.N.H. Alexandre, J.G.L. Neto, M.B. Sales, P. G. de, S. Junior, A.L.B. de Oliveira, M.C.M. de Souza, J.C.S. dos Santos, A Comprehensive Review on the Use of Metal–Organic Frameworks (MOFs) Coupled with Enzymes as Biosensors, Electrochem 3 (2022) 89–113, https://doi.org/10.3390/electrochem3010006.
[42] D. Remonatto, R.H. Miotti Jr., R. Monti, J.C. Bassan, A.V. de Paula, Applications of immobilized lipases in enzymatic reactors: a review, Process Biochem 114 (2022) 1–20, https://doi.org/10.1016/j.procbio.2022.01.004.
[43] D. Remonatto, J.V. Oliveira, J.M. Guisan, D. Oliveira, J. Ninow, G. Fernandez-Lorente, Immobilization of eversa lipases on hydrophobic supports for ethanolysis of sunflower oil solvent-free, Appl. Biochem. Biotechnol. 194 (2022) 2151–2167, https://doi.org/10.1007/s12010-021-03774-8.
[44] U.M.F. de Oliveira, L.J.B. Lima de Matos, M.C.M. de Souza, B.B. Pinheiro, J.C. S. dos Santos, L.R.B. Gonçalves, Efficient biotechnological synthesis of flavor esters using a low-cost biocatalyst with immobilized Rhizomucor miehei lipase, Mol. Biol. Rep. 46 (2019) 597–608, https://doi.org/10.1007/s11033-018-4514-z.
[45] R.M. Bezerra, R.R.C. Monteiro, D.M.A. Neto, F.F.M. da Silva, R.C.M. de Paula, T.L. G. de Lemos, P.B.A. Fechine, M.A. Correa, F. Bohn, L.R.B. Gonçalves, J.C.S. dos Santos, A new heterofunctional support for enzyme immobilization: PEI functionalized Fe3O4 MNPs activated with divinyl sulfone. Application in the immobilization of lipase from Thermomyces lanuginosus, Enzym. Microb. Technol. 138 (2020), 109560, https://doi.org/10.1016/j.enzmictec.2020.109560.
[46] N.S. Rios, E.G. Morais, W. dos Santos Galvão, D.M. Andrade Neto, J.C.S. dos Santos, F. Bohn, M.A. Correa, P.B.A. Fechine, R. Fernandez-Lafuente, L.R. B. Gonçalves, Further stabilization of lipase from Pseudomonas fluorescens immobilized on octyl coated nanoparticles via chemical modification with bifunctional agents, Int. J. Biol. Macromol. 141 (2019) 313–324, https://doi.org/10.1016/j.ijbiomac.2019.09.003.
[47] M. Rüsch Gen. Klaas, S. Warwel, Complete and partial epoxidation of plant oils by lipase-catalyzed perhydrolysis, Ind. Crops Prod. 9 (1999) 125–132, https://doi.org/10.1016/S0926-6690(98)00023-5.
[48] R. de, C.S. Schneider, L.R.S. Lara, T.B. Bitencourt, M. da, G. Nascimento, M.R. dos, S. Nunes, Chemo-enzymatic epoxidation of sunflower oil methyl esters, J. Braz. Chem. Soc. 20 (2009) 1473–1477, https://doi.org/10.1590/S0103-50532009000800013.
[49] H. Lin, J.Y. Liu, H.B. Wang, A.A.Q. Ahmed, Z.L. Wu, Biocatalysis as an alternative for the production of chiral epoxides: a comparative review, J. Mol. Catal. B Enzym. 72 (2011) 77–89, https://doi.org/10.1016/j.molcatb.2011.07.012.
[50] S. Sun, X. Ke, L. Cui, G. Yang, Y. Bi, F. Song, X. Xu, Enzymatic epoxidation of Sapindus mukorossi seed oil by perstearic acid optimized using response surface methodology, Ind. Crops Prod. 33 (2011) 676–682, https://doi.org/10.1016/j.indcrop.2011.01.002.
[51] S. Sun, G. Yang, Y. Bi, H. Liang, Enzymatic epoxidation of corn oil by perstearic acid, J. Am. Oil Chem. Soc. 88 (2011) 1567–1571, https://doi.org/10.1007/s11746-011-1820-1.
[52] T. Vlček, Z.S. Petrović, Optimization of the chemoenzymatic epoxidation of soybean oil, J. Am. Oil Chem. Soc. 83 (2006) 247–252, https://doi.org/10.1007/s11746-006-1200-4.
[53] H.L. Bonazza, R.M. Manzo, J.C.S. dos Santos, E.J. Mammarella, Operational and thermal stability analysis of thermomyces lanuginosus lipase covalently immobilized onto modified chitosan supports, Appl. Biochem. Biotechnol. 184 (2018) 182–196, https://doi.org/10.1007/s12010-017-2546-9.
[54] J.J. Virgen-Ortíz, J.C.S. dos Santos, C. Ortiz, Á. Berenguer-Murcia, O. Barbosa, R. C. Rodrigues, R. Fernandez-Lafuente, Lecitase ultra: a phospholipase with great potential in biocatalysis, Mol. Catal. 473 (2019), 110405, https://doi.org/10.1016/j.mcat.2019.110405.
[55] K. da, S. Moreira, A.L.B. de Oliveira, L.S. d M. Júnior, R.R.C. Monteiro, T.N. da Rocha, F.L. Menezes, L.M.U.D. Fechine, J.C. Denardin, S. Michea, R.M. Freire, P.B. A. Fechine, M.C.M. Souza, J.C.S. dos Santos, Lipase from rhizomucor miehei immobilized on magnetic nanoparticles: performance in fatty acid ethyl ester (FAEE) optimized production by the taguchi method, Front. Bioeng. Biotechnol. 8 (2020), https://doi.org/10.3389/fbioe.2020.00693.
[56] L. Fernandez-Lopez, R. Bartolome-Cabrero, M.D. Rodriguez, C.S. Dos Santos, N. Rueda, R. Fernandez-Lafuente, Stabilizing effects of cations on lipases depend on the immobilization protocol, RSC Adv. 5 (2015) 83868–83875, https://doi.org/10.1039/c5ra18344h.
[57] A. Melo, F. Silva, J. dos Santos, R. Fernández-Lafuente, T. Lemos, F. Dias Filho, Synthesis of benzyl acetate catalyzed by lipase immobilized in nontoxic chitosan-polyphosphate beads, Molecules 22 (2017) 2165, https://doi.org/10.3390/molecules22122165.
[58] N.S. Rios, D.M.A. Neto, J.C.S. dos Santos, P.B.A. Fechine, R. Fernández-Lafuente, L. R.B. Gonçalves, Comparison of the immobilization of lipase from Pseudomonas fluorescens on divinylsulfone or p-benzoquinone activated support, Int. J. Biol. Macromol. 134 (2019) 936–945, https://doi.org/10.1016/j.ijbiomac.2019.05.106.
[59] R.R.C. Monteiro, P.J.M. Lima, B.B. Pinheiro, T.M. Freire, L.M.U. Dutra, P.B. A. Fechine, L.R.B. Gonçalves, M.C.M. de Souza, J.C.S. Dos Santos, R. Fernandez-Lafuente, Immobilization of lipase a from Candida antarctica onto Chitosan-coated magnetic nanoparticles, Int. J. Mol. Sci. 20 (2019), https://doi.org/10.3390/ijms20164018.
[60] E.A. Manoel, M. Pinto, J.C.S. Dos Santos, V.G. Tacias-Pascacio, D.M.G. Freire, J. C. Pinto, R. Fernandez-Lafuente, Design of a core-shell support to improve lipase features by immobilization, RSC Adv. 6 (2016) 62814–62824, https://doi.org/10.1039/c6ra13350a.
[61] M. Samavi, S. Rakshit, Utilization of microbial oil from poplar wood hemicellulose prehydrolysate for the production of polyol using chemo-enzymatic epoxidation, Biotechnol. Bioprocess Eng. 25 (2020) 327–335, https://doi.org/10.1007/s12257-019-0416-8.
[62] F. Björkling, H. Frykman, S.E. Godtfredsen, O. Kirk, Lipase catalyzed synthesis of peroxycarboxylic acids and lipase mediated oxidations, Tetrahedron 48 (1992) 4587–4592, https://doi.org/10.1016/S0040-4020(01)81232-1.

[63] A. Demirbas, Methylation of wood fatty and resin acids for production of biodiesel, Fuel 90 (2011) 2273–2279, https://doi.org/10.1016/j.fuel.2011.02.037.
[64] J.M.R. Da Silva, T.B. Bitencourt, M.A. Moreira, M. Da Graça Nascimento, Enzymatic epoxidation of β-caryophyllene using free or immobilized lipases or mycelia from the Amazon region, J. Mol. Catal. B Enzym. 95 (2013) 48–54, https://doi.org/10.1016/j.molcatb.2013.05.021.
[65] W.S.D. Silva, A.A.M. Lapis, P.A.Z. Suarez, B.A.D. Neto, Enzyme-mediated epoxidation of methyl oleate supported by imidazolium-based ionic liquids, J. Mol. Catal. B Enzym 68 (2011) 98–103, https://doi.org/10.1016/j.molcatb.2010.09.019.
[66] X. Zhang, X. Wan, H. Cao, R. Dewil, L. Deng, F. Wang, T. Tan, K. Nie, Chemo-enzymatic epoxidation of Sapindus mukurossi fatty acids catalyzed with Candida sp. 99–125 lipase in a solvent-free system, Ind. Crops Prod. 98 (2017) 10–18, https://doi.org/10.1016/j.indcrop.2017.01.013.
[67] H. Hosney, E.G. Al-Sakkari, A. Mustafa, I. Ashour, I. Mustafa, A. El-Shibiny, A cleaner enzymatic approach for producing non-phthalate plasticiser to replace toxic-based phthalates, Clean. Technol. Environ. Policy 22 (2020) 73–89, https://doi.org/10.1007/s10098-019-01770-5.
[68] U. Törnvall, C. Orellana-Coca, R. Hatti-Kaul, D. Adlercreutz, Stability of immobilized Candida antarctica lipase B during chemo-enzymatic epoxidation of fatty acids, Enzym. Microb. Technol. 40 (2007) 447–451, https://doi.org/10.1016/j.enzmictec.2006.07.019.
[69] W.S. Galvão, B.B. Pinheiro, L.R.B. Golçalves, M.C. de Mattos, T.S. Fonseca, T. Regis, D. Zampieri, J.C.S. dos Santos, L.S. Costa, M.A. Correa, F. Bohn, P.B. A. Fechine, Novel nanohybrid biocatalyst: application in the kinetic resolution of secondary alcohols, J. Mater. Sci. 53 (2018) 14121–14137, https://doi.org/10.1007/s10853-018-2641-5.
[70] D.M. Liu, C. Dong, Recent advances in nano-carrier immobilized enzymes and their applications, Process Biochem 92 (2020) 464–475, https://doi.org/10.1016/j.procbio.2020.02.005.
[71] S. Zahirinejad, R. Hemmati, A. Homaei, A. Dinari, S. Hosseinkhani, S. Mohammadi, F. Vianello, Nano-organic supports for enzyme immobilization: Scopes and perspectives, , Colloids Surf. B Biointerfaces 204 (2021), 111774, https://doi.org/10.1016/j.colsurfb.2021.111774.
[72] Y.L. Nunes, F.L. de Menezes, I.G. de Sousa, A.L.G. Cavalcante, F.T.T. Cavalcante, K. da Silva Moreira, A.L.B. de Oliveira, G.F. Mota, J.E. da Silva Souza, I.R. de Aguiar Falcão, T.G. Rocha, R.B.R. Valério, P.B.A. Fechine, M.C.M. de Souza, J.C. S. dos Santos, Chemical and physical Chitosan modification for designing enzymatic industrial biocatalysts: how to choose the best strategy? Int. J. Biol. Macromol. 181 (2021) 1124–1170, https://doi.org/10.1016/j.ijbiomac.2021.04.004.
[73] J. Chapman, A.E. Ismail, C.Z. Dinu, Industrial applications of enzymes: recent advances, techniques, and outlooks, Catalysts 8 (2018) 238, https://doi.org/10.3390/catal8060238.
[74] T. Ohra-Aho, J. Ropponen, T. Tamminen, Thermochemolysis using TMAAc and TMAH reagents as means to differentiate between free acids and esters, J. Anal. Appl. Pyrolysis 103 (2013) 31–35, https://doi.org/10.1016/j.jaap.2012.09.015.
[75] G.D. Yadav, K.Manjula Devi, A kinetic model for the enzyme-catalyzed self-epoxidation of oleic acid, J. Am. Oil Chem. Soc. 78 (2001) 347–351, https://doi.org/10.1007/s11746-001-0267-2.
[76] J. Meyer-Waßewitz, D. Elyorgun, C. Conradi, A. Drews, Dynamic modeling of the chemo-enzymatic epoxidation of & α-pinene and prediction of continuous process performance, Chem. Eng. Res. Des. 134 (2018) 463–475, https://doi.org/10.1016/j.cherd.2018.04.029.
[77] R. Anderson, D. Reid, P. Hart, A. Rudie, Hydrogen peroxide safe storage and handling, TAPPI Stand. Tech. Inf. Pap. Useful Methods, Norcross, GA (2010) 1–8.
[78] R.H. Myers, D.C. Monthgomery, C.M. Anderson-Cook, Response surface methodology: process and product optimization using designed experiments, Fourth Edi, Hoboken, N. Jersey (2016).
[79] P.K. Gamage, M.O. Brien, L. Karunanayake, Epoxidation of some vegetable oils and their hydrolysed products with peroxyformic acid - optimised to industrial scale 37 (2009) 229–240.
[80] N.T. Thuy, P.N. Lan, Epoxidation of vietnam rubber seed oil by using peroxophosphatotungstate catalyst complex based on Na2WO4/H3PO4/H2O2 with the presence of phase-transfer catalyst, Mol. Catal. 509 (2021), 111645, https://doi.org/10.1016/j.mcat.2021.111645.
[81] M. Kirpluks, E. Vanags, A. Abolins, S. Michalowski, A. Fridrihsone, U. Cabulis, High functionality bio-polyols from tall oil and rigid polyurethane foams formulated solely using bio-polyols, Mater. (Basel) 13 (2020) 1985, https://doi.org/10.3390/MA13081985.

7. pielikums
Appendix 7

Epoxidation of tall oil fatty acids and tall oil fatty acids methyl esters using the SpinChem® rotating bed reactor

Krzysztof Polaczek, Elīza Kauliņa, Ralfs Pomilovskis, Anda Fridrihsone, Miķelis Kirpļuks

Journal of Polymers and the Environment, 2022

Journal of Polymers and the Environment (2022) 30:4774–4786
https://doi.org/10.1007/s10924-022-02556-5

ORIGINAL PAPER

Epoxidation of Tall Oil Fatty Acids and Tall Oil Fatty Acids Methyl Esters Using the SpinChem® Rotating Bed Reactor

Krzysztof Polaczek[1] · Eliza Kaulina[2] · Ralfs Pomilovskis[2,3] · Anda Fridrihsone[2] · Mikelis Kirpluks[2]

Accepted: 10 August 2022 / Published online: 24 August 2022
© The Author(s) 2022

Abstract

Tall oil fatty acids are a second-generation bio-based feedstock finding application in the synthesis of polyurethane materials. The study reported tall oil fatty acids and their methyl esters epoxidation in a rotating packed bed reactor. The chemical structure of the synthesized epoxidized tall oil fatty acids and epoxidized tall oil fatty acids methyl ester were studied by Fourier-transform infrared spectroscopy. Average molecular weight and dispersity were determined from gel permeation chromatography data. The feasibility of multiple uses of the Amberlite® IRC120 H ion exchange resin as a catalyst was investigated. Gel permeation chromatography chromatograms of epoxidized tall oil fatty acids clearly demonstrated the formation of oligomers during the epoxidation reaction. The results showed that methylation of tall oil fatty acids allows obtaining an epoxidized product with higher relative conversion to oxirane and much smaller viscosity than neat tall oil fatty acids. Epoxidation in a rotating packed bed reactor simplified the process of separating the catalyst from the reaction mixture. The Amberlite® IRC120 H catalyst exhibited good stability in the tall oil fatty acids epoxidation reaction.

Graphical Abstract

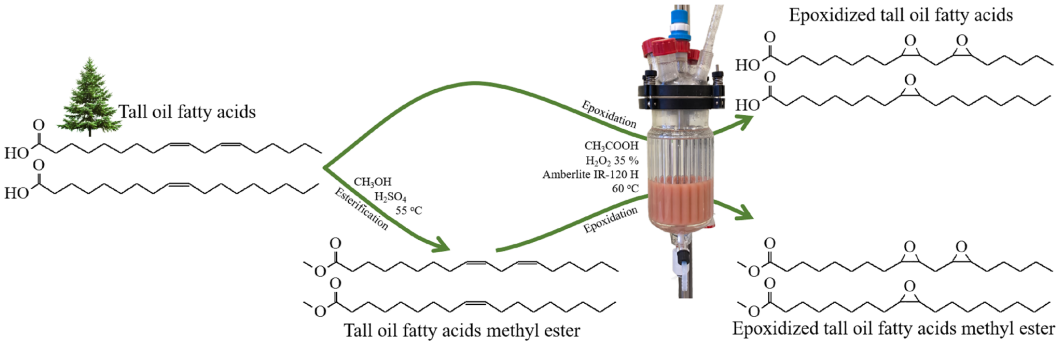

Keywords Tall oil fatty acids; tall oil methyl ester · Ion-exchange resin; epoxidation · Rotating bed reactor

✉ Krzysztof Polaczek
krzysztof.polaczek@doktorant.pk.edu.pl

[1] Department of Chemistry and Technology of Polymers, Cracow University of Technology, Warszawska 24, 31-155, Cracow, Poland

[2] Polymer Laboratory, Latvian State Institute of Wood Chemistry, Dzerbenes st. 27, Riga 1006, Latvia

[3] Institute of Technology of Organic Chemistry, Faculty of Materials Science and Applied Chemistry, Riga Technical University, P. Valdena St. 3/7, Riga 1048, Latvia

Introduction

The synthesis of polymeric materials with the principles of sustainability and cleaner production has been a widely researched topic in recent years. These principles are intended to reduce the environmental impact of products and production by reducing the use of fossil-based raw materials and replacing them with bio-based or waste/recycled

resources; reducing energy consumption through the use of more efficient processes and equipment; reducing or eliminating toxic and harmful raw materials; reducing the amount and toxicity of waste [1].

A widely available bio-based raw material with high potential in chemical synthesis is crude tall oil (CTO). CTO is a by-product of the wood pulp industry generated at an average rate of 30–50 kg per 1000 kg of processed wood [2]. World production of CTO is between 1.6 and 2 million tonnes/year, of which approximately 650 000 tonnes/year is produced in Europe [3]. CTO contains 30–50 wt.% of free fatty acids (mainly oleic and linolic acid), 15–35 wt.% of rosin acids and residues composed of sterols, fatty alcohols, phenols and hydrocarbons. CTO can be burned as an alternative to heavy fuel oil. However, CTO also can be used as a high-value feedstock for chemical syntheses after separation into various fractions, i.e. tall oil fatty acids (TOFA) and tall oil rosins (TOR). TOR are used as an ingredient in printing inks, adhesives, soaps, detergents, emulsifiers, sealing waxes and soldering fluxes [4]. TOFA is mainly used as a feedstock to produce tall oil fatty acids methyl ester (TOFAME) used as an alternative to diesel fuel [5]. TOFA can also be converted to hydrocarbons by hydrodeoxygenation/decarboxylation reactions [6, 7].

Moreover, TOFA also has been investigated as a potential raw material for the synthesis of bio-based polyols (bio-polyols). Polyols, conventionally petrochemical based, are one of the main components for the production of polyurethanes [8, 9]. The global market for polyols in 2019 was US$26.2 billion, and further growth is expected [10]. Commercially produced polyols are mainly made from non-renewable petrochemical feedstocks. In recent years, there has been an increase in the availability of commercial bio-polyols made from vegetable oils such as castor oil, soybean oil and palm oil [10, 11].

TOFA has several advantages in comparison to vegetable oil-based polyols. A significant advantage of TOFA is the high iodine value (about 155 g I_2/100 g) compared to vegetable oils (e.g., the iodine value of palm oil is 44–58 g I_2/100 g; the iodine value of rapeseed oil is 94–120 g I_2/100 g; the iodine value of soybean oil is 117–143 g I_2/100 g [12]). The higher iodine value indicates more unsaturated double bonds in the structure of fatty acids that can be chemically modified [13]. Moreover, TOFA is a second-generation feedstock and do not pose a concern about competition with food and feed supplies.

The most commonly used method for synthesizing bio-polyols from TOFA is a two-step process of epoxidation followed by oxirane ring-opening with proton donors [14]. The classical Prilezhaev epoxidation method uses peroxycarboxylic acids formed *in-situ* to oxidize the double bonds. Formic acid or acetic acid and hydrogen peroxide are most commonly used in this process [15]. The main disadvantage of the epoxidation of fatty acids is that the carboxyl groups of fatty acids react with hydrogen peroxide to form peroxy fatty acids which act as oxygen carriers, leading to extensive oxirane ring-opening and formation of oligomeric products [16, 17]. The use of heterogeneous catalysts such as acid ion exchange resins helps to reduce the occurrence of oxirane ring-opening side reactions compared to the use of heterogeneous catalysts such as H_2SO_4 [18, 19]. Heterogeneous catalysts can be easily separated from the reaction mixture, washed and reused, thus reducing process costs [20, 21].

A modern type of reactor that can facilitate the process of separating the catalyst from the reaction mixture is the rotating packed bed reactor (RBR), in which the catalyst is separated from the rest of the reaction mixture. The mixing occurs due to the centrifugal force generated by a rotating catalyst container. The use of the RBR leads to reduced energy consumption and the water needed to separate the catalyst from the reaction mixture. The literature describes studies where RBR was used for epoxidation of vegetable oils using ion exchange resin under conventional heating [22], oleic acid, TOFA and distilled tall oil under microwave irradiation [23], as well as epoxidation of oleic acid in the presence of ultrasound irradiation [24].

Polymer laboratory at Latvian State Institute of Wood Chemistry has studied the epoxidation of TOFA before. Kirpluks et al. studied the epoxidation process of TOFA under conventional heating [9, 17]. Studies on the epoxidation of TOFA using in-situ formed peracetic acid, catalyzed by the Amberlite® IRC120 H ion exchange resin, have confirmed that the resulting epoxidized TOFA is a mixture of monomers, dimers, trimers and oligomers [14, 17, 19]. Thus, the bio-polyols synthesized from ETOFA exhibited high viscosity, which significantly limits their potential application. The high viscosity of bio-polyols is undesirable as it complicates the large-scale production of rigid polyurethane foams [14].

The objective of this article was to compare the epoxidation of neat TOFA and their methyl ester with the use of an RBR reactor. Esterification of TOFA could help to reduce the occurrence of undesirable side reactions. The epoxidation reactions were carried out using varying catalyst content of 10, 15, 20 and 25 wt.%. The stability and reusability of the catalyst were also tested. The following characteristics were determined for obtained products: epoxy value, acid value and viscosity. The chemical structure of epoxidized TOFA and epoxidized TOFAME were studied by Fourier transform infrared spectroscopy and gel permeation chromatography.

Materials and Methods

Materials

The following reagents were used for synthesizing epoxidized TOFA and epoxidized TOFAME: TOFA (trade name

"FOR2") with a high content of fatty acids (> 96%), low content of rosin acids (1.9%), and unsaponifiables (1.8%) was ordered from Forchem Oyj (Rauma, Finland). The initial acid and iodine values for TOFA were 198 ± 1 mg KOH/g and 155 ± 1 g I_2/100 g, respectively. Acetic acid (AcOH), puriss. p.a., ACS reagent, reag. ISO, reag. Ph. Eur., ≥ 99.8% was ordered from Fluka (Seelze, Germany). Ethyl acetate (EtOAc), puriss., meets the analytical specifications of Ph. Eur., BP, NF, ≥ 99.5% (GC) was ordered from Riedel–de Haen (Seelze, Germany). Amberlite® IRC120 H, strongly acidic, hydrogen form, hydrogen peroxide (H_2O_2) 35%, methanol (MeOH), puriss. p.a., ACS reagent, reag. ISO, reag. Ph. Eur., ≥ 99.8% from Riedel–de Haen (Seelze, Germany), and sulfuric acid (H_2SO_4), puriss., meets the analytical specifications of Ph. Eur., BP, 95–97% were ordered from Sigma-Aldrich (Steinheim, Germany).

The following reagents were used for the analysis of TOFA and synthesized products: potassium hydroxide (KOH), ACS reagent, ≥ 85%, pellets, potassium phthalate monobasic (KHP), ACS reagent, acidimetric standard, chloroform, puriss. p.a., reag. ISO, reag. Ph. Eur., 99.0–99.4% (GC), perchloric acid, puriss. p.a., ACS reagent, reag. ISO, reag. Ph. Eur., 70.0–72.0%, tetraethylammonium bromide, reagent grade, 98%, acetic anhydride, puriss. p.a., ACS reagent, reag. ISO, reag. Ph. Eur., ≥ 99% (GC), N,N-dimethylformamide (DMF), anhydrous, 99.8%, 4-(dimethylamino) pyridine (DMAP), ReagentPlus, ≥ 99%, and potassium iodide (KI), ACS reagent, ≥ 99.0% were obtained from Sigma-Aldrich (Steinheim, Germany). Methanol (MeOH), puriss. p.a., ACS reagent, reag. ISO, reag. Ph. Eur., ≥ 99.8%, and dichloromethane, puriss. p.a., ACS reagent, reag. ISO, ≥ 99.9% were ordered from Riedel–de Haen (Seelze, Germany). Hanus solution, volumetric 0.1 M IBr, acetic acid (AcOH), puriss. p.a., ACS Reagent, Reag. ISO, Reag. Ph. Eur., ≥ 99.8%, and crystal violet, an indicator for determining the redox potential, S. No.:785 were ordered from Fluka (Seelze, Germany). Cresol red, indicator grade, was obtained from Alfa Aesar (Kandel, Germany). Sodium thiosulfate 0.1 mol/l (0.1 N) was ordered from Chempur (Karlsruhe, Germany).

Synthesis of TOFAME

The methylation of TOFA was carried out in a 2 l three-necked round bottom flask. The flask was immersed in a water bath equipped with a stirrer, a thermocouple, and a reflux condenser. The reaction conditions were chosen based on literature data [25]. The reaction temperature was 55 °C, and the reaction time was 30 min. The molar ratio of methanol to TOFA double bonds was 6:1. Catalyst content was 0.5 wt.% of TOFA. At first, 900 g of TOFA was added to the flask. The flask was immersed in the water bath, and the catalyst-methanol mixture (4.5 g of H_2SO_4 and 600 g MeOH) was added to the TOFA and stirred (100 rpm) under reflux. The reaction start time was assumed when the mixture reached the set temperature of 55 °C. After the reaction was completed, the mixture was poured into a separating funnel, and about 100 ml EtOAc was added. The bottom water-waste phase was poured out. The upper organic phase consisting of TOFAME was washed four times with warm distilled water at a temperature of 55 °C and then dried using a rotatory vacuum evaporator.

Synthesis of Epoxidized TOFA and Epoxidized TOFAME

Epoxidation was carried out using TOFA and TOFAME, resulting in epoxidized tall oil fatty acids (ETOFA) and epoxidized tall oil fatty acids methyl ester (ETOFAME). The synthesis scheme is given in Fig. 1.

The epoxidation of TOFA was carried out in a 1200 ml RBR, model V3 manufactured by Spinchem® (Sweden), as shown in Fig. 1. The reaction vessel is made of borosilicate glass. The rotating bed with a diameter of 70 mm and a height of 30 mm, the catalyst separation filter with a porosity of 104 µm and the shaft are made of stainless steel. The RBR was equipped with a heating/cooling jacket and a bottom drain. A thermocouple, dropping funnel, and a reflux condenser were attached to the 5-neck lid. A rotating bed filled with ion exchange resin was also used as a stirrer. The epoxidation of TOFA was carried out using peroxyacetic acid generated *in-situ* in the reaction of AcOH and H_2O_2 and using ion exchange resin as a catalyst. The molar ratio of TOFA double bonds to H_2O_2 to AcOH was 1.0:1.5:0.5. The mass of the catalyst was kept constant (40 g), while variable catalyst content of 10, 15, 20, and 25 wt.% in relation to the TOFA content was used.

At first, the calculated amount of TOFA and AcOH was added to the reactor. The initial set temperature of the jacket was 40 °C. The speed of the RBR was set to 400 rpm, and the mixture was started to stir. The calculated mass of H_2O_2 was added to the dropping funnel. After the reaction mixture reached a temperature of 40 °C, H_2O_2 was added during 60 min. The reaction temperature was increased by 5 °C at intervals of 15 min, finally setting the reaction temperature to 60 °C and running the reaction for 7 h total. The temperature of the reaction mixture did not exceed the set temperature by more than 2 °C. During the epoxidation, small amounts of product were collected every h by the bottom drain of RBR for analysis. Products were washed by adding EtOAc and warm distilled water at a temperature of 55 °C. The organic phase was washed 3 times with the addition of distilled water in a separating funnel. Products were dried using a rotatory vacuum evaporator to remove water and EtOAc residues. Fresh ion exchange resin was used for every

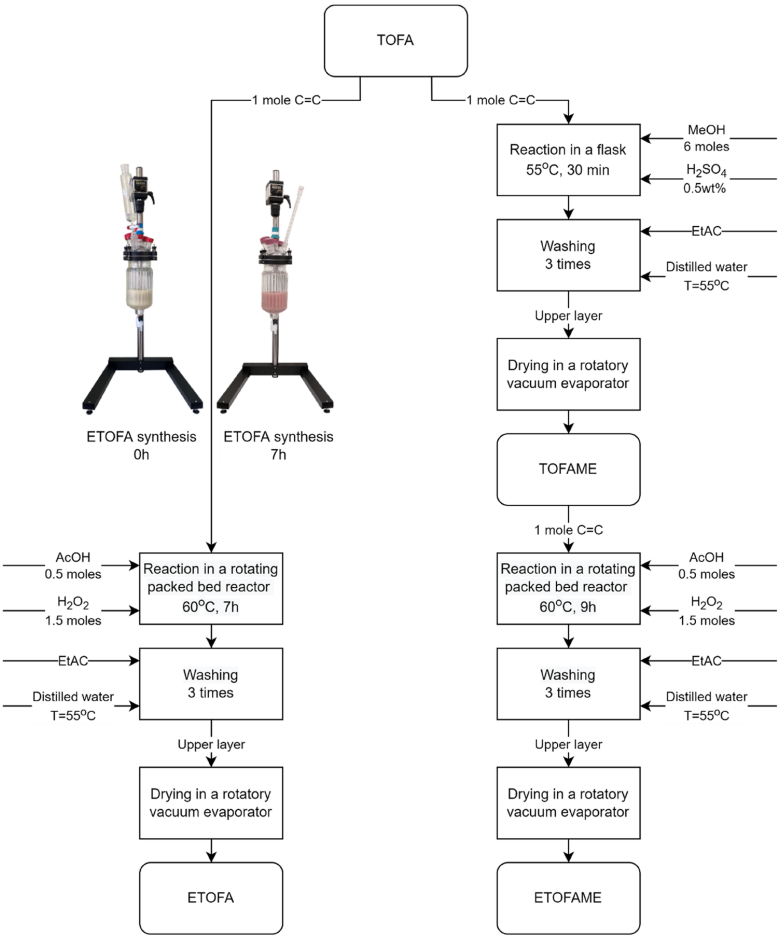

Fig. 1 The synthesis scheme of epoxidized TOFA or TOFAME

reaction. Reagent weights for TOFA or TOFAME epoxidation are given in Table 1.

The epoxidation synthesis of TOFAME was carried out in the same way as the TOFA epoxidation reaction. The overall reaction time was extended to 9 h to obtain additional information about the synthesis.

Reusability of Amberlite® IRC120 H Ion Exchange Resin in the Epoxidation of TOFA

Ten epoxidation reactions were performed to determine the reusability of the catalyst. Syntheses of ETOFA were carried out as described in Sect. "Synthesis of Epoxidized TOFA and Epoxidized TOFAME" with the difference that the catalyst was not removed from the synthesis media. The catalyst load for TOFA epoxidation was 20 wt.%. The reaction time was reduced to 4 h. The design of the RBR reactor allows the catalyst to be separated from the reaction mixture without any losses and additional operations such as filtration, washing and drying, as is the case when a batch reactor is used [19]. Separation of the reaction mixture from the catalyst in

Table 1 Reagent weights for TOFA or TOFAME epoxidation

Catalyst content*, wt.%	TOFA or TOFAME, g	H_2O_2, g	AcOH, g
10	400.0	356.1	74.1
15	266.7	237.4	49.4
20	200.0	178.1	37.0
25	160.0	142.4	29.6

*Catalyst content as weight percent from TOFA or TOFAME

the RBR reactor involves solely pouring it out through the bottom drain.

Methods of Analysis

The iodine value (IV) was determined according to ISO 3961:2018, and it is calculated by using Eq. (1).

$$IV = \frac{\left(V_b - V_s\right) \cdot c_t \cdot 12.69}{m_s} gI_2/100g \quad (1)$$

where V_b and V_s are volumes of sodium thiosulfate required for the blank and the sample, in ml, c_t is the concentration of sodium thiosulfate, in mol/l, m_s is the mass of the sample, in g. 12.96 is the conversion factor from milliequivalents sodium thiosulfate to grams of iodine.

Iodine value was used to determine fatty acid unsaturation ($n_{db,}$ moles of double bonds in gram of oil) by using Eq. (2).

$$n_{db} = \frac{IV}{M_{I_2} \cdot 100} mol/g \quad (2)$$

where M_{I2} is the molar mass of I_2, in g/mol.

The epoxy value (EV) (the content of oxirane rings) was determined according to ASTM D1652-11(2019) standard. Epoxy group content in moles per 100 g of oil was calculated by using Eq. (3).

$$EV = \frac{V_t \cdot c_t}{m_s \cdot 10} mol/100g \quad (3)$$

where V_t is volume, in ml, of titrant used, c_t is titrant concentration, in mol/l, m_s is mass of the sample.

The percentage of relative conversion of unsaturated bonds to oxirane (RCO) was calculated by Eq. (4) [26].

$$RCO = \frac{OO_{ex}}{OO_{th}} \cdot 100\% \quad (4)$$

where OO_{ex} is the experimentally determined content of oxirane (%), calculated by Eq. (5). The OO_{th} is the theoretical maximum oxirane content of oxirane in 100 g of fatty acids (%), which was calculated by Eq. (6).

$$OO_{ex} = A_O \cdot EV\% \quad (5)$$

where A_o is the atomic mass of oxygen.

$$OO_{th} = \frac{\left(\frac{IV_0}{2A_i}\right) \cdot A_o}{100 + \left(\frac{IV_0}{2A_i}\right) \cdot A_o} \cdot 100 \quad (6)$$

where A_i is the atomic mass of iodine, and IV_o is the initial iodine value of the fatty acid sample.

The relative ethylenic unsaturation (REU) was calculated by Eq. (7):

$$REU = \left(\frac{IV_{ex}}{IV_o}\right) \cdot 100\% \quad (7)$$

where IV_o is the initial iodine value, and IV_{ex} is the remaining iodine value during synthesis.

Hydroxyl value (HV) was determined according to ISO 4629–2:2016 standard and calculated by Eq. (8).

$$HV = \frac{\left(V_b - V_s\right) \cdot c_t \cdot 56.106}{m_s} mgKOH/g \quad (8)$$

where V_b, V_s are volumes, in ml, of potassium hydroxide required for the blank and the sample, respectively, c_t is the concentration of KOH, in mol/l m_s is the mass of the sample, in g. 56.106 is the molar mass of KOH, g/mol.

Acid value (AV) was determined according to ASTM D1980-87(1998) standard and calculated by Eq. (9).

$$AV = \frac{V_t \cdot c_t \cdot 56.106}{m_s} mgKOH/g \quad (9)$$

where V_t is the volume of titrant used, in ml, c_t is the concentration of KOH, in mol/l, m_s is the mass of the sample, in g. 56.106 is the molar mass of KOH, g/mol.

From the determined relative conversion to oxirane (Eq. 4) and relative ethylenic unsaturation (Eq. 7), the selectivity (S) of TOFA and TOFAME epoxidation reaction was calculated according to Eq. 10.

$$S = \frac{RCO}{100\% - REU} \quad (10)$$

The viscosity was measured at 25 °C using the Thermo Science HAAKE (Medium–High Range Rotational Viscometer, Thermo Fisher Scientific, Waltham, MA, USA).

The spectroscopic analysis of the chemical structure of the precursors and products was carried out using a Fourier-transform infrared spectrometer (FTIR) model iS50 (Thermo Fisher Scientific, Waltham, MA, USA) at a resolution of 4 cm^{-1} (32 scans) in the infrared range of 4000–500 cm^{-1}. The FTIR data were collected using an attenuated total reflectance (ATR) accessory with a diamond crystal.

An Agilent Infinity 1260 HPLC system (Agilent Technologies, Inc., Santa Clara, CA, USA) with degasser, autosampler, refractive index (RI) detector, and MALS (miniDAWN) detector was used to perform gel permeation chromatography (GPC) analysis. The analysis was performed using two GPC analytical columns connected in series: PLgel Mixed-E (3 uL, 300 × 7.5 mm). The flow rate was 1 ml/min, and the temperature of the RI detector was 35 °C. A total of two duplicate trials were carried out.

Results and Discussion

The epoxidations of TOFA and TOFAME were carried out using peracetic acid generated *in-situ* by the reaction of acetic acid and hydrogen peroxide. The kinetic curves of RCO increase depending on the applied catalyst content are presented in Fig. 2.

In the case of TOFA epoxidation (Fig. 2a), the application of 10 wt.% catalyst content resulted in RCO of 42.5% over a period of 6 h and a decrease in RCO to 40.1% at the seventh hour of the reaction, which corresponds to an EV of 0.237 mol/100 g and 0.223 mol/100 g, respectively. The reduction in the RCO implies that the oxirane ring-opening reactions occurred more intensively than the formation of new epoxy groups after the sixth hour. The increase in the catalyst content led to an increase in RCO to 47.5% after 7 h of the reaction (EV of 0.262 mol/100 g), 49.1% (EV of 0.275 mol/100 g), and 50.4% (EV of 0.281 mol/100 g) for 15, 20 and 25 wt.% of the catalyst content, respectively. The maximum RCO was reached after 5 h of reaction for the 15 and 20 wt.% of the catalyst content, while for the 25 wt.% of the catalyst content after 4 h of reaction. In a comparable experiment conducted in a batch reactor, the maximum RCO value achieved after 5 h of reaction at 20 wt.% catalyst content was 42.9% [19].

The kinetic curves of TOFAME are shown in Fig. 2b. The obtained epoxidized TOFAME exhibited significantly higher RCO in relation to TOFA of 65.2% (EV = 0.337 mol/100 g), 78.6% (EV = 0.406 mol/100 g), 81.0% (EV = 0.419 mol/100 g), 81.2% (EV = 0.420 mol/100 g) for catalyst content of 10, 15, 20 and 25 wt.%, respectively. Methylation of TOFA contributed to reducing side reactions caused by the opening of oxirane rings with a carboxyl group. All kinetic curves except the reaction catalyzed by 10 wt.% catalyst content showed virtually no increase in RCO after 7 h of the epoxidation reaction, which may be caused by side reactions occurring due to the presence of small amounts of fatty acids or by the reactions with acetic acid, peracetic acid, hydrogen peroxide or water [27].

For the TOFAME epoxidation (Fig. 2b), an RCO of about 50% is achieved between 2 and 3 h of reaction at catalyst content > 15 wt.%. In comparison, the same RCO was achieved between 4 and 6 h for TOFA epoxidation at the same catalyst concentrations. The shorter epoxidation time leads to lower costs of the epoxidation process.

The intensity of side reactions is affected by the content of carboxyl groups in the fatty acid. The synthesized TOFAME had an average AV of 39.95 mg KOH/g (the average AV of TOFA was 198.03 mg KOH/g), indicating that not all carboxyl groups were esterified. Figure 3 shows the change in AV during the epoxidation reactions of TOFA (Fig. 3a) and TOFAME (Fig. 3b). The decrease in AV during epoxidation confirmed that carboxyl groups took part in side reactions by opening oxirane rings. The most significant changes in AV were observed for the TOFA epoxidation catalyzed with 25 wt.% catalyst content.

Application of heterogeneous catalysts such as functionalized acidic ion exchange resin in epoxidation reaction provides higher selectivity and reduces side reactions compared to homogeneous catalysts [26]. Small molecules of organic acids can easily diffuse into the structure of porous acidic ion exchange resin, where the formation of peracetic acid occurs. Larger-sized molecules, such as triglycerides, can penetrate the catalyst structure much more restrictedly; thus, the generated oxirane rings are protected from attack by protons confined to the catalyst matrix [28]. The intensive occurrence of side reactions in TOFA epoxidation may suggest that due to their small size, TOFA molecules (about

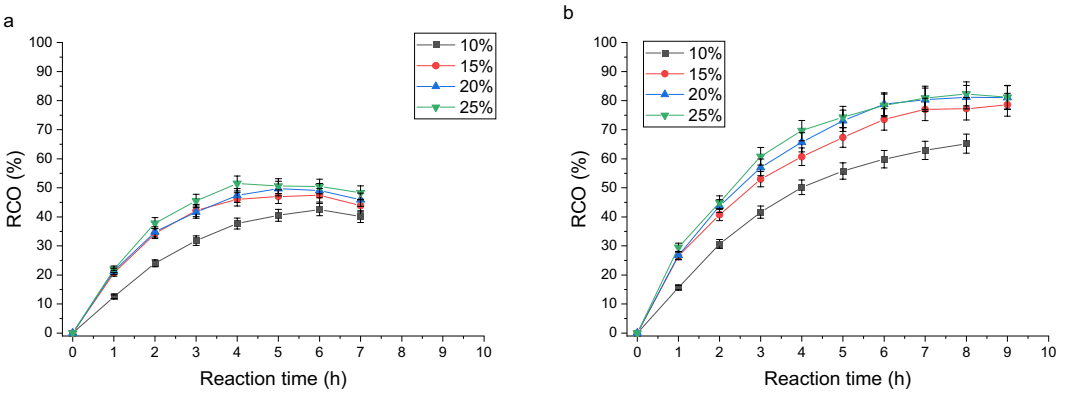

Fig. 2 RCO of TOFA **(a)** and TOFAME **(b)** at different catalyst content (wt.%)

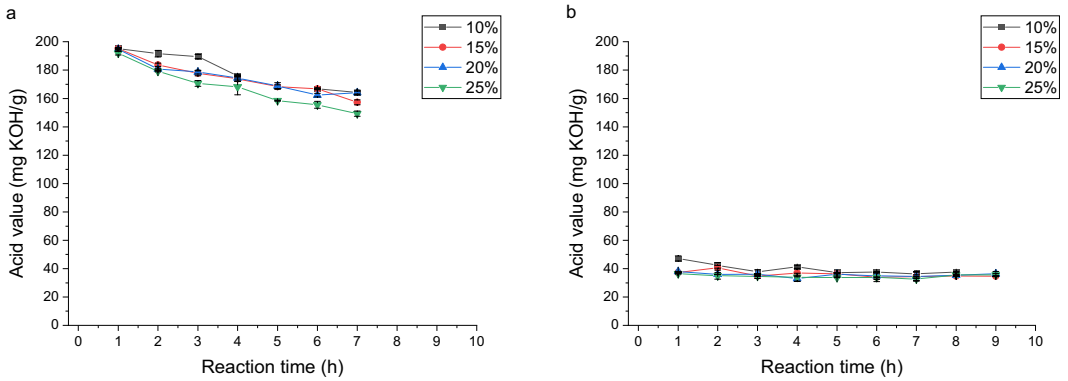

Fig. 3 The change in AV of the TOFA **(a)** and TOFAME **(b)** during the epoxidation process at different catalyst content (wt.%)

3 times smaller than triglyceride) penetrated the catalyst structure.

The TOFA and TOFAME epoxidation reaction may be also influenced by unsaturated fatty acids' composition and chemical structure. Lawer-Yolar et al. reported TOFA composition of 57.7% oleic acid, 35.4% linoleic acid and other mainly saturated fatty acids [25]. Keskin et al. [5] reported TOFA composition of 52.7% oleic acid, 38.3% linolenic acid, 6.9% linolenic acid and 2.1% stearic acid.

A study on the kinetics of the epoxidation of a high-linolenic triglyceride catalyzed by an ion exchange resin showed that the chemical groups (unsaturated and oxirane) at the 9th and 12th positions possess lower reactivity compared to the reactivity of the same groups at the 15th position. Chemical groups at the 15th position are not affected by steric and electronic effects of the glycerol center that highly affected the closer groups (at the 9th and 12th positions). The opening of the epoxy group at the 15th position can cause steric hindrance affecting the epoxidation of the rest of the double bonds but also preventing any interaction between organic acid and the epoxy groups, thus preventing their cleavage [29]. TOFA and TOFAME do not contain glycerol center, which could interact sterically and electrically with chemical groups at the 9th, 12th and 15th positions. However, in the case of TOFA epoxidation reactions, intensive oligomerization reactions leading to an increase in the molecular weight of the molecule can cause a steric hindrance preventing epoxidation of the remaining unsaturated bonds. Such phenomenon, together with the occurrence of side reactions of oxirane ring opening, can be responsible for the low RCO of TOFA epoxidation. The lower AV in the case of TOFAME reduces the formation of dimers and trimer responsible for steric hindrance thus a significantly higher RCO is achieved.

According to La Scala and Wool, rate constants of epoxidation of fatty acids methyl ester increased as the level of unsaturation increased, therefore oleic acid should undergo relatively slower epoxidation compared to linoleic and linolenic acids. An explanation for this phenomenon is that as the number of unsaturated bonds increases, the electron density increases, resulting in an increase in the reaction rate constant [30].

The change in REU over time at different catalyst content is presented in Fig. 4. The REU of TOFA (Fig. 4a) ranged from 10 to 27% and decreased with increasing catalyst content after 7 h of reaction. The lower the REU value, the more double bonds have reacted. At the same time, low RCO of TOFA (Fig. 2a) (from 40 to 48% depending on catalyst content) combined with low REU confirmed the effect of a high content of carboxyl groups (high AV) on the intensity of the oxirane ring-opening side reaction. The REU of TOFAME (Fig. 4b) ranged from 20 to 33.5% after 7 h of reaction. It was observed that increasing the catalyst content for TOFAME above 15 wt.% has no significant effect on the REU value.

The chemical structures of TOFA during the epoxidation reaction were investigated using FTIR spectroscopy. The overall FTIR of TOFA spectra are shown in Fig. 5a. The =C–H double bond stretching peak with the maximum at 3009 cm^{-1} (Fig. 5a) disappeared during the reaction, while the stretching peak at 823 cm^{-1} originating from the –C–O–C– epoxy groups appeared (Fig. 5a). The close-up of the C–O–C oxirane ring stretching vibration peak (Fig. 5c) shows the gradual increase of epoxy group content in the TOFA structure. The intensity of the epoxidation reaction decreased with time, which correlates with the RCO data (Fig. 2a). The gradual decrease of the =C–H stretching bond at 3009 cm^{-1} is shown in Fig. 5b. The peak practically disappeared, confirming previous REU results (Fig. 4a). Figure 5d shows the decreasing intensity of the stretching peak of the carboxyl groups –C=O at 1707 cm^{-1} while increasing the

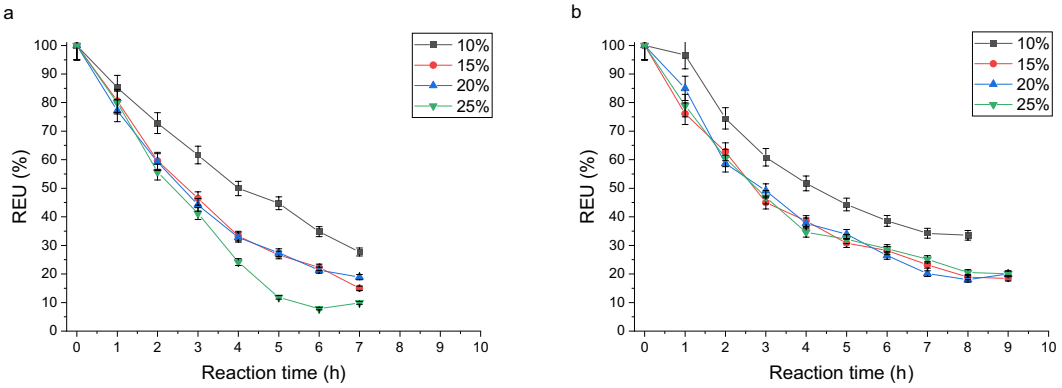

Fig. 4 REU of TOFA **(a)** and TOFAME **(b)** at different catalyst content (wt.%)

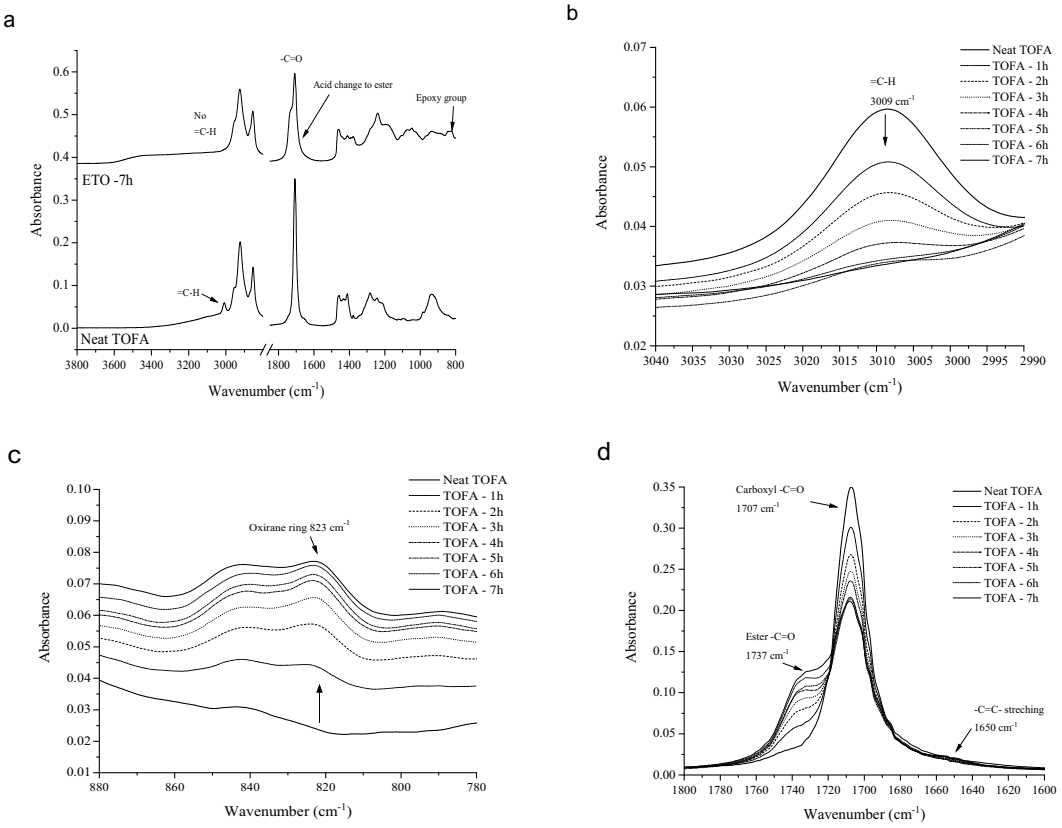

Fig. 5 FTIR spectra during TOFA epoxidation over time at 20 wt.% of the catalyst content; **a** overall FTIR spectra; **b** change of double bond absorption band, 3009 cm^{-1}, **c** change of oxirane ring vibration, 823 cm^{-1}, **d** change of carboxyl –C=O stretching vibration absorption band, 1707 cm^{-1}; ester –C=O stretching vibration absorption band, 1737 cm^{-1} and –C=C– stretching vibration band, 1650 cm^{-1}

intensity of the stretching peak vibrations of the ester groups –C = O at 1737 cm^{-1}. This indicates that the carboxyl group of TOFA opens the epoxy group with the formation of an ester group in dimers and molecules with multiples of TOFA molecular weight.

FTIR analysis of TOFAME and its epoxidation products was also performed. The overall FTIR spectra are shown in Fig. 6a. Similar to the TOFA, the = C–H double bond stretching peak at 3009 cm^{-1} (Fig. 6b) disappears almost completely during the reaction while the stretching –C–O–C– epoxy groups peak at 823 cm^{-1} increased (Fig. 6c). Figure 6d shows a close-up of the region of the carboxyl and ester group peak bands. The disappearance of the –C = O carboxyl group peak bands at 1707 cm^{-1} results in the gradual uncovering of the ester group peak band and the shift towards lower wavenumbers.

The initial presence of carboxyl group peak bands confirms their incomplete conversion during the esterification process. Nevertheless, the occurrence of side reactions affecting the increase of molecular weight and viscosity of the products was significantly reduced.

Figure 7a shows the change in TOFA viscosity during the epoxidation with different catalyst content. The initial viscosity of TOFA was 27.26 mPa•s. The resulting epoxidized TOFA synthesized with a catalyst content of 10 wt.% had a viscosity of 956.93 mPa•s. Higher catalyst content led to products with higher viscosities of 2168.00, 1736.10 and 1836.50 mPa•s for synthesis with catalyst content of 15, 20 and 25 wt.%, respectively.

The change in viscosity during TOFAME epoxidation is shown in Fig. 7b. The initial viscosity of TOFAME was 7.36 mPa•s. After 9 h of reaction (2 h longer than TOFA),

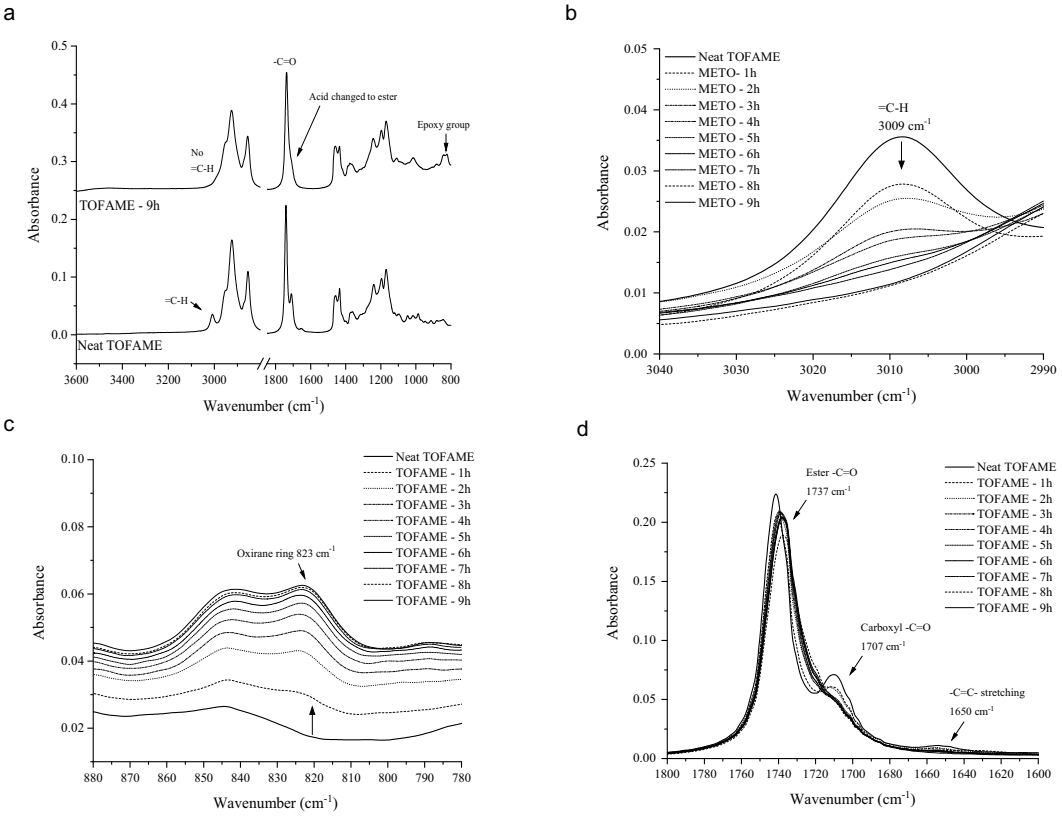

Fig. 6 FTIR spectra during TOFAME epoxidation over time at 20 wt.% of the catalyst content; **a** overall FTIR spectra; **b** change of double bond absorption band, 3009 cm^{-1}, **c** change of oxirane ring vibration, 823 cm^{-1}, **d** change of carboxyl –C = O stretching vibration absorption band, 1707 cm^{-1}; ester –C = O stretching vibration absorption band, 1737 cm^{-1} and –C = C = stretching vibration band, 1650 cm^{-1}

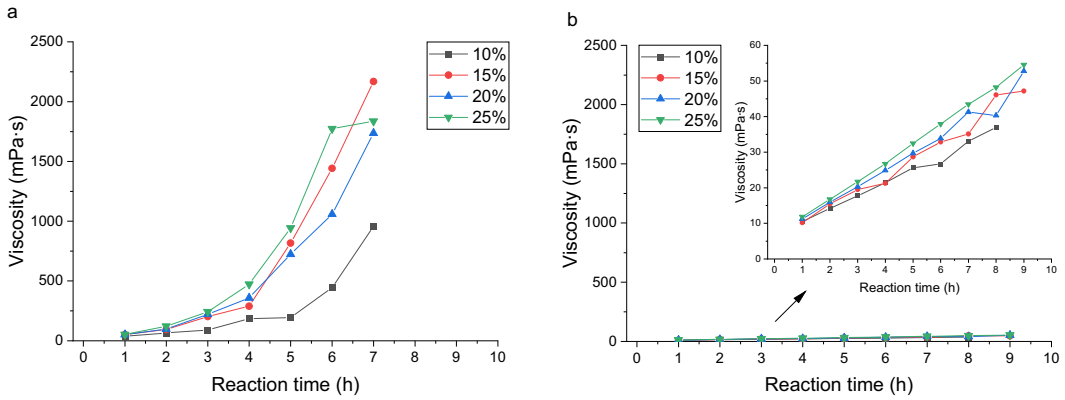

Fig. 7 The viscosity of TOFA **(a)** and TOFAME **(b)** at different catalyst content (wt.%)

the final viscosity ranged from 36.94 mPa•s to 54.55 mPa•s for the reaction catalyzed by 10 wt.% and 25 wt.% catalyst content, respectively. The resulting ETOFAME, despite its high EV, exhibited very low viscosities, being only slightly higher than the initial TOFA viscosity (27.26 mPa•s).

TOFA and TOFAME samples synthesized at 25 wt.% of the catalyst content were analyzed using GPC chromatography. It was necessary to follow the changes in molecular weight to analyze the course of the synthesis and determine the optimal duration of the synthesis. The GPC chromatograms are shown in Fig. 8. During TOFA epoxidation (Fig. 8a), a significant reduction in peak intensity with a retention time of ~ 15.30 min corresponding to the monomer content is observed. At the same time, the intensity of the peaks characterizing the content of dimers (retention time ~ 14.15 min) and trimers (retention time ~ 13.10 min) increased significantly. This indicates side reactions that occur during epoxidation involving oxirane ring-opening with the carboxyl group of fatty acid. The chromatogram also showed an increase in the peak at retention time ~ 14.90 min during the process, corresponding to by-products formed during the epoxidation process by oxirane ring-opening with AcOH.

Figure 8b characterizes content during TOFAME epoxidation. The changes in peak intensity are relatively small compared to the TOFA epoxidation process. Although the peak corresponding to the dimers is clearly observed, it is significantly lower in intensity than in the case of TOFA epoxidation, which means that they are formed in much lower content. Significantly fewer by-products, such as

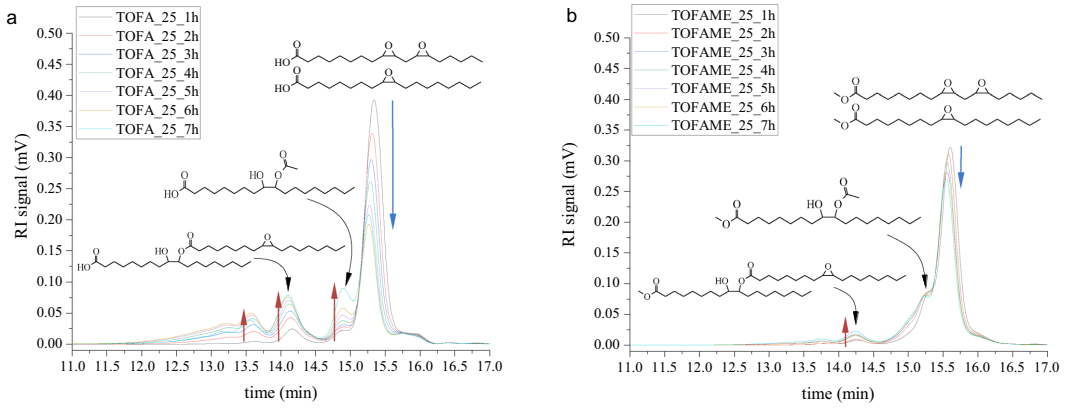

Fig. 8 GPC chromatograms during epoxidation over time at the catalyst content of 25 wt.%; **a** TOFA epoxidation **b** TOFAME epoxidation

dimers and trimers, are formed. The formation of dimers and trimers increases the viscosity of the product and thus makes it difficult to use it in further processing. Therefore, preventing the formation of these undesirable by-products during the synthesis is a significant benefit.

Polydispersity characterizes the molecular weight distribution. The change of polydispersity is shown in Fig. 9. In the case of TOFA epoxidation, the polydispersity increased significantly during the first h of epoxidation, reaching 1.8 in the 4th h. In contrast, the change in dispersity during the oxidation of TOFAME was less pronounced. It indicated greater homogeneity of TOFAME epoxidation products and smaller width of the molecular weight distribution.

Table 2 summarizes the physico-chemical properties of epoxidized TOFA and TOFAME at optimal synthesis time, which is considered to be the time when the reaction reached the highest RCO.

The selectivity of the TOFAME epoxidation reaction was about 0.98–1.00, while the TOFA epoxidation selectivity was 0.61–0.67. It was lower due to the occurance of side reactions involving oxirane ring-opening with a carboxyl group of fatty acid. It was found that the catalyst content of 20 wt.% of is sufficient to obtain products with high EV. Increasing the catalyst content to 25 wt.% did not lead to a significant increase in EV for both TOFA and TOFAME epoxidations. A lower catalyst content can reduce the cost of the epoxidation process and is consistent with cleaner production principles. The reusability and easy separation of the catalyst from the reaction products is especially important for the cost-effectiveness of the industrial scale process [21]. The further investigation consisted of conducting ten epoxidation reactions and determining the feasibility of using ion exchange resin as a catalyst multiple times.

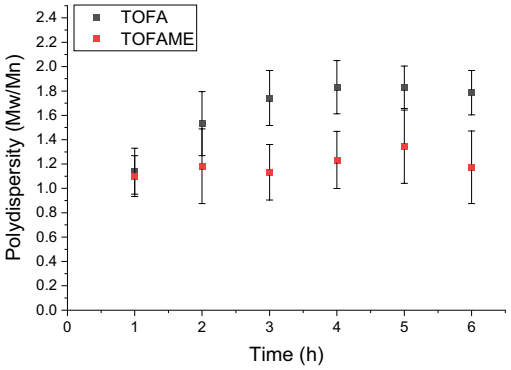

Fig. 9 Change of dispersity during epoxidation over time at the catalyst content of 25 wt.%

Figure 10 summarises the RCO and REU of 10 successive TOFA epoxidation reactions at 20 wt.% catalyst content. The results indicated good catalyst stability: the RCO was 48.2–41.9%, and the REU % was 32.2–36.3%. In a comparable experiment conducted in a batch reactor at 20 wt.% catalyst content, the RCO value after 10th reuse of the catalyst was reduced from 41.5 to 35.3% [19]. In the study by Aguilera et al. [23], the RCO of tall oil epoxidation in an isothermal batch reactor in four consecutive reactions was 42–45%.

By performing a linear approximation of the RCO and assuming a minimum value of 30% (EV approx. 0.18 mol/100 g), it can be concluded that the reusability of the catalyst in the TOFA epoxidation reaction is about 25 reactions. The use of TOFAME for the preparation of epoxidized derivatives with similar EVs to TOFA can lead to a significant extension of the catalyst lifetime.

Conclusions

A series of TOFA and TOFAME epoxidation reactions were carried out in the RBR reactor using Amberlite® IRC120 H catalyst. Results showed that methylation of TOFA allows obtaining a product with a higher

Table 2 Summary of the physico-chemical properties of epoxidized TOFA and TOFAME at optimal synthesis time

Catalyst content(wt.%)	Optimal synthesis time (h)	RCO (%)	REU (%)	EV (mol/100 g)	S	Viscosity (mPa•s)
TOFA epoxidation						
10	6	42.51	34.81	0.24	0.65	445.13
15	6	47.46	22.33	0.26	0.61	1442.7
20	5	49.75	27.41	0.27	0.68	723.06
25	4	51.52	24.18	0.28	0.67	472.36
TOFAME epoxidation						
10	8	65.22	33.53	0.33	0.98	36.94
15	7	78.61	23.18	0.40	~1.00	35.12
20	7	81.21	20.13	0.42	~1.00	41.26
25	7	82.34	25.15	0.42	~1.00	43.43

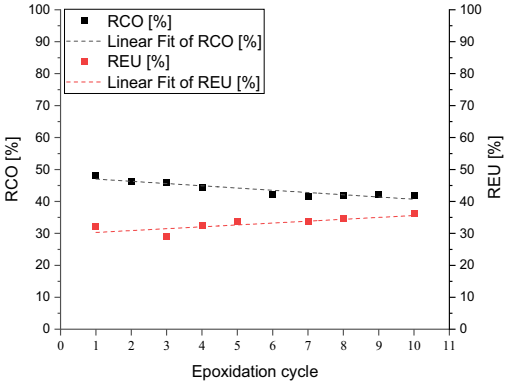

Fig. 10 The RCO and REU of TOFA at catalyst content of 20 wt.% of the successive cycles of epoxidation

epoxy value (TOFA: 0.223–0.281 mol/100 g; TOFAME 0.337–0.420 g/mol and smaller viscosity (TOFA: 956.93–2168.00 mPa•s; TOFAME: 36.94–54.55 mPa•s). The selectivity of TOFAME epoxidation reaction was higher than the selectivity of TOFA epoxidation. It was found that 20 wt.% of the Amberlite® IRC120 H is sufficient to obtain products with high epoxy value. Increasing the catalyst content to 25 wt.% did not significantly increase epoxy value for both TOFA and TOFAME epoxidations. Conducting the epoxidation reaction in the RBR reactor facilitated the separation process and provided the opportunity of reusing the catalyst. The Amberlite® IRC120 H catalyst was found to exhibit good stability in the TOFA epoxidation reaction. The relative conversion to oxirane decreased from 48.2 to 41.9% over 10 subsequent reactions. It was found that the conversion of double bonds to oxiranes in the TOFA epoxidation reaction carried out in the RBR reactor was higher than when a batch reactor was used. The produced TOFAME epoxy derivatives characterized by very low viscosity and high epoxy value are more suitable to be used as raw material for the synthesis of bio-polyols than TOFA epoxy derivatives.

Author Contributions KP: Writing—Original Draft, Investigation, Visualization; EK: Investigation, Visualization; RP: Investigation, Visualization; AF: Writing—Review & Editing, Funding acquisition, Project administration; MK: Conceptualization, Resources, Visualization, Funding acquisition, Supervision.

Funding This research was funded by ERDF project No. 1.1.1.1/20/A/098 "100% Bio-based thermal insulation polymer development".

Declarations

Conflict of Interest The authors declare that they have no competing interests as defined by Springer, or other interests that might be perceived to influence the results and/or discussion reported in this paper.

Open Access This article is licensed under a Creative Commons Attribution 4.0 International License, which permits use, sharing, adaptation, distribution and reproduction in any medium or format, as long as you give appropriate credit to the original author(s) and the source, provide a link to the Creative Commons licence, and indicate if changes were made. The images or other third party material in this article are included in the article's Creative Commons licence, unless indicated otherwise in a credit line to the material. If material is not included in the article's Creative Commons licence and your intended use is not permitted by statutory regulation or exceeds the permitted use, you will need to obtain permission directly from the copyright holder. To view a copy of this licence, visit http://creativecommons.org/licenses/by/4.0/.

References

1. Satish JG, Nagesha N (2018) Cleaner production: a brief literature review. Mater Today Proc 5:17944–17951. https://doi.org/10.1016/j.matpr.2018.06.124
2. Aryan V, Kraft A (2021) The crude tall oil value chain: global availability and the influence of regional energy policies. J Clean Prod 280:124616. https://doi.org/10.1016/j.jclepro.2020.124616
3. Vevere L, Fridrihsone A, Kirpluks M, Cabulis U (2020) A review of wood biomass-based fatty acids and rosin acids use in polymeric materials. Polymers (Basel) 12:1–17. https://doi.org/10.3390/polym12112706
4. Konwar LJ, Mikkola JP, Bordoloi N et al (2018) Sidestreams from bioenergy and biorefinery complexes as a resource for circular bioeconomy. Elsevier B.V. https://doi.org/10.1016/B978-0-444-63992-9.00003-3
5. Keskin A, Yaşar A, Gürü M, Altiparmak D (2010) Usage of methyl ester of tall oil fatty acids and resinic acids as alternative diesel fuel. Energy Convers Manag 51:2863–2868. https://doi.org/10.1016/j.enconman.2010.06.025
6. Konwar LJ, Oliani B, Samikannu A et al (2022) Efficient hydrothermal deoxygenation of tall oil fatty acids into n-paraffinic hydrocarbons and alcohols in the presence of aqueous formic acid. Biomass Convers Biorefinery 12:51–62. https://doi.org/10.1007/s13399-020-01103-3
7. Knuuttila P, Kukkonen P, Hotanen U (2015) Method and apparatus for preparing fuel components from crude tall oil. US Patent No. 9024095 B2
8. Kairytė A, Kirpluks M, Ivdre A et al (2018) Cleaner production of polyurethane foam: replacement of conventional raw materials, assessment of fire resistance and environmental impact. J Clean Prod 183:760–771. https://doi.org/10.1016/j.jclepro.2018.02.164
9. Kirpluks M, Vanags E, Abolins A et al (2019) Chemo-enzymatic oxidation of tall oil fatty acids as a precursor for further polyol production. J Clean Prod 215:390–398. https://doi.org/10.1016/j.jclepro.2018.12.323
10. Sardon H, Mecerreyes D, Basterretxea A et al (2021) From lab to market: current strategies for the production of biobased polyols. ACS Sustain Chem Eng 9:10664–10677. https://doi.org/10.1021/acssuschemeng.1c02361
11. Maisonneuve L, Chollet G, Grau E, Cramail H (2016) Vegetable oils: a source of polyols for polyurethane materials.

OCL—Oilseeds fats, Crop Lipids. https://doi.org/10.1051/ocl/2016031
12. Xia Y, Larock RC (2010) Vegetable oil-based polymeric materials : synthesis, properties, and applications. Green Chem. https://doi.org/10.1039/c0gc00264j
13. Uschanov P, Heiskanen N, Mononen P et al (2008) Synthesis and characterization of tall oil fatty acids-based alkyd resins and alkyd-acrylate copolymers. Prog Org Coatings 63:92–99. https://doi.org/10.1016/j.porgcoat.2008.04.011
14. Abolins A, Pomilovskis R, Vanags E et al (2021) Impact of different epoxidation approaches of tall oil fatty acids on rigid polyurethane foam thermal insulation. Materials (Basel) 14:1–17. https://doi.org/10.3390/ma14040894
15. Meng Y, Taddeo F, Aguilera AF et al (2021) The lord of the chemical rings: catalytic synthesis of important industrial epoxide compounds. Catalysts. https://doi.org/10.3390/catal11070765
16. Omonov TS, Kharraz E, Curtis JM (2016) The epoxidation of canola oil and its derivatives. RSC Adv 6:92874–92886. https://doi.org/10.1039/c6ra17732h
17. Kirpluks M, Vanags E, Abolins A et al (2020) High functionality bio-polyols from tall oil and rigid polyurethane foams formulated solely using bio-polyols. Materials (Basel) 13:38–53. https://doi.org/10.3390/MA13081985
18. Kurańska M, Beneš H, Prociak A et al (2019) Investigation of epoxidation of used cooking oils with homogeneous and heterogeneous catalysts. J Clean Prod 236:117615. https://doi.org/10.1016/j.jclepro.2019.117615
19. Abolins A, Kirpluks M, Vanags E et al (2020) Tall oil fatty acid epoxidation using homogenous and heterogeneous phase catalysts. J Polym Environ 28:1822–1831. https://doi.org/10.1007/s10924-020-01724-9
20. Mungroo R, Pradhan NC, Goud VV, Dalai AK (2008) Epoxidation of canola oil with hydrogen peroxide catalyzed by acidic ion exchange resin. J Am Oil Chem Soc 85:887–896. https://doi.org/10.1007/s11746-008-1277-z
21. Miceli M, Frontera P, Macario A, Malara A (2021) Recovery/reuse of heterogeneous supported spent catalysts. Catalysts. https://doi.org/10.3390/catal11050591
22. Wai PT, Jiang P, Shen Y et al (2019) Catalytic developments in the epoxidation of vegetable oils and the analysis methods of epoxidized products. RSC Adv 9:38119–38136. https://doi.org/10.1039/c9ra05943a
23. Freites Aguilera A, Rahkila J, Hemming J et al (2020) Epoxidation of tall oil catalyzed by an ion exchange resin under conventional heating and microwave irradiation. Ind Eng Chem Res 59:10397–10406. https://doi.org/10.1021/acs.iecr.0c01288
24. Freites Aguilera A, Hämäläinen R, Eränen K et al (2021) Prilezhaev epoxidation of oleic acid in the presence and absence of ultrasound irradiation. J Chem Technol Biotechnol 96:1874–1881. https://doi.org/10.1002/jctb.6706
25. Lawer-Yolar G, Dawson-Andoh B, Atta-Obeng E (2021) Synthesis of biodiesel from tall oil fatty acids by homogeneous and heterogeneous catalysis. Sustain Chem 2:206–221. https://doi.org/10.3390/suschem2010012
26. Dinda S, Goud VV, Patwardhan AV, Pradhan NC (2011) Selective epoxidation of natural triglycerides using acidic ion exchange resin as catalyst. Asia-Pacific J Chem Eng 6:870–878. https://doi.org/10.1002/apj.466
27. Petrović ZS, Zlatanić A, Lava CC, Sinadinović-Fišer S (2002) Epoxidation of soybean oil in toluene with peroxoacetic and peroxoformic acids - Kinetics and side reactions. Eur J Lipid Sci Technol 104:293–299. https://doi.org/10.1002/1438-9312(200205)104:5%3c293::AID-EJLT293%3e3.0.CO;2-W
28. Musante RL, Grau RJ, Baltanás MA (2000) Kinetic of liquid-phase reactions catalyzed by acidic resins: the formation of peracetic acid for vegetable oil epoxidation. Appl Catal A Gen 197:165–173. https://doi.org/10.1016/S0926-860X(99)00547-5
29. Kousaalya AB, Beyene SD, Ayalew B, Pilla S (2019) Epoxidation kinetics of high-linolenic triglyceride catalyzed by solid acidic-ion exchange resin. Sci Rep 9:1–12. https://doi.org/10.1038/s41598-019-45458-8
30. La Scala J, Wool RP (2002) Effect of FA composition on epoxidation kinetics of TAG. JAOCS, J Am Oil Chem Soc 79:373–378. https://doi.org/10.1007/s11746-002-0491-9

Publisher's Note Springer Nature remains neutral with regard to jurisdictional claims in published maps and institutional affiliations.

Ralfs Pomilovskis Rīgas Tehniskajā universitātē (RTU) ieguvis inženierzinātņu bakalaura grādu ķīmijas tehnoloģijā (2018) un dabaszinātņu maģistra grādu ķīmijā (2020). No 2017. gada strādā Latvijas Valsts koksnes ķīmijas institūtā sākotnēji Biorafinēšanas laboratorijā, kurā izstrādājis arī bakalaura un maģistra darbu par levoglikozenona iegūvi katalītiskās ātrās pirolīzes procesā, bet kopš 2020. gada – Polimēru laboratorijā ķīmijas inženiera amatā, nododoties polimērmateriālu izstrādei un pētniecībai. 2022. gadā ievēlēts par RTU Ķīmijas un ķīmijas tehnoloģijas institūta zinātnisko asistentu. Patlaban profesionālajā jomā galvenokārt fokusējas uz Maikla komponentu sintezēšanu no talejļas taukskābēm un to izmantošanu dažādu polimērmateriālu ieguvei.

Ralfs Pomilovskis obtained a Bachelor's degree in Chemical Technology (2018) and a Master's degree in Chemistry (2020) from the Riga Technical University. Since 2017, he has been working at the Latvian State Institute of Wood Chemistry, initially in the Biorefinery Laboratory, where he also developed his bachelor's and master's theses about levoglucosenone production in the catalytic fast pyrolysis process, since 2020 – in the Polymer Laboratory as a chemical engineer, devoting himself to the development and research of polymer materials. In 2022, he was appointed as a research assistant at the Institute of Chemistry and Chemical Technology of Riga Technical University. In the professional field, he is now focusing mainly on synthesising the Michael components from tall oil fatty acids and using them to produce various polymer materials.